Scientific Computation

Bernard Shizgal

Spectral Methods in Chemistry and Physics

Applications to Kinetic Theory and Quantum Mechanics

Springer

Spectral Methods in Chemistry and Physics

Scientific Computation

More information about this series at http://www.springer.com/series/718

Bernard Shizgal

Spectral Methods in Chemistry and Physics

Applications to Kinetic Theory and Quantum Mechanics

Springer

Bernard Shizgal
University of British Columbia
Vancouver, BC
Canada

ISSN 1434-8322
Scientific Computation
ISBN 978-94-017-9453-4 ISBN 978-94-017-9454-1 (eBook)
DOI 10.1007/978-94-017-9454-1

Library of Congress Control Number: 2014955993

Springer Dordrecht Heidelberg New York London

Printed on acid-free paper

Springer Science+Business Media B.V. Dordrecht is part of Springer Science+Business Media (www.springer.com)

Preface

Spectral and pseudospectral methods have become increasingly popular as higher order methods for the solution of partial differential and integral equations (Azaïez et al. 2013). A spectral method refers to the representation of the solution of some problem in a basis set of orthogonal functions, whereas a pseudospectral approach, sometimes referred to as a collocation, is based on the representation of the solution with the function values at a set of discrete points. For the smooth solutions of particular problems, these methods can provide exponential convergence of the solutions versus the number of basis functions or the number of grid points retained.

Books devoted to these methods include the monographs by Shen et al. (2011), Kopriva (2009), Hesthaven et al. (2007) and the new edition of the book by Canuto et al. (2006). Other textbooks include those by Peyret (2002), Deville et al. (2002), Boyd (2001), Trefethen (2000), Shu (2000), Fornberg (1996), Funaro (1992), Guo (1998) and Gottlieb and Orszag (1977).

In view of the availability of texts on spectral/pseudospectral methods, it might be appropriate to question whether another book on this subject is justfied. The aforementioned books are devoted primarily to problems in fluid mechanics and to the solutions of the Navier-Stokes, Helmholtz, Poisson equations and related problems most often for bounded intervals. At the present time, a textbook that covers the fundamental aspects of spectral and pseudospectral methods with applications to problems in chemistry and physics does not exist.

The main objective is to provide the basic concepts of spectral and pseudo-spectral methods to the solution of problems in diverse fields of interest to a wide audience, and to demonstrate the improved convergence obtained with nonclassical basis functions for certain problems. Perhaps the first application of a collocation method in physics was the solution of the integro-differential radiative transfer equation by Chandrasekhar (1944, 1960) based on Gauss-Legendre quadrature points. There are many applied problems in chemistry, physics, astrophysics, engineering, biology, economics and other fields for which spectral/pseudospectral methods can be used to advantage.

The basic mathematics and numerical methods used in the book are presented in Chaps. 1–4, whereas Chaps. 5 and 6 summarize the applications of spectral and

pseudospectral methods to several specialized topics in nonequilibrium statistical mechanics and quantum mechanics. A brief overview of the background physics is provided for some of the topics.

Chapter 1 presents the basic concepts of spectral space and physical space for the representations of functions and the unitary transformation between the two spaces. A Hilbert space is defined as are hermitian operators, Sturm-Liouville eigenvalue problems and the Rayleigh-Ritz variational theorem, which might also be referred to as a method of weighted residuals or a Galerkin method. A personal historical summary of the development of pseudospectral methods in chemistry and physics is also presented with an overview of the topics in the book.

Chapter 2 provides the fundamental mathematics used throughout the book. The construction of orthogonal polynomials in terms of the three term recurrence relation is discussed. The numerical instability inherent in the Gram-Schmidt orthogonalization to construct basis sets is demonstrated with applications to Legendre, Hermite and the nonclassical Rys polynomials. Numerical round-off errors in scientific computations can sometimes be very subtle as is demonstrated in several applications. Lagrange interpolation is introduced as the basis for Newton-Cotes integration algorithms and Gaussian quadrature. The Gaussian quadrature points are the eigenvalues of the Jacobi matrix, the matrix representation of the continuous multiplicative coordinate operator and defined in terms of the recurrence coefficients in the three term recurrence relation. From a quantum mechanical perspective, the Jacobi matrix is the discrete approximation to the continuous eigenvalues of the coordinate operator. The quadrature weights are determined from the eigenvectors of the Jacobi matrix.

In addition to a summary of the properties of the classical polynomials, several nonclassical basis sets such as the Maxwell polynomials orthogonal with respect to weight function $w(x) = x^p e^{-x^2}$ on the semi-infinite axis, the Rys polynomials with $w(x) = e^{-cx^2}$ on the interval $[-1, 1]$ and bimodal polynomials with $w(x) = \exp(-(x^4/(4\epsilon) - x^2/(2\epsilon)))$ for both the infinite and semi-infinite axes are presented. These polynomial basis sets and associated quadratures are used in kinetic theory, quantum mechanics and chemical kinetics. Alternate interpolation algorithms such as the sinc function, B-splines and radial basis functions are also discussed.

In Chap. 3, the convergence of the integration algorithms of Chap. 2 versus the number of quadrature points is compared for integrals that occur for several physical systems. The systems include chemical and nuclear reaction rates, the integral over the "cusp" in the Boltzmann integral collision operator as well as for quantum mechanical scattering phase shifts. The calculation of matrix elements of multiplicative operators, namely the collision frequency in the Boltzmann equation and the interaction potential in the Schrödinger equation are compared. Several challenging integrals such as integrals with oscillating integrands and electron repulsion integrals in quantum chemistry are reviewed. The last section describes the discrete matrix representation of derivative operators employed in pseudospectral methods. The exact pseudospectral solutions of Sturm-Liouville eigenvalue equations for the classical polynomials is demonstrated.

Chapter 4 illustrates spectral convergence in the expansion of selected functions in different basis sets. The expansions of simple Gaussians, as well as the Kappa distribution of space physics, in Hermite and Laguerre polynomials are presented with an analysis of the spectral convergence. Fourier series expansions are included and applied to the construction of wave packets in quantum mechanics and the resolution of a free induction decay curve typical in Fourier Transform spectroscopy. Also presented is the resolution of the oscillations at a jump discontinuity, known as the Gibbs phenomenon, that arise in the Fourier series representation of a piecewise continuous function. A brief description of the Runge phenomenon is also discussed.

In Chap. 5, the applications to the solution of integral equations with particular emphasis on the Boltzmann equation of kinetic theory are presented. The use of spectral and pseudospectral methods in the determination of the eigenvalue spectra of the linearized (one component) and linear (two component) integral collision operators is presented. The spectra of both operators consist of discrete and continuous eigenvalues as can also occur for the eigenvalue spectrum of the Hamiltonian in the Schrödinger equation for particular potentials. A brief summary is provided of the Chapman-Enskog method of solution of the Boltzmann equation that yields the integral equations that define the transport coefficients in a dilute gas. The relaxation of initial nonequilibrium distributions, including anisotropic initial distributions, is studied versus the mass ratio of the two components in a binary gaseous mixture. The classic Milne problem of astrophysics and kinetic theory is presented and applied to a study of the nonequilibrium effects associated with the escape of light atoms from planetary atmospheres. As can be ascertained from this overview, there are several different applications included and the presentation shifts quickly from topic to topic.

Chapter 6 consists of applications of spectral and pseudospectral methods for the solution of the Fokker-Planck equation (Risken and Till 1996) in nonequilibrium statistical mechanics and the Schrödinger equation (Liboff 2002) in quantum mechanics. Fokker-Planck equations can be transformed to Schrödinger equations and the potentials that result belong to supersymmetric quantum mechanics (Comtet et al. 1985; Dutt et al. 1988; Cooper et al. 1995). The nonclassical basis sets and quadrature points are chosen based on the equilibrium probability density functions for the Fokker-Planck equations. Fokker-Planck equations for Brownian motion, for relaxation in the disparate mass limits of the linear Boltzmann equation known as the Rayleigh and Lorentz limits and for models of cis-trans isomerization reactions are solved with both spectral and pseudospectral methods. Pseudospectral methods are used for the solution of Sturm-Liouville eigenvalue problems for simple systems. With the appropriate choice of weight function, a quadrature can be constructed for which the pseudospectral representation of the Hamiltonian in the Schrödinger equation does not include an explicit reference to the potential. As is the case for Chap. 5, the topics in this chapter also change quickly from topic to topic.

I have deliberately limited the use of acronyms as they are often not unique. A good example is DFT which can be either Density Functional Theory or Discrete Fourier Transform. In kinetic theory, BGK refers to the Bhatnager-Gross-Krook

model of the Boltzmann collision operator, whereas in plasma physics it signifies Bernstein-Green-Kruskal solitary waves. The subject matter of the book spans several disciplines and the use of acronyms would defeat the purpose of reaching a broad audience.

I have provided in footnotes very brief biographies of the scientists and mathematicians who have provided the mathematical and physical concepts upon which much of the current research is based. As an example, Josiah Willard Gibbs (1839–1903) is familiar to mathematicians for his contributions to the understanding of the slow convergence of the Fourier series for functions with jump discontinuities leading to oscillations referred to as the Gibbs phenomenon. Gibbs is very well known to chemists and physicists as a thermodynamicist and his name is associated with the Gibbs free energy and for his contributions to entropy concepts in physical systems. The biography of Gibbs at aps.org mentions that, "When his publications were read, they were considered too mathematically complex for most chemists and too scientific for many mathematicians". Much of the current applied work by chemists and physicists could not be done without the mathematics developed by mathematicians and scientists. More detailed and interesting discourses of the contributions of many people and their personal careers can be found on the Internet and published biographies.

MATLAB® codes are provided for many of the numerical results reported in the book. These were developed on a 64 bit personal computer with an Intel i5 CPU at 2.50 GHz and 8 GB RAM. The computational time in most cases was of the order of several seconds and usually less than one minute. The codes in some instances are not completely vectorized and a few "for" loops remain. As a consequence, the codes are hopefully more transparent to the user for a very small cost in the computational time. Although several short MATLAB codes are listed in the text, the vast majority of the codes were finalized after submission of the manuscript. The codes and accompanying documentation are available at www.springer.com and at spectralmethods.chem.ubc.ca.

The book is intended for use by upper year undergraduates, graduate students as well as established researchers working on applied problems in chemistry, physics, astrophysics, space science, plasma physics, biology, engineering and in other related fields. The large bibliography provided is to current research in these diverse fields. Although many mathematical results are proved and the fundamental principles are illustrated with numerical examples, the presentation is utilitarian and not meant to be mathematically rigorous. I provide references to textbooks and review papers where more rigorous mathematical approaches are presented. I have also included very brief derivations of the integral and/or differential equations defining the physical problems considered with references to more detailed discussions. The large bibliography provided is the evidence of the wide applicability of spectral/pseudospectral methods in science and engineering.

This book is the result of 30 years of research employing spectral and pseudospectral methods for the solution of a wide range of different physical problems. I have not benefited from the opportunity to teach this material to several cohorts of undergraduate and/or graduate students. However, I am indebted to

numerous graduate students, postdoctoral fellows and other collaborators, who are cited in the references provided, for their contributions to this research. I am also very grateful to several colleagues who proofread portions of a preliminary version of the book. The people involved are Patrick Casasm-Chenaï, Daniel Hubert, Joseph Lemaire, Joseph Lo, Norman McCormick, Gren Patey, Viviane Pierrard, Bob Snider and Larry Viehland. My heartfelt thanks are extended especially to Daniel Baye, Livio Gibelli, Jae-Hun Jung, Konstantin Kabin and Mark Thachuk for their conscientious reading of several chapters. The many constructive comments of these people are very much appreciated and their contributions to the book cannot be underestimated. However, I am solely responsible for any errors that remain and I encourage readers of the book to report any further corrections to me at shizgal@chem.ubc.ca. A list of errata and MATLAB codes will be posted periodically at the websites provided. I thank Maria Bellantone and Mieke van der Fluit at Springer for their advice and their extreme patience with this project. Very special thanks to my wife, Judy, for putting up with my preoccupation with this effort for several years.

Vancouver, Canada Bernard Shizgal
October 2014

References

Azaïez, M., El Fekih, H., Hesthaven, J.S.: Spectral and High Order Methods for Partial Differential Equations-ICOSAHOM 2012. Springer, Berlin (2013)

Boyd, J.P.: Chebyshev and Fourier Spectral Methods. Dover, New York (2001)

Canuto, C., Hussaini, M.Y., Quarteroni, A., Zang, T.A.: Spectral Methods: Fundamentals in Single Domains. Springer, New York (2006)

Chandrasekhar, S.: On the radiative equilibrium of a stellar atmosphere II. Astrophys. J. **100**, 76–86 (1944)

Chandrasekhar, S.: Radiative Transfer. Dover, New York (1960)

Comtet, A., Bandrauk, A.D., Campbell, D.K.: Exactness of semiclassical bound-state energies for supersymmetric quantum-mechanics. Phys. Lett. B. **150**, 159–162 (1985)

Cooper, F., Khare, A., Sukhatme, U.: Supersymmetry and quantum mechanics. Phys. Rep. **251**, 267–385 (1995)

Deville, M.O., Fisher, P.F., Mund, E.H.: High Order Methods for Incompressible Fluid Flow. Cambridge University Press, Cambridge (2002)

Dutt, R., Khare, A., Sukhatme, U.P.: Supersymmetry, shape invariance and exactly solvable potentials. Am. J. Phys. **56**, 163–168 (1988)

Fornberg, B.: A Practical Guide to Pseudospectral Methods. Cambridge University Press, Cambridge (1996)

Funaro, D.: Polynomial Approximation of Differential Equations. Springer, Berlin (1992)

Gottlieb, D., Orszag, S.: Numerical Analysis of Spectral Methods: Theory and Applications. SIAM, Philadelphia (1977)

Guo, B.-Y.: Spectral Methods and Their Applications. World Scientific, Singapore (1998)

Hesthaven, J.S., Gottlieb, S., Gottlieb, D.: Spectral Methods for Time Dependent Problems. Cambridge University Press, Cambridge (2007)

Kopriva, D.A.: Implementing Spectral Methods for Partial Differential Equations Algorithms for Scientists and Engineers. Springer, Berlin (2009)
Liboff, R.L.: Introductory Quantum Mechanics, 4th edn. Addison-Wesley, New York (2002)
Peyret, R.: Spectral Methods for Incompressible Viscous Flow. Springer, New York (2002)
Risken, H., Till, F.: The Fokker-Planck Equation: Methods of Solution and Applications, 2nd edn. Springer, Berlin (1996)
Shen, J., Tang, T., Wang, L.-L.: Spectral Methods: Algorithms, Analysis and Applications. Springer, Berlin (2011)
Shu, C.: Differential Quadrature and Its Application in Engineering. Springer, Berlin (2000)
Trefethen, L.N.: Spectral Methods in MATLAB. SIAM, Philadelphia (2000).

Contents

Chapter 1
Introduction to Spectral/Pseudospectral Methods

Abstract This chapter introduces the basic principles of spectral/pseudospectral methods for the solution of partial differential and/or integral equations that serve to model a large number of physical processes in chemistry and physics. The first part of the chapter defines the spectral space representation of functions and the transformation to the physical space representation. A Hilbert space is defined as well as the definition of self-adjoint operators that occur in quantum mechanics and kinetic theory. The Rayleigh-Ritz variational principle and the method of weighted residuals are discussed. An historical summary of the development of pseudospectral methods in chemistry and physics is presented together with an outline of the book. The science, the mathematical models and the computer algorithms are interrelated.

1.1 Introduction

This book describes current spectral and pseudospectral methods for the solution of partial differential and/or integral equations that model a large number of systems and processes in chemistry and physics with many applications to biology, engineering, astrophysics and space science. We consider physical systems and processes that are modeled theoretically with the principles of quantum mechanics and kinetic theory. This introduction provides an overview of several physical systems for which spectral and pseudospectral methods are used to solve the differential and/or integral equations that define the problems.

The basic mathematical tools are briefly presented in Sects. 1.2 and 1.3. A more detailed presentation of the mathematics and numerical algorithms is presented in Chap. 2. There are also many comprehensive discussions of this material in the bibliography provided.

A personal historical summary of the development of pseudospectral methods with applications to physical problems in chemistry, physics, biology and engineering is presented in Sect. 1.4. This is a very broad subject that cannot be covered in detail in a single volume. The many references provided form a very important additional resource to the material presented here. This large bibliography also demonstrates the widespread use of the mathematical/numerical methods that are described.

B. Shizgal, *Spectral Methods in Chemistry and Physics*, Scientific Computation,
DOI 10.1007/978-94-017-9454-1_1

Quantum theory (Messiah 1961; Liboff 2002) based on the Schrödinger [1] equation provides the theoretical description of numerous systems in chemistry and physics. An important problem in quantum chemistry is the calculation of the electronic energy states for a molecule taking into account the electron-nuclei and electron-electron Coulombic interactions for fixed positions of the nuclei (Sherrill 2010). This is referred to as electronic structure theory (Szabo and Ostlund 1996; Friesner 1991; Helgaker et al. 2000; Levine 2009) and includes density functional theory (Jones and Gunnarsson 1989; Morgan 1996; Tsuneda 2014).

The potential from the solution of the electronic problem is used in the Schrödinger equation for the motion of the nuclei and provides the rotational and vibrational states of the molecule (Friesner et al. 1993; Light and Carrington 2000; Koput et al. 2001). A complementary problem concerns the quantum description for the continuum or scattered states that are of concern in collision theory (Child 1996; Taylor 2012) especially as applied to theoretical chemical kinetics and photochemistry (Cassam-Chenaï and Liévin 2012; Balint-Kurti 2008; Burke 2011). These applications and many others (Hu et al. 2002; Baye et al. 2008; Amore et al. 2009; Heyl and Thirumalai 2010) are active areas of research in chemistry and physics requiring efficient computational algorithms.

Statistical mechanics can be divided into equilibrium and non-equilibrium statistical mechanics which includes kinetic theory. Kinetic theory is based on the Boltzmann[2] equation (Liboff 2003; Kremer 2010) or the Fokker[3]-Planck[4] equation (Chandrasekhar 1949; Risken and Till 1996) for the particle distribution functions that define, for example, the transport coefficients in a dilute gas as well as chemical reaction rates including nuclear reactions. For collision dominated gaseous systems, the Chapman[5]-Enksog[6] method (Chapman and Cowling 1970) of solution of the Boltzmann equation yields the macroscopic equations of fluid mechanics and in

[1] Erwin Schrödinger (1887–1961) was an Austrian physicist who worked on fundamental aspects of quantum theory and developed the equation that bears his name. He also made important contributions to statistical mechanics and thermodynamics and had an interest in biology and philosophy. He was awarded the 1933 Nobel Prize for his development of wave mechanics in quantum theory.

[2] Ludwig Eduard Boltzmann (1844–1906) was an Austrian physicist who made significant contributions to statistical mechanics and proposed the kinetic equation that bears his name. The equilibrium particle distribution is the Maxwell-Boltzmann distribution.

[3] Adrian Fokker (1887–1972) was a Dutch physicist and made contributions to relativity in addition to statistical mechanics. The Fokker-Planck equation used to model numerous processes in physics, astrophysics, chemistry, finance and biology bears his name. He also made numerous contributions to music theory.

[4] Max Planck (1858–1947) was a German physicist and was awarded the 1918 Nobel Physics Prize for his contributions to quantum theory. Planck and Fokker independently derived the Fokker-Planck equation of statistical physics.

[5] Sydney Chapman (1888–1970) was a British mathematician and geophysicist developed the Chapman-Enksog method of solution of the Boltzmann equation and contributed to the theory of stochastic processes. He also made many fundamental contributions to geophysics.

[6] David Enskog (1884–1947) was a Swedish mathematical physicist who contributed to the kinetic theory of gases with the method of solution developed with Chapman.

particular the Navier[7]-Stokes[8] equation. This complements the usual derivation of the equations of fluid mechanics in terms of mass, momentum and energy conservation (Kundu et al. 2012; Durran 2010). Spectral and pseudospectral methods have been extensively applied to problems in fluid mechanics (Gottlieb and Orszag 1977; Peyret 2002; Canuto et al. 2006b).

We consider a large number of systems that includes radiative and neutron transport, astrophysics, plasma physics and space science that can be described with kinetic theory. We do not consider applications of equilibrium statistical mechanics to liquids and electrochemistry that are currently studied primarily with Monte Carlo simulations (Car and Parrinello 1985; Landau and Binder 2009). The direct simulation Monte Carlo method (Bird 1994) used for many rarefied gas dynamical problems is not discussed.

The vast number of applications of kinetic theory in many different fields is truly remarkable. If the particles of interest are photons, the Boltzmann equation is replaced with a radiative transfer equation and we find applications to the transport of radiation in atmospheric science (Liou 2002; Thomas and Stamnes 2002), radio therapy (Gifford et al. 2006) and astrophysics (Chandrasekhar 1949). The evolution of stars in globular clusters can be studied with the Fokker-Planck equation with the interstellar gravitational Coulomb interactions (Lightman and Shapiro 1978; Chavanis 2006; Binney and Tremaine 2008) analogous to the use in plasma physics (Birdsall and Langdon 2005; Anderson et al. 2004; Peeters and Strintzi 2008). The development of nuclear reactors (Hebert 2009) requires kinetic theory to understand the thermalization and transport of neutrons (Davison 1957; Williams 1966), and nuclear reaction rates (Atenzi and Meyer-Ter-Vehn 2004).

There are also important applications to the escape of atoms from planetary atmospheres (Fahr and Shizgal 1983; Shizgal and Arkos 1996) as well as the loss of charged particles from the earth (Lie-Svendsen and Rees 1996; Pierrard and Lemaire 1998) and the sun (Echim et al. 2011). A complementary problem is the escape of stars from a globular cluster (Spitzer and Härm 1958; Lemou and Chavanis 2010) and relativistic astrophysics (Bonazzola et al. 1999; Grandclément and Novak 2009). We will not be able to consider all of these applications. However, we will provide some of the basic concepts with concern to the numerical modeling of particular systems with spectral and pseudospectral methods.

In each application, the physical problem is approximated with a mathematical model which for most applications requires a numerical solution of partial differential or integral equations. The objectives can be summarized in the flow chart in Fig. 1.1. We consider a mathematical model which provides an approximate description of the physical system. A numerical algorithm is developed to solve the differential or integral equations for the model. The results are compared with observations

[7] Claude Louis Navier (1785–1836) was a French mathematician who worked in engineering science with emphasis on bridge building and also made basic contributions to fluid mechanics. He was a student and colleague of Fourier.

[8] Sir George Gabriel Stokes (1819–1903) was a Irish/English mathematical physicist and made fundamental contributions to fluid dynamics including Stokes' law and Navier-Stokes equation.

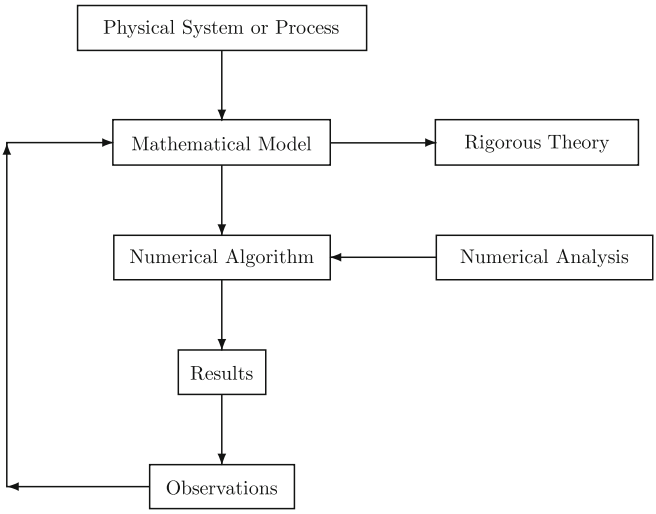

Fig. 1.1 Flow diagram of the modelling of physical systems or processes

and revisions to the mathematical model are made as required. There are often more rigorous mathematical treatments for much simplified models of the physical system. There are many discussions with concern to the numerical analysis of the algorithms used. We will not consider in detail these theoretical aspects but we will provide references to research papers that complement the presentation. The objective is to provide a utilitarian approach for the use of spectral and pseudospectral methods.

Computer power has become readily available and inexpensive and fairly large complex systems can be modeled numerically with ease. The advances made in this area parallels advances made in the development of numerical methods and algorithms for the numerical solution for a large number of applied problems. Our main objective in this book is to demonstrate the ease of use of spectral and pseudospectral methods in the efficient numerical modeling of many systems and processes.

1.2 Spectral and Pseudospectral Methods

We provide in this section a brief overview of spectral and pseudospectral methods. The origin of the terminology, "spectral" is not entirely clear but probably arises from the original use of Fourier[9] sines and cosines as basis functions (Gottlieb and Orszag 1977; Brown and Churchill 1993) especially in connection with a time series analysis and the fundamental frequencies of a process, namely the "spectrum" (Shen et al. 2011).

[9] Jean Baptiste Joseph Fourier (1768–1830) was a French mathematician and physicist best known for the development of Fourier series and the solution of differential equations notably heat transfer.

Spectral methods are generally based on the representation of a real, continuous, "well-behaved" function, $f(x)$, on some interval not necessarily bounded as an expansion in an orthonormal set of functions, $P_n(x)$, that is,

$$f(x) = \sum_{n=0}^{\infty} a_n P_n(x), \quad x \in [a, b] \tag{1.1}$$

where the polynomials are orthonormal

$$\int_a^b w(x) P_n(x) P_m(x) dx = \delta_{nm}, \tag{1.2}$$

with respect to some appropriate weight function, $w(x)$, and the Kronecker[10] delta is defined by

$$\delta_{nm} = \begin{cases} 1, & m = n \\ 0, & m \neq m. \end{cases} \tag{1.3}$$

Examples of such polynomial basis sets are the well-known classical polynomials listed in Chap. 2, Table 2.1 and several nonclassical polynomials in Table 2.2. Whereas the non-classical polynomials are constructed to be orthonormal as in Eq. (1.2), the classical polynomials are generally not normalized to unity.

The term "pseudospectral" refers to the solution of the defining equations on a grid of discrete points, $\{x_i\}$, and the solution, $f(x_i)$, as determined at the grid points. This is often referred to as a collocation. Pseudospectral methods are discussed further in Sect. 1.4.

1.2.1 The Spectral Space Representation

We approximate the function of interest, $f(x)$, with the finite sum

$$f^{(N)}(x) = \sum_{n=0}^{N-1} a_n P_n(x), \quad x \in [a, b] \tag{1.4}$$

where with the orthonormality condition, Eq. (1.2), the expansion coefficients are given by

$$a_n = \int_a^b w(x) P_n(x) f(x) dx, \tag{1.5}$$

[10] Leopold Kronecker (1823–1891) was a German mathematician who specialized in algebra and number theory. His studies of mathematics was originally a hobby and he did not hold a university position untill 1883 at the University of Berlin.

and occasionally referred to as the generalized Fourier coefficients. The a_n coefficients, Eq. (1.5), represent the "spectral space representation" of $f(x)$. We choose an appropriate basis set so that the series Eq. (1.1) provides an accurate approximation of $f(x)$ with a small number of terms. If the method is efficient, the absolute values of the coefficients, $|a_n|$, should decrease rapidly with increasing n as will be demonstrated for particular functions and basis sets in Chap. 4.

An alternate choice of basis functions are the functions $p_n(x) = \sqrt{w(x)}P_n(x)$, orthonormal according to

$$\int_a^b p_n(x)p_m(x)dx = \delta_{nm}. \tag{1.6}$$

We have the alternate expansion

$$f^{(N)}(x) = \sum_{n=0}^{N-1} b_n p_n(x), \tag{1.7}$$

with the expansion coefficients,

$$b_n = \int_a^b f(x)p_n(x)dx. \tag{1.8}$$

We can also choose the expansion

$$f^{(N)}(x) = w(x)\sum_{n=0}^{N-1} c_n P_n(x), \tag{1.9}$$

for which the expansion coefficients are

$$c_n = \int_a^b f(x)P_n(x)dx.$$

The convergence of the expansions Eqs. (1.4), (1.7) and (1.9) (each designated with the same $f^{(N)}$(x)!) can be very different as dependent on the behaviour of $f(x)$. Several examples are presented in Chap. 4. For basis sets with unit weight function such as Legendre polynomials and Fourier sines and cosines, these expansions are identical.

The main concern regarding the approximations Eqs. (1.4), (1.7) and (1.9) is whether the series converges and how quickly. Often these two concerns are unrelated except when the series does not converge and then the rapidity of the convergence is irrelevant. The knowledge that the series expansion is convergent does not provide the practical information as to how many terms, N, are required for the approximation, $f^{(N)}(x)$, to be a good approximation to the function, $f(x)$.

There are many discussions of the mathematics concerning the convergence of such expansions. The interested reader can consult several references (Cheney 1966; Rivlin 1969; Trefethen 2013) for a more detailed mathematical treatment of this subject. A discussion of approximation theory from an historical perspective is provided by Steffens (2006).

A very important aspect of approximation theory (Pinkus 2000) is how to measure the difference between $f(x)$ and $f^{(N)}(x)$. We measure the error of the series expansion, Eq. (1.4), with the least squares norm, that is,

$$E_2^{(N)} = \int_a^b w(x)\Big[f(x) - f^{(N)}(x)\Big]^2 dx. \tag{1.10}$$

We write out the square in Eq. (1.10) and use Eq. (1.4) that is

$$\begin{aligned} E_2(N) = &\int_a^b w(x) f^2(x) dx - 2\sum_{n=0}^{N-1} a_n \int_a^b w(x) P_n(x) f(x) dx \\ &+ \sum_{n=0}^{N-1}\sum_{m=0}^{N-1} a_n a_m \int_a^b w(x) P_n P_m dx. \end{aligned} \tag{1.11}$$

With the orthonormality of the basis functions in the last term and the minimization of $E_2(N)$ with respect to all a_n, that is

$$\frac{\partial E_2^{(N)}}{\partial a_n} = 0, \tag{1.12}$$

give the same expansion coefficients as obtained using orthogonality, Eq. (1.5). With Eq. (1.5) in (1.11)

$$E_2^{(N)} = \|f\|^2 - \sum_{n=0}^{N-1} a_n^2, \tag{1.13}$$

where the norm of the function is defined as

$$\|f\|^2 = \int_a^b w(x) f^2(x) dx < \infty, \tag{1.14}$$

and which must be finite. Since $E_2^{(N)} \geq 0$, Bessel's inequality follows as

$$\sum_{n=0}^{N-1} a_n^2 \leq \|f\|. \tag{1.15}$$

For $N \to \infty$, we have Parseval's theorem

$$\sum_{n=0}^{N-1} a_n^2 = \|f\|^2. \tag{1.16}$$

A more detailed mathematical proof of the results, Eqs. (1.15) and (1.16), can be found in the book by Brown and Churchill (1993) on Fourier series expansions.

Another important result is obtained with Eq. (1.8) substituted into Eq. (1.7) which gives

$$f(x) = \int_a^b f(x') \sum_{n=0}^{\infty} p_n(x) p_n(x') dx', \tag{1.17}$$

where

$$\sum_{n=0}^{\infty} p_n(x) p_n(x') = \delta(x - x'), \tag{1.18}$$

and $\delta(x - x')$ is the Dirac delta function defined in terms of the integral

$$\int_0^{\infty} f(x') \delta(x - x') dx' = f(x). \tag{1.19}$$

The basis set $\{p_n\}$ is then considered to be "complete" and Eq. (1.18) is referred to as the completeness relation.

1.2.2 The Physical Space Representation

We have referred to the set of expansion coefficients $\{a_n\}$ in the expansion, Eq. (1.1), as the spectral space representation of the function. The expansion coefficients are determined from orthogonality, Eq. (1.5). In Chap. 2, we introduce Gaussian[11] quadratures for the efficient evaluation of integrals. This is the algorithm

$$\int_a^b w(x) F(x) dx \approx \sum_{i=1}^{N} w_i F(x_i), \tag{1.20}$$

[11] Carl Friedrich Gauss (1777–1855) was a German mathematician and physical scientist. He was a child prodigy and made many fundamental contributions to geometry, number theory and algebra at a very young age. He is also well known for his work on planetary science, geomagnetism and Gaussian probability distributions.

where the set of "quadrature points" $\{x_i\}$ are the roots $P_N(x_i) = 0$ and $\{w_i\}$ are the corresponding set of "quadrature weights". The polynomials that define the quadrature are orthogonal with respect to $w(x)$ as given by Eq. (1.2). With Eq. (1.20), in (1.5), the Gaussian quadrature approximation of the $\{a_n\}$ coefficients is

$$a_n = \sum_{i=1}^{N} w_i P_n(x_i) f_(x_i). \tag{1.21}$$

The set of function values, $f_i \equiv f(x_i)$, is the representation of $f(x)$ in the "physical space representation" and can be written as

$$f_i = \sum_{n=0}^{N-1} a_n P_n(x_i). \tag{1.22}$$

We label the first grid point and the first expansion coefficient as x_1 and a_0, respectively. Equations (1.21) and (1.22) are the transformations from physical space to spectral space and from spectral space to physical space, respectively.

This transformation can by symmetrized with the definition $\hat{f}_i = \sqrt{w_i} f_i$ and gives

$$\begin{aligned} \hat{f}_i &= \sum_{n=0}^{N-1} a_n \sqrt{w_i} P_n(x_i), \quad i = 1, 2, \ldots, N, \\ a_n &= \sum_{j=1}^{N} \sqrt{w_j} P_n(x_j) \hat{f}_j, \quad n = 0, 1, \ldots, N-1. \end{aligned} \tag{1.23}$$

The transformation matrix between the spectral space representation a_n and the physical space representation $\hat{f}_i$ is defined by

$$T_{in} = \sqrt{w_i} P_n(x_i), \tag{1.24}$$

and we rewrite Eq. (1.23) as

$$\begin{aligned} \hat{f}_i &= \sum_{n=0}^{N-1} T_{in} a_n, \\ a_n &= \sum_{i=1}^{N} T_{ni} \hat{f}_i. \end{aligned} \tag{1.25}$$

With the second of these equations for a_n substituted in the first, gives

$$\hat{f}_i = \sum_{j=1}^{N} \left(\sum_{n=0}^{N-1} T_{in} T_{nj} \right) \hat{f}_j. \tag{1.26}$$

The transformation matrix **T** is unitary, that is,

$$\sum_{n=0}^{N-1} T_{in} T_{nj} = \delta_{ij} \tag{1.27}$$

which is equivalent to

$$\begin{aligned} w_i \sum_{n=0}^{N-1} P_n^2(x_i) &= 1, \quad i = j, \\ \sum_{n=0}^{N-1} P_n(x_j) P_n(x_i) &= 0, \quad i \neq j, \end{aligned} \tag{1.28}$$

valid for all N.

With the substitution of Eq. (1.21) into (1.4) and interchange of the summations, we obtain the basic interpolation result

$$f^{(N)}(x) = \sum_{i=1}^{N} I_i(x) f(x_i), \tag{1.29}$$

where the interpolation function is given by

$$I_i^{(N)}(x) = w_i \sum_{n=0}^{N-1} P_n(x) P_n(x_i), \tag{1.30}$$

which satisfies,

$$I_i^{(N)}(x_j) = \delta_{ij}, \tag{1.31}$$

referred to as the "Cardinality" condition. What is remarkable is that this result is satisfied for any N, consistent with Eq. (1.27). These interpolation functions play a central role in pseudospectral methods of solution.

It is of interest to notice that the interpolation functions, Eq. (1.30), are orthogonal, that is,

$$\begin{aligned} \int_a^b w(x) I_i(x) I_j(x) dx &= w_i w_j \sum_{n=0}^{N-1} P_n(x_i) P_n(x_j), \\ &= \delta_{ij}, \end{aligned} \tag{1.32}$$

where the orthonormality of the basis functions, $P_n(x)$, has been used. The use of similar basis function interpolants has been employed by Baye (2006) and co-workers

(Baye and Heenen 1986; Baye and Vincke 1999; Baye et al. 2002) in the development of the Lagrange mesh method for the solution of differential equations, notably the Schrödinger equation. A more detailed discussion is presented in Chap. 6 with comparisons made with other pseudospectral methods.

1.2.3 A Hilbert Space

In this section, we present a few elementary principles associated with the use of a Hilbert space. We first make comparison with a real vector space defined by the set of three mutually perpendicular unit cartesian vectors $\mathbf{e}_x$, $\mathbf{e}_y$ and $\mathbf{e}_z$. We define a scalar or dot product between these unit vectors as $\mathbf{e}_\alpha \cdot \mathbf{e}_\beta = \delta_{\alpha\beta}$, $(\alpha, \beta) \equiv (x, y, z)$. An arbitrary vector can be represented by $\mathbf{v} = v_x\mathbf{e}_x + v_y\mathbf{e}_y + v_z\mathbf{e}_z$ where v_x, v_y and v_z are the cartesian components of $\mathbf{v}$, given by $v_x = \mathbf{e}_x \cdot \mathbf{v}$, by $v_y = \mathbf{e}_y \cdot \mathbf{v}$ and by $v_z = \mathbf{e}_z \cdot \mathbf{v}$. The scalar or dot product of two different vectors is $\mathbf{u} \cdot \mathbf{v} = u_x v_x + u_y v_y + u_x v_z$ and is zero if the vectors are orthogonal. The length of a vector or the *norm* is defined in terms of the scalar product $||\mathbf{v}|| = \sqrt{\mathbf{v} \cdot \mathbf{v}} = \sqrt{v_x^2 + v_y^2 + v_z^2} \geq 0$ with the equality if and only if $\mathbf{v} = 0$. The distance between two vectors is simply the norm $||\mathbf{v} - \mathbf{u}||$. This cartesian space is said to be linear since $\mathbf{u} \cdot (a\mathbf{v}_1 + b\mathbf{v}_2) = a\mathbf{u} \cdot \mathbf{v}_1 + b\mathbf{u} \cdot \mathbf{v}_2$. Moreover, we can define a linear operator $\mathbf{R}$ which transforms or maps one vector into another, that is $\mathbf{u} = \mathbf{R} \cdot \mathbf{v}$. In the $(\mathbf{e}_x, \mathbf{e}_y, \mathbf{e}_z)$ representation, the operator $\mathbf{R}$ is the familiar three-dimensional rotation matrix. We consider this space as complete as we can express any vector as a linear combination of the three unit vectors.

We consider a Hilbert[12] space with the orthogonal basis functions $p_n(x)$, $n = 0, 1, \ldots, \infty$ as unit vectors that are in general complex. We introduce the Dirac[13] *bra*, $\langle n|$, and *ket*, $|n\rangle$ notation (Messiah 1961) to make the connection with a vector space clearer by associating the basis function, $p_n(x)$, with the symbolic vector $|n\rangle$. The basis functions, $p_n(x)$, are in fact the components of the vector $|n\rangle$ in the coordinate representation of basis vectors $|x\rangle$, such that

$$|n\rangle = \int p_n(x)|x\rangle dx. \tag{1.33}$$

There is also the dual space of complex vectors written as $\langle m|$ and the scalar product satisfies, $\langle m|n\rangle = \langle n|m\rangle^*$, where the asterisk denotes the complex conjugate. Thus we

[12] David Hilbert (1862–1943) was a German mathematician who worked on many fundamental problems including functional analysis and integral equations with a deep interest in mathematical physics.

[13] Paul Adrien Maurice Dirac (1902–1984) was an English mathematical physicist who shared the 1933 Nobel Physics Prize with Irwin Schrödinger for their contributions to atomic theory. He made seminal contributions to quantum mechanics and relativity.

consider the representation of the function $f(x)$ or the vector $|f\rangle$ in terms of the basis functions or unit vectors. We include N basis functions and obtain the approximation $|f^{(N)}\rangle$ given by,

$$|f^{(N)}\rangle = \sum_{n=0}^{N-1} c_n |n\rangle, \tag{1.34}$$

where the expansion coefficients are obtained from the projection of $|n\rangle$ onto $|f\rangle$, that is

$$c_n = \langle n|f\rangle \equiv \int_a^b p_n^*(x) f(x) dx. \tag{1.35}$$

Although we have written $p_n^*(x)$ in Eq. (1.35), for most of the applications considered the basis functions are real. We include linear differential operators denoted by L and the eigenvalue problem of the form

$$L|\psi_n\rangle = \lambda_n |\psi_n\rangle, \tag{1.36}$$

where λ_n is the eigenvalue, assumed to be discrete. We will find it useful to also denote the scalar product as

$$\langle f|g\rangle = \int_a^b w(x) f^*(x) g(x) dx, \tag{1.37}$$

with the weight function $w(x)$. The matrix element of some operator, L, is denoted by

$$\langle f|Lg\rangle = \int_a^b w(x) f^*(x) Lg(x) dx. \tag{1.38}$$

For the scalar products, $\langle f|g\rangle$ and $\langle f|Lg\rangle$, the weight function is not shown explicitly to simplify the notation. We summarize the properties of a Hilbert space for our purposes as

1. $\langle f|ag + bh\rangle = a\langle f|g\rangle + b\langle f|h\rangle$, a and b are numbers,
2. $\langle f|g\rangle = \langle g|f\rangle^*$,
3. $\langle f|f\rangle \geq 0$,
4. $||f|| = \langle f|f\rangle = 0$ if and only if $f = 0$.
5. $L(|f\rangle + |g\rangle) = L|f\rangle + L|g\rangle$, L is a linear operator.

More detailed discriptions of a Hilbert space are in the book by Helmberg (2008) and especially Chap. 6 in the book by Hunter and Nachtergaele (2001).

1.2.4 Hermitian and Self-adjoint Operators: The Sturm-Liouville Problem

Consider the eigenvalue problem

$$L\psi_n(x) = \lambda_n \psi_n(x), \tag{1.39}$$

where L is a linear operator which includes the Hamiltonian for a quantum problem or the linear integral operator in the Boltzmann equation or the differential Fokker-Planck operator. The eigenfunction, $\psi_n(x)$, defined on the interval $[a, b]$ is subject to two homogeneous boundary conditions which are linear combinations of the value of the function and derivative at the two interval end points and are of the form

$$\begin{aligned} A_1\psi_n(a) + B_1\psi_n'(a) &= 0, \\ A_2\psi_n(b) + B_2\psi_n'(b) &= 0, \end{aligned} \tag{1.40}$$

where for $A_k = 0$ we have a Neumann boundary condition and if $B_k = 0$ we have a Dirichlet boundary condition.

The Hermitian conjugate or the adjoint of L denoted by $L^\dagger$ is defined by the eigenvalue problem

$$L^\dagger \psi_m^*(x) = \lambda_m^* \psi_m^*(x). \tag{1.41}$$

The Hermitian conjugate of the matrix representative of an operator with elements L_{nm} is the complex conjugate of each element of the transpose matrix, that is L_{mn}^*.

We now show that for a self-adjoint operator, the eigenvalues, λ_n, are real and the eigenfunctions, $\psi_n(x)$, of different eigenvalues are orthogonal. Multiply Eq. (1.41) by $\psi_n(x)$ and Eq. (1.39) by $\psi_m^*(x)$, subtract the two equations and integrate to get

$$\int_a^b \left[\psi_n(x) L^\dagger \psi_m^*(x) - \psi_m^*(x) L\psi_n(x)\right] dx = (\lambda_m^* - \lambda_n) \int_a^b \psi_m^*(x)\psi_n(x)dx \tag{1.42}$$

If L, is self-adjoint or Hermitian, the left hand side of Eq. (1.42) is zero. Thus the right hand side of Eq. (1.42) is also zero. If $m = n$ we have that $\lambda_n^* = \lambda_n$ since the integral is not zero. The eigenvalues of a self-adjoint operator are real. For $n \neq m$ we have the orthogonality of the eigenfunctions, that is,

$$\int_a^b \psi_m^*(x)\psi_n(x)dx = \gamma_n \delta_{nm}, \tag{1.43}$$

where the norm is

$$\gamma_n = ||\psi_n||^2 = \int_a^b \psi_n^2(x)dx. \tag{1.44}$$

The Sturm[14]-Liouville[15] problem (Pryce 1993; Al-Gwaiz 2008) is the eigenvalue problem defined by the differential equation

$$L\psi_n(x) = \frac{d}{dx}\left[p(x)\frac{d\psi_n(x)}{dx}\right] + q(x)\psi_n(x) = \lambda_n w(x)\psi_n(x), \tag{1.45}$$

where $p(x)$, $q(x)$ are real and $w(x) > 0$ is a real weight function. The interval may be bounded, $x \in [a, b]$, semi-infinite $x \in [0, \infty)$, or infinite $x \in (-\infty, \infty)$. Any linear second order differential equation can be written in this form. The classical polynomials such as the Legendre, Hermite and Laguerre polynomials defined in Chap. 2 satisfy Sturm-Liouville eigenvalue equations. These polynomials are often chosen as the basis functions in spectral solutions of particular problems. Alternatively, the quadrature weights and points associated with these classical polynomials are used in pseudospectral solutions.

To show that L defined by Eq. (1.45) is self-adjoint, we consider the matrix element

$$\langle\phi|L|\psi\rangle = \int_a^b \phi(x)\left[p(x)\psi'(x)\right]' dx + \int_a^b q(x)\phi(x)\psi(x)dx, \tag{1.46}$$

and perform an integration by parts for the first integral on the right hand side. The result is

$$\langle\phi|L|\psi\rangle = p(x)\psi'(x)\phi'(x)\Big|_a^b - \int_a^b p(x)\psi'(x)\phi'(x)dx + \int_a^b q(x)\phi(x)\psi(x)dx. \tag{1.47}$$

The boundary term is zero owing to the chosen boundary conditions, Eqs. (1.40), and

$$\langle\phi|L|\psi\rangle = \langle\psi|L|\phi\rangle.$$

Thus the Sturm-Liouville operator, L, is self-adjoint, and the importance of the specified boundary conditions is clear. The Schrödinger and the Fokker-Planck eigenvalue equations are Sturm-Liouville problems and considered in Chap. 6. In Chap. 5, we consider the eigenvalues of the integral collision operator of the Boltzmann equation.

[14] Jacques Charles François Sturm (1803–1855) was a French mathematician who made important contributions to algebra and the numerical evaluation of the roots of polynomials. The differential eigenvalue equation that bears his name defines the classical polynomials.

[15] Joseph Liouville (1809–1882) was a French mathematician who made fundamental contributions to complex analysis, algebra, mechanics, and many other topics. He is well known for Liouville's theorem in classical Hamiltonian mechanics.

1.2.5 Rayleigh-Ritz Variational Theorem

We are interested in solving the operator eigenvalue problem

$$L|\psi_n\rangle = \lambda_n|\psi_n\rangle, \tag{1.48}$$

where L is a self-adjoint positive definite operator in a square integrable Hilbert space of real functions. The Rayleigh[16]-Ritz[17] variational approach is based on the representation of the eigenvectors $|\psi_n\rangle$ in terms of N orthogonal vectors $|k\rangle$ each weighted linearly with a variational parameter, a_k. Thus we write,

$$|\psi_n\rangle = \sum_{k=0}^{N-1} a_k|k\rangle, \tag{1.49}$$

where $\langle k|\ell\rangle = \delta_{k\ell}$. A functional dependent on the set of variational parameters, a_k, is defined by

$$\begin{aligned} F(\{a_k\}) &= \langle\psi_n|L|\psi_n\rangle - \lambda\langle\psi_n|\psi_n\rangle, \\ &= \sum_{k=0}^{N-1}\sum_{\ell=0}^{N-1}\left[a_k a_\ell L_{k\ell} - \lambda a_k^2\right], \end{aligned} \tag{1.50}$$

where $L_{k\ell} = \langle k|L|\ell\rangle$ are the matrix elements of the operator in the chosen basis set. We determine the extremum of $F(\{a_k\})$ with respect to the set of expansion coefficients $\{a_k\}$ by setting

$$\frac{\partial F(\{a_k\})}{\partial a_k} = 0. \tag{1.51}$$

The result is the set of linear equations for the variational parameters, a_k, that is,

$$\sum_{k=0}^{N-1} a_k\left[L_{k\ell} - \lambda\delta_{k\ell}\right] = 0, \tag{1.52}$$

and the eigenvalues are the roots of the "secular" equation resulting from the requirement that the solution of homogeneous linear equations, Eq. (1.52), exists, that is

$$\det\left[\mathbf{L}^{(N)} - \Lambda\right] = 0, \tag{1.53}$$

---

[16] John William Strutt, third Baron Rayleigh (1842–1919) was an English physicist who discovered argon for which he was awarded 1904 Nobel Physics Prize. His named is associated with kinetic theory, electrodynamics, light scattering, sound propagation and other subjects.

[17] Walther Ritz (1878–1909) was a Swiss theoretical physicist. His name is associated with the Rydberg Ritz combination principle for atomic spectral lines and the Rayleigh-Ritz variational method.

where the matrix Λ is diagonal, $\Lambda_{k\ell} = \lambda_k \delta_{k\ell}$. Equation (1.53) is the secular equation, a polynomial of degree N in λ and the roots are λ_k.

A good overall discussion of the different approximation methods for applications in physics and engineering can be found in the book by Finlayson (1972). The review paper by Finlayson and Scriven (1966) with 187 references provides an overview of the development of these methods. A more rigrous mathematical discussion has been presented by Hill (1985).

The Rayleigh-Ritz variational theorem has been applied extensively in numerous fields including quantum mechanics (Bhattacharyya 2009), kinetic theory (Cuperman et al. 1982; Driessler 1981; Present and Morris 1969; Snider 1964; Shizgal and Karplus 1971; Bobylev and Cercignani 1999), radio science (Sarkar 1983) and other fields. The common aspect of all these applications is the approximate representation of the solution of a differential equation in a set of orthogonal basis functions.

1.3 An Overview of Spectral Methods

In Chap. 2, we develop the basic concepts of spectral and pseudospectral methods with application to physical problems. In this section, we provide an overview of the development of these methods which are discussed in greater detail in the chapters that follow.

We consider the time dependent differential equation,

$$\frac{\partial f(x,t)}{\partial t} = Lf(x,t) + S(x) \quad x \in [a,b], \tag{1.54}$$

where L is a linear operator and $S(x)$ is a source term. We impose Dirichlet boundary conditions, $f(a,t) = 0, f(b,t) = 0$ and provide an initial condition $f(x,0) = g(x)$. The operator L could be the operator in the linear Boltzmann equation, Eq. (5.41), or in a Fokker-Planck equation, Eq. (6.7). The eigenvalue problem $L\psi_n(x) = \lambda_n \psi_n(x)$ is of interest for the time dependent solution of Eq. (1.54). We are also interested in a similar eigenvalue problem for the Schrödinger equation, Eq. (6.78), defined with a linear self-adjoint Hamiltonian operator H.

For these problems, we approximate the solution in terms of the finite expansion in a set of orthonormal functions, $p_n(x) = \sqrt{w(x)}P_n(x)$, Eq. (1.7), involving N terms and we have the Nth approximation to $f(x,t)$, that is

$$f^{(N)}(x,t) = \sum_{n=0}^{N-1} b_n(t) p_n(x). \tag{1.55}$$

We discuss the choice of basis set from the large set of classical and nonclassical polynomials in Chap. 2. This choice determines the rate of convergence of the expansion, Eq. (1.55).

The initial values of the expansion coefficients are provided from the expansion of the initial condition, that is,

$$g(x) = \sum_{n=0}^{N-1} b_n(0) p_n(x). \tag{1.56}$$

With the substitution of Eq. (1.56) into (1.54), we have that

$$\sum_{n=0}^{N-1} p_n(x) \frac{db_n(t)}{dt} = \sum_{n=0}^{N-1} b_n(t) L p_n(x) + S(x). \tag{1.57}$$

The departure of the approximate solution from the actual solution is measured by the "residue" defined by

$$\begin{aligned} R_N(x,t) &= \frac{\partial f^{(N)}(x,t)}{\partial t} - L f^{(N)}(x,t) - S(x), \\ &= \sum_{n=0}^{N-1} p_n(x) \frac{db_n(t)}{dt} - \sum_{n=0}^{N-1} b_n(t) L p_n(x) - S(x). \end{aligned} \tag{1.58}$$

The method of weighted residuals (Finlayson and Scriven 1966; Finlayson 1972) is a procedure to calculate $b_n(t)$ so as to minimize the residual $R_N(x,t)$ in some average way. We impose the condition that the residue is minimized subject to

$$\int_a^b t(x) R_N(x,t) dx = 0, \tag{1.59}$$

where there are several different choices for the "test" function $t(x)$ and each choice gives rise to a different approximation. If we choose $t(x) = p_n(x)$, $n = 0, 1, \ldots, N-1$, the partial differential equation is converted to a set of N coupled ordinary differential equations, that is,

$$\frac{db_m(t)}{dt} = \sum_{n=0}^{N-1} L_{mn} b_n(t) + s_m \quad m = 0, 1, \ldots, N-1, \tag{1.60}$$

where the matrix representation of L in this basis set is,

$$L_{mn} = \int_a^b p_m(x) L p_n(x) dx, \tag{1.61}$$

and

$$s_n = \int_a^b p_n(x) S(x) dx, \tag{1.62}$$

are the expansion coefficients for the source term, $S(x)$. This approach is referred to as a spectral or a "Galerkin"[18] solution.

The set of coupled ordinary differential equations, Eq. (1.60), can be advanced in time from the initial values, $c_n(0)$, with the appropriate time integration algorithm. An important aspect regarding the stability of the direct time integration of the set of equations, Eq. (1.60), is the eigenvalue spectrum of the matrix, L_{mn}, and the condition number, $\kappa(\mathbf{L}) = \lambda_{max}/\lambda_{min}$.

The condition number is also very important with regards to the inversion of the steady state matrix equations

$$\sum_{n=0}^{N-1} L_{nm} C_m = -s_n \quad m = 0, 1, \ldots, N-1, \tag{1.63}$$

for the time independent coefficients denoted by C_m. If the condition number of the matrix $\mathbf{L}$ is large, the inversion of Eq.(1.63) can be contaminated with numerical errors. We can also consider the related eigenvalue problem

$$\sum_{n=0}^{N-1} L_{nm} d_m = \lambda_n d_n \quad n = 0, 1, \ldots, N, \tag{1.64}$$

for the eigenvalues, λ_n, and eigenvector coefficients $\mathbf{d}$ with the proviso that the eigenvalue spectrum of the operator L is discrete.

For the Boltzmann, Fokker-Planck and Schrödinger equations, the linear operators involved can have discrete spectra, or a combination of a discrete spectrum plus a continuum or just a continuum. We discuss these properties of eigenvalue problems with specific applications in Chaps. 5 and 6 (Reinhardt 1979).

1.4 The Development of Pseudospectral Methods in Chemistry and Physics: An Overview of the Book

A preliminary introduction to pseudospectral methods is provided by the eigenvalue problem

$$\int_a^b k(x, y)\psi_n(y)dy = \lambda_n \psi_n(x), \tag{1.65}$$

where the integral operator on the left hand side is defined by the kernel, $k(x, y)$, which is assumed to be well behaved in both arguments. The integral equation

[18] Boris Galerkin (1871–1945) was a Russian mathematician and developed the Galerkin method for solving partial differential equations associated with problems in mechanical engineering.

is reduced to a set of linear equations with the use of the appropriate quadrature. Equation (1.20), defined with the quadrature points, $\{x_i\}$. The result is

$$\sum_{i=1}^{N} W_i k(x_j, x_i)\psi_n(x_i) = \lambda_n \psi_n(x_j), \tag{1.66}$$

where $W_i = w_i/w(x_i)$ and $w(x)$ is the weight function that defines the polynomials, Eq. (1.2). The eigenfunctions are evaluated at the set of quadrature points and are represented by the physical space representation, $\psi_n(x_i)$. Extensive use of this pseudospectral method is discussed in Chap. 5 for the solution of the Boltzmann equation.

For differential equations, a derivative matrix operator is derived in Chap. 2 in terms of the interpolation function, Eq. (2.32),

$$D_{ij} = \left.\frac{dI_i^{(N)}(x)}{dx}\right|_{x=x_i}, \tag{1.67}$$

as well as an analogous matrix operator for the second derivative. Second order differential equations such as the Fokker-Planck and Schrödinger equations can be reduced to linear algebraic equations or time dependent ordinary differential equations. Pseudospectral methods are used extensively in Chaps. 5 and 6. The history of the development of pseudospectral methods in chemistry, physics and other fields is outlined in Table 1.1. This chronology of events is a personal view and people with different backgrounds may well have other interpretations.

As discussed in Chap. 5, the first use of a pseudospectral method appears to be the work of Wick (1943) and Chandrasekhar (1944) in the solution of

Table 1.1 The development of pseudospectral methods in chemistry and physics

1943	Gaussian quadrature solution for Radiative Transfer	Wick (1943)
1944	Gaussian quadrature solution for Radiative Transfer	Chandrasekhar (1944)
1953	The Discrete Ordinate Method (DOM) in Neutron Transport	Carlson (1955)
1972	Differential Quadrature (DQ)	Bellman et al. (1972)
1973	Spline methods for the Schrödinger equation	Shore (1973, 1975)
1977	Numerical Analysis of Spectral Methods	Gottlieb and Orszag (1977)
1982	Nonclassical basis functions for the Boltzmann equation	Shizgal (1981a)
1984	A DOM for the solution of differential equations	Shizgal and Blackmore (1984)
1985	Pseudospectral methods for electronic structure	Friesner (1985)
1985	Discrete Variable Representation (DVR)	Light et al. (1985)
1985	Fourier techniques	Schwartz (1985)
1986	Lagrange mesh method	Baye and Heenen (1986)
1987	Spectral methods in fluid mechanics	Canuto et al. (1998)

the integro-differential radiative transfer equation (Chandrasekhar 1960). They introduced Gauss-Legendre quadratures to reduce the radiative transfer equation to a set of linear ordinary differential equations. The problem was originally considered by Milne[19] (Milne 1930) as a problem in astrophysics as well as in rarefied gas dynamics where it is referred to as a half-space problem (Williams 1971; Cercignani 1988). A spectral solution of the Milne problem based on the Boltzmann equation is discussed in Chap. 5 (Lindenfeld and Shizgal 1983) and a pseudospectral method of solution for an electron Fokker-Planck equation was presented by Vasenkov and Shizgal (2000).

The radiative transfer and neutron transport community exploited the pseudospectral approach (Chandrasekhar 1960; Rybicki 1996) and it was referred to as the Discrete Ordinate Method (DOM) (Carlson 1955). Other designations are the S_N (Lathrop 1992) and P_N methods (Liou 2002; Thomas and Stamnes 2002). The S_N method appears to refer to the "segmentation" of the interval of interest with N quadrature points and can be considered as a spectral element method (Deville et al. 2002) or a discontinuous Galerkin method (Cockburn et al. 2000) originally developed in neutron transport theory (Reed and Hill 1973). The P_N method refers to a spectral method with the expansion of the angular dependence of the velocity distribution functions in Legendre polynomials (Liou 2002; Thomas and Stamnes 2002). Similar Laguerre and Hermite expansions of functions that occur in kinetic theory are presented in Chap. 4.

The pseudospectral solution of differential equations is based on the global approximation of the derivative operator in terms of the function values on a grid. Interpolation, Eq. (1.30), and the discrete matrix derivative operator, Eq. (1.67), are the basis for the development of these collocation type solutions of differential equations. Bellman et al. (1972) developed the differential quadrature (DQ) method for the solution of differential equations. This appears to be the first introduction of pseudospectral methods applied primarily to problems in engineering (Shu 2000). Pseudospectral methods based on the discrete physical space representation of derivative operators is presented in Chap. 3, Sect. 3.9.2 and defined with the Lagrange interpolation in Chap. 2, Sect. 2.3.1.

The numerical methods of solution based on B-Splines (Shore 1973) also belong to the class of collocation Galerkin type solutions for quantum problems (Bachau et al. 2001) as well as for the Boltzmann equation (Pitchford and Phelps 1982; Siewert 2002; Khurana and Thachuk 2012) and many other applications. The introduction of spectral methods with Fourier and Chebyshev basis functions for fluid mechanics problems was developed by Gottlieb and Orszag (1977).

Shizgal and Blackmore (1984) applied a combination of the Gaussian quadratures for integrals, Eq. (1.20), and the discrete physical space matrix representations for derivatives, Eq. (1.67), for the solution of the integro-differential Boltzmann equation, presented in Chap. 5. A nonclassical quadrature based on polynomials orthogonal with weight function, $w(x) = x^p e^{-x^2}, \quad x \in [0, \infty)$, was used (Shizgal 1981a). The

[19] Edward Arthur Milne (1896–1950) was a British astrophysicist and mathematician who contributed to stellar structure and the thermodynamics of stars.

method of Gaussian quadrature for the evaluation of integrals is used to solve integral equations (Delves and Mohamed 1985; Jerri 1999; Eskola 2012) and is referred to as the Nyström method. Gaussian quadratures are developed in Chap. 2 and applied to the numerical evaluation of integrals in Chap. 3 and to the determination of the eigenvalue spectra for the collision operators of the Boltzmann equation in Chap. 5.

Nonclassical polynomials and associated quadratures were subsequently applied to the Fokker-Planck and Schrödinger equations and referred to as the quadrature discretization method (Shizgal and Chen 1996, 1997; Lo and Shizgal 2006, 2008a). The choice of basis functions arises from the transformation of the Fokker-Planck equation to a Schrödinger equation with potentials that belong to the class of problems in supersymmetric quantum mechanics (Comtet et al. 1985; Dutt et al. 1988). The pseudospectral algorithms discussed in Chap. 6, Sect. 6.3.2, provide a representation of the Hamiltonian in the Schrödinger equation that is not contaminated by nonphysical ghost levels (Wei 1997; Willner et al. 2004; Kallush and Kosloff 2006).

Friesner (1985) applied pseudospectral methods to the solution of the electronic structure equations (the Schrödinger equation) for the electronic states of the neon atom following on the pioneering work of Gottlieb and Orszag (1977) on spectral methods for fluid mechanics. For the quantum chemistry community involved with the calculation of the vibrational states of polyatomic molcules, pseudospectral methods originated from the quadrature evaluation of matrix elements of a multiplicative operator, namely the potential in the Schrödinger equation (Harris et al. 1965; Dickinson and Certain 1968). Following on this work, Light and coworkers (Hamilton and Light 1986; Bacic and Light 1989; Light and Carrington 2000) developed a pseudospectral method referred to as the Discrete Variable Representation (DVR).

Baye (1995, 2006) and coworkers (Baye and Heenen 1986; Baye and Vincke 1999; Baye et al. 2002) developed the Lagrange mesh method for similar quantum problems. Mention should be made of the work of Schwartz (1985) on Fourier methods. The second derivative operator representation in this paper was later reported by Colbert and Miller (1992) and Amore (2006).

In Chap. 3, we discuss the representations of multiplicative operators for both kinetic theory as well as for quantum problems and the transformation between spectral space and physical space, Eq. (1.25). This provides insight into the success of pseudospectral methods from the inexact calculation of matrix elements of the potentials in the Schrödinger equation (Baye et al. 2002; Szalay et al. 2012).

Fourier methods for quantum problems were developed by Balint-Kurti and coworkers (Marston and Balint-Kurti 1989; Balint-Kurti and Pulay 1995; Stare and Balint-Kurti 2003) and by Kosloff (Kosloff and Kosloff 1983; Kosloff 1993, 1994). Mention should be made of the distributed approximating functional (DAF) method of Hoffman et al. (1998) and the discrete singular convolution (DSC) method (Wei 2000a, b; Amore et al. 2009).

In Chap. 5, we employ Gaussian quadratures for the representation of integral operators such as in the Boltzmann equation (Shizgal and Blackmore 1983; Sospedra-Alfonso and Shizgal 2012). Quadratures are used to reduce integral equations to algebraic form. In Chap. 6, interpolation serves to define a matrix derivative operator

to reduce differential equations such as the Fokker-Planck and Schrödinger equations to algebraic equations. In both situations, nonclassical basis functions are often used. The original version of the book by Canuto et al. (1998), which has since been republished in two volumes (Canuto et al. 2006a, b), is noted in the table as representative of the many textbooks on spectral methods in fluid dynamics that have been referenced in the Preface.

References

Al-Gwaiz, M.A.: Sturm-Liouville Theory and its Applications. Springer, Berlin (2008)
Amore, P.: A variational Sinc collocation method for strong-coupling problems. J. Phys. A: Math. Gen. **39**, L349–L355 (2006)
Amore, P., Fernandez, F.M., Saenz, R.A., Salvo, K.: Collocation on uniform grids. J. Phys. A: Math. Theor. **42**, 115302 (2009)
Anderson, D., Lisak, M., Andersson, F., Fülöp, T.: Slowing down dynamics of fast particles in plasmas via the Fokker-Planck equation. Nucl. Sci. Eng. **146**, 99–105 (2004)
Atenzi, S., Meyer-Ter-Vehn, J.: The Physics of Inertial Fusion. Clarendon Press, Oxford (2004)
Bachau, H., Cormier, E., Decleva, P., Hansen, J.E., Martin, F.: Application of B-Splines in atomic and molecular physics. Rep. Prog. Phys. **64**, 1815–1942 (2001)
Bacic, Z., Light, J.C.: Theoretical methods for rovibrational states of floppy molecules. Annu. Rev. Phys. Chem. **40**, 469–498 (1989)
Balint-Kurti, G.G.: Time-dependent and time-independent wavepacket approaches to reactive scattering and photodissociation dynamics. Int. Rev. Phys. Chem. **27**, 507–539 (2008)
Balint-Kurti, G.G., Pulay, P.: A new grid-based method for the direct computation of excited molecular vibrational-states: test application to formaldehyde. J. Mol. Struct. (Theochem) **341**, 1–11 (1995)
Baye, D.: Constant-step Lagrange meshes for central potentials. J. Phys. B: At. Mol. Opt. Phys. **28**, 4399–4412 (1995)
Baye, D.: Lagrange-mesh method for quantum-mechanical problems. Phys. Stat. Sol. B **243**, 1095–1109 (2006)
Baye, D., Heenen, P.H.: Generalized meshes for quantum-mechanical problems. J. Phys. A: Math. Gen. **19**, 2041–2059 (1986)
Baye, D., Vincke, V.: Lagrange meshes from nonclassical orthogonal polynomials. Phys. Rev. E **59**, 7195–7199 (1999)
Baye, D., Hesse, M., Vincke, M.: The unexplained accuracy of the Lagrange-mesh method. Phys. Rev. E **65**, 026701 (2002)
Baye, D., Vincke, M., Hesse, M.: Simple and accurate calculations on a Lagrange mesh of the hydrogen atom in a magnetic field. J. Phys. B: At. Mol. Opt. Phys. **41**, 055005 (2008)
Bellman, R.E., Kashef, B.G., Casti, J.: Differential quadrature: a technique for the rapid solution of nonlinear partial differential equations. J. Comput. Phys. **10**, 40–52 (1972)
Bhattacharyya, B.: Bounds on the ground state energy: application of the variational principle. Am. J. Phys. **77**, 44–47 (2009)
Binney, J., Tremaine, S.: Galactic Dynamics, 2nd edn. Princeton University Press, New Jersey (2008)
Bird, G.A.: Molecular Gas Dynamics and the Direct Simulation of Gas Flows. Clarendon, Oxford (1994)
Birdsall, C.K., Langdon, A.B.: Plasma Physics via Computer Simulation. Taylor and Francis, New York (2005)

Bobylev, A.V., Cercignani, C.: On the rate of entropy production for the Boltzmann equation. J. Stat. Phys. **94**, 603–618 (1999)
Bonazzola, S., Gourgoulhon, E., Marck, J.-A.: Spectral methods in general relativistic astrophysics. J. Comput. Appl. Math. **109**, 433–473 (1999)
Brown, J.W., Churchill, R.V.: Fourier Series and Boundary Value Problems. McGraw Hill, New Jersey (1993)
Burke, P.G.: R-Matrix Theory of Atomic Collisions: Application to Atomic, Molecular and Optical Processes. Springer, New York (2011)
Canuto, C., Hussaini, M.Y., Quarteroni, A., Zang, T.A.: Spectral Methods in Fluid Dynamics. Springer, New York (1998)
Canuto, C., Hussaini, M.Y., Quarteroni, A., Zang, T.A.: Spectral Methods: Evolution to Complex Geometries and Applications to Fluid Mechanics. Springer, New York (2006a)
Canuto, C., Hussaini, M.Y., Quarteroni, A., Zang, T.A.: Spectral Methods: Fundamentals in Single Domains. Springer, New York (2006b)
Car, R., Parrinello, M.: Unified approach for molecular dynamics and density functional theory. Phys. Rev. Lett. **55**, 2471–2474 (1985)
Carlson, B.G.: Solution of the Transport Equation by S_n Approximation. Technical Report LA-1891, Los Alamos Scientific Laboratory (1955)
Cassam-Chenaï, P., Liévin, J.: Ab initio calculation of the rotational spectrum of methane vibrational ground state. J. Chem. Phys. **136**, 174309 (2012)
Cercignani, C.: The Boltzmann Equation and its Applications. Springer, New York (1988)
Chandrasekhar, S.: On the radiative equilibrium of a stellar atmosphere II. Astrophys. J. **100**, 76–86 (1944)
Chandrasekhar, S.: Brownian motion, dynamical friction, and stellar dynamics. Rev. Mod. Phys. **21**, 383–388 (1949)
Chandrasekhar, S.: Radiative Transfer. Dover, New York (1960)
Chapman, S., Cowling, T.G.: The Mathematical Theory of Nonuniform Gases. Cambridge University Press, Cambridge (1970)
Chavanis, P.H.: Relaxation of a test particle in systems with long-range interactions: diffusion coefficient and dynamical friction. Eur. J. Phys. B **52**, 61–82 (2006)
Cheney, E.W.: Introduction to Approximation Theory. McGraw-Hill, New York (1966)
Child, M.S.: Molecular Collision Theory. Dover, New York (1996)
Cockburn, B., Karniadakis, G.E., Shu, C.-W.: Discontinuous Galerkin Methods: Theory, Computation and Applications. Springer, Berlin (2000)
Colbert, D.T., Miller, W.H.: A novel discrete variable representation for quantum-mechanical reactive scattering via the S-Matrix Kohn method. J. Chem. Phys. **96**, 1982–1991 (1992)
Comtet, A., Bandrauk, A.D., Campbell, D.K.: Exactness of semiclassical bound-state energies for supersymmetric quantum-mechanics. Phys. Lett. B **150**, 159–162 (1985)
Cuperman, S., Weiss, J., Dryer, M.: A variational derivation of the velocity distribution functions for nonequilibrium, multispecies, weakly interacting, spherically symmetric many-body systems. J. Stat. Phys **29**, 803–812 (1982)
Davison, B.: Neutron Transport. Oxford University Press, Oxford (1957)
Delves, L.M., Mohamed, J.L.: Computational Methods for Integral Equations. Cambridge University Press, Cambridge (1985)
Deville, M.O., Fisher, P.F., Mund, E.H.: High Order Methods for Incompressible Fluid Flow. Cambridge University Press, Cambridge (2002)
Dickinson, A.S., Certain, P.R.: Calculation of matrix elements for one-dimensional quantum-mechanical problems. J. Chem. Phys. **49**, 4209–4211 (1968)
Driessler, W.: On the spectrum of the Rayleigh piston. J. Stat. Phys. **24**, 595–606 (1981)
Durran, D.R.: Numerical Methods for Fluid Dynamics: With Applications to Geophysics. Springer, Berlin (2010)
Dutt, R., Khare, A., Sukhatme, U.P.: Supersymmetry, shape invariance and exactly solvable potentials. Am. J. Phys. **56**, 163–168 (1988)

Echim, M.M., Lemaire, J., Lie-Svendsen, O.: A review on solar wind modeling: kinetic and fluid aspects. Surv. Geophys. **32**, 1–70 (2011)
Eskola, L.: Geophysical Interpretation Using Integral Equations. Springer, Netherlands (2012)
Fahr, F.J., Shizgal, B.: Modern exospheric theories and their observational relevance. Rev. Geophys. Space Phys. **21**, 75–124 (1983)
Finlayson, B.A.: The Method of Weighted Residuals and Variational Principles. Academic Press, New York (1972)
Finlayson, B.A., Scriven, L.E.: The method of weighted residuals—a review. Appl. Mech. Rev. **19**, 735–748 (1966)
Friesner, R.A.: Solution of self-consistent field electronic structure equations by a pseudospectral method. Chem. Phys. Lett. **116**, 39–43 (1985)
Friesner, R.A.: New methods for electronic structure calculations on large molecules. Annu. Rev. Phys. Chem. **42**, 341–367 (1991)
Friesner, R.A., Bentley, J.A., Menou, M., Leforestier, C.: Adiabatic pseudospectral methods for multidimensional vibrational potentials. J. Chem. Phys. **99**, 324–335 (1993)
Gifford, K.A., Horton Jr, J.L., Wareing, T.A., Failla, G., Mourtada, F.: Comparison of a finite-element multigroup discrete-ordinates code with Monte Carlo for radiotherapy calculations. Phys. Med. Biol. **51**, 2253–2265 (2006)
Gottlieb, D., Orszag, S.: Numerical Analysis of Spectral Methods: Theory and Applications. SIAM, Philadelphia (1977)
Grandclément, P., Novak, J.: Spectral methods for numerical relativity. Living Rev. Relativ. **12**(1), 103 (2009)
Hamilton, I.P., Light, J.C.: On distributed Gaussian bases for simple model multidimensional vibrational problems. J. Chem. Phys. **84**, 306–317 (1986)
Harris, D.O., Engerholm, G.G., Gwinn, W.D.: Calculation of matrix elements for one-dimensional quantum-mechanical problems and the application to anharmonic oscillators. J. Chem. Phys. **43**, 1515–1517 (1965)
Hebert, A.: Applied Reactor Physics. Presse Int. Polytechnique, Montréal (2009)
Helgaker, T., Jorgensen, P., Olsen, J.: Molecular Electronic Structure Theory. Wiley, New York (2000)
Helmberg, G.: Introduction to Spectral Theory in Hilbert Space. Dover, New York (2008)
Heyl, J.S., Thirumalai, A.: Pseudo-spectral methods for atoms in strong magnetic fields. Mon. Not. R. Astron. Soc. **407**, 590–598 (2010)
Hill, R.N.: Rates of convergence and error estimation formulas for the Rayleigh-Ritz variational methods. J. Chem. Phys. **83**, 1173–1196 (1985)
Hoffman, D.K., Wei, G.W., Zhang, D.S., Kouri, D.J.: Interpolating distributed approximating functionals. Phys. Rev. E **57**, 6152–6160 (1998)
Hu, X.G., Ho, T.S., Rabitz, H., Askar, A.: Multivariate radial basis interpolation for solving quantum fluid dynamical equations. Comput. Math. Appl. **43**, 525–537 (2002)
Hunter, J.K., Nachtergaele, B.: Applied Analysis. World Scientific, Singapore (2001)
Jerri, A.J.: Introduction to Integral Equations with Applications, 2nd edn. Wiley, New York (1999)
Jones, R.O., Gunnarsson, O.: The density functional formalism, its applications and prospects. Rev. Mod. Phys. **61**, 689–746 (1989)
Kallush, S., Kosloff, R.: Improved methods for mapped grids: applied to highly excited vibrational states of diatomic molecules. Chem. Phys. Lett. **433**, 221–227 (2006)
Khurana, S., Thachuk, M.: A numerical solution of the linear Boltzmann equation using cubic B-splines. J. Chem. Phys. **136**, 094103 (2012)
Koput, J., Carter, S., Handy, N.C.: Ab initio prediction of the vibrational-rotational energy levels of hydrogen peroxide and its isotopomers. J. Chem. Phys. **115**, 8345–8350 (2001)
Kosloff, R.: The fourier method. In: Cerjan, C. (ed.) Numerical Grid Methods and Their Application to Schrödinger's Equation, pp. 175–194. Kluwer Academic, The Netherlands (1993)
Kosloff, R.: Propagation methods for quantum molecular dynamics. Annu. Rev. Phys. Chem. **45**, 145–178 (1994)

Kosloff, D., Kosloff, R.: A Fourier method solution for the time-dependent Schrödinger-equation as a tool in molecular dynamics. J. Comput. Phys. **52**, 35–53 (1983)
Kremer, G.M.: An Introduction to the Boltzmann Equation and Transport Processes in Gases. Springer, New York (2010)
Kundu, P., Cohen, I.M., Dowling, D.R.: Fluid Mechanics, 6th edn. Academic Press, Waltham (2012)
Landau, D.P., Binder, K.: A Guide to Monte Carlo Simulations in Statistical Physics, 3rd edn. Cambridge University Press, Cambridge (2009)
Lathrop, K.D.: The early days of the S_N method. Trans. Am. Nucl. Soc. **66**, 241–242 (1992)
Lemou, M., Chavanis, P.H.: Escape of stars from gravitational clusters in the Chandrasekhar model. Phys. A **389**, 1021–1040 (2010)
Levine, I.N.: Quantum Chemistry, 6th edn. Prentice Hall, New Jersey (2009)
Liboff, R.L.: Introductory Quantum Mechanics, 4th edn. Addison-Wesley, New York (2002)
Liboff, R.L.: Kinetic Theory: Classical, Quantum, and Relativistic Descriptions, 3rd edn. Springer, New York (2003)
Lie-Svendsen, O., Rees, M.H.: An improved kinetic model for the polar outflow of a minor ion. J. Geophys. Res. **101**, 2415–2433 (1996)
Light, J.C., Carrington Jr, T.: Discrete variable representations and their utilization. Adv. Chem. Phys. **114**, 263–310 (2000)
Light, J.C., Hamilton, I.P., Lill, J.V.: Generalized discrete variable approximation in quantum mechanics. J. Chem. Phys. **82**, 1400–1409 (1985)
Lightman, A.P., Shapiro, S.L.: The dynamical evolution of globular clusters. Rev. Mod. Phys. **50**, 437–481 (1978)
Lindenfeld, M.J., Shizgal, B.: The Milne problem: a study of the mass dependence. Phys. Rev. **A27**, 1657–1670 (1983)
Liou, K.N.: An Introduction to Atmospheric Radiation. Elsevier, Amsterdam (2002)
Lo, J.Q.-W., Shizgal, B.D.: Spectral convergence of the quadrature discretization method in the solution of the Schrödinger and Fokker-Planck equations: comparison with Sinc methods. J. Chem. Phys. **125**, 194108 (2006)
Lo, J.Q.-W., Shizgal, B.D.: An efficient mapped pseudospectral method for weakly bound states: vibrational states of He_2, Ne_2, Ar_2 and Cs_2. J. Phys. B: At. Mol. Opt. Phys. **41**, 185103 (2008)
Marston, C.C., Balint-Kurti, G.G.: The Fourier grid Hamiltonian method for bound state eigenvalues and eigenfunctions. J. Chem. Phys. **91**, 3571–3576 (1989)
Messiah, A.: Quantum Mechanics, vol. I. North Holland, Amsterdam (1961)
Milne, E.A.: Thermodynamics of the stars. Handbuch der Astrophysik **3**, 65–255 (1930)
Morgan, J.D.: Thomas-Fermi and other density—functional theories. In: Drake, G.W.F. (ed.) Atomic, Molecular and Optical Physics Handbook, pp. 233–242. AIP Press, New York (1996)
Peeters, A.G., Strintzi, D.: The Fokker-Planck equation, and its application in plasma physics. Ann. Phys. (Berlin) **17**, 142–157 (2008)
Peyret, R.: Spectral Methods for Incompressible Viscous Flow. Springer, New York (2002)
Pierrard, V., Lemaire, J.: A collisional model of the polar wind. J. Geophys. Res. **103**, 11701–11709 (1998)
Pinkus, A.: Weierstrass and approximation theory. J. Approx. Theory **107**, 1–66 (2000)
Pitchford, L.C., Phelps, A.V.: Comparative calculations of electron-swarm properties in N_2 at moderate E/N values. Phys. Rev. A **25**, 540–554 (1982)
Present, R.D., Morris, B.M.: Variational solution of the chemical kinetic Boltzmann equation. J. Chem. Phys. **50**, 151–160 (1969)
Pryce, J.D.: Numerical Solution of Sturm-Liouville Problems. Oxford University Press, Oxford (1993)
Reed, W. H., Hill T.R.: Triangular Mesh Methods for the Neutron Transport Equation. Technical Report LA-UR-73-479, Los Alamos Scientific Laboratory (1973)
Reinhardt, W.P.: L^2 discretization of atomic and molecular electronic continua: moment, quadrature and J-matrix techniques. Comput. Phys. Commun. **17**, 1–21 (1979)

Risken, H., Till, F.: The Fokker-Planck Equation: Methods of Solution and Applications, 2nd edn. Springer, Berlin (1996)
Rivlin, T.J.: An Introduction to the Approximation of Functions. Blaisdell Publishing Co., Toronto (1969)
Rybicki, G.B.: Radiative transfer. J. Astrophys. Astron. **17**, 95–112 (1996)
Sarkar, T.K.: A note on the variational method (Rayleigh-Ritz), Galerkin's methods and the method of weighted residuals. Radio Sci. **18**, 1207–1224 (1983)
Schwartz, C.: High-accuracy approximation techniques for analytic functions. J. Math. Phys. **26**, 411–415 (1985)
Shen, J., Tang, T., Wang, L.-L.: Spectral Methods: Algorithms, Analysis and Applications. Springer, Berlin (2011)
Sherrill, C.D.: Frontiers in electronic structure theory. J. Chem. Phys. **132**, 110902 (2010)
Shizgal, B.: A Gaussian quadrature procedure for the use in the solution of the Boltzmann equation and related problems. J. Comput. Phys. **41**, 309–328 (1981)
Shizgal, B., Blackmore, R.: Eigenvalues of the Boltzmann collision operator for binary gases and relaxation of anisotropic distributions. Chem. Phys. **77**, 417–427 (1983)
Shizgal, B., Blackmore, R.: A discrete ordinate method of solution of linear boundary value and eigenvalue problems. J. Comput. Phys. **55**, 313–327 (1984)
Shizgal, B., Karplus, M.: Nonequilibrium contributions to the rate of reaction. II. Isolated multicomponent systems. J. Chem. Phys. **54**, 4345–4356 (1971)
Shizgal, B.D., Arkos, G.G.: Nonthermal escape of the atmospheres of Venus, Earth, and Mars. Rev. Geophys. **34**, 483–505 (1996)
Shizgal, B.D., Chen, H.: The quadrature discretization method (QDM) in the solution of the Schrödinger equation with nonclassical basis functions. J. Chem. Phys. **104**, 4137–4150 (1996)
Shizgal, B.D., Chen, H.: The quadrature discretization method in the solution of the Fokker-Planck equation with nonclassical basis functions. J. Chem. Phys. **107**, 8051–8063 (1997)
Shore, B.W.: Solving the radial Schrödinger equation by using cubic-spline basis functions. J. Chem. Phys. **58**, 3855–3866 (1973)
Shore, B.W.: B-spline expansion bases for excited states and discretized scattering states. J. Chem. Phys. **63**, 3835–3840 (1975)
Shu, C.: Differential Quadrature and Its Application in Engineering. Springer, Berlin (2000)
Siewert, C.E.: On computing the Chapman-Enskog functions for viscosity and heat transfer and the Burnett functions. JQRST **74**, 789–796 (2002)
Snider, R.F.: Variational methods for solving the Boltzmann equation. J. Chem. Phys. **41**, 591–595 (1964)
Sospedra-Alfonso, R., Shizgal, B.D.: Henyey-Greenstein model in the shape relaxation of dilute gas mixtures. Trans. Theory Stat. Phys. **41**, 368–388 (2012)
Spitzer, L.J., Härm, R.: Evaporation of stars from open clusters. Astrophys. J. **127**, 544–550 (1958)
Stare, J., Balint-Kurti, G.G.: Fourier grid Hamiltonian method for solving the vibrational Schrödinger equation in internal coordinates: theory and test applications. J. Phys. Chem. A **107**, 7204–7214 (2003)
Steffens, K.G.: The History of Approximation Theory, from Euler to Bernstein. Birkhäuser, Boston (2006)
Szabo, A., Ostlund, N.S.: Modern Quantum Chemistry, Introduction to Advanced Electronic Structure Theory. Dover, New York (1996)
Szalay, V., Szidarovsky, T., Czakó, G., Császár, A.G.: A paradox of grid-based representation techniques: accurate eigenvalues from inaccurate matrix elements. J. Math. Chem. **50**, 636–651 (2012)
Taylor, J.R.: Scattering Theory: the quantum Theory on Nonrelativistic Collisions. Dover, New York (2012)
Thomas, G.E., Stamnes, K.: Radiative Transfer in the Atmosphere and Ocean. Cambridge University Press, Cambridge (2002)
Trefethen, L.N.: Approximation Theory and Approximation Practice. SIAM, Philadelphia (2013)

Tsuneda, T.: Density Functional Theory in Quantum Chemistry. Springer, New York (2014)
Vasenkov, A., Shizgal, B.D.: Nonhydrodynamic aspects of electron transport near a boundary: the milne problem. Phys. Rev. E **63**, 016401 (2000)
Wei, H.: Ghost levels and near-variational forms of the discrete variable representation: application to H_2O. J. Chem. Phys. **106**, 6885–6900 (1997)
Wei, G.W.: Solving quantum eigenvalue problems by discrete singular convolution. J. Phys. B: At. Mol. Opt. Phys. **33**, 343–352 (2000a)
Wei, G.W.: Wavelets generated by using discrete singular convolution kernels. J. Phys. A: Math. Gen. **33**, 8577–8596 (2000b)
Wick, G.C.: Über ebene diffusionsprobleme. Z. Phys. **121**, 702–718 (1943)
Williams, M.M.R.: The Slowing Down and Thermalization of Neutrons. North-Holland, Amsterdam (1966)
Williams, M.M.R.: Mathematical Methods in Particle Transport Theory. Wiley-Interscience, New York (1971)
Willner, K., Dulieu, O., Masnou-Seeuws, F.: Mapped grid methods for long-range molecules and cold collisions. J. Chem. Phys. **120**, 548–561 (2004)

Chapter 2
Polynomial Basis Functions and Quadratures

Abstract Spectral and pseudospectral methods in chemistry and physics are based on classical and nonclassical orthogonal polynomials defined in terms of a three term recurrence relation. The coefficients in the three term recurrence relations for the nonclassical polynomials can be calculated with the Gautschi-Stieltjes procedure. The round-off errors that occur with the use of Gram-Schmidt orthogonalization procedure is demonstrated for both classical and nonclassical polynomials. The trapezoidal, Simpson's and Newton-Cotes integration rules are derived as are the Fejér, Clenshaw-Curtiss, Gauss-Lobatto and Gauss-Radau algorithms. Sinc interpolation based on Fourier sine basis functions is compared with the Lagrange interpolation. Nonclassical Maxwell and Bimodal polynomials orthogonal on the infinite domain with respect to weight functions $w(x) = x^2 \exp(-x^2)$ and $x^2 \exp[-(x^4/4\epsilon - x^2/2\epsilon)]$, respectively, are introduced for kinetic theory problems. The Gaussian quadrature rule based on the nonclassical Rys polynomials orthogonal with respect to the weight function $w(x) = e^{-cx^2}$, $x \in [-1,\ 1]$, used to evaluate integrals in molecular quantum mechanics is presented. For $c \to 0$ and $c \to \infty$, the Rys polynomials are the Legendre and scaled Hermite polynomials, respectively. Two dimensional quadratures, such as the Lebedev cubature, are used to evaluate two dimensional integrals in density functional theory for electronic structure calculations as well as for the nonlinear Boltzmann equation in kinetic theory. The Stieltjes moment problem is related to the inversion of moment data in chemical physics to reconstruct photoelectron cross sections.

2.1 Introduction

A spectral method of solution of partial differential and integral equations is based on the expansion of the solution in a basis set of linearly independent functions. The choice of basis set for a particular problem is dictated in part by both the interval of interest and the anticipated behaviour of the solutions. Table 2.1 lists several classical polynomials orthogonal with respect to weight function $w(x)$ on the specified interval $[a, b]$. The Fourier sine and cosine basis functions are also included. The list in the table is not exhaustive but it does summarize the most frequently used orthogonal basis sets. Except for the sine and cosine basis sets and the Hermite functions, $h_n(x)$, the other basis functions are all polynomials.

B. Shizgal, *Spectral Methods in Chemistry and Physics*, Scientific Computation,
DOI 10.1007/978-94-017-9454-1_2

Table 2.1 Classical orthogonal basis functions

$[a, b]$	$w(x)$	Name	Symbol	N_n
$[-1,\ 1]$	1	Legendre	$P_n(x)$	$2/(2n+1)$
$[-1,\ 1]$	$1/\sqrt{1-x^2}$	Chebyshev	$T_n(x)$	$\pi\ \ (n=m=0)$
				$\pi/2\ \ (n=m\neq 0)$
$[-1,\ 1]$	$(1-x^2)^{\lambda-\frac{1}{2}}$	Gegenbauer	$C_n^{(\lambda)}(x)$	$\frac{2^{1-2\lambda}\pi\Gamma(n+2\lambda)}{n!(n+\lambda)\Gamma^2(\lambda)}$
$[-1,\ 1]$	$(1-x)^\alpha(1-x)^\beta$	Jacobi	$P_n^{(\alpha,\beta)}(x)$	$\frac{2^{\alpha+\beta+1}}{2n+\alpha+\beta}\frac{\Gamma(n+\alpha+1)\Gamma(n+\beta+1)}{n!\Gamma(n+\alpha+\beta+1)}$
$[-1,\ 1]$	1	Sine	$\sin(n\pi x)$	1
$[-1,\ 1]$	1	Cosine	$\cos(n\pi x)$	1
$[-\infty, \infty]$	e^{-x^2}	Hermite	$H_n(x)$	$2^n\sqrt{\pi}n!$
$[-\infty, \infty]$	1	Hermite	$h_n(x)=e^{-x^2/2}H_n(x)$	$2^n\sqrt{\pi}n!$
$[0, \infty]$	$x^\alpha e^{-x}$	Associated Laguerre	$L_n^{(\alpha)}(x)$	$\frac{\Gamma(n+\alpha+1)}{n!}$
$[0, \infty]$	$x^{2\alpha+1}e^{-x^2}$	Sonine	$S_\alpha^{(n)}(x^2)$	$\frac{\Gamma(n+\alpha+1)}{2n!}$

$\Gamma(\alpha)=\int_0^\infty x^{(1-\alpha)}e^{-x}dx$ is the Gamma function

A set of basis functions normalized to unity can be defined by dividing the basis functions above by $\sqrt{N_n}$. These polynomials arise in the solution of a variety of physical problems, especially in kinetic theory and quantum mechanics. The Legendre[1] polynomials are the eigenfunctions for the rotational states of a diatomic molecule with a fixed interatomic distance, that is a rigid rotor. The Hermite[2] polynomials are the eigenfunctions for the quantum harmonic oscillator representing the vibrational states of a diatomic molecule with a quadratic interatomic potential. The associated Laguerre[3] polynomials occur in the definition of the eigenfunctions of the radial Schrödinger equation for the hydrogen atom.

The Sonine[4] polynomials are used for the solution of the Boltzmann[5] equation and the calculation of the transport properties of a dilute gas (Chapman and Cowling 1970; Ferziger and Kaper 1972; Liboff 2003; Kremer 2010). For a repulsive pair potential that varies as the inverse 4th power of the interparticle separation, the

[1] Adrian Marie Legendre (1752–1833) studied mathematics and physics in France and is known for the method of least squares for fitting data, the Legendre transform in classical mechanics.

[2] Charles Hermite (1822–1901) was a French mathematician who contributed to number theory and algebra and one of his students was Henri Poincaré.

[3] Edmond Nicolas Laguerre (1834–1886) was a French mathematician who contributed to geometry and complex analysis.

[4] Nikolay Yakovlevich Sonin (1849–1915) was a Russian mathematician who made substantial contributions to the theory of orthogonal polynomials and cylindrical functions.

[5] Ludwig Eduard Boltzmann (1844–1906) was an Austrian theoretical physicist who made unique contributions to kinetic theory, statistical mechanics and radiation physics. He derived the Boltzmann equation of kinetic theory and the H-theorem which is the basis for the use of entropy to explain the approach to equilibrium.

Sonine polynomials are the eigenfunctions of the linear collision operator of the Boltzmann equation, as discussed in Chaps. 3 and 5. The product of the cross section and the relative speed for this model is independent of the relative speed and the collision operator is simplified as recognized by Maxwell[6]; hence the name Maxwell molecules for this model. In kinetic theory, the Sonine polynomials are functions of the "reduced speed", $x = \sqrt{mv^2/2k_BT}$, where m is the mass of the gaseous particle, $\mathbf{v}$ is the velocity, k_B is the Boltzmann constant and T is the temperature. The Laguerre polynomials, as used in kinetic theory, are very similar and are functions of the "reduced energy" $y = mv^2/2k_BT$.

The Gegenbauer[7] polynomials occur in potential theory and harmonic analysis and also for the resolution of the Gibbs phenomenon (Gottlieb and Shu 1997; Shizgal and Jung 2003) as discussed in Chap. 4. The Gegenbauer polynomials are the Legendre and Chebyshev[8] polynomials for $\lambda = \frac{1}{2}$ and $\lambda = 0$, respectively. The classical orthogonal polynomials listed in Table 2.1 are the eigenfunctions of second order differential operators of the Sturm-Liouville type (Al-Gwaiz 2008) and also possess many well known properties such as a generating function.

Table 2.2 lists several non-classical polynomials for which a very limited set of properties are known in stark contrast with the classical polynomials. Gautschi (1994) noted three decades ago that there has not been widespread use of nonclassical orthogonal polynomials and encouraged their use. Since then, there has been increased research on the use of nonclassical polynomials for spectral and pseudospectral solutions of differential and integral equations applied to many fields. The nonclassical weight functions determine the distribution of the quadrature points within the interval of interest which may resolve the pseudospectral solutions of particular problems (Byrd and Galant 1970; Garcia 1999; Baye and Vincke 1999; Chen and Shizgal 2001; Shizgal 2002). The table provides a brief but not exhaustive summary of the research to date. A brief overview of recent works follows with more detailed discussions and applications provided in Chaps. 3–6.

The Maxwell polynomials were introduced long ago for the solution of problems in kinetic theory (Gross et al. 1957) and neutron transport (Desai and Nelkin 1966), and subsequently considered independently by several researchers (Steen et al. 1969; Galant 1969; Shizgal 1981; Gautschi 1984, 2009). These nonclassical polynomials (for $p = 0$, 1 and 2) have found widespread use in numerous applications in kinetic theory (Sospedra-Alfonso and Shizgal 2012a), Fokker-Planck transport (Blackmore and Shizgal 1985a), polar wind modelling (Pierrard and Lemaire 1998), tethered

[6] James Clerk Maxwell (1831–1879) was a Scottish mathematical physicist who made exceptional contributions to kinetic theory, electromagnetism and optics. He was responsible for the Maxwell equations which are the basis for the behavior of electric and magnetic fields in numerous physical situations.

[7] Leopold Bernhard Gegenbauer (1849–1903) was an Austrian mathematician who specialized in algebra and made important contributions to function theory and developed the Gegenbauer polynomials for his doctoral thesis.

[8] Pafnuty Lvovich Chebyshev (1821–1894) was a Russian mathematician who worked in probability and number theory, and developed the polynomials named after him while interested in linkages that converted rotational motion into rectilinear motion in steam engines.

Table 2.2 Non-classical orthogonal basis functions

$[a, b]$	$w(x)$	Name	Symbol	N_n
$[0, \infty]$	$x^p e^{-x^2}$	Maxwell	$M_n^{(p)}(x)$	1
$[0, \infty]$	e^{-x^4}	Druvesteyn[a]	$D_n(x)$	1
$[0, \infty]$	$\exp[-a(x - x_0)^2]$	Gaussian	$G_n(x)$	1
$[0, \infty]$	$\exp[-5x + 6e^{-x}]$	Morse[b]	$M_n(x)$	1
$[0, \infty]$	$x^5 e^{-x^4/16}$	Schrödinger equation[c]	None	1
$[-\infty, \infty]$	$e^{-(x^4/4 - x^2/2)/\epsilon}$	Bimodal[d]	$B_n(x)$	1
$[0, \infty]$	$x^2 e^{-(x^4/4 - x^2/2)/\epsilon}$	Bimodal half-range	$\hat{B}_n(x)$	1
$[-1, 1]$	e^{-cx^2}	Rys[e]	$J_n(x, c)$	1
$[0, 1]$	e^{-cx^2}	Rys	$R_n(x, c)$	1
$[0, 1]$	$\ln^2(x)$	Multi-Exponential[f]	$E_n(x)$	1
$[0, 1]$	$e^{-c/x}$	Radiative Transfer[g]	$R_n(x)$	1
$[0, \infty]$	$\left(\frac{x}{e^{cx}-1}\right)^p$	Bose-Einstein[h]	$Be_n(x)$	1
$[0, \infty]$	$\left(\frac{1}{e^{cx}+1}\right)^p$	Fermi-Dirac[h]	$Fd_n(x)$	1

[a] See Sect. 3.7.5 in Liboff (2003), (Chen and Shizgal 2001)
[b] Model vibrational Morse potential $V(x) = 9(e^{-2x} - 2e^{-x})$ (Chen and Shizgal 2001)
[c] Potential is $V(x) = \frac{x^6}{64} - x^2 + \frac{15}{4x^2}$ (Shizgal and Chen 1996)
[d] Blackmore and Shizgal (1985a), Shizgal and Chen (1997), Lo and Shizgal (2006)
[e] Dupuis et al. (1976), Rys et al. (1983)
[f] Gill and Chien (2003)
[g] Gander and Karp (2001)
[h] Gautschi (1993)

satellite analysis (Williams 2011), Fermi liquids (Warringa and Sedrakian 2011) heat transfer (Graur and Polikarpov 2009), satellite re-entry, (Li and Zhang 2009) and other applications. For $p = 0$, the Maxwell polynomials, often referred to as the half-space Hermite polynomials, permit the efficient application of boundary conditions for a rarefied gas dynamical problem (Gibelli 2012).

The Druvesteyn distribution function (see Liboff 2003, p. 236) is the steady distribution for electrons in a background gas under the influence of a steady electrostatic field with a hard sphere cross section for electron-atom collisions. For realistic cross sections, the steady distribution function is the Davydov distribution function. These distributions are displaced to higher energies with an increase in the electrostatic field. These physical distribution functions are used as weight functions to define nonclassical polynomials (Wannier 1971; Chen and Shizgal 1998, 2001) and associated quadratures.

Gaussian weight functions, $w(x) = \exp[-a(x - x_0)^2]$, have been used to define nonclassical quadratures for the solution of the electron Fokker-Planck equation and the associated Schrödinger equation for a mixture of an inert gas and a strongly attaching electron gas (Shizgal 1987). As a consequence of the attachment heating of the electrons, the steady state distribution is non-Maxwellian and displaced to

higher energies. With the appropriate choice of parameters in the Gaussian weight functions, quadrature points can be constructed to be densely distributed in some interval of interest.

Gaussians have been used as basis functions for the solution of the vibrational Schrödinger equation (Garashchuk and Light 2001; Karabulut and Kalay 2005). In Chap. 6, nonclassical basis functions defined by Morse potentials are used to solve the Schrödinger equation for the vibrational energy states of diatomic molecules. Extensive use is made of potentials, such as the Morse potential, that belong to the class of potential functions in supersymmetric quantum mechanics (Comtet et al. 1985; Dutt et al. 1988; Cooper et al. 1995) which serve to define nonclassical weight functions.

The bimodal polynomials have been used to solve the Fokker-Planck equation which models a chemical reaction with a bistable potential separating reactants from products (Blackmore and Shizgal 1985a; Shizgal and Chen 1997; Lo and Shizgal 2006) with a barrier height controlled by ϵ. The Rys polynomials (Dupuis et al. 1976; King and Dupuis 1976; Rys et al. 1983) provide an efficient technique for electronic structure calculations by providing a quadrature for integrals over Gaussian orbitals (Dupuis and Marquez 2001; Schneider and Nygaard 2002). Gill and Chien (2003) developed a nonclassical quadrature based on the weight function $w(x) = \ln^2(x)$, $x \in [0, 1]$ for radial integrals that occur in density functional theory. Gander and Karp (2001) developed a quadrature for use in radiative transfer theory and quadratures for integrals with logarithmic singularities have been reported by Beebe and Ball (2007).

For the most part, the use of nonclassical quadratures as discussed in the previous paragraphs has been very limited by comparison to the use of quadratures based on the classical polynomials. We discuss in Chaps. 5 and 6 the applications of these quadrature rules to the solution of differential and integral equations such as the Boltzmann, Fokker-Planck and Schrödinger equations (Blackmore and Shizgal 1985a; Baye and Heenen 1986; Light and Carrington 2000; Baye 2006; Lo and Shizgal 2008).

In Sect. 2.3.4, we present the basis for the Gaussian quadrature numerical evaluation of integrals. Perhaps the first use of a quadrature rule after Gauss (1814) in a pseudospectral application was by Wick (1943) and later by Chandrasekhar (1960) in the solution of a radiative transfer equation discussed in Chap. 5.

2.2 Gram-Schmidt Orthogonalization and Three Term Recurrence Relations

Given a weight function, $w(x)$, and an interval of interest, $x \in [a, b]$, an orthogonal polynomial basis can be constructed from the linearly independent set of monomials, $1, x, x^2, \ldots, x^n$. The procedure, which is known as the Gram[9]-

[9] Jorgen Pedersen Gram (1850–1916) was a Danish mathematician and number theorist.

Schmidt[10] orthogonalization, is based on the monic polynomials

$$Q_n(x) = \sum_{k=0}^{n-1} q_{nk} x^k + x^n, \tag{2.1}$$

for which the coefficient of x^n is unity. Given $Q_n(x)$, the next member of the set $Q_{n+1}(x)$ is determined by making it orthogonal to all the n lower order $Q_n(x)$ polynomials and determining the normalization, γ_n

$$\int_a^b w(x) Q_n Q_m dx = \gamma_n \delta_{nm}. \tag{2.2}$$

The procedure begins with $Q_0(x) = 1$ with the normalization $\gamma_0 = \int_a^b w(x)dx$. The next member of the set is then $Q_1(x) = q_{10} + x$. The requirement that it be orthogonal to Q_0 gives

$$q_{10} = -\frac{1}{\gamma_0} \int_a^b w(x) x dx,$$

and the normalization is $\gamma_1 = \int_a^b Q_1^2(x)dx$. The next polynomial in the set is $Q_2(x) = q_{20} + q_{21}x + x^2$. The requirement that this be orthogonal to Q_0 and Q_1 leads to two equations for the two coefficients q_{20} and q_{21}.

This procedure requires the moments of the weight function

$$\mu_n = \int_a^b w(x) x^n dx. \tag{2.3}$$

We can continue this process to generate successively higher order polynomials and the analogous set of orthonormal polynomials

$$P_n(x) = \frac{Q_n(x)}{\sqrt{\gamma_n}}, \tag{2.4}$$

not to be confused with Legendre polynomials that we will later write as $P_\ell(x)$.

This approach is algebraically cumbersome and the more efficient approach is the Gautschi-Stieltjes procedure discussed in Sect. 2.3.6. The Gram-Schmidt orthogonalization method is described to illustrate an example of an algorithm that is numerically ill-conditioned and unstable. The numerical algorithms used for scientific applications can be seriously contaminated with round-off errors. It is important to

[10] Erhard Schmidt (1876–1959) was a German mathematician who made contributions to functional analysis with his advisor David Hilbert.

recognize the origin of such numerical instabilities and to develop well conditioned algorithms (Quarteroni et al. 2010; Gautschi 2011).

Consider the monic polynomials up to $Q_n(x)$ with $\langle Q_m|Q_n\rangle = 0$ for $m < n$. We use the "bra" and "ket" notation introduced in Chap. 1. It is understood that the scalar product written in this way is defined with the weight function $w(x)$ as in Eq. (2.2). The next polynomial in the set, $Q_{n+1}(x)$, can be generated from $xQ_n(x)$ and therefore we write,

$$xQ_n(x) = Q_{n+1}(x) + \sum_{k=0}^{n} c_{nk} Q_k(x), \tag{2.5}$$

where the coefficients are determined by taking the scalar product of Eq. (2.5) with $Q_k(x)$, that is

$$c_{nk} = \frac{1}{\gamma_n}\langle Q_n|x|Q_k\rangle, \tag{2.6}$$

where Eq. (2.2) has been used. Since $xQ_k(x)$ is a polynomial of order $k+1$, $c_{nk} = 0$ for $k = 0, 1, \ldots (n-2)$ and Eq. (2.5) can be rewritten as

$$xQ_n = Q_{n+1} + \alpha_n Q_n + \beta_n Q_{n-1}, \tag{2.7}$$

where the coefficients have been redefined, that is, $c_{n,n} = \alpha_n$ and $c_{n,n-1} = \beta_n$. The scalar product of this equation with Q_n is

$$\langle Q_n|x|Q_n\rangle = \alpha_n \gamma_n, \tag{2.8}$$

so that

$$\alpha_n = \frac{\langle Q_n|x|Q_n\rangle}{\gamma_n} = \langle P_n|x|P_n\rangle. \tag{2.9}$$

where Eq. (2.4) has been used. The scalar product of Eq. (2.7) with Q_{n-1} gives

$$\langle Q_{n-1}|x|Q_n\rangle = \beta_n \gamma_{n-1}. \tag{2.10}$$

Similarly, the scalar product of $Q_n(x)$ with Eq. (2.7) and n replaced with $n-1$, gives

$$\gamma_n = \langle Q_n|x|Q_{n-1}\rangle, \tag{2.11}$$

so that with Eq. (2.10)

$$\beta_n = \frac{\gamma_n}{\gamma_{n-1}}. \tag{2.12}$$

Equation (2.7) can be rewritten as

$$\boxed{Q_{n+1} = (x - \alpha_n)Q_n - \beta_n Q_{n-1},} \tag{2.13}$$

or in terms of the polynomials normalized to unity,

$$\boxed{xP_n = \sqrt{\beta_{n+1}}P_{n+1} + \alpha_n P_n + \sqrt{\beta_n}P_{n-1},} \tag{2.14}$$

where the recurrence coefficients, α_n and β_n are given by Eqs. (2.9) and (2.12), respectively.

Equations (2.13) and (2.14) together with the definitions of α_n and β_n are central to the theoretical development of orthogonal polynomials. If the recurrence relation Eq. (2.14), is squared, multiplied by $w(x)$ and integrated, we obtain another recurrence relation that gives β_{n+1} in terms of the lower order coefficients, that is,

$$\langle x^2 P_n^2 \rangle = \beta_{n+1} + \alpha_n^2 + \beta_n. \tag{2.15}$$

This relationship is used in an application later in this chapter.

We have an algorithm for the generation of a polynomial basis set defined by a weight function and the interval of interest. We combine the Gram-Schmidt orthogonalization with the three term recurrence relation. With $Q_{-1}(x) = 0$, $Q_0(x) = 1$ and $Q_1(x) = x$, we can evaluate $\gamma_0 = \langle Q_0|Q_0\rangle$, $\gamma_1 = \langle Q_1|Q_1\rangle$, $\alpha_1 = \langle P_1|x|P_1\rangle$ and $\beta_1 = \gamma_1/\gamma_0$. The next monic polynomial, $Q_2(x)$, can then be evaluated with the three term recurrence relation, Eq. (2.13), as well as γ_2, α_2, β_2 and hence $Q_3(x)$. Unfortunately, this approach eventually breaks down for some n owing to large round-off errors for both classical and nonclassical polynomials. This occurs in the calculation of γ_n, the normalization of the monic polynomial, Q_n, as shown later. However, the calculation can be done algebraically with MAPLE. We adopt both approaches in the construction of the classical Legendre and Hermite polynomials, and the nonclassical Rys polynomials.

2.2.1 Legendre and Hermite Polynomials

For polynomials over a symmetric interval, $[-a, a]$, defined with an even weight function, $w(-x) = w(x)$, we have that $\alpha_n = \langle xP_n^2\rangle = 0$ and $\beta_n = \gamma_n/\gamma_{n-1}$. Among many different polynomial basis sets, this includes the Legendre polynomials, P_ℓ on $[-1,\ 1]$ with weight function $w(x) = 1$ and the Hermite polynomials on $[-\infty, \infty]$ with weight functions $w(x) = \exp[-x^2]$. We consider their construction based on the Gram-Schmidt procedure so as to illustrate a numerical instability inherent in the approach. A discussion of the bimodal polynomials for which $\alpha_n = 0$ is provided in Sect. 2.5.2.

The Gram-Schmidt procedure involves writing the nth monic polynomial in terms of the lower order orthogonal polynomials Q_k, $k = 0, 1, \ldots (n-1)$, that is,

$$Q_n(x) = \sum_{k=0}^{n-1} c_{n,k} P_k(x) + x^n. \tag{2.16}$$

The requirement that Q_n be orthogonal to all the lower order P_k functions gives

$$c_{n,k} = -\langle x^n | P_k \rangle, \tag{2.17}$$

and the normalization can be written as

$$\gamma_n = \mu_{2n} - \sum_{k=0}^{n-1} c_{n,k}^2. \tag{2.18}$$

The data required for the Gram-Schmidt procedure are the moments of the weight function, Eq. (2.3). A numerical problem with the subtraction in Eq. (2.18) can be anticipated as the two quantities on the right hand side can become large and nearly equal.

The moments defined by Eq. (2.3) for the Legendre weight function are

$$\mu_n = \int_{-1}^{1} x^n dx = \begin{cases} \frac{2}{n+1} & n \text{ even}, \\ 0 & n \text{ odd}. \end{cases} \tag{2.19}$$

For the Hermite weight function, the moments are

$$\mu_n = \int_{-\infty}^{\infty} e^{-x^2} x^n dx = \begin{cases} \Gamma(n + \frac{1}{2}) & n \text{ even}, \\ 0 & n \text{ odd}. \end{cases} \tag{2.20}$$

The lower order polynomials can be determined with these moments. Table 2.3 summarizes the procedure up to Q_4. The monic polynomials are alternately odd and even and thus $c_{n,k} \neq 0$ unless n and k are both even or odd. With the recurrence relation, Eq. (2.14), and the definition Eq. (2.17) we have that

$$c_{n,k} = \sqrt{\beta_{k+1}} c_{n-1,k+1} + \sqrt{\beta_k} c_{n-1,k-1}. \tag{2.21}$$

Table 2.3 Gram-Schmidt orthogonalization procedure

n	Polynomial	Coefficients	γ_n	Hermite $\gamma_n/\sqrt{\pi}$	Legendre γ_n
0	$Q_0 = 1;\ P_0 = Q_0/\sqrt{\gamma_0}$		μ_0	1	2
1	$Q_1 = x;\ P_1 = Q_1/\sqrt{\gamma_1}$		μ_2	1/2	2/3
2	$Q_2 = c_{2,0}P_0 + x^2$	$c_{2,0} = -\mu_2/\sqrt{\mu_0}$	$\mu_4 - \mu_2^2/\mu_0$	1/2	8/45
3	$Q_3 = c_{3,1}P_1 + x^3$	$c_{3,1} = -\mu_4/\sqrt{\mu_2}$	$\mu_6 - \mu_4^2/\mu_2$	3/4	8/175
4	$Q_4 = c_{4,0}P_0 + c_{4,2}P_2 + x^4$	$c_{4,0} = -\mu_4/\sqrt{\mu_0}$			
		$c_{4,2} = -(\mu_6\mu_0 - \mu_2\mu_4)/\mu_0\sqrt{\mu_2}$	$\mu_8 - c_{4,0}^2 - c_{4,2}^2$	3/2	128/11,025

The lower order coefficients, $c_{n,k}$, for a given n are easily calculated as shown in Table 2.3. The subsequent coefficients for k up to $n-1$ are determined from the recurrence relation, Eq. (2.21). Finally the normalization, γ_n, is determined with Eq. (2.18). It is well known that the Gram-Schmidt procedure is numerically unstable and the current approach will break down as a consequence of the computation of the norm with Eq. (2.18). The polynomials are defined with the recurrence coefficient β_n as given by Eq. (2.12) in terms of the normalizations.

With a symbolic algebraic software such as MAPLE, the numerical instability can be avoided. The MAPLE code for Legendre polynomials is shown in Listing 2.1. The numerical values of β_n that result are shown in the second column of Table 2.4 and converted to rational form in the third column. By inspection, the numerical value of the numerator varies as n^2 and the denominator varies as $4n^2-1$. The normalizations, γ_n, are listed in the fourth column and the rapid decrease with increasing n is evident. These are also converted to rational form in the last column. We have thus generated the Legendre polynomials with the moment information and the three term recurrence relation.

In Table 2.4, we show the results of the numerical calculation of the normalizations with Eq. (2.18) and the recurrence, Eq. (2.21). The first column lists the moments, μ_{2n} whereas the second the sum, $\sum_{k=0}^{n-1} c_{n,k}^2$, both of which become nearly equal with increasing n. The ill-conditioned nature of the Gram-Schmidt procedure is self evident by the round-off error that arises from the subtraction of these nearly equal quantities to give the small norm. The underlined digits in bold for $c_{n,k}$ show the significant figures that determine γ_n.

Listing 2.1 MAPLE code for Gram-Schmidt Generation of Legendre Polynomials

```
restart; Digits:=40; N:=8; wt:=1.0;
g[0]:=int(wt,x=-1..1);  beta[0]:=0;
Q[0]:=1; Q[1]:=x;
for i from 2 to 51 do
g[i-1]:=int(wt*Q[i-1]^2,x=-1..1); beta[i-1]:=g[i-1]/g[i-2];
convert(g[i-1],'rational');
Q[i]:=simplify(x*Q[i-1] - beta[i-1]*Q[i-2]):
convert((beta[i-1]),'rational'); end
```

A similar study for the Hermite polynomials is summarized in Tables 2.6 and 2.7. The exact lower order normalizations, γ_n (in units of $\sqrt{\pi}$), are shown in Table 2.6 whereas the details of the iterative Gram-Schmidt construction is shown in Table 2.7. By contrast to the results for Legendre polynomials in Table 2.5, in this case both the moments of the weight function in the second column and $\sum_{k=0}^{n-1} c_{n,k}^2$ in the third column increase dramatically with n. The normalization, γ_n, is the difference of these large quantities and although also large it is several orders of magnitude smaller and round-off errors occur, albeit for somewhat larger n than shown for the Legendre polynomials in Table 2.5. For the Hermite polynomials, one can determine from the results in Table 2.6 that $\beta_n = n/2$ consistent with the known recurrence relation Eq. (2.114).

The round-off errors that we have demonstrated arise from the finite arithmetic precision of computers. This is a very important aspect of scientific computations and

Table 2.4 Gram-Schmidt procedure for Legendre polynomials with MAPLE

n	$\beta_n = \frac{n^2}{4n^2-1}$		$\gamma_n = \beta_n \gamma_{n-1}$	
0	0	0	2	2
1	0.3333333333	1/3	0.2666666667	2/3
2	0.266666667	4/15	0.1777777778	8/45
3	0.2571428571	9/35	0.0457142857	8/175
4	0.2539682540	16/63	0.0116099773	128/11,025
5	0.2525252525	25/99	0.0029318125	128/43,659
6	0.2517482517	36/143	0.0007380787	512/693,693
7	0.2512820513	49/195	0.0001854659	512/2,760,615
8	0.2509803922	64/255	0.0000465483	32,768/703,956,825
9	0.2507739938	81/323	0.0000116731	32,768/2,807,136,475
10	0.2506265664	100/399	0.0000029256	131,072/44,801,898,141

Table 2.5 Iterative Gram-Schmidt procedure for Legendre polynomials

n	μ_{2n}	$\sum_{k=0}^{n-1} c_{n,k}^2$	$\gamma_n^{numerical}$	$\gamma_n^{numerical}/\gamma_n^{exact}$
4	0.2222222222222222	0.2106122448979591	0.11609977 (−1)	1.0000000000
8	0.1176470588235294	0.1176**005105142636**	0.46548309 (−4)	1.0000000000
12	0.0800000000000000	0.0799998**164533769**	0.18354662 (−6)	0.9999999993
16	0.0606060606060606	0.060606059**8856000**	0.72046063 (−9)	0.9999987444
18	0.0540540540540541	0.05405405400**89528**	0.45101305 (−10)	0.9999705423
20	0.0487804878048780	0.048780487802**0550**	0.28230959 (−11)	1.0001642759
21	0.0465116279069767	0.046511627906**2742**	0.70253525 (−12)	0.9950102337
22	0.0444444444444444	0.044444444444**2586**	0.18589297 (−12)	1.0525869822
23	0.0425531914893617	0.042553191489**365**	0.25202063 (−13)	0.5705396358

$\gamma_n^{numerical} = \mu_{2n} - \sum_{k=0}^{n-1} c_{n,k}^2$

Table 2.6 Gram-Schmidt procedure for Hermite polynomials with MAPLE

n	$[\gamma_n = \beta_n \gamma_{n-1}]/\sqrt{\pi}$	
0	1	1
1	0.50000	1/2
2	0.50000	1/2
3	0.75000	3/4
4	1.50000	3/2
5	3.75000	15/4
6	11.2500	45/4
7	39.3750	315/8
8	157.500	315/2
9	708.750	2,835/4
10	3,543.75	14,175/4

Table 2.7 Iterative Gram-Schmidt procedure for Hermite polynomials

n	μ_{2n}	$\sum_{k=0}^{n-1} c_{n,k}^2$	$\gamma_n^{numerical}$	$\gamma_n^{numerical}/\gamma_n^{exact}$
4	0.1403440729348341 (5)	0.1375524581196581 (5)	0.2791614815176053 (3)	1.0000000000
8	0.1403440729348341 (5)	0.1375524581196581 (5)	0.2791614815176053 (3)	1.0000000000
12	0.1368433654655659 (9)	0.136**6360880655389** (9)	0.2072774000270069 (6)	1.0000000000
16	0.5189998453040125 (13)	0.5189**432585738031** (13)	0.5658673020947266 (9)	1.0000000000
20	0.5406242982335074 (18)	0.54062 **01857928796** (18)	0.4112440627840000 (13)	1.0000000024
24	0.1259906343072937 (24)	0.125990 **5687591398** (24)	0.6554815390180966 (17)	0.9999994339
26	0.7871264878348175 (26)	0.787126 **3813197458** (26)	0.1065150717740922 (20)	0.9999930657
28	0.5736184280096233 (29)	0.5736184 **078792427** (29)	0.2013038066556109 (22)	0.9999449868
30	0.4822696933490908 (32)	0.48226968 **89723022** (32)	0.4376788620142886 (24)	0.9995866131
32	0.4633406078851389 (35)	0.463340606 **8040431** (35)	0.1081095786141925 (27)	0.9955827253
33	0.1505856975626702 (37)	0.150585697 **3806734** (37)	0.1819967576228392 (28)	1.0157641582
34	0.5044620868349450 (38)	0.504462086 **5474933** (38)	0.2874517700748905 (29)	0.9437246513

$\gamma_n^{numerical} = \mu_{2n} - \sum_{k=0}^{n-1} c_{n,k}^2$

must be treated seriously. Round-off errors can quickly contaminate computations in a more subtle manner than what we have demonstrated in these sections with the user perhaps unaware of its occurrence. Excellent discussions of the finite precision of computers and the potential deleterious effects on scientific computations have been provided in Chap. 1 of the book by Gautschi (2011) and in Sect. 1.2 in the book by Quarteroni et al. (2010).

2.2.2 The Rys Polynomials

In molecular quantum chemistry computer codes (Reine et al. 2012; Helgaker et al. 2000), most of the computational time of the simulations is the numerical evaluation of a very large number of integrals discussed in Chap. 3. The integrals that are calculated can be reduced to the form

$$I_n(c) = \int_0^1 P_n(x^2) e^{-cx^2} dx, \tag{2.22}$$

where $P_n(x^2)$ is a polynomial in x^2 of degree n, and n and c can vary considerably for different integrals that occur in the calculations. The research activity in this field to develop computationally efficient algorithms is intense (Rys et al. 1983; Becke 1988; Lindh et al. 2001; Chien and Gill 2006; Matsuyama and Koga 2010; Mitani 2011; Asadchev and Gordon 2012).

One approach for the numerical evaluation of such integrals is to consider a quadrature based on the nonclassical Rys polynomials (Dupuis et al. 1976; King and Dupuis 1976; Rys et al. 1983; Lindh et al. 1991) orthogonal according to

$$\int_0^1 e^{-cx^2} R_n(x) R_m(x) dx = \delta_{nm}. \tag{2.23}$$

We refer to these polynomials as half-range owing to their definition on the interval $x \in [0, 1]$ as discussed in Sect. 2.5.3. Half-range Legendre polynomials discussed in Sect. 2.4.2 are used in radiative transfer. Half-range Hermite polynomials $x \in [0, \infty)$ are used in kinetic theory (Gibelli 2012; Ghiroldi and Gibelli 2014). The half-range and full range Legendre polynomials are related by a simple variable transformation owing to the unit weight function, $w(x) = 1$.

In this section, we are concerned with the full-range nonclassical Rys polynomials, $J_n(x)$, orthogonal on $[-1, 1]$, that is

$$\int_{-1}^1 e^{-cx^2} J_n(x) J_m(x) dx = \delta_{nm}. \tag{2.24}$$

The recurrence coefficients $\alpha_n = 0$ owing to the definition of the polynomials over a symmetric interval with even weight function. This is not the case for the half-range Rys polynomials defined by Eq. (2.23) for which $\alpha_n \neq 0$.

The Rys polynomials, $J_n(x)$, approach the Legendre polynomials for $c \to 0$. Alternatively, if the substitution $y = x\sqrt{c}$ is made, then the orthogonality relation, Eq. (2.24), is equivalent to

$$\frac{1}{\sqrt{c}} \int_{-\sqrt{c}}^{\sqrt{c}} e^{-y^2} J_n(y\sqrt{c}) J_m(y\sqrt{c}) dy = \delta_{nm}, \tag{2.25}$$

and the Rys polynomials approach the scaled Hermite polynomials as $c \to \infty$.

We use the Gram-Schmidt procedure to construct these polynomials from the moments of the weight function defined by

$$\mu_n = \int_{-1}^{1} e^{-cx^2} x^n dx, \tag{2.26}$$

with the expectation that round-off error will contaminate the calculations. With an integration by parts, one can show that the moments satisfy the recurrence relation

$$\mu_n = \frac{n-1}{2c} \quad \mu_{n-2} - \frac{1}{c} e^{-c}, \tag{2.27}$$

and can be calculated given the first member

$$\mu_0 = \sqrt{\frac{\pi}{c}} \mathrm{erf}(c). \tag{2.28}$$

where the complementary error function is $\mathrm{erf}(x) = 1 - \mathrm{erf}(x)$ and $\mathrm{erf}(x) = (2/\sqrt{\pi}) \int_0^x \exp(-t^2) dt$.

The recursion relation for the moments is unstable owing to the substraction that occurs in Eq. (2.27). The roundoff error that occurs is subtle as there is a loss of almost one digit with each iteration. The analytic results for lower order moments can be obtained by hand from the recurrence relation or with a short MAPLE program. If the recurrence relation is used successively such that the subtraction is left to the end of the calculation, the roundoff error that occurs is more obvious as illustrated in Table 2.8. The result is that increased numerical precision is required to accurately calculate the moments. The "exact" result in the table is determined with MAPLE. This exact result for a higher order moment can be used with Eq. (2.27) as a downward recursion which is stable (King and Dupuis 1976; Sagar and Smith 1992).

With the moments of the weight function calculated in either of the methods described above, the basis set cannot be constructed with the Gram-Schmidt procedure owing to the round-off error that occurs with the calculation of the normalization. Useful results (not shown) can be obtained only up to approximately $n = 20$.

Table 2.8 Illustration of the round-off error in the recursive calculation of μ_n for the Rys polynomials, Eq. (2.27) of the moments of the weight function $\exp(-cx^2)$ with $c = 1$

			Numerical	Exact
$\mu_{10} =$	$\frac{9!!}{2^5}\sqrt{\pi}\,\mathrm{erf}(1)$	$-\frac{1915}{2^4 e}$		
	44.10930034423397	−44.03057061520700	= 0.07872972902697	0.07872972902697
$\mu_{20} =$	$\frac{19!!}{2^{10}}\sqrt{\pi}\,\mathrm{erf}(1)$	$-\frac{1329151345}{2^9 e}$		
	955014.5969999168	−955014.5586540446	= 0.0383458722	0.03834587218263
$\mu_{30} =$	$\frac{29!!}{2^{15}}\sqrt{\pi}\,\mathrm{erf}(1)$	$-\frac{12566760954932644}{2^{14} e}$		
	282168762050.6263	−282168762050.6010	= 0.0253	0.025259470041296

Table 2.9 Gram-Schmidt procedure for Rys polynomials; $c = 1$

n	β_n	γ_n
1	0.2537041018	0.3789446916
2	0.2754960710	0.1043977737
3	0.2618831608	0.0273400189
4	0.2556247772	0.0069887863
5	0.2532295876	0.0017697675
6	0.2521168628	0.0004461882
7	0.2515016521	0.0001122171
8	0.2511224677	0.0000281802
9	0.2508714069	0.0000070696
10	0.2506963412	0.0000017723

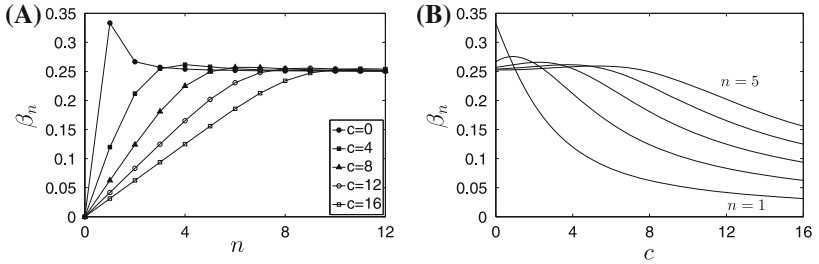

Fig. 2.1 (**A**) Variation of β_n versus n for Rys polynomials $J_n(x)$ for $c = 0, 4, 8, 12$ and 16; Legendre polynomials correspond to $c = 0$ and Hermite polynomials for $c \to \infty$. (**B**) Variation of β_n versus c for Rys polynomials $J_n(x)$ for $n = 1$–5

The lower order values of β_n and γ_n are shown in Table 2.9 and the similarity with the results for the Legendre polynomials in Table 2.4 is clear.

The variation of β_n versus n and c is shown in Fig. 2.1. For the larger values of c, the variation of β_n versus n is smooth and $\lim_{n\to\infty} \beta_n \to 1/4$. This behavior suggests that an efficient fitting procedure may be possible for β_n versus n and c (Clarke

and Shizgal 1993) that may prove useful in the construction of quadratures for the evaluation of integrals, Eq. (2.22). We discuss in Sects. 2.5.3 and 3.8.1 the application of Rys polynomials to the calculation of these integrals and their use in quantum chemistry computer codes and for the evaluation of electron repulsion integrals.

The techniques discussed above are interesting but they are not generally applicable to different classes of weight functions. Each weight function presents a new problem that may not be amenable to a similar analysis and it is anticipated that the results would also lead to unstable recurrence relations. The stable approach that works for arbitrary weight function is the Gautschi-Stieltjes[11] procedure described in Sect. 2.3.6.

2.3 Numerical Integration Algorithms

The Lagrange interpolation, discussed in the section that follows, is the basis for the construction of algorithms for numerical integration. It also provides the discrete physical space representation of derivative operators used in pseudospectral applications discussed in Sect. 3.9.2. In Sect. 2.3.3, the derivation of the Newton[12]-Cotes[13] integration rules which includes the trapezoidal and Simpson's rules is provided. Gaussian quadrature rules are derived and the Gautschi-Stieltjes procedure for the calculation of the quadrature points and weights from the diagonalization of the Jacobi matrix is presented. The Jacobi matrix is the matrix representation of the multiplicative coordinate operator.

2.3.1 Polynomial and Lagrange Interpolation

A common problem is the need to calculate the missing entries in a table of data of some quantity y_i versus x_i. Suppose we have N function values, $y_1, y_2, \ldots, y_N$ for $x_1, x_2, \ldots x_N$. We are interested in interpolating within the tabulated data to determine missing values of y for specific values of x, and we assume that there is a functional relationship giving $y = f(x)$.

Spectral and pseudospectral methods are based on numerical interpolation (Davis 1963; Boyd 2001). Meijering (2002) has provided an excellent historical account of the development of interpolation with particular application to image process-

[11] Thomas Joannes Stieltjes (1856–1894) was a Dutch mathematician and contributed the mathematics of continued fractions and the Stieltjes moment problem. He is also known for the Reimann-Stieltjes integral.

[12] Sir Isaac Newton (1642–1727) was an English physicist and mathematician that made original contributions to classical mechanics, optics, calculus and to other fields.

[13] Roger Cotes (1682–1716) was an English mathematician who worked closely with Isaac Newton and developed the quadrature rules that bear their names.

ing (Meijering et al. 1999; Thévenaz 2000). A short pedagogical discussion is also presented by Prandoni and Vetterli (2009). The discussion in this section overlaps the discussion of Sinc interpolation in Sect. 2.6.1.

A simple interpolation is to assume that the dependence of $y = f(x)$ is linear between successive entries in the table of data. This linear interpolation is given by

$$f(x) \approx f_1(x) = f(x_1)\frac{x - x_2}{x_1 - x_2} + f(x_2)\frac{x - x_1}{x_2 - x_1}, \quad x_1 < x < x_2. \tag{2.29}$$

If x_1 and x_2 are a pair of successive entries in the table, then for $x = x_1$ the second term is zero and the coefficient of $f(x_1)$ is unity. Similarly, for $x = x_2$, the coefficient of $f(x_1)$ is zero and that of $f(x_2)$ is unity. The interpolation returns the tabulated entries exactly. Equation (2.29) can be rewritten, after some algebra, as $f_1(x) = a_1 + b_1 x$.

The interpolation can be improved by increasing the degree of the interpolating functions which are polynomials. The quadratic approximation is given by

$$f(x) \approx f_2(x) = f(x_1)\frac{(x - x_3)(x - x_2)}{(x_1 - x_3)(x_1 - x_2)} + f(x_2)\frac{(x - x_3)(x - x_1)}{(x_2 - x_3)(x_2 - x_1)} + f(x_3)\frac{(x - x_1)(x - x_2)}{(x_3 - x_1)(x_3 - x_2)}. \tag{2.30}$$

The coefficient of $f(x_1)$ is zero for x equal to x_2 or x_3, and unity for $x = x_1$. A similar behaviour is observed for the coefficients of $f(x_2)$ and $f(x_3)$ so that the interpolation returns the tabulated values exactly. This interpolation can be written, after some algebra, as a quadratic, that is, $f_2(x) = a_2 + b_2 x + c_2 x^2$.

This can be generalized to an Nth order interpolation by writing

$$f(x) \approx f_N(x) = \sum_{i=1}^{N} f(x_i)\ell_i(x), \tag{2.31}$$

where the interpolating polynomials are defined by

$$\ell_i(x) = \prod_{j=1, j\neq i}^{N} \frac{x - x_j}{x_i - x_j}, \tag{2.32}$$

and $\ell_i(x)$ depends on N. We do not show this dependence to keep the notation simple. This polynomial interpolation is referred to the as Lagrange[14] interpolation. The interpolating polynomials have been constructed so that

$$\ell_i(x_j) = \delta_{ij}, \tag{2.33}$$

[14] Joseph-Louis Lagrange (1736–1813) was an Italian mathematician and astronomer and made significant contributions to analysis, number theory, classical and celestial mechanics.

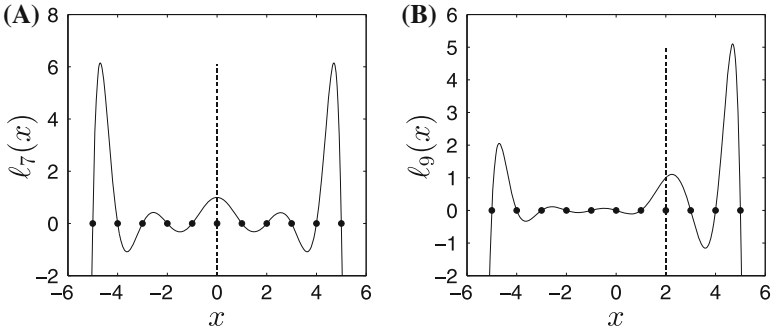

Fig. 2.2 The Lagrange interpolation functions $\ell_i(x)$ for (**A**) $i = 7$ and (**B**) $i = 9$ for a uniform grid $x_j = -7 + j,\ j = 1, 2, \ldots, 11$. The *solid symbols* identify the grid points for which $\ell_i(x_j) = 0, i \neq j$ and the *vertical dashed line* at x_i for which $\ell_i(x_i) = 1$. The Sinc interpolation for the same grid is shown in Fig. 2.10

known as the Cardinality condition and the functions $\ell_j(x)$ are referred to as Cardinal functions. By construction, the interpolation gives the exact values of $f(x)$ at the grid points x_i which need not be equidistant. The variation of the Lagrange interpolants, $\ell_7(x)$ and $\ell_9(x)$, for a uniform grid of 11 points is shown in Fig. 2.2. The interpolant has roots at all the grid points, $x_j \neq x_i$, except for the one point $x_i = x_j$ where it is unity.

The Lagrange polynomial, Eq. (2.32), is unique once the grid points are chosen. It can be constructed in terms of orthogonal polynomials. If we choose the nonuniform grid points, x_i, corresponding to the quadrature points defined as the roots of the Nth order polynomial, $P_N(x_i) = 0$, that is

$$P_N(x) = \prod_{j=1}^{N} (x - x_j), \tag{2.34}$$

the Lagrange interpolant can be written as

$$\ell_i(x) = \frac{P_N(x)}{(x - x_i)P'_N(x_i)}. \tag{2.35}$$

The term $(x - x_i)$ in the denominator of Eq. (2.35) deleted in the product in Eq. (2.32) cancels with the corresponding term in $P_N(x)$ and the denominator in Eq. (2.32) is precisely $P'_N(x_i)$; see Eq. (2.30) for an example.

2.3.2 Trapezoidal and Simpson's Integration Rules

The interpolation introduced in the preceding section can be used to derive approximate integration rules. We present here a synthesis of the discussions that can be found elsewhere (Ralston and Rabinowitz 2001; Talman 2006; Cheney and Kincaid

2008). These integration rules can in general be written in the form

$$\int_a^b f(x)dx \approx I_N = \sum_{i=1}^{N} w_i f(x_i), \tag{2.36}$$

where $x_i \in [a, b]$ are a set of grid points in the interval of interest and w_i are the corresponding weights.

The function, $f(x)$, can be approximated with Eq. (2.29) within the interval $[a, b]$. We choose a uniform grid of N points, that is, $(x_1, x_1 + h, x_1 + 2h, \ldots, x_N - h, x_N)$, with spacing $h = (b - a)/(N - 1)$, and $a = x_1$ and $b = x_N$. With the linear interpolation given by Eq. (2.29), the integral $\int_{x_1}^{x_2} f(x)dx$ is the sum of the two linear interpolating polynomials, Eq. (2.29), over the interval of width h, and

$$\begin{aligned}
\int_{x_1}^{x_1+h} \ell_1(x)dx &= \int_{x_1}^{x_1+h} \frac{x - x_2}{x_1 - x_2}dx = \frac{h}{2}, \\
\int_{x_1}^{x_1+h} \ell_2(x)dx &= \int_{x_1}^{x_1+h} \frac{x - x_1}{x_2 - x_1}dx = \frac{h}{2}.
\end{aligned} \tag{2.37}$$

Thus the weights are the same for all intervals of the same length between adjacent points of width h in the interval $[x_1, x_2]$ as shown in Table 2.10 for $m = 1$. We apply this result to each interval, sum over the N intervals and get the trapezoidal rule,

$$I_N = \frac{1}{h}\left[\frac{f_1}{2} + \sum_{i=2}^{N-1} f_i + \frac{f_N}{2}\right]. \tag{2.38}$$

The coefficient of the interior points is unity as there are two contributions to f_i from adjacent intervals whereas there is only one contribution from each of the interval boundaries.

If we choose a quadratic fit to $f(x)$ with three successive grid points (x_1, x_2, x_3) we then have to evaluate the integrals of the three quadratic interpolating polynomials

Table 2.10 Newton Cotes coefficients and the Lagrange interpolation of order m

m	Integration rule	Formula	Error
1	Trapezoidal	$\frac{h}{2}[f_1 + f_2]$	$\frac{h^3}{12} f^{(2)}(\xi)$
2	Simpson's	$\frac{h}{3}[f_1 + 4f_2 + f_3]$	$\frac{h^5}{90} f^{(4)}(\xi)$
3	Simpson's 3/8	$\frac{3h}{8}[f_1 + 3f_2 + 3f_3 + f_4]$	$\frac{3h^5}{80} f^{(4)}(\xi)$
4	Milne rule	$\frac{2}{45}[7f_1 + 32f_2 + 12f_3 + 32f_47 + f_5]$	$\frac{8h^7}{945} f^{(6)}(\xi)$

in Eq. (2.30) over an interval of length $2h$, that is

$$\begin{aligned}
\int_{x_1}^{x_1+2h} \ell_1(x)dx &= \int_{x_1}^{x_1+2h} \frac{(x-x_3)(x-x_2)}{(x_1-x_3)(x_1-x_2)}dx = \frac{h}{3}, \\
\int_{x_1}^{x_1+2h} \ell_2(x)dx &= \int_{x_1}^{x_1+2h} \frac{(x-x_3)(x-x_1)}{(x_3-x_2)(x_1-x_2)}dx = \frac{4h}{3}, \\
\int_{x_1}^{x_1+2h} \ell_3(x)dx &= \int_{x_1}^{x_1+2h} \frac{(x-x_1)(x-x_2)}{(x_3-x_1)(x_3-x_2)}dx = \frac{h}{3}.
\end{aligned} \tag{2.39}$$

The integrals above are straightforward and provide the weights for each interval. The integral over the entire interval $[a, b]$ is evaluated by adding the contributions from consecutive intervals of width $2h$ and the result is the Simpson's[15] integration rule

$$I_N = \frac{h}{3}\left[f_1 + 4f_2 + 2f_3 + \cdots + 4f_{N-2} + 2f_{N-1} + f_N\right]. \tag{2.40}$$

The factor 2 arises because of the contributions from the 3rd point of one interval and the 1st point from the following interval, except for the interval boundaries, and N is odd. These integration rules for orders 1 and 2 are summarized in Table 2.10 together with two other higher order methods discussed in the next section.

2.3.3 Newton-Cotes Integration Rules; Error Analysis

The approximation of integrals based on interpolating polynomials of order 3 and 4 yield the the Simpson's 3/8 rule and the Milne rule. These higher order integrations are collectively referred to as the Newton-Cotes integration rules. The integrals required are similar to Eqs. (2.37) and (2.39) and can be done with a hand calculation. The procedure is straightforward but the integrals required involve some algebra and a short MAPLE code can be written to evaluate the integrals exactly. For interpolating polynomials of degree $n = 3$ and 4, we obtain the Simpson's 3/8 and Milne rules as shown in Table 2.10.

Error estimates for these integration algorithms can be determined. We consider an elementary interval of m grid points with $x \in [x_1, x_m]$ with uniform spacing h so that $x_i = x_1 + (i-1)h$, $i = 1, 2, \ldots m$. We seek the remainder, $R(x)$, in the Lagrange interpolation with m grid points and write Eq. (2.31) as

$$f(x) = f_m(x) + R(x). \tag{2.41}$$

[15] Thomas Simpson (1710–1761) was a British mathematician and his name is associated with this approximation of integrals. He was not the first to develop this algorithm.

The function $F(z)$, with z different from x, is defined as

$$F(z) = [f(z) - f_m(z)] - [f(x) - f_m(x)]\frac{P_m(z)}{P_m(x)}. \tag{2.42}$$

where $P_m(x)$ is given by Eq. (2.34) with $m = N$. Since the Lagrange interpolation is exact at the grid points, $R(x_i) = 0$ and the roots of $F(z)$ are $z = x$ and $z = x_i$, and thus $F(z)$ has $m + 1$ roots. If we differentiate $F(z)$ m times with respect to z and set $f^{(m)}(z) \equiv d^m f(z)/dz^m$, we have that,

$$F^{(m)}(z) = [f^{(m)}(z) - f_m^{(m)}(z)] - [f(x) - f_m(x)]\frac{P_m^{(m)}(z)}{P_m(x)}, \tag{2.43}$$

where $f_m^{(m)}(z) = 0$ and $P_m^{(m)}(z) = m!$. Thus, $F^{(m)}(z)$ has at least one root at $z = \xi$ in the interval $[x_1, x_m]$. With these results in Eq. (2.43) and $R(x_i) = 0$, we have that

$$R(x) = \frac{f^{(m)}(\xi)}{m!}P_m(x), \quad x_1 < \xi < x_m. \tag{2.44}$$

The main value of this result is that the error depends on $f^{(m)}(x)$ and the integration rules are exact for functions of degree $m - 1$ or less. The error in the integration algorithms is therefore

$$\epsilon_m = \frac{f^{(m)}(\xi)}{m!}\int_{x_1}^{x_m} P_m(x)dx. \tag{2.45}$$

We make the change of variable $y = [x - (m - 1)h/2]$ so that the integration is over the symmetric interval $[-mh/2, mh/2]$. With this change of variable, the lower order polynomials are given by

$$P_m(y) = \begin{cases} (y^2 - \frac{h^2}{4}), & m = 2, \\ y(y^2 - h^2), & m = 3, \\ (y^2 - \frac{9h^2}{4})(y^2 - \frac{h^2}{4}), & m = 4, \\ y(y^2 - h^2)(y^2 - 4h^2), & m = 5, \end{cases} \tag{2.46}$$

and are either even or odd, that is, $P_m(-y) = (-1)^m P_m(y)$ and the roots are symmetric about the midpoint of the interval. The integrals in Eq. (2.45) are elementary and are explicitly given by

$$\epsilon_m = \frac{f^{(m)}(\xi)}{m!}\int_{-mh/2}^{mh/2} P_m(y)dy = \begin{cases} \frac{h^2}{12}f^{(2)}, & m = 2, \\ 0, & m = 3, \\ \frac{3h^5}{80}f^{(4)}, & m = 4, \\ 0, & m = 5. \end{cases} \tag{2.47}$$

A short MAPLE code can be used to perform the elementary integrations and obtain the error estimates as given by Eq. (2.47) for arbitrary m. The surprising result is that for Simpson's rule with $m = 3$ (and for all odd m) the integrals of $P_m(y)$ are zero.

This development gives the error estimates for m even and a separate treatment is required for m odd. We calculate the error estimate for Simpson's rule with $m = 3$ by first writing the algorithm,

$$\int_{x_1}^{x_1+2h} f(x)dx \approx \frac{h}{3}\left[f(x_1) + 4f(x_1+h) + f(x_1+2h)\right]. \tag{2.48}$$

With the expansion of the last two terms on the right hand side with a Taylor series, we get

$$\int_{x_1}^{x_1+2h} f(x)dx \approx 2hf(x_1) + 2h^2 f^{'}(x_1) + \frac{4}{3}h^3 f^{''}(x_1) + \frac{2}{3}h^4 f^{(3)}(x_1) + \frac{100}{3\times 5!}h^5 f^{(4)}(x_1) + \cdots \tag{2.49}$$

With the definition

$$G(x) = \int_{x_1}^{x} f(t)dt, \tag{2.50}$$

where $G^{'}(x) = f(x)$, the expansion of $G(x_1 + 2h)$ gives

$$G(x_1+2h) \approx 2hf(x_1) + 2h^2 f^{'}(x_1) + \frac{4}{3}h^3 f^{''}(x_1) + \frac{2}{3}h^4 f^{(3)}(x_1) + \frac{32}{5!}h^5 f^{(4)}(x_1) + \cdots \tag{2.51}$$

Equations (2.49) and (2.51) yield the result

$$\epsilon_2 = \left[\frac{100}{3\times 5!} - \frac{32}{5!}\right]h^5 f^{(4)}(x_1) = -\frac{1}{90h^5} f^{(4)}(x_1). \tag{2.52}$$

The procedure for developing higher order quadrature rules should be clear. The algebra involved to evaluate the elementary integrations can be tedious. We summarize the results in Table 2.10. Also provided in the table are the error estimates which depend on the interval width h and a bound on the mth order derivative evaluated at some point ξ within the interval. The result that the error for the trapezoidal rule depends on $f^{(2)}$ is reasonable, showing that this is exact for linear functions. However, it is surprising that the error for Simpson's rule based on a quadratic approxima-

tion shows that the error depends on $f^{(4)}$ and that it is exact for functions of order 3 as is the next algorithm for Simpson's 3/8 rule. The use of the results in the table requires the analytic evaluation of a higher order derivative. The value of ξ in the interval is not specified. The main interest in these results is that the errors depend on $f^{(m)}$, so that the different integration rules are exact for functions of degree $m-1$ or less.

2.3.4 Gaussian Quadrature

The Lagrange interpolation is the basis for a very efficient algorithm for the evaluation of integrals as developed by Gauss (1814). The main difference with the Newton-Cotes algorithms is that the grid points used are not uniform and the quadrature can be exact for higher order polynomials. We consider the nodes, x_i, as the roots of the polynomial $P_N(x)$ of degree N from the set $\{P_n(x)\}$ orthogonal with respect to weight function $w(x)$.

We consider a second polynomial, $q(x)$, of degree equal to or less than $2N-1$ and the interpolant,

$$q_N(x) = \sum_{i=1}^{N} \ell_i(x) q(x_i), \tag{2.53}$$

where $\ell_i(x)$ is given by Eq. (2.35) and satisfies the Cardinality condition, Eq. (2.33). The difference between the polynomial $q(x)$ and the interpolant $q_N(x)$ is

$$E(x) = q(x) - q_N(x), \tag{2.54}$$

where $E(x_i) = 0$ by construction. Since $E(x)$ is a polynomial of degree less than or equal to $2N-1$, we define

$$E(x) = d_{N-1}(x) P_N(x), \tag{2.55}$$

where $d_{N-1}(x)$ is a polynomial of degree $N-1$. Thus, the integral of the original polynomial, $q(x) = E(x) + q_N(x)$, weighted by $w(x)$ is

$$\int_a^b w(x) q(x) dx = \int_a^b w(x) q_N(x) dx + \int_a^b w(x) d_{N-1}(x) P_N(x) dx. \tag{2.56}$$

The second integral on the right vanishes owing to the orthogonality of $P_N(x)$ with the polynomial $d_{N-1}(x)$ of degree $N-1$ and with $E(x_i) = 0$, the integral is

$$\int_a^b w(x) q(x) dx = \sum_{i=1}^{N} q(x_i) \int_a^b w(x) \ell_i(x) dx. \tag{2.57}$$

This last result can be written as

$$\int_a^b w(x)q(x)dx = \sum_{i=1}^{N} w_i q(x_i), \tag{2.58}$$

where the w_i are the quadrature weights defined by

$$\boxed{w_i = \int_a^b w(x)\ell_i(x)dx.} \tag{2.59}$$

The error, $E(x)$, in the Lagrange interpolation for a polynomial of degree no greater than $2N-1$ is orthogonal to $P_N(x)$ that defines the nodes x_i. Therefore, this Gaussian quadrature based on N nodes is exact for polynomials of degree no greater than $2N-1$. We now require an explicit expression for the weights, w_i, which is developed in the next section.

2.3.5 The Christoffel-Darboux Relation and Quadrature Weights

We need an important result, the Christoffel[16]-Darboux[17] relation, so as to evaluate the quadrature weights defined by Eq. (2.59) in a more explicit form. The Christoffel-Darboux relation also serves to demonstrate several other relations discussed later. The three term recurrence relation is rewritten as a function of x and again versus y

$$\begin{aligned} xP_k(x) &= \sqrt{\beta_{k+1}}P_{k+1}(x) + \alpha_k P_k(x) + \sqrt{\beta_k}P_{k-1}(x), \\ yP_k(y) &= \sqrt{\beta_{k+1}}P_{k+1}(y) + \alpha_k P_k(y) + \sqrt{\beta_k}P_{k-1}(y). \end{aligned} \tag{2.60}$$

Multiply the first by $P_k(y)$ and the second by $P_k(x)$ and then subtract the two equations. The terms in α_k cancel and

$$\begin{aligned} (x-y)P_k(y)P_k(x) = &\sqrt{\beta_{k+1}}\left[P_k(y)P_{k+1}(x) - P_k(x)P_{k+1}(y)\right] \\ &+ \sqrt{\beta_k}\left[P_k(y)P_{k-1}(x) - P_k(x)P_{k-1}(y)\right]. \end{aligned} \tag{2.61}$$

---

[16] Elwin Bruno Christoffel (1829–1900) was a German mathematician and physicist who made important advances in differential geometry of surfaces, conformal maps, potential theory and mathematical physics.

[17] Jean-Gaston Darboux (1842–1917) was a French mathematician who worked primarily in geometry, orthogonal surfaces and mathematical analysis.

If both sides are summed from $k = 0$ to $k = n$, the two terms in square brackets on the right hand side cancel except for the term with $k = N$, and the result is the Christoffel-Darboux relation

$$\sum_{k=0}^{N} P_k(y)P_k(x) = \frac{\sqrt{\beta_{N+1}}}{x-y}[P_N(y)P_{N+1}(x) - P_N(x)P_{N+1}(y)]. \tag{2.62}$$

We use Eq. (2.62) to derive an expression for the weights, w_i, in the quadrature evaluation of integrals. If $y = x_i$ in Eq. (2.62) where x_i are the quadrature nodes, that is $P_N(x_i) = 0$, the sum on the left hand side terminates at $k = N - 1$. We then multiply this equation by $w(x)P_0(x)$ and integrate over the interval. This procedure projects out the term in $k = 0$ on the left hand side which is unity and

$$\sqrt{\beta_{N+1}}P_{N+1}(x_i)\int_a^b \frac{w(x)P_N(x)}{x-x_i}dx = -1. \tag{2.63}$$

If the definition of the interpolating polynomial, Eq. (2.35), is used to express

$$P_N(x)/(x-x_i) = \ell_i(x)P'_N(x_i),$$

then Eq. (2.63) can be rewritten as

$$\sqrt{\beta_{N+1}}P_{N+1}(x_i)P'_N(x_i)\int_a^b w(x)\ell_i(x)dx = -1, \tag{2.64}$$

and with Eq. (2.59) we have the final desired result

$$\boxed{w_i = -\frac{1}{\sqrt{\beta_{N+1}}P_{N+1}(x_i)P'_N(x_i)}.} \tag{2.65}$$

This a very useful result for later discussions. If we set $x = y$ and use l'Hopital's rule in Eq. (2.62), we get

$$\sum_{k=0}^{N} P_k^2(x) = \sqrt{\beta_{N+1}}[P_N(x)P'_{N+1}(x) - P'_N(x)P_{N+1}(x)]. \tag{2.66}$$

If we now combine Eq. (2.66) with $x = x_i$ and Eq. (2.65), the weights are given by

$$w_i = \frac{1}{\sum_{k=0}^{N-1} P_k(x_i)^2}. \tag{2.67}$$

The numerical evaluation of the quadrature points, x_i, and weights, w_i, is presented in the next section.

2.3.6 The Gautschi-Stieltjes Procedure, the Jacobi Matrix

The Gautchi-Stieltjes method was suggested by Golub and Welsch (1969) and developed further by Gautschi in a series of papers (Gautschi 1985, 1996, 2004, 2007) and is applicable to almost any weight function. The development here parallels the discussions in other references (Davis and Rabinowitz 1975; Gautschi 1981, 1994; Kythe and Schaferkotter 2004; Canuto et al. 2006; Gil et al. 2007; Kopriva 2009). The method is stable, efficient and based on the recurrence relation for the monic polynomials defined by Eq. (2.1). The recurrence coefficient α_n given by Eq. (2.9) is rewritten explicitly as

$$\alpha_n = \frac{\int_a^b w(x) x Q_n^2(x) dx}{\int_a^b w(x) Q_n^2(x) dx}, \tag{2.68}$$

and similarly the coefficient β_n is,

$$\beta_n = \frac{\int_a^b w(x) Q_n^2(x) dx}{\int_a^b w(x) Q_{n-1}^2(x) dx} = \frac{\gamma_n}{\gamma_{n-1}}. \tag{2.69}$$

The calculation begins with $Q_{-1}(x) = 0$ and $Q_0(x) = 1$ from which α_0 is calculated from Eq. (2.9). Equation (2.1) gives $Q_1(x)$ and α_1 and β_1 are evaluated with Eqs. (2.68) and (2.69). The success of the method relies on the accurate evaluation of the integrals in Eqs. (2.68) and (2.69) with very high precision. This is accomplished with a higher order multidomain quadrature procedure and in each domain the Fejér quadrature discussed in Sect. 2.4.10 is used.

The Jacobi matrix defined by Eq. (2.71) below plays a very important role in the theory of orthogonal polynomials and it appears in almost all the papers on this subject. It can be introduced in a variety of different ways. We here consider the matrix representation of the multiplicative coordinate operator, x, as discussed in quantum mechanics textbooks. This is given by the matrix elements $\langle P_n|x|P_m\rangle$ in some basis set $\{P_n(x)\}$. If we employ the three term recursion relation, Eq. (2.14), it is easy to see that

$$\langle P_n|x|P_m\rangle = \sqrt{\beta_{m+1}}\delta_{n,m+1} + \alpha_m\delta_{n,m} + \sqrt{\beta_m}\delta_{n,m-1}. \tag{2.70}$$

These are the elements of the tridiagonal Jacobi matrix which is given by,

$$\mathbf{J} = \begin{pmatrix} \alpha_0 & \sqrt{\beta_1} & 0 & 0 & 0 & \cdots & 0 \\ \sqrt{\beta_1} & \alpha_1 & \sqrt{\beta_2} & 0 & 0 & \cdots & 0 \\ 0 & \sqrt{\beta_2} & \alpha_2 & \sqrt{\beta_3} & 0 & \cdots & 0 \\ 0 & 0 & \sqrt{\beta_3} & \alpha_3 & \sqrt{\beta_4} & \cdots & 0 \\ \vdots & \vdots & \vdots & \vdots & \vdots & \cdots & \vdots \\ 0 & 0 & 0 & 0 & 0 & \sqrt{\beta_N} & \alpha_N \end{pmatrix}. \tag{2.71}$$

We now show how the quadrature points and weights can be determined with the numerical diagonalization of **J** as discussed by Davis and Rabinowitz (1975). If we define the vectors

$$\mathbf{R}(x) = [P_0(x), P_1(x), \ldots P_{N-1}(x)]^t \quad \text{and} \quad \mathbf{e} = [0, 0, \ldots, 1]^{\mathrm{t}}, \tag{2.72}$$

where t denotes the transpose, the three term recurrence relation, Eq. (2.14), can be written in vector form as

$$x\mathbf{R}(x) = \mathbf{J} \cdot \mathbf{R}(x) + \alpha_N P_N(x)\mathbf{e}. \tag{2.73}$$

With the definition of the quadrature points as the N roots, x_i, given by $P_N(x_i) = 0$, we have that

$$\mathbf{J} \cdot \mathbf{R}(x_i) = x_i \mathbf{R}(x_i), \tag{2.74}$$

and the quadrature points are the eigenvalues of the Jacobi matrix.

As for the weights, we first denote

$$\mathbf{U}(x_i) = \sqrt{w_i}\mathbf{R}(x_i) = [u_{0i}, u_{1i}, \ldots, u_{(N-1)i}]^t,$$

as the normalized eigenvector of **J** where the first component of the ith eigenvector is u_{0i}. With Eq. (2.65), the result

$$w_i \sum_{k=0}^{N-1} P_k^2(x_i) = \sqrt{w_i}\mathbf{R}^t(x_i) \cdot \sqrt{w_i}\mathbf{R}(x_i) = 1 \tag{2.75}$$

represents the normalization of **U**. If we focus on the first component of the ith eigenvector, u_{0i}, for which $P_0(x) = 1/\sqrt{\gamma_0}$ and $\mu_0 = \gamma_0$, we have the result

$$w_i = \mu_0 u_{0i}^2. \tag{2.76}$$

MATLAB codes to evaluate the quadrature points, x_i, and weights, w_i, for the classical polynomials are very compact and fast (Gautschi 1985, 1994; Weideman and Reddy 2000). An alternate efficient calculation of the quadrature weights is given by Eq. (2.67). In the next section, we summarize the properties of the classical orthogonal polynomials.

2.4 The Classical Polynomials; Recurrence Coefficients and Quadratures

The numerous mathematical properties and relationships for the classical polynomials are readily available in standard textbooks and tables such as the Handbook of Mathematical Functions (Abramowitz and Stegun 1964). We present some properties of the classical polynomials used in other sections of the book. In particular, we are interested in the recurrence coefficients which define the Jacobi matrix, Eq. (2.71).

Table 2.11 Recurrence coefficients for classical polynomials

Polynomial	$w(x)$	Interval	α_n	β_n
Legendre	1	$[-1, 1]$	0	$\frac{n^2}{4n^2-1}$
Associated Legendre	1	$[-1, 1]$	0	–
Hermite	e^{-x^2}	$(-\infty, \infty)$	0	$\frac{n}{2}$
Laguerre	e^{-x}	$[0, \infty)$	$2n+1$	n^2
Associated Laguerre	$x^\alpha e^{-x}$	$[0, \infty)$	$2n+\alpha+1$	$n(n+\alpha)$
Gegenbauer	$(1-x^2)^{\lambda-\frac{1}{2}}$	$[-1, 1]$	0	$\frac{n(n+2\lambda-1)}{4(n+\lambda)(n+\lambda-1)}$
Jacobi	$(1-x)^\alpha(1+x)^\beta$	$[-1, 1]$	Eq. (2.77)	Eq. (2.78)
Chebyshev	$\sqrt{1-x^2}$	$[-1, 1]$	0	$\frac{1}{4}$

The diagonalization of the Jacobi matrix yields the quadrature points as the eigenvalues and the quadrature weights in terms of the first component of the ith eigenvector as given by Eq. (2.76).

The recurrence coefficients for the classical polynomials are provided in Table 2.11. It is important to note that these recurrence coefficients are derived from the recurrence relations for the classical polynomials normalized to unity in accordance with Eq. (2.14). The parameters α and β in the weight functions for the associated Legendre and Laguerre polynomials as well as for the Jacobi polynomials should not be confused with the α_n and β_n recurrence coefficients.

The recurrence coefficients for the Jacobi polynomials are too long to fit in the table and are given by,

$$\alpha_n = \frac{\alpha^2 - \beta^2}{(2n+\alpha+\beta+2)(2n+\alpha+\beta)}, \tag{2.77}$$

$$\beta_n = \frac{2}{(2n+\alpha+b)}\sqrt{\frac{n(n+\alpha)(n+\beta)(n+\alpha+\beta)}{(2n+\alpha+\beta+1)(2n+\alpha+\beta-1)}}, \tag{2.78}$$

In the sections that follow, we list some of the lower order polynomials for each of the commonly used classical polynomials, the recurrence relations and the Sturm-Liouville equation, which can be written as a Schrödinger equation discussed in Chap. 6, Sect. 6.7.

2.4.1 Legendre Polynomials

The Legendre polynomials satisfy the orthogonality condition

$$\int_{-1}^{1} P_\ell(x) P_{\ell'} dx = \frac{2}{2\ell+1}\delta_{\ell\ell'}. \tag{2.79}$$

The first few members of the set are

$$P_0(x) = 1, \quad P_1(x) = x, \quad P_2(x) = \frac{1}{2}(3x^2 - 1), \quad P_3(x) = \frac{1}{2}(5x^3 - 3x),$$

$$P_4(x) = \frac{1}{8}(35x^4 - 30x^2 + 3), \quad P_5(x) = \frac{1}{8}(63x^5 - 70x^3 + 15x), \tag{2.80}$$

and the parity is even for ℓ even and odd for ℓ odd. The recurrence relation for the Legendre polynomials normalized as in Eq. (2.79) is

$$xP_\ell(x) = \frac{1}{2\ell + 1}\Big[(\ell + 1)P_{\ell+1}(x) + \ell P_{\ell-1}(x)\Big]. \tag{2.81}$$

This recurrence relation is often used to calculate the matrix elements of operators in kinetic theory and quantum mechanics. The Gauss-Legendre quadrature points and weights associated with these polynomials are easily evaluated with the diagonalization of the Jacobi matrix defined in Eq. (2.71) and the recurrence coefficients are in Table 2.11.

The Legendre polynomials satisfy a Sturm–Liouville eigenvalue problem of the form

$$\frac{d}{dx}\Big[(1 - x^2)\frac{dP_\ell}{dx}\Big] = -\ell(\ell + 1)P_\ell, \tag{2.82}$$

which is analogous to the Schrödinger equation for the rotational states of a diatomic nonvibrating molecule referred to as a rigid rotor and ℓ is the angular momentum quantum number.

The Legendre polynomials are often employed in kinetic theory to express the departure of the velocity distribution function, $f(\mathbf{v})$, from spherical symmetry, that is,

$$f(\mathbf{v}) = \sum_{\ell=0}^{\infty} f_\ell(v)P_\ell(\mu), \tag{2.83}$$

where the argument of the Legendre polynomials is $\mu = \cos\theta$ and θ gives the orientation of $\mathbf{v}$ relative to the polar axis. This representation arises in the kinetic theory of gases to describe the drift of charged particles (electrons or ions) through a background gas under the influence of a spatially homogeneous electrostatic field or to calculate the ion or electron mobility versus the electrostatic field strength (Pitchford and Phelps 1982; McMahon and Shizgal 1985; Mason and McDaniel 1988; Viehland 1994). In space physics, θ is the angle between the particle velocity and the Earth's geomagnetic field and it is referred to as the "pitch angle". Legendre polynomials have been used in climate models (North 1975), image inversion in photoionization (Garcia et al. 2004) and many other applications.

The transport of radiation through some medium such as a planetary atmosphere or interstellar matter is described with the radiative transfer equation discussed in Chap. 5. The intensity of radiation, $I(\tau, \mu)$ depends on direction of propagation as

denoted by $\mu = \cos\theta$ and the position as specified in terms of the optical depth, τ. The radiative intensity is expanded in a series of Legendre polynomials, that is,

$$I(\tau, \mu) = \sum_{\ell=0}^{\infty} C_\ell(\tau) P_\ell(\mu), \tag{2.84}$$

analogous to Eq. (2.83) and this method is referred to as a P_N method in the radiative transfer community. Similar expansions in Legendre polynomials are employed in the relaxation of anisotropic velocity distributions (Shizgal and Blackmore 1983) and in the Milne problem (Lindenfeld and Shizgal 1983).

2.4.2 Half Range Legendre Polynomials

In the field of radiative transfer (Garcia and Siewert 1996; Garcia and Ono 1999), it has often been found advantageous to split the interval $[-1,\ 1]$ into two subintervals, namely $[-1, 0]$ and $[0, 1]$. This is done to better fit boundary conditions at $\mu = 0$. Thus, the half-range (hr) Legendre polynomials are defined orthogonal on $[0, 1]$ and are easily derived from the full range polynomials. With the transformation $y = (x + 1)/2$, we get the half-range Legendre polynomials

$$\begin{aligned}
P_0^{(hr)}(y) &= 1,\\
P_1^{(hr)}(y) &= 2y - 1,\\
P_2^{(hr)}(y) &= 6y^2 - 6y + 1,\\
P_3^{(hr)}(y) &= 20y^3 - 30y^2 + 12y - 1),\\
P_4^{(hr)}(y) &= 70y^4 - 140y^3 + 90y^2 - 20y + 1,\\
P_5^{(hr)}(y) &= 252y^5 - 630y^4 + 560y^3 - 210y^2 + 30y - 1,
\end{aligned} \tag{2.85}$$

orthogonal according to

$$\int_0^1 P_k^{(hr)}(y) P_\ell^{(hr)}(y) dy = \frac{1}{2\ell + 1}\delta_{k\ell}. \tag{2.86}$$

The quadrature points are derived from the quadrature points for the full range Legendre polynomials, that is, $\mu_i^{(hr)} = (\mu_i + 1)/2$ and the weights are $w_i^{(hr)} = w_i/2$.

A collocation method in radiative transfer theory (Thomas and Stamnes 2002) based on quadrature points is referred to as a "discrete ordinate method" or the S_N method. It appears that this notation is derived from "segmentation" (Carlson 1953) and discussed by Lathrop (1992). If the method is based on the half-range Legendre weights and points it is often called a "double Gauss method" (Sykes 1951; Garcia and Siewert 1996; Garcia and Ono 1999; Thomas and Stamnes 2002).

This linear transformation from full range to half range polynomials can be done for the Legendre polynomials owing to the unit weight function, $w(x) = 1$. This is not the case for half range Hermite polynomials which are the associated Maxwell polynomials with $p = 0$. There is no relationship between the half range Rys polynomials discussed in Sect. 2.2.2 or the half range Chebyshev polynomials employed by Garcia and Ono (1999) in terms of the corresponding full range polynomials.

2.4.3 Associated Legendre Polynomials

It is appropriate to also introduce the associated Legendre polynomials that arise in particular in the solution to the Schrödinger equation for the hydrogen atom, Sect. 2.4.6, and in many other applications. The associated Legendre polynomials $P_\ell^m(x)$ satisfy a Sturm-Liouville problem similar to Eq. (2.82) given by

$$\frac{d}{dx}\Big[(1-x^2)\frac{dP_\ell^m}{dx}\Big] - \frac{m^2}{1-x^2}P_\ell^m = -\ell(\ell+1)P_\ell^m, \tag{2.87}$$

where m is the "magnetic" quantum number. These are the eigenfunctions of the square of the angular momentum operator, L^2, with eigenvalues $\ell(\ell+1)$ and are orthogonal according to,

$$\int_{-1}^{1} P_\ell^m(x)P_{\ell'}^m(x)dx = \frac{2(\ell+m)!}{(2\ell+1)(\ell-m)!}\delta_{\ell,\ell'}. \tag{2.88}$$

They satisfy the recurrence relation given by,

$$xP_\ell^m(x) = \frac{1}{2\ell+1}\Big[(\ell-m+1)P_{\ell+1}^m(x) + (\ell+m)P_{\ell-1}^m(x)\Big]. \tag{2.89}$$

For $m = 0$, these reduce to the corresponding relations for the Legendre polynomials.

2.4.4 The Spherical Harmonics

The spherical harmonics are basis functions in the spherical polar angles (θ, ϕ) that are constructed as a direct product of the associated Legendre polynomials and the Fourier functions $e^{\pm im\phi}$. The Fourier functions are the eigenfunctions of the z-component of the angular momentum operator, L_z, as discussed in Sect. 2.4.6 and defined by the eigenvalue problem,

$$\frac{d^2\Phi_m(\phi)}{d\phi^2} = -m^2\Phi(\phi). \tag{2.90}$$

where $\Phi(\phi + 2\pi) = \Phi(\phi)$. We define the spherical harmonic functions as

$$Y_{\ell m}(\theta, \phi) = \sqrt{(2\ell + 1)\frac{(\ell - m)!}{(\ell + m)!}} P_\ell^m(\cos\theta) e^{im\phi}, \tag{2.91}$$

which are orthonormal,

$$\int_{\phi=0}^{2\pi} \int_{\theta=0}^{\pi} Y^*_{\ell,m}(\theta, \phi) Y_{\ell',m'}(\theta, \phi) \sin\theta d\theta d\phi = \delta_{\ell,\ell'}\delta_{m,m'}, \tag{2.92}$$

and the asterisk denotes the complex conjugate. The integrations over θ and ϕ are often written in terms of the spherical solid angle Ω where $d\Omega = \sin\theta d\theta d\phi$. The spherical harmonic functions are the simultaneous eigenfunctions of the operators, L^2 and L_z which commute, as discussed in Sect. 2.4.6.

In molecular quantum mechanics, spherical integrals of the form,

$$I_{\mathbf{r}} = \int R(\mathbf{r}) d\mathbf{r}, \tag{2.93}$$

are required. These can be separated as a radial integral over r and an angular integral over (θ, ϕ), that is

$$\begin{aligned} I_{\mathbf{r}} &= \int_0^\infty R(r) r^2 dr, \\ R(r) &= \int_{\phi=0}^{2\pi} \int_{\theta=0}^{\pi} f(r, \theta, \phi) \sin\theta d\theta d\phi. \end{aligned} \tag{2.94}$$

We discuss and compare in Chap. 3 the various quadratures that have been used for radial integrals over r (Gill and Chien 2003; El-Sherbiny and Poirier 2004; Chien and Gill 2006) and the angular integral over (θ, ϕ). The angular integrals are often evaluated with Lebedev cubatures (Lebedev 1977; Haxton 2007) There is considerable interest to develop efficient quadrature procedures for such integrals.

2.4.5 Associated Laguerre and Sonine Polynomials

The associated Laguerre polynomials denoted by $L_n^{(\alpha)}(y)$ are defined on $y \in [0, \infty)$ orthogonal with respect to the weight function $w(y) = y^\alpha e^{-y}$, that is,

$$\int_0^\infty y^\alpha e^{-y} L_n^{(\alpha)}(y) L_m^{(\alpha)}(y) dy = \frac{\Gamma(n + \alpha + 1)}{n!}, \tag{2.95}$$

The first members of this set are,

$$
\begin{aligned}
L_0^{(\alpha)}(y) &= 1, \qquad L_1^{(\alpha)}(y) = \alpha - y + 1, \\
L_2^{(\alpha)}(y) &= \frac{y^2}{2} - (\alpha+2)y + \frac{(\alpha+1)(\alpha+2)}{2}, \\
L_3^{(\alpha)}(y) &= -\frac{y^3}{6} + \frac{(\alpha+3)y^2}{2} + \frac{(\alpha+2)(\alpha+3)y}{2} \\
&\quad + \frac{(\alpha+1)(\alpha+2)(\alpha+3)}{6},
\end{aligned}
\tag{2.96}
$$

and they satisfy the recurrence relation

$$
L_n^{(\alpha)}(y) = \left(2 + \frac{\alpha - y - 1}{n}\right) L_{n-1}^{(\alpha)}(y) - \left(1 + \frac{\alpha - 1}{n}\right) L_{n-2}^{(\alpha)}(y). \tag{2.97}
$$

These polynomials are related to the eigenfunctions of the radial Schrödinger equation for the hydrogen atom. They are the eigenfunctions of the integral collision operator of the Boltzmann equation for the Maxwell molecule collision model discussed in Chap. 5. The Maxwell molecule model corresponds to a repulsive particle interaction potential that varies as r^{-4} where r is the particle separation (Chapman and Cowling 1970). The Laguerre polynomials are also the eigenfunctions of a hard sphere Fokker-Planck operator in the Rayleigh limit (Andersen and Shuler 1964), discussed in Chap. 6, Sect. 6.1.4.

The MATLAB code for the calculation of the associated Gauss-Laguerre quadrature points and weights with the diagonalization of the Jacobi matrix Eq. (2.71) defined in terms of the recurrence coefficients in Table 2.11 is provided in Listing 2.2. The MATLAB code sets up and diagonalizes the symmetric Jacobi matrix, $\mathbf{J}$, in terms of $\alpha_n = 2n + \alpha + 1$ on the diagonal and $\beta_n = n(n+\alpha)$ on the upper and lower off-diagonals.

Listing 2.2 MATLAB code lag_ptswts.m calculates the associated Laguerre quadrature points and weights

```
function [pt,wt]=lagptwt2(n,alf)
format long e
xn=[0:1:n-1];
a=2*xn+alf+1; rtb=sqrt(xn.*(xn+alf)); rtb(1)=[];
J=diag(rtb,-1)+diag(a)+diag(rtb,1);
[f,lambda]=eig(J); pt=diag(lambda);
wt=gamma(alf+1)*f(1,:).^2;
ptwt=[pt,wt']
```

The numerical results for the Laguerre quadrature points and weights obtained with this code agree to 16 significant figures with the tabulated values in Table 25.9 by Abramowitz and Stegun (1964). There is also agreement with the results reported by Concus et al. (1963) as well as the results obtained with the code mp.GaussRule.m

provided at http://www.advanpix.com/. The calculation of 100 weights and points on a PC with an Intel i5 CPU @ 2.50 GHz requires approximately 0.01 s.

In kinetic theory (Chapman and Cowling 1970; Kremer 2010), the basis set that is often used are the Sonine polynomials which are very similar to the Laguerre polynomials. The independent variable is the particle speed, $v = |\mathbf{v}|$, where $\mathbf{v}$ is the velocity of a particle. A dimensionless reduced speed is defined, that is, $x = v\sqrt{m/2k_BT_b}$ where k_B is the Boltzmann constant and T_b is the temperature of the gas. The associated Sonine polynomials are written as $S_\alpha^{(n)}(x^2)$. The Sonine polynomials for $\alpha = 1/2$ occur frequently (Shizgal and Karplus 1970; Shizgal and Dridi 2010) and are orthogonal as given by

$$\int_0^\infty x^2 e^{-x^2} S^{(n)}(x^2) S^{(m)}(x^2) dx = \frac{\Gamma(n+3/2)}{2n!}\delta_{nm}. \tag{2.98}$$

where α is not shown explicitly. We use this notation in Chap. 5. Owing to the similarity with the Laguerre polynomials, the Sonine polynomials are referred to as the Sonine-Laguerre polynomials.

2.4.6 Quantum Mechanics of the Hydrogen Atom

We consider the quantum mechanical description of the discrete energy states of the hydrogen atom or other one electron ion. This is a two body problem involving an electron interacting with a positively charged nucleus where their relative position is given by the vector $\mathbf{r}$ with spherical polar coordinates r, θ, ϕ. The mathematical problem involves the calculation of the eigenfunctions and eigenvalues of the Schrödinger equation. The classical orthogonal polynomials are used for the description of the physics. Detailed discussions can be found in numerous textbooks on quantum mechanics (Karplus and Porter 1970; Szabo and Ostlund 1996; Liboff 2002; Levine 2009; Tsuneda 2014).

The Schrödinger equation for a one electron atomic system is

$$H\psi_{n\ell m}(r,\theta,\phi) = -\frac{\hbar^2}{2m_e}\nabla^2\psi_{n\ell m}(r,\theta,\phi) - \frac{Zq_e^2}{r} = E_n\psi_{n\ell m}(r,\theta,\phi), \tag{2.99}$$

where m_e and q_e are the electron mass and charge, respectively, and $\hbar = h/2\pi$ where h is the Planck constant. The Hamiltonian, H, consists of the kinetic energy operator, $\hbar^2\nabla^2/2m_e$ and the Coulomb potential, Zq_e^2/r, where Zq_e is the nuclear charge. The final result has been anticipated as the eigenfunctions are denoted with the three quantum numbers (n, ℓ, m) and the energy eigenvalues, E_n, depend only on n.

The correspondence between classical and quantum mechanics associates the linear momentum with the operator $p_x = -i\hbar\frac{\partial}{\partial x}$ (and two other operators for p_y and p_z). Thus, the quantum mechanical representation of the classical angular momentum

defined by $\mathbf{L} = \mathbf{r} \times \mathbf{p}$, where $\mathbf{p}$ is the linear momentum is given by,

$$\begin{aligned} Ł_x &= \frac{\hbar}{i}\left(y\frac{\partial}{\partial z} - z\frac{\partial}{\partial y}\right), \\ L_y &= \frac{\hbar}{i}\left(z\frac{\partial}{\partial x} - x\frac{\partial}{\partial z}\right), \\ L_z &= \frac{\hbar}{i}\left(x\frac{\partial}{\partial y} - y\frac{\partial}{\partial x}\right). \end{aligned} \tag{2.100}$$

The square of the total angular momentum operator is

$$\mathbf{L}^2 = L_x^2 + L_y^2 + L_z^2. \tag{2.101}$$

The three mutually commuting operators in H, L_z and L^2, where the commutator of two operators A and B is defined by $[A, B] = AB - BA$ have the same set of eigenfunctions. The analogy in linear algebra is that of two symmetric matrices that commute and can be diagonalized with the same rotation operator; that is, they have the same set of eigenvectors.

With the explicit expression for ∇^2 in spherical polar coordinates, the Schrödinger equation is

$$-\frac{\hbar^2}{2m_e}\left[\frac{1}{r^2}\frac{\partial}{\partial r}[r^2\frac{\partial\psi_{n,\ell,m}}{\partial r}] + \frac{L^2}{2\mu r^2}\psi_{n,\ell,m}\right] - \frac{Zq_e^2}{r}\psi_{n,\ell,m} = E_n\psi_{n,\ell,m}, \tag{2.102}$$

where

$$L^2 = \hbar^2\left[\frac{1}{\sin\theta}\frac{\partial}{\partial\theta}\left(\sin\theta\frac{\partial}{\partial\theta}\right) + \frac{1}{\sin^2\theta}\frac{\partial^2}{\partial\phi^2}\right]. \tag{2.103}$$

In this coordinate system, $L_z = \frac{\hbar}{i}\frac{\partial}{\partial\phi}$. The eigenvalue problem for L^2 leads to a separation of the variables θ and ϕ by analogy with the rigid rotor problem, Eq. (2.82). This is very similar to the situation here except for the added term in $\frac{\partial^2}{\partial\phi^2}$. The eigenfunctions of L^2 are expressed as the product of functions of the form $P_\ell^{(m)}(\theta)\Phi_m(\phi)$.

With this representation,

$$\frac{\sin\theta}{P_\ell^{(m)}}\frac{\partial}{\partial\theta}\left(\sin\theta\frac{\partial P_\ell^{(m)}}{\partial\theta}\right) + \ell(\ell+1)\sin^2\theta = -\frac{1}{\Phi_m}\frac{d^2\Phi_m}{d\phi^2} = -m^2. \tag{2.104}$$

where

$$\Phi(\phi) = Ce^{im\phi}. \tag{2.105}$$

and m is an integer so that $\Phi(\phi + 2\pi) = \Phi(\phi)$.

With the substitution $x = \cos\theta$ we have the differential equation for the associated Legendre polynomials in the form of a Sturm-Liouville eigenvalue problem,

Eq. (2.87). We summarize the results so far in terms of the spherical harmonic functions, $Y_{\ell,m}(\theta, \phi)$, Eq. (2.91), orthonormal as given by Eq. (2.92). We have determined the simultaneous eigenfunctions of the commuting operators H, L^2 and L_z as given by

$$\psi_{n\ell m}(r, \theta, \phi) = R_{n\ell}(r) Y_\ell^{(m)}(\theta, \phi) \tag{2.106}$$

With this form for the eigenfunctions, the differential equation for the radial functions, $R_{n\ell}(r)$, is

$$-\frac{\hbar^2}{2mr^2}\frac{d}{dr}\left(r^2\frac{dR_{n\ell}(r)}{dr}\right) + \frac{\hbar^2\ell(\ell+1)}{2mr^2}R_{n\ell}(r) - \frac{Zq_e^2}{r}R_{n\ell}(r) = E_n R_{n\ell}(r) \tag{2.107}$$

With the change of the independent radial variable

$$\rho = r\sqrt{\frac{8m_e|E_n|}{\hbar^2}}, \tag{2.108}$$

the radial equation is

$$\frac{d^2R_{n\ell}(\rho)}{d\rho^2} + \frac{2}{\rho}\frac{dR_{n\ell}(\rho)}{d\rho} - \left[\frac{\ell(\ell+1)}{\rho^2} + \frac{Zq_e^2}{\hbar\rho}\sqrt{\frac{m_e}{2|E_n|}} - \frac{1}{4}\right]R_{n\ell}(\rho) = 0. \tag{2.109}$$

After some algebra, the solution of this differential equation can be written in terms of the associated Laquerre polynomials, that is,

$$R_{n\ell}(\rho) = \rho^\ell L_{n\ell}(\rho) e^{-\rho/2}. \tag{2.110}$$

The hydrogen atom "orbitals" given by Eqs. (2.106) and (2.110) or variants are used as the basis functions for the solution of the Schrödinger equation for more complicated atoms and molecules.

2.4.7 Hermite Polynomials

The Hermite polynomials, $H_n(x)$, are defined on $x \in (-\infty, \infty)$ orthogonal with respect to weight function $w(x) = e^{-x^2}$, that is,

$$\int_{-\infty}^{\infty} e^{-x^2} H_n(x) H_m(x) dx = \sqrt{\pi} 2^n n! \delta_{nm}. \tag{2.111}$$

The first few members of the set are,

$$\begin{aligned} &H_0(x) = 1, \quad H_1(x) = 2x, \quad H_2(x) = 4x^2 - 2, \\ &H_3(x) = 8x^3 - 12x, \quad H_4(x) = 16x^4 - 48x^2 + 12. \end{aligned} \tag{2.112}$$

and satisfy recurrence relations

$$\begin{aligned} H_{n+1}(x) &= 2xH_n(x) - 2nH_{n-1}(x), \\ H_{n+1}(x) &= 2xH_n(x) - \frac{dH_n(x)}{dx}, \\ \frac{dH_n(x)}{dx} &= 2nH_{n-1}(x). \end{aligned} \tag{2.113}$$

The orthonormal Hermite polynomials, $h_n(x) = e^{-x^2/2}H_n(x)/\sqrt{\sqrt{\pi}2^n n!}$, satisfy the recurrence relation

$$xh_n(x) = \sqrt{\beta_{n+1}}h_{n+1}(x) - \sqrt{\beta_n}h_{n-1}(x), \tag{2.114}$$

with $\beta_n = n/2$. The Gaussian quadrature weights and points are easily evaluated with the MATLAB code provided in Listing 2.3. The quadrature weights and points computed with this MATLAB code agree with the values provided in Table 25.10 of Abramowitz and Stegun (1964).

The Hermite polynomials satisfy the Sturm-Liouville equation,

$$-\frac{d}{dx}\left[e^{-x^2}H_n'(x)\right] = 2ne^{-x^2}H_n(x), \tag{2.115}$$

The eigenfunctions of the Schrödinger equation for an harmonic oscillator with a quadratic potential, $V(x) = x^2$, are the $h_n(x)$ functions that is

$$-\frac{d^2h_n(x)}{dx^2} + x^2h_n(x) = (2n+1)h_n(x), \tag{2.116}$$

with the energy eigenvalue in dimensionless units is equal to $(2n + 1)$.

Listing 2.3 MATLAB code herm_ptswts.m for the Hermite quadrature points and weights

```
function [pt wt]=hermptwt(n)
format long e
xn=[1:1:n]; rtb=sqrt(xn/2); rtb(n)=[];
J=diag(rtb,-1)+diag(rtb,1);
[f,lambda]=eig(J); pt=diag(lambda);
wt=sqrt(pi)*f(1,:).^2;
ptwt=[pt,wt'];
```

The Hermite polynomials are often used as a basis set for quantum mechanical problems, the solution of the Vlasov equation of plasma physics (Schumer and Holloway 1998; Gibelli et al. 2010), the kinetic theory of ion drift in gases (Viehland 1994), in signal processing (Alp and Arikan 2012) and many other applications. A very important use of Hermite polynomials is in the solution of the Boltzmann equation for rarefied gases with the thirteen moment method developed by Grad (1949).

With Eq. (2.65), we have an important result for the quadrature weights for a quadrature of order N used in Chap. 3, that is,

$$w_i = -\sqrt{\frac{2}{N+1}}\frac{\sqrt{2(N+1)}2^N N!\sqrt{\pi}}{H_{N+1}(x_i)H'_N(x_i)} = \frac{2^{N+1}N!\sqrt{\pi}}{H^2_{N+1}(x_i)}, \tag{2.117}$$

where the recurrence relation

$$H'_n(x)\Big|_{x=x_i} = 2x_i H_N(x_i) - H_{N+1}(x_i) = -H_{N+1}(x), \tag{2.118}$$

has been used and $H_N(x_i) = 0$ by virtue of the definition of the quadrature points.

2.4.8 Gegenbauer Polynomials

The Gegenbauer polynomials are a subset of the Jacobi polynomials with $\alpha = \beta = \lambda - 1/2$ and have applications to potential theory and harmonic analysis. They reduce to Legendre polynomials for $\lambda = 1/2$ and to Chebyshev polynomials for $\lambda = 0$. It is useful to note the explicit expressions for the lower order Gegenbauer polynomials. These are,

$$\begin{aligned} &C^\lambda_0(x) = 1, \quad C^\lambda_1(x) = 2\lambda x, \quad C^\lambda_2(x) = 2\lambda(\lambda+1)x^2 - \lambda, \\ &C^\lambda_3(x) = \frac{4\lambda}{3}(\lambda+1)(\lambda+2)x^3 - 2\lambda(\lambda+1)x, \end{aligned} \tag{2.119}$$

and satisfy the orthogonality relation

$$\frac{1}{h^\lambda_\ell}\int_{-1}^{1}(1-x^2)^{\lambda-1/2}C^\lambda_\ell(x)C^\lambda_k(x)dx = \delta_{\ell,k}. \tag{2.120}$$

The normalization h^λ_ℓ is

$$h^\lambda_\ell = \frac{2^{1-2\lambda}\pi\Gamma(\ell+2\lambda)}{\ell!(\ell+\lambda)[\Gamma(\lambda)]^2}. \tag{2.121}$$

The recurrence relation for the Gegenbauer polynomials is given by

$$(\ell+2)C^\lambda_{\ell+2} = 2(\lambda+\ell+1)xC^\lambda_{\ell+1} - (2\lambda+\ell)C^\lambda_\ell. \tag{2.122}$$

These relationships for the Gegenbauer polynomials are used for the resolution of the Gibbs phenomenon presented in Chap. 4.

2.4.9 Chebyshev Polynomials; Fourier Cosine Basis Functions

We define the Chebyshev polynomials in terms of the non-polynomial cosine functions, $\cos(n\theta)$, defined on the interval $x \in [0, \pi]$ and orthogonal as given by

$$\int_0^\pi \cos(n\theta)\cos(m\theta)d\theta = \begin{cases} 0 & n \neq m, \\ \pi & n = m = 0, \\ \frac{\pi}{2} & n = m \neq 0. \end{cases} \tag{2.123}$$

This orthogonality relation can be verified with the use of the addition formulae $\cos(\theta_1)\cos(\theta_2) = \frac{1}{2}[\cos(\theta_1 + \theta_2) + \cos(\theta_1 - \theta_2)]$. We introduce the Fourier cosine orthogonality to construct the Chebyshev polynomials. A more complete discussion of Fourier series is presented in Chap. 4.

Chebyshev polynomials together with Fourier basis functions are the basis sets of choice used for fluid dynamics and related problems (Gottlieb and Orszag 1977; Boyd 2001; Peyret 2002; Canuto et al. 2006).

The definition of the Chebyshev polynomials is

$$T_n(x) = \cos(n\theta), \qquad x = \cos\theta. \tag{2.124}$$

With the well known identities for $\cos(n\theta)$, that is $\cos(2\theta) = 2\cos^2(\theta) - 1)$, $\cos(3\theta) = 4\cos^3(\theta) - 3\cos(\theta)$, etc. one can easily show that the lower order Chebyshev polynomials are given by

$$\begin{aligned} &T_0(x) = 1, \quad T_1(x) = x, \quad T_2(x) = 2x^2 - 1, \quad T_3(x) = 4x^3 - 3x, \\ &T_4(x) = 8x^4 - 8x^2 + 1, \quad T_5(x) = 16x^5 - 20x^3 + 5x. \end{aligned} \tag{2.125}$$

With the change of variable, $x = \cos\theta$, in Eq. (2.123), the Chebyshev polynomials are orthogonal in accordance with

$$\int_{-1}^{1} \frac{1}{\sqrt{1-x^2}} T_n(x)T_m(x)dx = c_n \frac{\pi}{2}\delta_{nm}, \tag{2.126}$$

where

$$c_n = \begin{cases} 2 & n = 0 \\ 1 & n \geq 1 \end{cases}. \tag{2.127}$$

The recurrence relation for the Chebyshev polynomials is

$$T_{n+1}(x) = 2xT_n(x) - T_{n-1}, \tag{2.128}$$

The quadrature points of order N for this basis set are easily determined as the roots of $\cos(N\theta_i) = 0$ given by $\theta_i = (2i-1)\pi/2N$, $i = 1, 2, \ldots, N$, so that the

Gauss-Chebyshev quadrature points are

$$x_i = \cos\left[(2i-1)\frac{\pi}{2N}\right] \qquad i = 1, 2, \ldots N. \tag{2.129}$$

With Eq. (2.65) for the quadrature weights and noting the normalization of the Chebyshev polynomials, we have that

$$w_i = -\frac{\pi}{T_{n+1}(x_i)T'_N(x_i)}. \tag{2.130}$$

The definition, Eq. (2.124), thus yields

$$T'_N(x) = \frac{N\sin(N\theta)}{\sin(\theta)}. \tag{2.131}$$

We evaluate $T_{N+1}(x)$ at the quadrature nodes, that is

$$\begin{aligned} T_{N+1}(x_i) &= \cos[(N+1)\theta_i] \\ &= \cos(N\theta_i)\cos(\theta_i) - \sin(N\theta_i)\sin(\theta_i) \\ &= -\sin(\theta_i), \end{aligned} \tag{2.132}$$

where $\cos(N\theta_i) = 0$ and $\sin(N\theta_i) = 1$. Thus with Eq. (2.131) evaluated at x_i, we have the result

$$T_{N+1}(x_i)T'_N(x_i) = -N. \tag{2.133}$$

With this result in Eq. (2.130), the weights in the quadrature are given by

$$w_i = \frac{\pi}{N}. \tag{2.134}$$

Equations (2.129) and (2.130) define the Gauss-Chebyshev quadrature defined by

$$\int_{-1}^{1} \frac{1}{\sqrt{1-x^2}} f(x)dx \approx \sum_{i=1}^{N} w_i f(x_i) \tag{2.135}$$

The Sturm-Liouville equation for the Chebyshev polynomials is

$$\sqrt{1-x^2}\frac{d}{dx}\left[\sqrt{1-x^2}\frac{dT_n(x)}{dx}\right] = -n^2 T_n(x). \tag{2.136}$$

2.4.10 *Fejér Quadratures*

The presentation here is adapted from the discussion in Davis and Rabinowitz (1975). The Fejér[18] quadrature is based on the Chebyshev nodes, defined by $T_N(x_i) = 0$, Eq. (2.129), with $w(x) = 1$ in Eq. (2.58). The quadrature approximation is then given by

$$\int_{-1}^{1} f(x)dx \approx \sum_{i=1}^{N} w_i f(x_i), \tag{2.137}$$

with the quadrature weights, w_i, obtained with Eq. (2.35) in Eq. (2.59) with the result

$$w_i = \frac{1}{T'_N(x_i)} \int_{-1}^{1} \frac{T_N(x)}{x - x_i} dx. \tag{2.138}$$

We now use the Christoffel-Darboux relation, Eq. (2.62), with $y = x_i$ and use $T_N(x_i) = 0$ on both sides of the equation so that the sum terminates at $N - 1$. The first term in the sum is written separately and with $\sqrt{\beta_{N+1}} = 1/2$ the result with the Christoffel-Darboux relation is

$$2\left[1 + \sum_{k=1}^{N-1} T_k(x)T_k(x_i)\right] = -T_{N+1}(x_i)\frac{T_N(x)}{x - x_i}. \tag{2.139}$$

With the substitution of $T_N(x)/(x - x_i)$ obtained from Eq. (2.139) in Eq. (2.138) and with Eq. (2.133), the quadrature weights, Eq. (2.138), are given by

$$w_i = \frac{2}{N}\left[1 + \sum_{k=1}^{N-1} T_k(x_i) \int_{-1}^{1} T_k(x)dx\right]. \tag{2.140}$$

The integral above is evaluated as

$$\int_{-1}^{1} T_k(x)dx = \int_{0}^{\pi} \cos(k\theta)\sin(\theta)d\theta = \begin{cases} \frac{2}{1-k^2} & \text{k even,} \\ 0 & \text{k odd.} \end{cases} \tag{2.141}$$

[18] Leopold Fejér (1880–1959) was a Hungarian mathematician noted for his work on harmonic analysis and Fourier series. He was the thesis advisor of John von Neumann, Paul Erdös, George Pólya and Pál Turán.

With $k = 2j$ and $T_{2j}(x_i) = \cos(2jx_i)$, the final result for the quadrature weights is

$$w_i = \frac{2}{N}\left[1 - \sum_{j=1}^{N/2} \frac{\cos(2jx_i)}{4j^2 - 1}\right]. \tag{2.142}$$

The Fejér quadrature rule is used for the multidomain quadratures in the Gautschi-Stieltjes calculation of the recurrence coefficients, α_n and β_n (Gautschi 1985, 1994).

2.4.11 The Clenshaw-Curtis Quadrature

The Clenshaw-Curtis quadrature (Clenshaw and Curtis 1960) is also based on the integral Eq. (2.137) with $w(x) = 1$. The integrand is expanded in Chebyshev polynomials

$$f(x) = \sum_{n=0}^{\infty} a_n T_n(x). \tag{2.143}$$

The orthogonality of the Chebyshev polynomials, Eq. (2.126), gives the expansion coefficients

$$a_n = \frac{2}{\pi}\int_{-1}^{1} \frac{1}{\sqrt{1-x^2}} f(x)T_n(x)dx. \tag{2.144}$$

The change of variable, $x = \cos(\theta)$, gives

$$a_n = \frac{2}{\pi}\int_{0}^{\pi} f(\cos(\theta))\cos(n\theta)d\theta. \tag{2.145}$$

With the expansion Eq. (2.143), the desired integral, Eq. (2.137) is evaluated as the integral of the Chebyshev polynomial, Eq. (2.141), so that

$$\int_{-1}^{1} f(x)dx = a_0 + \sum_{n=1}^{\infty} \frac{2a_{2n}}{1-4n^2}. \tag{2.146}$$

The Clenshaw-Curtiss quadrature is based on the truncation of the infinite series in Eq. (2.146)

$$\int_{-1}^{1} f(x)dx \approx a_0 + \sum_{n=1}^{N/2} \frac{2a_{2n}}{1-4n^2}, \tag{2.147}$$

and the evaluation of the expansion coefficients with a trapezoidal rule based on a uniform grid of $N+1$ points, $\theta_i = i\pi/N$ with step size $h = \pi/N$. In accordance with Eq. (2.38), the expansion coefficients are given by

$$a_n = \frac{2}{N}\left[\frac{f(1)}{2} + \sum_{i=2}^{N-1} f\left[\cos[\frac{i\pi}{N}\right]\cos(\frac{ni\pi}{N}) + \frac{f(-1)}{2}(-1)^n\right]. \tag{2.148}$$

The integral is thus given by a variant of the Fejér quadrature with two points at the interval boundaries, namely $x_1 = -1$ and $x_N = 1$ analogous to the Lobatto quadratures of the next section. The interior quadrature points are the extrema of the $T_{N-1}(x)$,

$$x_i = \cos(\frac{(i-1)\pi}{N-1}, \quad i = 1, 2, \ldots, N \tag{2.149}$$

If the a_{2n} coefficients given by Eq. (2.148) are substituted into Eq. (2.147) and the result can be written as a quadrature, Eq. (2.58). The Clenshaw-Curtiss quadrature is with the points $x_i = (i-1)\pi/(N-1)$. An explicit expression can be written for the weights with Eqs. (2.146) and (2.148) which depend on whether N is even or odd.

We do not provide these explicitly and refer readers to the MATLAB code clencurt.m provided by Trefethen (2000). Additional works on the Clenshaw-Curtiss quadrature have been reported (Gentleman 1972; Waldvogel 2006; Calabrò and Esposito 2009). The quadrature has been used in the evaluation of the scattering phase shifts for quantum collision cross sections (Kennedy and Smith 1967; Cohen 1978) and for classical scattering cross sections (Viehland and Chang 2010). Error estimates for these quadratures have been discussed (ÓHara and Smith 1968) and also compared with Gaussian quadratures (Trefethen 2008; Calabrò and Esposito 2009).

2.4.12 *Gauss-Lobatto and Gauss-Radau Quadrature Algorithms*

In collocation methods, it is often necessary to have quadrature points at the boundaries of the interval of interest so as to impose boundary conditions. The extremum values of the Gauss-Legendre quadrature points do not coincide with the interval boundaries for the interval $[-1, 1]$. The quadrature points referred to as the Gauss-Legendre-Lobatto are constructed so that $x_1 = -1$ and $x_N = 1$.

The Lobatto quadratures are often used in pseudospectral calculations for simulations in fluid mechanics (Peyret 2002; Canuto et al. 2006) but are also used in other applications (Herman and Conway 1996). This technique is generally applied to problems defined on a bounded domain such as $x \in [-1,\ 1]$ for which Legendre, Chebyshev or Jacobi quadratures are used. The method has been applied to optimal control problems (Garg et al. 2009) and for numerical simulations of tethered satellites (Williams 2011). The method can also be used for non-classical basis sets (Shizgal 2002).

The Gauss-Lobatto[19] quadrature points and weights associated with the weight function $w(x)$ are based on the set of polynomials $q_n(x)$ which are orthogonal with respect to $w(x)(1-x^2)$, that is,

$$\int_{-1}^{1} w(x)(1-x^2)q_n(x)q_m(x)dx = \delta_{n,m}. \tag{2.150}$$

We use $q_n(x)$ to distinguish this set from the polynomials, $P_\ell(x)$, orthonormal with respect to $w(x)$. The set of Gauss quadrature points, $\{\tilde{x}_k, k = 2, \ldots N-1\}$, interior to $[-1, 1]$ obtained with the diagonalization of the Jacobi matrix for $w(x)(1-x^2)$ are the roots of $q_{N-1}(x)$. The corresponding weights are $\{\tilde{w}_k\}$. The Lobatto quadrature formula for $w(x)$ of order N is

$$\int_{-1}^{1} w(x)f(x)dx \approx v_0 f(-1) + v_N f(1) + \sum_{k=1}^{N-1} v_k f(\tilde{x}_k). \tag{2.151}$$

where the N quadrature points are $(\tilde{x}_1 \equiv -1, \tilde{x}_2, \ldots, \tilde{x}_{N-1}, \tilde{x}_N \equiv 1)$.

The quadrature points can be shown to be the roots of the derivative of the Legendre polynomial. If we multiply the Sturm-Liouville equation, Eq. (2.82), by $P_\ell(x)$ and use orthogonality on the right hand side and integrate by parts on the left hand side, we find that $q_n(x) \equiv P_n'(x)$.

The Gauss-Lobbato weights, v_k are given in terms of the Gauss quadrature weights, $\tilde{w}_k$, that is, $v_k = \tilde{w}_k/(1-\tilde{x}_k^2)$ for $k = 2, \ldots, N-1$. The two weights associated with the ends of the interval can be determined by requiring that the first two moments of $w(x)$ are determined exactly with the quadrature, that is,

$$\int_{-1}^{1} w(x)dx = v_1 + v_N + \sum_{k=1}^{N-1} v_k \tag{2.152}$$

and

$$\int_{-1}^{1} w(x)xdx = -v_1 + v_N + \sum_{k=1}^{N-1} v_k\tilde{x}_k \tag{2.153}$$

This gives two equations for v_1 and v_N and the Lobatto-quadrature is fully specified.

The positive Lobatto-Legendre quadrature points for $N = 10$ are listed in Table 2.12 together with the associated weights in comparison with the Gauss-Legendre points and weights. Explicit expressions for the quadrature points and weights appear in many of the books on spectral methods (Boyd 2001; Peyret 2002;

[19] Rehuel Lobatto (1797–1866) was a Dutch mathematician known primarily for the Gauss-Lobatto quadrature.

Table 2.12 Comparison of the Lobatto-Legendre and the Gauss-Legendre quadrature points, $N = 10$

Lobatto-Legendre		Gauss-Legendre	
$\tilde{x}_k$	v_k	x_k	w_k
0.16527896	0.32753976	0.14887434	0.29552422
0.47792495	0.29204268	0.43339539	0.26926672
0.73877387	0.22488934	0.67940957	0.21908636
0.91953391	0.13330599	0.86506337	0.14945135
1.00000000	0.02222222	0.97390653	0.66671344

Canuto et al. 2006; Kopriva 2009). There are MATLAB codes provided by other authors for the evaluation of Lobatto-Legendre and Lobatto-Chebyshev quadrature points and weights (Shen et al. 2011; Gautschi 1985, 1994). The codes provided here for general positive nonclassical weight functions can be used efficiently for the classical polynomials and yield the same numerical results as do the explicit formulae provided in the textbooks cited.

We have shown that Gaussian quadratures with N points are exact for polynomials of order $2N - 1$. In particular, the orthogonality of the polynomials is computed exactly with N points, that is,

$$\sum_{k=1}^{N} w_k P_n(x_k) P_m(x_k) = \delta_{nm}. \tag{2.154}$$

Analogously, the discrete form of the completeness relation is exact, that is,

$$w_k \sum_{n=0}^{N} P_n(x_k) P_n(x_\ell) = \delta_{k\ell} \tag{2.155}$$

and these relationships are used to define the unitary transformation, $\mathbf{T}$, between physical and spectral spaces discussed in Chap. 1.

However, the Lobatto quadrature is only exact for polynomials of order $N - 2$ and the normalization of the polynomial of order $N - 1$ is given by

$$S_{N-1} = \sum_{k=1}^{N} v_k q_N^2(\tilde{x}_k) \neq 1. \tag{2.156}$$

If the Nth order polynomial is renormalized with S_N, there is a modified discrete "completeness" identity analogous to Eq. (2.155),

$$v_k \left(\sum_{n=0}^{N-2} q_n(\tilde{x}_i) q_n(\tilde{x}_j) + \frac{q_{N-1}(\tilde{x}_j) q_{N-1}(\tilde{x}_j)}{S_N} \right) = \delta_{ij}, \tag{2.157}$$

and a unitary transformation between spectral space and physical space exists (Hesthaven 1998).

Table 2.13 Comparison of Radau-Laguerre and Gauss-Laguerre quadrature points, $N = 10$, $\alpha = 1/2$

Radau-Laguerre		Gauss-Laguerre	
$\tilde{x}_k$	w_k	$\tilde{x}_k$	w_k
0.00000000	0.35926778 (−1)	0.22987298	0.17547082
0.49469154	0.31262035	0.92448155	0.35522338
1.47402112	0.34308717	2.09941046	0.25268356
2.97365694	0.15621514	3.78288087	0.86356103 (−1)
5.03607835	0.34472913 (−1)	6.01991803	0.15109778 (−1)
7.72862347	0.37177539 (−2)	8.88034760	0.13282156 (−2)
11.1593223	0.18325258 (−3)	12.4748324	0.54187800 (−4)
15.5123604	0.35435841 (−5)	16.9908473	0.87374758 (−6)
21.1450926	0.19557860 (−7)	22.7910029	0.40196999 (−8)
28.9761533	0.1357736 (−10)	30.8064059	0.2292222 (−11)

The Gauss-Radau quadrature specifies one fixed point, generally the origin. Radau-Legendre quadratures has been used in the solution of the Poisson equation to facilitate the application of boundary conditions (Chen et al. 2000). The calculation of the Gauss-Radau quadratures requires a minor change in the MATLAB codes used for the Gauss quadratures in that all that needs to be changed is the last diagonal element in the Jacobi matrix, **J**. The procedure is very well described in the papers by Golub (1973) and by Gautschi (2000). For the Radau-Laguerre quadrature, the last diagonal element of the Jacobi matrix is given by $J_{N-1,N-1} = N - 1$. A comparison of the Radau-Laguerre and Gauss-Laguerre quadratures is in Table 2.13.

2.5 Nonclassical Basis Functions

Table 2.2 lists several non-classical polynomials used in pseudospectral solutions of the Boltzmann, Fokker-Planck and Schrödinger equations, as well as for the solutions of other differential/integral equations. Gautschi (1994) noted two decades ago the slow adoption of spectral methods based on non-classical basis sets.

2.5.1 Maxwell Polynomials

In the kinetic theory of gases, the distribution of particle velocities, $f(\mathbf{v}, \mathbf{r}, t)$, plays a central role. The distribution function depends on seven variables; the three components of the particle velocity, **v**, three position variables, **r**, and the time, t. At complete equilibrium in the absence of external forces, spatial gradients, or chemical reactions, the distribution function is the Maxwell-Boltzmann distribution function given by

$$F(v) = n_b \left(\frac{m}{2\pi k_B T_b}\right)^{3/2} \exp(-\frac{mv^2}{2k_B T_b}), \tag{2.158}$$

where m is the mass of the particles and k_B is the Boltzmann constant. The distribution function is normalized to the total density n_b

$$n_b = 4\pi \int_0^\infty F(v) v^2 dv, \tag{2.159}$$

and the temperature, T_b, is the average kinetic energy given by

$$\frac{3}{2} n_b k_B T_b = 4\pi \int_0^\infty F(v) \frac{mv^2}{2} v^2 dv. \tag{2.160}$$

The Maxwellian distribution function is isotropic in velocity space and depends on $|\mathbf{v}|$.

The subject of kinetic theory impacts on numerous fields including transport phenomena in gaseous systems, neutron transport, nuclear engineering, plasma physics, space science, aerosol science, granular matter physics, as well many aspects of astrophysics including the kinetic theory of star clusters. In almost all these applications, the distribution function is not a Maxwellian and the goal of numerical simulation is to determine the extent of the departure from equilibrium. These simulations are based on a transport equations for the distribution function, such as the Boltzmann and or Fokker-Planck equations. These transport equations are generally differential or integro-differential equations. Their solution is obtained by various numerical methods including finite difference and spectral/pseudospectral methods as well as Monte-Carlo simulations (Bird 1994) and particle-in-cell methods (Birdsall and Langdon 1984).

The most often used basis set in kinetic theory are the Sonine-Laguerre polynomials (Chapman and Cowling 1970; Ferziger and Kaper 1972) expressed in the reduced energy, $y = mv^2/2k_B T_b$. The Maxwellian can be written as the weight function $w(y) = \sqrt{y} e^{-y}$ for which the basis set is the Laguerre polynomials, $L_n^{(1/2)}$ listed in Table 2.11. These are equivalent to the Sonine polynomials, $S_{(1/2)}^{(n)}(x^2)$, written in terms of the reduced speed $x = \sqrt{mv^2/2k_B T_b}$. If the distribution function is factored into three components, one for each of the three cartesian velocity components, that is, v_x, v_y and v_z, the weight function for each velocity component is $w(x) = e^{-x^2}$ $x = mv_z^2/2k_B T_b \in (-\infty, \infty)$, and the basis set corresponds to the Hermite polynomials. These basis functions occur in the well-known Grad moment method for the solution of the Boltzmann equation (Grad 1949, 1958; Struchtrup 2005) and for calculations of ion mobilities in gases (Mason and McDaniel 1988; Viehland 1994).

Maxwell polynomials, $M_n^{(p)}(x)$, are nonclassical basis functions orthonormal with respect to $w(x) = x^p e^{-x^2}$, $x \in [0, \infty]$ that is,

$$\int_0^\infty x^p e^{-x^2} M_n^{(p)}(x) M_m^{(p)}(x) dx = \delta_{mn} \tag{2.161}$$

that have also been used extensively in kinetic theory. The polynomials with $p = 0$ are referred to as the half-range Hermite polynomials and are not equivalent to the Hermite polynomials defined on the infinite axis. They were first introduced by Gross and Ziering (1958) for the calculation of the heat conduction in a rarefied gas, and also by Baltz (1969). The Maxwell polynomials were employed in neutron transport theory by Desai and Nelkin (1966) and Desai (1966) and constructed by Shizgal (1979) and by Risken and Voigtlaender (1984) for the relaxation of electrons in a monatomic gas as modelled with a Fokker-Planck equation. Gauss quadrature rules based on Maxwell polynomials with $p = 0$ were also considered (Huang and Giddens 1968; Galant 1969; Steen et al. 1969). The quadratures based on the Maxwell polynomials were employed by Shizgal (1981) for the solution of the Boltzmann equation. A recent application to a rarefied gas dynamical problem was reported by Gibelli (2012).

Recurrence relations for the recurrence coefficients α_n and β_n in the three term recurrence relation for $p = 2$, Eq. (2.14) can be derived as follows. To simplify the notation the explicit dependence of $M_n^{(p)}$ on p is now omitted. If the Christoffel-Darboux relation, Eq. (2.66) is multiplied by $xw(x)$ and integrated, one finds that

$$\sum_{k=0}^{n} \alpha_k = \sqrt{\beta_{n+1}} \langle x^2 M'_{n+1} M_n \rangle = 2\sqrt{\beta_{n+1}} \langle x^2 M_{n+1} M_n \rangle, \tag{2.162}$$

where an integration by parts has been performed on the middle term and the integral $\langle x M_{n+1} M'_n \rangle = 0$, since xM'_n, a polynomial of degree n is orthogonal to M_{n+1}. The Dirac notation used earlier is employed again. With repeated use of the three term recurrence relation, Eq. (2.14), and the orthogonality relation, we get

$$\sum_{k=0}^{n} \alpha_k = 2\beta_{n+1}(\alpha_n + \alpha_{n+1}). \tag{2.163}$$

A second recurrence relation for the recurrence coefficients can be derived with Eq. (2.15). The integral $\langle xM_n^2 \rangle$ can be evaluated by taking the average of the Christoffel-Darboux relation, Eq. (2.66), and the result is

$$(n+1) = \sqrt{\beta_{n+1}} \langle M'_{n+1} M_n \rangle = \langle x M_{n+1} M'_{n+1} \rangle, \tag{2.164}$$

where the second equality results by multiplying Eq. (2.14) by M'_{n+1} and with n replaced by $n + 1$. An integration by parts yields

$$\langle x M_n M'_n \rangle = -\frac{p+1}{2} + \langle x^2 M_n^2 \rangle, \tag{2.165}$$

and a third recurrence relation for β_{n+1} in terms of β_n and α_n is,

$$\beta_{n+1} + \alpha_n^2 + \beta_n = n + \frac{p+1}{2}. \tag{2.166}$$

The relations Eqs. (2.163) and (2.166) are two equations for the set of recurrence coefficients α_n and β_n. The recurrence is begun with $\alpha_0 = 2/\sqrt{\pi}$ and $\alpha_1 = 4(4-\pi)/(\sqrt{\pi}(3\pi-8))$, $\beta_0 = 0$ and $\beta_1 = 3/2-\alpha_0^2$. Equation (2.166) is used for β_{n+1} and α_{n+1} is calculated with Eq. (2.163). However simple these relationships they prove to be numerically unstable. This is another example where round-off error can contaminate a numerical algorithm that appears innocent.

In Table 2.14, the results obtained with these recurrence relations are compared with those determined with the Gautschi-Stieltjes procedure. The first column shows α_n with the Gautschi-Stieltjes method in comparison with the result with the recursion relations, Eqs. (2.163) and (2.166). The disagreement between the two results is highlighted with the underlined portion in the second column. The rapid loss in precision of the two results is very clear. A similar comparison of the β_n coefficients is shown in the next two columns. The loss of precision is machine dependent. Clarke and Shizgal (1993) employed asymptotic methods to determine the recurrence coefficients accurately with partial success. Ball (2003) derived recurrence relations very similar to (2.163) and (2.166) and judiciously rearranged the equations to iterate them appropriately without significant round-off error. Shizgal (1981) originally employed multiple precision arithmetic to evaluate the recurrence coefficients accurately.

The Gautschi-Stieltjes method provides accurate results for a large class of weight functions. The MATLAB codes ab_maxwell_p0.m and ab_maxwell_p2.m calculate the recurrence coefficients for $p = 0$ and 2, respectively. The results for 100 recurrence coefficients agree to 13 significant figures with those reported by Gautschi (2004) (example 1.13 and the file abhrhermite.dat, $p = 0$). The timing for the calculation is less than 0.1 sec. A short list of the recurrence coefficients for the polynomials, $M_n^{(0)}(x)$ is shown in Table 2.15. The recurrence coefficients for the Hermite

Table 2.14 Recurrence coefficients for Maxwell polynomials, $M_n^{(2)}(x)$, for $w(x) = x^2 e^{-x^2}$, $x \in [0, \infty)$

n	α_n		β_n	
	Gautschi-Stieltjes	Eqs. (2.163) and (2.166)	Gautschi-Stieltjes	Eqs. (2.163) and (2.166)
0	0.22676046	0.22676046	1.35966300	1.35966304
1	0.42455596	0.42455596	1.57050690	1.57050686
2	0.60895224	0.60895224	1.76189660	1.76189657
3	0.78676825	0.78676825	1.93706160	1.93706157
4	0.96102423	0.96102423	2.09900070	2.09900068
5	1.13317190	1.13317191	2.25007810	2.25007811
6	1.30397660	1.30397**58**	2.39210110	2.39210112
7	1.47387550	1.47387**63**	2.52645780	2.5264**541**
8	1.64313570	1.6431**3735**	2.65422970	2.6542**2471**
9	1.81192880	1.811**95384**	2.77627460	2.776**20316**
10	1.98037030	1.980**74217**	2.89328340	2.89**227120**

Table 2.15 Recurrence coefficients for Maxwell polynomials, $M_n^{(0)}(x)$ with $w(x) = e^{-x^2}$ $x \in [0, \infty)$; For Hermite polynomials $\alpha_n = n/2$ and $\beta_n = 0$

n	α_n	β_n
0	0.5641895835478	0.0000000000000
1	0.9884253928468	0.1816901138162
2	1.2859676193639	0.3413251289594
3	1.5247208440801	0.5049621529880
4	1.7301922743095	0.6702641946396
5	1.9134998431431	0.8361704992803
6	2.0806203364008	1.0023478510110
7	2.2352283805046	1.1686711647443
8	2.3797824435047	1.3350829222423
9	2.5160256434438	1.5015525993448
10	2.6452479250570	1.6680623621881

polynomials are $\alpha_n = 0$ and $\beta_n = n/2$. Quadrature points and weights for Maxwell polynomials for all values of p can be efficiently computed for various orders with the Gautschi-Stieltjes evaluation of the recurrence coefficients and diagonalization of the Jacobi matrix.

In Fig. 2.3 we compare the Maxwell polynomial, $M_{10}^{(2)}(x)$, $x \in [0, \infty)$, with the Laguerre polynomial, $L_{10}^{(1/2)}(y)$, $y \in [0, \infty)$. It is important to notice that the Laguerre polynomial is shown versus $\sqrt{y}$ and the polynomial is far more extended if shown versus y. The symbols in the figures denote the quadrature points. The quadrature points, y_i, are more sparsely distributed and extend to larger y as shown in Table 2.16 for both weight functions with $N = 10$. Table 2.16 lists the quadrature points and weights for both polynomials. The table illustrates the very different distribution of the quadrature points and the very small weights, w_i, for the Laguerre polynomials in comparison to the weights for the Maxwell polynomials. This is clear from the results in Table 2.17 which compares quadrature nodes for the two polynomials for $N = 6$. It is interesting to note that there is no relationship between the quadrature points $\sqrt{y_i}$ and x_i. We will demonstrate very different convergence results for these basis sets in Chaps. 3, 5 and 6.

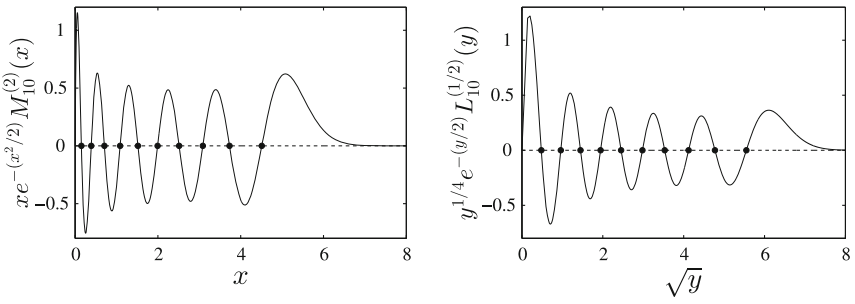

Fig. 2.3 Maxwell polynomial, $M_{10}^{(2)}(x)$, versus x on the *left* and Laguerre polynomial, $L_{10}^{(1/2)}(y)$, versus $\sqrt{y}$ on the *right*; *symbols* denote the quadrature points with $N = 10$

Table 2.16 Quadratures nodes, x_i, for Maxwell polynomial ($M_{10}^{(2)}(x)$) and y_i, for Laguerre polynomial $L_{10}^{(1/2)}(y)$, corresponding to the graphs in Fig. 2.3

	Maxwell		Laguerre	
i	x_i	w_i	y_i	w_i
1	0.1512	0.4326 (−2)	0.2299	0.1755
2	0.3901	0.3675 (−1)	0.9245	0.3552
3	0.7075	0.1064	2.0994	0.2527
4	1.0880	0.1473	3.7829	0.8636 (−1)
5	1.5171	0.1044	6.0199	0.1511 (−1)
6	1.9921	0.3728 (−1)	8.8803	0.1328 (−2)
7	2.5120	0.6240 (−2)	12.4748	0.5419 (−4)
7	2.5120	0.6240 (−2)	12.4748	0.5419 (−4)
8	3.0842	0.4244 (−3)	16.9908	0.8738 (−6)
9	3.7294	0.8811 (−5)	22.7910	0.4020 (−8)
10	4.5089	0.2708 (−7)	30.8064	0.2292 (−11)

Table 2.17 The positive quadrature points for the Hermite polynomial, $H_{12}(x)$, and the quadratures points for the Maxwell polynomial, $M_6^{(0)}(x)$, which is the half-range Hermite polynomial

	H_{12}		$M_6^{(0)}$
i	x_i	i	x_i
7	0.3142	1	0.0786
8	0.9476	2	0.3867
9	1.5977	3	0.8664
10	2.2795	4	1.4657
11	3.0206	5	2.1727
12	3.8897	6	3.0368

There is also no relationship between the Maxwell polynomials ($p = 0$) polynomials and the Hermite polynomials, $H_n(x)$, even for the set of even polynomials $H_{2n}(x)$ and symmetric on the infinite interval. The Maxwell polynomial $M_{10}^{(0)}(x)$ and $H_{20}(x)$ for $0 < x < \infty$ are compared in Fig. 2.4 with the quadrature points shown as the solid symbols and listed in Table 2.17. It is clear the Maxwell quadrature points are distributed closer to the origin than the positive Hermite quadrature points.

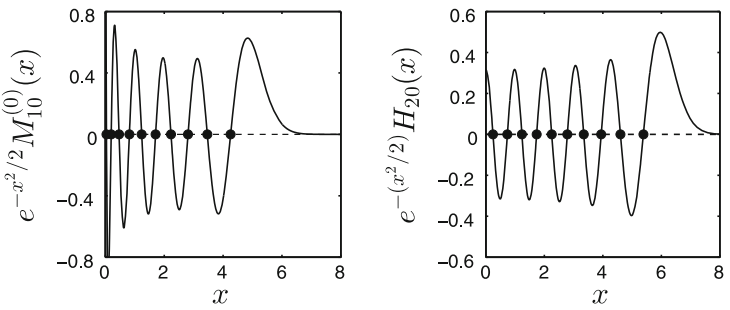

Fig. 2.4 Maxwell polynomial, $M_{10}^{(0)}(x)$, on the *left* and the Hermite polynomial, $H_{20}(x)$, for $x \in [0, 8]$, on the *right*; *symbols* denote the roots

2.5.2 The Bimodal Polynomials

In Chap. 6, we introduce a class of chemical reactions for which the reactant and products exist in two distinct potential minima separated by a barrier. The dynamics of such systems have been treated with Fokker-Planck equations that possess bimodal steady distribution functions (Blackmore and Shizgal 1985a, b; Montgomery et al. 1979; Hänggi et al. 1990; Shizgal and Chen 1997; Borromeo and Marchesoni 2005; Lo and Shizgal 2006). Similar Fokker-Planck equations have also been used to model climate (Nicolis and Nicolis 1981; Nicolis 1982), optical bistability (Bonifacio et al. 1978; Schenzle and Brand 1979; Blackmore et al. 1986) and stochastic resonance (Gammaitoni et al. 1998).

The steady state distributions of these systems exhibit two stable states and the equilibrium probability density can be modelled with the weight function

$$w(x) = \exp\left[-\frac{1}{\epsilon}\left(\frac{x^4}{4} - \frac{x^2}{2}\right)\right], \qquad x \in (-\infty, \infty). \tag{2.167}$$

shown in Fig. 2.5 with two maxima at $x = \pm 1$ and the shape varies with the parameter ϵ. With decreasing ϵ the peaks get narrower and the weight function is localized about $x = \pm 1$. The bimodal polynomials, $B_n(x)$ with $x \in [-\infty, \infty]$, are orthogonal with respect to this weight function

$$\int_{-\infty}^{\infty} w(x) B_n(x) B_m(x) dx = \delta_{nm}, \tag{2.168}$$

and are also localized as shown in Fig. 2.6.

The β_n recursion coefficients for these polynomials satisfy the recurrence relation (Blackmore and Shizgal 1985a),

$$\beta_{n+2} = \frac{(n+1)\epsilon}{\beta_{n+1}} - \beta_{n+1} - \beta_n + 1, \tag{2.169}$$

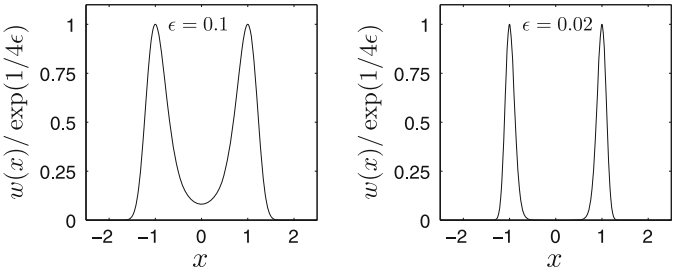

Fig. 2.5 The bimodal weight function $w(x) = \exp\left(-[x^4/4\epsilon - x^2/2\epsilon]\right)$ relative to $\exp(1/4\epsilon)$ versus x for $\epsilon = 0.1$ and $\epsilon = 0.02$

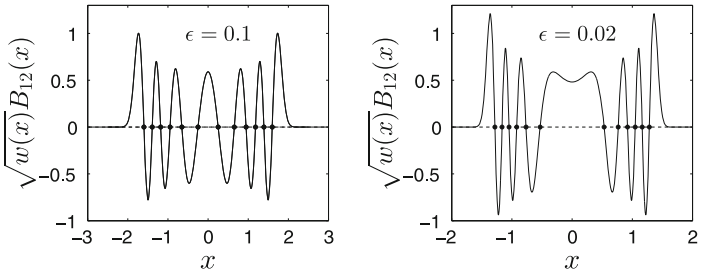

Fig. 2.6 Bimodal polynomial, $B_{12}(x)$ versus x and ϵ; *solid symbols* denote the quadrature points

Table 2.18 Quadrature nodes for bimodal polynomials for the positive roots versus the parameter ϵ in the weight function

i	$\epsilon = 0.1$	$\epsilon = 0.02$	$\epsilon = 0.005$
1	0.250927	0.5313424	0.8130843
2	0.6539267	0.7651935	0.8973338
3	0.9463795	0.9201875	0.9658537
4	1.181996	1.047651	1.027887
5	1.391344	1.164084	1.088161
6	1.59881	1.282431	1.152341

which suffers from round-off errors owing to the subtractions. Equation (2.169) is derived with the Christoffel-Darboux relation and the three term recursion relation. We can determine the moments μ_n with MAPLE. From this moment information, the normalizations γ_n, the recursion coefficients β_n and the polynomial basis set can be calculated. Alternatively, we can use the Gautschi-Stieltjes procedure and calculate the β_n recursion coefficients and the polynomials by recursion, Eq. (2.14). The non-monotonic variation of β_n is shown in Fig. 2.7. For large n, there is a transition from an oscillatory behaviour to a smoother asymptotic result for larger n (Clarke and Shizgal 1993).

The quadrature points determined from the diagonalization of the Jacobi matrix are densely distributed in the vicinity of the peaks of the weight function as shown

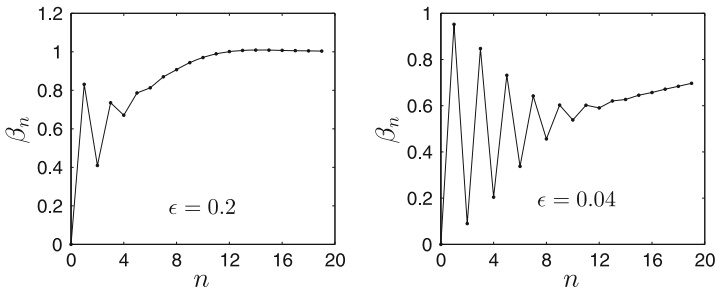

Fig. 2.7 Variation of β_n for the bimodal polynomials

by the solid symbols in Fig. 2.6. These are listed in Table 2.18, with the first two columns corresponding to Fig. 2.6. The polynomials orthogonal with this weight function are also concentrated in the region $x = \pm 1$. These attributes of the quadratures provide for rapidly convergent solutions of the Fokker-Planck equation for isomerization reactions in liquids discussed in Chap. 6. We also make use of half-range bimodal basis functions defined with the same weight function but for the semi-infinite interval.

2.5.3 Rys Polynomials; Full-Range and Half-Range

The Schrödinger equation for the electronic energy states of a molecule is the basis for electronic structure calculations in quantum chemistry (Szabo and Ostlund 1996; Helgaker et al. 2000; Sherrill 2010; Reine et al. 2012; Parrish et al. 2013; Tsuneda 2014). This is an extremely technical subject and we cannot consider here all the details of the calculations involved. Our purpose is to illustrate the use of quadratures based on the nonclassical Rys polynomials. This quadrature is employed in quantum chemistry computer codes including commercial products (Carsky and Polasek 1998; Lindh et al. 1991; Asadchev and Gordon 2012; Sandberg and Rinkevicius 2012). Further details are provided in Chap. 3.

The basis functions used in quantum chemistry are often constructed from Gaussians of the form,

$$\phi(\mathbf{r}) = x^{n_1} y^{n_2} z^{n_3} e^{-a\mathbf{r}^2}, \tag{2.170}$$

where x, y and z are the cartesian components of $\mathbf{r}$ measured from the position of a nucleus of an atom or molecule. The matrix elements of the Coulomb potential in the Hamiltonian for an atom or molecule are calculated for two such Gaussians, one for each electron at $\mathbf{r}_1$ and $\mathbf{r}_2$ and the electron repulsion integral is given by

$$\langle ij|\frac{1}{r_{12}}|k\ell\rangle = \int\int \phi_i(\mathbf{r}_1)\phi_j(\mathbf{r_1})\left(\frac{1}{r_{12}}\right)\phi_k(\mathbf{r}_2)\phi_\ell(\mathbf{r_2})d\mathbf{r}_1 d\mathbf{r}_2, \tag{2.171}$$

where $r_{12} = |\mathbf{r}_1 - \mathbf{r}_2|$ where the subscripts such as i on $\phi_i(\mathbf{r_1})$ is a shorthand for all the parameters that define the orbital. The main steps in the reduction of this six-dimensional integral involves writing the reciprocal of r_{12} as the integral,

$$\frac{1}{r_{12}} = \frac{2}{\sqrt{\pi}}\int_0^\infty e^{-(r_{12}t)^2} dt. \tag{2.172}$$

The product of two Gaussians is then written as a single Gaussian which is easily demonstrated by completing the square of the argument.

The change of variable

$$t^2 = \frac{x^2}{a + x^2}, \tag{2.173}$$

transforms the integration from $t \in (0, \infty)$ to $x \in [0, 1]$. After some considerable reductions, the electron repulsion integral, Eq. (2.171), is written in terms of sums of integrals of the form

$$I_L(c) = \int_0^1 f_L(x^2) e^{-cx^2} dx, \tag{2.174}$$

where $f_L(x^2)$ is a polynomial of degree $2L$ and an even function. The parameter c depends on the parameters of the Gaussian functions used and varies considerably from integral to integral. Further details of these calculations for Gaussian type orbitals in electronic structure calculations is presented in the book by Helgaker et al. (2000) and also in Chap. 3. The brief discussion here is to provide the reader with some background for the occurrence of integrals of the type in Eq. (2.174). In typical applications, a very large number of integrals, Eq. (2.171), are evaluated and thus the interest to reduce the computational cost.

In Sect. 2.2.2, we demonstrated the ill-conditioned Gram-Schmidt procedure with the construction of the full-range Rys polynomials, $J_n(x)$, defined on the interval $x \in [-1, 1]$. We here consider the half-range nonclassical polynomials, $R_n(x)$, with $x \in [0, 1]$ defined by the orthonormality

$$\int_0^1 e^{-cx^2} R_n(x) R_m(x) dx = \delta_{nm}, \tag{2.175}$$

The quadrature points associated with these polynomials do not coincide with the positive quadrature points and weights defined by the polynomials $J_n(x)$, Eq. (2.24).

The α_n and β_n recurrence coefficients are calculated with the Gautschi-Stieltjes procedure. The integrals, Eqs. (2.68) and (2.69), are evaluated by dividing the interval into many subintervals and evaluating the integral in each subinterval with a Fejér quadrature as suggested by Gautschi (1985, 1994). The MATLAB code ab_Rys.m can be used for this calculation. The quadrature points and weights are then calculated with the diagonalizaton of the Jacobi matrix, Eq. (2.71) (Golub and Welsch 1969). The quadrature based on either the full-range or half range Rys polynomials can be calculated with the same code by inputing either $x_{min} = -1$ or 0. For the full-range polynomials $\alpha_n = 0$ as discussed in Sect. 2.2.2 whereas these coefficients are finite for the half-range polynomials.

The variation of β_n versus n was shown in Fig. 2.1 for the full-range Rys polynomials. The variation of α_n and β_n for the half-range polynomials is shown in Fig. 2.8. The quadrature points and weights calculated with this code reproduces the values in Tables 1 and 2 in the work of Schneider and Nygaard (2002) for the full-range with $\alpha_n = 0$.

The results for $N = 40$ and $c = 0$, 10 and 20, agree to the eight significant figures with the results shown in Tables 1 and 2 in the paper by Schneider and Nygaard (2002). For $c = 10$ and $N = 26$, we calculate the weights and points in complete

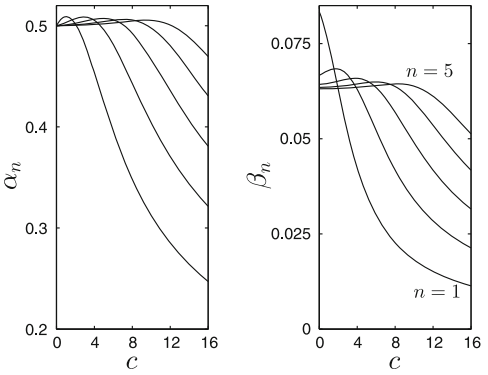

Fig. 2.8 Variation of α_n and β_n versus c for Rys polynomials $R_n(x)$ for $n = 1$ to 5, and $x \in [0, 1]$. Half-Range Legendre polynomials correspond to $c = 0$ and half-range Hermite polynomials for $c \to \infty$

agreement with the results reported by Sagar and Smith (1992) in their Table 4. The quadrature points defined by $J_{20}(x)$ in the interval [0, 1] shown in Fig. 2.9 and Table 2.19 do not coincide with the quadrature points in [0, 1] defined by $R_{10}(x)$. The integrand in Eq. (2.174) is even and consequently only the positive quadrature points associated with $J_n(x)$ for n even are used in the numerical evaluation of Eq. (2.174). The quadrature points for the full range quadrature are more densely distributed at $x \approx 1$ whereas the half range quadrature points are more densely distributed at $x \approx 0$. The weights for the two quadrature rules also differ as shown in the table. However, for $c = 0$, for which the Rys polynomials, $J_n(x, 0)$, are the Legendre polynomials, the quadrature points for the half-range (hr) Legendre polynomials, x_i^{hr}, defined on [0, 1] can be calculated from the full-range (fr) quadrature points, x_i^{fr}, on $[-1, 1]$ as given by the transformation of the intervals, that is $x_i^{hr} = (x_i^{fr} + 1)/2$. The half-range Legendre polynomials have found widespread application in the theory of radiative transfer which we discuss at greater length in Chap. 5. A comparison of the Rys quadrature rules is presented in Chap. 3.

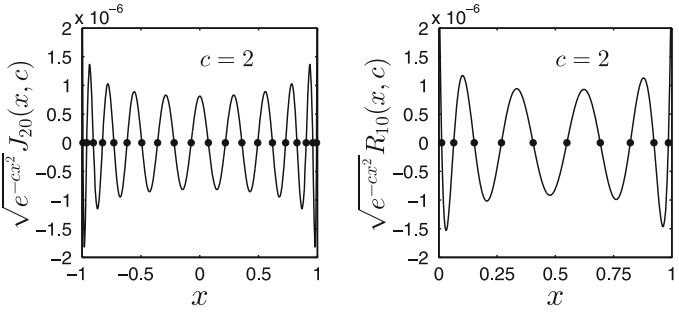

Fig. 2.9 Variation of the Rys polynomials $\sqrt{w(x)}J_{20}(x)$ on $[-1, 1]$ and $\sqrt{w(x)}R_{10}(x)$ on [0, 1]

Table 2.19 Quadrature points and weights for Rys polynomials; c = 2

n	Quadrature points		Quadrature weights	
	$J_{20}(x)$	$R_{10}(x)$	$J_{20}(x)$	$R_{10}(x)$
1	0.07299	0.01244	0.014421	0.031758
2	0.21768	0.06420	0.130255	0.070372
3	0.35851	0.15219	0.106726	0.099041
4	0.49278	0.26879	0.080009	0.110693
5	0.61759	0.40472	0.055537	0.102518
6	0.72991	0.54976	0.036182	0.079753
7	0.82656	0.69279	0.022376	0.052868
8	0.90436	0.82164	0.013126	0.030434
9	0.96042	0.92320	0.007009	0.015194
10	0.99241	0.98493	0.002709	0.005514

2.5.4 Additional Examples of Nonclassical Quadratures

In this section, we further demonstrate the efficient use of the Gautschi-Stieltjes procedure for the generation of quadratures based on nonclassical weight functions and we discuss several examples. Other examples are in the book by Gautschi (2004). The first is the weight function

$$w(x) = e^{-\frac{3}{2x}}, \qquad x \in [0, 1], \tag{2.176}$$

proposed by Gander and Karp (2001) for use in radiative transfer problems that we consider in Chap. 5. The authors report that the method of moments for the calculation of polynomial recurrence relations and quadrature points is numerically unstable as we have seen with the Gram-Schmidt orthogonalization. However, they also report that the Gautschi-Stieltjes procedure is unstable and show in Table 3 of their paper the errors they compute for the α_n and β_n recurrence coefficients presumably arising from numerical instabilities. Thus, they claim that these two classical methods for continuous measures fail and it is impossible to compute the Gauss quadrature.

Instead, they use MAPLE and the method proposed by Boley and Golub (1987) based on the discrete measures of the weight function to calculate accurate values of the recurrence coefficients reported in Table 2. However it is not clear why the Gautschi-Stieltjes procedure fails in contradiction to the code ab_rad_transf.m which provides the recurrence coefficients in agreement with the results in Table 2 of the paper by Gander and Karp (2001). The authors also report results with four other weight functions but specific applications to radiative transfer problems were not considered (Garcia 1999).

The evaluation of radial integrals that arise in the application of density functional theory in molecular electronic structure calculations is a very important endeavor (Gill and Chien 2003; El-Sherbiny and Poirier 2004). In Chap. 3, we present a comparison of several different quadratures that involve interval mappings and the use

of classical quadratures although Gill and Chien (2003) introduced a nonclassical weight function defined by

$$w(x) = \ln^2 x, \qquad x \in [0, 1]. \tag{2.177}$$

The recurrence coefficients for this weight function can be accurately calculated with the Gautschi-Stieltjes procedure. The quadrature points and weights are then determined from the diagonalization of the Jacobi matrix and are in agreement with the results provided at http://rsc.anu.edu.au/~pgill/multiexp.phpp2008.

The third example of a nonclassical weight function arises from the role of Kappa distributions (Maksimovic et al. 1997; Shizgal 2007) in space physics. We discuss the nonconvergence of the expansion of the Kappa distribution in Laguerre polynomials in Chap. 4 and the derivation of this distribution from a particular Fokker-Planck equation in Chap. 6.

Magnus and Pierrard (2008) discuss the calculation of the recurrence coefficients for the weight function

$$w(x) = \frac{|x|^A}{\left[1 + \left(\frac{x}{C}\right)^{2r}\right]^B}, \qquad x \in (-\infty, \infty), \tag{2.178}$$

which is a variant of the Kappa distribution

$$f_\kappa(x) = \frac{x^2}{(1 + \frac{x^2}{\kappa})^{\kappa+1}}, \qquad x \in [0, \infty), \tag{2.179}$$

and reduces to the Kappa distribution with $A = 2$, $B = \kappa + 1$, $C = \kappa$, $r = 1$ and the change of domain. The κ distribution tends to a Maxwellian for $\kappa \to \infty$. One feature of the Kappa distribution is that all the moments are not defined and in particular the temperature and normalization are not defined for $\kappa \leq 3/2$ and 1/2, respectively. Thus, it cannot be used as a weight function to define a set of nonclassical polynomials. Magnus and Pierrard (2008) consider the weight function, Eq. (2.178), and provide a number of recurrence relations for the β_n recurrence coefficients which all prove to be numerically unstable even for the particular values, $r = 1$ and 2. It is the very slow decay of these weight functions for $x \to \pm\infty$ analogous to the Kappa distribution that is responsible for these numerical instabilities. Of particular interest is that for the special case $B = C \to \infty$, the weight function, Eq. (2.178) reduces to $w(x) = |x|^A e^{-x^2}$ which defines the relativistic Hermite polynomials related to the Gegenbauer polynomials (Nagel 1994). Further work is required to develop new quadratures that may prove useful in space plasma physics.

In Sect. 2.7, we consider the Stieltjes moment method which is defined as the problem of recovering a weight function from a finite number of the moments. One such application is the work of Langhoff et al. (1976) which is directed towards the reconstruction of photoabsorption distributions from experimental measurements

of the moments. In order to benchmark their inversion procedure, they choose the distribution

$$w(x) = 1 - \frac{2}{\pi}\left[\frac{\sqrt{\frac{1}{x}-1}}{3}\left(2x^2 - 5x\right) + \tan^{-1}\left(\sqrt{\frac{1}{x}-1}\right)\right], \quad x \in [0,1], \tag{2.180}$$

and report recurrence coefficients

$$\begin{aligned} \alpha_n &= \frac{4n^2-3}{2(4n^2-1)}, \\ \beta_n &= \frac{(2n+3)(2n-1)}{[4(2n+1)]^2}. \end{aligned} \tag{2.181}$$

for the polynomials

$$q_n(x) = (x - \alpha_n)q_{n-1}(x) - \beta_{n-1}(x)q_{n-2}(x), \tag{2.182}$$

orthogonal with respect to $w(x)$, Eq. (2.180). The α_n and β_n coefficients define a Jacobi matrix and hence a set of quadrature weights and points. The reconstruction of the weight function can be done discretely from the quadrature points (Clarke and Shizgal 1993) as given by

$$w(\tilde{x}_i) = \frac{w_{i+1} + w_i}{2(x_{i+1} - x_i)} \tag{2.183}$$

where $\tilde{x}_i = (x_{i+1} - x_i)/2$. Langhoff et al. (1976) report the reconstruction of the weight function, Eq. (2.180), from the quadrature points and weights as shown in Fig. 1 of their paper.

2.6 Sinc Interpolation, Cubic B-Splines and Radial Basis Functions

In Sect. 2.3.1, we discussed the Lagrange interpolation and it forms the basis for the Newton-Cotes integration rules for a uniform grid as well as the nonuniform Gaussian quadratures based on orthogonal polynomials. As mentioned previously, and as we will discuss in Chap. 3, interpolation is the basic tool to define derivative operators in physical space and their application to the solution of partial differential equations. In this section, we present several alternate interpolation procedures that are also discussed in standard references (Press et al. 2007; Cheney and Kincaid 2008; Burden and Faires 2011).

2.6.1 Sinc Interpolation

Our main concern in this chapter is with the Lagrange interpolation of Sect. 2.3.1 and the nonuniformly distributed quadrature points that arise with orthogonal polynomials. Quite generally, spectral methods involve the use of Fourier or Chebyshev basis functions. We consider in this section Fourier basis functions discussed in greater detail in Chap. 4 and the corresponding quadrature.

We note that the roots of $\sin(y)$ are at $y_k = \pm k\pi$, $k = 0, 1, 2, \ldots$ We thus define $p(x) = \sin(\pi x)$ with an infinite number of uniformly distributed integer roots, $x_k = k$ for $k = 0, \pm 1, \pm 2, \ldots$, that is,

$$p(x) = \sin(\pi x) = \pi x \prod_{k=1}^{\infty} \left(1 - \frac{x^2}{k^2}\right), \qquad x \in (-\infty, \infty), \tag{2.184}$$

with roots at $x_k = k$ for $k = 0, \pm 1, \pm 2, \ldots$ Equation (2.184) is Item 1.431.1 in Gradshteyn and Ryzhik (2007). In terms of the polynomial $p(x)$, the Lagrange interpolant as in Eq. (2.31) is

$$\begin{aligned} \ell_k(x) &= \frac{p(x)}{(x - x_k)p'(x_k)}, \\ &= \frac{\sin(\pi x)}{\pi(x - x_k)}, \\ &= \operatorname{sinc}(x - x_k), \end{aligned} \tag{2.185}$$

where we have used $p'(x_k) = \pi \cos(\pi x_k) = \pi$, $\sin(\pi x_k) = \sin[\pi(x - x_k)]$ and the sinc function is defined by $\operatorname{sinc}(x) = \frac{\sin(\pi x)}{\pi x}$. The original work on sinc interpolation is due to Whittaker (1929a, 1927) and discussed in detail by Stenger (1993).

In view of the definition of the sinc function, we easily verify that $\ell_k(x)$ defined by Eq. (2.185) satisfies the cardinality condition, $\ell_k(x_j) = \delta_{kj}$ arising from the result that

$$\operatorname{sinc}(x_j - x_k) = \begin{cases} 1, & j = k, \\ 0, & j \neq k. \end{cases} \tag{2.186}$$

For $j \neq k$, $\sin[\pi(x_j - x_k)] = 0$, and for $j = k$, l'Hopital's rule is used. Thus we have the sinc-interpolation of some function of the form

$$f(x) = \sum_{k=-\infty}^{\infty} f(x_k)\operatorname{sinc}(x - x_k), \tag{2.187}$$

where the nodes are the integers, $x_k = k$, $k = 0, \pm 1, \pm 2, \ldots$ In this case, there are an infinite number of nodes along the real axis.

The variation of the sinc functions is shown in Fig. 2.10 with the same grid as used for the Lagrange interpolation in Fig. 2.2. The Lagrange interpolation based on

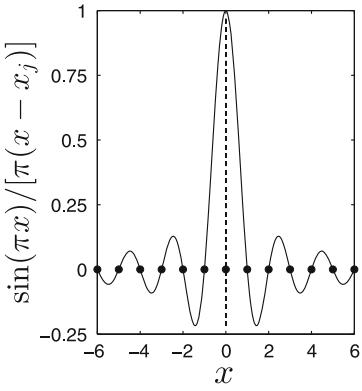

Fig. 2.10 Variation of the sinc function, $\mathrm{sinc}(x) = \sin(\pi x)/[\pi(x - x_j)]$, defined for 11 points [−6:1:6] and $x_j = 0$. The Lagrange interpolation on the same grid is shown in Fig. 2.2

polynomials discussed in Sect. 2.3.1 is usually a polynomial of degree N determined from $N + 1$ data. In both cases, the interpolant reproduces the given data exactly. For the sinc interpolation, the spacing between grid points does not have to be unity as assumed. If we define $y = xh$, the spacing between grid points in y is $y_{k+1} - y_k = h$. With this substitution we have that

$$f(y) = \sum_{k=-\infty}^{\infty} f(\frac{y_k}{h})\mathrm{sinc}(\frac{y - y_k}{h}). \tag{2.188}$$

It is clear that the formalism introduced for polynomials does not apply to this basis set of trigonometric functions. There is no three term recurrence relation and the quadrature rules employed previously do not apply in this case. The quadrature or grid points in this case are uniformly distributed and the weights are not specified. The weights are defined by any quadrature based on uniformly distributed grid points. Thus the trapezoidal or Simpson's rules or other Newton-Cotes algorithms can be used. There have been numerous applications of the sinc interpolation to the solution of the Fokker-Planck and Schrödinger equations (Colbert and Miller 1992; Wei 2000; Amore 2006) and Fishers equation (Wei 1999; Al-Khaled 2001; Zhao and Wei 2003; Olmos and Shizgal 2006). The sinc interpolation features prominently in digital signal processing (Blackledge 2006; Meijering et al. 1999; Meijering 2002).

2.6.2 Cubic B-Splines:

Our discussion of interpolation would not be complete without a comparison with cubic splines and B-Splines that are used in many applied problems. We return to the problem of interpolating within a table containing pairs of values $\{x_i, y_i \equiv f(x_i), \quad i = 1, \ldots, N\}$. We wish to determine the function value $y_k = f(x_k)$ for the independent variable at x_k. The Lagrange interpolation discussed in Sect. 2.3.1

is a global polynomial based method and may not be accurate for functions that vary rapidly in some small subinterval. We could divide the domain into unequal subdomains and use different Lagrange interpolants in each domain. However, the resulting interpolation can have discontinuous first and second derivatives at the subdomain boundaries.

We introduce the cubic polynomial, $S_i(x)$, in *each* subinterval (x_i, x_{i+1}) to interpolate the numerical values in the table. We impose the requirements that (1) the function values are returned exactly, that is $y_i = S(x_i)$, (2) the first derivative $y_i' \equiv df(x)/dx|_{x=x_i}$ is continuous at the interval boundaries and (3) the second derivative $y_i'' \equiv d^2 f(x)/dx^2|_{x=x_i}$ is also continuous. With this local fitting procedure, we anticipate an approximation to the function that will be smoother with fewer oscillations as compared with the Lagrange interpolation over the whole interval $[a, b]$. In the B spline literature (Prenter 1975), the grid points, $\{x_i\}$, are referred to as *knots*.

We consider representing $S_i(x)$ as a cubic in x but instead we begin by noting that the second derivative, $S_i''(x)$ is linear in x (Press et al. 2007). We thus consider a linear interpolation of the second derivative, that is,

$$S_i''(x) = y_i'' \frac{x - x_{i+1}}{x_i - x_{i+1}} + y_{i+1}'' \frac{x - x_i}{x_{i+1} - x_i}. \tag{2.189}$$

It is important to mention that the input data is strictly the table of values x_i and y_i and the second derivatives in Eq. (2.189) are not provided. We generate the desired cubic by integrating twice,

$$S_i(x) = \frac{y_i''}{6} \frac{(x - x_{i+1})^3}{(x_i - x_{i+1})} + A(x - x_i) + \frac{y_{i+1}''}{6} \frac{(x - x_i)^3}{(x_{i+1} - x_i)} + B(x - x_{i+1}). \tag{2.190}$$

The first requirement, (1), gives the two equations $y_i = S_i(x_i)$ and $y_{i+1} = S_i(x_{i+1})$. These two conditions give the values of the constants A and B in Eq. (2.190), that is,

$$\begin{aligned} A &= \frac{y_i}{x_{i+1} - x_i} - \frac{y_{i+1}''}{6}(x_{i+1} - x_i), \\ B &= \frac{y_i}{x_i - x_{i+1}} - \frac{y_i''}{6}(x_i - x_{i+1}). \end{aligned} \tag{2.191}$$

With the substitution of Eq. (2.191) in Eq. (2.190), we get the cubic equation

$$\begin{aligned} S_i(x) = \frac{y_i''}{6} \frac{(x - x_{i+1})^3}{(x_i - x_{i+1})} + \left[\frac{y_{i+1}}{x_{i+1} - x_i} - \frac{y_{i+1}''}{6}(x_{i+1} - x_i) \right] (x - x_i) \\ + \frac{y_{i+1}''}{6} \frac{(x - x_i)^3}{(x_{i+1} - x_i)} + \left[\frac{y_i}{x_i - x_{i+1}} - \frac{y_i''}{6}(x_i - x_{i+1}) \right] (x - x_{i+1}). \end{aligned} \tag{2.192}$$

As for the continuity of the first derivatives, we equate the first derivative as calculated for the interval (x_{i-1}, x_i) and the first derivative calculated for the interval (x_i, x_{i+1}),

both at the interval boundary $x = x_i$. With $S'_{i-1}(x)$ evaluated from Eq. (2.192) we find after some algebra that

$$S'_i(x_i) = (x_i - x_{i+1})\frac{y''_i}{3} - (x_{i+1} - x_i)\frac{y''_i}{6} + \frac{y_{i+1} - y_i}{x_{i+1} - x_i},$$
$$S'_{i-1}(x_i) = (x_i - x_{i-1})\frac{y''_i}{3} - (x_{i-1} - x_i)\frac{y''_{i-1}}{6} + \frac{y_i - y_{i-1}}{x_i - x_{i-1}}, \tag{2.193}$$

and by imposing continuity of the first derivative, $S'_i(x_i) = S'_{i-1}(x_i)$, we get

$$(x_i - x_{i-1})y''_{i-1} + 2(x_{i+1} - x_{i-1})y''_i + (x_{i+1} - x_i)y''_{i+1}$$
$$= 6\left[\frac{y_{i+1} - y_i}{x_{i+1} - x_i} - \frac{y_i - y_{i-1}}{x_i - x_{i-1}}\right]. \tag{2.194}$$

Equation (2.194) represents a tridiagonal matrix for the unknown second derivatives y''_i in terms of the input data, $\{x_i, y_i\}$, on the right hand side as well as the matrix elements in terms of the interval lengths $h_i = x_{i+1} - x_i$. The solution of this matrix equations gives y''_i and thus we have the cubic fit in each interval defined with Eq. (2.192).

However, since we have N points we have only specified continuity of the first and second derivatives at the $N - 2$ interior points and the conditions at the interval ends at x_1 and x_N have not been specified. If the second derivatives at these points are known, which is usually not the case, then these are simply added to the conditions at x_1 and x_N. There are several different choices that can be made in the absence of this information. One can set $y''_1 = y''_N = 0$ and then solve Eq. (2.194). This choice is referred to as a natural spline which in the absence of the required second derivative values is expedient but one must exercise caution.

2.6.3 B-Splines

Closely related to the use of cubic splines for the interpolation of data are the family of functions known as B-Splines defined locally and used in the solution of integral and differential equations in many different fields discussed at the end of this section. They are used as a non-orthogonal set of linearly independent basis functions of increasing degree over a finite interval. For the set of nodes at $x_i = i, i = 0, 1, 2, \ldots, k)$, the first member of the set of B-splines is

$$B^{(1)}(x) = \begin{cases} 1 & x \in [0, 1] \\ 0 & \text{otherwise.} \end{cases} \tag{2.195}$$

The second member of the set is the piecewise continuous linear function defined by

$$B^{(2)}(x) = \begin{cases} x & x \in [0,1] \\ 2-x & x \in [1,2] \\ 0 & \text{otherwise.} \end{cases} \tag{2.196}$$

The third member of degree 2 spans three intervals and is given by,

$$B^{(3)}(x) = \frac{1}{2}\begin{cases} x^2 & x \in [0,1] \\ -2x^2+6x-3 & x \in [1,2] \\ (3-x)^2 & x \in [2,3] \\ 0 & \text{otherwise,} \end{cases} \tag{2.197}$$

and is zero at $x = 0$ and $x = 3$. The polynomial in the interval $x \in [1, 2]$ can be determined by requiring continuity of the functions and the derivatives at $x = 1$ and 2. Alternatively, it can be evaluated with the recursion relation

$$B^{(k)}(x) = \frac{x}{k-1}B^{(k-1)}(x) + \frac{k-x}{k-1}B^{(k-1)}(x). \tag{2.198}$$

As for $k = 4$, the polynomials in the first and last intervals can be written down easily. With the use of the recursion relation, the polynomials in the remaining two intervals can be obtained and the B-Spline of order 4 is,

$$B^{(4)}(x) = \frac{1}{6}\begin{cases} x^3 & x \in [0,1] \\ -3x^3+12x^2-12x+4 & x \in [1,2] \\ 3x^3-24x^2+60x-44 & x \in [2,3] \\ (4-x)^3 & x \in [3,4] \\ 0 & \text{otherwise.} \end{cases} \tag{2.199}$$

This local function is defined by four uniformly spaced grid points over a finite interval. The grid spacing, h, has been set to unity and the B-spline spans four grid points. We show in Fig. 2.11 four such B-Splines by taking the fundamental spline in the interval $x \in [0, 4]$ and translating it by one grid spacing to the right three times.

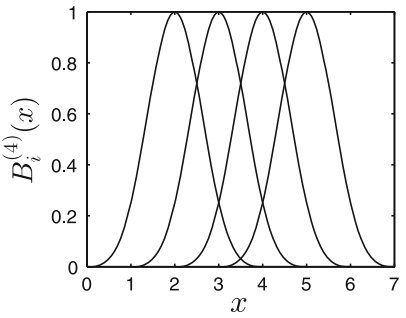

Fig. 2.11 Four B-spline functions of order 3 versus x measured in units of the grid spacing h

The B-Spline functions are local and not orthogonal and the integral over a pair of B-Spline functions defines an overlap matrix,

$$S_{ij} = \int_a^b B_i(x)B_j(x)dx. \tag{2.200}$$

As can be seen from Fig. 2.11, the overlap of a particular B-Spline function is with four other B-Spline functions two to the left and two to the right. The overlap matrix for B-Splines of order 4 is therefore pentadiagonal. A review of current work in atomic and molecular physics with B-Spline basis functions has been provided by Bachau et al. (2001). The application of B-Splines to the solution of the Schrödinger equation has been developed long ago (Shore 1973, 1975; O'Niel and Reinhardt 1978). There have also been several applications to kinetic theory and the study of electron transport in molecular gases (Pitchford et al. 1981), transport coefficients (Siewert 2002) and relaxation in hard sphere gases (Khurana and Thachuk 2012).

2.6.4 Radial Basis Functions

The developments in the previous sections, have been based largely on the Lagrange interpolation with polynomial basis functions in one dimension. A two dimensional application would involve the direct product of the two one dimensional spaces. For trigonometric basis functions, that is Fourier series discussed in greater detail in Chap. 5, the interpolation on the real line is in terms of the sinc function that we have discussed. Another type of interpolation that has important applications in many different areas is based on radial basis functions. It is important to mention that these are not orthogonal "basis functions".

A radial basis function, $\phi(r)$, depends on a one dimensional radial variable r. The radial variable measures the distance from some reference point $\mathbf{x}_0$ to $\mathbf{x}$, that is $r = \|\mathbf{x} - \mathbf{x}_0\| = \sqrt{x^2 - x_0^2}$, that is the Euclidean distance. Given the function $\phi(r)$, for which there are several choices as listed in Table 2.20, the basic interpolating radial basis function is

$$f_N(x) = \sum_{i=1}^{N} a_i \phi(r_i), \tag{2.201}$$

where $r_i = \|\mathbf{x} - \mathbf{x_i}\|$ and x_i are distinct positions. Given a set of data points for $f(x)$, that is $f_i = f(x_i)$, the expansion coefficients, a_i are determined such that $f_N(x_i) = f_i$, and are the solution of the matrix equation,

$$\sum_{j=1}^{N} A_{ij} a_j = f_i, \tag{2.202}$$

where $A_{ij} = \phi(\|\mathbf{x_j} - \mathbf{x_i}\|)$.

Table 2.20 Commonly used radial basis functions

Radial basis function	Name
$\phi(r) = r^3$	Cubic
$\phi(r) = r^5$	Quintic
$\phi(r) = r^3$	Cubic
$\phi(r) = \exp(-r^2)$	Gaussian
$\phi(r) = r^2 \log r$	Thin plate spline

The common forms of radial basis functions are in the table. An excellent discussion of radial basis functions is in the thesis by Sturgill (2009). A thorough discussion can be found in the book by Buhmann (2004). The technique is an interpolation analogous in some respects to splines and wavelets. Other useful discussions can be found in several recent research articles (Fornberg et al. 2002, 2004; Fasshauer and Zhang 2007) including interpolation for multidimensional problems (Sturgill 2009), resolution of the Runge phenomena (Boyd 2010) as well as the Gibbs phenomenon (Jung et al. 2011), comparison with finite difference differentiation (Boyd and Wang 2009) and quantum fluid dynamical equations (Hu et al. 2000, 2002). The applications of this interpolation technique include medical imaging, thermodynamics, quantum mechanics (Trahan and Wyatt 2003), engineering systems and fluid mechanics (Shu et al. 2003).

2.7 Moment Methods for Orthogonal Polynomials and the Stieltjes Moment Problem

In Sects. 2.2–2.2.2, we discussed the role of the moments of the weight function in the construction of orthogonal polynomials and the corresponding Gaussian quadratures. In this section, we reconsider this problem as there is a close connection between the classic moment problem (to be defined) and analogous work in chemical physics. The construction of orthogonal polynomials from the moments of the weight function will be contaminated with round-off errors.

The monic polynomial, $Q_n(x)$, is written as a series in the monomials, 1, $x, x^2, \ldots, x^n$, that is

$$Q_n(x) = \sum_{k=0}^{n} a_{nk} x^k, \tag{2.203}$$

where by definition $a_{nn} = 1$. Since x^m can be written in terms of the polynomials of order less than n, the scalar product with x^m with $m < n$ gives

$$\langle x^m | Q_n \rangle = \sum_{k=0}^{n} a_{nk} \mu_{m+k} = 0, \qquad m < n. \tag{2.204}$$

For the case $m = n$, Eq. (2.16) gives

$$x^n = Q_n(x) - \sum_{k=0}^{n-1} c_{n,k} P_k(x). \tag{2.205}$$

where $\langle P_k | P_n \rangle = \delta_{kn}$. We take the scalar product of Eq. (2.205) with $Q_n(x)$ and since $\langle Q_n | P_k \rangle = 0, k = 0, 1, \ldots, n-1$ we find that

$$\langle x^n | Q_n \rangle = \sum_{k=0}^{n} a_{nk} \mu_{n+k} = \gamma_n. \tag{2.206}$$

Equations (2.204) and (2.206) can be rewritten as the linear set of equations for the a_{nk} coefficients, that is,

$$\begin{pmatrix} \mu_0 & \mu_1 & \mu_2 & \cdots & \mu_n \\ \mu_1 & \mu_2 & \mu_3 & \cdots & \mu_{n+1} \\ \vdots & \vdots & \vdots & & \vdots \\ \mu_{n-1} & \mu_n & \mu_{n-1} & \cdots & \mu_{2n-1} \\ \mu_n & \mu_{n+1} & \mu_{n+2} & \cdots & \mu_{2n} \end{pmatrix} \begin{pmatrix} a_{n0} \\ a_{n1} \\ \vdots \\ a_{n,n-1} \\ a_{nn} \end{pmatrix} = \begin{pmatrix} 0 \\ 0 \\ \vdots \\ 0 \\ \gamma_n \end{pmatrix}. \tag{2.207}$$

Equation (2.207) cannot be used to determine the polynomials as the normalization γ_n is required. Rather we use this set of equations with a known value of γ_n to verify the value of the coefficient $a_{nn} = 1$ versus the size of the matrix. We study the solution of the moment equations, Eq. (2.207), versus the size of the matrix, the condition number and the value of a_{nn} in comparison with the exact value $a_{nn} = 1$. The results are shown in Table 2.21 for Legendre and Hermite polynomials.

It is clear that the condition numbers increase dramatically with increasing n and the solution of the matrix equation breaks down for $n \approx 10$ for Legendre polynomials and for $n \approx 15$ for Hermite polynomials with much larger condition numbers for the Hermite case. These results are anticipated from our earlier analyses and consistent with other similar discussions (Gautschi 2004).

In this chapter, we have focussed on the construction of a set of orthognonal polynomials and quadrature rules starting from a given weight function. We have used the numerical methods developed by Golub and Welsch (1969) and Gautschi (1985, 1996) based on the recurrence coefficients α_n and β_n in the three term recurrence relation, Eq. (2.14), and the diagonalization of the Jacobi matrix, Eq. (2.71). This approach is efficient and accurate as we have demonstrated for a large number of different classical and nonclassical weight functions.

However, inspite of the numerical instabilities involved in the construction of a polynomial basis set directly from the moments, mathematical theory of orthogonal polynomials has been based on moment theory and in particular the Stieltjes moment problem. This refers to the inverse problem of determining the weight function from a knowledge of the power moments $\mu_n = \int_a^b w(x) x^n dx$, which has a long history (Shohat and Tamarkin 1943; Akhiezer 1965; Chihara 1989).

Table 2.21 Condition number and solution of the moment equations, Eq. (2.207)

n	Legendre		Hermite	
	Condition number	a_{nn}	Condition number	a_{nn}
2	1.41×10^{1}	1.00000000	3.87	1.00000000
3	3.58×10^{2}	1.00000000	6.78×10^{1}	1.00000000
4	1.02×10^{4}	1.00000000	4.23×10^{3}	1.00000000
5	3.07×10^{5}	1.00000000	4.83×10^{5}	1.00000000
6	9.44×10^{6}	1.00000000	8.55×10^{7}	1.00000000
7	2.96×10^{8}	1.00000000	2.15×10^{10}	1.00000000
8	9.39×10^{9}	0.99999992	7.22×10^{12}	1.00000000
9	3.00×10^{11}	0.99999823	3.11×10^{15}	1.00000000
10	9.68×10^{12}	0.99997208	1.66×10^{18}	0.99999993
11	3.13×10^{14}	0.99882357	1.89×10^{20}	0.99999941
12	9.86×10^{15}	0.94434728	1.17×10^{23}	0.99999679
13	1.42×10^{17}	0.31755343	5.09×10^{25}	0.99999238
14	2.29×10^{17}	0.07350753	2.84×10^{27}	1.00004565
15	–	–	4.66×10^{31}	1.00055745
16	–	–	5.24×10^{32}	0.99822421
17	–	–	2.27×10^{35}	0.90941239
18	–	–	2.29×10^{38}	0.46249017
19	–	–	9.61×10^{39}	0.21464113
20	–	–	1.57×10^{43}	0.38678474

The main purpose for introducing the discussion here is the application to analogous problems in chemical physics (Gordon 1968; Wheeler 1974; Corcoran and Langhoff 1977; Reinhardt 1979). We will not cover this subject in great depth but it is important to point out the relationship of these separate workings on a common problem with different perspectives and objectives. An excellent overview with an historical list of references was provided by Müller-Plathe and Diercksen (1989).

The matrix defined by Eq. (2.207) is known as a Hankel matrix and the recursion coefficients can be written in terms of these matrices (Gautschi 2007; Golub and Meurant 2009). This approach leads, as might be anticipated, to algorithms that are fraught with round-off errors and are not of practical use. Consequently, alternate procedures based on the determination of the moments with other orthogonal polynomials, known as "modified moments" (Gautschi 1970; Sack and Donavan 1972; Wheeler 1974) that provide stable algorithms have been developed.

These methods have important applications in the determination of unknown weight functions or spectral densities from the power moments (Gordon 1968). This inversion of the moment problem has been applied to the determination of photoabsorption cross sections from limited moment spectral data (Langhoff et al. 1976; Corcoran and Langhoff 1977; Reinhardt 1979; Hermann and Langhoff 1983). One aspect of these works is that the authors are considering quantum problems involving emission and/or absorption of a free electron and thus the continuum spectrum of the

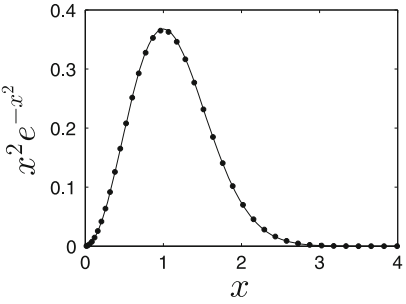

Fig. 2.12 Reconstruction of the Maxwell weight function, $w(x) = x^2 e^{-x^2}$ shown as the *solid curve* from the quadrature points and weights, $w(x_i) = (w_{i+1} + w_i)/[2(x_{i+1} - x_i)]$ shown as the *filled circles*

Hamiltonian for the system is studied. The associated eigenproblems are solved by the expansion of the eigenfunctions in a finite basis set and the continuum eigenfunctions cannot be treated rigorously as we will discuss for the Boltzmann, Fokker-Planck and the Schrödinger equations in Chaps. 5 and 6.

Of particular interest is the reconstruction of the weight function from a knowledge of the moments of the weight function or equivalently the recursion coefficients in the three term recurrence relation (Langhoff et al. 1976). To illustrate this process, we choose the recurrence coefficients for the Maxwell polynomials and the discrete form of the weight function, that is

$$w(\tilde{x}_i) = \frac{w_{i+1} + w_i}{2(x_{i+1} - x_i)}. \tag{2.208}$$

where $\tilde{x}_i = (x_i + x_{i+1})/2$. The solid curve in Fig. 2.12 is $w(x) = x^2 e^{-x^2}$ and the filled circles are calculated with Eq. (2.208).

2.8 Two Dimensional Integrals and Cubatures

The calculation of two dimensional integrals of the type

$$I_{2D} = \int_a^b \int_c^d f(x, y) dx dy, \tag{2.209}$$

can be estimated with a direct product of the two spaces, that is we use two grids $\{x_i\}$ and $\{y_i\}$ and estimate the integral as the double quadrature sum

$$I_{2D}^{(N_1,N_2)} = \sum_{i=1}^{N_1} \sum_{j=1}^{N_2} w_i w_j f(x_i, y_j), \tag{2.210}$$

which involves $N_1 \times N_2$ function evaluations and the computational cost of the algorithm can be high, especially if we extend this direct product to more that two

dimensions. The integral in Eq. (2.209) is over the square in the $x-y$ plane defined by the points (a, c), (b, c), (b, d) and (a, d). Obviously, if $f(x, y)$ factors into separate functions of x and y, the integral reduces to the product of two one-dimensional integrals. Occasionally, a suitable variable change accomplishes this factorization.

A more efficient algorithm for a two-dimensional integral involves a single summation of the form

$$\iint_A f(x, y)dxdy \approx \sum_{i-1}^{N} w_i f(x_i, y_i), \tag{2.211}$$

where A is the area in the $x - y$ plane analogous to the rectangle in the example in Eq. (2.209) and (x_i, y_i) are the coordinates of a point in the area A. Quadrature formulas of this form are referred to as "cubatures" (Cools 2002, 2003) whereas for a one-dimensional integral the numerical approximation is a quadrature. If a Simpson's rule or a Gaussian quadrature is used for each dimension in Eq. (2.212), the quadrature points are well defined and the weights can be deduced in terms of products of the weights in each dimension (Burden and Faires 2011). The analogue cubature in three dimensions is a rule of the form

$$\int_V \iint f(x, y, z)dxdydz \approx \sum_{i-1}^{N} w_i f(x_i, y_i, z_i). \tag{2.212}$$

The literature on this subject is extensive and was begun long ago by Clerk-Maxwell (1877) as noted by Hammer and Wymore (1957) and Hammer and Stroud (1958). These two older references provide a useful discussion of the construction of these quadrature rules. Cools (1997) has provided a very readable review of the origin of cubature formulae and also provides some elementary examples originally presented by Stroud (1971).

There are many applications of cubatures including spectral element methods in fluid mechanics (Pasquetti and Rapetti 2004), the computation of the solid angle integrations for radial integrals in the theory of molecular electronic structure (Lebedev 1977; Haxton 2007), density functional theory (El-Sherbiny and Poirier 2004), and with a finite difference discretization of the non-linear Boltzmann equation (Kabin and Shizgal 2003; Sospedra-Alfonso and Shizgal 2012b). For the solution of the vibrational Schödinger equation (Avila and Carrington Jr. 2009; Avila and Carrington 2013; Lauvergnat and Nauts 2014), a Smolyak algorithm similar to cubature quadratures is used to reduce the dimensionality of the direct product basis sets.

References

Abramowitz, M., Stegun, I.A.: Handbook of Mathematical Functions with Formulas, Graphs, and Mathematical Tables. U.S. Government Printing Office, Washington (1964)
Akhiezer, N.I.: The Classical Moment Problem. Oliver and Boyd, London (1965)
Al-Gwaiz, M.A.: Sturm-Liouville Theory and Its Applications. Springer, Berlin (2008)

Al-Khaled, K.: Numerical study of Fisher's reaction-diffusion equation by the Sinc collocation method. J. Comput. Appl. Math. **137**, 245–255 (2001)
Alp, Y.K., Arikan, O.: Time-frequency analysis of signals using support adaptive Hermite-Gaussian expansions. Digit. Signal Process. **22**, 1010–1023 (2012)
Amore, P.: A variational Sinc collocation method for strong-coupling problems. J. Phys. A: Math. Gen. **39**, L349–L355 (2006)
Andersen, K., Shuler, K.E.: On the relaxation of a hard sphere Rayleigh and Lorentz gas. J. Chem. Phys. **40**, 633–650 (1964)
Asadchev, A., Gordon, M.S.: Mixed-precision evaluation of two-electron integrals by Rys quadrature. Comput. Phys. Commun. **183**, 1563–1567 (2012)
Avila, G., Carrington Jr, T.: Nonproduct quadrature grids for solving the Schrödinger equation. J. Chem. Phys. **131**, 174103 (2009)
Avila, G., Carrington Jr, T.: Solving the Schrödinger equation using Smolyak interpolants. J. Chem. Phys. **139**, 134114 (2013)
Bachau, H., Cormier, E., Decleva, P., Hansen, J.E., Martin, F.: Application of B-splines in atomic and molecular physics. Rep. Prog. Phys. **64**, 1815–1942 (2001)
Ball, J.S.: Half-range generalized Hermite polynomials and the related Gaussian quadratures. SIAM J. Numer. Anal. **40**, 2311–2317 (2003)
Baltz, R.V.: Ein funktionensystem für zeit-und energieabhängige thermalisierungsprobleme. Atomkernergie (ATKE) **14–33**, 179–181 (1969)
Baye, D.: Lagrange-mesh method for quantum-mechanical problems. Phys. Stat. Sol. B **243**, 1095–1109 (2006)
Baye, D., Heenen, P.H.: Generalized meshes for quantum-mechanical problems. J. Phys. A: Math. Gen. **19**, 2041–2059 (1986)
Baye, D., Vincke, V.: Lagrange meshes from nonclassical orthogonal polynomials. Phys. Rev. E **59**, 7195–7199 (1999)
Becke, A.D.: A multicenter numerical integration scheme for polyatomic molecules. J. Chem. Phys. **88**, 2547–2553 (1988)
Beebe, N.H.F., Ball, J.S.: Algorithm 867: QUADLOG-A package of routines for generating Gauss—related quadrature for two classes of logarithmic weight functions. ACM. Trans. Math. Softw. **33**, 1–30 (2007)
Bird, G.A.: Molecular Gas Dynamics and the Direct Simulation of Gas Flows. Clarendon, Oxford (1994)
Birdsall, C.K., Langdon, A.B.: Plasma Physics via Computer Simulation. McGraw-Hill, New York (1984)
Blackledge, J.M.: Digital Signal Processing: Mathematical and Computational Methods, Software Development and Applications. Woodhead, Chichester (2006)
Blackmore, R., Shizgal, B.: Discrete ordinate method of solution of Fokker-Planck equations with nonlinear coefficients. Phys. Rev. A **31**, 1855–1868 (1985a)
Blackmore, R., Shizgal, B.: A solution of Kramers equation for the isomerization of n-butane in CCl_4. J. Chem. Phys. **83**, 2934–2941 (1985b)
Blackmore, R., Weinert, U., Shizgal, B.: Discrete ordinate solution of a Fokker-Planck equation in laser physics. Trans. Theory Stat. Phys. **15**, 181–210 (1986)
Boley, D., Golub, G.H.: A survey of matrix inverse eigenvalue problems. Inverse Probl. **3**, 595–622 (1987)
Bonifacio, R., Gronchi, M., Lugiato, L.A.: Photon statistics of a bistable absorber. Phys. Rev. A **18**, 2266–2279 (1978)
Borromeo, M., Marchesoni, F.: Asymmetric probability densities in symmetrically modulated bistable devices. Phys. Rev. E **71**, 031105 (2005)
Boyd, J.P.: Chebyshev and Fourier Spectral Methods. Dover, New York (2001)
Boyd, J.P.: Six strategies for defeating the Runge phenomenon in Gaussian radial basis functions on a finite interval. Comput. Math. Appl. **60**, 3108–3122 (2010)

Boyd, J.P., Wang, L.: Truncated Gaussian RBF differences are always inferior to finite-differences of the same stencil width. Commun. Comput. Phys. **5**, 42–60 (2009)
Buhmann, R.D.: Radial Basis Functions. Cambridge University Press, Cambridge (2004)
Burden, R.L., Faires, J.D.: Numerical Analysis, 9th edn. Brooks/Cole, Boston (2011)
Byrd, P.F., Galant, D.C.: Gauss Quadrature Rules Involving Some Nonclassical Weight Functions. Technical Report TN D-5785, NASA, 1–42 (1970)
Calabrò, F., Esposito, A.C.: An evaluation of Clenshaw-Curtis quadrature rule for integration w.r.t. singular measures. J. Comput. Appl. Math. **229**, 120–128 (2009)
Canuto, C., Hussaini, M.Y., Quarteroni, A., Zang, T.A.: Spectral Methods: Fundamentals in Single Domains. Springer, New York (2006)
Carlson, B.G.: Solution of the Transport Equation by S_N Approximation. Technical Report LA-1891, Los Alamos Scientific Laboratory (1953)
Carsky, P., Polasek, M.: Evaluation of molecular integrals in a mixed Gaussian and plane-wave basis by Rys quadrature. J. Comput. Phys. **143**, 266–277 (1998)
Chandrasekhar, S.: Radiative Transfer. Dover, New York (1960)
Chapman, S., Cowling, T.G.: The Mathematical Theory of Nonuniform Gases. Cambridge University Press, Cambridge (1970)
Chen, H., Shizgal, B.D.: The quadrature discretization method (QDM) in the solution of the Schrödinger equation. J. Math. Chem. **24**, 321–343 (1998)
Chen, H., Shizgal, B.D.: A spectral solution of the Sturm-Liouville equation: comparison of classical and nonclassical basis sets. J. Comput. Appl. Math. **136**, 17–35 (2001)
Chen, H.L., Su, Y.H., Shizgal, B.D.: A direct spectral collocation Poisson solver in polar and cylindrical coordinates. J. Comput. Phys. **160**, 453–469 (2000)
Cheney, W., Kincaid, D.: Numerical Methods and Computing, 6th edn. Brooks/Cole Publishing Company, Pacific Grove (2008)
Chien, S.-H., Gill, P.M.W.: SG-0: a small standard grid for DFT quadrature on large systems. J. Comput. Chem. **27**, 730–739 (2006)
Chihara, T.S.: Hamburger moment problems and orthogonal polynomials. Trans. Am. Math. Soc. **315**, 189–293 (1989)
Clarke, A.S., Shizgal, B.D.: On the generation of orthogonal polynomials using asymptotic methods for recurrence coefficients. J. Comput. Phys. **104**, 140–149 (1993)
Clenshaw, C., Curtis, A.R.: A method for the numerical integration on an automatic computer. Numer. Math. **2**, 197–205 (1960)
Clerk-Maxwell, J.: On approximate multiple integration between limits of summation. Camb. Philos. Soc. Proc. **3**, 39–47 (1877)
Cohen, J.S.: Rapid accurate calculation of JWKB phase-shifts. J. Chem. Phys. **68**, 1841–1843 (1978)
Colbert, D.T., Miller, W.H.: A novel discrete variable representation for quantum-mechanical reactive scattering via the S-Matrix Kohn method. J. Chem. Phys. **96**, 1982–1991 (1992)
Comtet, A., Bandrauk, A.D., Campbell, D.K.: Exactness of semiclassical bound-state energies for supersymmetric quantum-mechanics. Phys. Lett. B **150**, 159–162 (1985)
Concus, P., Cassatt, D., Jaehnig, G., Melby, E.: Tables for the evaluation of $\int_0^\infty x^\alpha e^{-x} f(x)dx$ by Gauss-Laguerre quadrature. Math. Comput. **17**, 245–256 (1963)
Cools, R.: Constructing cubature formulae: the science behind the art. Acta Numer. **6**, 1–54 (1997)
Cools, R.: Advances in multidimensional integration. J. Comput. Appl. Math. **149**, 1–12 (2002)
Cools, R.: An encyclopaedia of cubature formulas. J. Complex. **19**, 445–453 (2003)
Cooper, F., Khare, A., Sukhatme, U.: Supersymmetry and quantum mechanics. Phys. Rep. **251**, 267–385 (1995)
Corcoran, C.T., Langhoff, P.W.: Moment-theory approximations for nonnegative spectral densities. J. Math. Phys. **18**, 651–657 (1977)
Davis, P.J.: Interpolation and Approximation. Blaisdell, London (1963)
Davis, P.J., Rabinowitz, P.: Methods of Numerical Integration. Academic Press, New York (1975)
Desai, R.C.: Non-Gaussian corrections to Van Hove's $G_s(r, t)$ for a monatomic gas. J. Chem. Phys. **44**, 77–86 (1966)

Desai, R.C., Nelkin, M.: Atomic motions in a rigid sphere gas as a problem in neutron transport. Nucl. Sci. Eng. **24**, 142–152 (1966)
Dupuis, M., Marquez, A.: The Rys quadrature revisited: a novel formulation for the efficient computation of electron repulsion integrals over Gaussian functions. J. Chem. Phys. **114**, 2067–2078 (2001)
Dupuis, M., Rys, J., King, H.F.: Evaluation of molecular integrals over Gaussian basis functions. J. Chem. Phys. **65**, 111–116 (1976)
Dutt, R., Khare, A., Sukhatme, U.P.: Supersymmetry, shape invariance and exactly solvable potentials. Am. J. Phys. **56**, 163–168 (1988)
El-Sherbiny, A., Poirier, R.A.: An evaluation of the radial part of the numerical integration commonly used in DFT. J. Comput. Chem. **25**, 1378–1384 (2004)
Fasshauer, G.E., Zhang, J.G.: On choosing optimal shape parameters for RBF approximation. Numer. Algorithms **45**, 345–368 (2007)
Ferziger, J.H., Kaper, H.G.: Mathematical Theory of Transport Processes in Gases. North-Holland Publisher, Amsterdam (1972)
Fornberg, B., Driscoll, T.A., Wright, G., Charles, R.: Observations on the behavior of radial basis function approximations near boundaries. Comput. Math. Appl. **43**, 473–490 (2002)
Fornberg, G., Wright, G., Larsson, E.: Some observations regarding interpolants in the limit of flat radial basis functions. Comput. Math. Appl. **47**, 37–55 (2004)
Galant, D.: Gauss quadrature rules for the evaluation of $(2/\sqrt{\pi}) \int_0^\infty \exp(-x^2) f(x)dx$. Math. Comput. **23**, 674 (1969)
Gammaitoni, L., Hänggi, P., Jung, P., Marchesoni, F.: Stochastic resonance. Rev. Mod. Phys. **70**, 223–287 (1998)
Gander, M.J., Karp, A.H.: Stable computation of high order Gauss quadrature rules using discretization for measures in radiation transfer. JQRST **68**, 213–223 (2001)
Garashchuk, S., Light, J.C.: Quasirandom distributed Gaussian bases for bound problems. J. Chem. Phys. **114**, 3929–3939 (2001)
Garcia, R.D.M., Siewert, C.E.: A stable shifted-Legendre projection scheme for generating P_N boundary conditions. Am. Nucl. Energy **23**, 321–332 (1996)
Garcia, R.D.M.: The application of non-classical orthogonal polynomials in particle transport theory. Prog. Nucl. Energy **35**, 249–273 (1999)
Garcia, R.D.M., Ono, S.: Improved discrete ordinate calculations for an approximate model of neutral particle transport in ducts. Nucl. Sci. Eng. **133**, 40–54 (1999)
Garcia, G.A., Nahon, L., Powis, I.: Two-dimensional charged particle image inversion using polar basis function expansion. Rev. Sci. Instrum. **75**, 4989–4996 (2004)
Garg, D., Patterson, M.A., Hager, W.W., Rao, A.V., Benson, D., Huntingdon, G.T.: An overview of three pseudospectral methods for the numerical solution of the optimal control problems. Astrodynamics **135**, 475–487 (2009)
Gauss, C.F.: Methodus nova integralium valores per approximationem inveniendi. Comment. Soc. Reg. Scient. Gotting. Recent. **3**, 39–76 (1814)
Gautschi, W.: On the construction of Gaussain quadrature rules from modified moments. Math. Comput. **24**, 245–260 (1970)
Gautschi, W.: A survey of Gauss-Christoffel quadrature formulae. In: Butzer, P.L., Fehér, F. (eds.) E. B. Christoffel, pp. 72–147. Birkhaüser Verlag, Basel (1981)
Gautschi, W.: Discrete approximations to spherically symmetric distributions. Numer. Math. **44**, 53–60 (1984)
Gautschi, W.: Orthogonal polynomials-constructive theory and applications. J. Comput. Appl. Math. **12**, 61–76 (1985)
Gautschi, W.: On the computation of generalized Fermi-Dirac and Bose-Einstein integrals. Comput. Phys. Commun. **74**, 233–238 (1993)
Gautschi, W.: Algorithm 726: ORTHOPOL—a package of routines for generating orthogonal polynomials with Gauss-type quadrature rules. ACM Trans. Math. Softw. **20**, 21–62 (1994)

Gautschi, W.: Orthogonal polynomials: applications and computation. Acta Numerica **5**, 45–119 (1996)
Gautschi, W.: Gauss-Radau formulae for Jacobi and Laguerre weight functions. Math. Comput. Simulat. **54**, 403–412 (2000)
Gautschi, W.: Orthogonal Polynomials Computation and Approximation. Oxford University Press, Oxford (2004)
Gautschi, W.: A guided tour through my bibliography. Numer. Algorithms **45**, 11–35 (2007)
Gautschi, W.: Variable-precision recurrence coefficients for nonstandard orthogonal polynomials. Numer. Algorithms **52**, 409–418 (2009)
Gautschi, W.: Numerical Analysis, 2nd edn. Birkhäuser, New York (2011)
Gentleman, W.M.: Implementing Clenshaw-Curtis quadrature. I Methodology and experience. Commun. ACM **15**, 337–342 (1972)
Ghiroldi, G.P., Gibelli, L.: A direct method for the Boltzmann equation based on a pseudo-spectral velocity space discretization. J. Comput. Phys. **258**, 568–584 (2014)
Gibelli, L.: Velocity slip coefficients based on the hard-sphere Boltzmann equation. Phys. Fluids **24**, 022001 (2012)
Gibelli, L., Shizgal, B.D., Yau, A.W.: Ion energization by wave-particle interactions: comparison of spectral and particle simulation solutions of the Vlasov equation. J. Comput. Phys. **59**, 2566–2581 (2010)
Gil, A., Segura, J., Temme, N.M.: Numerical Methods for Special Functions. SIAM, Philadelphia (2007)
Gill, P.M.W., Chien, S.-H.: Radial quadrature for multiexponential integrands. J. Comput. Chem. **24**, 732–740 (2003)
Golub, G.H.: Some modified matrix eigenvalue problems. SIAM Rev. **15**, 318–334 (1973)
Golub, G.H., Welsch, J.H.: Calculation of Gauss quadrature rules. Math. Comput. **23**, 221–230 (1969)
Golub, G.H., Meurant, G.: Matrices, Moments and Quadrature with Applications. Princeton University Press, Princeton (2009)
Gordon, R.G.: Error bounds in equilibrium statistical mechanics. J. Math. Phys. **9**, 655–663 (1968)
Gottlieb, D., Orszag, S.: Numerical Analysis of Spectral Methods: Theory and Applications. SIAM, Philadelphia (1977)
Gottlieb, D., Shu, C.-W.: On the Gibbs phenomenon and its resolution. SIAM Rev. **39**, 644–668 (1997)
Grad, H.: On the kinetic theory of rarefied gases. Commun. Pure Appl. Math. **2**, 331–407 (1949)
Grad, H.: Principles of the kinetic theory. Handbook of Physics, pp. 205–294. Springer, Berlin (1958)
Gradshteyn, I.S., Ryzhik, I.M.: Tables of Integrals, Series and Products. Elsevier, Amsterdam (2007)
Graur, I.A., Polikarpov, A.P.: Comparison of different kinetic models for the heat transfer problems. Heat Mass Transf. **46**, 237–244 (2009)
Gross, E.P., Jackson, E.A., Ziering, S.: Boundary value problems in kinetic theory of gases. Ann. Phys. **1**, 141–167 (1957)
Gross, E.P., Ziering, S.: Kinetic theory of linear shear flow. Phys. Fluids **1**, 215–224 (1958)
Hammer, P.C., Wymore, A.W.: Numerical evaluation of multiple integrals I. Math. Comput. **11**, 59–67 (1957)
Hammer, P.C., Stroud, A.H.: Numerical evaluation of multiple integrals II. Math. Comput. **12**, 272–280 (1958)
Hänggi, P., Talkner, P., Borkovec, M.: Reaction rate theory: fifty years after Kramers. Rev. Mod. Phys. **62**, 251–341 (1990)
Haxton, D.J.: Lebedev discrete variable representation. J. Phys. B: At. Mol. Opt. Phys. **40**, 4443–4451 (2007)
Helgaker, T., Jorgensen, P., Olsen, J.: Molecular Electronic Structure Theory. Wiley, New York (2000)

Herman, A.L., Conway, B.A.: Direct optimization using collocation based on high-order Gauss-Lobatto quadrature rules. J. Guid. Control Dyn. **19**, 592–599 (1996)
Hermann, M.R., Langhoff, P.W.: Explicit Hilbert space representation of Schrödinger states: definitions and properties of Stieltjes-Tchebycheff orbitals. J. Math. Phys. **24**, 541–547 (1983)
Hesthaven, J.S.: Integration preconditioning of pseudospectral operators. I. Basic linear operators. SIAM J. Numer. Anal. **35**, 1571–1593 (1998)
Hu, X.G., Ho, T.S., Rabitz, H., Askar, A.: Solution of the quantum fluid dynamical equations with radial basis function interpolation. Phys. Rev. E **61**, 5967–5976 (2000)
Hu, X.G., Ho, T.S., Rabitz, H., Askar, A.: Multivariate radial basis interpolation for solving quantum fluid dynamical equations. Comput. Math. Appl. **43**, 525–537 (2002)
Huang, A.B., Giddens, D.P.: A new table for a modified (half-range) Gauss-Hermite quadrature with an evaluation of integral. J. Math. Phys. **47**, 213–218 (1968)
Jung, J.-H., Gottlieb, S., Kim, S.O.: Iterative adaptive RBF methods for detection of edges in two-dimensional functions. Appl. Numer. Math. **61**, 77–91 (2011)
Kabin, K., Shizgal, B.D.: Exact evaluation of collision integrals for the nonlinear Boltzmann equation. AIP Conf. Proc. **663**, 35–42 (2003)
Karabulut, H., Kalay, M.: Distributed Gaussian discrete variable representation. J. Quant. Chem. **104**, 16–28 (2005)
Karplus, M., Porter, R.N.: Atoms and Molecules: An Introduction for Students of Physical Chemistry. Benjamin, New York (1970)
Kennedy, M., Smith, F.J.: The efficient computation of JWKB phase shifts. Mol. Phys. **13**, 443–448 (1967)
Khurana, S., Thachuk, M.: A numerical solution of the linear Boltzmann equation using cubic B-splines. J. Chem. Phys. **136**, 094103 (2012)
King, H.F., Dupuis, M.: Numerical integration using Rys polynomials. J. Comput. Phys. **21**, 144–165 (1976)
Kopriva, D.A.: Implementing Spectral Methods for Partial Differential Equations Algorithms for Scientists and Engineers. Springer, Berlin (2009)
Kremer, G.M.: An Introduction to the Boltzmann Equation and Transport Processes in Gases. Springer, New York (2010)
Kythe, P.K., Schaferkotter, M.R.: Handbook of Computational Methods for Integration. Chapman and Hall/CRC, London (2004)
Langhoff, P.W., Corcoran, C.T., Sims, J.S., Weinhold, F., Glover, R.M.: Moment-theory of photoabsorption and dispersion profiles in atoms and ions. Phys. Rev. A **14**, 1042–1056 (1976)
Lathrop, K.D.: The early days of the S_N method. Am. Nucl. Soc. Trans. **66**, 241–242 (1992)
Lauvergnat, D., Nauts, A.: Quantum dynamics with sparse grids: a combination of Smolyak scheme and cubature. Application to methanol in full dimensionality. Spectrochim. Acta. Part A **119**, 18–25 (2014)
Lebedev, V.I.: Spherical quadrature formulas exact to orders 25–29. Sib. Math. J. **18**, 132–142 (1977)
Levine, I.N.: Quantum Chemistry, 6th edn. Prentice Hall, New Jersey (2009)
Li, Z.-H., Zhang, H.-X.: Gas-kinetic numerical studies of three-dimensional complex flows on spacecraft re-entry. J. Comput. Phys. **228**, 1116–1138 (2009)
Liboff, R.L.: Introductory Quantum Mechanics, 4th edn. Addison-Wesley, New York (2002)
Liboff, R.L.: Kinetic Theory: Classical, Quantum, and Relativistic Descriptions, 3rd edn. Springer, New York (2003)
Light, J.C., Carrington Jr, T.: Discrete variable representations and their utilization. Adv. Chem. Phys. **114**, 263–310 (2000)
Lindenfeld, M.J., Shizgal, B.: The Milne problem: a study of the mass dependence. Phys. Rev. **A27**, 1657–1670 (1983)
Lindh, U., Ryu, U., Liu, B.: The reduced multiplication scheme of the Rys quadrature and new recurrence relations for auxiliary function based two-electron integral evaluation. J. Chem. Phys. **95**, 5889–5897 (1991)

Lindh, R., Malmqvist, P.A., Gagliardi, L.: Molecular integrals by numerical quadrature. I. Radial integrals. Theor. Chem. Acta **106**, 178–187 (2001)
Lo, J.Q.-W., Shizgal, B.D.: Spectral convergence of the quadrature discretization method in the solution of the Schrödinger and Fokker-Planck equations: comparison with Sinc methods. J. Chem. Phys. **125**, 194108 (2006)
Lo, J.Q.-W., Shizgal, B.D.: An efficient mapped pseudospectral method for weakly bound states: vibrational states of He_2, Ne_2, Ar_2 and Cs_2. J. Phys. B: At. Mol. Opt. Phys. **41**, 185103 (2008)
Magnus, A.P., Pierrard, V.: Formulas for the recurrence coefficients of orthogonal polynomials related to Lorentzian-like weights. J. Comput. Appl. Math. **219**, 431–440 (2008)
Maksimovic, M., Pierrard, V., Lemaire, J.: A kinetic model of the solar wind with Kappa distributions in the corona. Astron. Astrophys. **324**, 725–734 (1997)
Mason, E.A., McDaniel, E.W.: Transport Properties of Ions in Gases. Wiley, New York (1988)
Matsuyama, H., Koga, T.: Inner and outer radial density functions in singly-excited $1sn\ell$ states of the He atom. J. Comp. Appl. Math. **233**, 1584–1589 (2010)
McMahon, D.R.A., Shizgal, B.: Hot-electron zero-field mobility and diffusion in rare-gas moderators. Phys. Rev. A **31**, 1894–1905 (1985)
Meijering, E.H.W., Niessen, W.J., Viergever, M.A.: The Sinc-approximating kernels of classical polynomial interpolation. IEEE Int. Conf. Image Process. **3**, 652–656 (1999)
Meijering, E.: A chronology of interpolation: from ancient astronomy to modern signal and image processing. Proc. IEEE **90**, 319–342 (2002)
Mitani, M.: An application of double exponential formula to radial quadrature grid in density functional calculation. Theor. Chem. Acc. **130**, 645–669 (2011)
Montgomery, J.A., Chandler, D., Berne, B.J.: Trajectory analysis of a kinetic theory for isomerization dynamics in condensed phases. J. Chem. Phys. **70**, 4056–4066 (1979)
Müller-Plathe, F., Diercksen, G.H.F.: Molecular photoionization cross sections by moment theory. An introduction. In: Canuto, S., Castro, J.D., Paixao, F.J. (eds.) Electronic Structure of Atoms and Molecules, pp. 1–29. World Scientific, Singapore (1989)
Nagel, B.: The relativistic Hermite polynomial is a Gegenbauer polynomial. J. Math. Phys. **35**, 1549–1554 (1994)
Nicolis, C.: Stochastic aspects of climatic transitions—response to a periodic forcing. Tellus **34**, 1–9 (1982)
Nicolis, C., Nicolis, G.: Stochastic aspects of climatic transitions—additive fluctuations. Tellus **33**, 225–234 (1981)
North, G.R.: Theory of energy-balance climate models. J. Atmos. Sci. **32**, 2033–2043 (1975)
ÓHara, H., Smith, F.J.: Error estimation in the Clenshaw-Curtis quadrature formula. Comput. J. **11**, 213–219 (1968)
Olmos, D., Shizgal, B.D.: A pseudospectral method of solution of Fishers equation. J. Comput. Appl. Math. **193**, 219–242 (2006)
O'Niel, S.V., Reinhardt, W.P.: Photoionization of molecular hydrogen. J. Chem. Phys. **69**, 2126–2142 (1978)
Parrish, R.M., Hohenstein, E.G., Martnez, T.J., Sherrill, C.D.: Discrete variable representation in electronic structure theory: quadrature grids for least-squares tensor hypercontraction. J. Chem. Phys. **138**, 194107 (2013)
Pasquetti, R., Rapetti, F.: Spectral element methods on triangles and quadrilaterals: comparisons and applications. J. Comput. Phys. **198**, 349–362 (2004)
Peyret, R.: Spectral Methods for Incompressible Viscous Flow. Springer, New York (2002)
Pierrard, V., Lemaire, J.: A collisional kinetic model of the polar wind. J. Geophys. Res. **103**, 11701–11709 (1998)
Pitchford, L.C., ONeil, S.V., Rumble Jr., J.R.: Extended Boltzmann analysis of electron swarm experiments. Phys. Rev. A **23**, 294–304 (1981)
Pitchford, L.C., Phelps, A.V.: Comparative calculations of electron-swarm properties in N_2 at moderate E/N values. Phys. Rev. A **25**, 540–554 (1982)

Prandoni, P., Vetterli, M.: From Lagrange to Shanon. . . and back: another look at sampling. IEEE Signal Process. Mag. **28**, 138–144 (2009)
Prenter, P.M.: Splines and Variational Methods. Wiley, New York (1975)
Press, W.H., Teukolsky, S.A., Veterling, W.T., Flannery, B.P.: Numerical Recipes: The Art of Scientific Computing. Cambridge University Press, New York (2007)
Quarteroni, A., Saleri, F., Gervasio, P.: Scientific Computing with MATLAB and Octave, 3rd edn. Springer, New York (2010)
Ralston, A., Rabinowitz, P.: A First Course in Numerical Analysis. Dover, New York (2001)
Reine, S., Helgaker, T., Lindh, R.: Multi-electron integrals. WIREs Comput. Mol. Sci. **2**, 290–303 (2012)
Reinhardt, W.P.: L^2 discretization of atomic and molecular electronic continua: moment, quadrature and J-matrix techniques. Comput. Phys. Commun. **17**, 1–21 (1979)
Risken, H., Voigtlaender, K.: Solutions of the Fokker-Planck equation describing thermalization of neutrons in a heavy gas moderator. Z. Phys. B—Condens. Matter **54**, 253–262 (1984)
Rys, J., Dupuis, M., King, H.F.: Computation of electron repulsion integrals using the Rys quadrature method. J. Comput. Chem. **4**, 154–175 (1983)
Sack, R.A., Donavan, A.F.: An algorithm for Gaussian quadrature given modified moments. Numer. Math. **18**, 465–478 (1972)
Sagar, P.R., Smith, V.H.: On the calculation of Rys polynomials and quadratures. Int. J. Quant. Chem. **42**, 827–836 (1992)
Sandberg, J.A.R., Rinkevicius, Z.: An algorithm for the efficient evaluation of two-electron repulsion integrals over contracted Gaussian-type basis functions. J. Chem. Phys. **137**, 234105 (2012)
Schenzle, A., Brand, H.: Multiplicative stochastic processes in statistical physics. Phys. Rev. A **20**, 1628–1647 (1979)
Schneider, B.I., Nygaard, N.: Orthogonal functions, discrete variable representation and generalized Gauss quadratures. J. Phys. Chem. A **106**, 10773–10776 (2002)
Schumer, J.W., Holloway, J.P.: Vlasov simulations using velocity-scaled Hermite representations. J. Comput. Phys. **144**, 626–661 (1998)
Shen, J., Tang, T., Wang, L.-L.: Spectral Methods: Algorithms Analysis and Applications. Springer, Berlin (2011)
Sherrill, C.D.: Frontiers in electronic structure theory. J. Chem. Phys. **132**, 110902 (2010)
Shizgal, B.: Eigenvalues of the Lorentz Fokker-Planck equation. J. Chem. Phys. **70**, 1948–1951 (1979)
Shizgal, B.: A Gaussian quadrature procedure for the use in the solution of the Boltzmann equation and related problems. J. Comput. Phys. **41**, 309–328 (1981)
Shizgal, B., Blackmore, R.: Eigenvalues of the Boltzmann collision operator for binary gases and relaxation of anisotropic distributions. Chem. Phys. **77**, 417–427 (1983)
Shizgal, B., Karplus, M.: Nonequilibrium contributions to the rate of reaction. I. Perturbation of the velocity distribution function. J. Chem. Phys. **52**, 4262–4278 (1970)
Shizgal, B.: Electron distribution functions for electron attachment to SF_6 and model systems. Chem. Phys. Lett. **138**, 65–70 (1987)
Shizgal, B.D., Chen, H.: The quadrature discretization method (QDM) in the solution of the Schrödinger equation with nonclassical basis functions. J. Chem. Phys. **104**, 4137–4150 (1996)
Shizgal, B.D., Chen, H.: The quadrature discretization method in the solution of the Fokker-Planck equation with nonclassical basis functions. J. Chem. Phys. **107**, 8051–8063 (1997)
Shizgal, B.D.: Spectral methods based on nonclassical basis functions: the advection-diffusion equation. Comput. Fluids **31**, 825–843 (2002)
Shizgal, B.D., Jung, J.-H.: Towards the resolution of the Gibbs phenomena. J. Comput. Appl. Math. **161**, 41–65 (2003)
Shizgal, B.D.: Suprathermal particle distributions in space physics: Kappa distributions and entropy. Astrophys. Space Sci. **312**, 227–237 (2007)
Shizgal, B.D., Dridi, R.: Maple code for the calculation of the matrix elements of the Boltzmann collision operators for mixtures. Comput. Phys. Commun. **181**, 1633–1640 (2010)

Shohat, J.A., Tamarkin, J.D.: The Problem of Moments. American Mathematical Society, New York (1943)
Shore, B.W.: Solving the radial Schrödinger equation by using cubic-spline basis functions. J. Chem. Phys. **58**, 3855–3866 (1973)
Shore, B.W.: B-spline expansion bases for excited states and discretized scattering states. J. Chem. Phys. **63**, 3835–3840 (1975)
Shu, C., Ding, H., Yeo, K.S.: Local radial basis function-based differential quadrature method and its application to solve two-dimensional incompressible Navier-Stokes equations. Comput. Methods Appl. Mech. Eng. **192**, 941–954 (2003)
Siewert, C.E.: On computing the Chapman-Enskog functions for viscosity and heat transfer and the Burnett functions. JQRST **74**, 789–796 (2002)
Sospedra-Alfonso, R., Shizgal, B.D.: Henyey-Greenstein model in the shape relaxation of dilute gas mixtures. Trans. Theory Stat. Phys. **41**, 368–388 (2012a)
Sospedra-Alfonso, R., Shizgal, B.D.: Hot atom populations in the terrestrial atmosphere. A comparison of the nonlinear and linearized Boltzmann equation. AIP Conf. Proc. **1501**, 91–98 (2012b)
Steen, N.M., Byrne, G.D., Gelbard, E.M.: Gaussian quadratures for the integrals $\int_0^\infty \exp(-x^2) f(x)dx$ and $\int_0^b \exp(-x^2) f(x)dx$. Math. Comput. **23**, 661–671 (1969)
Stenger, F.: Numerical methods based on Sinc and analytic functions. Springer Ser. Comput. Math. **20**, 91–96 (1993)
Stroud, A.H.: Approximate Calculation of Multiple Integrals. Prentice Hall, Engelwood Cliffs (1971)
Struchtrup, H.: Macroscopic Transport Equations for Rarefied Gas Flows: Approximation Methods in Kinetic Theory. Springer, New York (2005)
Sturgill, D.: Variable shape parameter strategies in radial basis function methods. Ph.D. thesis, Marshall University, West Virginia, USA (2009)
Sykes, J.B.: Approximate integration of the equation of transfer. Mon. Not. Roy. Astron. Soc. **111**, 377–386 (1951)
Szabo, A., Ostlund, N.S.: Modern Quantum Chemistry: Introduction to Advanced Electronic Structure Theory. Dover, New York (1996)
Talman, L.A.: Simpson's rule is exact for quintics. Am. Math. Mon. **113**, 144–155 (2006)
Thévenaz, P.: Interpolation revisited. IEEE Trans. Med. Imaging **19**, 739–758 (2000)
Thomas, G.E., Stamnes, K.: Radiative Transfer in the Atmosphere and Ocean. Cambridge University Press, Cambridge (2002)
Trahan, C.J., Wyatt, R.E.: Radial basis function interpolation in the quantum trajectory method: optimization of the multi-quadric shape parameter. J. Comput. Phys. **185**, 27–49 (2003)
Trefethen, L.N.: Spectral Methods in MATLAB. SIAM, Philadelphia (2000)
Trefethen, L.N.: Is Gauss quadrature better than Clenshaw-Curtis? SIAM Rev. **50**, 67–87 (2008)
Tsuneda, T.: Density Functional Theory in Quantum Chemistry. Springer, New York (2014)
Viehland, L.A.: Velocity distribution functions and transport coefficients of atomic ions in atomic gases by a Gram-Charlier approach. Chem. Phys. **179**, 71–92 (1994)
Viehland, L.A., Chang, Y.: Transport cross sections for collisions between particles. Comput. Phys. Commun. **181**, 1687–1696 (2010)
Waldvogel, J.: Fast construction of the Fejér and Clenshaw-Curtis quadrature rules. BIT Numer. Math. **46**, 195–202 (2006)
Wannier, G.H.: Derivation of the Davydov distribution from the Boltzmann equation. Am. J. Phys. **39**, 281–285 (1971)
Warringa, H.J., Sedrakian, A.: Vortex formation in a rotating two-component Fermi gas. Phys. Rev. A **84**, 023609 (2011)
Wei, G.W.: Discrete singular convolution for the solution of the Fokker Planck equation. J. Chem. Phys. **110**, 8930–8942 (1999)
Wei, G.W.: Solving quantum eigenvalue problems by discrete singular convolution. J. Phys. B: At. Mol. Opt. Phys. **33**, 343–352 (2000)

Weideman, J.A.C., Reddy, S.C.: A MATLAB differentiation matrix suite. ACM Trans. Math. Softw. **26**, 465–519 (2000)
Wheeler, J.C.: Modified moments and Gaussian quadratures. Rocky Mt. J. Math. **4**, 287–296 (1974)
Whittaker, J.M.: The Fourier theory of the Cardinal function. Proc. Roy. Soc. Edinb. **1**, 169–176 (1929a)
Whittaker, J.M.: On the Cardinal function of interpolation theory. Proc. Roy. Soc. Edinb. **1**, 41–46 (1927)
Wick, G.C.: Über ebene diffusions-probleme. Z. Phys. **121**, 702–718 (1943)
Williams, P.: Quadrature discretization method in tethered satellite control. Appl. Math. Comput. **217**, 8223–8235 (2011)
Zhao, S., Wei, G.W.: Comparison of the discrete singular convolution and three other numerical schemes for solving Fisher's equation. SIAM J. Sci. Comput. **25**, 127–147 (2003)

Chapter 3
Numerical Evaluation of Integrals and Derivatives

Abstract The numerical evaluation of integrals referred to as a quadrature is an important aspect of a large number of applied problems in science and engineering. In Chap. 2, we derived several different methods for the numerical evaluation of integrals. These include the trapezoidal and Simpson's rules, the higher order Newton-Cotes algorithms, the Clenshaw-Curtis scheme and the Gauss quadrature methods based on classical and nonclassical polynomials. In this chapter, general principles for the accurate and efficient numerical evaluation of integrals that occur in the modeling of physical systems are provided. This is the basis for an efficient numerical method of solution of integral equations discussed in Chap. 5. The physical systems considered vary considerably from section to section and a brief introduction is provided in each case with numerous references to textbooks and current research publications. We consider radial integrals that occur in density functional theory, integrals for chemical and nuclear fusion rate coefficients and also for the solution of the Boltzmann equation. The numerical evaluation of matrix elements in kinetic theory and quantum mechanics is also presented with important implications for pseudospectral methods. The latter section of the chapter is devoted to the pseudospectral method for numerical differentiation based on the Lagrange and Sinc interpolants. The numerical solution of Sturm-Liouville differential eigenvalue problems for the classical polynomials is also presented.

3.1 Numerical Evaluation of Integrals

The integration of a smooth slowing varying integrand is generally not difficult. With the speed of current personal computers, almost any one-dimensional integral can be evaluated to almost machine accuracy in a finite time. It is well known that a specific numerical method might be efficient for a particular type of integral and not for others. One can always propose a method adapted to work very well for a certain class of integrals but that performs poorly when applied to other integrals.

There have been several discussions of automatic integrators (Davis and Rabinowitz 1975; Lyness 1983) which evaluate one-dimensional integrals for a given integrand, interval and accuracy desired. These automatic integrators have found

B. Shizgal, *Spectral Methods in Chemistry and Physics*, Scientific Computation,
DOI 10.1007/978-94-017-9454-1_3

some success but are not flawless, as discussed by Lyness (1983). A comprehensive presentation of computational methods for integration with a large number of examples was provided by Kythe and Schaferkotter (2004).

The main objective of this chapter is to present techniques for the evaluation of integrals that arise in physical problems, The precision required will be high but not necessarily of machine accuracy. Specific examples will include radial integrals that arise in density functional theory, electron repulsion integrals in quantum chemistry, integrals in kinetic theory applications and in the evaluation of chemical and nuclear reaction rates, integrals for the efficient evaluation of semi-classical phase shifts in atom-atom scattering and other applications. Often the integrals desired generally have smooth well behaved integrands but in the simulations for which they are required there are a large number of such integral evaluations and thus an efficient scheme is desired. We emphasize the use of Gauss quadratures based on non-classical polynomials.

In kinetic theory, the Boltzmann collision operator is the sum of an integral operator with a well-defined kernel and the collision frequency which is a multiplicative operator. Similarly, the Hamiltonian in the Schrödinger equation is the sum of the kinetic energy second derivative operator and a multiplicative potential function. We consider the calculation of the spectral matrix representations of such multiplicative operators, that is, matrix elements of functions that arise in kinetic theory (Hoare and Kaplinsky 1970; Shizgal and Fitzpatrick 1974; Lindenfeld and Shizgal 1979; Loyalka et al. 2007) and in quantum mechanics (Harris et al. 1965; Dickinson and Certain 1968; Gallas 1980; Bordoni and Manini 2007).

An important example is the matrix representative of the coordinate operator which is the Jacobi matrix, Eq. (2.71). The eigenvalues of this multiplicative operator are the Gaussian quadrature points for the specified weight function and represent the continuous spectrum of the coordinate operator on the specified interval. These continuous eigenvalues do not converge to discrete values with an increase in the number of quadrature points.

The matrix elements of such multiplicative operators can sometimes be calculated exactly in a particular basis set with algebraic methods or approximately by using an appropriate Gaussian quadrature. Harris et al. (1965) and Dickinson and Certain (1968) considered the quadrature evaluation of matrix elements of the potential in the Schrödinger equation. The research lead to the development of a pseudospectral method (Hamilton and Light 1986; Light and Carrington Jr. 2000) for the solution of the Schrödinger equation, primarily for the calculation of the vibrational states of polyatomic molecules.

In quantum chemistry, there is an ongoing interest in the efficient numerical evaluation of three-dimensional integrals over spherical coordinates, (r, θ, ϕ). The theoretical modelling of polyatomic molecules requires the accurate computation of a very large number of similar integrals (Treutler and Ahlrichs 1995; Mura and Knowles 1996; Lindh et al. 2001; Gill and Chien 2003; El-Sherbiny and Poirier 2004; Kakhiani et al. 2009; Mitani 2011). This is an important concern for researchers in quantum chemistry involved with electronic structure calculations. The integration

over solid angle, (θ, ϕ), is generally considered with a cubature separately from the integration over the radial variable, r. In Sect. 3.4.2, the details of the integration of radial integrals is discussed with several examples.

The solution of the Boltzmann equation with a collocation method involves the integral over a kernel which can have a sharp cusp (Gibble and Gallagher 1991; Rogers and Berman 1991; Bovino et al. 2011; Kharchenko et al. 1998; Sospedra-Alfonso and Shizgal 2012). We address the problem of the integration over the cusp for the solution of the Boltzmann equation and similar integral equations discussed in greater detail in Chap. 5. We briefly discuss the challenges presented by oscillatory integrals in physics as well as several integrals that are largely devoid of any physical application (Bornemann et al. 2004).

Pseudospectral methods (Fornberg 1996; Canuto et al. 2006) applied to a multitude of applied problems in diverse fields are defined in terms of global discrete derivative matrix operators generally based on some interpolant. These methods provide first and second order finite derivative matrix operators in physical space and reduce partial differential equations to ordinary differential equations. We will apply these matrix derivative operators to the solution of Sturm-Liouville eigenvalue problems that define the classical polynomials. We also consider the application of pseudospectral methods to the solution of the Fokker-Planck and Schrödinger equations in Chap. 6. There are also finite difference methods (LeVeque 2007; Burden and Faires 2011) that are local representations of the derivative.

3.2 Some General Principles for the Numerical Evaluation of Integrals

We are concerned with the numerical evaluation of a one-dimensional integral of the form

$$I = \int_a^b f(x)dx, \tag{3.1}$$

with the assumption that the antiderivative, $F(x)$ defined by $dF(x)/dx = f(x)$ is not known analytically. If $F(x)$ is known analytically, then the problem reduces to

$$I = \int_a^b f(x)dx = F(b) - F(a). \tag{3.2}$$

Since $F(x)$ is generally not known, we consider a numerical approximation to the integral I. In some cases, $F(x)$ is known but expressed in terms of a very complicated function, such as the hypergeometric function, whose evaluation is perhaps more difficult than the numerical calculation of the integral.

For numerical integration, it is important to know in detail the behaviour of the integrand $f(x)$. Of primary interest is the smoothness of $f(x)$ as governed by the continuity of $f(x)$ and its derivatives. If $f(x)$ is continuous, but $df(x)/dx$ is not, special attention is required for the numerical evaluation of I to be accurate as we will show. If $x \in [0, \infty)$ and $f(x)$ decays too slowly as $x \to \infty$, the numerical algorithm chosen must be adapted to take this behaviour into account. Other examples include an integrand that oscillates about zero as $x \to \infty$ or perhaps as $x \to 0$ and the value of I is small. Other special cases include integrands that have singularities in the domain of integration for which a Cauchy principal value is required. For certain functions, a simple variable change $x \to y$, referred to as a mapping, can transform the integrand to a more manageable form suitable for a particular quadrature.

3.3 Scaling Quadrature Points and Weights

For quadratures defined by polynomials on the infinite and semi-infinite intervals such as the Laguerre, Hermite and Maxwell polynomials, an important mapping is the scale change, $z = sx$, to redistribute the quadrature points so as to better capture the integrand. The scaling of quadrature points on the semi-infinite interval for Gauss-Maxwell quadrature with weight function $w(x) = x^2 e^{-x^2}$ often involves this variable change, $z = sx$, and the integral is calculated with the algorithm

$$\begin{aligned} I &= \int_0^\infty G(z)dz = s\int_0^\infty G(sx)dx = s\int_0^\infty x^2 e^{-x^2}\frac{G(sx)}{x^2 e^{-x^2}}dx, \\ &\approx \sum_{i=1}^{N} \frac{sw_i}{x_i^2 e^{-x_i^2}} G(sx_i) = \sum_{i=1}^{N} W_i G(sx_i), \end{aligned} \tag{3.3}$$

where the "big" weights are given by $W_i = sw_i/w(x_i)$.

The variable $z = \sqrt{mv^2/2k_BT}$ in the Maxwell weight function is the reduced particle speed with m the particle mass, k_B the Boltzmann constant and T the temperature of the gas. We interpret this mapping in terms of an arbitrary temperature, T_s, different from T so that $x = \sqrt{mv^2/2k_BT_s}$ where the scaling parameter is identified as $s^2 = T_s/T$. This scaling technique has been used in the solution of the Boltzmann equation (Shizgal 1981), the Schrödinger equation (Baye and Heenen 1986; Lo and Shizgal 2008), the Vlasov equation (Schumer and Holloway 1998; Gibelli et al. 2010) and is the basis for the two-temperature model for the solution of the Boltzmann equation for ion mobilities (Mason and McDaniel 1988) in ion-atom binary gases. In the sections that follow, we apply this important technique (Holway 1967; Tang 1993; Holloway 1996; Ordzywolek 2011) to the calculation of radial integrals in density functional theory and to several other applications.

3.4 Integrals in Density Functional Theory

The efficient evaluation of integrals is particularly relevant to the calculation of the electronic energy states of atoms and molecules. Electronic structure modeling in quantum chemistry involves the solution of the Schrödinger equation for the electronic state of a many electron atom or molecule. We provide a very brief overview of this subject to motivate the specific applications in subsequent sections and refer readers to several texts (Karplus and Porter 1970; Szabo and Ostlund 1996; McQuarrie and Simon 1997; Helgaker et al. 2000; Levine 2009; Tsuneda 2014) and research papers (Rys et al. 1983; El-Sherbiny and Poirier 2004; Sandberg and Rinkevicius 2012; Reine et al. 2012; Becke 2014) for a more complete description of this subject and the numerical challenges presented.

The Hamiltonian for the Schrödinger equation is the sum of the electron kinetic energy operators, the electron-nuclei and the electron-electron Coulomb interactions. The only systems for which exact results exist are the hydrogen atom, and one-electron ions such as He^+ (Drake 1999; Drake et al. 2002) and H_2^+ (Cassar and Drake 2004).

The quantum state of the hydrogen atom is represented by the wave function $\psi_{n\ell m}(r, \Omega)$ in spherical polar coordinates (r, Ω), $\Omega = (\theta, \phi)$. We showed in Sect. 2.4.6 that the wavefunction for the H-atom separates into the spherical harmonic basis functions $Y_{\ell m}(\Omega) = P_\ell^m(\cos\theta)e^{im\phi}$ and the associated Laguerre polynomials, so that,

$$\psi_{n\ell m}(\rho, \Omega) = N_{n\ell} \exp(-\rho/2)\rho^\ell L_{n-\ell-1}^{(2\ell+1)}(\rho) Y_{\ell m}(\Omega), \tag{3.4}$$

where $\rho = 2r/na_0$, $a_0 = \hbar^2/m_e Z_e^2$ is the Bohr[1] radius and $N_{n\ell}$ is a normalization such that the wave functions are orthonormal,

$$\iint \psi_{nlm}^* \psi_{n'l'm'} r^2 dr d\Omega = \delta_{nn'}\delta_{\ell\ell'}\delta_{mm'}.$$

The spherical harmonic and Laguerre basis functions were discussed in Sects. 2.4.4 and 2.4.5, respectively. In the absence of external fields and spin dependent interactions, the electronic energy states depend only on the principal quantum number n, and the energy is given by $E_n = -e^2/2a_0n^2$.

The basis functions for the solution of the Schrödinger equation for many electron atoms and molecules are often derived from the eigenfunctions ("orbitals") of the H-atom. The basis functions chosen must be antisymmetric with respect to the exchange of any pair of electrons in order to satisfy the symmetry properties of fermions. The representation of the Hamiltonian in these basis sets is then required and the calculation of the electron-electron pair repulsion integrals presents an ongoing numerical challenge as discussed in Sect. 3.8.1.

An important development in the field was the adoption of an approximate formalism originally developed independently by Thomas (1927) and Fermi (1927)

[1] Niels Henrik David Bohr (1885–1962) was a Danish physicist who made fundamental contributions to quantum theory and in particular to the Bohr model of the hydrogen atom. He received the Nobel Prize in Physics in 1922.

for the statistical mechanics of an electron gas and later applied to atomic structure theory (Parr 1983; Parr and Gosh 1986). The electronic ground state is viewed as dependent on the electron density, $\rho(\mathbf{r})$, rather than on the multidimensional electron wavefunction. For many electron systems, the electron density is formally expressed by the integral of the square of the many electron wave function, that is,

$$\rho(\mathbf{r}) = \int |\Psi(\mathbf{r}_1, \mathbf{r}_2, \ldots, \mathbf{r}_n|^2 d\mathbf{r}_1 \mathbf{r}_2 \ldots \mathbf{r}_{n-1}. \tag{3.5}$$

The electron-electron and electron-nuclei interactions are then expressed in terms of the density. A variational formalism is applied to the Schrödinger equation written in terms of the electron density appearing as a functional. The theoretical foundations were established by Hohenberg and Kohn (1964) and Kohn and Sham (1965). Excellent reviews of the Thomas-Fermi model and density functional theory are available (Lieb 1981; Jones and Gunnarsson 1989; Morgan 1996) where the original references can be found.

Density functional theory is now routinely employed in electronic structure simulations. The details of this theoretical approach are well beyond the scope of this book. A more complete exposition of this theoretical formalism is available in several textbooks and reviews (Parr 1983; Jones and Gunnarsson 1989; Fiolhais et al. 2003; Burke 2012).

3.4.1 Mapping the Semi-infinite Interval $r \in [0, \infty)$ to $x \in [-1, 1]$

Much of the work on spectral methods (Fornberg 1996; Boyd 2001; Peyret 2002; Canuto et al. 2006; Hesthaven et al. 2007) is based on Fourier series, Chebyshev and Legendre polynomials. Chebyshev polynomials are very closely related to a Fourier series and often referred to as a "Fourier series in disguise" as discussed in Chap. 2. In the next section, we review the evaluation of radial integrals that arise in density functional theory applied to quantum chemistry. The integrals over the semi-infinite domain are often mapped onto the finite interval $[-1, 1]$ as summarized in Table 3.1, and Chebyshev or Legendre quadratures are then used.

Table 3.1 Different mappings of the semi-infinite interval $r \in [0, \infty)$ to $x \in [-1, 1]$

Reference	Mapping
Boyd (1982), Treutler and Ahlrichs (1995)	$x = 1 - 2e^{-r/s}$
Murray et al. (1993)	$x = 2\sqrt[m]{1 - e^{-r/s}} - 1$
Boyd (1987), Becke (1988)	$x = \frac{r-s}{r+s}$
Mura and Knowles (1996)	$x = 2\sqrt{r/(r-s} - 1$
Linear map	$x = \frac{2r}{r_{max}} - 1;\ r \in [0, r_{max}]$

The parameter s is a scaling factor

The accuracy of the different mappings can be tested with the numerical calculation of two integrals on the semi-infinite domain given by

$$\int_0^\infty r^2 e^{-r^2} M_5^2(r) dr = 1,$$

$$\int_0^\infty r^2 e^{-r^2} M_4(r) M_5(r) dr = 0, \tag{3.6}$$

for which the integrands are shown in Fig. 3.1.

Figure 3.1(A) shows the integrand for the normalization of the Maxwell polynomial $M_5(r)$ with respect to the weight function, $w(r) = r^2 e^{-r^2}$, $r \in [0, \infty)$. The integral of this function is the norm which is unity. Figure 3.1(B) shows the integrand for the product of the polynomials $M_4(r)$ and $M_5(r)$ which are orthogonal and the integral for this integrand is zero. We have changed notation from x (originally reduced speed) to r (a radial coordinate) and in the current context we use $x \in [-1, 1]$ as the new variable obtained with variable change or mapping.

These two integrals, one of degree 10 and the other of degree 9, can be done exactly to machine accuracy with the Maxwell ($p = 2$) quadrature points of order 6 shown by the symbols in the graphs. This is a remarkable demonstration of the power of Gaussian quadratures albeit for polynomial integrands. This is no surprise.

This exact quadrature would not be obvious simply from the graphs of the integrands. One could consider the numerical calculation of the integral in Fig. 3.1(A) as the sum of six integrals, each evaluated with a quadrature between the zeros of the function suitably transformed to $[-1, 1]$. The last interval would have to be trun-

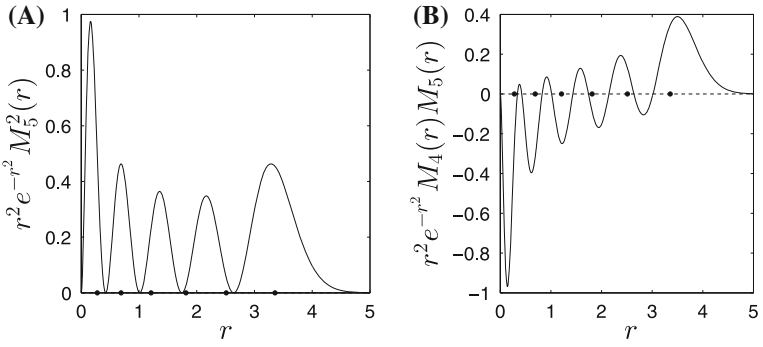

Fig. 3.1 (**A**) The variation of $r^2 e^{-r^2} M_5^2(r)$ and (**B**) $r^2 e^{-r^2} M_4(r) M_5(r)$ versus r. The polynomials $M_n(r)$ are orthogonal with the Gauss-Maxwell weight function $w(r) = r^2 e^{-r^2}$, $r \in [0, \infty)$. The integral of the function on the left is 1 and for the function on the right it is zero. The *closed circles* are the quadrature points for the Gauss-Maxwell quadrature for which the integrals in Eq. (3.6) are calculated to machine accuracy with $N = 6$

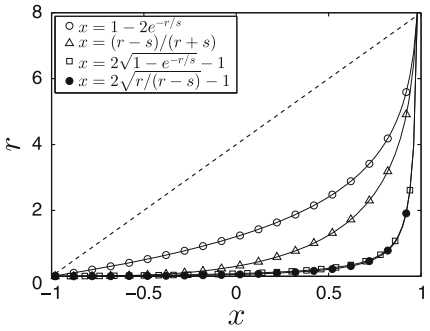

Fig. 3.2 Different variable transformations or mappings from $r \in [0, \infty)$ to $x \in [-1, 1]$ as summarized in Table 3.1. The *dashed line* is the linear map. The scale factor s is chosen such that $r_{max} = 8$ for which the integrands in Fig. 3.1 are considered to be very small

cated at some sufficiently large r_{max}. The integral of the function in Fig. 3.1(B) could also be calculated by evaluating the ten integrals between nodes in the same way. The integrals from node to node can be evaluated with a Chebyshev or Legendre quadrature or a Simpson's rule. This is a commonly used technique for oscillatory integrals.

Five mappings that transform the radial variable $r \in [0, \infty)$ to $x \in [-1, 1]$ are listed in Table 3.1 and shown in Fig. 3.2. A Gauss-Legendre quadrature is then used to evaluate the integrals. These mappings are used in spectral methods (Boyd 1982, 1987) and in particular for the evaluation of integrals in density functional theory. There have been several reviews with numerical comparisons (Lindh et al. 2001; Gill and Chien 2003; El-Sherbiny and Poirier 2004).

The linear map (dashed line) with a truncation at $r = 8$ beyond which there is an insignificant contribution to the integrals does not bias the distribution of quadrature points other than the original clustering near the ends of the interval. An exponential map (open circles) proposed independently by Boyd (1982) and Treutler and Ahlrichs (1995) distributes more quadrature points at small r than at large r. There could be an additional flexibility in the mappings with the use of the scaling parameter which has been chosen as $s = 1$. The main concern is the manner in which the mapping distributes quadrature points and whether the details of the integrand have been captured. A comparison of the distribution of quadrature points for the mappings in Table 3.1 was presented in Fig. 1 of Gill and Chien (2003).

We choose two test integrals of this type to study the different mappings from $[0, \infty)$ to $[-1, 1]$ that have been used as summarized in Table 3.1, namely

$$\langle M_4^2 \rangle = \int_0^\infty r^2 \exp(-r^2) M_4^2 dr = 1,$$
$$\langle M_6^2 \rangle = \int_0^\infty r^2 \exp(-r^2) M_6^2 dr = 1. \tag{3.7}$$

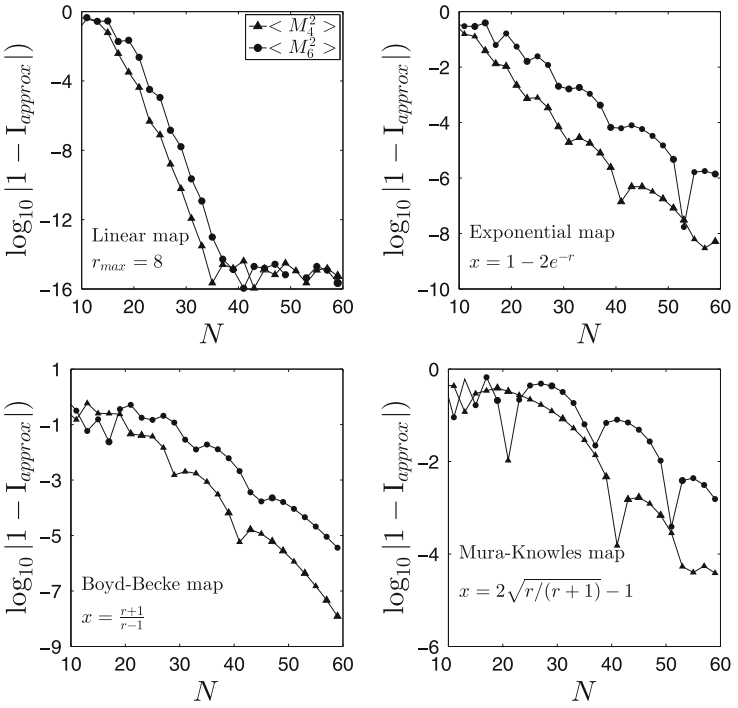

Fig. 3.3 The variation of the relative error for the integrals $\langle M_n^2 \rangle = \int_0^\infty r^2 e^{-r^2} M_n^2(r) = 1$ for $n = 4$ and 6 with four different mappings. The relative error is shown versus the number of Legendre quadrature points, N. The definitions of the mappings are given in Table 3.1

The variation of the relative error for the numerical evaluation of these integrals versus the number of quadrature points, N, is shown for several mappings in Fig. 3.3. The relative error $\log_{10}[1 - I_{approx}]$ for the linear map provides the most rapid convergence. The error with the exponential map is comparable to that with the Boyd-Becke map. The Mura-Knowles map provides the slowest convergence. The different convergence rates depend on the distribution of quadrature points in the transformed interval $[-1, 1]$. These normalization integrals can be evaluated exactly with the Gauss-Maxwell quadrature (p = 2) with $N = 5$ and $N = 7$ quadrature points, respectively.

3.4.2 Radial Integrals in Density Functional Theory

Electron structure calculations in quantum chemistry and density functional theory for polyatomic molecules require the calculation of a large number of three dimensional integrals over a sphere of the form

$$I_{3D} = \int F(\mathbf{r}) d\mathbf{r}, \tag{3.8}$$

where the vector **r** is defined in terms of the three spherical polar coordinates (r, θ, ϕ). The three dimensional integral can be split into an angular integral

$$f(r) = \int_0^{2\pi} \int_0^{\pi} F(r, \theta, \phi) \sin\theta d\theta d\phi, \tag{3.9}$$

over θ and ϕ and the radial integral

$$I_{radial} = \int_0^{\infty} f(r) r^2 dr. \tag{3.10}$$

The angular integral is often evaluated with an algorithm that reduces the two dimensional integral to a single quadrature sum referred to as a cubature (Stroud and Secrest 1966; Lebedev 1977; Cools 2003; Haxton 2007) as discussed in Chap. 2, Sect. 2.8.

There have been several numerical experiments of the calculation of I_{radial} with $f(r)$ approximated by a sum of Gaussians to model the radial variation of the electron density in simple systems such as the inert gas atoms. The mappings from $r \in [0, \infty)$ to $x \in [-1, 1]$ in Table 3.1 have been used (Becke 1988; Murray et al. 1993; Treutler and Ahlrichs 1995; Mura and Knowles 1996; Lindh et al. 2001; Gill and Chien 2003; El-Sherbiny and Poirier 2004; Kakhiani et al. 2009). These studies demonstrate the intense interest in the development of efficient numerical algorithms for the calculation of these three dimensional integrals, Eq. (3.8).

Lindh et al. (2001) considered the integral of a simple (normalized) Gaussian given by,

$$\frac{2\alpha^{(\ell+3)/2}}{\Gamma[(\ell+3)/2]} \int_0^{\infty} r^{\ell} e^{-\alpha r^2} r^2 dr = 1. \tag{3.11}$$

They employed the mappings in Table 3.1 and studied the calculation of this elementary integral for a range of values of α and ℓ versus the number of quadrature points, N. For the integral of the Gaussian in Eq. (3.11), the Gauss-Maxwell quadrature with $p = 2$ provides an exact result for this integral (with $\ell = 0$) and a scale factor $s = 1/\sqrt{\alpha}$.

We evaluate this integral with the Gauss-Maxwell quadrature and the scaling procedure given by Eq. (3.3). The variation of the relative error, defined by

$$\text{Relative Error} = \left| 1 - \frac{I_{approx}}{I_{exact}} \right|, \tag{3.12}$$

versus the scaling parameter s is shown in Fig. 3.4. The integral is evaluated to machine accuracy for $s = 1/\sqrt{\alpha}$ which for $\alpha = 4$ occurs at $s = 0.5$. For $N = 2$ and 4, the range of s values for which the integral is evaluated exactly (to machine accuracy) in the vicinity of $s = 0.5$ is narrower than for the $N = 8$ and 10. It is clear from the graph that there are values of $s > 1/2$, at the inverted cusps, for which the

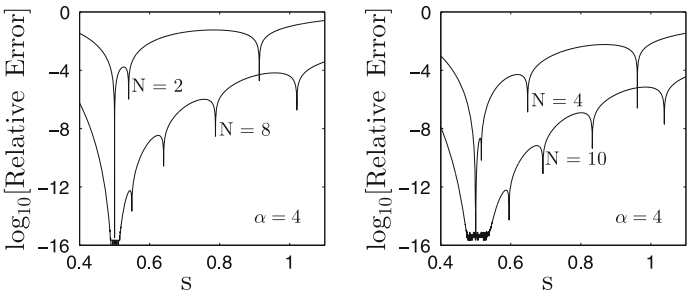

Fig. 3.4 The variation of the relative error for the integral of the Gaussian in Eq. (3.11) versus the scale factor s with the number of Maxwell quadrature points equal to N. The integral is evaluated to machine accuracy for $s = 1/\sqrt{\alpha} = 0.5$ for which the quadrature is exact

integral is also evaluated exactly. This occurs because the error in the integration can overestimate or underestimate the exact value and $(I_{approx} - I_{exact})$ oscillates about zero as s varies. It is difficult to determine a priori where these "roots" of $I_{approx} - I$ versus s occur. We will demonstrate this behaviour versus the scaling parameter in the evaluation of other integrals.

The variation of the relative error for the integral in Eq. (3.11) with the Maxwell quadrature is shown in Fig. 3.5 versus N for $s = 1/2$, $\alpha = 4$ and several values of ℓ. The integral is evaluated to machine accuracy for $\ell = 6$, 8, 10 and 14, with N = 4, 5, 6, and 8 quadrature points, respectively. This is not a surprising result as the Gauss-Maxwell integration of a polynomial of degree $2N - 1$ is exact with N quadrature points. The Gaussian in Eq. (3.11) is essentially the Gauss-Maxwell weight function.

The functional forms chosen to simulate realistic radial integrands in Eq. (3.10) include a simple Gaussian

$$f_1(r) = e^{-ar^2}, \tag{3.13}$$

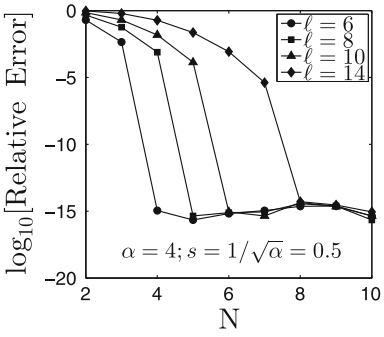

Fig. 3.5 The variation of the relative error for the Gaussian in Eq. (3.11) versus the number of Maxwell quadrature points N for $s = 1$, $\alpha = 4$ and several ℓ values. For $\ell = 6$, 8, 10 and 14, the integrals are evaluated to machine accuracy with N = 4, 5, 6, and 8 quadrature points, respectively. This is consistent with the exactness of the Gauss-Maxwell quadrature for polynomials of order $2N - 1$

which is essentially Eq. (3.11). Also studied are the integrands which are the sum of two Gaussians

$$f_2(r) = \left[e^{-r^2} + ae^{-ar^2}\right], \tag{3.14}$$

and the sum of three Gaussians

$$f_3(r) = \left[e^{-r^2} + ae^{-ar^2} + be^{-br^2}\right]. \tag{3.15}$$

Almost all of the algorithms proposed by different authors to date involve the mapping of the semi-infinite interval, $[0, \infty)$ to the new integration variable $x \in [-1, 1]$ and a quadrature appropriate for the new interval is chosen. These mappings are summarized in Table 3.1. These numerical experiments have been carried out for $a = 10$ and $b = 100$. The quadratures chosen for $x \in [-1, 1]$ are generally Gauss-Legendre, Gauss-Chebyshev and Gauss-Jacobi quadratures.

The variation of the relative error versus the number of Gauss-Maxwell quadrature points, N, for the evaluation of the integrand with a sum of two and three Gaussians, Eqs. (3.14) and (3.15), are shown in Fig. 3.6(A), (B), respectively, for several values of the scaling parameter, s. For the smaller values of s the variation of $\log_{10}$(Relative Error) versus N is almost linear as shown by the dashed lines and also summarized in Table 3.2 for both integrands. The relative error oscillates with N and the linear variation is not accurate for the larger s values.

A Laguerre quadrature which does not involve the mapping to $[-1, 1]$ has also been used as well as a nonclassical quadrature based on the weight function $w(x) = \ln^2 x$ for $x \in [-1, 1]$ (Gill and Chien 2003). The quadrature points and weights for this weight function are easily calculated with a MATLAB code. A comparison and summary of the results of these studies were provided by Gill and Chien (2003) and El-Sherbiny and Poirier (2004). The relative errors obtained vary considerably and are for the most part in the range $-2 \rightarrow -4$ for N in the range $11 \rightarrow 17$. The accuracies

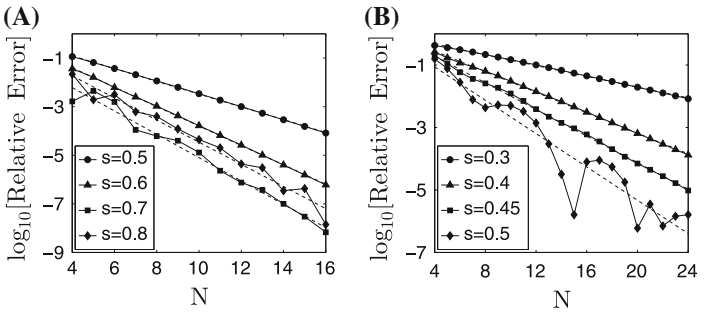

Fig. 3.6 (**A**) The variation of the relative error versus the number of quadrature points N for the integrand in Eq. (3.14) with $a = 10$ and several values of the scaling parameter s. (**B**) The variation of the relative error versus the number of quadrature points N for the integrand in Eq. (3.15) with $a = 10$ and $b = 100$ and several values of the scaling parameter s. The *dashed lines* are the linear fits to the numerical result

Table 3.2 Spectral fits to the convergence of $\log_{10}[|1 - I(N)/I_{exact}|] = A(s)N + B(s)$ and the scaling parameter s

s	A(s)	B(s)
$f_2(r) = [e^{-r^2} + 10e^{-10r^2}]$		
0.5	−0.2630	0.1471
0.6	−0.3996	0.1991
0.7	−0.4804	−0.2947
0.8	−0.4554	0.0915
$f_3(r) = [e^{-r^2} + 10e^{-10r^2} + 100e^{-100r^2}]$		
0.3	−0.08630	0.01899
0.4	−0.01643	0.01015
0.45	−0.02132	0.01369

of the quadratures proposed for the integration of the radial densities for the three atoms mentioned are in the approximate range $-5 \rightarrow -8$ with N up to 25.

In Table 3.3, we compare the results with the Gauss-Maxwell quadrature with the nonclassical Multiexp quadrature of Gill and Chien (2003). Both algorithms converge quickly with a small number of quadrature points with the Gauss-Maxwell quadrature

Table 3.3 Convergence of the integration of $f_2(r)$ and $f_3(r)$, Eqs. (3.14) and (3.15) with the Maxwell quadrature ($p = 2$) and the Multiexp nonclassical quadrature by Gill and Chien (2003) with weight function $w(x) = \ln^2(x)$, $x \in [0, 1]$

N	$I(N)$ (s=0.74)	$\log_{10}$(Relative Error)	$I(N)$	$\log_{10}$(Relative Error)
	$w(r) = r^2 e^{-r^2}$; $r \in [0, \infty)$		$w(x) = \ln^2(x)$; $x \in [-1, 1]$	
$f_2(r) = [e^{-r^2} + 10e^{-10r^2}]$				
3	0.586161143	−2.30	0.586777664	−2.22
5	0.581900828	−2.64	0.585623383	−2.39
7	0.583287168	−4.08	0.585623383	−2.39
9	0.583232448	−5.00	0.583206200	−4.26
11	0.583238398	−6.58	0.583228705	−4.79
13	0.583238252	−7.81	0.583238660	−6.15
15	0.583238238	−8.09	0.583238152	−6.80
$f_3(r) = [e^{-r^2} + 10e^{-10r^2} + 100e^{-100r^2}]$				
3	0.471897196	−0.606	0.586885435	−1.19
5	0.578862504	−1.11	0.622404076	−2.09
7	0.622639519	−2.11	0.634521349	−1.95
9	0.624246729	−2.28	0.625215372	−2.43
11	0.625501911	−2.49	0.628005273	−3.14
13	0.627361813	−3.52	0.627477032	−3.94
15	0.627548579	−5.79	0.627559616	−4.80

converging slightly faster. The value of s is optimized for the Gauss-Maxwell quadrature. It appears that it is more efficient to develop quadratures on the semi-infinite interval and avoid the mapping to the interval $x \in [-1, 1]$.

3.5 Chemical and Nuclear Reaction Rate Coefficients

In this section, we consider integrals that arise in the calculation of equilibrium reaction rates for chemical and nuclear fusion reactions. The theoretical calculation of reactive cross sections involves a classical or quantal treatment of the collision dynamics between the reactants with a specified interparticle interaction. The macroscopic rate coefficient is then the average of the reactive cross section with Maxwellian distributions for the colliding particles (Ross and Mazur 1961; Truhlar and Wyatt 1976; Chatfield et al. 1991). An important endeavor is the development of efficient algorithms for the calculation of rate coefficients of chemical reactions for numerous applications in shock waves (Brun 2009), in atmospheric science (Seinfeld and Pandis 2006), for nuclear fusion reactions in astrophysics (Clayton 1968) and nuclear fusion machines (Atenzi and Meyer-Ter-Vehn 2004).

3.5.1 Equilibrium Rate Coefficient for Chemical Reactions

The temperature dependence of the binary reactive rate coefficient, $k(T)$, for gas phase chemical reactions as well as nuclear fusion reactions is given in terms of the energy dependence of the total reactive cross section, $\sigma_r(E)$, versus the relative translational energy of the reactants E, and the equilibrium Maxwell-Boltzmann distribution functions of the colliding pair of particles, $F_1(v_1)$ and $F_2(v_2)$, respectively, of the form

$$F(v) = \left[\frac{m}{2\pi k_B T}\right]^{3/2} e^{-mv^2/2k_B T}, \tag{3.16}$$

and normalized according to $4\pi \int_0^\infty F(v)v^2 dv = 1$. In Eq. (3.16), the temperature of the gas is T, k_B is the Boltzmann constant and $m = m_1$ or $m = m_2$ for the particle masses. The temperature dependence of the reactive rate coefficient is given by the average of the reactive flux $g\sigma_r(E)$ over all particle velocities weighted with the distribution functions, that is,

$$k(T) = \iint F_1(v_1)F_2(v_2)g\sigma_r(E)d\mathbf{v}_1 d\mathbf{v}_2, \tag{3.17}$$

where the relative velocity is $\mathbf{g} = \mathbf{v}_2 - \mathbf{v}_1$. We transform to relative velocity, $\mathbf{g}$, and center of mass, $\mathbf{G}$, that is,

$$\begin{aligned} \mathbf{g} &= \mathbf{v}_2 - \mathbf{v}_1, \\ \mathbf{G} &= \frac{m_1\mathbf{v}_1 + m_2\mathbf{v}_2}{m_1 + m_2}. \end{aligned} \tag{3.18}$$

The total kinetic energy can be expressed in terms of G and g given by

$$m_1 v_1^2 + m_2 v_2^2 = m_0 G^2 + \mu g^2, \tag{3.19}$$

where $m_0 = m_1 + m_2$ and the reduced mass is $\mu = m_1 m_2 / m_0$. The Jacobian of the transformation is unity so that $d\mathbf{v_1} d\mathbf{v_2} = d\mathbf{G} d\mathbf{g}$. The integral over G that results from this transformation is

$$4\pi \int_0^\infty e^{-m_0 G^2/k_B T} G^2 dG = 2\pi \left[\frac{2k_B T}{m_0}\right]^{3/2} \Gamma(\tfrac{3}{2}), \tag{3.20}$$

where $\Gamma(\alpha) = \int_0^\infty e^{-x} x^{\alpha-1} dx$ is the Gamma function. Two useful identities for the Gamma function are $\Gamma(n+1) = n\Gamma(n) = n!$ and $\Gamma(\frac{1}{2}) = \sqrt{\pi}$.

With Eq. (3.20), Eq. (3.17) can be reduced to a single integral over g, that is

$$k(T) = 4\pi \left(\frac{\mu}{2\pi k_B T}\right)^{3/2} \int_0^\infty e^{-\mu g^2/2k_B T} \sigma_r(E) g^3 dg, \tag{3.21}$$

or in terms of relative energy $E = \mu g^2/2$,

$$k(T) = \sqrt{\frac{8}{\pi\mu}} \frac{1}{(k_B T)^{3/2}} \int_0^\infty e^{-E/k_B T} E \sigma_r(E) dE. \tag{3.22}$$

These are standard results that can be found in many texts on chemical kinetics and kinetic theory (McQuarrie and Simon 1997; Gombosi 1994; Kremer 2010; Liboff 2003). The thermal average in Eq. (3.22) is the last step in a detailed theoretical calculation that involves the interaction potential between the reactants followed by the classical or quantal scattering calculation of the reactive cross section (Chatfield et al. 1991).

The temperature dependence of $k(T)$ is determined by the energy dependence of the reactive cross section $\sigma_r(E)$. In fact, one can view $k(T)$ as the Laplace transform of $E\sigma_r(E)$. There are many applications that we can consider each with a different reactive cross section $\sigma_r(E)$. We first consider a simple model system for reactions with activation energy referred to as the line-of-centers reactive cross section given by

$$\sigma_r(E) = \begin{cases} 0, & E \le E^*, \\ \sigma_d(1 - \frac{E^*}{E}), & E > E^*. \end{cases} \tag{3.23}$$

The activation energy is denoted by E^* and there are no reactive collisions if $E < E^*$. For this simple model, the integral in Eq. (3.17) can be done analytically and the result is,

$$k(T) = \sigma_d \sqrt{\frac{8k_B T_b}{\pi\mu}} e^{-E^*/k_B T}, \tag{3.24}$$

where σ_d is a hard sphere cross section.

There is an ongoing effort to determine reactive cross sections experimentally as well as theoretically for a large number of different systems for a wide range of applications. We consider here just one such physically realistic process, namely the collision dissociation reaction $O + O_2$ with applications to planetary atmospheres (Johnson and Tully 2002). The analytic fit to the theoretical scattering results is

$$\sigma_r(E) = \sigma_0 \frac{(E - E_t)^a}{E_0 + E^b}, \tag{3.25}$$

where $\sigma_0 = 4.51$, $E_t = 14.5\,\text{eV}$, $E_0 = 0.21$, $a = 1.03$ and $b = 1.31$. The cross section is in $10^{-16}\,\text{cm}^2$ with E in eV. The variation with energy of this cross section is shown in Fig. 3.7 in comparison with the line-of-centers cross section with the threshold energy $E_t = 1.8\,\text{eV}$ in order to fit the cross sections near threshold.

For such reactions with activation energy, we transform the integral over energy in Eq. (3.17) to an integration over reduced energy $y = E/k_BT$ from which the integral is zero for $y < y_t = E_t/k_BT$. With the additional transformation to $z = y - y_t$ we get the rate coefficient in a form suitable for integration with Gauss-Laguerre quadratures, that is,

$$k(T) = \sqrt{\frac{8k_BT}{\pi\mu}} \left[y_t e^{-y_t} \int_0^\infty e^{-z} \sigma[(z + y_t)k_BT]dz \right.$$
$$\left. + e^{-y_t} \int_0^\infty z e^{-z} \sigma[(z + y_t)k_BT]dz \right]. \tag{3.26}$$

The first integral suggests the use of Laguerre quadratures based on $L_n^{(\alpha)}(z)$ with $\alpha = 0$ and the second with $\alpha = 1$. The weights and points for each can also be scaled.

In Table 3.4, we show the convergence of the rate coefficient versus the number of Gauss-Laguerre quadrature points for several different scale factors, s. Also shown

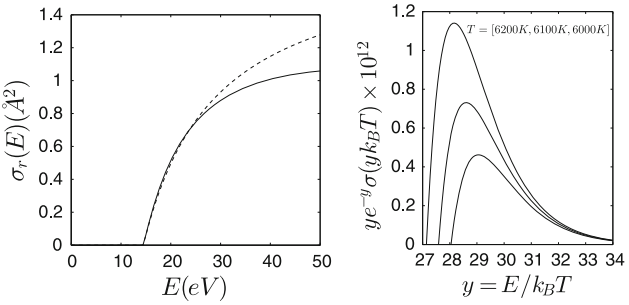

Fig. 3.7 (*Left panel*) Reactive cross section for collisional dissociation for $O + O_2$, Eq. (3.25) (*solid line*) in comparison with the line of centers cross section (*dashed line*; $E^* = E_t$, $\sigma_d = 1.8\,\text{Å}^2$). (*Right panel*) Integrand in Eq. (3.22) versus the reduced energy, $y = E/k_BT$)

Table 3.4 Convergence of the integration Eq. (3.26) for the O + O_2 reactive cross section, Eq. (3.25), for $T = 6{,}000$ K with a Simpson's rule (SR) integration and the Gauss-Laguerre quadrature for three scalings, s

N	SR	N	$s = 1$	$s = 0.8$	$s = 0.5$
20	1.243617	6	1.257290	1.257398	1.257416
40	1.257156	12	1.257497	1.257522	1.257546
60	1.257661	18	1.257533	1.257544	1.257555
80	1.257671	24	1.257546	1.257551	1.257557
120	1.257625	30	1.257551	1.257555	1.257559
200	1.257586	40	1.257556	1.257558	1.257560
300	1.257572	50	1.257558	1.257559	1.257560

The rate coefficient is in units of $10^{-12}\sqrt{8k_BT/\pi\mu}$

is the convergence with a Simpson's rule. One difficulty with the Simpson's rule integration is the truncation of the grid at some sufficiently large z_{max}. There are therefore two convergence parameters, the number of grid points, N and z_{max}.

The rate of convergence of the integrals is much slower with the Simpson's rule in comparison with the Gauss-Laguerre quadrature. The change with scale factor improves the quadrature result for the smaller N values.

3.5.2 *Rate Coefficients for Fusion Reactions; Non-resonant Cross Sections*

The accurate calculation of nuclear reaction rate coefficients is a very important for solar and big bang nucleosynthesis (Clayton 1968; Angula 1999; Descouvemont et al. 2004; Bertulani et al. 2013) as well as for nuclear fusion machines (Haubold and John 1981; Heidbrink and Sadler 1994; Atenzi and Meyer-Ter-Vehn 2004). There is considerable research work on the accurate computation of nuclear reaction rates versus the ambient temperature. For time dependent evolutionary simulations, the rate coefficients need be evaluated numerous times as the temperature evolves with time.

In this section, we consider nuclear fusion reactions for which the non-resonant reactive cross sections are of the form

$$\sigma_r(E) = \frac{S(E)}{E} e^{-B/\sqrt{E}}, \tag{3.27}$$

where B is a constant and $S(E)$, often referred to as the astrophysical S-factor, is a slowly varying function of E. There is another important resonant contribution to fusion reactions which we do not consider. The equilibrium rate coefficient from the average of the reactive cross section with the Maxwellian distribution of

relative energies is given by Eq. (3.22). With the reduced energy $y = E/k_BT$, the rate coefficient is given by

$$k(T) = S_0\sqrt{\frac{8}{\pi\mu k_B T}}I, \tag{3.28}$$

where $S(E)$ is set to a constant, S_0, and the energy average of the cross section can be written in terms of the dimensionless integral

$$I = \int_0^\infty e^{-y-b/\sqrt{y}}dy, \tag{3.29}$$

with $b = B/\sqrt{k_BT}$.

We are interested in the numerical evaluation of the integral in Eq. (3.29). The S_0 and B values of some representative nuclear fusion reactions in stellar interiors are shown in Table 3.5. The details of the integration in Eq. (3.29) are shown in Fig. 3.8(A) as the product of the decreasing Maxwellian and the increasing cross section. The integrand is shown as the Gaussian curve.

The integral in Eq. (3.29) is often approximated with the method of stationary phase also referred to as the saddle-point method (Clayton 1968; Atenzi and Meyer-Ter-Vehn 2004). This is the Gaussian approximation to the bell-shaped curves in Fig. 3.8 which involves the Taylor expansion of the argument of the exponential in

Table 3.5 Representative nuclear fusion reactions (barn $= 10^{-24}$ cm^2)

Reaction	$S(0)$ (keV barn)	B ($\sqrt{\text{keV}}$)
$\text{D} + \text{T} \rightarrow \alpha + \text{n}$	1.2×10^4	34.38
$\text{T} + \text{T} \rightarrow \alpha + 2\text{n}$	138	38.45
$\text{p} + \text{p} \rightarrow \text{D} + \text{e}^+ + \nu$	4.0×10^{-22}	22.20

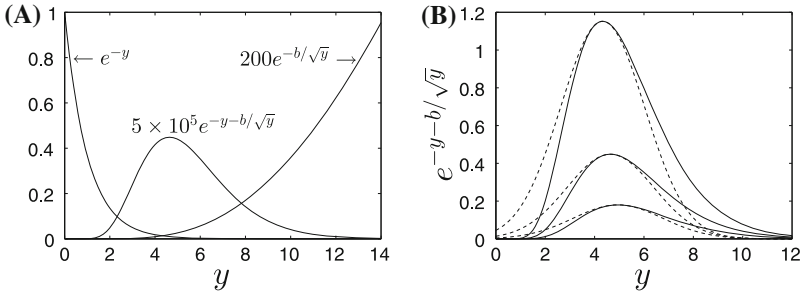

Fig. 3.8 (**A**) The product of decaying Maxwellian distribution and the rising nuclear cross section for $b = 20$. The thermally averaged rate coefficient is the area under the Gaussian shaped curve. (**B**) Integrands for Eq. (3.29) for b = 18, 20 and 22, from *top curve* to *bottom curve*. The *dashed curves* are the Gaussian approximations to the actual integrands used in the approximate evaluation of the integral with the saddle-point or stationary phase method as discussed in the text. The exact integrands, Eq. (3.29), are shown by the *solid curves*

Eq. (3.29) up to the quadratic term. The maximum of the function $f(y) = y + b/\sqrt{y}$ occurs at $y_m = \sqrt[3]{b^2/4}$ and the second derivative is $f''(y_m) = \frac{3}{4} b/y_m^{5/2}$. With the extension of the lower limit of the integral to $-\infty$, the analytic evaluation of the integral of the resulting Gaussian, gives the approximate result

$$I_{approx} = \sqrt{\frac{4\pi}{3y_m}} e^{-y_m - b\sqrt{y_m}}. \tag{3.30}$$

The Gaussian approximations to the integrand for $b = 18$, 20 and 22 are shown by the dashed curves in Fig. 3.8(B). The exact value of the integral can be determined with MAPLE and a comparison of the exact value with the approximation, Eq. (3.30), is shown in Table 3.6 versus b. The Gaussian approximation is accurate to several percent.

We use a Simpson's rule integration to estimate the integral in Eq. (3.29). The variation of the accuracy versus the number of integration points, N, is shown in Fig. 3.9 for three different values of y_{max} that defines the integration interval $[0, y_{max}]$. Figure 3.9(A) shows an oscillatory variation of the relative error versus N and there are sharp minima at specific N values for each y_{max}.

Table 3.6 The error of the Gaussian approximation to the integral $I = \int_0^\infty \exp(-y - b/\sqrt{y})dy$, Eq. (3.30), and the exact value computed with MAPLE

b	I_{exact}	I_{approx}	$\log_{10}\|(I_{exact} - I_{approx})/I_{exact}$
5	0.11854108456183054492994 0 (−1)	1.106 (−2)	−1.18
10	0.56743703833918910589037 3 (−3)	5.425 (−4)	−1.36
18	0.10122934702409988290546 9 (−4)	0.9815 (−5)	−1.52
20	0.40689157785203254674699 9 (−5)	3.953 (−6)	−1.55
22	0.16819070586396057456700 2 (−5)	1.637 (−6)	−1.56

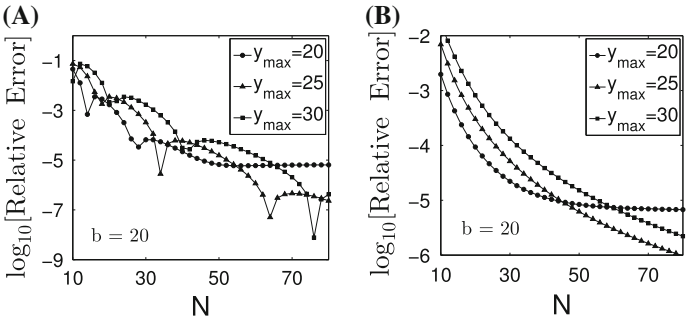

Fig. 3.9 Variation of $\log_{10}$[relative error] versus the number of integration points, N, for the Simpson's rule evaluation of the integral, Eq. (3.29) for $b = 20$. (**A**) Integration interval is $[0, y_{max}]$, (**B**) Integration intervals $[0, \sqrt[3]{b^2/4}]$ and $[\sqrt[3]{b^2/4}, y_{max}]$ where the peak in the Gaussian approximation occurs at $y_0 = \sqrt[3]{b^2/4}$ and N integration points in each interval

Figure 3.9(B) shows the results with a Simpson's rule integration using two intervals, namely $[0, \sqrt[3]{b^2/4}]$ and $[\sqrt[3]{b^2/4}, y_{max}]$ where the peak in the Gaussian approximation occurs at $y_0 = \sqrt[3]{b^2/4}$. The relative error is comparable to that with the full integral and half the number of points but the variation versus N appears monotonic. For the smaller values of N, the accuracy decreases with increasing y_{max} owing to the larger step size. For $y_{max} = 20$, the accuracy attains an asymptotic value because the "tail" of the integrand has not been sampled. This improves with the larger y_{max} values. This exercise illustrates the difficulties of the Simpson's rule on the semi-infinite axis requiring y_{max} to be specified.

We also carry out a comparison of the numerical evaluation of the integral in Eq. (3.29) with a Laguerre quadrature defined by $w(y) = e^{-y}$, and with a quadrature based on the Maxwell weight with $p = 1$ that is, $w(x) = xe^{-x^2}$ with the change of variable $y = x^2$. An important aspect is the distribution of points within the integrand shown in Fig. 3.8. Thus the quadrature points must be scaled so as to be predominantly within the bell shaped curve of the integrand. The results with the Gauss-Laguerre and Gauss-Maxwell quadratures shown in Fig. 3.10 converge much faster versus N than the Simpson's rule integration. The sharp minima in Fig. 3.10

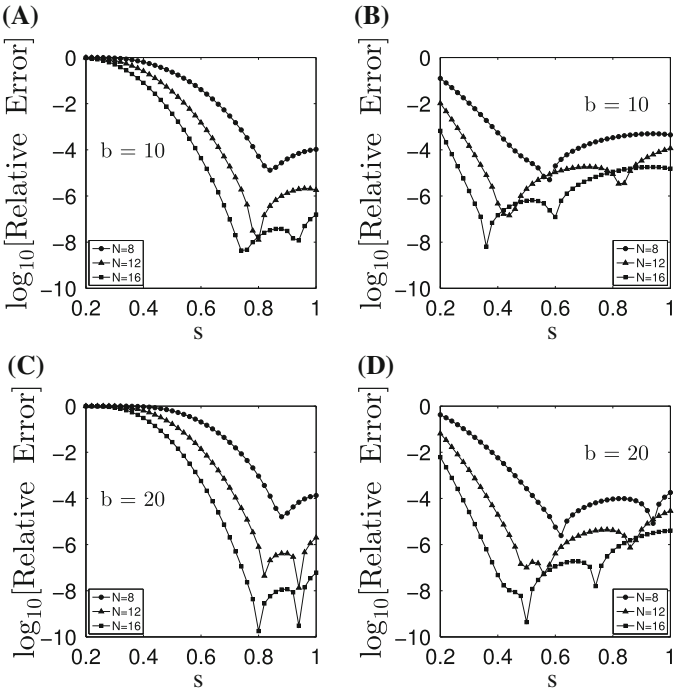

Fig. 3.10 The variation of the $\log_{10}$[relative error] versus the scale factor s for the integral $I = \int_0^\infty \exp(-y - b/\sqrt{y})dy$: (**A**) and (**C**) Gauss-Maxwell quadrature; $w(x) = x\exp(-x^2)$. (**B**) and (**D**) Laguerre quadrature based on $w(y) = \exp(-y)$. The exact value of the integral is calculated with MAPLE listed in Table 3.6

versus the scaling parameter s arise from the change in sign of $I_{approx} - I_{exact}$. Thus, there are several values of the scaling factor for which the numerical result is exact.

There have been several approximate analytical results for the energy integral with the cross section Eq. (3.27) and an energy dependent $S(E)$ which is often expanded in a power series about $E = 0$, that is,

$$S(E) = S(0) + \sum_{n=1}^{N} \frac{1}{n!} \frac{dS(E)}{dE}\bigg|_{E=0} E^n. \tag{3.31}$$

With Eq. (3.31), the reaction rate involves integrals of the form

$$I_n = \int_0^\infty y^n e^{-y-\hat{b}/\sqrt{y}} dy. \tag{3.32}$$

This type of parametrization of the cross section and the subsequent analytical approximation of the integrals was carried out by several groups (Haubold and John 1981; Hussein and Pato 1997; Ueda et al. 2000; Mathai and Haubold 2002). This approach yields the integrals in terms of the Meijer G-function related to the hypergeometric function.

We do not pursue this approach here and consider an efficient quadrature evaluation of the integral in Eq. (3.22) with an alternate fit to $S(E)$ in the form of a Padé approximant (Bosch and Hale 1992) of the form

$$S(E) = \frac{a_1 + E(a_2 + E(a_3 + E(a_4 + Ea_5)))}{1 + E(b_1 + E(b_2 + E(b_3 + Eb_4)))}. \tag{3.33}$$

The cross section parameters for some of the more important fusion reactions are provided in Table IV of the review paper by Bosch and Hale (1992). With the change of variable $x^2 = E/k_BT$, the integral in Eq. (3.22) is appropriate for the Gauss-Maxwell quadrature with $p = 1$.

In Table 3.7 we show the rapid convergence of the rate coefficients, $k(T)$, for three nuclear fusion reactions with the Gauss-Maxwell ($p = 1$) quadrature. A small number of quadrature points of the order of 10 yields more accurate results than the corresponding empirical fits of the rate coefficients versus temperature by Bosch and Hale (1992).

3.6 Integrals in Collision Theory and Kinetic Theory

The theoretical description of collisional processes represents an important research effort in chemical physics. This includes the theoretical calculations of reactive cross sections for chemical and nuclear reactions, photoionization, collisional energy transfer and many other applications. In kinetic theory, the collision operator in the Boltzmann equation for translational energy is defined by the differential collision cross section for binary collisions for atom-atom, electron-atom and ion-atom pairs.

Table 3.7 Convergence of the nuclear reaction rate coefficient, $k(T)$ in cm^3s^{-1} with the thermal average of the cross section in Eq. (3.33) and the parameters in Table VII of Bosch and Hale (1992)

$k_BT(keV)$	N	^{3}He(d, p)^{4}He	D(d, p)T	D(d, n)^{3}He
1	4	0.2353 (−26)	0.98921 (−22)	9.6908 (−23)
	6	2.8176 (−26)	0.99971 (−22)	9.8165 (−23)
	8	2.9488 (−26)	1.0015 (−22)	9.8340 (−23)
	10	2.9571 (−26)	1.0013 (−22)	9.8328 (−23)
	12	2.9575 (−26)		9.8326 (−23)
	14	2.9576 (−26)		
Bosch and Hale (1992)		3.057 (−26)	1.017 (−22)	9.933 (−23)
10	4	1.6792 (−19)	5.8566 (−19)	6.0804 (−19)
	6	1.6301 (−19)	5.8523 (−19)	6.0798 (−19)
	8	1.6286 (−19)	5.8486 (−19)	6.0766 (−19)
	10	1.6288 (−19)	5.8492 (−19)	
	12		5.8491 (−19)	
Bosch and Hale (1992)		2.126 (−19)	5.781 (−19)	6.023 (−19)
50	4	3.4347 (−17)	9.9370 (−18)	1.1349 (−17))
	6	3.4255 (−17)	9.9725 (−18)	1.1378 (−17)
	8	3.4241 (−17)	9.9668 (−18)	1.1373 (−17)
	10	3.4244 (−17)	9.9678 (−18)	1.1374 (−17)
Bosch and Hale (1992)		5.554 (−17)	9.838 (−18)	1.133 (−17)

The Maxwell weight function $w(x) = x\exp(-x^2)$ is used in the energy integration. The rate coefficients quoted by Bosch and Hale (1992) are taken from their Table VIII

Inelastic collisions between molecules with internal energy transfer are also important processes (McCourt et al. 1991; Brun 2009) as well as inelastic electron or ion atom/molecule collisions (Burke and Joachain 1995; Burke 2011) but these topics are beyond the scope of this book.

In the next five subsections, we consider the quadratures involved in the evaluation of (1) the reactive and elastic collision frequencies, (2) the integration over the cusp in the kernel of the Boltzmann equation, (3) the shear viscosity for a simple gas, (4) the eigenvalues of the collision operator in the Boltzmann equation for the special model referred to as Maxwell molecules and (5) the Jeffries-Wentzel-Brillouin-Kramers (JWKB) approximation to the quantal phase shifts used in the calculation of atom-atom collision cross sections. Some but not all of the physical results discussed are derived in detail and the references provided should be consulted for a better understanding of each topic.

3.6.1 The Reactive and Elastic Collision Frequencies

In the previous sections we showed the relationship between the energy dependence of the reactive cross section and the temperature dependence of the reactive rate

coefficient for reactions of chemical interest as well as for fusion reactions. In this section, we express the reactive rate coefficient in terms of the speed dependence of the reactive collision frequency by assuming that one reactant is distributed in speed with a Maxwellian distribution whereas the distribution function of the second component is not specified. We thus integrate over the velocity of the species m_2 taken to be at equilibrium but we do not transform to centre of mass and relative velocity coordinates as done in the previous section.

We write the reactive rate coefficient as

$$k(T) = \int f_1(v_1) R(v_1) d\mathbf{v}_1, \tag{3.34}$$

where the reactive collision frequency is defined by

$$R(v_1) = \int F(v_2) \sigma_r(E) g d\mathbf{v}_2. \tag{3.35}$$

The analogous elastic collision frequency, $Z(v_1)$, is

$$Z(v_1) = \int F(v_2) \sigma_{el}(E) g d\mathbf{v}_2, \tag{3.36}$$

with the total elastic cross section denoted by $\sigma_{el}(E)$. This elastic collision frequency occurs in the collision operator of the Boltzmann equation. The spectral properties of the linear and linearized operators are considered in detail in Chap. 5, and the elastic collision frequency plays an important role as demonstrated later.

The distribution function of reactant labeled 1, $f_1(v_1)$, is unspecified whereas $F(v_2)$ is a Maxwell-Boltzmann distribution function. We define reduced velocity variables

$$\mathbf{z} = \mathbf{g}\sqrt{\frac{\mu}{2k_BT}}, \qquad \mathbf{x}_i = \mathbf{v}_i\sqrt{\frac{m_i}{2k_BT}}, \qquad i = 1, 2 \tag{3.37}$$

so that

$$R(x_1) = \frac{1}{\pi}\sqrt{\frac{2k_BT}{\pi\mu}} \int e^{-x_2^2} \sigma_r(E) z d\mathbf{x}_2. \tag{3.38}$$

With the change of variable in Eq. (3.38) from x to z where the reduced relative velocity is $\mathbf{z} = \sqrt{M_1}\mathbf{x_2} - \sqrt{M_2}\mathbf{x_1}$ and the mass fractions are $M_1 = m_1/(m_1 + m_2)$ and $M_2 = m_2(m_1 + m_2)$, we have that

$$R(x_1) = 2\sqrt{\frac{2k_BT}{\pi\mu}} M_1^{-\frac{3}{2}} \int_0^\infty e^{-(z^2 + M_2 x_1^2)/M_1} \left[\int_{-1}^{1} e^{-2\sqrt{M_2} z x_1 \hat{\mu}/M_1} d\hat{\mu} \right] \sigma_r(E) z^3 dz. \tag{3.39}$$

The 2π factor results from the integration over the azimuthal angle of $\mathbf{z}$ relative to $\mathbf{x}_1$ as the polar axis and $\hat{\mu} = \cos\theta$ where θ is the angle between $\mathbf{z}$ and $\mathbf{x}_1$. The integration over $\hat{\mu}$ is elementary and we find that,

$$R(x_1) = \sqrt{\frac{2k_BT}{\pi\mu}} \frac{1}{\sqrt{M_1M_2x_1}} \left[G(-x_1) - G(x_1)\right], \tag{3.40}$$

where

$$G(x_1) = \int_0^\infty e^{-(z+\sqrt{M_2}x_1)^2/M_1} \sigma_r(E) z^2 dz. \tag{3.41}$$

To evaluate $R(x_1)$, the energy dependence of the reactive cross section must be specified and in the first instance we choose the line-of-centers model, Eq. (3.23), for which we have

$$G(x_1) = \sigma_d \sqrt{M_1} \left[M_1 I_2 - 2\sqrt{M_1M_2} I_1 + (M_2x_1 - \epsilon) I_0\right], \tag{3.42}$$

where the I_n integrals are defined by

$$I_n = \int_{t_0}^\infty e^{-t^2} t^n dt, \tag{3.43}$$

where $t_0 = (\sqrt{\epsilon} + \sqrt{M_2}x_1)/M_1$. These integrals are determined by iteration with

$$I_0 = \frac{\sqrt{\pi}}{2} \mathrm{erfc}(t_0),$$

and

$$I_{n+1} = \frac{1}{2}\left[e^{-t_0^2} t_0^n + nI_{n-1}\right].$$

The variation of the reactive collision frequency for this line-of centers cross section versus reduced energy, x_1^2, for several mass ratios is shown in Fig. 3.11. The mass ratio decreases from $m_1/m_2 = 100$ to $m_1/m_2 = 10^{-4}$ as shown in the graph and Table 3.8. The reactive collision frequency changes form with mass ratio and the numerical evaluation of the integral

$$k(T) = \int_0^\infty x^2 e^{-x^2} R(x) dx, \tag{3.44}$$

for the rate coefficient must take this mass ratio variation into account. A straightforward application of the quadrature based on the Maxwellian weight, $w(x) = x^2 e^{-x^2}$,

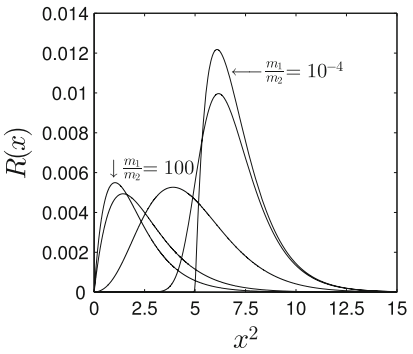

Fig. 3.11 The reactive collision frequency $R(x)$ in units of $\sqrt{2k_BT/\pi\mu}$ versus reduced energy, $x^2 \equiv x_1^2 = mv_1^2/2k_BT$ for reduced threshold energy $\epsilon^* = 5$ for the line-of-centers cross section, Eq. (3.23), and for several mass ratios m_1/m_2 (see Table 3.8). For $m_1/m_2 \to 0$, $R(x) \to 2e^{-x^2}\sigma_r(x^2k_BT)$ and increases rapidly near the threshold energy for small mass ratios m_1/m_2

Table 3.8 The relative error of the Gauss-Maxwell quadrature approximation ($w(x) = x^2e^{-x^2}$) to the integral $I = \int_0^\infty x^2 \exp(-x^2)R(x)dx$ for the line-of-centers cross section, Eq. (3.23)

m_1/m_2	0.0001	0.05	1	10	100
N	Accuracy $= \log[\|1 - I(N)/I_{exact}\|]$				
4	−0.300	−0.521	−4.34	−6.65	−10.5
6	−0.379	−0.731	−4.56	−10.3	−14.3
8	−0.552	−1.08	−6.17	−14.3	
10	−0.806	−1.66	−7.88		
12	−1.73	−1.98	−9.64		
14	−0.878	−1.87	−11.5		
16	−0.945	−2.69	−14.0		
18	−1.01	−2.45	−14.9		
20	−1.16	−3.14			

The exact value is $I_{exact} = e^{-\epsilon^*}$, $\epsilon^* = 5$; The integrals are in units of $\sqrt{2k_BT/\pi\mu}$

yields excellent results for the larger mass ratios but does not capture the integrand for the small mass ratios as shown in Table 3.8. The results for the two smallest mass ratios in the table are very poor and understandably so. Much better results can be obtained with the appropriate translation of the quadrature points so that the first point is just below the threshold energy.

For $\epsilon^* = 0$, the reactive collision frequency reduces to the well-known elastic collision frequency,

$$Z(x) = \pi d^2 \sqrt{\frac{k_BT_b}{2M}} \left[(2\sqrt{\gamma x} + \frac{1}{\sqrt{\gamma x}}) \frac{\sqrt{\pi}}{2} \text{erf}(\sqrt{\gamma x}) + e^{-\gamma x} \right]. \tag{3.45}$$

This collision frequency appears in the Boltzmann collision operator, Eq. (3.46), and is in part the origin of the continuous portion of the eigenvalue spectrum of the collision operator (Hoare and Kaplinsky 1970). In Sect. 3.9.2, we consider the calculation of matrix elements of the multiplicative operator, $Z(x)$. We compare the matrix representation in Laguerre polynomials with the representation in Maxwell polynomials. We compare the calculation of the matrix elements of the elastic collision frequency with the calculation of the matrix elements of the potential in the Schrödinger equation. The matrix elements of the coordinate operator (Harris et al. 1965; Dickinson and Certain 1968) featured prominantly in the development of pseudospectral methods in chemical physics (Light and Carrington Jr. 2000).

3.6.2 Integration Over a Cusp; the Boltzmann Equation

In Chap. 5, we consider the solution of integral equations, in particular the Boltzmann equation, with a kernel $K(x, y)$ defined later. The kernel in this integral equation exhibits a cusp for $x = y$ with a derivative discontinuity at this point. We use a pseudospectral or collocation method (Jerri 1999; Kythe and Puri 2002) to solve the integral equation which requires the integration over the cusp with a chosen quadrature. Other examples of this type of integral equation include Love's integral equation for a circular parallel plate capacitor (Love 1949; Bartlett and Corle 1985; Kumar 2010; Pastore 2011) and a weakly singular Volterra integral equation with sharp gradients reported by Isaacson and Kirby (2011) as well as for quantum mechanical modelling of crystalline solids (Pask et al. 2012). In this section, we consider numerical experiments that involve the integration over the cusp in the kernel for the Boltzmann equation.

We consider a two component system with one component of mass m dilutely dispersed in a second component of mass M which is at equilibrium and at a constant temperature, T_b. The nonequilibrium distribution function, $f(\mathbf{v}, t)$, in the absence of external fields and spatial gradients is given by the linear Boltzmann equation

$$\frac{\partial f(\mathbf{v}, t)}{\partial t} = \int K(\mathbf{u}, \mathbf{v}) f(\mathbf{u}, t) d\mathbf{u} - Z(|\mathbf{v}|) f(\mathbf{v}, t), \tag{3.46}$$

where $K(\mathbf{u}, \mathbf{v})$ is a kernel that describes the change in the distribution function owing to collisions between the two species (Chapman and Cowling 1970; Kapral and Ross 1970; Ferziger and Kaper 1972; Kharchenko et al. 1997) and is known for arbitrary differential cross section as given explicitly by Eq. (7) in Sospedra-Alfonso and Shizgal (2012). The kernel depends on the mass ratio of the two components defined by $\gamma = M/m$.

The distribution function can be anisotropic and it is often represented as an expansion in Legendre polynomials, that is

$$f(\mathbf{v}, t) = \sum_{\ell=0}^{\infty} f_\ell(v, t) P_\ell(\mu), \tag{3.47}$$

where $\mu = \cos\theta$ and θ is the angle between $\mathbf{v}$ and the polar axis in velocity space. We consider the relaxation of isotropic and anisotropic distributions in Chap. 5, Sects. 5.6.3 and 5.7.1, respectively. In Chap. 6, Sect. 6.3, we consider the relaxation of electrons in inert gas atoms with the Fokker-Planck equation which is the limiting form of the Boltzmann equation for $\gamma \to \infty$. This mass ratio limit is referred to as the Lorentz limit as discussed in detail later. The other mass ratio limit is the Rayleigh limit, namely $\gamma \to 0$.

If the distribution function of species m is assumed isotropic, only the spherically symmetric component $f_0(v, t)$ in Eq. (3.47) is of concern. In terms of the reduced energies $x = mu^2/2k_BT_b$ and $y = mv^2/2k_BT_b$, respectively, the isotropic distribution satisfies the Boltzmann equation,

$$\frac{\partial f_0(y,t)}{\partial t} = \int_0^\infty k_0(x,y) f_0(x,t) dx - Z(y) f_0(y,t). \tag{3.48}$$

The kernel $k_0(x, y)$ is the spherical component of $K(\mathbf{u}, \mathbf{v})$.

The kernel for the hard sphere differential cross section, $\sigma = d^2/4$, is known as the Wigner[2]-Wilkins[3] kernel and was originally used to describe neutron slowing down (Wigner and Wilkins 1944). The Wigner-Wilkins kernel (Andersen and Shuler 1964; Hoare and Kaplinsky 1970; Hoare 1971) is given by

$$k_{ww}(x,y) = \tfrac{1}{2}AQ^2\sqrt{\frac{\pi}{x}}\Big[\operatorname{erf}(Q\sqrt{y} - R\sqrt{x}) + e^{x-y}\operatorname{erf}(R\sqrt{y} + Q\sqrt{x}) \pm \Big(\operatorname{erf}(Q\sqrt{y} - R\sqrt{x} + e^{x-y}\operatorname{erf}(R\sqrt{y} - Q\sqrt{x})\Big)\Big], \tag{3.49}$$

where $A = \pi d^2 n_b\sqrt{k_BT_b/2M}$, $Q = \frac{1}{2}(\gamma^{-1/2} + \gamma^{1/2})$, $R = \frac{1}{2}(\gamma^{-1/2} - \gamma^{1/2})$ and n_b is the density of the background gas of particles of mass M. It is useful to note for later reference that the corresponding kernel for realistic differential cross sections is known and involves two integrations over the scattering angle and relative energy (Kapral and Ross 1970; Sospedra-Alfonso and Shizgal 2012, 2013).

The steady state solution is the equilibrium Maxwellian distribution in dimensionless energy units, (see Eq. (3.16)), that is

$$\hat{F}(y) = \frac{2}{\sqrt{\pi}}\sqrt{y}e^{-y}.$$

There are two important physical principles that yield the dependence of the collision frequency, $Z(y)$, versus the reduced energy, y, originally defined by Eq. (3.36).

---

[2] Eugene Paul Wigner (1902–1995), was an Hungarian American theoretical physicist and mathematician who was awarded the Nobel Prize in Physics in 1963 for his fundamental work on the quantum mechanics of elementary particles and symmetries.

[3] Jesse Ernest Wilkins, Jr. (1923–2011) was an African American nuclear physicist and mathematician who contributed to the Manhattan project and nuclear fission reactions.

The first is conservation of number density so that the integral of Eq. (3.48) gives zero that is, $\partial/\partial t[\int_0^\infty f_0(y,t)\sqrt{y}dy] = 0$, as $f_0(y,t)$ is normalized to unity, and we have that,

$$Z(y) = \int_0^\infty k_0(y,x)dx. \tag{3.50}$$

The second principle is the detailed balance condition at equilibrium (Hoare and Kaplinsky 1970) so that $\partial f_0/\partial t = 0$ for $f_0 = \hat{F}$, that is,

$$Z(y) = \frac{1}{\hat{F}(y)} \int_0^\infty k_0(x,y)\hat{F}(x)dx. \tag{3.51}$$

The Maxwellian distributions in Eq. (3.51) symmetrize the kernel, that is

$$G_0(x,y) = \frac{\hat{F}(x)}{\hat{F}(y)} k_0(x,y) = G_0(y,x). \tag{3.52}$$

The Wigner-Wilkins kernel for the special case of equal masses, $\gamma = 1$, is

$$\begin{aligned} k_{ww}(x,y) &= \tfrac{1}{2}AQ^2\sqrt{\frac{\pi}{x}}\,\mathrm{erf}(\sqrt{y}), \quad y < x, \\ &= \tfrac{1}{2}AQ^2\sqrt{\frac{\pi}{x}}e^{x-y}\,\mathrm{erf}(\sqrt{x}), \quad y > x. \end{aligned} \tag{3.53}$$

The three dimensional plot of the symmetrized Wigner-Wilkins kernel for $\gamma = 1$ is shown in Fig. 3.12 (top left graph). The variation of $G(x, y_0)$ versus x for $y_0 = 1, 2, 3, 4$ and 5 for $\gamma = 0.0001$, 1 and 1,000 is shown in the other three graphs. For $\gamma = 1$, the kernel versus x for each y_0 is much wider than the very narrow cusps for the two disparate mass ratios on the right hand graphs.

It is clear that the kernel is sharply peaked at the disparate mass limits, which are referred to as the Lorentz and Rayleigh limits as discussed previously. This is a result of the small energy transfers in a collision between particles of very different mass. This property of the kernel concerning velocity changing collisions has been reported frequently in the literature (Shizgal and Lindenfeld 1979; Liao et al. 1980; Berman et al. 1986; Rogers and Berman 1991; Gibble and Gallagher 1991; Shapiro 2000; Belai et al. 2007; McGuyer et al. 2012) and impacts on many applications and on Doppler spectroscopy in particular. Examples of a similar localized nature of the kernel in the Boltzmann equation for realistic cross sections are shown in Fig. 4 of Bovino et al. (2011) and Fig. 5 of Zhang et al. (2007).

Our interest in this section is the calculation of the collision frequency with Eq. (3.51). It is clear that in the disparate mass limits a single quadrature for all values of y_0 would be inefficient if the integration algorithm does not take into account the position and width of the cusp over a small interval $[x_{min}, x_{max}]$.

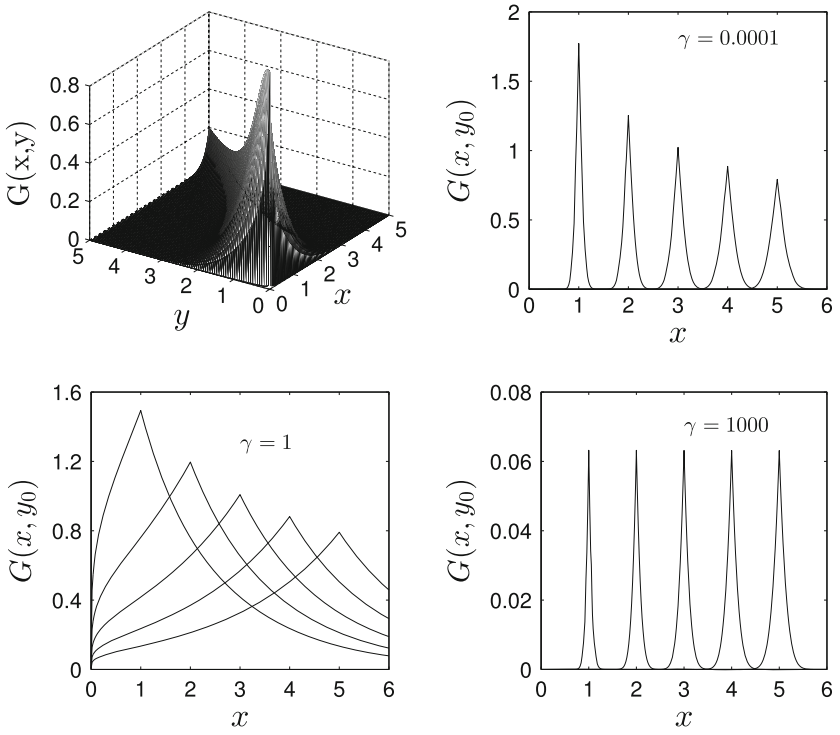

Fig. 3.12 (*Upper left panel*) The three dimensional surface of the Wigner-Wilkins kernel, Eq. (3.53) for equal masses, $\gamma = 1$. Variation of the kernel for fixed argument, $y_0 = 1$, 2, 3, 4 and 5 versus x for $\gamma = 0.0001$, 1 and 1,000

We consider the extreme mass ratio $\gamma = 1{,}000$, shown in Fig. 3.12 and choose a Simpson rule quadrature to evaluate the integral. In view of the localized nature of the kernel, we consider a narrow interval that brackets the cusp at y_0.

In Fig. 3.13(A), we show for $\gamma = 100$, $y_0 = 1$, the variation of the relative error with a Simpson rule algorithm versus the number of grid points, N, $x_{min} = 0$ and different values of x_{max}. The grid spacing is the same for all x_{max} and as expected the number of integration points required to achieve convergence decreases with x_{max}. The initial decrease in the relative error is rapid for small values of N for all values of x_{max}. In spite of the localized nature of the kernel, the interval has to be sufficiently wide to capture the "tails" on either side of the cusp.

In Fig. 3.13(B), we show for $y_0 = 5$ the variation of the relative error versus the number of grid points, N, for different values of x_{max} with $x_{min} = 0$ (dashed curves) and $x_{min} = 3$ (solid curves). The smaller interval about $y_0 = 5$ gives the more rapid convergence as expected with also a rapid convergence even for small values of N. For all the results shown in Fig. 3.13 there is a grid point at the cusp. The grid spacing, h, is varied as given by $h = 1/m$, and m varies from 10 to 400 in increments of 10. These aspects of the integration over the kernel are important with regard the

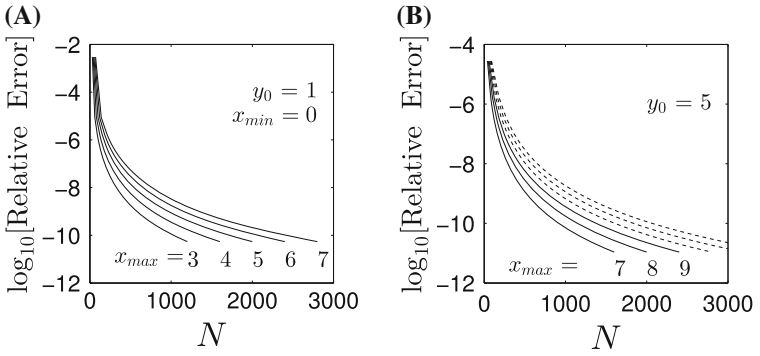

Fig. 3.13 Variation of $\log_{10}$[relative error] for the Simpson rule integration of the symmetrized Wigner-Wilkins kernel $G_0(x, y_0)$, Eq. (3.52) for $\gamma = 1{,}000$. (**A**) $y_0 = 1$; integration is over the interval $x \in [0, x_{max}]$; (**B**) $y_0 = 5$; integration is over the interval $x \in [3, x_{max}]$ (*solid curve*) and $x \in [0, x_{max}]$ (*dashed curve*). In each case, the grid spacing is given by $h = 1/m$ with $m =$ [10:10:400]

solution of the time dependent Boltzmann equation, Eq. (3.48), discussed in Chap. 5. However, the choice $\gamma = 1{,}000$ is extreme.

We compare further the results just discussed with integrations that divide the integration interval into two subintervals $x \in [0, y_0]$ and $x \in [y_0, x_{max}]$. We use a Simpson rule integration in both subdomains as well as a Legendre quadrature for each subdomain with the appropriate change of variable. The results for the Simpson rule integration are shown in Fig. 3.14(A) for $y_0 = 1$ (solid curves) and the two intervals [0, 3] and [0, 2] with convergence faster for the smaller interval. The results

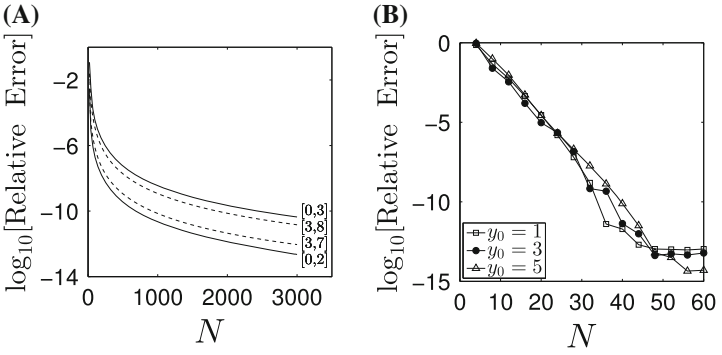

Fig. 3.14 Variation of $\log_{10}$[relative error] for the integration of the symmetrized Wigner-Wilkins kernel $G_0(x, y_0)$, Eq. (3.52) for $\gamma = 1{,}000$. (**A**) Simpson rule integration with $N/2+1$ points in each of the intervals $[0, y_0]$ and $[y_0, x_{max}]$ for $y_0 = 1$ (*solid curves*) and $y_0 = 5$ (*dashed curves*). The intervals used are shown next to the curves. (**B**) Legendre quadrature integration over the intervals $[x_{min}, y_0]$ and $[y_0, x_{max}]$ for $y_0 = 1$, 3 and 5 with $N/2$ points in the intervals [0, 2], [2, 5] and [3, 8], respectively, that bracket y_0

for $y_0 = 5$ (dashed curves) are very similar with the smaller interval providing faster convergence. We notice an initial rapid convergence versus N with a small number of quadrature points as also shown in Fig. 3.13. By contrast with Fig. 3.13, there are $N/2$ points in each interval and many more points between the origin and y_0. Also the grid spacing changes with N as given by $h = 1/m$ with m chosen as before.

In Fig. 3.14(B), the results the Gauss-Legendre quadrature in the two intervals $[x_{min}, y_0]$ and $[y_0, x_{max}]$ with $N/2$ quadrature points in each interval are shown. It is very clear that the Gauss-Legendre quadrature is far superior to the Simpson rule algorithm with results similar for all y_0 provided that the integration domain brackets the cusp. A similar comparison of Simpson and trapezoidal rules for integrations over a cusp were discussed by Secrest and Johnson (1966) in their modelling of atom-diatomic collisional energy transfer.

We consider the Gauss-Maxwell quadrature with $w(x) = x^2 e^{-x^2}$ where $x = \sqrt{mv^2/2k_BT_b}$ is the reduced speed rather than the reduced energy. We calculate $Z(x_i)$ where x_i is the ith quadrature point of the quadrature of order N. This approach does not take into account the cusp in the kernel and we cannot expect the convergence to yield the very small relative errors as in Figs. 3.13 and 3.14. The collision frequency at each x_i calculated with the same set of $N = 80$ quadrature points is shown in Fig. 3.15. The best agreement between the exact and numerical collision frequencies is for mass ratio unity. The departures for the larger and smaller mass ratios arise from the more narrow cusp. The errors are largest for the larger quadrature points as a small number of quadrature points are distributed to the right of the cusp. The calculation of $Z(x_{80} = 14.012)$ does not include the contributions beyond x_{80}. However, this is precisely the approach used, with this or other quadratures, to reduce the integral equation, Eq. (3.46) to a set of coupled ordinary differential equations as discussed further in Chap. 5.

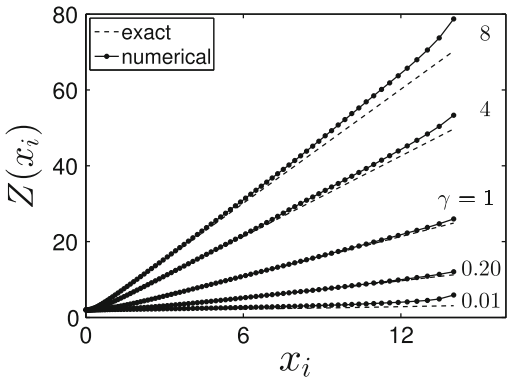

Fig. 3.15 Comparison of the exact hard sphere collision frequency, $Z(x)$ (*dashed curves*) in units of $\pi d^2\sqrt{k_BT_b/2m}$, Eq. (3.45), with the numerical integration (*solid curves*) of the Wigner-Wilkins kernel with the Gauss-Maxwell quadrature ($p = 2$, $N = 80$) for several mass ratios. The symbols show each of the 80 quadrature points and $x = \sqrt{mv^2/2k_BT_b}$ is the reduced speed

3.6.3 Viscosity of a Simple Gas

The Chapman-Enskog method of solution of the Boltzmann equation for a one component gas discussed in Chap. 5 is the basis for the calculation of the transport coefficients (Hirschfelder et al. 1954; Huang 1967; Chapman and Cowling 1970; Ferziger and Kaper 1972). For the calculation of the viscosity, the method assumes a small departure of the velocity distribution function from a Maxwellian owing to a small velocity gradient. This perturbation of the distribution function is given by the solution of the linearized Boltzmann equation, Eq. (5.45). The integral collision operator in the Boltzmann equation is defined by the differential scattering cross section for binary collisions of the gaseous particles. We assume that the particle collisions are described by a hard sphere cross section and the integral Boltzmann equation is then given by Eq. (5.88).

The shear viscosity of a simple gas in reduced units is given by

$$\nu = \frac{16\sqrt{2}}{15} \int_0^\infty e^{-x^2} x^4 B(x) dx, \tag{3.54}$$

as defined in recent publications (Siewert 2002; Sharipov and Bertoldo 2009). We direct our attention to the numerical integration of the integral in Eq. (3.54) given the function $B(x)$ which is determined with the solution of the Boltzmann equation for viscosity (Loyalka et al. 2007).

Loyalka et al. (2007) employed an expansion of the distribution function in the Laguerre (or Sonine) polynomials and used *Mathematica* to algebraically obtain extremely accurate converged solutions to the Boltzmann equation with up to 150 terms and provided the function $B(x)$ in Table 5 of their paper. This is essentially the Galerkin solution of the integral equation. Their work serves as an excellent benchmark and they report the viscosity to 34 significant figures, that is $\nu = 0.44902780628789243460904948953465 45$.

We use a spline fit of $B(x)$ from the data provided in Table 5 of Loyalka et al. (2007) which has 44 data points for $x \in [0, 6]$. The values of $B(x)$ are available only up to $x = 6$, but beyond this point the integrand is less than 10^{-15}. With the weight factor $w(x) = x^2 \exp(-x^2)$ in the integrand, it would appear that an optimal quadrature is the one based on the Maxwell polynomials with $p = 2$.

Thus we consider the integral in Eq. (3.54) with the quadratures based on the Maxwell and Laguerre polynomials and we also include a Simpson's rule for comparison. In this case since the data for $B(x)$ is limited up to $x_{max} = 6$ the Simpson's rule is defined on the interval $[0, 6]$. Also, for the higher order quadratures, the Laguerre quadrature points can be greater than 6^2 so that these have to be scaled as in Eq. (3.3) such that the last point is at $y = 36$ which occurs for $N > 10$. The quadrature point x_N for the Maxwell quadrature and y_N for the Laguerre quadratures for orders $N = 3$ to 10 are compared in Table 3.9. The Laguerre quadrature points are far more diffuse in reduced energy than the Maxwell quadrature in reduced speed for the same N. A similar comparison was shown in Chap. 2.

Table 3.9 The quadrature points, x_N and y_N, for the listed Nth order Gaussian quadratures

	N	3	4	5	6	7	8	9	10
Maxwell ($p = 2$)	x_N	2.220	2.640	3.014	3.356	3.671	3.967	4.245	4.509
Laguerre ($\alpha = 3/2$)	y_N	8.471	11.71	15.05	18.46	21.92	25.43	28.98	32.55

The Laguerre quadrature points are far more diffuse than the Maxwell quadrature points with the same N

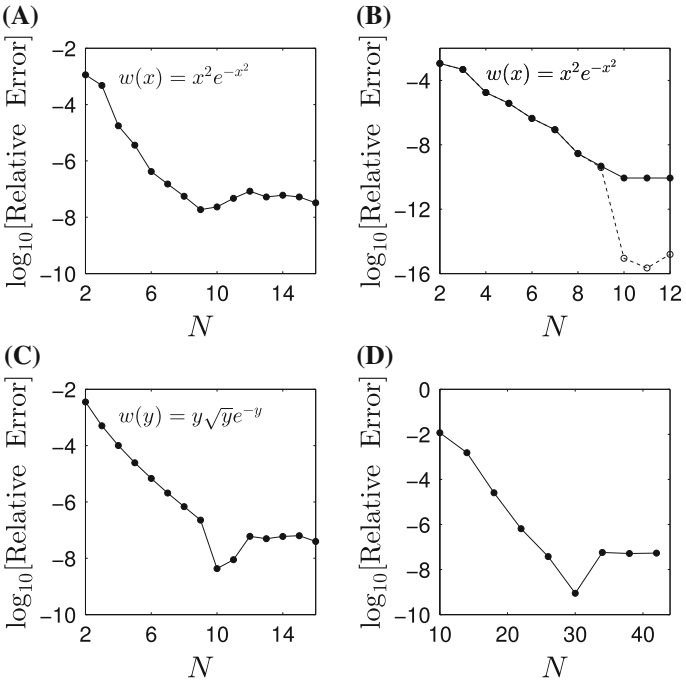

Fig. 3.16 Convergence of the integral for the viscosity of a simple hard sphere gas, Eq. (3.54). (**A**) Gauss-Maxwell quadrature with spline fit to the data in Table 5 of Loyalka et al. (2007); (**B**) Gauss-Maxwell quadrature with a 16th order polynomial fit to the data in Table 5 of Loyalka et al. (2007); *dashed curve* uses the "exact" value with the polynomial fit; (**C**) Gauss-Laguerre quadrature ($\alpha = 3/2$); (**D**) Simpson's rule

A comparison of the convergence of the viscosity, given by Eq. (3.54) versus the number of quadrature points for these three algorithms is shown in Fig. 3.16. Figure 3.16(A), (B) are the results for Gauss-Maxwell ($p = 2$) with a spline fit of the data in Table 5 of Loyalka et al. (2007). For the dashed curve in Fig. 3.16(B), the exact value from the polynomial fit is used so that machine accuracy obtained is expected. The results with the Gauss-Laguerre quadrature in Fig. 3.16(C) are comparable to those with the Gauss-Maxwell quadrature above. The moderately rapid convergence of the relative errors for this integral for all quadratures are anticipated for this very smooth integrand. In Chap. 5, Sect. 5.4.5, we consider the solution of the Boltzmann integral equation for $B(x)$ and the calculation of the shear viscosity in comparison with the spline method of solution used by Siewert (2002).

3.6.4 Eigenvalues of the Boltzmann Collision Operator for Maxwell Molecules

In the kinetic theory of gases, the model system based on the atom-atom power law repulsive interaction of the form $V_{MM}(r) = \kappa/r^4$, where r is the atom-atom separation, is referred to as "Maxwell molecules" and κ determines the strength of the interaction. The model was introduced by James Clerk Maxwell[4] long ago as reviewed by Santos (2009). This model is of major significance to the history of the kinetic theory of gases. In spite of the nonphysical nature of this repulsive interaction potential, the model has been used over several decades in many applications (St.-Maurice and Schunk 1976, 1979; Hubert 1983; Shizgal and Hubert 1989; Sabbane et al. 2003; Napier and Shizgal 2008; Santos 2009). The attractive potential, $V(r) = -\kappa/r^4$, is a model for the long range ion atom interaction potential that provides an estimate of ion mobilities in neutral gases with solutions of the Boltzmann equation (McDaniel and Mason 1973; Mason and McDaniel 1988).

The eigenfunctions of the linearized one-component Boltzmann collision operator for the repulsive Maxwell molecule interaction are the direct product of the Sonine-Laguerre polynomials and the spherical harmonics. Thus, the Sonine-Laguerre polynomials have become the basis set of choice for kinetic theory problems. The Maxwell molecule model has also been employed in studies of the approach to equilibrium for the non-linear Boltzmann equation (Krook and Wu 1976; Ernst 1981; Bobylev 1984).

For the interparticle potential, $V_{MM}(r)$, the two body classical scattering problem can be solved exactly (Goldstein et al. 2000; Liboff 2003) and the dependence of the differential cross section on the relative speed, g, and scattering angle, θ, is given by

$$\sigma(g,\theta) = 2\sqrt{\frac{\kappa}{m}}\frac{1}{g}I_4(\theta). \tag{3.55}$$

The dependence on the scattering angle is given by

$$I_4(\theta) = -\frac{1}{\sin(\theta)}\frac{d\cot(2\phi)}{d\theta}, \tag{3.56}$$

with the scattering angle θ defined in terms of ϕ

$$\theta = \pi - 2\sqrt{\cos(\phi)}K(\sin^2\phi), \tag{3.57}$$

where

$$K(\sin^2\phi) = \int_0^{\pi/2}\frac{1}{[1-\sin^2\phi\sin^2\alpha]}d\alpha, \tag{3.58}$$

is the Elliptic integral.

[4] James Clerk Maxwell (1831–1879) was a Scottish mathematical physicist who made a large number of fundamental contributions to electromagnetic theory, kinetic theory and thermodynamics.

It is very important to notice that for this interaction the product $g\sigma(g,\theta)$ is independent of g (see Eq. (3.55)). An important consequence of this model is that the collision frequency $Z(v)$ that occurs in the collision operator in the Boltzmann equation as given by Eq. (3.35) is independent of the particle speed. The collision operator is greatly simplified and the eigenvalue spectrum of the operator is completely discrete.

It can be shown (Ford 1968; Foch and Ford 1970) that the eigenvalues, $\lambda_{n,\ell}$, of the linearized one-component collision operator for this interaction are given explicitly by the integral

$$\lambda_{n,\ell} = -4\pi\sqrt{\frac{\kappa}{m}}\int_0^{\pi} I_4(\theta)\Big[\cos^{2n+\ell}(\frac{\theta}{2})P_\ell[\cos(\frac{\theta}{2})] + \sin^{2n+\ell}(\frac{\theta}{2})P_\ell[\sin(\frac{\theta}{2}) - 1] - \delta_{n0}\delta_{\ell,0}\Big]\sin\theta d\theta. \tag{3.59}$$

We find it convenient to transform the integration variable from θ to ϕ so that the integral in Eq. (3.59) becomes

$$\lambda_{n,\ell} = 8\pi\sqrt{\frac{\kappa}{m}}\int_0^{\pi/4}\left[\frac{\cos^{2n+\ell}(\frac{\theta}{2})P_\ell[\cos(\frac{\theta}{2})] + \sin^{2n+\ell}(\frac{\theta}{2})P_\ell[\sin(\frac{\theta}{2}) - 1] - \delta_{n0}\delta_{\ell,0}}{\sin^2 2\phi}\right]d\phi, \tag{3.60}$$

and the angle θ is determined from ϕ as given by Eq. (3.57). In Fig. 3.17(A) we show the integrands of Eq. (3.60) versus ϕ for $\lambda_{n,0}$ with $n = 4$, 8, 12 and 16 and likewise in Fig. 3.17(B) we show the integrands for $\lambda_{0,\ell}$ with $\ell = 6$, 10, 14 and 16. There is a rapid variation near $\phi = \pi/4$ shown in Fig. 3.17(B).

We choose a Gauss-Legendre quadrature to calculate $\lambda_{n,\ell}$. The convergence of several eigenvalues versus the number of quadrature points increases with n and ℓ as shown in Tables 3.10 and 3.11. The results in the tables are in agreement with

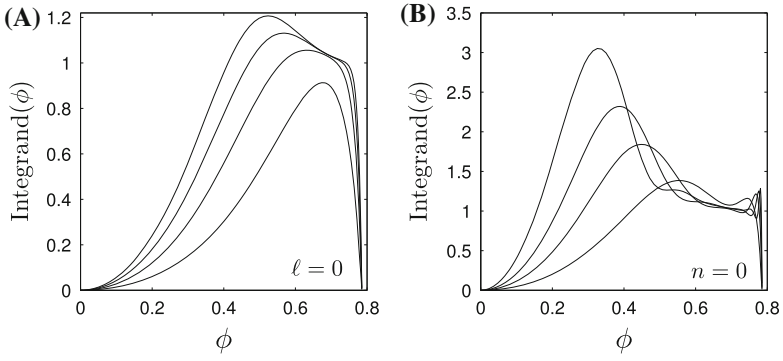

Fig. 3.17 The ϕ variation of the integrand in Eq. (3.60) for the Maxwell molecule eigenvalues, $\lambda_{n,\ell}$. (**A**) $\ell = 0$ and n from top to bottom is 16, 12, 8 and 4. (**B**) $n = 0$ and ℓ from top to bottom is 16, 14, 10 and 6

Table 3.10 Convergence of the Maxwell molecule eigenvalues, $\lambda_{n,0}$ with Gauss-Legendre quadratures

N	$\lambda_{4,0}$	$\lambda_{8,0}$	$\lambda_{12,0}$	$\lambda_{16,0}$
4	7.2473049826	10.6815741779	12.6401640971	13.9560579506
8	7.1404138296	10.3355659392	12.2873384173	13.7368118926
12	7.1402976496	10.3296515433	12.2624669303	13.6902870561
16	7.1402976448	10.3296443968	12.2622077369	13.6886563346
20	7.1402976448	10.3296443951	12.2622072790	13.6886437782
24		10.3296443951	12.2622072788	13.6886437520
32			12.2622072788	13.6886437519
40				13.6886437520

Table 3.11 Convergence of the Maxwell molecule eigenvalues, $\lambda_{0,\ell}$ with Gauss-Legendre quadratures

N	$\lambda_{0,6}$	$\lambda_{0,10}$	$\lambda_{0,14}$	$\lambda_{0,18}$
4	15.0278419641	18.9389440371	21.4348909276	25.4697236812
8	14.2744916100	19.4726281411	23.4800390873	26.5094667009
12	14.2628153767	19.3091338846	23.3459851156	26.8105457092
16	14.2628093775	19.3059204404	23.2863701647	26.7017149499
20	14.2628093771	19.3059159880	23.2852977701	26.6815970246
24		19.3059159869	23.2852954023	26.6812438552
32		19.3059159868	23.2852954009	26.6812426849
40			23.2852954011	26.6812426851
50				26.6812426847

the large number of eigenvalues reported by Alterman et al. (1962) to the significant figures shown and expressed in units of their $A_2 = 9.689818653\ \sqrt{\kappa/m}$, that is $\lambda_{02} = 0.6 \times 9.689818653\ \sqrt{\kappa/m} = 5.8138911918\sqrt{\kappa/m}$. The authors mention that the integrands in their work were highly oscillatory. They calculated the eigenvalues to 10 significant figures in triple precision with up to 96 Gauss-Legendre quadrature points. The lower order eigenvalues reported recently (Sabbane et al. 2003; Santos 2009) are also in agreement with the results reported here.

3.6.5 The JWKB Phase Shifts and Quantum Elastic Cross Sections

The calculation of the differential and total elastic cross sections for atom-atom collisions with a specified interatomic potential is important for the calculation of transport

coefficients for diffusion, viscosity, heat conduction and ion mobilities (Hirschfelder et al. 1954; Chapman and Cowling 1970; Ferziger and Kaper 1972; Mason and McDaniel 1988; Lemmon and Jacobsen 2004; Danailov et al. 2008; Oh 2013). Other applications include the relaxation to equilibrium of an initial nonequilibrium distribution of energetic atoms by collisional energy transfer (Nan and Houston 1992; Kharchenko and Dalgarno 2004; Zhang et al. 2007; Bovino et al. 2011; Sospedra-Alfonso and Shizgal 2013). Binary collision theory is based on either classical mechanics (Goldstein et al. 2000) or quantum mechanics (Child 1996; Burke 2011).

The quantum mechanical differential elastic cross section for binary collisions between two structureless particles is given in terms of the square of the scattering amplitude, $f(E, \theta)$, which depends on the center-of-mass relative energy, E, and the scattering angle, θ, that is

$$\sigma(E, \theta) = |f(E, \theta)|^2, \tag{3.61}$$

where the scattering amplitude can be expressed in terms of the phase shifts, $\delta_\ell(E)$,

$$f(E, \theta) = \frac{1}{k} \sum_{\ell=0}^{\infty} (2\ell + 1) e^{i\delta_\ell} \sin(\delta_\ell) P_\ell(\cos\theta), \tag{3.62}$$

and $P_\ell(\cos\theta)$ is the Legendre polynomial. In Eq. (3.62), $k = \sqrt{2\mu E/\hbar^2}$ is the wave number and μ is the reduced mass of the colliding pair. The phase shifts can be determined from a solution of the radial Schrödinger equation

$$\frac{1}{r^2}\frac{d}{dr}\left(r^2 \frac{du_{k,\ell}(r)}{dr}\right) + [k^2 - U(r) - \frac{\ell(\ell+1)}{r^2}]u_{k,\ell}(r) = 0 \tag{3.63}$$

where $U(r) = 2\mu V(r)/\hbar^2, k^2 = 2\mu E/\hbar^2$ and the interaction potential is $V(r)$, where r is the distance between the pair of particles considered. The Schrödinger equation is solved for the continuum scattering states with $E > 0$ and the asymptotic boundary condition on the radial wavefunction is

$$u_{k,\ell}(r) \underset{r\to\infty}{\sim} r\frac{\sin(kr - \ell\pi/2 - \delta_\ell)}{kr}, \tag{3.64}$$

which defines the phase shift δ_ℓ. A more detailed discussion of the theoretical approach can be found in several references (Bernstein 1966; Child 1996; Burke 2011; Taylor 2012).

With the scattering amplitude expressed as in Eq. (3.62), the total cross section is given by

$$\sigma_{total}(E) = 2\pi \int_0^\pi \sigma(E, \theta) \sin\theta d\theta = \frac{4\pi}{k^2} \sum_{\ell=0}^{\infty} (2\ell + 1) \sin^2 \delta_\ell(k). \tag{3.65}$$

For heavy particle collisions at high relative energies, many phase shifts contribute to the total cross section, Eq. (3.65), and the time consuming numerical integration

of the radial Shrödinger equation is not necessary in many situations. The Jeffreys-Wentzel-Kramers-Brillouin (JWKB) phase shift (Child 1996; Burke 2011) given by

$$\delta_\ell = \int_{r_0}^{\infty} \sqrt{\left[k^2 - \frac{(\ell+\frac{1}{2})^2}{r^2} - U(r)\right]} dr - \int_{r_1}^{\infty} \sqrt{k^2 - \frac{(\ell+\frac{1}{2})}{r^2}} dr, \tag{3.66}$$

provides a very good approximation. In Eq. (3.66), r_0 is the classical turning point given by the root of the square bracket term in the first integral. Analogously, $r_1 = \sqrt{(\ell+\frac{1}{2})^2/k^2}$ and we have made the familiar Langer modification (Langer 1937) by replacing $\ell(\ell+1)$ with $(\ell+\frac{1}{2})^2$.

With this very brief overview of semiclassical scattering theory, we now direct attention to our main concern here, namely the numerical evaluation of the phase shift as defined by Eq. (3.66). As with the previous applications discussed in this chapter, the nature of the integrand dictates the choice of numerical quadrature. In this application, it is important to notice that the integral depends on the choice for the potential, $V(r)$, the relative energy as given by k^2, the value of ℓ and the classical turning point, r_0.

We choose the diatom O-H which is important in the estimation of the escape of atomic species from planetary atmospheres (Shizgal 1999; Balakrishnan and Dalgarno 2003; Kharchenko and Dalgarno 2004; Jamieson et al. 2006) and in other applications (Wright and Donaldson 1985; Oneal and Neff 1997). The interaction potentials and collision dynamics were reported in detail in these references. For the purpose of the numerical comparisons presented here it is sufficient to choose the ground $X^2\Pi$ state of OH to be the Morse potential reported by Wright and Donaldson (1985) and given by

$$V(r) = D_e\left[1 - e^{-\beta(r-r_e)}\right]^2, \tag{3.67}$$

where $r_e = 1.821$ au, $D_e = 5.426\,\text{eV}$ and $\beta = 1.189\,(\text{au})^{-1}$ where $1\text{au} = 0.52917$ Å and 1 Å $= 10^{-8}$ cm. In Chap. 6, we will also consider the bound vibrational states of such diatomic molecules modelled with the Morse potential. There are many other choices for the interatomic potentials including a Lennard-Jones potential (Sospedra-Alfonso and Shizgal 2013) as well the results of quantum mechanical calculations of the electronic structure (Jamieson et al. 2006) for which the potential is often available in tabular rather than in analytic form (Shizgal 1999).

The methods that have been proposed to evaluate the integral in Eq. (3.66) include a modified Clenshaw-Curtis quadrature (Kennedy and Smith 1967), a Gauss-Mehler quadrature (Pack 1974), a Gauss-Legendre quadrature and a non-classical quadrature proposed by Cohen (1978) based on the weight function $w(x) = 1/\sqrt{1-x} \quad x \in [0, 1]$ (see Item 25.4.36 in Abramowitz and Stegun (1964)) with quadrature points and weights related to the Gauss-Legendre quadrature.

A comparison of the Gauss-Legendre and Gauss-Mehler quadratures in the numerical evaluation the integrals for δ_ℓ is presented. It is of interest to note that the use of the

Clenshaw-Curtis quadrature in this application resulted in a study of the convergence properties by O'Hara and Smith (1968) and later by Trefethen (2008).

A detailed comparison of different quadratures is made challenging owing to the variation of the integrand in Eq. (3.66) versus x that depends on the interaction potential, $V(r)$, the energy E and the value of ℓ. Except for the case of short ranged nuclear interactions, a moderately large number of partial waves must be calculated in order to get a converged cross section. Such cross sections for a variety of binary atomic pairs are used in several studies of the approach to equilibrium based on the Boltzmann equation (Bovino et al. 2009, 2011; Sospedra-Alfonso and Shizgal 2013) that we consider in detail in Chap. 5. There are also practical applications concerning gaseous transport properties (Oh 2013; Lemmon and Jacobsen 2004) as well for ion mobilities in gases (Mason and McDaniel 1988; Viehland 1994; Danailov et al. 2008).

The first step in the evaluation of the integral for the phase shift is the determination of the classical turning point which can be done with a simple search to bracket the root and then with a Newton-Raphson iteration to converge to the root. We show in Fig. 3.18 the variation of the "effective" potential, $V_{eff}(r) = V(r) + (\ell + \frac{1}{2})/r^2$ versus r for four values of ℓ at $E = 1.0\,\text{eV}$. For the two lowest ℓ values there is one innermost turning point whereas for $\ell = 60$ there are three turning points and for $\ell = 62$ there is one outermost turning point. We here only consider the one outermost turning point but there is an error introduced (Munn et al. 1964; Viehland and Chang 2010) which is related to the classical orbiting problem when the relative energy is close to the top of the centrifugal barrier depicted by the maximum in $V_{eff}(r)$ in Fig. 3.18.

We make the change of variable $x = r_0/r$ and recognize the classical impact parameter with $b = (\ell + \frac{1}{2})/k$. A very important connection between the semiclassical theory and the classical approach is the relationship between the variation of δ_ℓ versus ℓ and the scattering angle, $\chi(b)$ versus b, given by $\chi(b) = 2\partial\delta_\ell/\partial\ell$ (Child 1996; Viehland and Chang 2010). The phase shift in the new integration variable

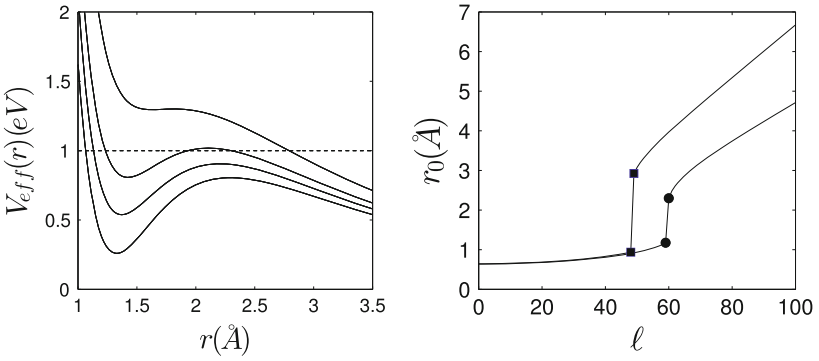

Fig. 3.18 (*Left hand side*) The effective potential $V_{eff}(r) = V(r) + \frac{(\ell+1/2)^2}{r^2}$ where $\ell = 56, 58, 60$ and 62 from bottom to top curves with $E = 1.0\,\text{eV}$ as the *dashed line*. The three turning points are clearly seen for $\ell = 60$. (*Right hand side*) The classical turning points, r_0 versus ℓ, for $E = 0.5\,\text{eV}$ (*square symbols*) and for $E = 1.0\,\text{eV}$. The symbols show the change in the classical turning from the innermost root to the outermost root

appropriate for Gauss-Legendre (GL) quadratures is given by,

$$\delta_\ell^{(GL)} = kr_0 \int_0^1 I_\ell^{(GL)}(x)dx + \frac{\pi[(\ell+\frac{1}{2}) - kr_0]}{2}, \tag{3.68}$$

where

$$I_\ell^{(GL)}(x) = \left[\sqrt{1 - \frac{(\ell+\frac{1}{2})x^2}{kr_0} - \frac{U(r_0/x)}{k^2}} - \sqrt{1-x^2}\right]\frac{1}{x^2}. \tag{3.69}$$

Pack (1974) suggested the use of a Gauss-Mehler quadrature which is a Chebyshev quadrature ($w(x) = 1/\sqrt{1-x^2}$) with only the positive quadrature points. The Gauss-Mehler quadrature points and weights are given by

$$x_i = \cos(\frac{i\pi}{2N+1}), \quad i = 1, \ldots N$$

$$w_i = \frac{(1-x_i^2)\pi}{2N+1}. \tag{3.70}$$

The algorithm is applied to the integral

$$\delta_\ell^{(GM)} = kr_0 \int_0^1 \frac{1}{\sqrt{1-x^2}} I_\ell^{(GM)}(x)dx + \frac{\pi[(\ell+\frac{1}{2}) - kr_0]}{2}, \tag{3.71}$$

where

$$I_\ell^{(GM)}(x) = (1-x^2)\left[\sqrt{1 - \frac{(\ell+\frac{1}{2})x^2}{kr_0} - \frac{U(r_0/x)}{k^2} - 1}\right]\frac{1}{x^2}. \tag{3.72}$$

It is readily shown that the derivative of the integrand is singular at $x = 1$.

The phase shifts for a range of energies and ℓ values were determined from the integral in Eq. (3.68) with a Gauss-Legendre quadrature. It is instructive to first show the energy dependence of the total cross section in Fig. 3.19(A). The actual value of the cross section is somewhat larger than previously reported for more realistic potentials for OH (Wright and Donaldson 1985; Shizgal 1999; Bovino et al. 2009, 2011). The differential cross section for $E = 0.5\,\text{eV}$ is shown in Fig. 3.19(B). The number of phase shifts required to get convergence of the cross sections increases with E and for the energy range shown in the figure up to 400 phase shifts were required. Thus a large number of phases shifts are required for the results shown in Fig. 3.19.

The details of the integrand in Eq. (3.68) vary considerably with E and ℓ and of course the choice of the potential. We choose two energies, $E = 0.5$ and $1.0\,\text{eV}$ and four ℓ values as shown in Fig. 3.20.

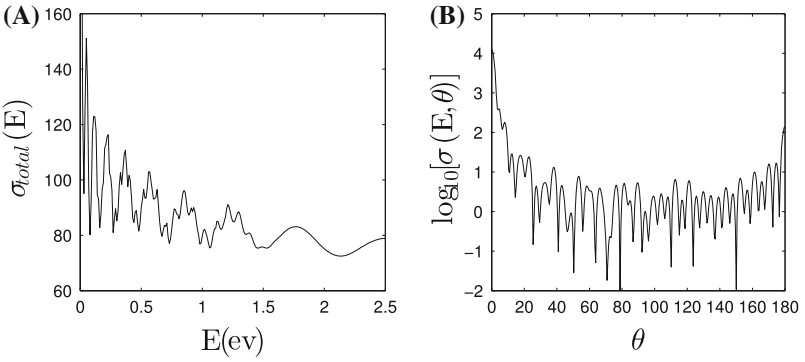

Fig. 3.19 (**A**) The total cross section in Å^2 versus relative energy, E, for O-H; (**B**) The differential cross section in Å^2 versus scattering angle for $E = 0.5\,\text{eV}$

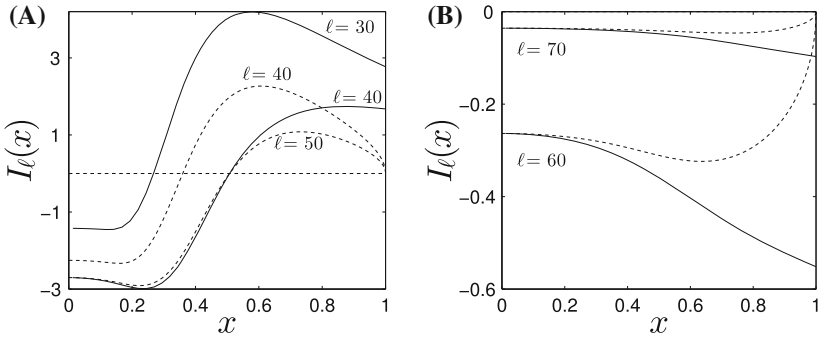

Fig. 3.20 The integrand, $I_\ell(x)$ for $E = 1.0\,\text{eV}$ for Gauss-Legendre quadrature (*dashed line*), Eq. (3.69), and Gauss-Mehler quadrature (*solid line*), Eq. (3.72)

Table 3.12 Convergence of the Gauss-Legendre evaluation of the JWKB phase shifts, Eq. (3.66), versus the number of quadrature points, N, at two energies

N	$E = 0.5\,\text{eV}$			$E = 1.0\,\text{eV}$		
	$\ell = 20$	$\ell = 50$	$\ell = 80$	$\ell = 20$	$\ell = 50$	$\ell = 80$
20	49.72877	1.73645	0.017339	41.81695	32.97958	0.37106
40	49.72806	1.73663	0.017342	41.81610	32.97880	0.36994
60	49.72799	1.73665	0.017342	41.81601	32.97871	0.36982
80	49.72797	1.73666		41.81599	32.97869	0.36979
100				41.81598	32.97868	0.36978

The convergence of the phase shifts with the Gauss-Legendre and Gauss-Mehler quadratures are shown in Tables 3.12 and 3.13, respectively. It is clear that the Gauss-Mehler quadrature outperforms the Gauss-Legendre quadrature. The convergence of the smaller phase shifts for the larger ℓ values is faster than for the larger phase

Table 3.13 Convergence of the Gauss-Mehler evaluation of the JWKB phase shifts, δ_ℓ, Eq. (3.66), versus the number of quadrature points, N, at two energies

N	$E = 0.5\,\text{eV}$			$E = 1.0\,\text{eV}$		
	$\ell = 20$	$\ell = 50$	$\ell = 80$	$\ell = 20$	$\ell = 50$	$\ell = 80$
6	49.72877	1.73645	0.017339	42.21144	32.94304	0.36977
8	49.72806	1.73663	0.017342	42.01845	32.97914	0.36977
12	49.72799	1.73665	0.017342	41.79747	32.97949	
16	49.72797	1.73666		41.81488	32.97895	
20				41.81665	32.97864	
30				41.81595	32.97868	
40				41.81597		

shifts for smaller ℓ values. The reason would appear to be the slower variation of the integrands for the Gauss-Mehler quadrature than for the Gauss-Legendre quadrature as seen in Fig. 3.20. This type of analysis was not considered in the review of the different quadratures by Cohen (1978). A more detailed comparison of the different quadrature procedures and for different potential forms would be useful.

It is important to point out that the numerical calculation of the total cross section with Eq. (3.65) as the integral of the differential cross section shown in Fig. 3.19 would require a very fine grid of points in order to capture the detailed structure. In this case a Simpson's rule would be the method of choice or an adaptive quadrature with subdivision of the domain. This is also the case for the calculation of the elastic collision frequency, Eq. (3.36) with the total cross section also shown in Fig. 3.19 in order to capture the detailed oscillations that occur.

3.7 The Calculation of Matrix Elements of Multiplicative Operators

The collision operator in the Boltzmann equation, Eq. (3.48), is the difference of the integral collision operator and the elastic collision frequency, $Z(y)$, defined by Eq. (3.50). The eigenvalue spectrum of the collision operator has in general a discrete set of eigenvalues as well as a continuum. Similarly, the Hamiltonian for a quantum problem can have bound states of negative energy (discrete eigenvalues) as well as scattering states of positive energy (continuum states). These eigenvalue spectra can be modelled approximately from the matrix representatives of the respective operators in suitable basis sets as discussed in the sections that follow.

In Chap. 1, we outlined the spectral Galerkin solution of differential and/or integral equations based on the method of weighted residuals (Finlayson and Scriven 1966; Finlayson 1972). The Boltzmann or Fokker-Planck equation for a spatially uniform

system in the absence of external forces is the time dependent equation of the form

$$\frac{\partial f(x,t)}{\partial t} = Lf(x,t) \quad x \in [a,b], \tag{3.73}$$

where L is a linear self-adjoint operator and an initial condition, $f(x,0) = g(x)$, is specified.

An approximate solution is given by the finite expansion in a set of orthonormal basis functions $P_n(x)$ where $P_n(x)$ are classical or nonclassical polynomials and $\int_a^b w(x)P_n(x)P_m(x)dx = \delta_{nm}$. We thus have the Nth order approximation to $f(x,t)$,

$$f^{(N)}(x,t) = \sum_{n=0}^{N-1} c_n(t)P_n(x). \tag{3.74}$$

The initial values, $c_n(0)$, are provided by the expansion of the initial condition, that is,

$$g(x) = \sum_{n=0}^{N-1} c_n(0)P_n(x). \tag{3.75}$$

The departure of the approximate solution from the actual solution is measured by the "residue" defined by

$$\begin{aligned} R_N(x,t) &= \frac{\partial f^{(N)}(x,t)}{\partial t} - Lf^{(N)}(x,t), \\ &= \sum_{n=0}^{N-1} P_n(x)\frac{dc_n(t)}{dt} - \sum_{n=0}^{N-1} c_n(t)LP_n(x). \end{aligned} \tag{3.76}$$

The method of weighted residuals (Finlayson and Scriven 1966; Finlayson 1972; Shen et al. 2011) is a procedure to calculate $c_n(t)$ so as to minimize the residual $R_N(x,t)$ in some average way. We impose the condition that the residue is minimized subject to

$$\int_a^b t(x)R_N(x,t)dx = 0, \tag{3.77}$$

where we choose the "test function" as $t(x) = w(x)P_m(x)$, $m = 0, 1, \ldots (N-1)$. The partial differential equation is approximated by the set of $N-1$ coupled ordinary differential equations with the Galerkin procedure, that is,

$$\frac{dc_m(t)}{dt} = \sum_{n=0}^{N-1} L_{mn}c_n(t) \quad m = 0, 1, \ldots, N-1, \tag{3.78}$$

where

$$L_{mn} = \int_a^b w(x) P_m(x) L P_n(x) dx, \tag{3.79}$$

is the matrix representative of the operator L in spectral space. An important consideration is the condition number of the matrix L_{mn} which determines the stability of the linear set of equations, Eq. (3.78), and their numerical time integration. The preceding discussion follows closely the presentation in Sect. 1.3.

The Nth order transformation from spectral space, c_n, to physical space, $f_i \equiv f(x_i)$, is given by

$$f_i = \sum_{n=0}^{N-1} T_{in}^{(N)} c_n. \tag{3.80}$$

The transformation matrix is defined by

$$T_{ni}^{(N)} = \sqrt{w_i} P_n(x_i) \quad i = 1, 2, \ldots N; \quad n = 0, 1, \ldots (N-1) \tag{3.81}$$

and is symmetric at all orders N, that is

$$\left(\mathbf{T}^{(N)}\right)^t \cdot \mathbf{T}^{(N)} = \mathbf{I}^{(N)}, \tag{3.82}$$

where ^{t} denotes the transpose of the real matrix of order N. Equation (3.82) written in component form is

$$\begin{aligned} \sum_{n=0}^{N-1} T_{in}^{(N)} T_{nj}^{(N)} &= \sqrt{w_i w_j} \sum_{n=0}^{N-1} P_n(x_i) P_n(x_j) \\ &= \sqrt{w_i w_j} \frac{\delta_{ij}}{\sqrt{w_i w_j}} \\ &= \delta_{ij}. \end{aligned} \tag{3.83}$$

which is exact to any order N. This is a direct consequence of the cardinality condition for the underlying interpolation at any order N.

In the following sections, we direct our attention to the calculation of the matrix elements of multiplicative operators denoted by $G(x)$. The matrix representative in some basis set is

$$G_{mn} = \int_a^b w(x) P_m(x) G(x) P_n(x) dx. \tag{3.84}$$

If this is approximated with the quadrature associated with the basis functions $P_n(x)$, then the Nth order approximation is

$$G_{mn}^{(N)} = \sum_{k=1}^{N} w_k P_m(x_k) G(x_k) P_n(x_k). \tag{3.85}$$

What is remarkable is that if we transform this (approximate) spectral space representation, $G^{(N)}_{nm}$, to the discrete space, G_{ij}, we have that

$$
\begin{aligned}
G_{ij} &= \sum_{n=0}^{N-1}\sum_{m=0}^{N-1} T_{in} G^{(N)}_{nm} T_{mj}, \\
&= \sum_{n=0}^{N-1}\sum_{m=0}^{N-1} \sqrt{w_i} P_n(x_i) \left[\sum_{k=1}^{N} w_k P_m(x_k) G(x_k) P_n(x_k)\right] \sqrt{w_j} P_m(x_j), \\
&= \sqrt{w_i w_j} \sum_{k=1}^{N} w_k G(x_k) [\sum_{n=0}^{N-1} P_n(x_j) P_n(x_k)][\sum_{m=0}^{N-1} P_m(x_i) P_m(x_k)], \\
&= \sqrt{w_i w_j} \sum_{k=1}^{N} w_k G(x_k) \frac{\delta_{jk}}{\sqrt{w_j w_k}} \frac{\delta_{ik}}{\sqrt{w_i w_k}}, \\
&= G(x_i)\delta_{ij}, \qquad (3.86)
\end{aligned}
$$

where the definition of T_{in} was used in the 2nd line and the "finite completeness" of the basis set in the 3rd line. The transform of the exact G_{nm} matrix elements would not give a diagonal physical space representation of the multiplicative operator as we demonstrate later.

For the Schrödinger equation, the multiplicative operator of interest is the potential, $V(x)$, in a one-dimensional Hamiltonian. The approximate calculation of the matrix elements of the potential function with a quadrature has served as the basis in chemical physics (Harris et al. 1965; Dickinson and Certain 1968) for the development of a pseudospectral or collocation solution of the Schrödinger equation (Light et al. 1985; Light and Carrington Jr. 2000) referred to as the Discrete Variable Representation (DVR).

An analogous procedure was developed by Shizgal (1981) and Shizgal and Blackmore (1984) for the Boltzmann equation and later applied to the Fokker-Planck and the Schrödinger equations (Shizgal and Chen 1996, 1997; Lo and Shizgal 2006, 2008). There is also the analogous Lagrange mesh method developed by Baye (1994, 2006) and coworkers (Baye and Heenen 1986; Baye et al. 2002). These methods of solution of the Schrödinger equation are studied in detail in Chap. 6. The objective in this section is to demonstrate the relationship of the spectral representation of multiplicative operators in an orthonormal basis set evaluated by quadrature and the physical space representation as described in Eq. (3.85).

For the Boltzmann equation the multiplicative operator is the collision frequency,

$$
Z_{nm} = \frac{2}{\sqrt{\pi}} \int_0^\infty w(y) P_n(y) Z(y) P_m(y) dy, \qquad (3.87)
$$

which depends on the mass ratio, $\gamma = M/m$. We will compare these calculations with similar calculations for the matrix elements of the potential in the Schrödinger equation of the form

$$V_{nm} = \int_0^\infty w(x) Q_n(x) V(x) Q_m(x) dx, \tag{3.88}$$

where $Q_n(x)$ are "appropriate" orthonormal basis functions. It should be clear that the choice of basis functions in different applications is crucial so as to get the "best" approximation to the operators. In Sect. 3.7.2, we consider the analogous calculation of the matrix elements of the potential in the Schrödinger equation for the quantum harmonic oscillator. It is the quadrature calculation of the matrix elements of the potential in the Schrödinger equation (Harris et al. 1965; Dickinson and Certain 1968) that inspired the discrete variable representation pseudospectral method in chemical physics (Light and Carrington Jr. 2000).

3.7.1 Matrix Representation of the Collision Frequency in Laguerre and Maxwell Polynomials

The collision operator of the Boltzmann equation, Eq. (3.48), includes the sum of the integral operator and the elastic collision frequency, $Z(y)$, Eq. (3.50) which for the hard sphere cross section is given by Eq. (3.45). The physical system of interest is the binary system of a test particle of mass m dilutely dispersed in a background gas of particles of mass M at equilibrium at temperature T_b. The mass ratio is $\gamma = M/m$.

We are interested in the analytic evaluation of the matrix elements of the collision frequency, $Z(y)$, for a binary gas with the hard sphere cross section. This calculation illustrates some of the techniques used in kinetic theory with the so-called moment method of solution which is a spectral solution of the Boltzmann equation with the distribution expanded in a basis set of functions. The basis set that is commonly used is the Sonine-Laguerre polynomials (Hoare and Kaplinsky 1970). The reason for this choice is that for a particular collisional model, namely for "Maxwell molecules", particles that interact with an inverse power law potential, $(V(r) \approx r^{-4})$, the collision frequency is a constant and the eigenvalue spectrum of the Boltzmann collision operator is discrete. Further details are discussed in Chap. 5.

The Sonine-Laguerre polynomials of order $\alpha = 1/2$ can be defined by their explicit polynomial representation,

$$L_n^{(\frac{1}{2})}(y) = \sum_{k=0}^{n} S_{nk} y^k, \tag{3.89}$$

where $y = mv^2/2k_BT_b$ is reduced energy and the coefficients are given by

$$S_{nk} = \frac{(-1)^k \Gamma(k+\frac{3}{2})}{\Gamma(n+\frac{3}{2})(n-k)!k!} y^k. \tag{3.90}$$

The $L_n^{(\frac{1}{2})}(y)$ basis functions are orthogonal as given by

$$\int_0^\infty \sqrt{y} e^{-y} L_n^{(\frac{1}{2})}(y) L_m^{(\frac{1}{2})}(y) dy = \frac{\Gamma(n+\frac{3}{2})}{n!} \delta_{nm}. \tag{3.91}$$

It is important to note that the coefficients in Eq. (3.90) alternate in sign owing to the factor $(-1)^k$.

With Eqs. (3.89) and (3.90), the matrix elements of the collision frequency, $Z(x)$, Eq. (3.45), are given by

$$Z_{nm} = \frac{A}{\sqrt{\gamma}} \sum_{k=0}^{n} \sum_{\ell=0}^{m} S_{nk} S_{m\ell} \int_0^\infty \sqrt{y} e^{-y} y^{(k+\ell)} \times \left(e^{-\gamma y} + \frac{\sqrt{\pi}}{2} \left[\frac{1}{\sqrt{\gamma y}} + 2\sqrt{\gamma y} \right] \mathrm{erf}(\sqrt{\gamma y}) \right) dy, \tag{3.92}$$

with $A = \pi d^2 \sqrt{k_B T_b / 2M}$. The integrals of powers of the collision frequency can be evaluated exactly in terms of two sets of integrals, defined by,

$$I_1(n) = \int_0^\infty y^n e^{-(\gamma+1)y} dy = \frac{1}{(\gamma+1)^{n+1}} \Gamma(n+1), \tag{3.93}$$

and

$$I_2(n) = \int_0^\infty y^n e^{-y} \mathrm{erf}(\sqrt{\gamma y}) dy, \tag{3.94}$$

which satisfies the recurrence relation

$$I_2(n) = n I_2(n-1) + \sqrt{\frac{\gamma}{\pi}} \frac{\Gamma(n+1)}{(\gamma+1)^{(n+1)}}. \tag{3.95}$$

The matrix elements can be written in terms of these integrals as given by

$$Z_{nm} = \frac{A}{\sqrt{\gamma}} \sum_{k=0}^{n} \sum_{\ell=0}^{m} S_{nk} S_{m\ell} \left[I_1(k+\ell+\tfrac{1}{2}) + \frac{1}{2}\sqrt{\frac{\pi}{\gamma}} I_2(k+\ell) + \sqrt{\pi\gamma} I_2(k+\ell+1) \right]. \tag{3.96}$$

As noted earlier, the terms in the sum in Eq. (3.96) alternate in sign and we can expect significant round-off errors for n and m of the order of 15–20. We only consider the lower order matrix elements.

The matrix elements of the collision operator are calculated exactly with Eqs. (3.93)–(3.96) and approximately by quadrature. An important consideration is the mass dependence of the collision frequency that is shown in Table 3.14.

The exact matrix elements for $\gamma = 1$ and order $N = 5$ in Table 3.14 are calculated with Eq. (3.96). The approximate results evaluated with only $N = 5$ quadrature points are shown in Table 3.15. If $Z(y)$ were unity, the matrix is diagonal with the diagonal elements equal to the normalization of the Laguerre polynomials and would require at least $N = (n + 1)/2$ quadrature points for their exact evaluation. Whereas the lower order matrix elements are in agreement (to 4 significant figures), the higher order matrix elements are not exact owing to the departure of $Z(y)$ from a polynomial of some finite order. The convergence of Z_{22} and Z_{44} is shown in Fig. 3.21 for much large numbers of quadrature points.

If we transform the "approximate" matrix representative, Table 3.15, to physical space we recover a diagonal matrix with the diagonal elements equal to $Z_{ij} = Z(y_i)\delta_{ij}$ which for $N = 5$ is represented by the vector

$$\frac{A}{\sqrt{\gamma}}[2.5681 \quad 3.3945 \quad 4.5452 \quad 5.9259 \quad 7.6095].$$

with the components equal to the "exact" $Z(y_i)$ values for the five Laguerre quadrature points 0.43140, 1.75975, 4.10447, 7.74670, 13.45768, in accordance with Eq. (3.86).

Table 3.14 Exact matrix elements, Z_{nm}, in units of $A/\sqrt{\gamma}$ for $\gamma = M/m = 1$, Eq. (3.96), of the hard sphere collision frequency Z(x)

n/m	0	1	2	3	4
0	3.1915	−0.6515	−0.0728	−0.0169	−0.0050
1	−0.6515	4.1224	−0.9961	−0.1273	−0.0331
2	−0.0728	−0.9961	4.8688	−1.2693	−0.1755
3	−0.0169	−0.1273	−1.2693	5.5103	−1.5018
4	−0.0050	−0.0331	−0.1755	−1.5018	6.0819

Table 3.15 Approximate matrix elements of the hard sphere collision frequency, $Z(x)$, in units of $A/\sqrt{\gamma}$ for $\gamma = M/m = 1$ evaluated with $N = 5$ Gauss-Laguerre quadrature points

n/m	0	1	2	3	4
0	3.1915	−0.6515	−0.0728	−0.0167	−0.0044
1	−0.6515	4.1225	−0.9958	−0.1261	−0.0292
2	−0.0728	−0.9958	4.8703	−1.2637	−0.1585
3	−0.0167	−0.1261	−1.2637	5.5297	−1.4388
4	−0.0044	−0.0292	−0.1585	−1.4388	6.3291

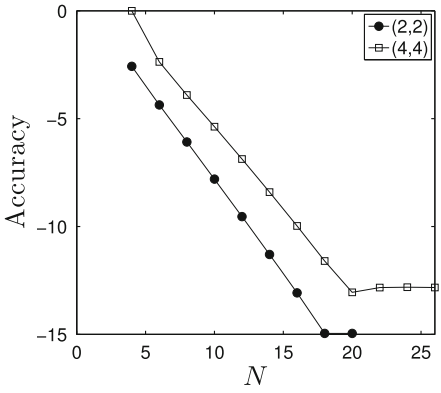

Fig. 3.21 The convergence of the diagonal matrix elements Z_{22} and Z_{44} versus the number of Laguerre quadrature points, N. The exact values are determined as given by Eqs. (3.93)–(3.96); Accuracy $= \log_{10} |1 - Z_{nn}^{(N)}/Z_{nn}|$

By contrast, the transform of the "exact" spectral space representation of Z_{nm} in Table 3.14 gives the "approximate" non-diagonal physical space representation,

$$\mathbf{T}^{\dagger} \cdot \mathbf{Z} \cdot \mathbf{T} = \frac{A}{\sqrt{\gamma}} \begin{pmatrix} 2.5540 & 0.0243 & -0.0296 & 0.0313 & -0.0308 \\ 0.0243 & 3.3527 & 0.0512 & -0.0544 & 0.0540 \\ -0.0296 & 0.0512 & 4.4822 & 0.0675 & -0.0676 \\ 0.0313 & -0.0544 & 0.0675 & 5.8527 & 0.0742 \\ -0.0308 & 0.0540 & -0.0676 & 0.0742 & 7.5333 \end{pmatrix}. \quad (3.97)$$

This remarkable result between the exact and quadrature evaluated matrix elements and the corresponding physical space representation might be unexpected, but it is consistent with the analysis given by Eq. (3.85). The variation of the matrix representation of the collision frequency with mass ratio is of interest and shown in Tables 3.16 and 3.17 for two different mass ratios.

For $M/m \to 0$, the Rayleigh limit, the matrix representative is becoming diagonal in this basis set, whereas in the larger mass limit, $M/m \to \infty$, the Lorentz limit, the off-diagonal elements are increasing.

It is of interest to examine the reduced energy dependence of the collision frequency in the Rayleigh limit for which $\gamma \to 0$. With the Taylor series expansion of

Table 3.16 Exact matrix elements in units of $A/\sqrt{\gamma}$ for $\gamma = M/m = 0.1$ with Eq. (3.96)

n/m	0	1	2	3	4
0	2.367	−0.088	−0.002	−0.000	−0.000
1	−0.088	2.507	−0.155	−0.004	−0.000
2	−0.002	−0.155	2.640	−0.217	−0.008
3	−0.000	−0.004	−0.217	2.767	−0.275
4	−0.000	−0.000	−0.008	−0.275	2.888

Table 3.17 Exact matrix elements in units of $A/\sqrt{\gamma}$ for $\gamma = M/m = 100$ with Eq. (3.96)

n/m	0	1	2	3	4
0	22.680	−9.167	−2.030	−0.930	−0.543
1	−9.167	33.945	−12.570	−2.693	−1.213
2	−2.030	−12.570	42.397	−15.191	−3.199
3	−0.930	−2.693	−15.191	49.443	−17.411
4	−0.543	−1.213	−3.199	−17.411	55.608

the exponential and error functions, we find that

$$Z(y) \overset{\gamma\to 0}{\approx} \frac{2A}{\sqrt{\gamma}}\left[1 - \frac{1}{3}\gamma y - \frac{1}{30}(\gamma y)^2 + \frac{1}{210}(\gamma y)^3 - \cdots\right]. \tag{3.98}$$

Therefore in this mass ratio limit, the Laguerre basis set is a good choice for the representation of $Z(y)$ as the collision frequency is approaching a polynomial in the reduced energy, y. In the Lorentz limit for which $\gamma \to \infty$ we use $\text{erf}(\sqrt{\gamma y}) = 1 - \text{erfc}(\sqrt{\gamma y})$ and with the asymptotic expansion of the $\text{erfc}(\sqrt{\gamma y})$, that is

$$\text{erfc}(y) = \frac{e^{-y^2}}{y\sqrt{\pi}}\left(1 - \frac{1}{2y^2} + \frac{3}{4y^4} - \frac{15}{8y^6} + \cdots + (-1)^n\frac{(2n-1)!!}{(2y^2)^n} + \cdots\right) \tag{3.99}$$

we get

$$Z(y) \overset{\gamma\to\infty}{\approx} A\left[\sqrt{\pi y}(1 + \frac{1}{2\gamma y}) - \frac{e^{-\gamma y}}{2(\gamma y)^2}\left[1 - \frac{3}{2\gamma y} + \frac{15}{4(\gamma y)^2}\cdots\right]\right]. \tag{3.100}$$

and the limiting dependence is $\sqrt{y}$ with the resulting slow convergence with Laguerre polynomials. On the other hand, if Z(y) is expressed in reduced speed $x = \sqrt{y}$, we recognize that the expansion in Maxwell polynomials would be exact with $N = 2$. This demonstrates the manner in which a particular problem dictates the optimal choice of basis functions, namely Laguerre polynomials for the Rayleigh limit and Maxwell polynomials for the Lorentz limit.

3.7.2 Matrix Representation of the Harmonic Oscillator Potential in Hermite Polynomials

An instructive calculation of the pseudopsectral representation of the Hamiltonian for the quantum harmonic potential is the evaluation of the matrix elements of the harmonic potential, $V(x) = x^2$ for the quantum harmonic oscillator problem, that is,

$$-\frac{d^2\psi_n}{dx^2} + x^2\psi_n(x) = \lambda_n\psi_n(x), \tag{3.101}$$

where $\lambda_n = 2n + 1$ in dimensionless units. The Hermite polynomials, Sect. 2.4.7, (Liboff 2002) are the eigenfunctions of the Hamiltonian and are a logical choice for the basis functions. The matrix representative of the potential in the set of basis functions $h_n(x) = e^{-x^2/2}H_n(x)/\sqrt{M_n}$, $M_n = \sqrt{\pi}2^n n!$ is given by

$$V_{nm} = \int_{-\infty}^{\infty} h_n(x)x^2 h_m(x)dx = \begin{cases} \frac{1}{2}(2n+1), & n = m, \\ \frac{1}{2}\sqrt{(n+1)(n+2)}, & n = m \pm 2, \\ 0, & \text{otherwise} \end{cases} \tag{3.102}$$

where we have used the recurrence relation

$$xH_n(x) = \frac{1}{2}[H_{n+1}(x) + 2nH_{n-1}(x)], \tag{3.103}$$

twice. We use M_N to denote the normalization factor of the Hermite polynomials to distinguish it from N.

We are interested in the evaluation of these matrix elements with the Gauss-Hermite quadrature, that is,

$$V_{nm}^{(N)} = \frac{1}{\sqrt{M_n M_n}} \sum_{i=1}^{N} w_i H_n(x_i)x_i^2 H_m(x_i). \tag{3.104}$$

The matrix V_{nm} without the term in x^2 in the integral in Eq. (3.102) represents the orthonormality of the basis functions. We can verify this result to order N with exactly N Gauss-Hermite quadrature points and weights since the largest element would be a polynomial of order $2N$ and the use of N quadrature points would yield an exact result. However, with the additional term in x^2 in Eq. (3.102), the matrix element $V_{N-1,N-1}^{(N)}$ in the bottom rightmost corner of the matrix is not calculated accurately with N quadrature weights and points. The error in this one matrix element can be determined exactly.

The matrix element $V_{N-1,N-1}^{(N)}$ of the potential for the harmonic oscilator is given by Eq. (3.104)

$$V_{N-1,N-1}^{(N)} = \frac{2}{M_{N-1}} \sum_{i=1}^{N/2} w_i x_i^2 H_{N-1}^2(x_i), \tag{3.105}$$

and the quadrature sum is twice the sum over the positive quadrature points. With $M_{N-1} = \sqrt{\pi}2^{N-1}(N-1)!$, the use of the recurrence relation, Eq. (3.103) and $H_N(x_i) = 0$ which defines the quadrature points, we get that,

$$\begin{aligned} V_{N-1,N-1}^{(N)} &= \frac{1}{M_{N-1}} \sum_{i=1}^{N} w_i H_{N-2}^2(x_i), \\ &= (N-1)^2 \frac{M_{N-2}}{M_{N-1}}, \\ &= \frac{N-1}{2}, \end{aligned} \tag{3.106}$$

where the quadrature sum is the normalization of H_{N-2} which is "exact" with N quadrature points. The approximate result, Eq. (3.106), should be compared with the exact result given by Eq. (3.102), that is

$$V_{N-1,N-1} = \frac{2N-1}{2}. \tag{3.107}$$

The transform of the "approximate" quadrature evaluated matrix representative gives the "exact" physical space representation of the potential as the diagonal matrix,

$$V_{ij} = \sum_{m=0}^{N-1}\sum_{n=0}^{N-1} T_{im} V_{nm}^{(N)} T_{mj} = x_i^2 \delta_{ij}. \tag{3.108}$$

This is expected as the transformation of the matrix representation of a multiplicative operator evaluated with an Nth order quadrature, namely $G_{nm}^{(N)}$ in Eq. (3.85) gives on transformation to physical space the diagonal representation, $G(x_i)\delta_{ij}$.

If the exact spectral representation of the harmonic oscillator potential is transformed to physical space it gives an inexact result. This can be seen by considering the transform of the difference of the two spectral space representations,

$$(\Delta V)_{nm} = \frac{N}{2}\delta_{m,N-1}\delta_{n,N-1}, \tag{3.109}$$

which is the null matrix except for the one element $V_{N-1,N-1} = N/2$. We transform the matrix, Eq. (3.109) to physical space and recognize that it is the last row of $\mathbf{T}$ that plays a role which is the vector with components

$$T_{N-1,j} = (-1)^{N+j}\frac{1}{\sqrt{N}}. \tag{3.110}$$

Thus we have analogous to Eq. (3.108)

$$\begin{aligned}(\Delta V)_{ij} &= \sum_{m=0}^{N-1}\sum_{n=0}^{N-1} T_{im}(\Delta V)_{nm} T_{mj} = \frac{N}{2}\sum_{n=0}^{N-1}\sum_{m=0}^{N-1} T_{in}T_{jm}\delta_{m,N-1}\delta_{n,N-1} \\ &= \frac{1}{2}(-1)^{i+j}.\end{aligned} \tag{3.111}$$

where Eqs. (3.109) and (3.110) have been used. These results were noted by others (Eq. 4.1 in Baye and Heenen (1986) and Eq. (14) in Szalay (1993)) and are important in connection with the convergence properties of pseudospectral methods in kinetic theory and also in quantum mechanics (Szalay et al. 2003). The analysis in this section explains in part the accuracy of pseudospectral methods based on approximate quadrature evaluated matrix elements (Baye et al. 2002; Szalay et al. 2012). Further details are presented in Sect. 6.7.3, in Chap. 6.

3.8 Challenging Integrals

We complete our discussion of the quadrature evaluation of integrals with a brief summary of some challenging integrals, the majority of which are characterized by integrands that oscillate and decay very slowly for $x \to \infty$ on the semi-infinite interval (Lyness 1985). Integrals with oscillatory integrands, especially those defined on the infinite or semi-infinite domains abound in the physical sciences and engineering (Safouhi 2001; Fornberg et al. 2002; Asheim et al. 2014). The use of the Distorted Wave Born Approximation (DWBA) for quantum inelastic cross sections (Rasch and Whelan 1997) leads to oscillatory integrands for the matrix elements between continuum eigenstates. A good example is the calculation of the rate of nuclear spin transitions in ^{3}He-^{3}He collisions (Shizgal 1973; Mullen and Richards 1990; Newbury et al. 1993). We also consider an integral from the SIAM 100-Digit Challenge (Bornemann et al. 2004) that exhibits a similar behaviour.

The numerical evaluation of the six-dimensional electron repulsion integrals that are required for molecular electronic structure calculations is summarized. In these simulations, many integrals are required so as to estimate the electronic states of atoms and molecules. There is a very large effort devoted to the efficient calculation of such integrals. Our discussion in this section is an overview of current work with emphasis on the choice of basis functions and the numerical calculation of the integrals that occur for the different choices. The use of nonclassical Rys quadratures is one of several different methods to calculate the integrals.

3.8.1 Molecular and Atomic Electronic Structure; Electron Pair Repulsion Integrals

The description of the electronic energies of an atom or molecule is based on the Schrödinger equation for the motion of the electrons and nuclei which interact via Coulomb potentials. Owing to the much smaller mass of the electrons relative to the nuclei, one can uncouple the electronic and nuclear motions in accordance with the Born[5]-Oppenheimer[6] approximation (Levine 2009; Szabo and Ostlund 1996). Thus one can write the Schrödinger equation for the electronic motion with the nuclei in fixed positions at $\mathbf{R}_n$ for the nucleus labelled by n. In this way, the Schrödinger equation is the eigenvalue problem

$$(H_{el} + V_{nn})\psi(\mathbf{r}_1, \mathbf{r}_2, \ldots, \mathbf{r}_n) = E_{el}(\mathbf{R_n})\psi(\mathbf{r}_1, \mathbf{r}_2, \ldots, \mathbf{r}_n), \tag{3.112}$$

[5] Max Born (1882–1970) was a German-British physicist and mathematician who made significant contributions to quantum mechanics, solid-state physics and optics, and won the 1954 Nobel Prize in Physics for the statistical interpretation of wavefunctions.

[6] Julius Robert Oppenheimer (1904–1967) was an American theoretical physicist and played a prominent role in the Manhattan Project for which he became known as the "father of the atomic bomb".

where $\mathbf{r_i}$ is the position vector of the ith electron. The electronic Hamiltonian is

$$H_{el} = -\frac{\hbar^2}{2m_e}\sum_i \nabla_i^2 - \sum_n \sum_i \frac{Z_n e^2}{|\mathbf{R}_n - \mathbf{r}_i|} + \sum_i \sum_{i>j} \frac{e^2}{|\mathbf{r}_j - \mathbf{r}_i|}, \tag{3.113}$$

where Z_n is the charge of the nth nucleus and e is the charge of the electron. The first term in Eq. (3.113) is the kinetic energy of the ith electron. The second term is the Coulomb interaction with the ith electron and the nth nucleus and the last term is the electron-electron repulsion between different electrons. The $\mathbf{R}_n$ positions relative to some space fixed axes are considered known. The rotational and vibrational states are the solution of the Schrödinger equation for the motion of the nuclei in the potential $E_{el}(\mathbf{R}_n)$ considered separately in Chap. 6.

The situation simplifies considerably if we consider atoms with one nucleus and in particular atomic hydrogen with one electron moving about a proton for which an analytic solution is known (Karplus and Porter 1970; Levine 2009; Liboff 2003). The eigenfunctions of the H-atom are

$$\psi_{n\ell m}(r, \theta, \phi) = R_{n\ell}(r) Y_\ell^{(m)}(\theta, \phi), \tag{3.114}$$

where $R_{n\ell}(r)$ can be written in terms of the associated Laguerre polynomials as discussed in Chap. 2, Sect. 2.4.6. These atomic orbitals are often used as the basis functions for larger molecular systems. Another one-electron system that can be solved analytically is H_2^+ (Wind 1965; Levine 2009; Liu and Zhao 2010). The Helium atom is the simplest two electron problem for which the Hamiltonian is,

$$H = -\frac{\hbar^2}{2m_e}\nabla_1^2 - \frac{\hbar^2}{2m_e}\nabla_2^2 - \frac{2e^2}{r_1} - \frac{2e^2}{r_2} + \frac{e^2}{|\mathbf{r}_1 - \mathbf{r}_2|}, \tag{3.115}$$

where the last term is the electron repulsion potential. This is a prototypical quantum system that provides some of the main concepts for quantum chemical problems (Karplus and Porter 1970; Levine 2009).

Our main interest is with respect to the quadrature evaluation of electron repulsion integrals which is central to quantum chemistry computer codes (Becke 1988; Lindh et al. 2001; Gill and Chien 2003; El-Sherbiny and Poirier 2004; Kakhiani et al. 2009; Mitani 2011). Any speed-up in the computational time of these integrals represents an enormous advance toward the treatment of larger molecular systems. The subject is very technical and it is not our intention to treat this in any detailed manner here. It has become a very computationally intensive problem that occupies the interests of a large number of computational theoretical chemists and physicists. Additional presentations of the problem are in several textbooks (Karplus and Porter 1970; Szabo and Ostlund 1996; Helgaker et al. 2000; Levine 2009; Tsuneda 2014) and review papers (Gill 1994; Reine et al. 2012). The objective is to introduce the reader to the ongoing efforts of many researchers in the development of efficient methods for the evaluation of integrals over the basis functions of electrons in atoms and molecules.

This subject area often involves very technical aspects of Fortran codes and the nomenclature for the basis sets used can be found in Chap. 3 in the book by Szabo and Ostlund (1996). This brief summary will hopefully provide the reader with the essential aspects as it relates to numerical quadratures and the evaluation of integrals.

The only exact solution of the Schrödinger equation is for the hydrogen atom and other one-electron atoms such as He^{+}, Li^{++}, etc. with a Hamiltonian which is separable and consequently with eigenfunctions that are expressed as a direct product of the associated Laguerre polynomials and the spherical harmonics, Eq. (3.4). In the absence of external fields, the allowed energy levels depend only on n. The eigenfunctions $\psi_{nlm}(r, \theta, \phi)$ are referred to as orbitals.

The Schrödinger equation for two-electron atoms such as He, is not separable in the same way owing to the Coulomb electron-electron interaction dependent on the distance, $r_{12} = |\mathbf{r_1} - \mathbf{r_2}|$ between the two electrons. There are several variational treatments for He that provide useful analytical approximations to the electronic ground eigenstate (Frankowski and Pekeris 1966; Levine 2009). The choice of basis functions is a key element in current computational methods in atomic electronic structure calculations. As always, the basis functions should be chosen so as to best describe the anticipated behaviour of the eigenfunctions and at the same time provide for an efficient numerical treatment.

For many electron atoms, one useful choice of basis functions or "orbitals" are those that mimic the orbitals for the single electron for the H-atom and are the product of a radial function $R_{n\ell}(r)$ and the spherical harmonic $Y_{\ell m}(\theta, \phi)$. One such basis function is the set of Slater[7]-type orbitals (STO) given by

$$\phi^{sto}_{n\ell m}(\mathbf{r}) = N_{n\ell m} r^{n-1} e^{-\alpha r} Y_{\ell m}(\theta, \phi), \tag{3.116}$$

where $N_{n\ell m}$ is a normalization and α is a parameter. An added complexity is that electrons are fermions with spin 1/2 states and the eigenfunctions must be made anti-symmetric with respect to an exchange of the two electrons. In order to reduce the Schrödinger equation for He to a set of matrix equations, a large number of matrix elements of the Hamiltonian between basis functions must be evaluated. The situation for He has been considered by numerous researchers and exact numerical results are known (Drake 1999; Drake et al. 2002) including the application of pseudospectral methods (Cassar and Drake 2004; Grabowski and Chernoff 2011). Electronic structure calculations for many electron atoms is an active area of research.

Another level of complexity occurs for diatomic molecules such as H_2 with two nuclei, that is "two centers", as shown in Fig. 3.22. The protons are at a fixed separation R in keeping with the Born-Oppenheimer approximation and the relative electron-electron distance is $r_{12} = |\mathbf{r_1} - \mathbf{r_2}|$. The other solid lines are the four electron-proton interactions. The two electrons can move in space and their positions specified with cartesian coordinates (x_1, y_1, z_1) and (x_2, y_2, z_2) or preferably in terms of spherical polar coordinates which is made difficult owing to the two centers.

[7] John Clarke Slater (1900–1976) was an American physicist who pioneered theoretical methods in atomic and molecular electronic structure.

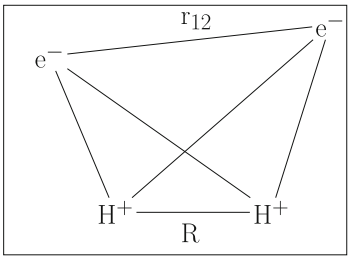

Fig. 3.22 Electron-electron separation is denoted by $r_{12} = |\mathbf{r_1} - \mathbf{r_2}|$ and then fixed separation of the protons by R. The other *solid lines* are the four electron-proton interactions

Thus, one of the main difficulties is the choice of coordinates and the basis functions in which to express the three-dimensional eigenfunctions. The ground state eigenenergy depends on the nuclear separation R and provides the potential $V(R)$ for the subsequent study of the nuclear motion or vibration. For H_2^+, with only one electron and no electron-electron repulsion the problem is simplified (Wind 1965). Further details of the theoretical treatment for this molecular ion can be found elsewhere (Cassar and Drake 2004; Levine 2009).

For molecular systems, the evaluation of matrix elements between Slater type orbitals is difficult and a better choice are the basis sets constructed from Gaussian type orbitals,

$$\phi^{gto}_{n\ell m}(\mathbf{r}) = N_{n\ell m} r^{\ell} e^{-\alpha r^2} Y_{\ell m}(\theta, \phi), \tag{3.117}$$

where the main difference with Slater type orbitals is the exponential dependence on r^2 rather than r. The main advantage is that the product of two Gaussians is another Gaussian which can be easily understood by completing the square of the argument of the exponential. Another suggestion for basis function are those discussed by Weniger (2009) referred to as B-functions with the radial portion expressed as a Bessel function. In this approach, we once again encounter integrals with oscillating integrands as discussed in Sect. 3.8.2 (Safouhi 2001). The importance of choosing the appropriate basis functions is clear.

In either case, the problem reduces to an expansion of the multi-electron ground state eigenfunction in these basis sets and the reduction of the Schrödinger equation to a set of linear equations for the eigenvalues. This is easier said than done. In the course of this calculation, the matrix elements of the kinetic energy operator and, in particular, of the electron-electron Coulomb repulsion potential must be calculated. These are integrals of the form

$$\langle ij|\frac{1}{r_{12}}|k\ell\rangle = \iint \phi_i(\mathbf{r_1})\phi_j(\mathbf{r_2})\frac{1}{r_{12}}\phi_k(\mathbf{r_1})\phi_\ell(\mathbf{r_1})d\mathbf{r_2}d\mathbf{r_2}. \tag{3.118}$$

These are 6-dimensional integrals with the position, r_i, of each basis function (or orbital) with reference to the position of a particular nucleus. Even for diatomic molecules, the numerical evaluation of these integrals is difficult and a large number

are required in a simulation of the electronic structure. It might be of interest for the reader to consult some original papers in which some of these integrals were evaluated analytically (Shavitt and Karplus 1965; Kern and Karplus 1965).

3.8.2 *Relaxation Times for ^{3}He-^{3}He Spin Exchange Collisions—Oscillatory Integrands*

The use of the distorted wave Born approximation to approximate transition probabilities for inelastic collision processes (Child 1996; Canto and Hussein 2013) yields integrals with oscillatory integrands. We choose to apply this theoretical approach to the nuclear spin-exchange that accompanies ^{3}He-^{3}He collisions. The distorted wave Born approximation applies to systems for which the interaction potential is the sum of two distinct potentials, a spherical potential, $V_0(r)$, that defines the elastic scattering of the He atoms and another much weaker spin dependent interaction, $\mathbf{V}_1(\mathbf{r}; \mathbf{I}_1, \mathbf{I}_2)$ that is responsible for the changes in the ^{3}He nuclear spin states, $\mathbf{I}_1$ and $\mathbf{I}_2$. With this assumption, the continuum scattering eigenfunctions are very well approximated with the solution of the Schrödinger equation with only $V_0(r)$.

The integrals required in the distorted wave Born approximation are the diagonal matrix elements between the radial wavefunctions $u_{k,\ell}(r)$, of the form $\int_0^\infty u_{k,\ell}^2/r^8 d\mathbf{r}$ or $\int_0^\infty u_{k,\ell}^2 e^{-\alpha r}/r^2 d\mathbf{r}$ for the spin dependent interactions (Shizgal 1973, 1974a). The radial wavefunction, $u_{k.\ell}(r)$, are the solutions of Eq. (3.63). However, the continuum radial eigenfunctions can also be approximated with the JWKB eigenfunctions. The difficulty with the numerical evaluation of these integrals is that the integrands are highly oscillatory and may decay slowly for $r \to \infty$. Shizgal (1974b) evaluated such integrals by searching for the roots of the integrands and evaluating the integrals between successive roots with a Gauss-Mehler quadrature. This technique provides acceptable results but the convergence of the partial sums is slow. The results compared favorably with the exact quantum results obtained with a direct numerical integration of the radial Schrödinger equation. Dickinson and Shizgal (1975) later employed a classical analogue to the JWKB approximation and found excellent agreement with the semi-classical and quantal results.

We will not discuss the details of these calculations but instead consider analogous integrals with the replacement of the radial wavefunctions with the plane wave analogues so that $u_{k,\ell}(r) \to j_\ell(kr)$ where $j_\ell(kr)$ is the spherical Bessel function (Abramowitz and Stegun 1964). A typical example is the integral

$$\int_0^\infty \frac{j_\ell^2(x)}{x} dx = \frac{1}{2\ell(\ell+1)}, \tag{3.119}$$

with the oscillatory integrand shown in Fig. 3.23. The partial sums of the integrals between the successive zeros (with 8 Gauss-Legendre quadrature points and weights) for the integral in Eq. (3.119) with $\ell = 5$ are 0.01556, 0.01600, 0.01618, 0.01630,

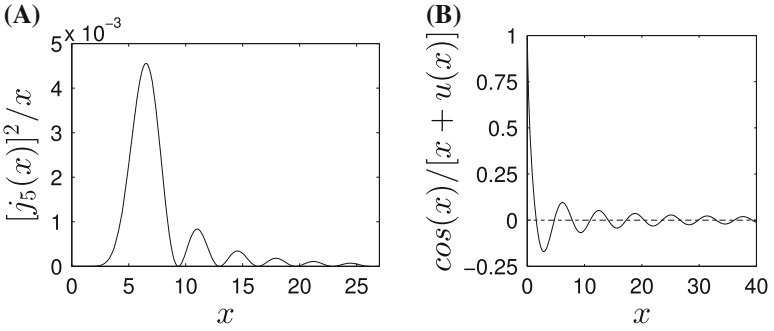

Fig. 3.23 (**A**) Integrand for the integral in Eq. (3.119) for $\ell = 5$; (**B**) The integrand for the integral, Eq. (3.120) in the SIAM 100-Digit Challenge (Gautschi 2008; Slevinsky and Safouhi 2008)

0.01637, 0.01643, etc. The exact value is 1/60 = 0.01666. More than 93 % of the contribution to the integral is from the first peak and the contributions from the remaining intervals are much smaller and decrease very slowly. For physical applications such as this one, the required accuracy is of several significant figures. Similar integrals involving the squares of Bessel functions occur in the reconstruction of temperature multipole spectrum of cosmic microwave background from measured data (Tomaschitz 2012, 2013) containing the squares of Bessel functions as in Eq. (3.119). An exhaustive discussion of the work on oscillatory integrands is beyond the scope of the book. The original treatment of quadratures for integrals of this type is Filon[8]'s sine and cosine formulae discussed in Sect. 4.11 of the book by Lindfield and Penny (2012). More advanced discussions can be found in recent papers (Iserles and Norsett 2005; Asheim et al. 2014).

3.8.3 The SIAM 100-Digit Challenge; a "Twisted Tail" Integral

It is useful to compare the previous discussion with the integral

$$I = \int_0^\infty \frac{\cos(x)}{x + u(x)} dx \tag{3.120}$$

arising from a change of variable from an original integral (Slevinsky and Safouhi 2008; Gautschi 2008) discussed by Laurie in Chap. 1 in the SIAM 100-Digit

[8] Louis Napoleon George Filon (1875–1937) was an English mathematician and worked in classical mechanics, elasticity and continuous media.

Challenge (Bornemann et al. 2004). In Eq. (3.120), $x = u(x)\ln[u(x)]$. The integrand in Eq. (3.120) is shown in Fig. 3.23(B) and shares some of the features of Fig. 3.23(A). The graph is drawn with the spline fit of a table of $u(x)$ versus x. Gautschi (2008) provides a numerical algorithm for the evaluation of this integral. The infinite domain is divided into subdomains with the end points at the roots of $\cos(x)$ that is $x_k = (2k+1)\pi/2$ so that the integral is represented as a sum over each subdomain. The integral in each sub-domain is evaluated with a Gauss-Legendre quadrature over the interval $[-1, 1]$ with the appropriate change of variable as done for the integral in Eq. (3.119). Gautschi also discusses the need to introduce a special acceleration scheme in the summation over subintervals as this series converges very slowly analogous to the results cited for Eq. (3.119).

Further details can be found in recent publications (Gautschi 2008; Slevinsky and Safouhi 2008). In contrast to the applications to physical problems where the precision required is often less than machine accuracy, the "challenge" for this example and others (Bornemann et al. 2004) is to evaluate the integral to 100 digits.

3.9 Numerical Evaluation of Derivatives

The numerical evaluation of the derivatives of a function is the basis of pseudospectral methods of solution of partial differential equations such as the Schrödinger equation and/or differential-integro equations such as the Boltzmann equation. The earliest collocation appears to be the solution of the radiative transfer equation by Wick (1943) and Chandrasekhar (1960). The technique of differential quadrature was later introduced by Bellman (Bellman et al. 1972; Shu 2000) based on either polynomials or Fourier basis sets. The monograph by Gottlieb and Orszag (1977) established the use of spectral methods with a finite basis set expansion and the relationship with a collocation.

Blackmore and Shizgal (1985) applied pseudospectral discretizations of derivatives together with quadratures for integrals to reduce the Boltzmann equation to linear algebraic form. The method was referred to as a discrete ordinate method analogous to the terminology in radiative and neutron transport (Chandrasekhar 1960; Liou 1973) and in kinetic theory (Robson et al. 1991; Robson and Prytz 1993). These discretization techniques were applied to the Schrödinger equation by Light and coworkers (Hamilton and Light 1986; Bacic and Light 1986; Light and Carrington Jr. 2000) and originated from considerations of the quadrature evaluation of matrix elements (Harris et al. 1965; Dickinson and Certain 1968) discussed in Sect. 3.7. The Lagrange mesh method developed by Baye (1994) and coworkers (Baye and Heenen 1986; Baye and Vincke 1999) is based on Lagrange interpolation. A personal chronology of the development of pseudospectral methods in chemistry and physics was provided in Table 1.1. The applications to the Boltzmann, Fokker-Planck and Schrödinger equations are presented in Chaps. 5 and 6.

3.9.1 Finite Difference Formulas for Derivatives

Finite difference methods for the evaluation of derivatives are often used for the solution of differential equations. We present a brief summary in comparison with pseudospectral methods. The finite difference first derivative of a function is simply an approximation to the definition of the derivative as the slope of the function at some point. The method is considered local as the derivative is approximated by neighbouring function values. Specifically, we evaluate the first derivative between uniformly spaced grid points, x_i and x_{i+1}, with $\Delta x = x_{i+1} - x_i$ as

$$\left.\frac{df}{dx}\right|_{x_i} \approx \frac{f(x_{i+1}) - f(x_i)}{\Delta x}. \tag{3.121}$$

Equation (3.121) is the forward finite difference whereas

$$\left.\frac{df}{dx}\right|_{x_i} \approx \frac{f(x_i) - f(x_{i-1})}{\Delta x}, \tag{3.122}$$

is the backward finite difference approximation to the first derivative. It is clear that this is a local method as only neighbouring grid points are involved. The third approximation is the centered difference formula given by,

$$\left.\frac{df}{dx}\right|_{x_i} \approx \frac{f(x_{i+1}) - f(x_{i-1})}{2\Delta x}. \tag{3.123}$$

The error in the above approximations to the first derivative is second order in Δx. Higher order estimates can also be provided. Further details can be found in Chap. 4 of Burden and Faires (2011) and Chap. 7 of Cheney and Kincaid (2008).

The approximation to the second derivative is derived from the expressions above and we have the second order estimate,

$$\left.\frac{d^2f}{dx^2}\right|_{x_i} \approx \frac{f(x_{i+1}) - 2f(x_i) + f(x_{i-1})}{(\Delta x)^2}. \tag{3.124}$$

The diffusion equation of the form

$$\frac{\partial n(x,t)}{\partial t} = \frac{\partial^2 n(x,t)}{\partial x^2} \tag{3.125}$$

can be discretized with Eq. (3.121) on the right-hand side in x and with Eq. (3.124) on the left hand side in t so that

$$\frac{n_i(t + \Delta t) - n_i(t)}{\Delta t} = \frac{n_{i+1}(t) - 2n_i(t) + n_{i-1}(t)}{(\Delta x)^2}. \tag{3.126}$$

where $n_i(t) \equiv n(x_i, t)$. The solution can be advanced in time with an Euler algorithm, that is

$$n_i(t + \Delta t) = n_i(t) + \left[\frac{n_{i+1}(t) - 2n_i(t) + n_{i-1}(t)}{(\Delta x)^2}\right]\Delta t, \tag{3.127}$$

which is initiated with the initial condition $n_i(0)$.

The differential operators in many different partial differential equations can be discretized in this way and the equations reduced to ordinary differential equations which are then advanced in time with an Euler scheme above or with higher order methods such as a Runge-Kutta scheme (Cheney and Kincaid 2008). An important aspect of these methods is the choice of the grid spacing in x and t, that is Δx and Δt. Further details on finite difference methods can be found in several textbooks (LeVeque 2007; Cheney and Kincaid 2008; Durran 2010). We use a finite difference method for the solution of the nonlinear Boltzmann equation in Chap. 5, Sect. 5.8 (Kabin and Shizgal 2003). We make use of the Chang and Cooper (1970) finite difference scheme for the solution of the Fokker-Planck equation in Chap. 6, Sect. 6.2.3.

3.9.2 Interpolation and Differentiation

In Chap. 2, Sect. 2.3.1, we discussed the role of interpolation in the development of quadrature procedures. A Lagrange interpolation was defined for the set of N points $\{x_i\}$ and the corresponding function values, $y_i = f(x_i)$. The Nth order Lagrange interpolant is of the form

$$f(x) \approx f^{(N)}(x) = \sum_{i=1}^{N} f(x_i) I_i(x), \tag{3.128}$$

where the interpolation function, $I_i(x)$, is constructed from orthogonal polynomials that is

$$I_i(x) = w_i \sum_{n=0}^{N-1} P_n(x) P_n(x_i), \tag{3.129}$$

and satisfy the Cardinality condition

$$I_i(x_j) = \delta_{ij}. \tag{3.130}$$

Thus the interpolation returns the exact values of the function values, $f(x_i)$, at each point x_i, as discussed in Sect. 2.3.1 and shown in Fig. 2.2.

It is clear that an approximation for the derivative of $f(x)$ is given by

$$\frac{df^{(N)}(x)}{dx} = \sum_{i=1}^{N} f(x_i) \frac{dI_i(x)}{dx}. \tag{3.131}$$

We thus identify the derivative matrix operator used in pseudospectral methods for the solution of differential equations as the derivative of the Lagrange interpolant, that is,

$$\begin{aligned}\hat{D}_{ij} &= \left.\frac{dI_j(x)}{dx}\right|_{x=x_i} \\ &= w_j \sum_{n=0}^{N-1} P_n'(x_i) P_n(x_j). \end{aligned} \tag{3.132}$$

It is straightforward to construct the discrete derivative matrix operator for classical and nonclassical polynomials from the recurrence coefficients α_n and β_n. The quadrature weights and points are calculated with the diagonalization of the Jacobi matrix, Eq. (2.71). The polynomials, $P_n(x)$, and the derivatives, $P_n^{'}(x)$ are determined by recurrence and the discrete derivative matrix operator is given by Eq. (3.132).

It follows that the second derivative matrix operator in physical space is given by

$$\hat{D}_{ij}^{(2)} = w_j \sum_{n=0}^{N-1} P_n''(x_i) P_n(x_j). \tag{3.133}$$

With Eq. (3.132), the approximation to the second derivative that appears in Eq. (3.133) is

$$P_n''(x_i) = \sum_{\ell=1}^{N} \hat{D}_{i\ell} P_n'(x_\ell). \tag{3.134}$$

We substitute Eq. (3.134) into (3.133) and get

$$\begin{aligned}\hat{D}_{ij}^{(2)} &= w_j \sum_{n=0}^{N} \left[\sum_{\ell=0}^{N} \hat{D}_{i\ell} P_n'(x_\ell) \right] P_n(x_j), \\ &= \sum_{\ell=0}^{N} \hat{D}_{i\ell} w_j \sum_{n=0}^{N} P_n'(x_\ell) P_n(x_j), \\ &= \sum_{\ell=0}^{N} \hat{D}_{i\ell} \hat{D}_{\ell j}. \end{aligned} \tag{3.135}$$

Thus the second derivative matrix operator is the matrix product of the first order derivative matrix operators.

We use nonclassical basis functions for the majority of the applications in Chaps. 5 and 6 and use the definition Eq. (3.132) to construct the derivative matrix operator. For some nonclassical weight functions it is possible to express the spectral space matrix elements, d_{nm}, in terms of the recurrence coefficients and then transform to

Table 3.18 References to explicit first and second derivative matrix operators

Basis	Quadrature	Reference	$\mathbf{D}^{(1)}$	$\mathbf{D}^{(2)}$
Fourier		Schwartz (1985)	Eq. (2)	Eq. (3)
		Baye and Heenen (1986)		Eq. (3.5)
		Colbert and Miller (1992)		Appendix
		Kokoouline et al. (1999)		Appendix
		Shen et al. (2011)	Eq. (2.34)	Eq. (2.37)
	Odd collocation	Peyret (2002)	Eq. (2.30)	Eq. (2.31)
	Even collocation	Peyret (2002)	Eq. (2.32)	Eq. (2.33)
Chebyshev	Gauss	Funaro (1992)	Eq. (7.2.14)	
	Gauss	Shen et al. (2011)	Eq. (3.231)	
	Lobatto	Peyret (2002)	Eq. (3.46)	Eq. (3.47)
	Lobatto	Canuto et al. (2006)	Eq. (2.4.33)	Eq. (2.4.36)
	Lobatto	Shen et al. (2011)	Eq. (3.228)	
	Radau	Shen et al. (2011)	Eq. (3.229)	
Legendre	Gauss	Funaro (1992)	Eq. (7.2.14)	
Jacobi	Gauss	Shen et al. (2011)	Eq. (3.164)	
	Gauss	Funaro (1992)	Eq. (7.2.12)	
	Lobatto	Shen et al. (2011)	Eq. (3.160)–(3.162)	
	Radau	Shen et al. (2011)	Eq. (3.163)	
Laguerre	Radau	Funaro (1992)	Eq. (7.2.15)	
	Gauss	Baye and Heenen (1986)		Eq. (3.17)
Hermite	Gauss	Baye and Heenen (1986)		Eq. (3.14)

the physical space representation as done for Maxwell polynomials (Shizgal and Blackmore 1984). In general, explicit expressions of the physical space derivative matrix operators, $\hat{D}_{ij}$ and $\hat{D}^{(2)}_{ij}$, for nonclassical polynomials are not available. Explicit expressions do exist for derivative operators for the classical polynomials and Table 3.18 provides a partial list to the references where these results can be found.

The Fourier basis is the basis set of choice especially for the second derivative operator representing the kinetic energy in the Hamiltonian for quantum problems. Other definitions of these derivative matrix operators were reported by Baye (1994), Barkley (1995) and by Szalay (1993). There is considerable overlap of the results reported in these references.

If the matrix elements of the derivative operator in spectral space

$$d_{nm} = \int_a^b w(x) P_n(x) \frac{dP_m(x)}{dx} dx, \tag{3.136}$$

is transformed to physical space with the transform, T_{ni}, then the derivative matrix operator in physical space is,

$$
\begin{aligned}
D_{ij} &= \sum_{n=0}^{N-1}\sum_{m=0}^{N-1} T_{in} d_{nm} T_{mj}, \\
&= \sum_{n=0}^{N-1}\sum_{m=0}^{N-1}\left[\sqrt{w_i}P_n(x_i)\right]\sum_{k=1}^{N} w_k P_n(x_k) P'_m(x_k)\left[\sqrt{w_j}P_m(x_j)\right], \\
&= \sqrt{w_i w_j}\left[\sum_{k=1}^{N} w_k \sum_{n=0}^{N-1} P_n(x_i)P_n(x_k)\right]\sum_{m=0}^{N-1} P'_m(x_k)P_m(x_j), \\
&= \sqrt{w_i w_j}\left[I_k(x_i)\right]\sum_{m=0}^{N-1} P'_m(x_k)P_m(x_j), \qquad (3.137)
\end{aligned}
$$

where in the second line we have used the definitions of d_{nm} and of T_{in} in the square brackets. In the third line, we have collected the separate sums over n and m and we recognize the interpolation function in square brackets as noted in the last line. Since $I_k(x_i) = \delta_{ki}$, we have that

$$
\boxed{D_{ij} = \sqrt{w_i w_j}\sum_{m=0}^{N-1} P'_m(x_i)P_m(x_j)}. \qquad (3.138)
$$

This is consistent with Eq. (3.132) since

$$
\hat{D}_{ij} = D_{ij}\sqrt{\frac{w_i}{w_j}}. \qquad (3.139)
$$

In the absence of explicit analytic expressions, we show the physical space first and second derivative matrix operators for Maxwell polynomials, ($w(x) = x^2 e^{-x^2}$), with $N = 5$ in Tables 3.19 and 3.20. The main objective is to show the potential round-off errors that can occur in the calculation of numerical derivatives with these matrix operators. The matrix elements alternate in sign and increase rapidly with N, especially for $\mathbf{D}^{(2)}$.

In Fig. 3.24, we show the first and second derivatives of $f(x) = e^{-x^4}$ and the numerical values as symbols with $N = 20$ and a scale factor $s = 0.3$ so to as

Table 3.19 First derivative operator, **D**, in physical space for Maxwell Polynomials, $w(x) = x^2 e^{-x^2}$

i/j	1	2	3	4	5
1	−3.8890	6.1977	−3.1580	0.9693	−0.1201
2	−0.6768	−0.8170	1.8841	−0.4389	0.0485
3	0.2644	−1.4443	0.5276	0.7112	−0.0588
4	−0.3160	1.3101	−2.7694	1.5640	0.2112
5	1.1631	−4.3053	6.8023	−6.2745	2.6143

Table 3.20 Second derivative operator, $\mathbf{D}^{(2)}$, in physical space for Maxwell Polynomials, $w(x) = x^2 e^{-x^2}$

i/j	1	2	3	4	5
1	9.6484	−22.8180	18.7915	−6.4661	0.8442
2	3.8783	−7.0327	3.1378	0.0515	−0.0349
3	−0.2042	3.2413	−5.6473	2.7466	−0.1364
4	−0.6386	2.1113	−0.8897	−1.7295	1.1467
5	5.2122	−18.5745	26.9635	−18.3623	4.7611

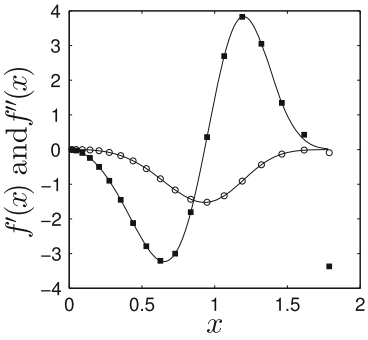

Fig. 3.24 Numerical values of $f'(x)$ (*circles*) and $f''(x)$ (*squares*) versus x for $f(x) = e^{-x^4}$ with Maxwell quadrature points with scaling factor $s = 0.3$. The *solid lines* are the exact results

to shorten the effective interval. The effect of the roundoff error in the second derivative is illustrated by the two quadrature points for $n = 18$ and $n = 19$ (solid circles) that deviate significantly from the exact result (solid curve). In fact, the error in the last point, $n = 20$, is too large to show on the graph. Similar round-off errors for physical space derivative matrix operators for Chebyshev polynomials was discussed in Sect. 3.3.4 in Peyret (2002). This was also discussed in greater detail by Baltensperger and Trummer (2003) who provided methods to reduce the errors. Additional detailed discussions of such errors were also reported in the solution of Fisher's equation (Olmos and Shizgal 2006). The errors for the pseudospectral methods based on the Maxwell polynomials in the semi-infinite axis are larger than for Chebyshev pseudospectral methods.

Shizgal and Blackmore (1984) calculated D_{kj} for Legendre polynomials normalized to unity with the transform of

$$d_{nm} = \begin{cases} \sqrt{(2n+1)(2m+1)}, & m > n, \quad \text{m + n odd}, \\ 0 & \text{otherwise}, \end{cases} \tag{3.140}$$

as given by the first line of Eq. (3.137). In Fig. 3.25, we show the variation of the absolute error in the calculation of the first and second derivatives of the oscillatory function

$$f(x) = \sin\left[3(\sinh(x) + (1-x)^2)\right]. \tag{3.141}$$

The convergence is moderately fast for this non-polynomial function and slow at the interval boundaries relative to the convergence in the middle part of the interval.

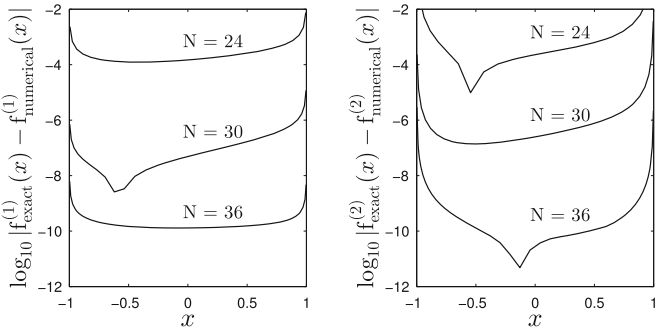

Fig. 3.25 Variation of the absolute error versus x for the numerical first derivative $\mathbf{f}^{(1)} = \mathbf{D} \cdot \mathbf{f}$ and numerical second derivative $\mathbf{f}^{(2)} = \mathbf{D}^{(2)} \cdot \mathbf{f}$ for $f(x) = \sin[3(\sinh(x) + (1+x)^2)]$ with $N = 24$, 30, and 36 Legendre quadrature points

A comparison with a fourth order finite difference differentiation was shown by Shizgal and Blackmore (1984).

3.9.3 Sturm-Liouville Eigenvalues Problems

The classical polynomials satisfy Sturm-Liouville eigenvalue problems and equivalent Schrödinger equations. We provide a detailed discussion of these problems in Chap. 6. In this section, we introduce the subject so as to show that only the first derivative matrix operator is required for such second order differential equations. To illustrate this result, we note that the Sturm-Liouville equation for Legendre polynomials is given by

$$-\frac{d}{dx}\left[(1-x^2)\frac{dP_\ell(x)}{dx}\right] = \ell(\ell+1)P_\ell(x), \tag{3.142}$$

which is equivalent to the Schrödinger equation for a rigid rotor, that is

$$-\frac{\hbar^2}{2I}\left[\frac{1}{\sin\theta}\frac{\partial}{\partial\theta}\left(\sin\theta\frac{\partial}{\partial\theta}\right)\right]\psi_\ell(\theta) = E_\ell\psi_\ell(\theta), \tag{3.143}$$

where I is the moment of the inertia of the diatomic molecule. The change of variable, $x = \cos\theta$ transforms Eq. (3.143) to Eq. (3.142) with $E_\ell = \ell(\ell+1)\frac{\hbar^2}{2I}$.

We wish to construct the physical space representation of the Sturm-Liouville operator on the left hand side of Eq. (3.142). We begin with the spectral space representation given by

$$L_{\ell\ell'} = -\int_{-1}^{1} P_\ell \frac{d}{dx}\left[(1-x^2)\frac{dP_{\ell'}(x)}{dx}\right]dx. \tag{3.144}$$

An integration by parts gives

$$\begin{aligned} L_{\ell\ell'} &= \int_{-1}^{1} (1-x^2) P'_\ell(x) P'_{\ell'}(x) dx, \\ &\approx \sum_{k=1}^{N} w_k (1-x_k^2) P'_\ell(x_k) P'_{\ell'}(x_k), \\ &= \sum_{k=1}^{N} w_k (1-x_k^2) \sum_{\alpha=1}^{N} \hat{D}_{k\alpha} P_\ell(x_\alpha) \sum_{\beta=1}^{N} \hat{D}_{k\beta} P'_\ell(x_\beta), \end{aligned} \tag{3.145}$$

where the integral for the matrix elements is evaluated by quadrature in the second line and the derivatives are evaluated with the derivative matrix operator in the third line. The transformation of $L_{\ell\ell'}$ to physical space with the transformation $T_{i\ell} = \sqrt{w_i} P_\ell(x_i)$ gives

$$\begin{aligned} L_{ij} &= \sum_{\ell=0}^{N-1} T_{i\ell} L_{\ell\ell'} T_{\ell' j}, \\ &= \sum_{k=1}^{N} w_k (1-x_k^2) \left[\sum_{\ell=0}^{N-1} \sqrt{w_i} P_\ell(x_i) \sum_{\alpha=1}^{N} \hat{D}_{k\alpha} P_\ell(x_\alpha) \right] \\ &\quad \times \left[\sum_{\ell'=0}^{N-1} \sqrt{w_j} P_{\ell'}(x_j) \sum_{\beta=1}^{N} \hat{D}_{k\beta} P_{\ell'}(x_\beta) \right]. \end{aligned} \tag{3.146}$$

We now use the discrete "completeness" relation

$$\sum_{\ell=0}^{N-1} P_\ell(x_i) P_\ell(x_\alpha) = \frac{\delta_{i\alpha}}{w_i}, \tag{3.147}$$

in each square bracket and the final result is

$$L_{ij} = \sum_{k=1}^{N} (1-x_k^2) D_{ki} D_{kj}, \tag{3.148}$$

where the definition Eq. (3.139) has been used. The eigenfunctions of $\mathbf{L}$ given by Eq. (3.148) for $N = 6$ calculated with a MATLAB code are shown by the solid symbols in Fig. 3.26. These coincide exactly with the solid line which is $P_5(x)$. The eigenvalues calculated in this way are "exactly" the rigid rotor eigenvalues, that is $\lambda_\ell = \ell(\ell+1)$.

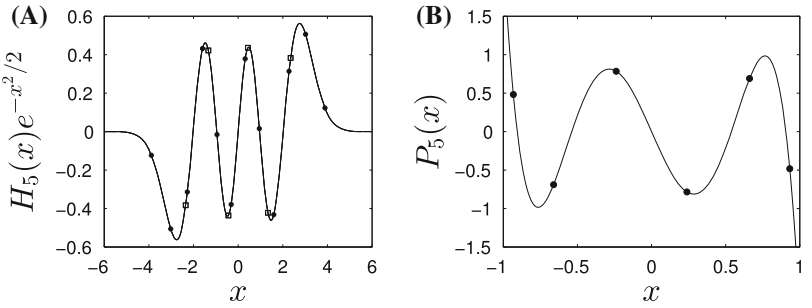

Fig. 3.26 (**A**) *Solid line* is the exact result for the orthonormal Hermite polynomial $H_5(x)e^{-x^2/2}$. The eigenfunctions of H_{ij} of Eq. (3.149) agree with the exact polynomial as shown by the *solid circles* for $N = 12$ and by the *squares* for $N = 6$. (**B**) *Solid line* is the exact result for the orthonormal Legendre polynomial $P_5(x)$. The eigenfunctions of L_{ij} of Eq. (3.148) agree with the exact polynomial as shown by *solid circles* for $N = 6$

Similarly, the eigenfunctions and eigenvalues for the harmonic oscillator are calculated with the diagonalization of the pseudospectral representation of the Schrödinger equation, that is

$$\boxed{H_{ij} = \sum_{k=1}^{N} D_{ki} D_{kj}} \tag{3.149}$$

with Gauss-Hermite quadratures.

This calculation provides N exact eigenvalues, $\lambda_n = 2n$, relative to the ground state and eigenfunctions that coincide with the Hermite functions $h_n(x)$. In Fig. 3.26, the symbols are the results obtained with the diagonalization of Eq. (3.149) and are in exact agreement with the polynomial $h_5(x) = H_5(x)e^{-x^2/2}$ shown by the solid lines for $N = 6$ and $N = 12$. This calculation for the quantum harmonic oscillator, based on Eq. (3.149), does not involve the calculation of the matrix elements of the harmonic potential (Colbert and Miller 1992; Baye and Heenen 1986).

The evaluation of the potential energy matrix elements by quadrature (Szalay 1993; Baye et al. 2002; Szalay et al. 2012) are of no concern with this pseudospectral approach. Moreover, there is no occurrence of nonphysical "ghost levels" (Wei 1997; Willner et al. 2004; Kallush and Kosloff 2006) as discussed further in Chap. 6, Sect. 6.7.3.

3.9.4 Discrete Singular Convolution; Whittaker's Sinc Interpolation

Fourier basis functions are traditionally associated with pseudospectral methods for the solution of partial differential equations, and the grids associated with Fourier methods are uniform grids. In Sect. 2.6.1, we introduced the sinc function (Whittaker 1929a, b; Stenger 1993)

$$S_k(x) = \frac{\sin[\frac{\pi}{h}(x - x_k)]}{\frac{\pi}{h}(x - x_k)}, \tag{3.150}$$

which satisfies the cardinality condition $S_k(x_j) = \delta_{jk}$. Thus we have the interpolation on a uniform grid of N points $x_k = x_{min} + h(k - 1)$, defined for the finite interval $[x_{min}, x_{xmax}]$ where the grid spacing is $h = (x_{max} - x_{min})/(N - 1)$, that is

$$f_N(x) \approx \sum_{k=0}^{N} S_k(x) f(x_k). \tag{3.151}$$

From the explicit differentiation of Eq. (3.151), the representation of the second derivative operator is,

$$D_{jk}^{(2)} = S_k''(x_j) = \begin{cases} -\frac{2(-1)^{j-k}}{(j-k)^2 h^2}, & j \neq k, \\ -\frac{\pi^2}{3h^2}, & j = k. \end{cases} \tag{3.152}$$

This representation of the second derivative operator has been used frequently for the solution of the Schrödinger equation (Schwartz 1985; Colbert and Miller 1992; Dulieu et al. 1997; Meijering et al. 1999; Boyd 2001; Wei 2000a, b; Amore 2006).

References

Abramowitz, M., Stegun, I.A.: Handbook of Mathematical Functions with Formulas, Graphs, and Mathematical Tables. US Government Printing Office (1964)

Alterman, Z., Frankowski, K., Pekeris, C.L.: Eigenvalues and eigenfunctions of the linearized Boltzmann collision operator for a Maxwell gas and for a gas of rigid spheres. Astophys. J. Suppl. **7**, 291–331 (1962)

Amore, P.: A variational Sinc collocation method for strong-coupling problems. J. Phys. A: Math. Gen. **39**, L349–L355 (2006)

Andersen, K., Shuler, K.E.: On the relaxation of a hard sphere Rayleigh and Lorentz gas. J. Chem. Phys. **40**, 633–650 (1964)

Angula, C., et al.: A compilation of charged-particle induced thermonuclear reaction rates. Nucl. Phys. A **656**, 3–183 (1999)

Asheim, A., Deano, A., Huybrechs, D., Wang, H.: A Gaussian quadrature rule for oscillatory integrals on a bounded interval. Discret. Contin. Dyn. Syst. **34**, 883–901 (2014)

Atenzi, S., Meyer-Ter-Vehn, J.: The Physics of Inertial Fusion. Clarendon Press, Oxford (2004)

Bacic, Z., Light, J.C.: Highly excited vibrational levels of floppy triatomic-molecules: a discrete variable representation—distributed Gaussian-basis approach. J. Chem. Phys. **85**, 4594–4604 (1986)

Balakrishnan, N., Dalgarno, A.: Nitric oxide production in collisions of hot O(^{3}P) atoms with N_2. J. Geophys. Res. **108**, 1065 (2003)

Baltensperger, R., Trummer, M.A.: Spectral differencing with a twist. SIAM J. Sci. Comput. **24**, 1465–1487 (2003)

Barkley, D.: Spiral meandering. In: Kapral, R., Showalter, K. (eds.) Chemical Waves and Patterns, pp. 163–189. Kluwer Academic, Norwell (1995)

Bartlett, D.F., Corle, T.R.: The circular parallel plate capacitor: a numerical solution for the potential. J. Phys. A: Math. Gen. **18**, 1337–1342 (1985)
Baye, D.: Lagrange bases for the Fourier, generalized Fourier and Riccati-Bessel grids. J. Phys. B: Atom. Mol. Opt. Phys. **27**, L187–L191 (1994)
Baye, D.: Lagrange-mesh method for quantum-mechanical problems. Phys. Stat. Sol. B **243**, 1095–1109 (2006)
Baye, D., Heenen, P.H.: Generalized meshes for quantum-mechanical problems. J. Phys. A: Math. Gen. **19**, 2041–2059 (1986)
Baye, D., Vincke, V.: Lagrange meshes from nonclassical orthogonal polynomials. Phys. Rev. E **59**, 7195–7199 (1999)
Baye, D., Hesse, M., Vincke, M.: The unexplained accuracy of the Lagrange-mesh method. Phys. Rev. E **65**, 026701 (2002)
Becke, A.D.: A multicenter numerical integration scheme for polyatomic molecules. J. Chem. Phys. **88**, 2547–2553 (1988)
Becke, A.D.: Perspective: fifty years of density-functional theory in chemical physics. J. Chem. Phys. **140**, 18A301 (2014)
Belai, O.Y., Schwartz, O.V., Shapiro, D.A.: Accuracy of one-dimensional collision integral in the rigid-sphere approximation. Phys. Rev. A **76**, 012513 (2007)
Bellman, R.E., Kashef, B.G., Casti, J.: Differential quadrature: a technique for the rapid solution of nonlinear partial differential equations. J. Comput. Phys. **10**, 40–52 (1972)
Berman, P.R., Haverkort, J.E.M., Woerdman, J.P.: Collision kernels and transport coefficients. Phys. Rev. A **34**, 4647–4656 (1986)
Bernstein, R.B.: Quantum effects in elastic molecular scattering. Adv. Chem. Phys. **10**, 75–134 (1966)
Bertulani, C.A., Fuqua, J., Hussein, M.S.: Big bang nucleosynthesis and non-Maxwellian distribution. Astrophys. J. **767**(63), 1–11 (2013)
Blackmore, R., Shizgal, B.: Discrete ordinate method of solution of Fokker-Planck equations with nonlinear coefficients. Phys. Rev. A **31**, 1855–1868 (1985)
Bobylev, A.V.: Exact solutions of the nonlinear Boltzmann equation and the theory of relaxation of a Maxwellian gas. Theor. Math. Phys. **60**, 820–841 (1984)
Bordoni, A., Manini, N.: An optimized algebraic basis for molecular potentials. J. Phys. Chem. A **111**, 12564–12569 (2007)
Bornemann, F., Laurie, D., Wagon, S., Waldvogel, J.: The SIAM 100-Digit Challenge: A Study in High-Accuracy Numerical Computing. SIAM, Philadelphia (2004)
Bosch, H.S., Hale, G.M.: Improved formulas for fusion cross sections and thermal reactivities. Nucl. Fusion **32**, 611–631 (1992)
Bovino, S., Zhang, P., Kharchenko, V., Dalgarno, A.: Trapping hydrogen atoms from a Neon-gas matrix: a theoretical simulation. J. Chem. Phys. **131**, 054302 (2009)
Bovino, S., Zhang, P., Kharchenko, V., Dalgarno, A.: Relaxation of energetic $S(^1D)$ atoms in Xe gas: comparison of ab initio calculations with experimental data. J. Chem. Phys. **135**, 024304 (2011)
Boyd, J.P.: The optimization of convergence for Chebyshev polynomial methods in an unbounded domain. J. Comput. Phys. **45**, 43–79 (1982)
Boyd, J.P.: Exponentially convergent Fourier-Chebyshev quadrature schemes on bounded and infinite domains. J. Sci. Comput. **2**, 99–109 (1987)
Boyd, J.P.: Chebyshev and Fourier Spectral Methods. Dover, New York (2001)
Brun, R.: Introduction to Reactive Gas Dynamics. Oxford University Press, Oxford (2009)
Burden, R.L., Faires, J.D.: Numerical Analysis, 9th edn. Brooks/Cole, Boston (2011)
Burke, P.G.: R-Matrix Theory of Atomic Collisions: Application to Atomic, Molecular and Optical Processes. Springer, New York (2011)
Burke, K.: Perspective on density functional theory. J. Chem. Phys. **136**, 150901 (2012)
Burke, P.G., Joachain, C.J.: Theory of Electron Atom Collisions Part 1: Potential Scattering. Springer, New York (1995)

Canto, L.F., Hussein, M.S.: Scattering Theory of Molecules, Atoms and Nuclei. Springer, New York (2013)
Canuto, C., Hussaini, M.Y., Quarteroni, A., Zang, T.A.: Spectral Methods: Fundamentals in Single Domains. Springer, New York (2006)
Cassar, M.M., Drake, G.W.F.: High precision variational calculations for H_2^+. J. Phys. B: At. Mol. Opt. Phys. **37**, 2485–2492 (2004)
Chandrasekhar, S.: Radiative Transfer. Dover, New York (1960)
Chang, J.S., Cooper, G.: A practical difference scheme for Fokker-Planck equations. J. Comput. Phys. **6**, 1–16 (1970)
Chapman, S., Cowling, T.G.: The Mathematical Theory of Nonuniform Gases. Cambridge University Press, Cambridge (1970)
Chatfield, D.C., Truhlar, D.G., Schwenke, D.W.: Benchmark calculations for thermal reaction rates. I. Quantal scattering theory. J. Chem. Phys. **94**, 2040–2044 (1991)
Cheney, W., Kincaid, D.: Numerical Methods and Computing, 6th edn. Brooks/Cole Publishing Company, Calif (2008)
Child, M.S.: Molecular Collision Theory. Dover, New York (1996)
Clayton, D.D.: Principles of Stellar Evolution and Nucleosynthesis. McGraw-Hill, New York (1968)
Cohen, J.S.: Rapid accurate calculation of JWKB phase-shifts. J. Chem. Phys. **68**, 1841–1843 (1978)
Colbert, D.T., Miller, W.H.: A novel discrete variable representation for quantum-mechanical reactive scattering via the S-Matrix Kohn method. J. Chem. Phys. **96**, 1982–1991 (1992)
Cools, R.: An encyclopaedia of cubature formulas. J. Complexity **19**, 445–453 (2003)
Danailov, D.M., Viehland, L.A., Johnson, R., Wright, T.G., Dickinson, A.S.: Transport of O^+ through Argon gas. J. Chem. Phys. **128**, 134302 (2008)
Davis, P.J., Rabinowitz, P.: Methods of Numerical Integration. Academic Press, New York (1975)
Descouvemont, P., Adahchour, A., Angulo, C., Coc, A., Vangioni-Flam, E.: Compilation and R-matrix analysis of Big Bang nuclear reaction rates. At. Data Nucl. Data Tables **88**, 203–236 (2004)
Dickinson, A.S., Certain, P.R.: Calculation of matrix elements for one-dimensional quantum-mechanical problems. J. Chem. Phys. **49**, 4209–4211 (1968)
Dickinson, A.S., Shizgal, B.: Comparison of classical and quantum continuum expectation values. Mol. Phys. **30**, 1221–1228 (1975)
Drake, G.W.F.: High precision theory of atomic Helium. Phys. Scr. **T83**, 82–92 (1999)
Drake, G.W.F., Cassar, M.M., Nistor, R.A.: Ground-state energies for helium, H^- and Ps^-. Phys. Rev. A **65**, 054501 (2002)
Dulieu, O., Kosloff, R., Masnou-Seeuws, F., Pichler, G.: Quasibound states in long-range alkali dimers: grid method calculation. J. Chem. Phys. **107**, 10633–10642 (1997)
Durran, D.R.: Numerical Methods for Fluid Dynamics: With Applications to Geophysics. Springer, Berlin (2010)
El-Sherbiny, A., Poirier, R.A.: An evaluation of the radial part of the numerical integration commonly used in DFT. J. Comput. Chem. **25**, 1378–1384 (2004)
Ernst, M.H.: Nonlinear model Boltzmann equations and exact solutions. Phys. Rep. **78**, 1–171 (1981)
Fermi, E.: Un metodo statistico per la determinazione di alcune priopriet dell'atomo. Rend. Accad. Naz. Lincei **6**, 602607 (1927)
Ferziger, J.H., Kaper, H.G.: Mathematical Theory of Transport Processes in Gases. North-Holland, Amsterdam (1972)
Finlayson, B.A.: The Method of Weighted Residuals and Variational Principles. Academic Press, New York (1972)
Finlayson, B.A., Scriven, L.E.: The method of weighted residuals—a review. Appl. Mech. Rev. **19**, 735–748 (1966)
Fiolhais, C., Marques, M.A.L., Nogueira, F.: A Primer in Density Functional Theory. Springer, Berlin (2003)

Foch, J.D., Ford, G.W.: The linear Boltzmann equation. In: de Boer, J., Uhlenbeck, G.E. (eds.) Studies in Statistical Mechanics, pp. 127–154. Elsevier, Holland (1970)
Ford, G.W.: Matrix elements of the linearized collision operator. Phys. Fluids **11**, 515–521 (1968)
Fornberg, B.: A Practical Guide to Pseudospectral Methods. Cambridge University Press, Cambridge (1996)
Fornberg, B., Driscoll, T.A., Wright, G., Charles, R.: Observations on the behavior of radial basis function approximations near boundaries. Comput. Math. Appl. **43**, 473–490 (2002)
Frankowski, K., Pekeris, C.L.: Logarithmic terms in the wave functions of two-electron atoms. Phys. Rev. **146**, 46–49 (1966)
Funaro, D.: Polynomial Approximation of Differential Equations. Springer, Berlin (1992)
Gallas, J.A.C.: Some matrix elements for Morse oscillator. Phys. Rev. A **21**, 1829–1834 (1980)
Gautschi, W.: The numerical evaluation of a challenging integral. Numer. Algorithms **49**, 187–194 (2008)
Gibble, K.E., Gallagher, A.: Measurements of velocity-changing collision kernels. Phys. Rev. A **43**, 1366–1380 (1991)
Gibelli, L., Shizgal, B.D., Yau, A.W.: Ion energization by wave-particle interactions: comparison of spectral and particle simulation solutions of the Vlasov equation. J. Comput. Phys. **59**, 2566–2581 (2010)
Gill, P.M.W.: Molecular integrals over Gaussian basis functions. Adv. Quant. Chem. **25**, 141–205 (1994)
Gill, P.M.W., Chien, S.-H.: Radial quadrature for multiexponential integrands. J. Comput. Chem. **24**, 732–740 (2003)
Goldstein, H., Poole, C., Safko, J.: Classical Mechanics. Addison Wesley, San Francisco (2000)
Gombosi, T.I.: Gaskinetic Theory. Cambridge University Press, Cambridge (1994)
Gottlieb, D., Orszag, S.: Numerical Analysis of Spectral Methods: Theory and Applications. SIAM, Philadelphia (1977)
Grabowski, P.E., Chernoff, D.F.: Pseudospectral calculation of helium wave functions, expectation values, and oscillator strength. Phys. Rev. A **84**, 042505 (2011)
Hamilton, I.P., Light, J.C.: On distributed Gaussian bases for simple model multidimensional vibrational problems. J. Chem. Phys. **84**, 306–317 (1986)
Harris, D.O., Engerholm, G.G., Gwinn, W.D.: Calculation of matrix elements for one-dimensional quantum-mechanical problems and the application to anharmonic oscillators. J. Chem. Phys. **43**, 1515–1517 (1965)
Haubold, H.J., John, R.W.: Analytical representation of the thermonuclear reaction rate and fusion energy production in a spherical plasma shock wave. Plasma Phys. **23**, 399–411 (1981)
Haxton, D.J.: Lebedev discrete variable representation. J. Phys. B: At. Mol. Opt. Phys. **40**, 4443–4451 (2007)
Heidbrink, W.W., Sadler, G.J.: The behaviour of fast ions in Tokamak experiments. Nucl. Fusion **34**, 535–615 (1994)
Helgaker, T., Jorgensen, P., Olsen, J.: Molecular Electronic Structure Theory. Wiley, New York (2000)
Hesthaven, J.S., Gottlieb, S., Gottlieb, D.: Spectral Methods for Time Dependent Problems. Cambridge University Press, Cambridge (2007)
Hirschfelder, J.O., Curtiss, C.F., Bird, B.: The Molecular Theory of Gases and Liquids. Wiley, New York (1954)
Hoare, M.R.: The linear gas. Adv. Chem. Phys. **20**, 135–214 (1971)
Hoare, M.R., Kaplinsky, C.H.: Linear hard sphere gas: variational eigenvalue spectrum of the energy kernel. J. Chem. Phys. **52**, 3336–3353 (1970)
Hohenberg, P., Kohn, W.: Inhomogeneous electron gas. Phys. Rev. **136**, B864–B871 (1964)
Holloway, J.P.: Spectral discretizations of the Vlasov-Maxwell equations. Trans. Theory Stat. Phys. **25**, 1–32 (1996)
Holway, L.H.: Time varying weight functions and the convergence of polynomial expansions. Phys. Fluids **10**, 35–48 (1967)

Huang, K.: Statistical Mechanics. Wiley, New York (1967)
Hubert, D.: Auroral ion velocity distribution function: generalized polynomial solution of Boltzmann's equation. Planet. Space Sci. **31**, 119–127 (1983)
Hussein, M.S., Pato, M.P.: Uniform expansion of the thermonuclear reaction rate formula. Braz. J. Phys. **27**, 364–372 (1997)
Isaacson, S.A., Kirby, R.M.: Numerical solution of linear Volterra integral equations of the second kind with sharp gradients. J. Comput. Appl. Math. **235**, 4283–4301 (2011)
Iserles, A., Norsett, S.P.: Efficient quadrature of highly oscillatory integrals using derivatives. Proc. R. Soc. A **461**, 1383–1399 (2005)
Jamieson, M.J., Dalgarno, A., Wei, L.: Elastic scattering of hydrogen and deuterium atoms by oxygen atoms. J. Geophys. Res. **111**, A06308 (2006)
Jerri, A.J.: Introduction to Integral Equations with Applications, 2nd edn. Wiley, New York (1999)
Johnson, R.E., Liu, M., Tully, C.: Collisional dissociation cross sections for $O + O_2$, $CO + N_2$, $O_2 + O_2$, $N + N_2$ and $N_2 + N_2$. Planet. Space Sci. **50**, 123–128 (2002)
Jones, R.O., Gunnarsson, O.: The density functional formalism, its applications and prospects. Rev. Mod. Phys. **61**, 689–746 (1989)
Kabin, K., Shizgal, B.D.: Exact evaluation of collision integrals for the nonlinear Boltzmann equation. AIP Conf. Proc. **663**, 35–42 (2003)
Kakhiani, K., Tsereteli, K., Tsereteli, P.: A program to generate a basis set adaptive radial quadrature grid for density functional theory. Comput. Phys. Commun. **180**, 256–268 (2009)
Kallush, S., Kosloff, R.: Improved methods for mapped grids: applied to highly excited vibrational states of diatomic molecules. Chem. Phys. Lett. **433**, 221–227 (2006)
Kapral, R., Ross, J.: Relaxation in a dilute binary gas mixture. J. Chem. Phys. **52**, 1238–1243 (1970)
Karplus, M., Porter, R.N.: Atoms and Molecules: An Introduction for Students of Physical Chemistry. Benjamin, Menlo Park (1970)
Kennedy, M., Smith, F.J.: The efficient computation of JWKB phase shifts. Mol. Phys. **13**, 443–448 (1967)
Kern, C.W., Karplus, M.: Gaussian-transform method for molecular integrals. II. Evaluation of molecular properties. J. Chem. Phys. **43**, 415–429 (1965)
Kharchenko, V., Dalgarno, A.: Thermalization of fast $O(^1D)$ atoms in the stratosphere and mesosphere. J. Geophys. Res. **109**, D18311 (2004)
Kharchenko, V., Tharamel, J., Dalgarno, A.: Kinetics of thermalization of fast nitrogen atoms beyond the hard sphere approximation. J. Atmos. Sol. Terr. Phys. **59**, 107–115 (1997)
Kharchenko, V., Balakrishnan, N., Dalgarno, A.: Thermalization of fast nitrogen atoms in elastic and inelastic collisions with molecules of atmospheric gases. J. Atmos. Terr. Phys. **60**, 95–106 (1998)
Kohn, W., Sham, L.J.: Self-consistent equations including exchange and correlation effects. Phys. Rev. **140**, A1133–A1138 (1965)
Kokoouline, V., Dulieu, O., Kosloff, R., Masnou-Seeuws, F.: Mapped Fourier methods for long-range molecules: application to perturbations in the $Rb_2(0_u^+)$ photoassociation spectrum. J. Chem. Phys. **110**, 9865–9876 (1999)
Kremer, G.M.: An Introduction to the Boltzmann Equation and Transport Processes in Gases. Springer, New York (2010)
Krook, M., Wu, T.T.: Formation of Maxwellian tails. Phys. Rev. Lett. **36**, 1107–1109 (1976)
Kumar, A.S.: An analytical solution to applied mathematics-related Loves equation using the Boubaker polynomials expansion scheme. J. Frankl. Inst. **347**, 1755–1761 (2010)
Kythe, P.K., Puri, P.: Computational Methods for Linear Integral Equations. Birkhauser, Berlin (2002)
Kythe, P.K., Schaferkotter, M.R.: Handbook of Computational Methods for Integration. Chapman and Hall/CRC, London (2004)
Langer, R.E.: On the connection formulas and the solutions of the wave equation. Phys. Rev. **51**, 669–676 (1937)

Lebedev, V.I.: Spherical quadrature formulas exact to orders 25–29. Sib. Mat. Zh. **18**, 132–142 (1977)
Lemmon, E.W., Jacobsen, R.T.: Viscosity and thermal conductivity equations for Nitrogen, Oxygen, Argon, and Air. Int. J. Thermophys. **25**, 21–69 (2004)
LeVeque, R.J.: Finite Difference Methods for Ordinary and Partial Differential Equations. SIAM, Philadelphia (2007)
Levine, I.N.: Quantum Chemistry, 6th edn. Prentice Hall, New Jersey (2009)
Liao, P.F., Bjorholm, J.E., Berman, P.R.: Effects of velocity-changing collisions on two-photon and stepwise-absorption spectroscopic line shapes. Phys. Rev. A **21**, 1927–1938 (1980)
Liboff, R.L.: Introductory Quantum Mechanics, 4th edn. Addison-Wesley, New York (2002)
Liboff, R.L.: Kinetic Theory: Classical, Quantum, and Relativistic Descriptions, 3rd edn. Springer, New York (2003)
Lieb, E.H.: Thomas-Fermi and related theories of atoms and molecules. Rev. Mod. Phys. **53**, 603–641 (1981)
Light, J.C., Carrington Jr, T.: Discrete variable representations and their utilization. Adv. Chem. Phys. **114**, 263–310 (2000)
Light, J.C., Hamilton, I.P., Lill, J.V.: Generalized discrete variable approximation in quantum mechanics. J. Chem. Phys. **82**, 1400–1409 (1985)
Lindenfeld, M.J., Shizgal, B.: Matrix elements of the Boltzmann collision operator for gas mixtures. Chem. Phys. **41**, 81–95 (1979)
Lindfield, G.R., Penny, J.E.T.: Numerical Methods Using MATLAB. Elsevier, Amsterdam (2012)
Lindh, R., Malmqvist, P.A., Gagliardi, L.: Molecular integrals by numerical quadrature I. Radial integration. Theor. Chem. Acta **106**, 178–187 (2001)
Liou, K.-N.: A numerical experiment on Chandrasekhar's discrete-ordinate method for radiative transfer: applications to cloudy and hazy atmospheres. J. Atmos. Sci. **30**, 1303–1326 (1973)
Liu, Q.-J., Zhao, W.-Q.: Iterative solution for groundstate of H_2^+ ion. Commun. Theor. Phys (Beijing, China). **53**, 57–62 (2010)
Lo, J.Q.-W., Shizgal, B.D.: Spectral convergence of the quadrature discretization method in the solution of the Schrödinger and Fokker-Planck equations: comparison with Sinc methods. J. Chem. Phys. **125**, 194108 (2006)
Lo, J.Q.-W., Shizgal, B.D.: An efficient mapped pseudospectral method for weakly bound states: vibrational states of He_2, Ne_2, Ar_2 and Cs_2. J. Phys. B: At. Mol. Opt. Phys. **41**, 185103 (2008)
Love, E.R.: The electrostatic field of two equal circular co-axial conducting disks. Q. J. Mech. Appl. Math. **2**, 428–451 (1949)
Loyalka, S.K., Tipton, E.L., Tompson, R.V.: Chapman-Enskog solutions to arbitrary order in Sonine polynomials I: simple, rigid-sphere gas. Physica A **379**, 417–435 (2007)
Lyness, J.N.: When not to use an automatic quadrature routine. SIAM Rev. **25**, 63–87 (1983)
Lyness, J.N.: Integrating some infinite oscillating tails. J. Comput. Appl. Math. **12**, 109–117 (1985)
Mason, E.A., McDaniel, E.W.: Transport Properties of Ions in Gases. Wiley, New York (1988)
Mathai, A.M., Haubold, H.J.: Review of mathematical techniques applicable in astrophysical reaction rate theory. Astrophys. Space Sci. **282**, 265–280 (2002)
McCourt, F.R.W., Beenakker, J.J.M., Köhler, W.E.E., Kuščer, I.: Nonequilibrium Phenomena in Polyatomic Gases Volume. 2: Cross Sections, Scattering, and Rarefied Gases. Oxford University Press, Oxford (1991)
McDaniel, E.W., Mason, E.A.: The Mobility and Diffusion of Ions in Gases. Wiley, New York (1973)
McGuyer, B.H., Marslann III, R., Olsen, B.A., Happer, W.: Cusp kernels for velocity-changing collisions. Phys. Rev. Lett. **108**, 183202 (2012)
McQuarrie, D.A., Simon, J.D.: Physical Chemistry: A Molecular Approach. University Science Books, California (1997)
Meijering, E.H.W., Niessen, W.J., Viergever, M.A.: The Sinc-approximating kernels of classical polynomial interpolation. IEEE Int. Conf. Image Proc. **3**, 652–656 (1999)

Mitani, M.: An application of double exponential formula to radial quadrature grid in density functional calculation. Theor. Chem. Acc. **130**, 645–669 (2011)
Morgan, J.D.: Thomas-Fermi and other density—functional theories. In: Drake, G.W.F. (ed.) Atomic, Molecular and Optical Physics Handbook, pp. 233–242. AIP Press, New York (1996)
Mullen, W.J., Laloë, F., Richards, M.G.: Longitudinal relaxation times for dilute quantum gases. J. Low Temp. Phys. **80**, 1–13 (1990)
Munn, R.J., Mason, E.A., Smith, F.J.: Some aspects of the quantal and semiclassical calculation of phase shifts and cross sections for molecular scattering and transport. J. Chem. Phys. **41**, 3978–3988 (1964)
Mura, M.E., Knowles, P.J.: Improved radial grids for quadrature in molecular density-functional calculations. J. Chem. Phys. **104**, 9848–9858 (1996)
Murray, C.W., Handy, N.C., Lamming, G.L.: Quadrature schemes for integrals of density functional theory. Mol. Phys. **78**, 997–1014 (1993)
Nan, G., Houston, P.L.: Velocity relaxation of S(^{1}D) by rare gases measured by Doppler spectroscopy. J. Chem. Phys. **97**, 7865–7872 (1992)
Napier, D.G., Shizgal, B.D.: Sound dispersion in single-component systems. Phys. A **387**, 4099–4118 (2008)
Newbury, N.R., Barton, A.S., Cates, G.D., Happer, W., Middleton, H.: Gaseous ^{3}He-^{3}He magnetic dipolar relaxation. Phys. Rev. A **48**, 4411–4420 (1993)
O'Hara, H., Smith, F.J.: Error estimation in the Clenshaw-Curtis quadrature formula. Comput. J. **11**, 213–219 (1968)
Oh, S.-K.: Modified Lennard-Jones potentials with a reduced temperature-correction parameter for calculating thermodynamic and transport properties: Noble gases and their mixtures (He, Ne, Ar, Kr, and Xe). J. Thermodyn. **2013**, 828620 (2013)
Olmos, D., Shizgal, B.D.: A pseudospectral method of solution of Fisher's equation. J. Comput. Appl. Math. **193**, 219–242 (2006)
O'Neal, D., Neff, J.E.: OH 1.563μ absorption from starspots on active stars. Astron. J. **113**, 1129–1137 (1997)
Ordzywolek, A.: Gaussian integration with rescaling abscissas and weights. Comput. Phys. Commun. **182**, 2533–2539 (2011)
Pack, R.T.: Space-fixed vs body-fixed axes in atom-diatomic molecule scattering. Sudden approximation. J. Chem. Phys. **60**, 633–639 (1974)
Parr, R.G.: Density functional theory. Annu. Rev. Phys. Chem. **34**, 631–656 (1983)
Parr, R.G., Gosh, S.W.: Thomas-Fermi theory for atomic systems. Proc. Natl. Acad. Sci. **83**, 3577–3579 (1986)
Pask, J.E., Sukumar, N., Monsavi, S.E.: Linear scaling solution of the all-electron Coulomb problem in solids. Int. J. Multiscale Comput. Eng. **10**, 83–99 (2012)
Pastore, P.: The numerical treatment of Love's integral equation having a small parameter. J. Comput. Appl. Math. **236**, 1267–1281 (2011)
Peyret, R.: Spectral Methods for Incompressible Viscous Flow. Springer, New York (2002)
Rasch, J., Whelan, C.T.: On the numerical evaluation of a class of integrals occurring in scattering problems. Comput. Phys. Commun. **101**, 31–46 (1997)
Reine, S., Helgaker, T., Lindh, R.: Multi-electron integrals. WIREs Comput. Mol. Sci. **2**, 290–303 (2012)
Robson, R.E., Prytz, A.: A discrete ordinate pseudo-spectral method: review and application from a physicist's perspective. Aust. J. Phys. **46**, 465–495 (1993)
Robson, R.E., Ness, K.F., Sneddon, G.E., Viehland, L.A.: Comment on the discrete ordinate method in the kinetic theory of gases. J. Comput. Phys. **92**, 213–229 (1991)
Rogers, G.L., Berman, P.R.: Exchange collision kernel. Phys. Rev. A **44**, 417–432 (1991)
Ross, J., Mazur, P.: Some deductions from a formal statistical mechanical theory of chemical kinetics. J. Chem. Phys. **35**, 19–28 (1961)
Rys, J., Dupuis, M., King, H.F.: Computation of electron repulsion integrals using Rys quadrature method. J. Comput. Chem. **4**, 154–157 (1983)

Sabbane, M., Tij, M., Santos, A.: Maxwellian gas undergoing a stationary Poiseuille flow in a pipe. Phys. A **327**, 264–290 (2003)
Safouhi, H.: The properties of sine, spherical Bessel and reduced Bessel functions for improving convergence of semi-infinite very oscillatory integrals: the evaluation of three-centre nuclear attraction integrals over B-functions. J. Phys. A: Math. Gen. **34**, 2801–2818 (2001)
Sandberg, J.A.R., Rinkevicius, Z.: An algorithm for the efficient evaluation of two-electron repulsion integrals over contracted Gaussian-type basis functions. J. Chem. Phys. **137**, 234105 (2012)
Santos, A.: Solutions of the moment hierarchy in the kinetic theory of Maxwell models. Contin. Mech. Thermodyn. **21**, 361–387 (2009)
Schumer, J.W., Holloway, J.P.: Vlasov simulations using velocity-scaled Hermite representations. J. Comput. Phys. **144**, 626–661 (1998)
Schwartz, C.: High-accuracy approximation techniques for analytic functions. J. Math. Phys. **26**, 411–415 (1985)
Secrest, D., Johnson, B.R.: Exact quantum-mechanical calculation of a collinear collision of a particle with a harmonic oscillator. J. Chem. Phys. **45**, 4556–4570 (1966)
Seinfeld, J.H., Pandis, S.N.: Atmospheric Chemistry and Physics: From Air Pollution to Climate Change, 2nd edn. Wiley, New York (2006)
Shapiro, D.A.: Spectral line narrowing in the Keilson-Storer model. J. Phys. B: At. Mol. Opt. Phys. **33**, L43–L49 (2000)
Sharipov, F., Bertoldo, G.: Numerical solution of the linearized Boltzmann equation for an arbitrary intermolecular potential. J. Comput. Phys. **228**, 3345–3357 (2009)
Shavitt, I., Karplus, M.: Gaussian-transform method for molecular integrals. I. Formulation of energy integrals. J. Chem. Phys. **43**, 398–414 (1965)
Shen, J., Tang, T., Wang, L.-L.: Spectral Methods: Algorithms Analysis and Applications. Springer, Berlin (2011)
Shizgal, B.: Kinetic theory calculation of NMR relaxation time for dilute ^{3}He gas. J. Chem. Phys. **58**, 3424–3431 (1973)
Shizgal, B.: Calculation of the NMR relaxation time for dilute ^{129}Xe gas. Chem. Phys. **5**, 464–470 (1974a)
Shizgal, B.: A method for the rapid calculation of matrix elements with highly oscillatory JWKB radial wavefunctions. Chem. Phys. Lett. **24**, 369–372 (1974b)
Shizgal, B.: A Gaussian quadrature procedure for the use in the solution of the Boltzmann equation and related problems. J. Comput. Phys. **41**, 309–328 (1981)
Shizgal, B.D.: An analysis of O-H interaction potentials, O-H and O-D cross sections and vibrational states. Planet. Space. Sci. **47**, 163–147 (1999)
Shizgal, B., Fitzpatrick, J.M.: Matrix elements of the linear Boltzmann collision operator for systems of two components at different temperatures. Chem. Phys. **6**, 54–65 (1974)
Shizgal, B., Lindenfeld, M.J.: Energy distribution function of translationally hot O(^3P) atoms in the atmosphere of earth. Planet. Space Sci. **27**, 1321–1332 (1979)
Shizgal, B., Blackmore, R.: A discrete ordinate method of solution of linear boundary value and eigenvalue problems. J. Comput. Phys. **55**, 313–327 (1984)
Shizgal, B., Hubert, D.: Nonequilibrium nature of ion distribution functions in the high latitude auroral ionosphere. In: Muntz, E.P., Weaver, D.P., Campbell, D.H. (eds.) Proceedings of the 16th International Symposium on Rarefied Gas Dynamics, pp. 3–22. AIAA, Washington (1989)
Shizgal, B.D., Chen, H.: The quadrature discretization method (QDM) in the solution of the Schrödinger equation with nonclassical basis functions. J. Chem. Phys. **104**, 4137–4150 (1996)
Shizgal, B.D., Chen, H.: The quadrature discretization method in the solution of the Fokker-Planck equation with nonclassical basis functions. J. Chem. Phys. **107**, 8051–8063 (1997)
Shu, C.: Differential Quadrature and Its Application in Engineering. Springer, Berlin (2000)
Siewert, C.E.: On computing the Chapman-Enskog functions for viscosity and heat transfer and the Burnett functions. JQRST **74**, 789–796 (2002)
Slevinsky, M., Safouhi, H.: Numerical treatment of a twisted tail using extrapolation methods. Numer. Algorithm **48**, 301–316 (2008)

Sospedra-Alfonso, R., Shizgal, B.D.: Henyey-Greenstein model in the shape relaxation of dilute gas mixtures. Trans. Theory Stat. Phys. **41**, 368–388 (2012)
Sospedra-Alfonso, R., Shizgal, B.D.: Energy and shape relaxation in binary atomic systems with realistic quantum cross sections. J. Chem. Phys. **139**, 044113 (2013)
St.-Maurice, J.-P., Schunk, R.W.: Use of generalized orthogonal polynomial solutions of Boltzmanns equation in certain aeronomy problems, Auroral ion velocity distributions. J. Geophys. Res. **81**, 2145–2154 (1976)
St.-Maurice, J.-P., Schunk, R.W.: Ion velocity distributions in the high-latitude ionosphere. Rev. Geophys. **17**, 99–134 (1979)
Stenger, F.: Numerical methods based on Sinc and analytic functions. Springer Series in Comp. Math. **20**, 91–96 (1993)
Stroud, A.H., Secrest, D.: Gaussian Quadrature Formulas. Prentice-Hall, New Jersey (1966)
Szabo, A., Ostlund, N.S.: Modern Quantum Chemistry, Introduction to Advanced Electronic Structure Theory. Dover, New York (1996)
Szalay, V.: Discrete variable representations of differential operators. J. Chem. Phys. **99**, 1978–1984 (1993)
Szalay, V., Szidarovsky, T., Czakó, G., Császár, A.G.: A paradox of grid-based representation techniques: accurate eigenvalues from inaccurate matrix elements. J. Math. Chem. **50**, 636–651 (2012)
Szalay, V., Czakó, G., Nagy, A., Furtenbacher, T., Császár, A.G.: On one-dimensional discrete variable representations with general basis functions. J. Chem. Phys. **119**, 10512–10518 (2003)
Tang, T.: The Hermite spectral method for Gaussian-type functions. SIAM J. Sci. Comput. **14**, 594–606 (1993)
Taylor, J.R.: Scattering Theory: The Quantum Theory on Nonrelativistic Collisions. Dover, New York (2012)
Thomas, L.H.: The calculation of atomic fields. Proc. Camb. Philos. Soc. **23**, 542–548 (1927)
Tomaschitz, R.: Multipole fine structure of the cosmic microwave background: reconstruction of the temperature power spectrum. Mon. Not. R. Astron. Soc. **427**, 1363–1383 (2012)
Tomaschitz, R.: Bessel integrals in epsilon expansion: squared spherical Bessel functions averaged with Gaussian power-law distributions. Appl. Math. Comput. **225**, 228–241 (2013)
Trefethen, L.N.: Is Gauss quadrature better than Clenshaw-Curtis? SIAM Rev. **50**, 67–87 (2008)
Treutler, O., Ahlrichs, R.: Efficient molecular numerical integration schemes. J. Chem. Phys. **102**, 346–354 (1995)
Truhlar, D.G., Wyatt, R.E.: History of H_3 kinetics. Annu. Rev. Phys. Chem. **27**, 1–43 (1976)
Tsuneda, T.: Density Functional Theory in Quantum Chemistry. Springer, New York (2014)
Ueda, M., Sargeant, A.J., Pato, M.P., Hussein, M.S.: Effective astrophysical S factor for nonresonant reactions. Phys. Rev. C **61**, 045801 (2000)
Viehland, L.A.: Velocity distribution functions and transport coefficients of atomic ions in atomic gases by a Gram-Charlier approach. Chem. Phys. **179**, 71–92 (1994)
Viehland, L.A., Chang, Y.: Transport cross sections for collisions between particles. Comput. Phys. Commun. **181**, 1687–1696 (2010)
Wei, H.: Ghost levels and near-variational forms of the discrete variable representation: application to H_2O. J. Chem. Phys. **106**, 6885–6900 (1997)
Wei, G.W.: Solving quantum eigenvalue problems by discrete singular convolution. J. Phys. B: At. Mol. Opt. Phys. **33**, 343–352 (2000a)
Wei, G.W.: Wavelets generated by using discrete singular convolution kernels. J. Phys. A: Math. Gen. **33**, 8577–8596 (2000b)
Weniger, E.J.: The strange history of B functions or how theoretical chemists and mathematicians do (not) interact. Int. J. Quant. Chem. **109**, 1706–1716 (2009)
Whittaker, J.M.: The Fourier theory of the Cardinal function. Proc. Roy. Soc. Edinb. **1**, 169–176 (1929a)
Whittaker, J.M.: On the Cardinal function of interpolation theory. Proc. Roy. Soc. Edinb. **1**, 41–46 (1929b)

Wick, G.C.: Über ebene diffusionsprobleme. Z. Phys. **121**, 702–718 (1943)
Wigner, E.P., Wilkins Jr, J.E.: Effect of temperature of the moderator on the velocity distribution of neutrons with numerical calculations for H as moderator. Technical Report AECD-2275, US Atomic Energy Commission (1944)
Willner, K., Dulieu, O., Masnou-Seeuws, F.: Mapped grid methods for long-range molecules and cold collisions. J. Chem. Phys. **120**, 548–561 (2004)
Wind, H.: Electron energy for H_2^+ in the ground state. J. Chem. Phys. **42**, 2371–2373 (1965)
Wright, J.S., Donaldson, D.J.: Potential energy and vibrational levels for local modes in water and acetylene. Chem. Phys. **94**, 15–23 (1985)
Zhang, P., Kharchenko, V., Dalgarno, A.: Thermalization of suprathermal N(^{4}S) atoms in He and Ar gases. Mol. Phys. **105**, 1487–1496 (2007)

Chapter 4
Representation of Functions in Basis Sets

Abstract The orthogonal basis sets most often used in spectral methods are the Chebyshev and Legendre polynomials on a bounded domain, or a Fourier basis set for periodic functions. We discuss in this chapter the expansions of Gaussian and Kappa distributions of kinetic theory in Hermite and Laguerre polynomials on the infinite and semi-infinite intervals, respectively. The spectral convergence properties of these expansions is demonstrated numerically and analytically. The expansions of $\sin(x)$ in Hermite polynomials, and of the Maxwellian distribution in Chebyshev polynomials are also considered. The basic principles of Fourier series are presented and applied to quantum mechanical wave packets as well as the analysis of free induction decay signals. The resolution of the Gibbs phenomenon with the Gegenbauer reconstruction method is compared with the inverse polynomial reconstruction method. A resolution of the Runge phenonmena is also presented.

4.1 Introduction

The spectral solutions of integral and partial differential equations are based on the finite expansions in a basis set. Spectral methods are used in many different fields including fluid mechanics (Gottlieb and Orszag 1977; Canuto et al. 2006), biology (Olmos and Shizgal 2006; Olmos 2010), economics (Tangman et al. 2008; Pindza et al. 2014), relativity (Grandclément and Novak 2009), satellite engineering (Williams 2011) and numerous other fields. In this chapter, the spectral convergence of the expansion of several different functions in basis sets is studied. The description of spectral (and pseudospectral) solutions of differential and integral equations, limited to physical problems based on the Boltzmann, Fokker-Planck, Kramers and the Schrödinger equations, as well as the equation for radiative transfer, are presented in Chaps. 5 and 6.

The basis sets commonly used are orthogonal polynomials and the periodic trigonometric functions. The choice of the basis functions depends on the problem studied. For a problem defined on a finite interval, the choice is generally Chebyshev, Legendre polynomials or trigonometric functions for periodic solutions. The most frequently used basis sets are listed in Table 2.1. Numerous mathematical identities

B. Shizgal, *Spectral Methods in Chemistry and Physics*, Scientific Computation,
DOI 10.1007/978-94-017-9454-1_4

are readily available for the classical polynomials (Abramowitz and Stegun 1964; Gradshteyn and Ryzhik 2007) and for each set there is a defining differential Sturm-Liouville eigenvalue problem (Jirari 1995; Al-Gwaiz 2008) discussed in Sect. 6.7. Nonclassical polynomials have also been used in many applications (Baye and Vincke 1999; Garcia 1999; Weideman 1999; Chen and Shizgal 2001; Lo and Shizgal 2008; Asadchev and Gordon 2012). By contrast, very few mathematical properties are known for the non-classical polynomials listed in Table 2.2.

A spectral method is based on the approximation of a function, $f(x)$, in a basis set. The Nth order polynomial approximation is given by

$$f^{(N)}(x) = \sum_{n=0}^{N} a_n P_n(x), \quad x \in [a, b], \tag{4.1}$$

where the basis functions, $P_n(x)$, are orthonormal with respect to a weight function, $w(x)$, that is

$$\int_a^b w(x) P_n(x) P_m(x) dx = \delta_{nm}.$$

A spectral method generally implies that if the function, $f(x)$, is sufficiently smooth, the absolute value of the coefficients, $|a_n|$, will decrease rapidly with n and the representation is efficient and accurate. There are proofs of the spectral convergence for certain problems that show an exponential decrease of the absolute value of the coefficients, $|a_n|$, with n (Gottlieb and Orszag 1977; Boyd 2001; Wang and Xiang 2012; Trefethen 2013).

In this chapter, we are concerned with the rate of convergence of the spectral representation of specific real functions, $f(x)$, in a basis set on a given interval. The Hermite and Laguerre polynomials are the basis sets of choice in many different applications in quantum theory (Boyd et al. 2003) and kinetic theory. We begin with a study of the convergence of expansions in Hermite polynomials on the infinite interval (Schumer and Holloway 1998; Alp and Arikan 2012) and Laguerre polynomials on the semi-infinite interval (Bao et al. 2008; Weniger 2009; Tatari and Haghighi 2014) as discussed in Sects. 4.3 and 4.5.

We consider Fourier series in some detail in Sect. 4.6.1 with particular attention given to the Gibbs' phenomenon (Gottlieb and Shu 1997; Driscoll and Fornberg 2001; Shizgal and Jung 2003; Jerri 2011; Gelb and Hines 2012). The expansion of a function on a finite interval in a Fourier series can lead to spurious oscillations, known as Gibbs phenomenon, at the discontinuous points where the function has a jump discontinuity. We also note the extensive use of Fourier series in the solution of numerous problems in quantum mechanics (Kosloff and Kosloff 1983; Kosloff 1993; Balint-Kurti and Pulay 1995; Balint-Kurti 2010), kinetic theory (Filbet et al. 2006; Filbet and Mouhot 2011), astrophysics (Bonazzola et al. 1999), geophysics (Durran 2010), signal and image processing (Blackledge 2006) and in many other fields.

4.2 Approximation of Functions in a Basis Set; The Least Squares Error

The representation of a given real function, $f(x)$, in a basis set, $\{P_n(x)\}$, orthonormal with respect to weight function, $w(x)$, is

$$f^{(N)}(x) = w(x) \sum_{n=0}^{N} a_n P_n(x). \tag{4.2}$$

The expansion coefficients are given by the integral

$$a_n = \int_I f(x) P_n(x) dx, \tag{4.3}$$

on some specified interval I. It is important to notice that the series expansion, Eq. (4.2), the weight function, $w(x)$, multiplies the series expansion and differs from Eq. (4.1). This choice is made with the expectation that $f(x)$ is not very different from $w(x)$ and hence the series expansion will converge quickly. This will become evident with the examples discussed in the sections that follow. A primary interest is the decrease of the expansion coefficients, $|a_n|$, versus n and how good is the approximation $f^{(N)}(x)$.

In kinetic theory, $w(x)$, is often the Maxwellian velocity distribution function, $F(x)$, Eq. (4.9), and the expansion Eq. (4.2) is often referred to as the expansion "about" a Maxwellian. The series expansion gives the correction to the Maxwellian owing to nonequilibrium processes (Mintzer 1965; Holway 1967).

There have been numerous discussions of approximation theory with different degrees of mathematical rigour (Davis 1963; Cheney 1966; Rivlin 1969; Boyd 2001; Trefethen 2013). One of the main results is the Weierstrass approximation theorem which states that every continuous function defined on a closed interval, $[a, b]$, can be uniformly approximated as closely as desired by a polynomial. An excellent historical account of approximation theory has been provided by Steffens (2006) and also by Pinkus (2000).

Given the approximation of the function, Eq. (4.2), how do we measure the accuracy of the approximation $f^{(N)}(x)$? How do we express the "distance" of $f^{(N)}(x)$ from $f(x)$? We could make use of the familiar method of least squares used to fit discrete data $\{x_i, y_i\}$ to a straight line, $y = ax + b$. In this case, the least squares fit is the one that minimizes the error

$$E(a, b) = \frac{1}{N} \sum_{i=1}^{N} [y_i - (ax_i + b)]^2,$$

with respect to a and b obtained with the inversion of the 2×2 matrix equation that is derived by setting $\partial E/\partial a = 0$ and $\partial E/\partial b = 0$ (Cheney and Kincaid 2008).

For the polynomial approximation in Eq. (4.2), we use the minimization of the global continuous least squares distance between $f(x)$ and $f^{(N)}(x)$ as given by

$$E_2(N) = \int_I \frac{1}{w(x)}\Big[f(x) - f^{(N)}(x)\Big]^2 dx, \tag{4.4}$$

where the definition of the norm is dictated by the form of Eq. (4.2) (Mintzer 1965). There are many other criteria that can be used to measure the closeness of $f^{(N)}(x)$ to $f(x)$ that serve to quantify the rate of convergence versus N. A comprehensive survey of different measures has been provided by Cha (2007) with particular emphasis to signal processing and image resolution. This includes the Kullback–Leibler entropy (Kullback and Leibler 1951) and other entropy functionals as a distance measure between a pair of probability density functions. We make use of entropy functionals in the study of the approach to statistical equilibrium in Chap. 6.

In this chapter, we study the way in which the choice of basis functions determines how well $f(x)$ is approximated by $f^{(N)}(x)$, and the rate of convergence versus the number of basis functions, N, retained. If the square in Eq. (4.4) is written out in full, then with Eq. (4.2) the least squares error is

$$E_2(N) = \int_I \frac{f^2(x)}{w(x)}dx - 2\sum_{n=0}^{N} a_n \int_I P_n(x) f(x) dx + \sum_{n=0}^{N}\sum_{m=0}^{N} a_n a_m \int_I w(x) P_n P_m dx. \tag{4.5}$$

With the orthonormality of the basis functions in the last term, the minimization of $E_2(N)$ with respect to all a_n, that is $\partial E_2(N)/\partial a_n = 0$ gives precisely the expansion coefficients derived with the orthogonality of the polynomials, Eq. (4.3), The first term in Eq. (4.5) must be finite, that is

$$\int_I \frac{f^2(x)}{w(x)}dx < \infty, \tag{4.6}$$

which for the infinite and semi-infinite intervals restricts the asymptotic dependence of $f(x)$, namely

$$\lim_{|x|\to\infty} \frac{f(x)}{\sqrt{w(x)}} \sim 0. \tag{4.7}$$

The function $f(x)$ must decay to zero faster than $\sqrt{w(x)}$ as $x \to \infty$ (Mintzer 1965; Leblanc and Hubert 1997). Thus we have from Eqs. (4.2) and (4.5)

$$E_2(N) = \int_I \frac{f^2}{w(x)}dx - \sum_{n=0}^{N} a_n^2 \tag{4.8}$$

with the understanding that the classical polynomials, Table 2.1, are normalized to unity. The integral in Eq. (4.8) defines the norm, which is consistent with the form of the expansion, Eq. (4.2).

4.3 Expansions in Hermite Polynomials; Spectral Convergence

For quantum and statistical mechanical problems, the domain of interest is either the infinite or semi-infinite interval and the functions of interest may be close to Gaussians. Thus we begin the illustration of spectral convergence with expansion of Gaussians in Hermite polynomials, $H_n(x)$, with $x \in (-\infty, \infty)$. Hermite polynomials are the eigenstates of the quantum harmonic oscillator which is a Sturm-Liouville eigenvalue problem. Expansions in Hermite polynomials are used for calculations of ion mobilities (Viehland 1994), in applications to astrophysics (Blinnikov and Moessner 1998), financial econometrics (Hurn et al. 2007), geophysics (Boyd 2001; Durran 2010), signal analysis (Alp and Arikan 2012), image processing (Martens 2006), stochastic processes (Risken and Till 1996), plasma physics (Schumer and Holloway 1998; Le Bourdiec et al. 2006; Gibelli et al. 2010) and other applications.

The kinetic theory of gases is based on the Boltzmann equation for the velocity distribution of electrons, protons, atoms, and ions in a large variety of physical situations for which only the translational energy of the particles is important. In space physics, where the effects of a magnetic field are important, it is often sufficient to consider the one dimensional distribution function, $f(v_z)$, as a function of the particle velocity, v_z, along the magnetic field direction.

We consider a one-dimensional distribution function assumed to be time independent and spatially homogeneous. It is defined such that the number of particles with velocities in the range $[v_z, v_z + dv_z]$, is $f(v_z)dv_z$. At complete equilibrium, the distribution is the well known one dimensional Maxwell-Boltzmann distribution given by

$$F(v_z) = \left(\frac{m}{2\pi k_B T_b}\right)^{1/2} e^{-\frac{mv_z^2}{2k_B T_b}}, \tag{4.9}$$

where m is the particle mass, k_B is the Boltzmann constant and T_b is the temperature of the gas. The distribution function is normalized to unit density, that is

$$\int_{-\infty}^{\infty} F(v_z)dv_z = 1, \tag{4.10}$$

and the temperature is defined in terms of the average energy

$$\frac{k_B T_b}{2} = \int_{-\infty}^{\infty} F(v_z)\frac{mv_z^2}{2}dv_z. \tag{4.11}$$

As is well known, each degree of freedom contributes $k_B T_b/2$ to the average energy. Were we to consider the three-dimensional distribution in $v = \sqrt{v_x^2 + v_y^2 + v_z^2}$ as we do later, the average energy is then $3k_B T_b/2$.

If there are external perturbations on the system, the distribution function may be different from the Maxwellian. There are integral or differential kinetic equations for these nonequilibrium distribution functions in different physical situations as discussed in Chaps. 5 and 6.

The solution of these kinetic equations can often be obtained with the expansion of the distribution function in Hermite polynomials of the form,

$$f^{(N)}(x) = se^{-s^2x^2} \sum_{n=0}^{N} c_n H_n(sx), \tag{4.12}$$

where the reduced speed is $x = v_z\sqrt{m/(2k_B T_b)}$, $s > 0$ is a scaling parameter and $w(sx) = e^{-s^2x^2}$ is the weight function for the scaled Hermite polynomials. The introduction of the scaling parameter has been shown to improve the convergence of such expansions (Holloway 1996; Schumer and Holloway 1998; Tang 1993; Fok et al. 2001; Le Bourdiec et al. 2006; Gibelli et al. 2010) as we later demonstrate in this chapter. This scaling procedure is analogous to the scaling of quadrature points discussed in Chap. 3, Sect. 3.3. For the solution of kinetic theory problems, it is often useful to choose the weight function to be as close to the actual anticipated distribution so that only a few terms in the sum, Eq. (4.2) are required.

4.3.1 An Asymmetric Hermite Expansion

In this and subsequent sections, we consider different expansions of a normalized dimensionless Maxwellian distribution, $f(x) = \sqrt{r/\pi}e^{-rx^2}$, at temperature T_0 with $r = T_b/T_0$. The first expansion that we consider is with the Hermite polynomials, $H_n(x)$, that is,

$$\sqrt{\frac{r}{\pi}}e^{-rx^2} = se^{-s^2x^2} \sum_{n=0}^{\infty} a_{2n} H_{2n}(sx), \tag{4.13}$$

which are orthogonal in accordance with

$$\int_{-\infty}^{\infty} e^{-s^2x^2} H_{2n}(sx) H_{2m}(sx) d(sx) = \delta_{nm}\sqrt{\pi}2^{2n}(2n)!. \tag{4.14}$$

Only even order Hermite polynomials occur in the sum as the function is even, $f(-x) = f(x)$. It is important to notice that the weight function, $w(sx) = \exp(-s^2x^2)$, occurs in front of the expansion, Eq. (4.13). The expansion of a

distribution about a zero order weight function that is a good approximation to the solution sought is a common technique in kinetic theory (Viehland 1994; Gibelli et al. 2010). The expansion, Eq. (4.13) is referred to as the asymmetric weight expansion employed in the solution of the Vlasov equation (Holloway 1996; Schumer and Holloway 1998).

If Eq. (4.13) is multiplied by $H_{2n}(sx)$ and integrated over x and the orthogonality relation is used, the expansion coefficients are

$$a_{2n} = \frac{\sqrt{r}}{\pi 2^{2n}(2n)!} \int_{-\infty}^{\infty} e^{-rx^2} H_{2n}(sx) dx. \tag{4.15}$$

We use the identity 7.373-2 from Gradshteyn and Ryzhik (2007), namely,

$$\int_{-\infty}^{\infty} e^{-z^2} H_{2n}(\beta z) dz = \sqrt{\pi} \frac{(2n)!}{n!} (\beta^2 - 1)^n, \tag{4.16}$$

to evaluate this integral. With the change of variable $z = x\sqrt{r}$ and $\beta = s/\sqrt{r}$ in Eq. (4.16), we find that,

$$a_{2n} = \frac{1}{n!\sqrt{\pi}} \left(\frac{s^2 - r}{4r} \right)^n. \tag{4.17}$$

The $E_2(N)$ error, Eq. (4.8), is given by

$$E_2(N) = \frac{r}{\pi} \int_{-\infty}^{\infty} e^{-(2r - s^2)x^2} dx - s\sqrt{\pi} \sum_{n=0}^{N} a_{2n}^2 (2n)! 2^{2n}, \tag{4.18}$$

where Eq. (4.15) and the normalization of the Hermite polynomials, Eq. (4.14), have been used. The integral in Eq. (4.18) is elementary and with the substitution of a_{2n} from Eq. (4.17) we have that

$$E_2(N) = \frac{r}{\sqrt{\pi(2r - s^2)}} - \frac{s}{\sqrt{\pi}} \sum_{n=0}^{N} \left(\frac{s^2 - r}{2r} \right)^{2n} \frac{(2n)!}{(n!)^2}. \tag{4.19}$$

For the special case, $s^2 = r$, the summation in Eq. (4.19) truncates at $n = 0$ and $E_2(N) = 0$ with $a_0 = 1/\sqrt{\pi}$ and $a_{2n} = 0, n \neq 0$. For $s = 1$ and several values of the temperature ratio, r, we show the variation of $\ln[E_2(N)]$ versus N in the left hand graph of Fig. 4.1. The exponential variation of $E_2(N)$ versus N, although not exact, is evident by the almost linear curves. Notice that with $s \geq \sqrt{2}r$ the integral in Eq. (4.18) and the series, Eq. (4.19), are not defined.

The symbols in Fig. 4.1 are the results obtained with Eq. (4.19) and the solid straight lines are the linear least squares fit to the curves. With $s = 1$, r must be

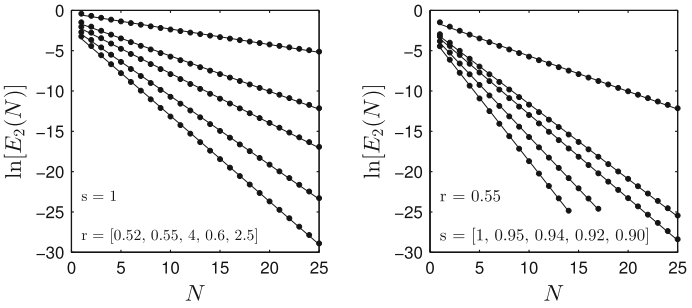

Fig. 4.1 Demonstration of spectral (that is exponential) convergence of the expansion of a Maxwellian $\sqrt{r/\pi}e^{-rx^2}$ at T_0 in Hermite polynomials, $H_{2n}(sx)$, about the weight function, $w(sx) = e^{-s^2x^2}$, with $x = v_z\sqrt{m/2k_BT_b}$ defined at T_b, $r = T_b/T_0$ and s is the scale factor. The *left hand graph* shows the spectral convergence for $s = 1$ and different values of r (from *top* to *bottom*) whereas the *right hand graph* is for $r = 0.55$ and different values of s (from *top* to *bottom*). The values $r = 4$ and 2.5 are equivalent to $r = 4/7$ and $5/8$, respectively. The *symbols* are the numerical results from Eq. (4.19) and the *straight lines* are linear least *squares* fits to the *symbols*. The slope of the lines are compared with the asymptotic estimates of Eq. (4.25) in Table 4.1

Table 4.1 Demonstration of spectral (exponential) convergence to accompany Fig. 4.1; $E_2(N) \approx Ce^{-AN}$

r	s	A from the linear fit	$A = -\sinh^{-1}[\frac{E_2(N+1)-E_2(N-1)}{2E_2(N)}]$	$A = -\ln[\frac{s^2-r}{r}]^2$
0.52	1	0.192	0.177	0.160
0.55	1	0.439	0.420	0.401
4.00	1	0.615	0.595	0.575
0.60	1	0.852	0.830	0.811
2.50	1	1.062	1.041	1.022
0.55	0.95	0.931	0.909	0.890
0.55	0.94	1.042	1.020	1.000
0.55	0.92	1.293	1.266	1.236
0.55	0.90	1.564	1.534	1.499

The slopes of the linear fit to each curve is shown in the third column. The fourth column provides an estimate of A with the last three points in the figures as discussed in the text. The fifth column is from the asymptotic analysis of Eq. (4.19); $\ln E_2(N) \approx -N \ln q - \ln\sqrt{N}+$ constant

greater than 0.50 for $E_2(N)$ to remain finite and for the convergence of the series Eq. (4.13). The criterion for the convergence of the expansion Eq. (4.13) is that $f(x)$ decays faster than $\sqrt{w(sx)}$, that is $\lim_{|x|\to\infty} f(x)/\sqrt{w(sx)} \to 0$ (Mintzer 1965; Holway 1967; Tang 1993; Leblanc and Hubert 1997; Gibelli et al. 2010).

The topmost curve with $r = 0.52$ in Fig. 4.1 demonstrates the slowest convergence for the r values chosen. The spectral convergence is clear for all the curves but the rate is dependent on r and s. The right hand graph of Fig. 4.1 shows the more rapid spectral convergence obtained by decreasing the scale factor below unity for $r = 0.55$

and s decreases from the top curve to the bottom curve. The values $r = 4$ and 2.5 are equivalent to $r = 4/7$ and $5/8$, respectively.

With the definition

$$q = \left(\frac{s^2 - r}{r}\right)^2, \tag{4.20}$$

and the approximate evaluation of the slope, the backward finite difference $E_2(N) - E_2(N-1)$ gives,

$$E_2(N) - E_2(N-1) = -\frac{s}{\pi}\frac{q^N}{4^N}\frac{(2N)!}{(N!)^2}. \tag{4.21}$$

It is useful to extract this (almost) exponential behaviour and for this purpose, we use Stirling's approximation in the form

$$n! \approx \sqrt{2\pi n}\left(\frac{n}{e}\right)^n, \tag{4.22}$$

so that in Eq. (4.21)

$$\frac{(2N)!}{(N!)^2} \approx \frac{4^N}{\sqrt{\pi N}}. \tag{4.23}$$

With this subtitution into Eq. (4.21)

$$E_2(N) - E_2(N-1) \overset{N\to\infty}{\approx} \frac{s}{\pi\sqrt{\pi N}} e^{-N\ln q} \tag{4.24}$$

and the final result is

$$\ln[E_2(N) - E_2(N-1)] \overset{N\to\infty}{\approx} -N\ln q + \ln(s/\sqrt{N}) + \text{constant}. \tag{4.25}$$

Table 4.1 shows the r and s variation of the different approximations to the slopes of the curves in Fig. 4.1. The third column is the slope from the linear fit whereas the values in the fourth column are derived from the assumption of an exponential dependence on N and the numerical centered finite difference evaluation of the derivative, that is

$$\frac{dE_2(N)}{dN} \approx \frac{e^{-A(N+1)} - e^{-A(N-1)}}{2e^{-AN}} = -\sinh(A). \tag{4.26}$$

The last column in the table is based on the asymptotic result, Eq. (4.25) with q given by Eq. (4.20). It is clear that the convergence is very close to exponential. Both the linear fit and the asymptotic result, columns 3 and 5 in the table, are approximations. They differ by about 20 % for the first entry and by 4 % for the last five entries. An important point is that exponential convergence does not necessarily mean that the convergence is rapid as demonstrated by the topmost curves in Fig. 4.1.

With the identity $x^2 = [H_2(x) + 2H_0(x)]/4$, the average energy of the Maxwellian distribution, Eq. (4.13), equivalently the average of the second moment of this distribution is

$$e_{avg} = \sqrt{\frac{r}{\pi}} \int_{-\infty}^{\infty} e^{-rx^2} x^2 dx = \frac{1}{2r}, \tag{4.27}$$

and is given exactly by the first two terms in the expansion, that is

$$e_{avg} = \frac{\sqrt{\pi}}{2s^2} (a_0 + 4a_2) . \tag{4.28}$$

With Eq. (4.17), the dimensionless average energy is confirmed, that is, $e_{avg} = 1/2r = T_0/2T_b$, even though the series approximation may not accurately approximate the distribution function.

4.3.2 A Symmetric Hermite Expansion; Spectral Convergence

An alternate expansion referred to as the symmetric weight expansion (Holway 1967; Tang 1993; Schumer and Holloway 1998; Gibelli et al. 2010) employs the functions $h_n(sx)$ given by

$$h_n(sx) = \frac{e^{-s^2x^2/2} H_n(sx)}{\sqrt{2^{2n}(2n)!\sqrt{\pi}}}, \tag{4.29}$$

orthogonal with unit weight function, that is,

$$\int_{-\infty}^{\infty} h_n(sx) h_m(sx) d(sx) = \delta_{nm}. \tag{4.30}$$

We use the expansion

$$\sqrt{\frac{r}{\pi}} e^{-rx^2} = s \sum_{n=0}^{\infty} b_{2n} h_{2n}(sx), \tag{4.31}$$

where the b_{2n} coefficients are given by orthogonality as

$$b_{2n} = \sqrt{\frac{r}{\pi}} \int_{-\infty}^{\infty} e^{-rx^2} h_{2n}(sx) dx. \tag{4.32}$$

If we define

$$b_{2n} = \frac{\hat{b}_{2n}}{\sqrt{2^{2n}(2n)!\sqrt{\pi}}}, \tag{4.33}$$

then

$$\hat{b}_{2n} = \sqrt{\frac{r}{\pi}} \int_{-\infty}^{\infty} e^{-(r+s^2/2)x^2} H_{2n}(sx)dx, \tag{4.34}$$

which with the identity, Eq. (4.16), we find that

$$\hat{b}_{2n} = \sqrt{\frac{2r}{(s^2+2r)}} \left(\frac{s^2-2r}{s^2+2r}\right)^n \frac{(2n)!}{n!}. \tag{4.35}$$

The least squares error is evaluated as in the previous section but without the weight function factor, that is

$$E_2(N) = \int_{-\infty}^{\infty} |f(x) - f^{(N)}(x)|^2 dx = \sqrt{\frac{r}{2\pi}} - s\sum_{n=0}^{N} \frac{\hat{b}_{2n}^2}{2^{2n}(2n)!\sqrt{\pi}}, \tag{4.36}$$

which with Eq. (4.35) is given by

$$E_2(N) = \sqrt{\frac{r}{2\pi}} - \frac{s}{\sqrt{\pi}} \left(\frac{2r}{2r+s^2}\right) \sum_{n=0}^{N} \left[\frac{s^2-2r}{2(s^2+2r)}\right]^{2n} \frac{(2n)!}{(n!)^2}. \tag{4.37}$$

It is clear from Eq. (4.37) that the expansion is exact for $s = \sqrt{2r}$. Since the distribution is expanded as given by Eq. (4.31), the condition, Eq. (4.6) is always satisfied.

The spectral convergence is shown in the left hand graph of Fig. 4.2 for $s = 1$ and different values of r much larger than those chosen in Fig. 4.1. The rate of convergence increases as the temperature ratio decreases. The variation in the rate of the spectral convergence is shown in the right hand graph for $r = 7$ for different values of the scaling parameter, s. It is clear that with the appropriate choice of the scaling parameter, the rate of convergence is accelerated.

Whereas the expansion Eq. (4.13) diverges for $s > \sqrt{2r}$ the expansion Eq. (4.31) converges for all s. However, with Eq. (4.31) the average energy defined by Eq. (4.27) is given by the series

$$e_{avg} = \frac{\sqrt{2\pi}}{4s^2} \sum_{n=0}^{N} \frac{\hat{b}_{2n}}{\sqrt{\pi}2^{2n}(2n)!} T_{2n}, \tag{4.38}$$

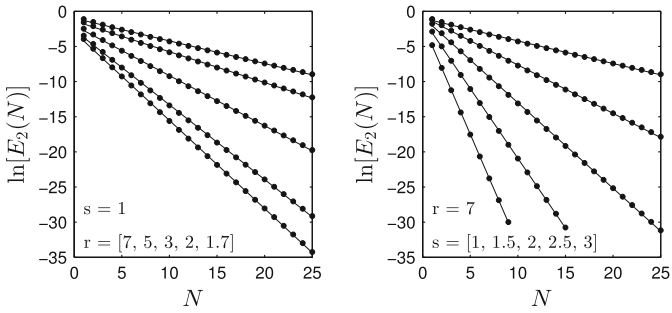

Fig. 4.2 Demonstration of spectral (that is exponential) convergence of the expansion of a Maxwellian $\sqrt{r/\pi}e^{-rx^2}$ at T_0 in Hermite polynomials, $h_{2n}(sx)$, with $x = \sqrt{mv_z^2/(2k_BT_b)}$ defined at T_b with $r = T_b/T_0$ and s is a scale factor. The *left hand frame* shows the spectral convergence for $s = 1$ and different values of r (from *top* to *bottom*) whereas the *right hand frame* is for $r = 7$ and different values of s (from *top* to *bottom*). The *symbols* are the numerical results from Eq. (4.37) and the *straight lines* are linear least *squares* fits to the *symbols*. In Table 4.2, the slopes of the *lines* are compared with the asymptotic results of Eq. (4.37)

Table 4.2 Demonstration of spectral convergence to accompany Fig. 4.2; $E_2(N) \approx Ce^{-AN}$ with $E(N)$ given by Eq. (4.37)

r	s	A from the linear fit	$A = -\sinh^{-1}[\frac{E_2(N+1)-E_2(N-1)}{2E_2(N)}]$	$A = -\ln[\frac{s^2-2r}{(s^2+2r)^2}]$
7	1	0.322	0.304	0.286
5	1	0.439	0.420	0.401
3	1	0.713	0.692	0.673
2	1	1.063	1.041	1.022
1.7	1	1.255	1.227	1.212
7	1.5	0.689	0.668	0.648
7	2.0	1.218	1.192	1.176
7	2.5	1.985	1.950	1.921
7	3.0	3.142	3.110	3.052

where

$$T_{2n} = \left(\frac{(2n+2)!}{(n+1)!} + (8n+2)\frac{(2n)!}{n!} + 8n(2n-1)\frac{(2n-2)!}{(n-1)!} \right). \tag{4.39}$$

The recurrence relation $xH_n = (H_{n+1} + 2nH_{n-1})/2$ has been used twice as well as the integral identity in Eq. (4.16). This result should be compared with approximation of the temperature, Eq. (4.28), with the asymmetric expansion, Eq. (4.13).

The convergence of the temperature is shown in the left hand graph of Fig. 4.3 for $r = 2$ and $s = 1$ calculated with Eqs. (4.38) and (4.39). The temperature in this case is not given in terms of a finite number of moments as in Eq. (4.28). The local

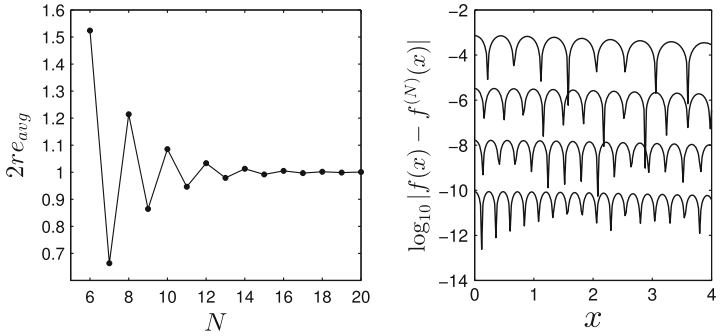

Fig. 4.3 (*Left graph*) Convergence of the average energy, $e_{avg} = 1/2r$, for the symmetric Hermite polynomial expansion in $h_{2n}(sx)$ of the Maxwellian, $f(x) = \sqrt{\frac{r}{\pi}}e^{-rx^2}$: with $r = 2$ and $s = 1$; (*Right graph*) the local convergence for $N = 20, 40, 60$ and 80 (from *top* to *bottom*)

convergence of the distribution is shown in the right graph of Fig. 4.3 for $r = 2$ and $s = 1$ and numerous cusps are evident (Boyd 2001). The convergence is more rapid as s increases and the result is exact for $s = \sqrt{2r}$; see Eq. (4.37).

The third column lists the slopes of the linear fits whereas the data in the fourth column are derived from the dependence on N given by Eq. (4.26). The last column is based on the asymptotic result, Eq (4.25), derived from Eq. (4.37) with $q = [(s^2 - 2r)/(s^2 + 2r)]^2$. The agreement between the results for the linear fit in column 3 and the asymptotic results in column 5 improves with an increase in s. Complementary discussions of this convergence analysis were also provided by Tang (1993) and Boyd (1987, 2001).

These spectral methods have been applied to the solution of the Vlasov equation for collisionless plasmas (Holloway 1996; Schumer and Holloway 1998; Gibelli and Shizgal 2006; Gibelli et al. 2010), in the representation of proton velocity distribution functions in stellar winds (Leblanc and Hubert 1997) and for the calculation of ion mobilities with solutions of the Boltzmann equation (Almeida et al. 2002). Numerical experiments with Hermite expansions analogous to those presented here and by Tang (1993) were also discussed at length by Le Bourdiec et al. (2006) with references to previous works.

4.3.3 Expansion of $\sin(x)$ *in Hermite Polynomials*

Gottlieb and Orszag (1977) and later Tang (1993) suggested from their studies of the expansion of a sine wave in Hermite polynomials that Hermite polynomials exhibit poor resolution properties. They considered the expansion

$$\sin(kx) = s \sum_{n=0}^{\infty} d_{2n+1} H_{2n+1}(sx), \tag{4.40}$$

where the parameter k is the wavenumber of the wave and the scaling parameter s is included (Tang 1993). With the orthogonality of the scaled Hermite polynomials, Eq. (4.14), and the change of integration variable $y = sx$, we have that

$$d_{2n+1} = \frac{1}{\sqrt{\pi} 2^{2n+1} (2n+1)!} \int_{-\infty}^{\infty} e^{-y^2} \sin(ky/s) H_{2n+1}(y) dy. \tag{4.41}$$

With item 7.388-1 in Gradshteyn and Ryzhik (2007),

$$\int_0^{\infty} e^{-x^2} \sin(\sqrt{2}\beta x) H_{2n+1}(x) dx = (-1)^n \sqrt{\pi} 2^{n-1/2} \beta^{2n+1} e^{-\beta^2/2}, \tag{4.42}$$

we get the result

$$d_{2n+1} = \frac{(-1)^n (k/s)^{2n+1} e^{-k^2/4s^2}}{2^{2n+2}(2n+1)!}. \tag{4.43}$$

where $\beta = k/(s\sqrt{2})$.

The approximation of the sine wave with the expansion in Hermite polynomials is shown in Fig. 4.4 for $N = 10, 20$ and 40 (from top to bottom in the figure) which resolve about 1, $2\frac{1}{2}$ and $4\frac{1}{2}$ oscillations, respectively. The solid curve is $\sin(x)$ and the symbols are the values computed from the expansion, Eq. (4.40). The fit breaks down after a few cycles of the sine wave depending on the number of terms retained in the Hermite expansion.

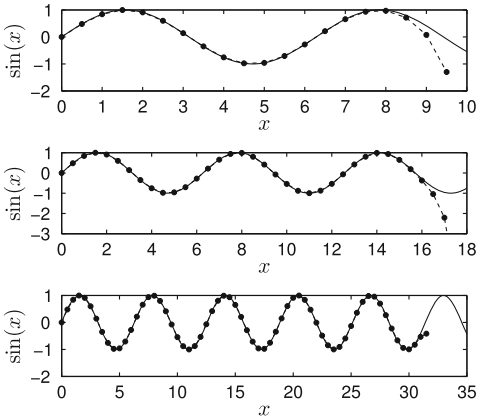

Fig. 4.4 Convergence of the expansion of $\sin(x)$ in Hermite polynomials, $H_{2n+1}(x)$ with $N = 10, 20$ and 40 (from *top* to *bottom*). The *solid curve* is $\sin(x)$ and the *symbols* are the values computed from the expansion in Eq. (4.40)

An analysis by Tang (1993) based on the asymptotic behaviour of the Hermite polynomials demonstrates that to resolve k wavelengths of the sine function requires of the order of $k^2/4$ Hermite functions. Figure 4.4 is similar to Figs. 3.11, 3.12 and 3.13 in Gottlieb and Orszag (1977) with results for the Laguerre polynomials. Their conclusion derived on the basis of the asymptotic behaviour of the Laguerre polynomials is that the Laguerre expansion requires approximately 9.06 polynomials per wavelength to achieve high accuracy.

Based on these observations, Gottlieb and Orszag (1977) conclude that this illustrates poor resolution properties for the Laguerre and Hermite polynomials and that these basis functions will not be of much practical value in applications of spectral methods. However we have noted otherwise in Sect. 4.3 that the Hermite basis functions may be the basis functions of choice in applications on the infinite domain.

4.4 Expansion of a Maxwellian with Chebyshev Polynomials

It is of interest to compare the expansions of the Maxwellian in Hermite polynomials on $(-\infty, \infty)$ with the expansion in Chebyshev polynomials which are defined on $[-1, 1]$. We consider the transformation of the infinite interval onto $[-1, 1]$ which can be done with many different mappings and the convergence of the expansion will depend on the choice (Boyd 1987; Shen and Yu 2012). We choose the map from $x \in (-\infty, \infty)$ to $y \in [-1, 1]$ of the form $x = y/(1 - y^2)$ and the expansion

$$\sqrt{\frac{r}{\pi}} e^{-ry^2/(1-y^2)^2} = \sum_{n=0}^{N} c_{2n+1} T_{2n+1}(y). \tag{4.44}$$

With the orthogonality of the Chebyshev polynomials

$$\int_{-1}^{1} \frac{1}{\sqrt{1-y^2}} T_n(y) T_m(y) = N_n \delta_{nm}, \tag{4.45}$$

the expansion coefficients are given by

$$c_{2n+1} = \frac{r}{\pi} \int_{-1}^{1} \frac{e^{-ry^2/(1-y^2)^2}}{\sqrt{1-y^2}} T_{2n+1}(y) dy, \tag{4.46}$$

which are evaluated with Chebyshev quadratures. The normalization of the Chebyshev polynomials, N_n, is given by Eq. (2.126). The least squares error is given by

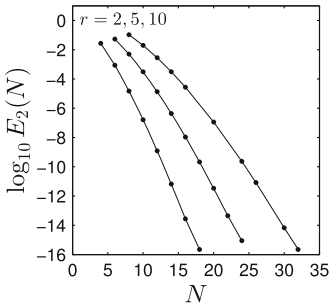

Fig. 4.5 Convergence of the expansion of a Maxwellian in Chebyshev polynomials, Eq. (4.44), with $r = T_b/T_0 = 2, 5$ and 10 (from *top* to *bottom*)

$$E_2(N) = \int_{-1}^{1} \frac{1}{\sqrt{1-y^2}} |f(y) - f^{(N)}(y)|^2 dy,$$

$$= \frac{r}{\pi} \int_{-1}^{1} \frac{e^{-2ry^2/(1-y^2)^2}}{\sqrt{1-y^2}} dy - \sum_{n=1}^{N} c_{2n+1}^2 N_{2n+1}. \tag{4.47}$$

The integral in the second line of Eq. (4.47) can be evaluated accurately with MAPLE. The $E_2(N)$ error is shown in Fig. 4.5 for $r = 2, 5,$ and 10. The rate of convergence is obviously slower for the larger r values and the curves are not nearly as linear as those for the expansion in Hermite polynomials shown in Figs. 4.1 and 4.2. Other mappings from $x \in (-\infty, \infty)$ to $y \in [-1, 1]$ will yield different results.

4.5 Expansion in Laguerre Polynomials

The associated Sonine-Laguerre polynomials, $L_n^{(\alpha)}(x)$, are the basis functions traditionally chosen for transport problems in gases. As discussed in Sect. 3.6.4, the Laguerre polynomials are the eigenfunctions of the linear Boltzmann collision operator for "Maxwell-molecules". These are particles that interact with a repulsive interaction potential that varies as the inverse fourth power of the relative separation of the atoms, r, that is $V(r) \propto r^{-4}$. The Laguerre polynomials are also the eigenfunctions of the radial Schrödinger equation for the hydrogen atom as discussed in Sect. 2.4.6 (Boyd et al. 2003). They are also used in many other spectral applications (Bao et al. 2008; Weniger 2008; Tatari and Haghighi 2014) and they define the quadratures (Evans 2005; Xiang 2012) on the semi-infinite domain.

4.5.1 Asymmetric Laguerre

The expansion of a Maxwellian at temperature T_0 about a Maxwellian at temperature T_b with the temperature ratio denoted by $r = T_b/T_0$ in Laguerre polynomials is

$$r^{3/2}\sqrt{y}e^{-ry} = sw(sy)\sum_{n=0}^{\infty} a_n L_n^{(1/2)}(sy), \quad y \in [0,\infty), \tag{4.48}$$

where $y = mv^2/(2k_BT_b)$ is the reduced energy, $w(sy) = \sqrt{sy}e^{-sy}$, and s is the scaling parameter. The associated Laguerre polynomial with $\alpha = 1/2$ is henceforth written simply as $L_n(sy)$. With the orthogonality condition,

$$\int_0^{\infty} \sqrt{sy}e^{-sy} L_n(sy) L_m(sy) d(sy) = \frac{\Gamma(n+\frac{3}{2})}{n!}\delta_{nm}, \tag{4.49}$$

the expansion coefficients are given by

$$a_n = \frac{n!}{\Gamma(n+\frac{3}{2})} r^{3/2} \int_0^{\infty} \sqrt{y}e^{-ry} L_n(sy) dy. \tag{4.50}$$

We make the change of variable $z = sy$ and get

$$a_n = \frac{n!}{\Gamma(n+\frac{3}{2})} \left(\frac{r}{s}\right)^{3/2} \int_0^{\infty} \sqrt{z}e^{-rz/s} L_n(z) dz. \tag{4.51}$$

With the result 7.414-8 in Gradshteyn and Ryzhik (2007), namely,

$$\int_0^{\infty} \sqrt{z}e^{-\beta z} L_n(z) dz = \frac{\Gamma(n+\frac{3}{2})}{n!\beta^{3/2}} \left(\frac{\beta-1}{\beta}\right)^n, \tag{4.52}$$

and with $\beta = r/s$, the expansion coefficients are given by

$$a_n = \left(\frac{r-s}{r}\right)^n. \tag{4.53}$$

For $r = s/2$, $a_n = (-1)^n$ and the series, Eq. (4.48) does not converge. Thus for $r > s/2$, $|a_n| < 1$ and the expansion Eq. (4.48) converges. This is consistent with the condition, Eq. (4.7), for the $E_2(N)$ error to be finite.

It is useful to set $s = 1$ and define $t = (r-1)/r$ so that the expansion becomes

$$\frac{e^{yt/(t-1)}}{(1-t)^{3/2}} = \sum_{n=0}^{\infty} L_n(y) t^n, \quad |t| < 1. \tag{4.54}$$

Equation (4.54) is recognized as the generating function for the Laguerre polynomials. The series converges provided that $|t| < 1$. Thus the expansion of a Maxwellian at

T_0 with a Maxwellian weight function at T_b is equivalent to the expansion of the generating function for Laguerre polynomials. The generating function in Eq. (4.54) serves as an important tool to calculate the matrix elements of the collision operator in the Boltzmann equation (Foch and Ford 1970; Shizgal and Karplus 1971; Gust and Reichl 2009; Shizgal and Dridi 2010).

The least squares error for the expansion, Eq. (4.48), is calculated as done in the previous sections and is given by

$$E_2(N) = \frac{1}{2}\sqrt{\frac{\pi}{s}}\frac{r^3}{(2r-s)^{3/2}} - s\sum_{n=0}^{N}\left(\frac{r-s}{r}\right)^{2n}\frac{\Gamma(n+3/2)}{n!}. \tag{4.55}$$

The variation of $E_2(N)$ is shown versus N in Fig. 4.6 for several values of r with $s = 1$ and for several values of s with $r = 0.54$. The topmost curves in both figures is for $r = 0.54$ close to the value for which the series expansion is not convergent. For the graph on the left, the convergence improves with increasing r. For the graph on the right, there is an improvement in the convergence with a decrease in the scaling parameter, s. On the right hand side of this figure, the topmost curve is for $r = 0.54$ and we see the dramatic improvement in the rate of convergence by decreasing the scaling parameter, s. Table 4.3 summarizes the slopes of the almost straight lines analogous to Tables 4.1 and 4.2.

There is a symmetric expansion in the Laguerre functions, $\ell_n(y) = \sqrt{\sqrt{y}e^{-y}}$ $L_n(y)$ (Hoare and Kaplinsky 1970) analogous to the expansion in Sect. 4.3.2. However, an analytical expression for the expansion coefficients is not available as for the other expansions considered. Although the coefficients can be determined numerically, the subsequent study of the convergence of the series is contaminated with the errors in the quadratures for the coefficients.

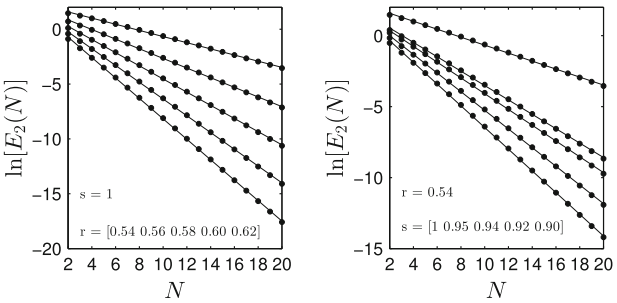

Fig. 4.6 Demonstration of spectral (that is exponential) convergence of the expansion of a Maxwellian, $r\sqrt{ry}e^{-ry}$, at T_0 in Laguerre polynomials about the function, $s\sqrt{sy}e^{-sy}$, with $y = mv^2/(2k_BT_b)$ defined at T_b with $r = T_b/T_0$ and s is the scale factor. The *left hand frame* shows the spectral convergence for $s = 1$ and different values of r (from *top* to *bottom*) whereas the *right hand frame* is for $r = 0.54$ and different values of s (from *top* to *bottom*). The *symbols* are the numerical results and the *straight lines* are linear least *squares* fits to the *symbols*. The slope of the *lines* are compared with the asymptotic results in Table 4.3

Table 4.3 Demonstration of spectral convergence with $E_2(N)$ given by Eq. (4.55); $E_2(N) \approx Ce^{AN}$ to accompany Fig. 4.6

r	s	A from linear fit	$A = -\sinh^{-1}[\frac{E_2(N+1)-E_2(N-1)}{2E_2(N)}]$	$A = -\ln[(\frac{r-s}{r})^2]$
0.54	1	0.281	0.298	0.321
0.56	1	0.439	0.458	0.482
0.58	1	0.600	0.621	0.646
0.60	1	0.765	0.786	0.811
0.62	1	0.931	0.954	0.979
0.54	0.95	0.507	0.527	0.551
0.54	0.94	0.556	0.576	0.600
0.54	0.92	0.657	0.678	0.703
0.54	0.90	0.765	0.786	0.811

4.5.2 Expansion of a Kappa Distribution in Laguerre Polynomials

The nonequilibrium distribution functions of atoms, ions or electrons in aeronomy and space physics in a multitude of different situations can exhibit large populations at high energies much in excess of that given by the Maxwellian at the local temperature. This includes energetic oxygen atoms in the atmospheres of the terrestrial planets, electrons and ions in the terrestrial ionosphere, as well as in the solar atmosphere (Collier 2004; Livadiotis and McComas 2009; Pierrard and Lazar 2010).

The theoretical analysis of these nonequilibrium situations, which occur as a consequence of many different processes and controlled by numerous physical parameters, is a complex problem. Nevertheless, many particle distributions in different environments can be remarkably well fitted to a Kappa distribution (Meyer-Vernet 2001; Hau and Fu 2007; Hellberg et al. 2009; Hau et al. 2009), given by

$$f_\kappa(y) = C_\kappa \sqrt{y} \left[\frac{1}{1 + \frac{y}{\kappa+1}} \right]^{\kappa+1}. \tag{4.56}$$

The distribution is normalized according to $4\pi \int_0^\infty f_\kappa(y) y^2 dy = 1$ which after the variable transformation, $z = y/(\kappa + 1)$ and use of the beta function,

$$B(p, q) = \int_0^\infty z^{p-1}/(1 - z)^{p+q} dz = \frac{\Gamma(p)\Gamma(q)}{\Gamma(p + q)} \tag{4.57}$$

gives the normalization

$$C_\kappa = \frac{\Gamma(\kappa + 1)}{[\sqrt{\pi(\kappa + 1)}]^3 \Gamma(\kappa - \frac{1}{2})}. \tag{4.58}$$

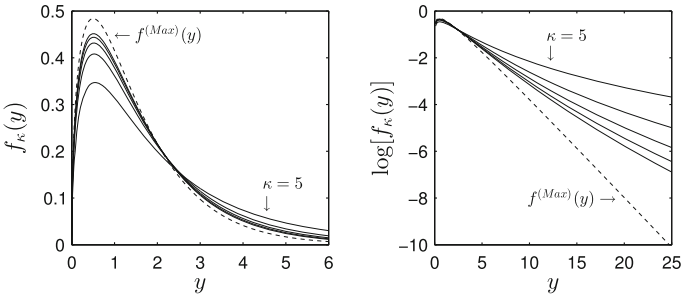

Fig. 4.7 (*Left panel*) Comparison of the Kappa distribution (*solid curves*) with a Maxwellian (*dashed curve*) for $\kappa = 5, 10, 15, 20$ and 25. The curve for $\kappa = 5$ is identified for which the departure from Maxwellian is the largest of those shown. (*Right panel*) The semi-logarithmic graph on the *right hand side* shows more clearly the increased population of energetic particles over the Maxwellian in the "tail" of the Kappa distribution. The Kappa distribution approaches the Maxwellian for $\kappa \rightarrow \infty$

The Kappa distribution is compared with a Maxwellian (dashed curve) in Fig. 4.7. In the limit $\kappa \rightarrow \infty$, $f_\kappa(y)$ approaches the Maxwellian. For finite κ, the Kappa distribution departs from a Maxwellian for sufficiently large reduced energies, y, and it is easily verified that $f_\kappa(y) \sim y^{-(\kappa+1)}$ as $y \rightarrow \infty$, that is as a power law.

The theoretical basis for the appearance of a Kappa distribution function is lacking although there is a large number of researchers who believe that it is indeed ubiquitous in nature (Leubner and Vörös 2005; Livadiotis and McComas 2009; Pierrard and Lazar 2010). The normalization of the distribution is not defined for $\kappa < \frac{1}{2}$, as is evident from Eq. (4.58).

The average thermal energy is $3k_B T_b/2$ where T_b is the temperature of the corresponding Maxwellian for $\kappa \rightarrow \infty$. This is given by the average of the reduced energy, y, and it can be shown, with the appropriate variable change used in the calculation of the norm, and with Eq. (4.57) that

$$\frac{T}{T_b} = \frac{\kappa + 1}{\kappa - \frac{3}{2}}, \tag{4.59}$$

which is not defined for $\kappa < \frac{3}{2}$. One can show that the nth moment of $f_\kappa(x)$ is infinite for $\kappa = n/2$. A justification for the existence of a Kappa distribution is the suggestion that this nonequilibrium distribution arises from a reformulation of statistical mechanics for particular nonequilibrium states in terms of a new entropy, referred to as the Tsallis nonextensive entropy (Tsallis 1995). There have been a large number of researchers in different research fields that have accepted this rationalization of the Kappa distribution although there have been objections (Nauenberg 2003; Tsallis 2004).

Our primary objective here is to consider the expansion of the Kappa distribution in Laguerre polynomials. We can anticipate some problems in view of the

nonexistence of the higher moments as dependent on the value of κ. We consider, as done previously, the expansion

$$f_\kappa^{(N)}(x) = s\sqrt{sy}e^{-sy}\sum_{n=0}^{N} c_n L_n(sy), \tag{4.60}$$

where from orthogonality

$$\begin{aligned} c_n &= s\frac{n!}{\Gamma(n+\frac{3}{2})}\int_0^\infty f_\kappa(y)L_n(sy)dy, \\ &\approx \frac{n!}{\Gamma(n+\frac{3}{2})}\sum_{i=0}^{M} W_i f_\kappa(y_i)L_n(sy_i), \end{aligned} \tag{4.61}$$

where $W_i = sw_i/[\sqrt{y_i}e^{-y_i}]$ are the big weights and M is the number of quadrature points.

In Fig. 4.8, we show the variation of c_n versus n for two moderately large values of κ. For both graphs, the coefficients are alternately positive and negative and eventually diverge for n beyond some value. This occurs at about $n = 10$ for $\kappa = 30$ and $n = 16$ for $\kappa = 50$. This is typical behaviour for an asymptotic series. We can expect a reasonable approximation to the Kappa distribution function as long as we are careful not to include too many terms.

In Fig. 4.9, the dashed curves represent the series approximation to the Kappa distribution, Eq. (4.60), for $\kappa = 30$ and $\kappa = 50$ with values of N for which the series expansion is about to diverge. For smaller values of N, the series expansion provides a reasonable approximation. The solid symbols in these graphs represent the Kappa distribution evaluated at the quadrature points for the value of N used. Only the first 8 or 10 quadrature points are shown as most are outside the range of y in the graphs with the choice $s = 1$. The series approximation gives the exact values at the quadrature points owing to the Cardinality condition but departs significantly from the Kappa distribution elsewhere.

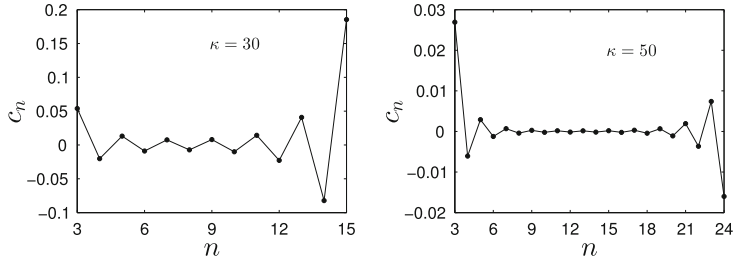

Fig. 4.8 Expansion coefficients, c_n, versus n for the Kappa distribution expanded in Laguerre polynomials for $\kappa = 30$ and $\kappa = 50$

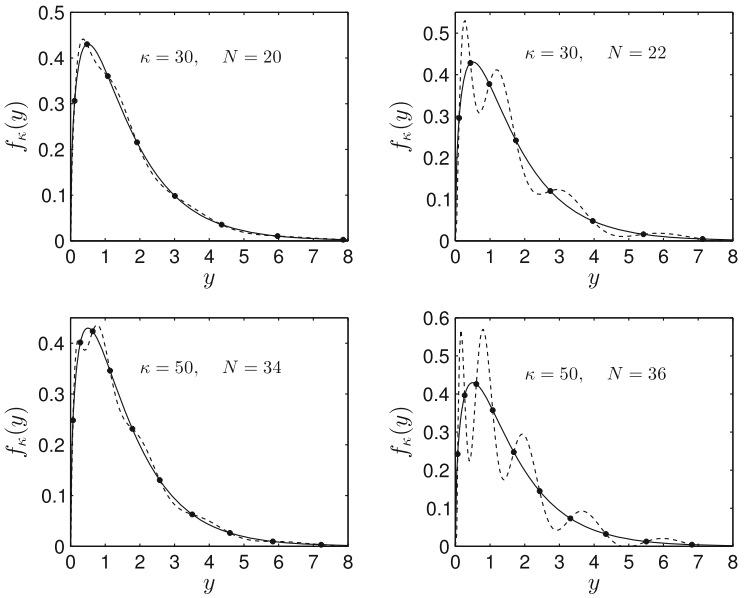

Fig. 4.9 The *solid curve* is the Kappa distribution with Eq. (4.56). The *dashed curves* represent the Laguerre series approximations, Eq. (4.60), with $\kappa = 30$ and $\kappa = 50$ for the values of N shown. The *solid symbols* are the values of the distribution evaluated at the quadrature points. Only 10 of 36 points are shown on the graph as the remaining quadrature points occur for $y > 8$

4.6 Representation of Functions in Periodic Fourier Series

In Sect. 4.3.3, we considered the expansion of $\sin(kx)$, $x \in [0, \infty)$, in Hermite polynomials and we concluded that the Hermite polynomials are not the optimal basis set for the sine function. The expansion of the Maxwellian considered in Sect. 4.4 in Chebyshev polynomials required a non-unique mapping of the semi-infinite interval to a bounded interval. We thus recognize that the choice of the basis set is of crucial importance for the convergence of particular functions. The basis set should be a "match" for the function.

The basis set appropriate for functions that vary periodically in space and/or time are the trigonometric sine and cosine functions, and the series expansion is referred to as a Fourier series. We consider the representation of a function, $f(x), x \in [-L, L]$, where the length of the interval can be unity ($L = 1$), a multiple of π ($L = n\pi$), or infinite for which $L \to \infty$. Almost every field of study in science and engineering involves applications based on a Fourier analysis. A classic application is the solution of partial differential and integral equations (Brown and Churchill 1993; Haberman 2013). Fourier methods parallel the use of polynomial basis sets as discussed in Chaps. 5 and 6.

Fourier series are also used to analyze oscillatory phenomena in many different fields such as spectral analysis (Hunter 2002), Fourier transform spectroscopy (Ernst and Anderson 1966), solar physics (Le Mouël et al. 2007; Petrovay 2010), astrophysics (Laskar 1993; Laskar and Correia 2009), stellar dynamics (Hunter 2002) as well as in finance (Duarte et al. 2010). In many instances, the main objective is to extract from a signal the fundamental frequencies of the wave motion in terms of a discrete Fourier transform (Briggs and Henson 1995; Blackledge 2006).

We also note the use of Fourier methods for the solution of problems in kinetic theory (Filbet et al. 2006), stochastic processes (van Kampen 2007; Paul and Baschnagel 2013) and quantum chemistry (Kosloff and Kosloff 1983; Colbert and Miller 1992; Kosloff 1993; Kokoouline et al. 1999; Stare and Balint-Kurti 2003; Amore et al. 2009). It is also useful to mention applications to the cosmic microwave background radiation (Chiang and Chen 2012) and relativity (Grandclément and Novak 2009). We are selective in our choice of applications and refer the reader to the references cited and textbooks on Fourier series (Lanczos 1966; Gottlieb and Orszag 1977; Boyd 2001; James 2002; Hanna and Rowland 2008) for further detailed discussions.

4.6.1 Fourier Series

The non-polynomial trignometric functions, $\sin(n\pi x)$ and $\cos(n\pi x)$, defined on the interval $x \in [-1, 1]$, are easily shown to be orthonormal according to

$$\begin{aligned}
\int_{-1}^{1} \sin(n\pi x)\sin(m\pi x)dx &= \delta_{nm}, \\
\int_{-1}^{1} \cos(n\pi x)\cos(m\pi x)dx &= \delta_{nm}, \\
\int_{-1}^{1} \sin(n\pi x)\cos(m\pi x)dx &= 0.
\end{aligned} \tag{4.62}$$

These orthogonality relations are verified with the use of the addition formulae for the trignometric functions, that is, $\sin(A)\sin(B) = \frac{1}{2}[\cos(A-B) - \cos(A+B)]$, $\cos(A)\cos(B) = \frac{1}{2}[\cos(A+B) + \cos(A-B)]$ and $\sin(A)\cos(B) = \frac{1}{2}[\sin(A+B) + \sin(A-B)]$. The approximation of a function $f(x)$ in this basis set is the Fourier series expansion given by,

$$f^{(N)}(x) = a_0 + \sum_{n=1}^{N-1} a_n \cos(n\pi x) + \sum_{n=1}^{N-1} b_n \sin(n\pi x). \tag{4.63}$$

By virtue of the orthogonality relations, the Fourier coefficients are given by

$$a_0 = \frac{1}{2}\int_{-1}^{1} f(x)dx,$$
$$a_n = \int_{-1}^{1} f(x)\cos(n\pi x)dx,$$
$$b_n = \int_{-1}^{1} f(x)\sin(n\pi x)dx. \tag{4.64}$$

If $f(x)$ is an even function, $f(-x) = f(x)$, then $b_n = 0$, $n = 1, \ldots, N-1$ and if $f(x)$ is an odd function, $f(-x) = -f(x)$, then $a_n = 0$, $n = 0, 1, \ldots, N-1$.

We denote sine and cosine basis functions collectively as

$$\phi_m(x) = \begin{cases} \frac{1}{2}, & m = 0, \\ \cos\left[\frac{1}{2}(2m+1)\pi x\right], & m \text{ odd}, \\ \sin\left[\frac{1}{2}m\pi x\right], & m \text{ even}. \end{cases} \tag{4.65}$$

so that Eq. (4.63) can be written as

$$f^{(N)}(x) = \sum_{m=0}^{N-1} c_m \phi_m(x). \tag{4.66}$$

The criterion we use to study the convergence of the Fourier series, Eq. (4.71), is the least squares distance, Eq. (4.5) and in particular Eq. (4.4). For Fourier series, with $w(x) = 1$, whether the expansion is written as in Eq. (4.1) or as in Eq. (4.2) is irrelevant. Minimization of the least squares error, Eq. (4.4), with $w(x) = 1$, gives the result

$$c_m = \int_{-1}^{1} f(x)\phi_m(x)dx, \quad m \neq 0$$
$$c_0 = \frac{1}{2}\int_{-1}^{1} f(x)dx, \quad m = 0. \tag{4.67}$$

analogous to Eq. (4.64). As before we anticipate that the coefficients $|c_m|$ decrease rapidly with m.

We do not present a rigorous proof of the convergence of a Fourier series as this has been presented by other authors (Gottlieb and Orszag 1977; Brown and Churchill 1993; Boyd 2001; Canuto et al. 2006). We note that the Fourier series of a piecewise continuous function converges for points within each subinterval and to the mean of the right and left hand limits of the function at the points of discontinuity. At the jump discontinuities, there can be oscillations referred to as the Gibbs phenomenon, discussed in detail in Sect. 4.7.

The least squares error associated with the expansion, Eq. (4.63), can be written as

$$E_2(N) = \|f\|^2 - \sum_{n=0}^{N-1} c_n^2, \tag{4.68}$$

where the norm of the function is defined by $\|f\|^2 = \int_{-1}^{1} f^2(x)dx$. Since $E_2(N) \geq 0$, we have Bessel's inequality, namely

$$\sum_{n=0}^{N-1} c_n^2 \leq \|f\|^2, \tag{4.69}$$

and in the limit $N \to \infty$ we have Parseval's theorem, that is

$$\sum_{n=0}^{\infty} c_n^2 = \|f\|^2. \tag{4.70}$$

These results are proved in several texts (Brown and Churchill 1993; James 2002; Kopriva 2009).

We consider the evaluation of the Fourier coefficients with a quadrature based on a uniform grid and we choose to compare the trapezoidal and Simpson's rule. We choose as an example the function $f(x) = x$ which we use in Sect. 4.7 to illustrate the Gibbs phenomenon. The Fourier sine series coefficients for $f(x) = x$ are $b_n = 2(-1)^{n+1}/(n\pi)$, also given by Eq. (4.134). A comparison of the convergence of the Simpson's and trapezoidal rule integrations give the approximation for $b_n^{(N_q)}$ versus the number of grid points N_q for $n = 1, 5, 9$ and 13 (from *bottom* to *top*) is shown in Fig. 4.10. The convergence is slower with the trapezoidal rule as expected and worsens for both algorithms with increasing n owing to the increasingly oscillatory sine integrand in Eq. (4.64). For the polynomial basis functions, the associated quadrature is defined by the roots, $P_N(x_i) = 0$. For the Fourier basis functions, the quadrature is defined by a uniform grid and the Newton-Cotes algorithms, Sect. 2.3.2.

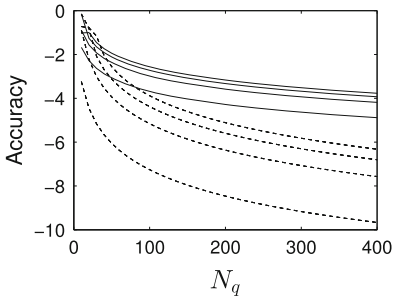

Fig. 4.10 The accuracy $= \log_{10} |b_n - b_n^{(N_q)}|$ versus the number of integration points, N_q, with a trapezoidal rule (*solid curves*) and a Simpson rule (*dashed curves*) for the numerical evaluation of the Fourier sine coefficient $b_n = 2(-1)^{n+1}/n\pi$ for $f(x) = x$, The values of n from *bottom* to *top curves* in each set are $n = 1, 5, 9$ and 13

4.6.2 Fourier Series in Complex Basis Functions

If we express the trigonometric functions as complex exponentials, $\sin(x) = [\exp(ix) - \exp(-ix)]/2i$ and $\cos(x) = [\exp(ix) + \exp(-ix)]/2$, we can rewrite Eq. (4.63) in the form

$$f^{(N)}(x) = \sum_{n=-N}^{N} c_n e^{in\pi x}, \tag{4.71}$$

where $i = \sqrt{-1}$, $c_n = \frac{1}{2}(a_n - ib_n)$, $c_{-n} = \frac{1}{2}(a_n + ib_n)$ and $c_{-n}^* = c_n$ where the asterisk denotes complex conjugation. Therefore

$$c_n = \frac{1}{2}\int_{-1}^{1} f(x) e^{-in\pi x} dx, \quad n \neq 0, \tag{4.72}$$

and $c_0 = a_0$. The orthonormality of the Fourier basis functions, Eq. (4.62), is rewritten as

$$\frac{1}{2}\int_{-1}^{1} e^{-in\pi x} e^{im\pi x} dx = \delta_{nm}. \tag{4.73}$$

The interval can be redefined to be $x \in [-L, L]$ and with the change of variable $y = xL$, Eqs. (4.71) and (4.62) can be written as

$$f^{(N)}(y) = \sum_{n=-N}^{N} c_n e^{in\pi y/L}, \tag{4.74}$$

$$c_n = \frac{1}{L}\int_{-L}^{L} f(y)e^{-in\pi y/L}dy, \tag{4.75}$$

and $c_0 = a_0/L$. With Eq. (4.63), the orthogonality of the Fourier basis functions, analogous to Eq. (4.73), is given by

$$\frac{1}{2L}\int_{-L}^{L} e^{-im\pi y/L}e^{in\pi y/L}dy = \delta_{nm}. \tag{4.76}$$

We identify the *wave-number* as $k_n = n\pi/L$ and consider $L \to \infty$ so as to introduce the Fourier basis function, $\phi_k(x) = \frac{1}{\sqrt{2\pi}}e^{ikx}$, with $x \in (-\infty, \infty)$ in Sect. 4.6.4.

4.6.3 Fourier Interpolation and Discrete Fourier Transforms

The spectral representation of the function $f(x)$ is the set of Fourier coefficients c_n. This is analogous to the expansions in polynomials, $P_n(x)$, orthonormal with respect to some weight function, $w(x)$, with quadrature points defined by $P_N(x_i) = 0$. For polynomial basis functions, the transformation, $\mathbf{T}$, between spectral space, $\{c_n\}$, and physical space, $\{f(x_i)\}$, is given by Eq. (1.25). It is important to note that this transformation is based on the *approximate* quadrature evaluation of the expansion coefficients and the transformation is unitary, Eq. (1.27), at any quadrature order.

In Sect. 2.6.1 we introduced the Sinc interpolation based on a uniform grid. In this section, we construct an interpolation function for Fourier sine basis functions analogous to the Lagrange interpolation for polynomials discussed in Sect. 2.3.1 and defined by Eq. (2.31) for polynomial basis functions.

We illustrate the analogous interpolation for Fourier basis functions with the expansion in a Fourier sine series that is

$$f(x) = \sum_{n=1}^{N} b_n \sin(n\pi x), \tag{4.77}$$

where b_n is given by Eq. (4.64) and as the integrand is even the integral is

$$b_n = 2\int_{0}^{1} f(x)\sin(n\pi x)dx. \tag{4.78}$$

With a trapezoidal integration for the integral with $N+1$ grid points, the Fourier coefficients are given by

$$b_n = \frac{2}{N} \sum_{i=2}^{N} f(x_i) \sin(n\pi x_i), \tag{4.79}$$

where the points $x_1 = 0$ and $x_{N+1} = 1$ do not contribute.

We substitute this approximate numerical result for b_n, Eq. (4.79), into (4.77) and get

$$f(x) = \frac{2}{N} \sum_{i=1}^{N} f(x_i) \sum_{n=1}^{N} \sin(n\pi x_i) \sin(n\pi x). \tag{4.80}$$

With Eq. (4.80), the interpolation function can be recognized as

$$\ell_i(x) = \frac{2}{N} \sum_{n=1}^{N} \sin(n\pi x_i) \sin(n\pi x), \tag{4.81}$$

which satisfies the cardinality condition $\ell_i(x_j) = \delta_{ij}$. This is shown in Fig. 4.11a with $N = 24$ and centered at $x_i = 0.5$.

This interpolation function resembles the Sinc interpolation in Fig. 2.10 although they are not identical. For $N = 6$, the two interpolations are given by

$$\ell_i^{sine}(x) = \frac{1}{3} \left[\sin(\pi x) - \sin(3\pi x) + \sin(5\pi x) \right], \tag{4.82}$$

and

$$\ell_i^{sinc}(x) = \frac{\sin[3\pi(2x-1)]}{3\pi(2x-1)}, \tag{4.83}$$

centred at $x_i = 0.5$. The differences in these interpolations near the interval boundaries are shown in Fig. 4.11b.

A comparison of several similar interpolations is discussed by Boyd (1992, 1999) and an interesting historical account is provided by Meijering (2002). The interpola-

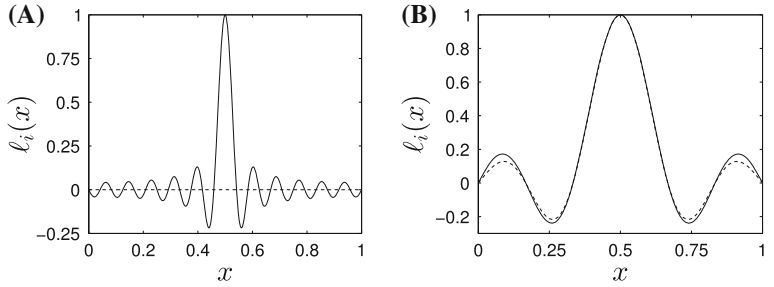

Fig. 4.11 (**A**) Interpolation function based on the sine basis functions, Eq. (4.81), with $N = 24$, $x_i = 0.5$. (**B**) Comparison of $\ell_i^{sine}(x)$ (*solid line*), Eq. (4.82), and $\ell_i^{sinc}(x)$ (*dashed line*), Eq. (4.83), with $N = 6$, $x_i = 0.5$

tion functions are at the basis of pseudospectral solutions of differential equations as discussed in Sect. 3.9.2 and summarized in Table 3.18 (Meyer 1970; Schwartz 1985; Baye and Heenen 1986; Colbert and Miller 1992; Amore et al. 2009). The interpolation functions provide the discrete first and second derivative matrix operators.

We apply a similar quadrature to the Fourier expansion, Eq. (4.74) and use a Riemann[1] sum (Cheney and Kincaid 2008; Burden and Faires 2011) to evaluate the expansion coefficients, c_n, Eq. (4.75), that is

$$c_n = \frac{1}{L}\sum_{k=-N}^{N} f_k e^{-in\pi k\Delta y/L} = \frac{1}{\sqrt{L}}\sum_{k=-N}^{N} f_k T_{kn}. \tag{4.84}$$

where $f_k \equiv f(x_k)$. Equation (4.84) defines the transformation between spectral space, $\{c_n\}$, and physical space, $\{f_k\}$, given by

$$T_{kn} = \frac{1}{\sqrt{L}} e^{-i\pi nk\Delta y/L}, \tag{4.85}$$

which is orthogonal, that is

$$\sum_{k=-N}^{N} T_{nk}^* T_{km} = \delta_{nm}, \tag{4.86}$$

and represents the discrete version of Eq. (4.73).

Whereas the analogous transform for polynomial basis sets, Eq. (1.24), of order N requires N^2 numerical operations, it is possible to efficiently program the discrete Fourier transform, Eq. (4.85), so to have a much smaller operation count of $N \log_{10} N$. This is achieved with the Fast Fourier Transform (FFT) algorithm generally credited to Cooley and Tukey (1965) but with earlier versions developed by Gauss and others. It should be noted that for one dimensional problems of moderate order the savings in computer time is not of practical significance because of the computational speed of current personal computers. There can be a substantial savings in the computational times for very large data sets.

4.6.4 Fourier Transforms

The discrete Fourier series can be extended to the expansion in the basis functions $\phi_k(x) = \exp(ikx)/\sqrt{2\pi}$, $x \in (-\infty, \infty)$, defined on the infinite interval, $x \in (-\infty, \infty)$, which are orthogonal in accordance with

[1] Georg Friedrich Bernhard Riemann (1826–1866) was a German mathematician who made fundamental contributions to topology, complex variables and integration.

$$\int_{-\infty}^{\infty} \phi_{k'}^*(x)\phi_k(x)dx = \delta(k-k'), \tag{4.87}$$

where the Dirac delta function is defined in the context of an integral, namely

$$\int_{-\infty}^{\infty} f(x')\delta(x'-x)dx' = f(x). \tag{4.88}$$

The Dirac delta function can be represented as the limit of several different functions. One example is the normalized Gaussian in the limit of vanishing width, that is

$$\delta(x) = \lim_{a\to 0} \frac{1}{a\sqrt{\pi}} e^{-x^2/a^2}. \tag{4.89}$$

The expansion of $f(x)$ in basis functions $\phi_k(x)$ is the integral

$$f(x) = \int_{-\infty}^{\infty} F(k)\phi_k(x)dk, \tag{4.90}$$

where the function $F(k)$ is the spectral space representation analogous to the expansion coefficients in Eq. (4.63) but parameterized by the continuous index k rather than the discrete integer n. It is determined in the same way using the orthogonality of the basis functions, that is

$$F(k) = \int_{-\infty}^{\infty} f(x')\phi_k^*(x')dx', \tag{4.91}$$

and is also consistent with convergence in the mean. With the substitution of $F(k)$ in Eq. (4.90) and use of the orthonormality, Eq. (4.87), we get that

$$\begin{aligned} f(x) &= \int_{-\infty}^{\infty} \left(\int_{-\infty}^{\infty} f(x')\phi_k^*(x')dx' \right) \phi_k(x)dk, \\ &= \frac{1}{2\pi} \int_{-\infty}^{\infty} f(x') \left(\int_{-\infty}^{\infty} e^{ik(x-x')}dk \right) dx', \\ &= \int_{-\infty}^{\infty} f(x')\delta(x-x')dx'. \end{aligned} \tag{4.92}$$

This result is the completeness condition for Fourier basis functions analogous to the result for polynomials, Eq. (2.155), in Chap. 2. The integral over k in the second line of Eq. (4.92) leading to $\delta(x - x')$ is a similar completeness condition for Fourier basis functions.

4.6.5 The Solution of the Diffusion Equation with Fourier Transforms

An example of the use of Fourier methods is the solution of the diffusion equation in one dimension

$$\frac{\partial N(x,t)}{\partial t} = D\frac{\partial^2 N(x,t)}{\partial x} \quad x \in (-\infty, \infty) \tag{4.93}$$

where $N(x,t)$ is a number density, D is the diffusion coefficient and the initial density is $N(x,0)$. The Fourier transform of the density is

$$n(k,t) = \frac{1}{\sqrt{2\pi}} \int_{-\infty}^{\infty} N(x,t) e^{-ikx} dx, \tag{4.94}$$

and of the time derivative, $\partial N(x,t)/\partial t$, is

$$\frac{\partial n(k,t)}{\partial t} = \frac{1}{\sqrt{2\pi}} \int_{-\infty}^{\infty} \frac{\partial N(x,t)}{\partial t} e^{-ikx} dx. \tag{4.95}$$

The Fourier transform of the differential equation is

$$\frac{\partial n(k,t)}{\partial t} = \frac{1}{\sqrt{2\pi}} \int_{-\infty}^{\infty} \frac{\partial^2 N(x,t)}{\partial x^2} e^{-ikx} dx, \tag{4.96}$$

and the left hand side is evaluated with two successive integration by parts to give

$$\begin{aligned} \frac{\partial n(k,t)}{\partial t} &= \frac{ik}{\sqrt{2\pi}} \int_{-\infty}^{\infty} \frac{\partial N(x,t)}{\partial x} e^{-ikx} dx, \\ &= -\frac{k^2}{\sqrt{2\pi}} \int_{-\infty}^{\infty} N(x,t) e^{-ikx} dx = -Dk^2 n(k,t). \end{aligned} \tag{4.97}$$

The representation of the diffusion equation in Fourier space is therefore

$$\frac{\partial n(k,t)}{\partial t} = -Dk^2 n(k,t). \tag{4.98}$$

The solution of this first order differential equation is

$$n(k,t) = n(k,0)e^{-Dk^2 t}. \tag{4.99}$$

The density is given by the inverse transform

$$N(x,t) = \frac{1}{\sqrt{2\pi}} \int_{-\infty}^{\infty} n(k,0)e^{-Dk^2 t + ikx} dk. \tag{4.100}$$

With $n(k,0)$ given by Eq. (4.94), we have that

$$N(x,t) = \frac{1}{2\pi} \int_{-\infty}^{\infty} \int_{-\infty}^{\infty} N(x',0)e^{-Dk^2 t + ik(x-x')} dk dx'. \tag{4.101}$$

The integral over k is calculated by completing the square in k, that is

$$N(x,t) = \frac{1}{2\pi} \int_{-\infty}^{\infty} N(x',0) \left[\int_{-\infty}^{\infty} e^{-Dt(k-\frac{x-x'}{4Dt})^2} dk \right] e^{-\frac{(x-x')^2}{4Dt}} dx', \tag{4.102}$$

and the integral over k gives $\sqrt{\pi/(Dt)}$. The general solution of the diffusion equation is

$$N(x,t) = \frac{1}{\sqrt{4\pi Dt}} \int_{-\infty}^{\infty} N(x',0)e^{-(x-x')^2/4Dt} dx'. \tag{4.103}$$

For an initial delta function distribution, $N(x,0) = \delta(x - x_0)$, the solution is

$$N(x,t) = \frac{1}{4\pi Dt} e^{-(x-x_0)^2/4Dt}. \tag{4.104}$$

We use this result to solve the Ornstein-Uhlenbeck Fokker-Planck equation in Chap. 6, Sect. 6.1.2.

4.6.6 Construction of a Quantum Wave Packet

We consider a superposition of plane waves so as to construct a wave that is localized in space about the origin generally referred to as a wave packet. We consider the following summation of cosines

$$f(x) = \frac{1}{N}\sum_{n=1}^{N} \cos(k_n \pi x), \tag{4.105}$$

each of unit amplitude but with slightly different wavenumbers as given by $k_n = k_0 + n\Delta$ with $k_0 = 100$, $\Delta = 0.5$ and $N = 100$. The result is the localized function shown in Fig. 4.12. In the figure, we see the constructive interference of the waves for $x \approx \pm 4$ and at $x \approx 0$. Elsewhere there is almost complete destructive interference of the individual waves. The peaks of $f(x_n) = 1$ occur at $x_n = \pm 2n/\Delta$ so for $\Delta = 1/2$, the peaks are at 0, ± 4, ± 8, ... for $n = 0, 1, 2, \ldots$

In quantum mechanics, the Fourier basis function, $\phi_k(x) = e^{ikx}/\sqrt{2\pi}$, is the plane wave representation in position space of a free particle with "wave number" k (Messiah 1961; Liboff 2002). This plane wave is an eigenfunction of the momentum operator $\hat{p} = -i\hbar\partial/\partial x$, that is

$$\hat{p}\phi_k(x) = -\frac{i\hbar}{\sqrt{2\pi}}\frac{\partial e^{ikx}}{\partial x} = \frac{\hbar k}{\sqrt{2\pi}}e^{ikx} \tag{4.106}$$

where $h = 2\pi\hbar$ is the Planck constant. We identify the eigenvalue as the momentum of the particle with $p = \hbar k$ which classically is $p = mv$ where m is the particle mass. The plane wave basis function is also an eigenfunction of the Hamiltonian operator, $\hat{H} = \hat{p}^2/2m$, that is

$$\hat{H}\phi_k(x) = -\frac{\hbar^2}{2m}\frac{d^2}{dx^2}\frac{e^{ikx}}{\sqrt{2\pi}} = \frac{\hbar^2 k^2}{2m}\phi_k(x) = E_k\phi_k(x) \tag{4.107}$$

with energy eigenvalues $E_k = \hbar^2 k^2/2m$.

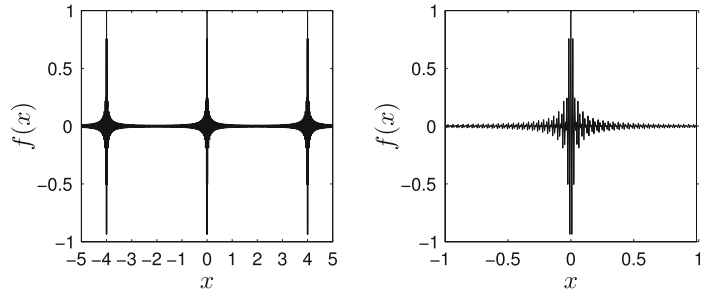

Fig. 4.12 Localized wave function formed from the summation of cosines, Eq. (4.105), with $k_n = k_0 + n\Delta$ with $k_0 = 100$, $\Delta = 1/2$ and $N = 100$

The plane wave is of infinite extent and we are interested in a quantum mechanical description of a particle that is localized in space and also moving with some velocity v analogous to a classical particle. This construction has important applications to current theoretical modelling of reactive processes including photoionization. Recent reviews were provided by Balint-Kurti (2003, 2008) with extensive references to the original works in this field. Some aspects for the direct solution of the time dependent Schrödinger equation have also been addressed (Russo and Smereka 2013, 2014).

A wavepacket is often modelled by assuming a Gaussian envelope for the wave as given by the wave function

$$\psi(x,0) = \frac{1}{\sqrt{\alpha\sqrt{\pi}}} e^{-x^2/2\alpha^2} e^{-ikx}. \tag{4.108}$$

This wave function can be constructed from the momentum wavefunction centered at $p = \hbar k$, given by

$$\phi(p,0) = \sqrt{\frac{\alpha}{\hbar\sqrt{\pi}}} \exp\left[-\frac{\alpha^2}{2\hbar^2}(\hbar k - p)^2\right]. \tag{4.109}$$

Notice that the widths of these two distributions are inversely related. We follow the presentation in Liboff (2002) and in Chap. 7 of the lecture notes by Ghosh[2] and write the time dependent momentum wave function as

$$\phi(p,t) = e^{-i\hat{H}t/\hbar}\phi(p,0) = \phi(p,0)e^{-ip^2t/2m\hbar}, \tag{4.110}$$

where $\phi(p,0)$ is an eigenstate of $\hat{H}$. We get the time dependence of the space wavefunction with the Fourier transform of Eq. (4.110), that is

$$\begin{aligned}\psi(x,t) &= \frac{1}{\sqrt{2\pi\hbar}} \int_{-\infty}^{\infty} e^{ipx/\hbar}\phi(p,t)dp, \\ &= \frac{1}{\sqrt{2\pi\hbar}}\sqrt{\frac{\alpha}{\hbar\sqrt{\pi}}} \int_{-\infty}^{\infty} e^{ipx/\hbar} \exp\left[-\frac{\alpha^2}{2\hbar^2}(\hbar k - p)^2 - \frac{ip^2t}{2m\hbar}\right] dp. \end{aligned} \tag{4.111}$$

We write the argument of the exponential as a quadratic in p and notice the integral

$$\int_{-\infty}^{\infty} \exp\left[-ap^2 + bp - c\right] dp = \sqrt{\frac{\pi}{a}} \exp(-c + b^2/4a), \tag{4.112}$$

[2] (http://www.phy.iitb.ac.in/dkg/qmech/Lecture7.pdf).

evaluated by completing the square in the argument of the exponential. With Eq. (4.112) and the definitions

$$\begin{aligned} a &= \frac{\alpha^2}{2\hbar^2} + \frac{it}{2m\hbar} = \frac{\alpha^2}{2\hbar^2}(1 + \frac{i\hbar t}{m\alpha^2}), \\ b &= \frac{ix + k\alpha^2}{\hbar}, \\ c &= \frac{\alpha^2 k^2}{2}, \end{aligned} \tag{4.113}$$

we get after some algebra the result

$$\psi(x,t) = \frac{1}{\sqrt{\alpha\sqrt{\pi}}(1 + it\hbar/m\alpha^2)} \exp\left[\frac{-x^2/2\alpha^2 - i[kx - \frac{\hbar k^2}{2m}t]}{1 + it\hbar/m\alpha^2}\right]. \tag{4.114}$$

It is confirmed that for $t = 0$ we recover $\psi(x, 0)$ given by Eq. (4.108). We show the real part of $\psi(x, t)$ as well as $|\psi(x, t)|^2$ in Fig. 4.13 at three different dimensionless times, where we have set $\alpha = 1$, $\hbar/m = 1$ and $k = 10$. The result is a wave packet moving in the positive x direction that spreads with time owing to the dispersion of the wave which resembles a classical particle with group velocity, $v_g = p/m$.

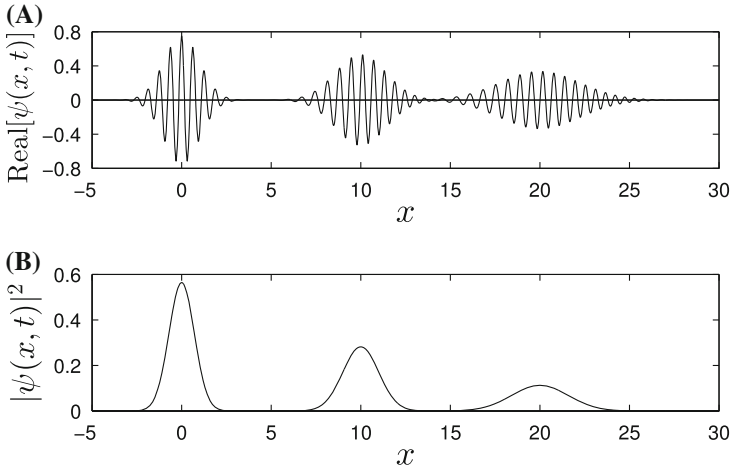

Fig. 4.13 Wave packet as given by Eq. (4.114) with $\alpha = 1$, $\hbar/m = 1$ and $k = 10$. The wave packets are shown for dimensionless times $t = 0$, 1 and 2

4.6.7 Fourier Transform Analysis of Time Series and Fourier Transform Spectroscopy

In Chap. 1, we defined spectral space as the set of expansion coefficients, Eq. (1.5), for the expansion of a function in a basis set of orthogonal functions, Eq. (1.1). In some instances, these are referred to as a generalized Fourier coefficients. The terminology carries over to the expansion of a function in the trigonometric Fourier basis functions where the a_n and b_n coefficients are the spectral space representation of the function. The physical space representation is as before $f(x_i)$. In the continuous situation we have the two spectral space representations with "coefficients" $F(k) \leftarrow f(x)$ where k is a wavenumber and "coefficients" $F(\omega) \leftarrow f(t)$ where ω is a frequency. We can decompose either the spatial variation or the time dependence of some quantity into its components.

Almost all types of spectroscopy in chemical physics are based on the Fourier transform of a free induction decay curve. Perhaps the best example to illustrate this technique is in the comparison of conventional mass spectrometry with the current Fourier transform ion cyclotron resonance spectrometry (Comisarow and Marshall 1974).

A charged particle executes a circular orbit in a uniform magnetic field, B, whereby the centripetal force is balanced by the magnetic force, that is,

$$\frac{mv^2}{r} = qBv \tag{4.115}$$

and the frequency of its circular motion is given by $\omega = B(q/m)$. In conventional mass spectrometry, the magnetic field is changed and the absorption of energy is measured when this resonance condition is achieved. The acquisition of data is slow with this technique (Comisarow 1993).

To illustrate the basic principles of Fourier transform spectrocopy, we construct a hypothetical free induction decay curve with four component waves of the form

$$f(t) = \sum_{k=1}^{4} A_k \cos(\omega_k t) e^{-t/\tau} \tag{4.116}$$

where we arbitrarily choose frequencies $\omega = (15, 25, 35, 45)$ radians/s and amplitudes $\mathbf{A} = [1\ 2\ 3\ 4]$, in arbitrary units with $\tau = 5$. The signal oscillates and also decays with time owing to a single relaxation process. The signal and the real part of the Fourier transform as calculated with MATLAB using real(fft($\mathbf{f}$)) with 1,024 discrete times $t_k = (15k/1{,}024)$, $k = 1, 2, \ldots, 1{,}024$ are chosen with $t \in [0, 15]$. The modelled free induction decay curve and the Fourier transform are shown in Fig. 4.14. As can be seen the frequency spectrum of the signal has been recovered.

There are numerous examples of the extraction of the fundamental frequencies of a signal. We mentioned the application of Fourier transform techniques to the study of solar activity, measured in terms of the number of sunsposts observed on the solar

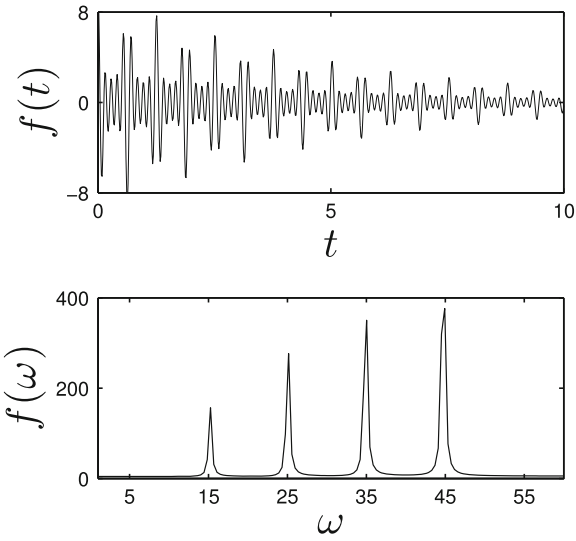

Fig. 4.14 (*Top*) Hypothetical free induction decay *curve* with four components. Equation (4.116) with $\omega = 15, 25, 35,$ and 45 radians/s. (*Bottom*) Real part of the Fourier transform of the signal above. The four input frequencies are recovered

surface. The sunspot number oscillates with a period of about 11 years (Petrovay 2010). The extraction of the periodic behaviour in solar activity has received considerable attention. The variation in solar activity can be found by searching the internet for sunspot.dat and the time series analysis is discussed in Chap. 8 in the book by Moler (2008).

4.7 Gibbs Phenomenon

The Gibbs[3] phenomenon is the overshoot that occurs at a jump discontinuity for a Fourier series approximation, Eq. (4.63), of a piecewise continuous function, $f(x)$. In two dimensions, a Fourier series is used to represent the image of an object which is often contaminated with these spurious oscillations. The resolution of the Gibbs phenomenon, that is the reconstruction of the function, $f(x)$, with the Fourier coefficients of the approximation, $f^{(N)}(x)$, has a large number of important practical applications in image reconstruction (Archibald and Gelb 2002; Dadkhahi et al. 2012), tomography (Gottlieb et al. 2000) and medical imaging (Kaur et al. 2007; Jung and Zhao 2012).

[3] Josiah Willard Gibbs (1839–1903) was an American physicist who made fundamental contributions to physics and mathematics, and to thermodynamics and statistical mechanics in chemistry where his name as associated for example with the Gibbs free energy and the Gibbs-Duhem equation. He is also know for his work on physical optics.

We illustrate the Gibbs phenomenon with the expansion of the step function,

$$f(x) = \begin{cases} -1, & -1 < x < 0, \\ 0, & x = 0, \\ 1, & 0 < x < 1. \end{cases} \tag{4.117}$$

This is an example of a function that is piecewise continuous on $[-1, 1]$. The derivative of the function is not continuous at the interval boundaries and the midpoint. The value of the function at the origin is defined to be the mean of the limits from the right and the left. Since the function is odd $a_n = 0$, and the Fourier series, Eq. (4.63), reduces to the sine series with odd $n = 2k - 1$ and $b_k = 4/[\pi(2k - 1)]$.

The Nth order Fourier sine series approximation to the step function is given by,

$$f^{(N)}(x) = \frac{4}{\pi} \sum_{k=1}^{N} \frac{\sin[(2k-1)\pi x]}{2k-1}. \tag{4.118}$$

The graph of $f^{(N)}(x)$ versus x in Fig. 4.15 for $N = 5$ shows the oscillatory approximation to $f(x)$. The oscillations persist for $N = 20$ with diminished amplitude in the middle portions of the intervals $[-1, 0]$ and $[0, 1]$. However, the oscillations in the vicinity of $x = 0$ and at $x = \pm 1$ do not decrease with an increase in the number of terms in Eq. (4.118) and move closer to the interval boundaries with almost constant amplitude. An instructive analysis of this behaviour is provided in Sect. 2.2 in Jerri (1998). Both approximations with $N = 5$ and $N = 20$ give $f^{(N)}(0) = 0$ as noted by the solid symbol, consistent with the point-wise convergence theorem. At the junp discontinuity, the Fourier series converges to the mean of the right and left limits of the function (Brown and Churchill 1993).

It is the oscillations at the discontinuous points that is referred to as the Gibbs phenomenon not to be confused with the Runge phenomenon discussed in Sect. 4.8. The resolution of the Gibbs phenomenon involves the reconstruction of $f(x)$ from a finite number of coefficients in the Fourier series, Eq. (4.63). In this section, we

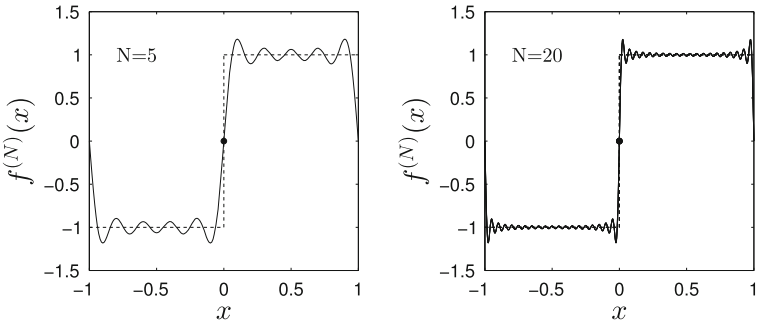

Fig. 4.15 The Fourier series approximation to a step function with $N = 5$ and 20

summarize some of the current methods employed to resolve Gibbs phenomenon in one and two dimensions. An important aspect of the reconstruction is to locate the boundaries at which the Gibbs phenomenon occurs and the technique is referred to as edge detection (Stefan et al. 2012).

Thus we have shown by example that the expansion of a piecewise continuous function on a finite interval in a Fourier series can lead to spurious oscillations at the interval boundaries where the function or its derivatives are not smooth (Lanczos 1966). This subject has had a long history beginning with the work by Wilbraham (1848) rediscovered by Gibbs as chronicled by several authors (Carlson 1925; Hewitt and Hewitt 1979). Jerri (1998) has suggested that the correct nomenclature should be the Gibbs-Wilbraham phenonemon.

This nonconvergence of a Fourier series contaminates numerous applications of Fourier series and the subject has been treated in several textbooks (Jerri 1998, 1999) and research papers (Gottlieb et al. 1992; Gottlieb and Shu 1997; Driscoll and Fornberg 2001; Shizgal and Jung 2003; Jung and Shizgal 2004, 2005, 2007; Jung 2007; Hrycak and Grchenig 2010; Kamm et al. 2010). Numerous methods have been suggested to resolve the Gibbs phenomenon such as spectral filtering (Adomaitis 2001) adaptive mollifiers (Tadmor and Tanner 2002), a Padé based algorithm (March and Barone 2000; Driscoll and Fornberg 2001), radial basis functions (Jung 2007) and spectral reprojection (Gelb and Tanner 2006; Adcock and Hansen 2012). A comprehensive review of all these methods is not possible in this book and the reader is directed to a review of the Gegenbauer reconstruction method (Gottlieb et al. 2011) and other methods in the book edited by Jerri (2011).

Gottlieb and co-workers (Gottlieb et al. 1992; Gottlieb and Shu 1997) developed a reconstruction method based on the re-expansion of the finite Fourier representation of a function in Gegenbauer polynomials that we refer to as the direct method. Shizgal and Jung (2003) developed a reconstruction algorithm which recovers polynomial functions exactly from their finite Fourier representation. This method is referred to as the inverse method (Jung and Shizgal 2004, 2005, 2007). It has also been referred to as the Inverse Polynomial Reconstruction Method (IPRM). The origin of the terminology concerning direct and inverse methods will be clarified in the sections that follow with a comparison of the two resolution procedures.

4.7.1 The Direct Method

We consider a piecewise continuous function, $f(x)$, on the interval $[-1, 1]$ expanded in a finite Fourier series, Eq. (4.63), where the Fourier coefficients are given by Eq. (4.64). We consider limited input data consisting of the first $2N+1$ *exact* Fourier coefficients a_k and b_k. The basic objective of a reconstruction procedure is to recover the function $f(x)$ from the input data.

We choose to expand the function in the Gegenbauer polynomials, $C_\ell^\lambda(x)$, discussed in Sect. 2.4.8

$$f(x) = \sum_{\ell=0}^{\infty} g_\ell C_\ell^\lambda(x), \tag{4.119}$$

where the g_ℓ coefficients depend on λ and are the *exact* Gegenbauer coefficients given by orthogonality, that is,

$$g_\ell = \frac{1}{h_\ell^\lambda} \int_{-1}^{1} (1-x^2)^{\lambda-1/2} C_\ell^\lambda(x) f(x) dx, \tag{4.120}$$

and h_ℓ^λ is the normalization.

The Gegenbauer reconstruction of $f^{(N)}(x)$, Eq. (4.63), is based on the expansion

$$\hat{f}_m(x) = \sum_{\ell=0}^{m} \hat{g}_\ell C_\ell^\lambda(x), \tag{4.121}$$

where the (approximate) Gegenbauer coefficients, $\hat{g}_\ell$, are given by,

$$\hat{g}_\ell = \frac{1}{h_\ell^\lambda} \int_{-1}^{1} (1-x^2)^{\lambda-1/2} C_\ell^\lambda(x) f^{(N)}(x) dx. \tag{4.122}$$

Notice that Eq. (4.122) refers to $f^{(N)}(x)$ whereas $f(x)$ appears in Eq. (4.120) and we have identified the expansion coefficients with $\hat{g}_\ell$ and g_ℓ, respectively.

An important aspect of the reconstruction procedure is that the summation in Eq. (4.121) is truncated at some sufficiently *small* value of $m < N$. Therefore we have denoted the reconstructed function by $\hat{f}_m(x)$. If this expansion is extended indefinitely, the result recovers the Gibbs phenomenon. Thus m must not be too large. It is important to note that the sum in Eq. (4.63) is up to $n = N - 1$.

We consider the expansion of the sine and cosine basis functions in the Gegenbauer polynomials, that is

$$\begin{aligned} \sin(k\pi x) &= \sum_{\ell=1}^{\infty} S_{k\ell} C_\ell^\lambda(x), \\ \cos(k\pi x) &= \sum_{\ell=0}^{\infty} W_{k\ell} C_\ell^\lambda(x), \end{aligned} \tag{4.123}$$

where the transformation matrices are

$$S_{k\ell} = \frac{1}{h_\ell^\lambda} \int_{-1}^{1} (1-x^2)^{\lambda-1/2} C_\ell^\lambda(x) \sin(k\pi x) dx,$$

$$W_{k\ell} = \frac{1}{h_\ell^\lambda} \int_{-1}^{1} (1-x^2)^{\lambda-1/2} C_\ell^\lambda(x) \cos(k\pi x) dx, \tag{4.124}$$

which can be evaluated analytically in terms of Bessel functions (Gottlieb and Shu 1997). This is the reason for choosing Gegenbauer polynomials. The work by Gottlieb and co-workers was based on a detailed numerical analysis of these coefficients and their relation to the *Gibbs condition* as defined previously and discussed by Gottlieb and coworkers (Gottlieb and Shu 1997; Gottlieb and Hesthaven 2001; Gottlieb et al. 2011).

With Eq. (4.63) substituted into Eq. (4.122) and the definition Eq. (4.124), we have that

$$\hat{g}_\ell = a_0 + \sum_{k=1}^{N} [a_k W_{k\ell} + b_k S_{k\ell}]. \tag{4.125}$$

Equation (4.125) is referred to as the *direct method* as the $\hat{g}_\ell$ coefficients are calculated with direct matrix multiplications.

Gottlieb et al. (1992) and Gottlieb and Shu (1997) showed, with a detailed numerical analysis, that a sufficient condition for spectral convergence of Eq. (4.121) versus N is that $\lambda = m = \beta N$, where $\beta = 2\pi/27 \approx 0.2327$. This relationship between λ, m and N is called the "Gibbs condition". In the numerical experiments carried out with the direct method, the choice $\lambda = m = N/4$ is made. The parameter λ can be chosen appropriately so as to optimize the Gegenbauer reconstruction procedure.

4.7.2 The Inverse Method; Odd Functions $f(-x) = -f(x)$

We demonstrate the reconstruction procedure with simple examples and consider odd functions, $f(-x) = -f(x)$, on the interval $[-1, 1]$. With the direct method, Eq. (4.125), for the approximate Gegenbauer coefficients reduces to

$$\boxed{\hat{g}_\ell = \sum_{k=1}^{N} b_k S_{k\ell},} \tag{4.126}$$

and the reconstructed function with Eq. (4.121).

We consider an alternate reconstruction procedure and note that the desired representation of the function is a *finite* expansion of Gegenbauer or other orthogonal polynomials, that is

$$\tilde{f}_m(x) = \sum_{odd\ \ell}^{m} \tilde{g}_\ell C_\ell^\lambda(x). \tag{4.127}$$

Therefore, instead of expanding the Fourier sines and cosines in the Gegenbauer basis as in Eq. (4.123), the approximate $\tilde{g}_\ell$ coefficients in Eq. (4.127) are determined by considering the representation of $\tilde{f}_m(x)$ in a Fourier sine series and then projecting out each Fourier mode. The underlying motivation for this approach is that the sought after representation of the function, Eq. (4.121), is a finite polynomial.

We consider the correspondence or projection

$$\sum_{odd\ \ell}^{\infty} \tilde{g}_\ell C_\ell^\lambda(x) \approx \sum_{k=1}^{N} b_k \sin(k\pi x), \tag{4.128}$$

made rigorous in subsequent papers (Jung and Shizgal 2004, 2005). With the orthogonality of the Fourier sine basis functions, the first m $\tilde{g}_\ell$ coefficients are given by,

$$\boxed{\sum_{odd\ \ell}^{m} \tilde{g}_\ell T_{\ell k} = b_k,} \tag{4.129}$$

where

$$T_{\ell k} = \int_{-1}^{1} C_\ell^\lambda(x) \sin(k\pi x) dx. \tag{4.130}$$

We note also the analogous transformation

$$V_{\ell k} = \int_{-1}^{1} C_\ell^\lambda(x) \cos(k\pi x) dx, \tag{4.131}$$

and the transformation matrices are

$$T_{kl} = \begin{cases} 0, & k = 0, \\ (-1)^{k+1} 4\lambda/(k\pi), & k \neq 0, \quad l = 1, \end{cases}$$

$$V_{kl} = \begin{cases} 1, & k = 0, \quad l = 0, \\ 0, & k \neq 0, \quad l = 0, \\ \frac{1}{l+\lambda}[C_{l+1}^\lambda(1) - C_{l-1}^\lambda(1)], & k = 0, \quad l \neq 0, \end{cases} \tag{4.132}$$

These results can be derived with the recurrence and differential recurrence relations as shown in the Appendix in Shizgal and Jung (2003).

Equation (4.129) defines the approximate $\tilde{g}_\ell$ coefficients that appear in Eq. (4.127). The matrix $T_{\ell k}$ is the transformation from the Gegenbauer space $\{g_\ell\}$ to the Fourier space $\{b_k\}$, whereas $S_{k\ell}$ is the transformation from the Fourier space to the Gegenbauer space.

The approximate Gegenbauer coefficients, $\tilde{g}_\ell$, are given by the inversion of Eq. (4.129) with $m = N$. We refer to this approach as the inverse method as the solution of Eq. (4.129) requires the inversion of a linear system. The projection of Eq. (4.128) onto the Fourier basis gives Eq. (4.129) whereas the projection onto the Gegenbauer basis gives Eq. (4.125) with $\tilde{g}_\ell$ replaced with $\hat{g}_\ell$. A more detailed discussion of these relationships was presented by Jung and Shizgal (2004).

4.7.3 The Inverse Method Is Exact for Polynomials

We choose the odd functions, $f_1(x) = x$ and $f_3(x) = x^3$, for which the exact Gegenbauer expansions are

$$\begin{aligned} x &= \frac{1}{2\lambda} C_1^\lambda(x), \\ x^3 &= \frac{3}{4\lambda(\lambda+2)} C_1^\lambda(x) + \frac{3}{4\lambda(\lambda+1)(\lambda+2)} C_3^\lambda(x), \end{aligned} \tag{4.133}$$

where we have used the explicit definitions of the lower order Gegenbauer polynomials in Chap. 2, Sect. 2.4.8. The exact Fourier sine coefficients are given by,

$$\begin{aligned} b_k^{(1)} &= \frac{2(-1)^{(k+1)}}{\pi k}, \\ b_k^{(3)} &= \frac{2(-1)^k}{\pi k}\left[\frac{6}{(\pi k)^2} - 1\right]. \end{aligned} \tag{4.134}$$

It is clear that the values of m in the Gegenbauer sum, Eq. (4.121), are $m = 1$ and $m = 3$, for $f_1(x)$ and $f_3(x)$, respectively, independent of λ. If the sum is taken to N, Eq. (4.121) recovers $f^{(N)}(x)$ contaminated with the Gibbs phenomenon.

We write the Gegenbauer polynomials as a finite power series, the expansion of x^ℓ in the polynomials, and the identity for the respective coefficients, that is

$$C_n^\lambda(x) = \sum_{\ell=0}^{n} G_{n\ell} x^\ell, \quad x^\ell = \sum_{k=0}^{\ell} H_{\ell k} C_k^\lambda(x), \quad \sum_{\ell=0}^{n} G_{n\ell} H_{\ell k} = \delta_{nk}. \tag{4.135}$$

The $H_{\ell k}$ coefficients are calculated for the lower order ℓ and k indices with the recurrence relation for $C_k^\lambda(x)$ provided in Chap. 2, Sect. 2.4.8.

We consider $f_p(x) = x^p$ (p odd), with Fourier coefficients

$$b_k^{(p)} = \int_{-1}^{1} x^p \sin(k\pi x) dx. \tag{4.136}$$

With the definition of $H_{\ell k}$ in the second of Eq. (4.135), the exact Gegenbauer coefficients for x^p are $g_\ell^{(p)} = H_{p\ell}$. Equation (4.129) is an identity with $\tilde{g}_\ell = H_{p\ell}$ and

$$\sum_{odd\ \ell}^{m} H_{p\ell} T_{\ell k} = b_k^{(p)}. \tag{4.137}$$

With the definition of $T_{\ell k}$, Eq. (4.130), and the first of Eq. (4.135), we have that

$$\sum_{odd\ \ell}^{m} H_{p\ell} \sum_{odd\ n}^{\ell} G_{\ell n} b_k^{(n)} = b_k^{(p)}. \tag{4.138}$$

With the third relation of Eq. (4.135), we get the result

$$\sum_{odd\ n}^{m} \delta_{p,n} b_k^{(n)} = b_k^{(p)}. \tag{4.139}$$

The linear system, Eq. (4.129), provides an *exact* relationship between the first m (exact) $b_k^{(p)}$ Fourier coefficients and the first m $\tilde{g}_\ell = g_\ell$ Gegenbauer coefficients, and the results are independent of λ.

We illustrate the previous results with the test function, $f_1(x) = x$. We require only one Fourier coefficient in Eq. (4.129)

$$\tilde{g}_1 T_{1,1} = b_1^{(1)}, \tag{4.140}$$

and obtain the *exact* resolution of the Gibbs phenomenon with $\tilde{g}_1 = g_1 = 1/2\lambda$.

For $f_3(x) = x^3$, the 2×2 linear system

$$\begin{aligned} \tilde{g}_1 T_{1,1} + \tilde{g}_3 T_{3,1} &= b_1^{(3)}, \\ \tilde{g}_1 T_{1,2} + \tilde{g}_3 T_{3,2} &= b_2^{(3)}. \end{aligned} \tag{4.141}$$

is solved. The Taylor coefficients, Eq. (4.141), are substituted into Eq. (4.141) which gives the system of equations

$$\begin{aligned} d_1 b_1^{(1)} + d_3 b_1^{(3)} &= b_1^{(3)}, \\ d_1 b_2^{(1)} + d_3 b_2^{(3)} &= b_2^{(3)}. \end{aligned} \tag{4.142}$$

A solution is $d_1 = 0$ and $d_3 = 1$ independent of λ. We write $\tilde{f}_p(x) = \sum_{odd\ n}^{m} d_n x^n$ with $d_n = \sum_{odd\ \ell}^{m} \tilde{g}_\ell G_{\ell,n}$ so that Eq. (4.129) for the Gegenbauer coefficients reduces to the linear system,

$$\sum_{odd\ n}^{m} d_n b_k^{(n)} = b_k, \tag{4.143}$$

for the Taylor coefficients independent of λ.

If the b_k coefficients on the right hand side of Eq. (4.143) are for $f_p(x) = x^p$ as given by Eq. (4.136), then Eq. (4.143) gives an exact result. One of the columns in the matrix $b_k^{(n)}$ is equal to the inhomogenous vector on the right hand side of Eq. (4.143) and $d_n = 1$ for $n = p$ and $d_n = 0$ for $n \neq p$. An important aspect of Eqs. (4.141)–(4.143) is that the exact b_k Fourier coefficients are considered as input. Therefore, the exact resolution of Gibbs phenomena requires that the exact $T_{k\ell}$ matrix elements be computed.

4.7.4 Numerical Comparisons

We compare the direct and inverse methods with numerical examples used previously (Gottlieb et al. 1992; Vozovoi et al. 1997) and the first one is the polynomial $f(x) = x^3 + x^6$ which is neither odd nor even. The $\tilde{g}_\ell$ coefficients with ℓ odd are obtained by inverting Eq. (4.129) and those with ℓ even are given by

$$\sum_{even\ \ell}^{m} \tilde{g}_\ell V_{\ell k} = a_k. \tag{4.144}$$

The matrices $T_{\ell k}$ and $V_{\ell k}$ are given by Eq. (4.132).

In Table 4.4, we show the Taylor coefficients, d_n, versus λ derived from the $\hat{g}_\ell$ coefficients, where the exact values are

$$d_n = \begin{cases} 0 & n \neq 3, \quad n \neq 6, \\ 1 & n = 3, \quad n = 6. \end{cases} \tag{4.145}$$

As demonstrated in the table, the inverse reconstruction of the function is exact. The L_∞ error defined by

$$L_\infty = \max_{-1 \leq x \leq 1} |f(x) - f_m(x)|,$$

is listed in the last column and is independent of λ. The convergence of the inverse approach is extremely rapid for this polynomial and requires only 6 terms in Eqs. (4.129) and (4.144).

Table 4.4 Inverse method; Taylor coefficients d_n versus λ for $f(x) = x^3 + x^6$; $(-n) \equiv 10^{-n}$; $m = 7$

λ	d_0	d_1	d_2	d_3	d_4	d_5	d_6	d_7	L_∞
$\frac{1}{2}$	0.132 (−15)	0.000000	−0.278 (−15)	1.0000	0.222 (−15)	0.000000	1.0000	0.000000	0.444 (−15)
1	0.798 (−16)	0.191 (−15)	0.222 (−15)	1.0000	0.444 (−15)	0.556 (−14)	1.0000	−0.389 (−14)	0.257 (−15)
2	−0.520 (−17)	0.209 (−15)	0.555 (−15)	1.0000	−0.155 (−14)	0.556 (−14)	1.0000	−0.389 (−14)	0.444 (−15)
4	0.183 (−15)	0.393 (−15)	−0.611 (−15)	1.0000	0.555 (−15)	0.103 (−13)	1.0000	−0.779 (−14)	0.133 (−14)
8	−0.316 (−15)	0.135 (−15)	0.125 (−14)	1.0000	0.111 (−15)	0.860 (−15)	1.0000	0.000000	0.666 (−15)

Reprinted from Shizgal and Jung (2003) with permission from Elsevier

The convergence of the Taylor coefficients versus N with the Gegenbauer reconstruction in Table 4.5 is much slower where the constraint $m = \lambda = N/4$ has been imposed. The L_∞ error decreases slowly with increasing N and for $N = 40$ it is not at machine accuracy with $m = 10$. It is clear with the results in Table 4.5 that if m is not large enough the reconstructed function with the direct method is inaccurate. Consider $f(x) = x^3 + x^6$ with $N = 20$ and $m = 5$ for which $L_\infty = 0.373$. If m is too large, then the reconstructed function will converge to $f^{(N)}$ and the Gibbs phenomenon is recovered, since $\lim_{m\to\infty} \hat{f}_m(x) = f^{(N)}(x)$.

The second test function is $f(x) = \cos[1.4\pi(x + 1)]$ with Fourier coefficients given by,

$$
\begin{aligned}
a_0 &= \frac{\sin(2.8\pi)}{(2.8\pi)}, \\
a_k &= \frac{1.4\pi(-1)^{(k+1)}}{(k\pi)^2} \frac{\sin(2.8\pi)}{(1 - (\frac{1.4}{k})^2)}, \\
b_k &= \frac{k\pi(-1)^k}{(1.4\pi)^2} \frac{(\cos(2.8\pi) - 1)}{(1 - (\frac{k}{1.4})^2)},
\end{aligned}
$$

The Taylor coefficients versus λ with the inverse method with $N = 12$ and $m = 23$ are shown in Table 4.6 which gives results independent of λ. The L_∞ error is close to machine accuracy. With only 23 Gegenbauer polynomials, the higher order Taylor coefficient d_{19} is unconverged and differs from the exact value by 0.53 %.

A comparison of the convergence of the direct and inverse methods for $f(x) = \cos[1.4\pi(x + 1)]$ is shown in Fig. 4.16. The inverse method provides a much faster convergence than the direct method. In Fig. 4.16b, we also show results for alternate weight functions. In addition to the Gegenbauer weight function, $w_g(x) = (1-x^2)^{\lambda-\frac{1}{2}}$, we use a modified Gegenbauer weight function, $w_m(x) = w_g(x)e^{-\alpha x^2}$ and a Gaussian weight function $w(x) = e^{-\beta x^2}$. The parameters λ, α and β in the weight function control the width of the weight functions about the origin. The orthogonal polynomials are constructed with the Gautschi-Stieltjes procedure discussed in Chap. 2, Sect. 2.3.6. For the Gegenbauer and modified Gegenbauer weight functions, $m = \lambda = N/4$. It is clear that the inverse method converges faster than the direct method with different polynomial basis sets.

The numerical calculations with the inverse method involve the inversion of Eqs. (4.129) and (4.144) for the $\tilde{g}_\ell$ coefficients. The reconstructed function is given by Eq. (4.127). The method gives remarkable results for the test functions studied. Alternatively, the $\tilde{g}_\ell$ coefficients can also be determined from the inversion of Eq. (4.125) or Eq. (4.144) for the equivalent Taylor coefficients. One important concern is the numerical invertibility of the matrices, $\mathbf{T}$ and $\mathbf{V}$. The condition numbers of these matrices increase rapidly with m and an accurate resolution of the Gibbs phenomenon with $L_\infty \leq 10^{-8}$ can be obtained for functions approximated by polynomials of order 25 or less. A method to mitigate the round-off errors that occur is described in the next section.

Table 4.5 Direct method; Taylor coefficients d_n versus N for $f(x) = x^3 + x^6$; $m = \lambda = N/4$

N	d_0	d_1	d_2	d_3	d_4	d_5	d_6	d_7	L_∞
4	0.802 (−1)	0.462 (0)	–	–	–	–	–	–	0.146 (1)
8	−0.314 (−1)	0.377 (0)	0.376 (0)	–	–	–	–	–	0.128 (1)
12	−0.179 (−1)	−0.677 (−3)	0.268 (0)	1.002652	–	–	–	–	0.752 (0)
16	0.372 (−2)	0.180 (−4)	−0.156 (0)	0.999909	0.833 (0)	–	–	–	0.319 (0)
20	0.260 (−2)	−0.134 (−4)	−0.125 (0)	1.000160	0.750 (0)	−0.317 (−3)	–	–	0.373 (0)
24	−0.111 (−7)	0.601 (−7)	0.669 (−6)	0.999999	−0.490 (−5)	0.305 (−5)	1.000010	–	0.559 (−5)
28	−0.809 (−10)	−0.257 (−6)	0.457 (−8)	1.000010	−0.292 (−7)	−0.322 (−4)	1.000000	0.430 (−4)	0.167 (−4)
32	−0.120 (−9)	−0.513 (−8)	0.129 (−7)	1.000000	−0.181 (−6)	−0.642 (−6)	1.000000	0.844 (−6)	0.595 (−6)
36	−0.897 (−12)	−0.461 (−8)	0.394 (−9)	1.000000	−0.587 (−8)	−0.180 (−5)	1.000000	0.586 (−5)	0.166 (−5)
40	0.135 (−11)	−0.243 (−9)	0.219 (−9)	1.000000	−0.525 (−8)	−0.964 (−7)	1.000000	0.322 (−6)	0.117 (−6)

Reprinted from Shizgal and Jung (2003) with permission from Elsevier

Table 4.6 Inverse method; Taylor coefficients d_n versus λ for $f(x) = \cos[1.4\pi(x+1)]$; $(-n) \equiv 10^{-n}$; $N = 12$, $m = 23$

λ/d_n	d_0	d_5	d_{10}	d_{15}	d_{19}	L_∞
$\frac{1}{2}$	−0.309017	0.130441 (2)	0.230674	−0.324243 (−2)	−0.129876 (−4)	0.7430 (−12)
1	−0.309017	0.130441 (2)	0.230674	−0.324245 (−2)	−0.130249 (−4)	0.1628 (−12)
2	−0.309017	0.130441 (2)	0.230674	−0.324244 (−2)	−0.130052 (−4)	0.2451 (−12)
4	−0.309017	0.130441 (2)	0.230674	−0.324250 (−2)	−0.130888 (−4)	0.1061 (−11)
8	−0.309017	0.130441 (2)	0.230674	−0.324241 (−2)	−0.129744 (−4)	0.1671 (−11)
Exact	−0.309017	0.130441 (2)	0.230674	−0.324247 (−2)	−0.130434 (−4)	–

Reprinted from Shizgal and Jung (2003) with permission from Elsevier

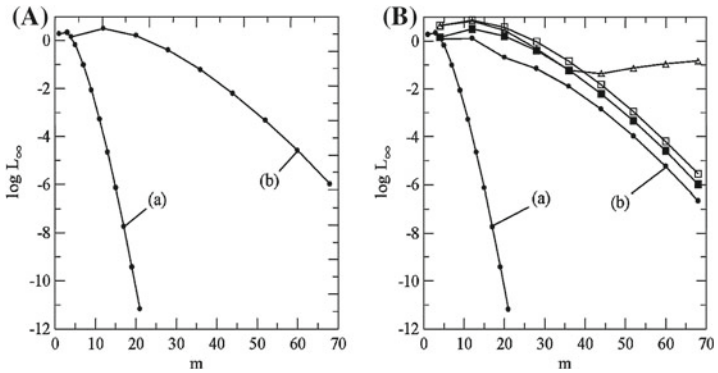

Fig. 4.16 The variation of the L_∞ error versus N for $f(x) = \cos[1.4\pi(x+1)]$; comparison of the direct and inverse methods. (**A**) Comparison of the inverse method and the direct method based on the Gegenbauer weight, $w_g(x) = (1-x^2)^{\lambda-\frac{1}{2}}$; (*a*) inverse method, (*b*) direct method; (**B**) Comparison of the inverse method and the direct method based on different weight functions: Gegenbauer weight function, $\lambda = N/4$ (*filled squares*); modifed Gegenbauer weight, $w_m(x) = w_g(x)e^{-\alpha x^2}$, $\lambda = N/4$ (*open squares*), $\alpha = 16$; *filled circles*, $\alpha = -16$; and a gaussian weight function $w(x) = e^{-\beta x^2}$, $\beta = 16$ (*triangles*). Reprinted from Shizgal and Jung (2003) with permission from Elsevier

4.7.5 Minimizing the Inverse Method Round-Off Errors

In Chap. 2, Sect. 2.2, we emphasized the manner in which round-off errors destroys the Gram-Schmidt orthogonalization procedure. Round-off errors generally occur when one attempts to subtract two very large numbers to give a desired result which is orders of magnitude smaller. We have also noted round-off errors of a different nature that occur in the calculation of the α_n and β_n coefficients for Maxwell polynomials from recurrence relations in Sect. 2.5.1. The inverse method for the resolution of the Gibbs phenomenon requires the inversion of the matrices **T** and **V** and the condition numbers of these matrices which increase with the matrix size determine the accuracy of the final results.

Table 4.7 Direct method; Taylor coefficients d_n versus λ for $f(x) = \cos[1.4\pi(x+1)]$; $(-n) \equiv 10^{-n}$; $N = 76, m = N/4 = 19$

λ	d_0	d_5	d_{10}	d_{15}	d_{19}	L_∞
$\frac{1}{2}$	−0.309029	−0.203631 (3)	0.151266 (2)	0.454691 (5)	0.566650 (4)	0.5352
1	−0.309016	−0.381491 (2)	−0.175522 (1)	0.123990 (5)	0.161670 (4)	0.2472
2	−0.309017	0.133678 (2)	−0.614139	−0.143695 (3)	−0.228711 (2)	0.2152 (−1)
4	−0.309017	0.130498 (2)	0.242121	−0.258823 (1)	−0.402494	0.1358 (−3)
6	−0.309017	0.130439 (2)	0.230461	0.166745	0.336778 (−1)	0.1112 (−3)
8	−0.309017	0.130441 (2)	0.230678	−0.118250 (−1)	−0.203508 (−2)	0.1500 (−4)
10	−0.309017	0.130441 (2)	0.230674	−0.279070 (−2)	0.112471 (−3)	0.1613 (−5)
14	−0.309017	0.130441 (2)	0.230674	−0.326321 (−2)	−0.173321 (−4)	0.6925 (−7)
18	−0.309017	0.130441 (2)	0.230674	−0.325798 (−2)	−0.181841 (−4)	0.2983 (−6)
Exact	−0.309017	0.130441 (2)	0.230674	−0.324247 (−2)	−0.130434 (−4)	–

Reprinted from Shizgal and Jung (2003) with permission from Elsevier

The inverse method is independent of the λ parameter in $C_\ell^\lambda(x)$; see Tables 4.4, 4.6 and 4.7. With the Legendre polynomial basis set, $P_\ell(x)$, corresponding to $\lambda = 1/2$, the inverse problem is

$$\mathbf{W} \cdot \tilde{\mathbf{g}} = \hat{\mathbf{f}}, \tag{4.146}$$

where the matrix $\mathbf{W}$ is

$$W_{k\ell} = \frac{1}{2} \int_{-1}^{1} e^{-ik\pi x} P_\ell(x) dx, \tag{4.147}$$

and is ill-condtioned.

The inversion of $\mathbf{W}$ is based on Gaussian elimination with partial pivoting. This method involves three steps, namely, (1) the Gaussian elimination with matrix operator $\mathbf{P}$ to construct the upper triangular matrix $\mathbf{U}$, (2) transformation of the Fourier coefficients $\hat{\mathbf{f}}$ to a new vector $\mathbf{h}$, and (3) inversion by backward substitution to get $\hat{\mathbf{g}}$. This is summarized by the three matrix operations,

$$\mathbf{U} = \mathbf{P} \cdot \mathbf{W}, \quad \mathbf{h} = \mathbf{P} \cdot \hat{\mathbf{f}}, \quad \mathbf{U} \cdot \hat{\mathbf{g}} = \mathbf{h}. \tag{4.148}$$

For the resolution of $f(x) = \cos[1.4\pi(x+1)]$, the various quantities in Eq. (4.148) are shown in Fig. 4.17 and the important result is the exponential decrease of h_k (purple curve) which is analogous to the behaviour of g_ℓ (red curve). If we were to use a test function that is a polynomial of degree m, then $g_\ell = 0$ for $\ell > m$, and h_k follows the same behaviour. The slower convergence of $\tilde{g}_\ell$ is also shown in Fig. 4.17. From the graph, we see that for $k > 24$, h_k is at machine accuracy and the values for large k represent random noise. Consequently with the inversion of $\mathbf{W}$, we get a rapid resolution of the Gibbs phenomenon versus N as shown by the circle symbols in Fig. 4.18a up to about $2N + 1 = 20$. Then with increasing N the

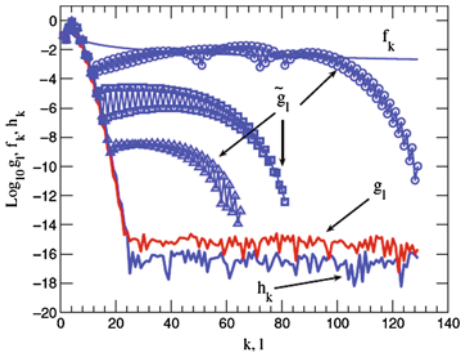

Fig. 4.17 The variation of f_k, g_ℓ, h_k and $\tilde{g}_\ell$ for $f(x) = \cos[1.4\pi(x+1)]$. $\hat{f}_k$ denotes the Fourier coefficients, g_ℓ the exact Legendre expansion coefficients, $\tilde{g}_\ell$ the expansion coefficients with the inverse method and h_k the mapped Fourier coefficients. The *symbols* △, □ and ◯ denote $\tilde{g}_\ell$ for $N = 32, 40$ and 64, respectively. Reprinted from Jung and Shizgal (2007) with permission from Elsevier

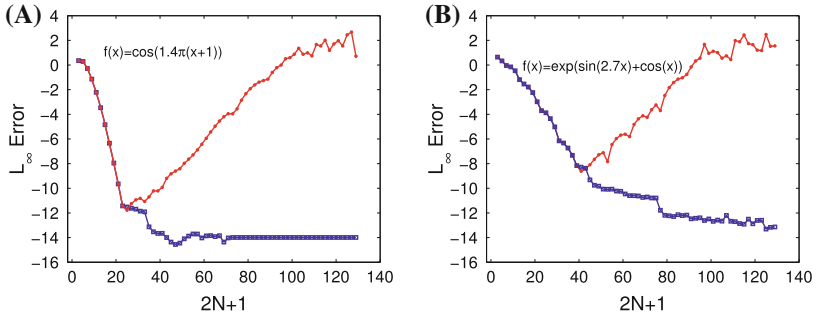

Fig. 4.18 The variation of L_∞ versus N arising from Gaussian elimination and partial pivoting with and without truncating **h**. The *red curves* denoted with *circle symbols* are the results without truncation whereas the *blue curves* denoted with *square symbols* are the results with truncation and the L_∞ remains at machine accuracy. Reprinted from Jung and Shizgal (2007) with permission from Elsevier

L_∞ error increases as shown by the red curves and circle symbols. A very similar behaviour is found for $f(x) = \exp[\sin(2.7x) + \cos(x)]$ in Fig. 4.18b.

Jung and Shizgal (2007) proposed a simple truncation by deleting from the vector **h** the small h_k components that ultimately lead to the increasing L_∞ values owing to the ill-conditioned **W** matrix. Thus we set $h_k = 0$ for $|h_k| \leq \epsilon$ where ϵ is taken close to but larger than the machine epsilon denoted by ϵ_M. With this fix, we find the improved variation of L_∞ with N as shown by the blue lines with the square symbols in Fig. 4.18. Hrycak and Grchenig (2010) have developed an alternate remedy for the ill-conditioned matrices with the inverse method by increasing the number of Fourier coefficients for a polynomial of degree n beyond the minimum required so that the Gibbs reconstruction becomes an overdetermined linear problem solved with

a least squares minimization. A similar approach using the pseudo-inverse, based on the statistical filter method, to reduce the round-off errors in the inverse method was proposed by Jung (2011).

4.7.6 Local Reconstruction and Image Resolution

Shizgal and Jung (2003) also considered a local reconstruction of piecewise continuous functions on subintervals with the inverse method applied to each subinterval. The generalization of the inverse method to two or more intervals is straightforward and is a slight modification of the methodology in Sect. 4.7.2. We consider the function

$$f(x) = \begin{cases} -(x+1), & x \leq 0, \\ (1-x)^6, & x > 0, \end{cases} \tag{4.149}$$

which is linear in the left domain and a polynomial of degree 6 in the right domain. We also consider the function

$$f(x) = \begin{cases} x^3 + x^6, & x \leq 0.45, \\ \cos[(1.4\pi(x+1)], & x > 0.45. \end{cases} \tag{4.150}$$

From the previous discussions, it is clear that the inverse method will provide an exact reconstruction in each subinterval. We show in Fig. 4.19 the Chebyshev ($\lambda = 0$)

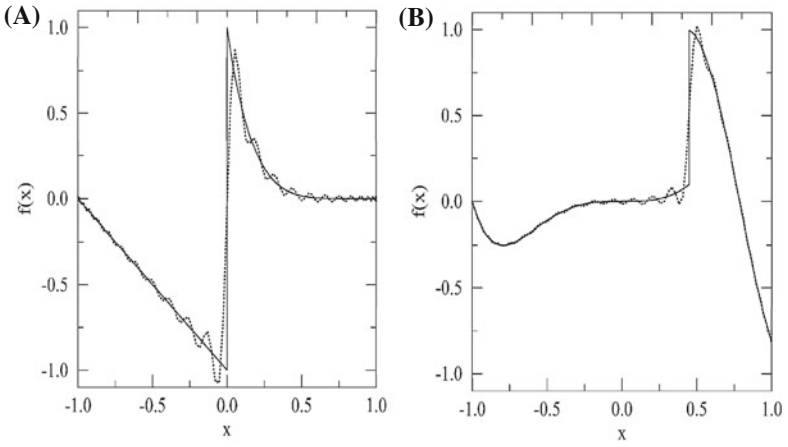

Fig. 4.19 (**A**) Reconstruction of $f(x) = -(x+1)$ if $x \leq 0$ and $(1-x)^6$ if $x > 0$. *Oscillatory curve* is the Chebyshev approximation with $N = 35$. (**B**) $f(x) = x^3 + x^6$ if $x \leq 0.45$ and $\cos[1.4\pi(x+1)]$ for $x > 0.45$. The *solid curves* are the reconstructed functions and indistinguishable from the original functions. Reprinted from Shizgal and Jung (2003) with permission from Elsevier

approximation with $N = 35$ as the dashed oscillatory curve and the reconstructed function as the solid curve which is indistinguishable from the exact result. However, it is very important to note that this reconstruction is done with a knowledge of the location of the discontinuities at the interval boundaries at $x = 0$ and $x = 0.45$.

The inverse method was also applied to the reconstruction of images in two dimensions and in particular the Shepp-Logan model for the brain (Jung and Shizgal 2005). Image reconstruction requires locating the points of discontinuity or edges, and edge detection has become an integral aspect of image restoration (Archibald and Gelb 2002; Stefan et al. 2012; Cochran et al. 2013). This research activity will undoubtedly play an important role in medical imaging (Kaur et al. 2007; Koay et al. 2007; Kamm et al. 2010; Dadkhahi et al. 2012).

4.8 The Runge Phenomenon

The Runge phenomenon is often discussed in conjunction with the Gibbs phenomenon and although there are similarities, they are different. The Runge phenomenon arises from the interpolation of a certain class of functions with a uniform grid. One such function is

$$f(x) = \frac{1}{1 + 25x^2}, \quad x \in [-1, 1]. \tag{4.151}$$

It is straightforward to do the interpolation in MATLAB and compare the interpolant with the exact result and this is shown in Fig. 4.20. The solid curves are for the function in Eq. (4.151). The dashed curves in the top graphs show the result of an interpolation with a uniform grid with $N = 8$ and $N = 14$ points, respectively. The bottom graph shows the results with the nonuniform Chebyshev points. The superior results with the Chebyshev quadrature points in comparison with the uniform grids is clear.

The Runge phenomenon has been analyzed in great detail by numerous workers and we provide a brief summary of some of the work done to date. Jung and Stefan (2011) analyzed the Runge phenomenon in a manner similar to the discussion in Sect. 4.7.5 for the minimization of the round-off error in the inversion of the matrices associated with the inverse method. Trefethen (2000) provides an insightful interpretation of the Runge phenomenon as the solution of the Poisson equation for a charge distribution. He points to the different charge distributions for the interpolation on the uniform grid in comparison with the Chebyshev grid. Boyd (2010) and coworkers (Boyd and Ong 2009, 2011) have carried out extensive studies with different strategies to overcome the Runge phenomenon. In spite of all the interest, the practical applications of these analyses have not been emphasized in the manner that the Gibbs phenomenon occupies an important role in medical imaging (Koay et al. 2007; Dadkhahi et al. 2012; Jung and Zhao 2012).

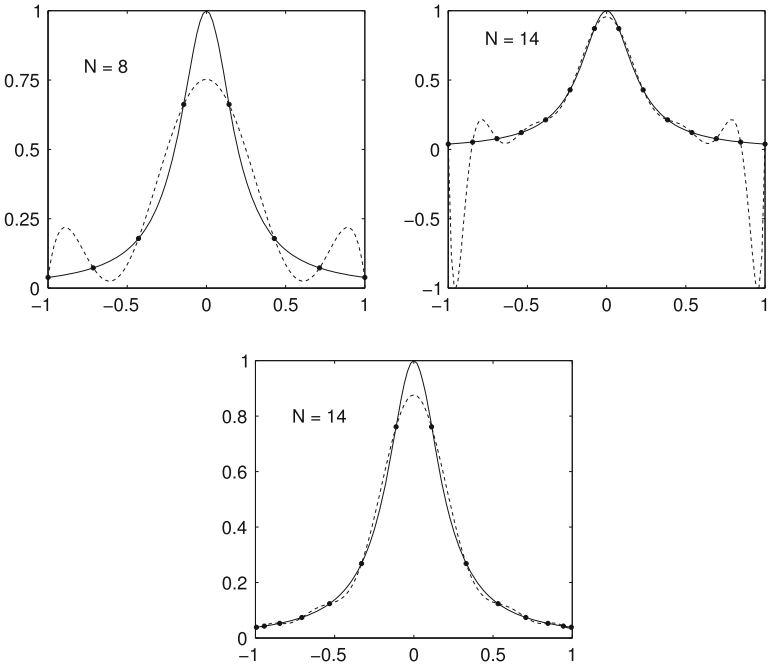

Fig. 4.20 The *solid curve* in each graph is Eq. (4.151) and the *dashed curve* is the interpolated function. (*Upper graphs*) The interpolation points (*solid symbols*) are uniformly distributed and the interpolation fails at the interval boundaries with increasing N as shown. (*Lower graphs*) The points (*solid symbols*) are the Chebyshev quadrature points, $x_i = \cos[(2i-1)\pi/2n]$, not distributed uniformly and there is convergence with increasing N

References

Abramowitz, M., Stegun, I.A.: Handbook of Mathematical Functions with Formulas, Graphs, and Mathematical Tables. US Government Printing Office (1964)

Adcock, B., Hansen, A.C.: Stable reconstructions in Hilbert spaces and the resolution of the Gibbs phenomenon. Appl. Comput. Harmon. Anal. **32**, 357–388 (2012)

Adomaitis, R.A.: Spectral filtering for improved performance of collocation discretization methods. Comput. Chem. Eng. **25**, 1621–1632 (2001)

Al-Gwaiz, M.A.: Sturm-Liouville Theory and Its Applications. Springer, Berlin (2008)

Almeida, P.G.C., Benilov, M.S., Naidis, G.V.: Calculation of ion mobilities by means of the two-temperature displaced-distribution theory. J. Phys. D: Appl. Phys. **35**, 1577–1584 (2002)

Alp, Y.K., Arikan, O.: Time-frequency analysis of signals using support adaptive Hermite-Gaussian expansions. Digit. Signal Process. **22**, 1010–1023 (2012)

Amore, P., Fernandez, F.M., Saenz, R.A., Salvo, K.: Collocation on uniform grids. J. Phys. A: Math. Theor. **42**, 115302 (2009)

Archibald, R., Gelb, A.: Reducing the effects of noise in image reconstruction. J. Sci. Comput. **17**, 167–180 (2002)

Asadchev, A., Gordon, M.S.: Mixed-precision evaluation of two-electron integrals by Rys quadrature. Comput. Phys. Commun. **183**, 1563–1567 (2012)

Balint-Kurti, G.G.: Wavepacket theory of photodissociation and reactive scattering. Adv. Chem. Phys. **128**, 249–301 (2003)
Balint-Kurti, G.G.: Time-dependent and time-independent wavepacket approaches to reactive scattering and photodissociation dynamics. Int. Rev. Phys. Chem. **27**, 507–539 (2008)
Balint-Kurti, G.G.: Wavepacket quantum dynamics. Theor. Chem. Acc. **127**, 1–17 (2010)
Balint-Kurti, G.G., Pulay, P.: A new grid-based method for the direct computation of excited molecular vibrational-states: test application to formaldehyde. J. Mol. Struct. (Theochem) **341**, 1–11 (1995)
Bao, W., Li, H., Shen, J.: A generalized Laguerre-Hermite pseudospectral method for computing symmetric and central vortex states in Bose-Einstein condensates. J. Comput. Phys. **227**, 9778–9793 (2008)
Baye, D., Heenen, P.H.: Generalized meshes for quantum-mechanical problems. J. Phys. A: Math. Gen. **19**, 2041–2059 (1986)
Baye, D., Vincke, V.: Lagrange meshes from nonclassical orthogonal polynomials. Phys. Rev. E **59**, 7195–7199 (1999)
Blackledge, J.M.: Digital Signal Processing: Mathematical and Computational Methods, Software Development and Applications. Woodhead, Cambridge (2006)
Blinnikov, S., Moessner, R.: Expansions for nearly Gaussian distributions. Astron. Astrophys. Suppl. Ser. **130**, 193–205 (1998)
Bonazzola, S., Gourgoulhon, E., Marck, J.-A.: Spectral methods in general relativistic astrophysics. J. Comput. Appl. Math. **109**, 433–473 (1999)
Boyd, J.P.: Exponentially convergent Fourier-Chebyshev quadrature schemes on bounded and infinite domains. J. Sci. Comput. **2**, 99–109 (1987)
Boyd, J.P.: A fast algorithm for Chebyshev, Fourier, and Sine interpolation onto an irregular grid. J. Comput. Phys. **103**, 243–257 (1992)
Boyd, J.P.: A numerical comparison of seven grids for polynomial interpolation on the interval. Comput. Math. Appl. **38**, 35–50 (1999)
Boyd, J.P.: Chebyshev and Fourier Spectral Methods. Dover, New York (2001)
Boyd, J.P.: Six strategies for defeating the Runge phenomenon in Gaussian radial basis functions on a finite interval. Comput. Math. Appl. **60**, 3108–3122 (2010)
Boyd, J.P., Ong, J.R.: Exponentially-convergent strategies for defeating the Runge phenomenon for the approximation of non-periodic functions, Part I: single-interval schemes. Commun. Comput. Phys. **5**, 484–497 (2009)
Boyd, J.P., Ong, J.R.: Exponentially-convergent strategies for defeating the Runge phenomenon for the approximation of non-periodic functions, part two: multi-interval polynomial schemes and multidomain Chebyshev interpolation. Appl. Numer. Math. **61**, 460–472 (2011)
Boyd, J.P., Rangan, C., Bucksbaum, P.H.: Pseudospectral methods on a semi-infinite interval with application to the hydrogen atom: a comparison of the mapped Fourier-sine method with Laguerre series and rational Chebyshev expansions. J. Comput. Phys. **188**, 56–74 (2003)
Briggs, W.L., Henson, V.E.: The DFT; An Owners Manual for the Discrete Fourier Transform. SIAM, Philadelphia (1995)
Brown, J.W., Churchill, R.V.: Fourier Series and Boundary Value Problems. McGraw Hill, New Jersey (1993)
Burden, R.L., Faires, J.D.: Numerical Analysis, 9th edn. Brooks/Cole, Boston (2011)
Canuto, C., Hussaini, M.Y., Quarteroni, A., Zang, T.A.: Spectral Methods: Fundamentals in Single Domains. Springer, New York (2006)
Carlson, H.S.: A historical note on Gibb's phenomenon in Fourier's series and integrals. Bull. Am. Math. Soc. **31**, 420–424 (1925)
Cha, S.-H.: Comprehensive survey on distance/similarity measures between probability density functions. Int. J. Math. Models Methods Appl. Sci. **1**, 300–307 (2007)
Chen, H., Shizgal, B.D.: A spectral solution of the Sturm-Liouville equation: comparison of classical and nonclassical basis sets. J. Comput. Appl. Math. **136**, 17–35 (2001)
Cheney, E.W.: Introduction to Approximation Theory. McGraw-Hill, New York (1966)

Cheney, W., Kincaid, D.: Numerical Methods and Computing, 6th edn. Brooks/Coll Publishing Company, California (2008)
Chiang, L.-Y., Chen, F.-F.: Direct measurement of the angular power spectrum of cosmic microwave background temperature anisotropies in the WAMP data. Astrophys. J. **751**, 1–6 (2012)
Cochran, C., Gelb, A., Wang, Y.: Edge detection from truncated Fourier data using spectral mollifiers. Adv. Comput. Math. **38**, 737–762 (2013)
Colbert, D.T., Miller, W.H.: A novel discrete variable representation for quantum-mechanical reactive scattering via the S-Matrix Kohn method. J. Chem. Phys. **96**, 1982–1991 (1992)
Collier, M.R.: Are magnetospheric suprathermal particle distributions (κ functions) inconsistent with maximum entropy considerations. Adv. Space Res. **33**, 2108–2112 (2004)
Comisarow, M.B.: Fundamental aspects of FT-ICR and applications to chemistry. Hyperfine Interact. **81**, 171–178 (1993)
Comisarow, M.B., Marshall, A.G.: Fourier transform ion cyclotron resonance spectroscopy. Chem. Phys. Lett. **25**, 282–283 (1974)
Cooley, J.W., Tukey, J.W.: An algorithm for the machine calculation of complex Fourier series. Math. Comput. **19**, 297–301 (1965)
Dadkhahi, H., Gotchev, A., Egiazarian, K.: Inverse polynomial reconstruction method in DCT domain. EURASIP J. Adv. Signal Process. **2012**, 1–23 (2012)
Davis, P.J.: Interpolation and Approximation. Blaisdell, London (1963)
Driscoll, T.A., Fornberg, B.: A Padé based algorithm for overcoming Gibbs phenomenon. Numer. Algorithms **26**, 77–92 (2001)
Duarte, F.B., Tenreiro Machado, J.A., Duarte, G.M.: Dynamics of the Dow Jones and the NASDAQ stock indexes. Nonlinear Dyn. **61**, 691–705 (2010)
Durran, D.R.: Numerical Methods for Fluid Dynamics: With Applications to Geophysics. Springer, Berlin (2010)
Ernst, R.R., Anderson, W.A.: Application of Fourier transform spectroscopy to magnetic resonance. Rev. Sci. Instrum. **37**, 93–102 (1966)
Evans, G.A.: Some new thoughts on Gauss-Laguerre quadrature. Int. J. Comput. Math. **82**, 721–730 (2005)
Filbet, F., Mouhot, C., Pareschi, L.: Solving the Boltzmann equation in $N\log_2 N$. SIAM J. Sci. Comput. **28**, 1029–1053 (2006)
Filbet, F., Mouhot, C.: Analysis of spectral methods for the homogeneous Boltzmann equation. Trans. Am. Math. Soc. **363**, 1947–1980 (2011)
Foch, J.D., Ford, G.W.: The linear Boltzmann equation. In: de Boer, J., Uhlenbeck, G.E. (eds.) Studies in Statistical Mechanics, pp. 127–154. Elsevier, Holland (1970)
Fok, J.C.M., Guo, B., Tang, T.: Combined Hermite spectral-finite difference method for the Fokker-Planck equation. Math. Comput. **71**, 1497–1528 (2001)
Garcia, R.D.M.: The application of non-classical orthogonal polynomials in particle transport theory. Prog. Nucl. Energy **35**, 249–273 (1999)
Gelb, A., Tanner, J.: Robust reprojection methods for the resolution of the Gibbs phenomenon. Appl. Comput. Harmon. Anal. **20**, 3–25 (2006)
Gelb, A., Hines, T.: Recovering exponential accuracy from non-harmonic Fourier data through spectral reprojection. J. Sci. Comput. **51**, 158–182 (2012)
Gibelli, L., Shizgal, B.D.: Spectral convergence of the Hermite basis function solution of the Vlasov equation, the free-streaming term. J. Comput. Phys. **219**, 477–488 (2006)
Gibelli, L., Shizgal, B.D., Yau, A.W.: Ion energization by wave-particle interactions: comparison of spectral and particle simulation solutions of the Vlasov equation. J. Comput. Phys. **59**, 2566–2581 (2010)
Gottlieb, D., Hesthaven, J.S.: Spectral methods for hyperbolic problems. J. Comput. Appl. Math. **128**, 83–131 (2001)
Gottlieb, D., Orszag, S.: Numerical Analysis of Spectral Methods: Theory and Applications. SIAM, Philadelphia (1977)

Gottlieb, D., Shu, C.-W.: On the Gibbs phenomenon and its resolution. SIAM Rev. **39**, 644–668 (1997)
Gottlieb, D., Gustafsson, B., Forssén, P.: On the direct Fourier method for computer tomography. IEEE Trans. Med. Imaging **19**, 223–232 (2000)
Gottlieb, D., Shu, C.-W., Solomonoff, A., Vandeven, H.: On the Gibbs phenomenon 1: recovering exponential accuracy from the Fourier partial sum of a nonperiodic analytic function. J. Comput. Appl. Math. **43**, 81–98 (1992)
Gottlieb, S., Jung, J.H., Kim, S.: A review of David Gottlieb's work on the resolution of the Gibbs phenomenon. Commun. Comput. Phys. **9**, 497–519 (2011)
Gradshteyn, I.S., Ryzhik, I.M.: Tables of Integrals, Series and Products. Elsevier, Amsterdam (2007)
Grandclément, P., Novak, J.: Spectral methods for numerical relativity. Living Rev. Relativ. **12**, 1–103 (2009)
Gust, E.D., Reichl, L.E.: Molecular dynamics simulation of collision operator eigenvalues. Phys. Rev. E **79**, 031202 (2009)
Haberman, R.: Applied Partial Differential Equations with Fourier Series and Boundary Value Problems, 5th edn. Prentice Hall, Upper Saddle River (2013)
Hanna, J.R., Rowland, J.H.: Fourier Series, Transforms, and Boundary Value Problems. Dover, New York (2008)
Hau, L.-N., Fu, W.-Z.: Mathematical and physical aspects of Kappa velocity distribution. Phys. Plasmas **14**, 110702 (2007)
Hau, L.-N., Fu, W.-Z., Chuang, S.-H.: Response to Comment on mathematical and physical aspects of Kappa velocity distribution. Phys. Plasmas **16**, 094702 (2009)
Hellberg, M.A., Mace, R.L., Baluku, T.K., Kourakis, I., Saini, N.S.: Comment on mathematical and physical aspects of Kappa velocity distribution. Phys. Plasmas **16**, 094701 (2009)
Hewitt, E., Hewitt, R.E.: The Gibbs-Wilbraham phenomenon: an episode in Fourier analysis. Arch. Hist. Exact Sci. **21**, 129–160 (1979)
Hoare, M.R., Kaplinsky, C.H.: Linear hard sphere gas: variational eigenvalue spectrum of the energy kernel. J. Chem. Phys. **52**, 3336–3353 (1970)
Holloway, J.P.: Spectral discretizations of the Vlasov-Maxwell equations. Trans. Theory Stat. Phys. **25**, 1–32 (1996)
Holway, L.H.: Time varying weight functions and the convergence of polynomial expansions. Phys. Fluids **10**, 35–48 (1967)
Hrycak, T., Grchenig, K.: Pseudospectral Fourier reconstruction with the modified inverse polynomial reconstruction method. J. Comput. Phys. **229**, 933–946 (2010)
Hunter, C.: Spectral analysis of orbits via discrete Fourier transforms. Space Sci. Rev. **102**, 83–99 (2002)
Hurn, A.S., Jeisman, J.I., Lindsay, K.A.: Seeing the wood for the trees: a critical evaluation of methods to estimate the parameters of stochastic differential equations. J. Financ. Econ. **5**, 390–455 (2007)
James, J.F.: A Student's Guide to Fourier Transforms, 2nd edn. Cambridge University Press, Cambridge (2002)
Jerri, A.J.: The Gibbs Phenomenon in Fourier Analysis, Splines and Wavelet Approximations. Kluwer, Boston (1998)
Jerri, A.J.: Introduction to Integral Equations with Applications, 2nd edn. Wiley, New York (1999)
Jerri, A.J.: Advances in Gibbs Phenomenon. Sampling, Potsdam (2011)
Jirari, A.: Second order Sturm-Liouville difference equations and orthogonal polynomials. Mem. Am. Math. Soc. **113**(542), (1995)
Jung, J.-H.: A note on the Gibbs phenomenon with multiquadric radial basis functions. Appl. Numer. Math. **57**, 213–229 (2007)
Jung, J.-H.: A hybrid method for the resolution of the Gibbs phenomenon. In: Hesthaven, J.S., Ronquist, E.M. (eds.) Lecture Notes in Computational Science and Engineering, pp. 219–227. Springer, Berlin (2011)

Jung, J.-H., Shizgal, B.D.: Generalization of the inverse polynomial reconstruction method in the resolution of the Gibbs phenomenon. J. Comput. Appl. Math. **172**, 131–151 (2004)
Jung, J.-H., Shizgal, B.D.: Inverse polynomial reconstruction of two dimensional Fourier images. J. Sci. Comput. **25**, 367–399 (2005)
Jung, J.-H., Shizgal, B.D.: On the numerical convergence with the inverse polynomial reconstruction method for the resolution of the Gibbs phenomenon. J. Comput. Phys. **224**, 477–488 (2007)
Jung, J.-H., Stefan, W.: A simple regularization of the polynomial interpolation for the resolution of the Runge phenomenon. J. Sci. Comput. **46**, 225–242 (2011)
Jung, K.-J., Zhao, T.: Parallel imaging with asymmetric acceleration to reduce Gibbs artifacts and to increase signal-to-noise ratio of the gradient echo echo-planar imaging sequence for functional MRI. Magn. Reson. Med. **67**, 419–427 (2012)
Kamm, J.R., Williams, T.O., Brock, J.S., Li, S.: Application of Gegenbauer polynomial expansions to mitigate Gibbs phenomenon in Fourier-Bessel series solutions of a dynamic sphere problem. Int. J. Numer. Meth. Biomed. Eng. **26**, 1276–1292 (2010)
Kaur, P., Kumaran, S.S., Tripathi, R.P., Khushu, S., Kaushik, S.: Protocol error artifacts in MRI: sources and remedies revisited. Radiography **13**, 291–306 (2007)
Koay, C.G., Sarlls, J.E., Özarslan, E.: Three-dimensional analytical magnetic resonance imaging phantom in the Fourier domain. Magn. Reson. Med. **58**, 430–436 (2007)
Kokoouline, V., Dulieu, O., Kosloff, R., Masnou-Seeuws, F.: Mapped Fourier methods for long-range molecules: application to perturbations in the $Rb_2(0_u^+)$ photoassociation spectrum. J. Chem. Phys. **110**, 9865–9876 (1999)
Kopriva, D.A.: Implementing Spectral Methods for Partial Differential Equations Algorithms for Scientists and Engineers. Springer, Berlin (2009)
Kosloff, R.: The Fourier method. In: Cerjan, C. (ed.) Numerical Grid Methods and Their Application to Schrödinger's Equation, pp. 175–194. Kluwer Academic, The Netherlands (1993)
Kosloff, D., Kosloff, R.: A Fourier method solution for the time-dependent Schrödinger equation as a tool in molecular dynamics. J. Comput. Phys. **52**, 35–53 (1983)
Kullback, S., Leibler, R.A.: On information and sufficiency. Ann. Math. Stat. **22**, 79–86 (1951)
Lanczos, C.: Discourse on Fourier Series. Hafner, New York (1966)
Laskar, J.: Frequency analysis for multi-dimensional systems. Global dynamics and diffusion. Physica D **67**, 257–281 (1993)
Laskar, J., Correia, A.C.M.: HD60532, a planetary system in a 3:1 mean motion resonance. Astron. Astrophys. **496**, L4–L8 (2009)
Le Bourdiec, S., de Vuyst, F., Jacquet, L.: Numerical solution of the Vlasov-Poisson system using generalized Hermite functions. Comput. Phys. Commun. **175**, 528–544 (2006)
Le Mouël, J.-L., Shnirman, M.G., Blanter, E.M.: The 27-day signal in sunspot number series and the solar dynamo. Sol. Phys. **246**, 295–307 (2007)
Leblanc, F., Hubert, D.: A generalized model for the proton expansion in astrophysical winds. I. The velocity distribution function representation. Astrophys. J. **483**, 464–474 (1997)
Leubner, M.P., Vörös, Z.: A nonextensive entropy approach to solar wind intermittency. Astrophys. J. **618**, 547–555 (2005)
Liboff, R.L.: Introductory Quantum Mechanics, 4th edn. Addison-Wesley, New York (2002)
Livadiotis, G., McComas, D.J.: Beyond Kappa distributions: exploiting Tsallis statistical mechanics in space plasmas. J. Geophys. Res. **114**, A11105 (2009)
Lo, J.Q.-W., Shizgal, B.D.: An efficient mapped pseudospectral method for weakly bound states: vibrational states of He_2, Ne_2, Ar_2 and Cs_2. J. Phys. B: At. Mol. Opt. Phys. **41**, 185103 (2008)
March, R., Barone, P.: Reconstruction of a piecewise constant function from noisy Fourier coefficients by Padé method. SIAM J. Appl. Math. **60**, 1137–1156 (2000)
Martens, J.: The Hermite transform: a survey. J. Appl. Signal Proc. **2006**, 1–20 (2006)
Meijering, E.: A chronology of interpolation: from ancient astronomy to modern signal and image processing. Proc. IEEE **90**, 319–342 (2002)
Messiah, A.: Quantum Mechanics, vol. I. North Holland, Amsterdam (1961)

Meyer, R.: Trigonometric interpolation method for one-dimensional quantum-mechanical problems. J. Chem. Phys. **52**, 2053–2059 (1970)
Meyer-Vernet, N.: Large scale structure of planetary environments: the importance of not being Maxwellian. Planet. Space Sci. **49**, 247–260 (2001)
Mintzer, D.: Generalized orthogonal polynomial solutions of the Boltzmann equation. Phys. Fluids **8**, 1076–1090 (1965)
Moler, C.: Numerical Computing in MATLAB. SIAM, Philadelphia (2008)
Nauenberg, M.: Critique of q-entropy for thermal statistics. Phys. Rev. E **67**, 036114 (2003)
Olmos, D.: Reflection and attachment of spirals at obstacles for the Fitzhugh-Nagumo and Beeler-Reuter models. Phys. Rev. E **81**, 041924 (2010)
Olmos, D., Shizgal, B.D.: A pseudospectral method of solution of Fisher's equation. J. Comput. Appl. Math **193**, 219–242 (2006)
Paul, W., Baschnagel, J.: Stochastic Processes. From Physics to Finance, 2nd edn. Springer, Berlin (2013)
Petrovay, K.: Solar cycle prediction. Living Rev. Sol. Phys. **7**, 6–59 (2010)
Pierrard, V., Lazar, V.: Kappa distributions: theory and applications in space plasmas. Sol. Phys. **267**, 153–174 (2010)
Pindza, E., Patidar, K.C., Ngounda, E.: Robust spectral method for numerical valuation of European options under Merton's jump-diffusion model. Numer. Methods Partial Differ. Equ. **30**, 1169–1188 (2014)
Pinkus, A.: Weierstrass and approximation theory. J. Approx. Theory **107**, 1–66 (2000)
Risken, H., Till, F.: The Fokker-Planck Equation: Methods of Solution and Applications, 2nd edn. Springer, Berlin (1996)
Rivlin, T.J.: An Introduction to the Approximation of Functions. Blaisdell Publishing Co., Toronto (1969)
Russo, G., Smereka, P.: The Gaussian wave packet transform: efficient computation of the semi-classical limit of the Schrödinger equation. Part 1. Formulation and the one dimensional case. J. Comput. Phys. **233**, 192–209 (2013)
Russo, G., Smereka, P.: The Gaussian wave packet transform: efficient computation of the semi-classical limit of the Schrödinger equation. Part 2. Multidimensional case. J. Comput. Phys. **257**, 1022–1038 (2014)
Schwartz, C.: High-accuracy approximation techniques for analytic functions. J. Math. Phys. **26**, 411–415 (1985)
Schumer, J.W., Holloway, J.P.: Vlasov simulations using velocity-scaled Hermite representations. J. Comput. Phys. **144**, 626–661 (1998)
Shen, J., Yu, H.: Efficient spectral sparse grid methods and applications to high dimensional elliptic equations II. Unbounded domains. SIAM J. Sci. Comput. **34**, A1141–A1164 (2012)
Shizgal, B., Karplus, M.: Nonequilibrium contributions to the rate of reaction. II. Isolated multi-component systems. J. Chem. Phys. **54**, 4345–4356 (1971)
Shizgal, B.D., Jung, J.-H.: Towards the resolution of the Gibbs phenomena. J. Comput. Appl. Math. **161**, 41–65 (2003)
Shizgal, B.D., Dridi, R.: Maple code for the calculation of the matrix elements of the Boltzmann collision operators for mixtures. Comput. Phys. Commun. **181**, 1633–1640 (2010)
Stare, J., Balint-Kurti, G.G.: Fourier grid Hamiltonian method for solving the vibrational Schrödinger equation in internal coordinates: theory and test applications. J. Phys. Chem. A **107**, 7204–7214 (2003)
Stefan, W., Viswanathan, A., Gelb, A., Renaut, R.: Sparsity enforcing edge detection method for blurred and noisy Fourier data. J. Sci. Comput. **50**, 536–556 (2012)
Steffens, K.G.: The History of Approximation Theory: From Euler to Bernstein. Birkhäuser, Boston (2006)
Tadmor, E., Tanner, J.: Adaptive mollifiers for high resolution recovery of piecewise smooth data from its spectral information. Found. Comput. Math. **2**, 155–189 (2002)

Tang, T.: The Hermite spectral method for Gaussian-type functions. SIAM J. Sci. Comput. **14**, 594–606 (1993)
Tangman, D.Y., Gopaul, A., Bhuruth, M.: Exponential time integration and Chebyshev discretisation schemes for fast pricing of options. Appl. Numer. Math. **58**, 1309–1319 (2008)
Tatari, M., Haghighi, M.: A generalized Laguerre-Legendre spectral collocation method for solving initial-boundary value problems. Appl. Math. Model. **38**, 1351–1364 (2014)
Trefethen, L.N.: Spectral Methods in MATLAB. SIAM, Philadelphia (2000)
Trefethen, L.N.: Approximation Theory and Approximation Practice. SIAM, Philadelphia (2013)
Tsallis, C.: Non-extensive thermostatics: brief review and comments. Physica A **221**, 277–290 (1995)
Tsallis, C.: Comment on Critique of q-entropy for thermal statistics. Phys. Rev. E **69**, 038101 (2004)
van Kampen, N.G.: Stochastic Processes in Physics and Chemistry, 3rd edn. North Holland, Amsterdam (2007)
Viehland, L.A.: Velocity distribution functions and transport coefficients of atomic ions in atomic gases by a Gram-Charlier approach. Chem. Phys. **179**, 71–92 (1994)
Vozovoi, L., Weill, A., Israeli, M.: Spectrally accurate solution of nonperiodic differential equations by the Fourier-Gegenbauer method. SIAM J. Numer. Anal. **34**, 1451–1471 (1997)
Wang, H., Xiang, S.: On the convergence rates of Legendre approximation. Math. Comput. **81**, 861–877 (2012)
Weideman, W.A.C.: Spectral methods based on non-classical polynomials. In: Gautschi, G., Golub, G.H., Opfer, G. (eds.) Approximations and Computation of Orthogonal Polynomials, pp. 239–251. Burkhauser, Basel (1999)
Weniger, E.J.: On the analyticity of Laguerre series. J. Phys. A: Math. Theor. **41**, 425207 (2008)
Weniger, E.J.: The strange history of B functions or how theoretical chemists and mathematicians do (not) interact. Int. J. Quant. Chem. **109**, 1706–1716 (2009)
Wilbraham, H.: On certain periodic functions. Camb. Dublin Math. J. **3**, 198–201 (1848)
Williams, P.: Quadrature discretization method in tethered satellite control. Appl. Math. Comput. **217**, 8223–8235 (2011)
Xiang, S.: Asymptotics on Laguerre or Hermite polynomial expansions and their applications in Gauss quadrature. J. Math. Anal. Appl. **393**, 434–444 (2012)

Chapter 5
Integral Equations in the Kinetic Theory of Gases and Related Topics

Abstract Integral equations occur in many areas of chemistry, physics and engineering. We consider in this chapter the integral equations that arise in radiative transfer theory and in the study of transport processes in dilute gases modeled with the Boltzmann equation. The first use of a collocation was the Gauss-Legendre quadrature for the solution of the integro-differential isotropic radiative transfer equation. The integral equations that are used to calculate the heat conductivity and viscosity of a dilute monatomic gas are derived with the Chapman-Enskog method of solution of the Boltzmann equation. The integral equations are solved with spectral and pseudospectral methods. These numerical methods are also used to calculate the eigenfunctions and eigenvalues for the linearized collision operator for a one component gas as well as for the linear collision operator for a binary mixture. The solution of the Boltzmann equation for many applications can be expressed in terms of the eigenfunctions and eigenvalues of the collision operators that in general possess an infinite number of discrete eigenvalues and a continuum. The eigenvalue spectra of these operators are calculated and discussed. A pseudospectral method of solution of the Boltzmann integral equation is used for the calculation of the nonequilibrium reaction rate for a model reactive system. A pseudospectral method is also used to solve the Chapman-Enskog integral equation that gives the viscosity of a dilute gas. The relaxation to equilibrium of an initial anisotropic nonequilibrium distribution for a binary gas mixture versus the mass ratio of the two components is studied. Also presented are the spectral solutions of Boltzmann equation for the Milne problem of rarefied gas dynamics, the escape of light atoms from a planetary atmosphere and the calculation of ion mobilities. Pseudospectral methods with nonclassical weight functions are used in some of these applications. The chapter concludes with the study of the relaxation to equilibrium of a one component gas as described by the nonlinear isotropic Boltzmann equation.

5.1 Introduction

Integral equations in which the desired function appears as an integrand in an integral operator occur in diverse subjects in science and engineering, and include such fields as radiative transfer theory (Chandrasekhar 1960), neutron transport (Kourganoff

B. Shizgal, *Spectral Methods in Chemistry and Physics*, Scientific Computation,
DOI 10.1007/978-94-017-9454-1_5

1963; Case and Zweifel 1967; Garcia 1999; Ganapol 2008), kinetic theory (Chapman and Cowling 1970), electromagnetic theory (Volakis and Sertel 2012), geophysics (Eskola 2012), quantum mechanics and scattering theory (Canto and Hussein 2013) and many other applications. Many partial differential equations can be transformed to integral equations with the appropriate Green's functions that satisfy the boundary conditions. There are several textbooks devoted to the solution of integral equations (Tricomi 1985; Delves and Mohamed 1985; Jerri 1999; Kythe and Puri 2002).

In this chapter, spectral and pseudospectral methods are applied to the solution of several different integral equations that arise in radiative transport and in kinetic theory based on the Boltzmann equation. Quadratures are used to reduce a linear integral equation to a set of coupled linear equations for the solution at the quadrature points. The first use of a similar collocation based on Gauss-Legendre quadratures was by Wick (1943) and Chandrasekhar (1944) for the solution of the radiative transfer equation (Chandrasekhar 1960). The overlap of radiative transfer theory with neutron transport also based on the Boltzmann equation is described in the books by Case and Zweifel (1967) and by Ganapol (2008). Recent historical reviews of these research areas were presented by Peraiah (1996) and Shore (2002). An historical account of the development of nuclear reactor theory based on the fundamental advances in radiative transfer and neutron transport was presented by Williams (2000). Although kinetic theory (Chapman and Cowling 1970) and neutron transport theory (Ganapol 2008) are based on the Boltzmann equation, there is a considerable difference in the notation employed. The book by Ganapol (2008) has an extensive bibliography to research papers and monographs on neutron transport theory.

We illustrate the application of spectral and pseudospectral methods to the solution of the integral equations for the Boltzmann equation of kinetic theory. A summary of the Chapman-Enskog method (Hirschfelder et al. 1954; Huang 1967; Chapman and Cowling 1970; Ferziger and Kaper 1972) is presented. This method is a special solution of the Boltzmann equation for a monatomic gas in the collision dominated regime constructed specifically for the calculation of the transport coefficients for diffusion, heat conduction and viscosity in terms of the differential cross sections describing binary collisions between particles. This formalism yields integral equations whose solutions present interesting applications for spectral methods.

The Chapman-Enskog method of solution of the Boltzmann equation provides a derivation of the hydrodynamic equations of fluid mechanics. This is an alternative approach to the methods based on control volumes and conservation principles presented in books on fluid dynamics (Fletcher 1991; Kundu et al. 2012). In physical situations where the gas density is very low and the mean free path, the average distance travelled between particle collisions, is comparable to or greater than the local scale length, the hydrodynamic equations are no longer valid and a kinetic theory treatment is required. This is the subject of rarefied gas dynamics (Sone 2007; Struchtrup 2005) and pertains to shock waves, aerodynamics, microfluidics (Gad-el-Hak 1999) and the high altitude regions of planetary atmospheres from which energetic atoms and ions can escape (Fahr and Shizgal 1983; Shizgal and Arkos 1996; Pierrard 2003; Echim et al. 2011). The direct simulation Monte Carlo method (Bird 1994) is often used to study such rarefied gaseous systems.

In this chapter, spectral and pseudospectral methods are used to study the spectral properties of the linearized collision operator defined by Eq. (5.41) as well as the analogous linear operator for a binary gas, Eq. (5.104). A spectral method is used to calculate the nonequilibrium effects that occur in a simple reactive system (Shizgal and Karplus 1970). The pseudospectral solutions of the Boltzmann equation for the viscosity in a one component gas (Siewert 2002; Sharipov and Bertoldo 2009) and the equilibration of nonequilibrium distributions in a binary gas are also described (Shizgal and Blackmore 1983).

The departure of distribution functions from spherical symmetry are considered in the applications to the Milne problem (Lindenfeld and Shizgal 1983) and for the escape of light species from a planetary atmosphere (Shizgal and Blackmore 1986). We review the development of spectral methods used to solve the Boltzmann equation for the drift of ions in a background gas under the influence of a uniform electrostatic field (Viehland 1994). In the last section, the nonlinear isotropic Boltzmann equation is used to study the approach to equilibrium of a one component gas and the relationship with the spectral properties of the linearized operator is discussed. A finite difference method is used which requires a cubature for the evaluation of the integral collision operator. A review of alternative methods based on spectral methods with both polynomial basis functions (Weinert et al. 1980; Ender et al. 2011) as well as Fourier methods (Filbet and Mouhot 2011; Wu et al. 2013) is presented.

5.2 Classes of Integral Equations and the Use of Quadratures

Fredholm integral equations of the 1st and 2nd kind (Delves and Mohamed 1985; Jerri 1999; Slevinsky and Safouhi 2008) are defined by

$$\int_a^b K(x, y) f(y) dy = S(x), \tag{5.1}$$

and

$$\int_a^b K(x, y) f(y) dy - g(x) f(x) = S(x), \tag{5.2}$$

respectively, where the kernel, $K(x, y)$, and the functions $g(x)$ and $S(x)$ are known. These integral equations can also be expressed as eigenvalue problems

$$\int_a^b K(x, y) \phi_n(y) dy = \lambda_n \phi_n(x), \tag{5.3}$$

and

$$\int_a^b K(x, y)\phi_n(y)dy - g(x)f(x) = \lambda_n \phi_n(x), \tag{5.4}$$

respectively. Volterra integral equations, which we do not consider, are similar with the upper boundary $b = x$.

The method of solution chosen for a particular problem depends on the behavior of the kernel versus x and y. If the kernel is well behaved in both variables, the solution can be easily computed. If there is a discontinuous lower order derivative or a strong singularity, then the numerical method to be used should be adapted to the particular behavior of the kernel. The types of singularities include a logarithmic singularity for which $K(x, y) = k(x, y)\log|x - y|$ or an algebraic singularity for which $K(x, y) = k(x, y)/|x - y|$. This aspect has been discussed by Atkinson and Shampine (2008) and MATLAB codes for the numerical solution of a large class of integral equations are readily available (Driscoll 2010).

Many current solution methods of integral equations involve the reduction of the integral equation to a set of algebraic equations with a suitable quadrature procedure with grid points $\{x_i\}$ and associated weights $\{w_i\}$ based on polynomials orthogonal with respect to weight function $w(x)$ on the interval $[a, b]$. With the use of a quadrature to perform the integral over y in Eq. (5.2), the integral operator is reduced to the sum over quadrature weights and points, that is

$$\sum_{i=1}^{N} W_i K(x, x_i) f(x_i) - g(x)f(x) = S(x), \tag{5.5}$$

where $W_i = w_i/w(x_i)$. If we evaluate this equation at the same set of grid points, we have the system of linear algebraic equations,

$$\sum_{i=1}^{N} W_i K(x_j, x_i) f(x_i) - g(x_j)f(x_j) = S(x_j). \tag{5.6}$$

Inversion of this set of linear equations gives the desired solution at the grid points. This is the method often used to solve integral equations and referred to as the Nyström method (Delves and Mohamed 1985; Kythe and Puri 2002). Obviously we need to know further details of the behavior of the kernel in order to choose the appropriate quadrature, and study the convergence of the solution.

To illustrate the method, this technique is used to solve the integral equation,

$$\int_{-1}^{1} \sinh(x + y)\phi(y)dy - \phi(x) = -x^2, \tag{5.7}$$

which is Example 2.2.2 from Kythe and Puri (2002). This equation has the exact solution

$$\phi_{exact}(x) = \alpha \sinh(x) + \beta \cosh(x) + x^2, \tag{5.8}$$

where $\alpha = 16e^3(e^2-5)/(1-34e^4+e^8)$, $\beta = [1+\frac{1}{4}(\frac{1}{e^2}-e^2)]\alpha$ and $e = 2.718282\ldots$ Since the domain is $x \in [-1, 1]$, we choose a Gauss-Legendre quadrature, for which $W_i = w_i$ and reduce the integral equation to a coupled set of linear algebraic equations for the solution evaluated at the quadrature points analogous to the linear set of equations, Eq. (5.6). We have that

$$\sum_{i=1}^{N} w_i \sinh(x_j + x_i)\phi^{(N)}(x_i) - \phi^{(N)}(x_j) = -x_j^2, \tag{5.9}$$

and the solution is represented by $\phi^{(N)}(x_i)$ at the N quadrature points. We measure the error of the numerical solution in comparison with the exact solution as given by the L^2 error

$$E_2^{(N)} = \sqrt{\frac{1}{N}\sum_{n=1}^{N}\left[\phi^{(N)}(x_i) - \phi_{exact}(x_i)\right]^2}. \tag{5.10}$$

The numerical solution of Eq. (5.9) and the $E_2^{(N)}$ error are computed with a MATLAB code. The variation of $\log_{10}[E_2^{(N)}]$ versus N is shown in Fig. 5.1. The solution converges to machine accuracy very quickly owing to the smooth, well behaved kernel and inhomogeneous term. The variation of the exact solution given by Eq. (5.8) is well approximated by a low order polynomial for $x \in [-1, 1]$ which explains the rapid convergence. There are numerous examples of such integral equations in Kythe and Puri (2002).

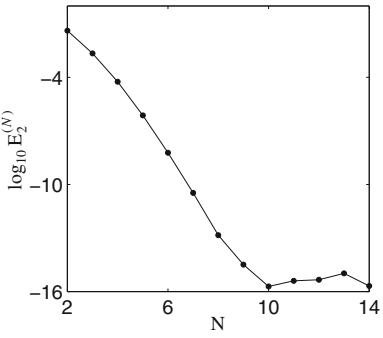

Fig. 5.1 Variation of the least squares error, $\log_{10} E_2^{(N)}$, for the integral equation, Eq. (5.7), versus the number of Gauss-Legendre quadrature points, N

5.3 Radiative Transfer and Neutron Transport Theory

The transfer of radiation in matter is an important aspect of atmospheric science and climate (Stamnes et al. 1988; Peraiah 1996; Liou 2002; Thomas and Stamnes 2002), astrophysics (Rybicki and Lightman 1979; Rybicki 1996), satellite remote sensing (Liang 2005), medical physics (Kan et al. 2013), neutron transport (Siewert 2000; Yilmazer and Kocar 2009) and other applications (Shore 2002). The propagation of radiation through a medium involves both absorption and reemission of the radiation. Radiative transfer theory is concerned with the variation of the radiative intensity with position in the medium, the direction of propagation as well as the frequency.

We consider the radiative transfer equation in recognition that almost every current publication in this field cites the original work by Chandrasekhar (1960). The numerical treatment introduced by Wick (1943) and developed further by Chandrasekhar (1960) is perhaps the first use of a quadrature, specifically the Gauss-Legendre quadrature, to reduce the radiative trnasfer equation, Eq. (5.14) to discrete form.

The system of interest is the plane-parallel atmosphere shown in Fig. 5.2. We define the radiative intensity, $I(z, \theta)$, with assumed azimuthal symmetry, as the energy contained in a pencil of radiation at position z moving in direction θ with respect to the polar direction. The intensity of radiation directed along z changes owing to the absorption of radiation by the medium, characterized by a mass attenuation coefficient, κ, and density $\rho(z)$. The change in incident intensity, I, directed at an angle θ with the vertical direction on traversing a slab of the medium of vertical thickness dz is

$$dI = -\kappa \rho I dz/\mu, \tag{5.11}$$

where $\mu = \cos\theta$. We now transform the vertical altitude, z, to optical depth, τ, defined by

$$d\tau = -\kappa \rho I dz, \tag{5.12}$$

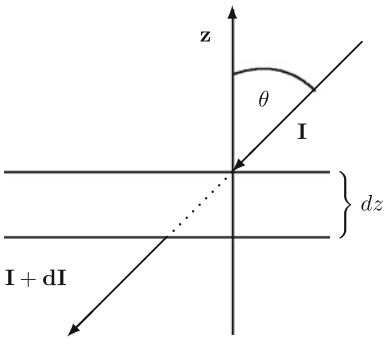

Fig. 5.2 Optical depth and radiative absorption

or in integral form

$$\tau(z) = \int_z^\infty \kappa\rho dz. \tag{5.13}$$

The integral of Eq. (5.11) in the absence of the emission of radiation from the medium gives the Beer-Lambert law,

$$I(\tau, \mu) = I(0)e^{-\tau(z)/\mu}.$$

In general, there is stimulated radiation emitted from the medium and the radiative intensity $I(\tau, \mu)$ is given by the radiative transfer equation,

$$\mu \frac{dI(\tau, \mu)}{d\tau} = I(\tau, \mu) - \frac{1}{2}\int_{-1}^{1} k(\mu, \mu')I(\tau, \mu')d\mu', \tag{5.14}$$

where the kernel, $k(\mu, \mu')$, accounts for the anisotropic absorption and reemission of radiation induced by the incident radiation.

With the assumption of isotropic scattering, that is $k(\mu, \mu') = 1$, we have the radiative transfer equation in the form

$$\mu \frac{dI(\tau, \mu)}{d\tau} = I(\tau, \mu) - \frac{1}{2}\int_{-1}^{1} I(\tau, \mu')d\mu'. \tag{5.15}$$

This is the simplest integro-differential equation of radiative transfer theory and is related to several other problems in rarefied gas dynamics. The radiative intensity, $I(\tau, \mu)$, varies with position, τ, and also with direction through μ. A collocation based on Gauss-Legendre quadratures is used to solve Eq. (5.15). The presentation follows the work in Chandrasekhar (1960) with a change in notation.

We use the quadrature on the interval $\mu \in [-1, 1]$ with $2N$ quadrature points μ_i, $i = \pm 1, \pm 2, \ldots, \pm N$ and corresponding weights w_i. We note that since the number of quadrature points is even, there is no point at $\mu = 0$. The discretized version of Eq. (5.14) is

$$\mu_i \frac{dI_i(\tau)}{d\tau} = I_i(\tau) - \frac{1}{2}\sum_{j=-N, j\neq 0}^{N} w_j I_j(\tau), \tag{5.16}$$

where $I_i(\tau) \equiv I(\tau, \mu_i)$. If the solution is assumed to be of the form, $I_i(\tau) = a_i e^{-\lambda\tau}$, then

$$a_i(1 + \mu_i\lambda) = \frac{1}{2}\sum_{j=-N, j\neq 0}^{N} w_j a_j = C, \tag{5.17}$$

with

$$a_i = \frac{C}{1 + \lambda\mu_i}, \tag{5.18}$$

which when substituted into Eq. (5.17) gives

$$1 = \frac{1}{2} \sum_{j=-N, j\neq 0}^{N} \frac{w_j}{1 + \lambda\mu_j} = \sum_{j=1}^{N} \frac{w_j}{1 - \lambda^2\mu_j^2}. \tag{5.19}$$

In the second equality we have used $w_{-j} = w_j$ and $\mu_{-j} = -\mu_j$. Because the sum of the weights is normalized to unity, $\sum_{j=1}^{N} w_j = 1$, $\lambda^2 = 0$ satisfies Eq. (5.19), which is the eigenvalue equation for the $2N - 2$ eigenvalues and two zero eigenvalues. The eigenvalues necessarily come in positive and negative pairs, $\pm\lambda_n, n = 1, 2, \ldots, N - 1$.

The roots of Eq. (5.19) each lie between the reciprocal of the quadrature points $[1/\mu_{i+1}, 1/\mu_i]$. A simple search combined with a bisection method gives the eigenvalues listed in Table 5.1. Alternatively, one can rewrite Eq. (5.19) as a polynomial of degree N and search for the roots of the polynomial (Kawabata et al. 1991). This can be numerically unstable for higher orders. The entries up to $N = 8$ agree with the limited results in Table VIII in Chandrasekhar (1960).

It is clear that the eigenvalues do not appear to converge to distinct values. The reason for this is that the discrete spectrum of the radiative transfer equation consists of only two zero eigenvalues. The remaining eigenvalues all lie in the continuum and hence there is no convergence. The mathematical properties of the continuum eigenfunctions have been the subject of considerable research (Case and Zweifel 1967; Liou 1973; McCormick and Kuščer 1973; Stamnes et al. 1988; Kuščer and McCormick 1991; Ven Den Eynde et al. 2007) (and references therein). In Sects. 5.5 and 5.6, we compare this behaviour with the spectral properties of the Boltzmann collision operators for a dilute monatomic gas that are characterized by an infinite number of discrete eigenvalues and a continuum.

Table 5.1 Eigenvalues of the radiative transfer equation, Eq. (5.14)

N	λ_1	λ_2	λ_3	λ_4	λ_5	λ_6	q
2	1.97203						0.6940
6	1.225211	3.202945					0.7039
8	1.103188	1.591779	4.458086				0.7069
10	1.059426	1.297814	1.987330	5.721175			0.7082
12	1.038632	1.183180	1.519150	2.394194	6.987899		0.7089
14	1.027106	1.125058	1.330224	1.752305	2.806740	8.256597	0.7094
						Exact[a]	0.710446

[a] Loyalka and Naz (2008)

We note that

$$I_i = b(\tau + s_i), \tag{5.20}$$

is also a solution to the radiative transfer equation, Eq. (5.14), which leads to the result

$$\mu_i = s_i - \frac{1}{2}\sum_{j=1}^{N} w_j s_j, \tag{5.21}$$

and satisfied by

$$s_i = q + \mu_i. \tag{5.22}$$

To ensure that the solution remains finite for large τ, the terms with positive λ_i must be eliminated from the solution. Thus the general solution is

$$I_i = b\left[\sum_{n=1}^{N-1} \frac{c_n e^{-\lambda_n \tau}}{1 + \mu_i \lambda_n} + \tau + \mu_i + q\right]. \tag{5.23}$$

The constants c_n $(n = 1, 2, \ldots, N-1)$ and q are determined with the boundary condition that there is no incident radiation at $\tau = 0$, that is,

$$I(0, \mu) = 0, \quad -1 \le \mu \le 0. \tag{5.24}$$

With this boundary condition, $c_{-n} = 0$ at $\tau = 0$ and

$$\sum_{n=1}^{N-1} \frac{c_n}{1 - \lambda_n \mu_i} - \mu_i + q = 0 \quad (i = 1, 2, \ldots, N), \tag{5.25}$$

which are N equations for the $N-1$ constants, c_n, and the extrapolation length, q. The physical significance of the extrapolation length is discussed later.

The results for q in Table 5.1 show that the convergence of the Gauss-Legendre quadrature is slow. This arises because the numerical method cannot provide a good fit to the boundary condition that requires that the radiative intensity vanishes on the half space $\mu \in [-1, 0]$. There have been many discussions and improvements and in particular the use of half-range Legendre polynomials referred to as the "double Gauss" method (Sykes 1951; Liou 1973; Stamnes et al. 1988; Ven Den Eynde et al. 2007).

Radiative transfer theory has its origins in astrophysics (Rybicki and Lightman 1979) and the interest to determine the intensity of the emergent radiation from a star and the observation that it decreases from the centre of the disc to the limb, a phenomenon known as limb darkening (Milne 1921). Thus, the radiative transfer

problem is often referred to as a Milne problem which has many different variants. We provide a very brief overview of the analysis and refer readers to the original reference (Chandrasekhar 1960) for further details. It is useful to define two moments of the radiative intensity, namely

$$F = 2\sum_{i=1}^{N-1} w_i \mu_i I_i,$$
$$K = \frac{1}{2}\sum_{i=1}^{N-1} w_i \mu_i^2 I_i, \tag{5.26}$$

and one can show that $F = 4b/3$, where b is the multiplicative constant in Eq. (5.23). We can also show that $K = F(\tau + q)/4$. The emergent intensity is then

$$I(0, \mu) = \frac{3}{4} F \sum_{k=1}^{N-1} \frac{c_k}{1 + \lambda_k \mu} + \mu + q, \tag{5.27}$$

which is one of the important results sought.

The emergent radiation can be related to the Chandrasekhar $H(\mu)$ function. This requires several new definitions and considerable but straightforward algebra (Chandrasekhar 1960). The result is the relation

$$I(0, \mu) = \frac{\sqrt{3}}{4} F H(\mu), \tag{5.28}$$

where the Chandrasekhar H function is the solution of the nonlinear integral equation

$$H(\mu) = 1 + \frac{1}{2} a H(\mu) \int_0^1 \frac{H(\mu')}{\mu + \mu'} d\mu'. \tag{5.29}$$

Although the detailed derivations have not been provided, this nonlinear integral equation is of considerable interest as the object of several different numerical solution methods. It has been solved with a Simpson's rule (Hiroi 1994), rational Chebyshev functions (Boyd 2005), analytic approximations (Davidović et al. 2008), polynomial approximations (Kawabata and Limaye 2011), integral representations (Jablonski 2013) and other approaches cited in these references. It is remarkable that there is continued interest almost 70 years after the original publication by Chandrasekhar and Breen (1947).

In Sect. 5.7.2, we consider the Milne problem of rarefied gas dynamics (see Fig. 5.16) for a binary hard sphere gas with a test particle of mass m dilutely dispersed in a background gas of mass M. The Milne problem reduces to the radiative transfer equation for the Lorentz limit, that is $M/m \to \infty$. We use a spectral method to solve the Milne problem based on the concepts developed in this section. A similar

Milne problem was studied with a Fokker-Planck equation for Coulomb collisions (Barrett et al. 1992) as well as in the modeling of the sheath problem in plasma physics (Vasenkov and Shizgal 2000). The Milne problem is the basis for a model of the escape of light atoms from a planetary atmosphere presented in Sect. 5.7.3 (Fahr and Shizgal 1983; Shizgal and Blackmore 1986).

Neutron transport theory is the study of the time and spatial dependence of the neutron velocity distribution function in different materials or moderators given a steady or pulsed source of neutrons. The theory is based on the Boltzmann equation for neutrons analogous to dilute gases. It remains a very active area of research for physicists, applied mathematicians and numerical analysts. Neutron transport has developed alongside work in radiative transfer theory (Kourganoff 1963). The distinction between the two fields is that in radiative transfer the photons move at the speed of light and for neutrons there is a speed distribution to determine. Often the radiative transfer problem noted in Eq. (5.14) is referred to as the "one speed" problem. This implies that the neutrons all move at the same speed as do photons. There are several standard references for both subjects (Davison 1957; Kourganoff 1963; Williams 1966; Case and Zweifel 1967; Thomas and Stamnes 2002). An historical account of the development of the subject was provided by Shore (2002).

5.4 The Boltzmann Equation and Transport Theory

The central quantity of interest in the kinetic theory of gases is the distribution function for a large collection or ensemble of particles without internal degrees of freedom representing some species such as electrons, ions, neutrons, photons, atoms, etc. At sufficiently low densities, the single particle distribution function, f($\mathbf{v}$, $\mathbf{r}$,t), is sufficient to describe the state of the system. The distribution function that depends on the three dimensional velocity, $\mathbf{v}$, the three dimensional position $\mathbf{r}$, and the time, t, is defined such that

$$f(\mathbf{v}, \mathbf{r}, t)\mathrm{d}\mathbf{v}\mathrm{d}\mathbf{r} = \text{ number of particles with velocity in } [\mathbf{v}, \mathbf{v} + \mathrm{d}\mathbf{v}] \text{ and position in } [\mathbf{r}, \mathbf{r} + \mathrm{d}\mathbf{r}] \text{ at time t.}$$

The Boltzmann equation is a seven dimensional nonlinear integro-differential equation for the one particle distribution function, $f(\mathbf{v}, \mathbf{r}, t)$, given by

$$\frac{\partial f}{\partial t} + \mathbf{v} \cdot \nabla f + \frac{\mathcal{F}}{m} \cdot \nabla_{\mathbf{v}} f = \int \int [f' f_1' - f f_1] g \sigma(g, \Omega) d\Omega d\mathbf{v_1}, \tag{5.30}$$

where the gradient operators are ∇ in $\mathbf{r}$ and $\nabla_{\mathbf{v}}$ in $\mathbf{v}$.

The three terms on the left hand side of this equation are collectively referred to as the drift term where $\mathcal{F}$ is an external force. The term on the right hand side is the nonlinear collision term parameterized by the elastic collision cross section, $\sigma(g, \Omega)$, where the relative velocity of a pair of particles is $\mathbf{g} = \mathbf{v}_1 - \mathbf{v}$ and Ω is the scattering

solid angle. The prime, $f' \equiv f(\mathbf{v}')$, denotes the post-collisional velocity, $\mathbf{v}'$, and is expressed in terms of the pre-collisional velocity, $\mathbf{v}$, as given by Eqs. (5.47)–(5.49). The kinetic theory of gases is an integral part of theoretical chemistry and physics (Hirschfelder et al. 1954; Liboff 2003; Kremer 2010).

A Boltzmann equation is used to model a large number of systems in astrophysics (Spitzer and Härm 1958; Lightman and Shapiro 1978; Buhmann 2004; Binney and Tremaine 2008), space science (Fahr and Shizgal 1983; Pierrard and Lazar 2010; Khazanov 2011), semiconductor physics (Jüngel 2009), nuclear reactor technologies (Hebert 2009), radiative transfer (Chandrasekhar 1960), radiotherapy (Kan et al. 2013) plasma physics (Boyd and Sanderson 2003), fusion machines (Atenzi and Meyer-Ter-Vehn 2004) and many more. The different systems and processes that can be studied with the Boltzmann equation or Boltzmann-like equations is truly remarkable.

The main objective of this section is to apply spectral and pseudospectral methods to the integral equations that arise in the application of the Boltzmann equation to several physical problems. A brief overview of the derivation of these integral equations in kinetic theory is provided in the sections that follow.

5.4.1 The Chapman-Enskog Method of Solution of the Boltzmann Equation for Transport Coefficients

The Chapman-Enskog method of solution of the Boltzmann equation was developed independently by Sydney Chapman[1] and David Enskog[2] for a particular purpose, namely the calculation of transport coefficients for a dilute monatomic gas. The transport coefficients are the diffusion coefficient, the viscosity and the heat conductivity. They serve to relate fluxes of particles, momentum and energy with the corresponding gradients. These relations between the fluxes and gradients such as Fourier's law for heat conduction (de Groot and Mazur 1984) are referred to as linear phenomenological laws. The Chapman-Enskog method provides a separate integral equation for each transport process. The transport coefficients, such as the viscosity discussed in Sect. 5.4.5, are expressed as integrals of the solution of a particular integral equation. The details of the Chapman-Enskog method are described in standard texts (Huang 1967; Chapman and Cowling 1970; Ferziger and Kaper 1972; Kremer 2010). A concise overview of the methodology follows.

A small departure from a Maxwellian is assumed to occur owing to small macroscopic drift velocity and/or temperature gradients. The distribution function is

[1] Sydney Chapman (1888–1970) was a British mathematician and geophysicist who developed the Chapman-Enksog method of solution of the Boltzmann equation and contributed to the theory of stochastic processes. He also made several fundamental contributions to geophysics.

[2] David Enskog (1884–1947) was a Swedish mathematical physicist who contributed to the kinetic theory of gases with the method of solution of the Boltzmann equation developed with Chapman.

written as a small perturbation of the "local" Maxwellian, $F[\mathbf{v}, n(\mathbf{r}, t), T(\mathbf{r}, t), W(\mathbf{r}, t)]$, parameterized by the particle density $n(\mathbf{r}, t)$, the temperature, $T(\mathbf{r}, t)$ and the flow velocity of the gas, $W(\mathbf{r}, t)$; see Eq. (5.32). With the assumption that the distribution is slightly perturbed from the local Maxwellian, F, we set

$$f(\mathbf{v}, \mathbf{r}, t) = F(\mathbf{v}, n, T, \mathbf{W})\Big[1 + \epsilon\phi(\mathbf{v})\Big], \tag{5.31}$$

where the parameter ϵ is taken to be very small and $\phi(\mathbf{v})$ is sought. Equation (5.31) is often extended as a power series in ϵ as discussed later.

The Chapman-Enskog method proceeds as follows. With the substitution of Eq. (5.31) in (5.30), the term zeroth order in ϵ is

$$\int\int [F'F_1' - FF_1] g\sigma(g, \Omega) d\Omega d\mathbf{v_1} = 0,$$

and defines the local Maxwellian,

$$F(v, n, \mathbf{W}, T) = n(\mathbf{r}, t)\left[\frac{m}{2\pi k_B T(\mathbf{r}, t)}\right]^{3/2} \exp\left[\frac{-m(\mathbf{v} - \mathbf{W}(\mathbf{r}, t))^2}{2k_B T(\mathbf{r}, t)}\right], \tag{5.32}$$

where k_B is the Boltzmann constant, m is the particle mass, and the number density, $n(\mathbf{r}, t)$, is defined by,

$$n(\mathbf{r}, t) = \int F_{LM}(\mathbf{v}, \mathbf{r}, t) d\mathbf{v}. \tag{5.33}$$

The local Maxwellian, Eq. (5.32), supports a flux and the drift or flow velocity, $\mathbf{W}(\mathbf{r}, t)$, is

$$\mathbf{W}(\mathbf{r}, t) = \frac{1}{n(\mathbf{r}, t)} \int F_{LM}(\mathbf{v}, \mathbf{r}, t) \mathbf{v} d\mathbf{v}. \tag{5.34}$$

The temperature, $T(\mathbf{r}, t)$, is a measure of the average thermal energy of the gas and is related to the diagonal element of the pressure tensor

$$\mathbf{P} = m \int f(\mathbf{v}, \mathbf{r}, t)(\mathbf{v} - \mathbf{W})(\mathbf{v} - \mathbf{W}) d\mathbf{v}, \tag{5.35}$$

and $\mathbf{P}^{(LM)} = p\mathbf{I}$ where $\mathbf{I}$ is the unit matrix and $p = nk_B T$ is the ideal gas law.

For nonequilibrium systems, there is a departure from the equilibrium Maxwell-Boltzmann distribution and the pressure tensor is of the form

$$\mathbf{P} = p\mathbf{I} + \mathbf{\Pi}. \tag{5.36}$$

where $\mathbf{\Pi}$ depends on the velocity gradients. If there is a temperature gradient present, then there is a heat flux defined as

$$\mathbf{q} = \frac{m}{2}\int f(\mathbf{v},\mathbf{r},t)(\mathbf{v}-\mathbf{W})(\mathbf{v}-\mathbf{W})^2 d\mathbf{v}. \tag{5.37}$$

The Boltzmann equation is rewritten with the collision term multiplied by the factor $1/\epsilon$ so as to explicitly take into account the assumption that the collision operator is dominant relative to the drift term, that is

$$\frac{\partial f}{\partial t} + \mathbf{v}\cdot\nabla f + \frac{\mathcal{F}}{m}\cdot\nabla_{\mathbf{v}} f = \frac{1}{\epsilon}\int\int [f' f_1' - f f_1] g\sigma(g,\Omega) d\Omega d\mathbf{v_1}. \tag{5.38}$$

The parameter ϵ is often identified as the Knudsen[3] number, the ratio of the mean-free-path, L_{mfp}, to some macroscopic length scale, H, that is $Kn = L_{mfp}/H$. In the collision dominated situation, $Kn \ll 1$.

The equation of order ϵ is obtained with the drift term evaluated with $f \to F$ and the collision operator linear in $\phi(v)$. To this order in ϵ, the derivatives in the drift term on the left hand side of the Boltzmann equation are evaluated implicitly through the $\mathbf{r}$ and t variation of $n(\mathbf{r},t)$, $T(\mathbf{r},t)$, $W(\mathbf{r},t)$ in the local Maxwellian, and $\phi(\mathbf{v})$ does not contribute.

In order to evaluate the left hand side of Eq. (5.30) in this way, we need the $(\mathbf{r},t)$ variation of n, $\mathbf{W}$ and T. These relations can be obtained by noting that the particle number, momentum and energy are conserved in a binary elastic collision. Thus, we multiply successively the Boltzmann equation by m, $m\mathbf{v}$ and $mv^2/2$, known as the "summational invariants", and integrate over $\mathbf{v}$. The integral over the collision operator multiplied by these quantities gives zero owing to their conservation. The details are provided in other texts (Hirschfelder et al. 1954; Chapman and Cowling 1970; Ferziger and Kaper 1972). The result of this calculation, after some algebra, of the so-called "equations of change", are the set of hydrodynamic, non-dissipative fluid dynamic equations, referred to as the Euler equations, given by

$$\begin{aligned} \frac{\partial\rho}{\partial t} + \nabla\cdot(\rho\mathbf{W}) &= 0, \\ \rho\frac{D\mathbf{W}}{Dt} + \nabla p &= \rho\mathcal{F}, \\ nk\frac{DT}{Dt} + \frac{3T}{2}(\nabla\cdot\mathbf{W}) &= 0, \end{aligned} \tag{5.39}$$

where $\rho(\mathbf{r},t) = mn(\mathbf{r},t)$ and

$$\frac{D}{Dt} = \frac{\partial}{\partial t} + \mathbf{W}\cdot\nabla.$$

[3] Martin Knudsen (1871–1949) was a Danish physicist known for his work on the kinetic theory of gases and the Knudsen number which measures the degree of rarefaction of dilute gases.

The term linear in ϵ which gives the integral equation for $\phi(\mathbf{v})$ involves the evaluation of the drift term with f replaced with F and the evaluation of the drift term operator on F implicitly using the Euler fluid equations. The result, after considerable tensorial algebra using the chain rule for the derivatives, is the integral equation

$$J(\phi) = F\left[(x^2 - 5/2)\mathbf{v} \cdot \nabla \ln T + 2(\mathbf{vv} - \frac{1}{3}v^2\mathbf{I}) : \nabla \mathbf{W}\right], \tag{5.40}$$

where $x = v\sqrt{m/2k_BT}$ is the reduced speed and the linearized collision operator is given by

$$J(\phi) = \int\int F_1 F\left[\phi_1' + \phi' - \phi_1 + \phi\right]\sigma(g,\theta)d\Omega d\mathbf{v}_1. \tag{5.41}$$

It can be shown that J is a negative definite self-adjoint rotationally invariant operator. The matrix representation of J in Legendre polynomials is diagonal as previously noted in the discussion of the quadrature evaluation of the eigenvalues for the Maxwell-molecule model in Chap. 3.

We now write the solution of Eq. (5.40) in the form

$$\phi = -\mathbf{A} \cdot \nabla \ln T - \mathbf{B} : \nabla \mathbf{W}, \tag{5.42}$$

where the vector $\mathbf{A}$ and tensor $\mathbf{B}$ are written as

$$\begin{aligned} \mathbf{A} &= A(v)\mathbf{v}, \\ \mathbf{B} &= B(v)\mathbf{v}^o\mathbf{v}, \end{aligned} \tag{5.43}$$

and $\mathbf{v}^o\mathbf{v} = \mathbf{vv} - \frac{1}{3}v^2\mathbf{I}$ is a traceless tensor. The functions $A(v)$ and $B(v)$ satisfy the integral equations,

$$J[A(v)\mathbf{v}] = (x^2 - 5/2)\mathbf{v}F, \tag{5.44}$$

and

$$J[B(v)\mathbf{v}^o\mathbf{v}] = 2\mathbf{v}^o\mathbf{v}F. \tag{5.45}$$

where $x = v\sqrt{m/2k_BT_b}$ is the reduced speed. The details of this calculation, which involve considerable tensorial algebra, are straightforward and can be found in standard references (Huang 1967; Chapman and Cowling 1970; Ferziger and Kaper 1972). An important aspect of the Chapman-Enskog method is that the solutions of the homogeneous equations corresponding to Eqs. (5.44) and (5.45), namely the "summational invariants", are orthogonal to the inhomogeneous functions in these integral equations. This ensures the existence of solutions. We will discuss this again in Sect. 5.4.4 for a simpler physical problem.

The solutions $A(v)$ and $B(v)$ are used to determine the temperature dependence of the heat conductivity and viscosity for a dilute gas given the differential cross section, $\sigma(g, \Omega)$, for binary particle collisions. The Sonine-Laguerre polynomials, $S_\alpha^{(n)}(x^2)$, are the basis functions almost always used to solve these integral equations with $\alpha = 3/2$ for Eq. (5.44) and $\alpha = 5/2$ for Eq. (5.45). This formalism forms the basis for the determination of interatomic potentials from measurements of transport coefficients (Hirschfelder et al. 1954; Pascal and Brun 1993; Oh 2013).

A different integral equation is solved for each transport process and the transport processes of different tensorial order do not couple, consistent with the Curie principle of irreversible thermodynamics (de Groot and Mazur 1984); see also (Andersen 1969) and Appendix A of Shizgal and Karplus (1970) where chemical reactions are included. Mixtures of gases can also be considered and the algebra becomes more involved. We note that theoretical descriptions of transport phenomena in polyatomic gases are available (Wang-Chang and Uhlenbeck 1951; Snider 1960; McCourt et al. 1991; Singh et al. 1996; Brun 2009). Our primary interest is the spectral and pseudospectral methods for the solution of the integral equations.

The Chapman-Enskog method provides to order ϵ the Navier-Stokes equations of fluid mechanics by including the dissipative transport terms in the "equations of change". The method is usually presented as a power series expansion in ϵ with terms of order ϵ^2 and ϵ^3 in addition to the term in ϵ in Eq. (5.31). This expansion is believed to be a type of asymptotic expansion where perhaps only the first few terms have physical meaning. At each level, the resulting hydrodynamic equations are modified, that is the Euler equations for zero order in ϵ, the Navier-Stokes equations of order ϵ and for higher orders in ϵ there are the Burnett and the Super-Burnett hydrodynamic equations (Grad 1949; Cercignani 1988). A very good overview of the effort to extend the description of gaseous flows to the larger Knudsen number regime was provided by Agarwal et al. (2001). This overlaps the approach developed by Grad (1949) and referred to as the Grad 13-moment method (Struchtrup 2005).

The breakdown of hydrostatic equilibrium and the Chapman-Enskog approach occurs in particular at high altitudes of the terrestrial atmopshere where collisions are infrequent (Fahr and Shizgal 1983). This also applies to the solar atmosphere for which there is a supersonic expansion of the stellar plasma, referred to as the solar wind. There are both fluid models (Parker 1965) and kinetic theory models (Lemaire and Scherer 1973) to describe the expansion of the solar atmosphere. This is another example of the need for a kinetic theory in the $Kn \approx 1$ regime (Lemaire 2010; Echim et al. 2011). The loss of ions from the terrestrial atmosphere at high latitudes along open magnetic field lines, referred to as the polar wind (Lemaire and Scherer 1970; Lie-Svendsen and Rees 1996; Pierrard and Lemaire 1998) is another example. There is an ongoing discussion as to the relationship of both fluid and kinetic models for the solar wind expansion (Parker 2010; Lemaire 2010) These discussions are important to note but are beyond the scope of this book. However, there is some overlap with the Milne problem in Sect. 5.7.2 and the escape of light atoms or ions from planetary atmospheres in Sect. 5.7.3.

5.4.2 The Linearized Collision Operator, J, in the Boltzmann Equation

A fundamental problem in the kinetic theory of gases is the relaxation of an initial nonequilibrium distribution to the equilibrium Maxwellian distribution. We consider a one component spatially uniform gaseous system for which the linearized Boltzmann equation in the absence of external fields is the initial value problem of the form

$$\frac{\partial f(\mathbf{v},t)}{\partial t} = J[f(\mathbf{v},t)]. \tag{5.46}$$

The kinematics of an elastic collision that relate the post-collisional ($\mathbf{v}'$) and pre-collisional ($\mathbf{v}$) velocity variables in Eq. (5.41) are required to define the collision operator, J, (Chapman and Cowling 1970; Cercignani 1988; Ferziger and Kaper 1972; Liboff 2003; Kremer 2010). In an elastic collision, depicted in Fig. 5.3, the relative velocity vector, $\mathbf{g}$, is rotated to the new orientation, $\mathbf{g}'$, while the magnitudes remain the same, that is $|\mathbf{g}'| = |\mathbf{g}|$ owing to energy conservation. The vector $\mathbf{k}$, referred to as the "apse-line vector", is the external bisector so that $\theta = \pi - 2\chi$. Thus, we have the relation

$$\mathbf{g}' = \mathbf{g} - 2(\mathbf{k}\cdot\mathbf{g})\mathbf{k}. \tag{5.47}$$

In terms of the centre of mass velocity

$$\mathbf{G} = \frac{m_1\mathbf{v}_1 + m_2\mathbf{v}_2}{m_1 + m_2}, \tag{5.48}$$

we have that

$$\begin{aligned} \mathbf{v}_1' &= \mathbf{g}' + \frac{m_1 + m_2}{m_1}\mathbf{G}, \\ \mathbf{v}_2' &= \mathbf{g}' - \frac{m_1 + m_2}{m_2}\mathbf{G}. \end{aligned} \tag{5.49}$$

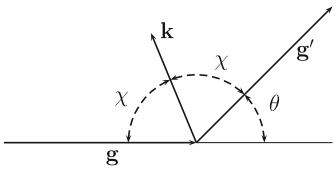

Fig. 5.3 Kinematics of an elastic collision; $\mathbf{g}$ and $\mathbf{g}'$ are the relative velocities before and after a collision, θ is the scattering angle, $\mathbf{k}$ is the external bisector of the angle between $\mathbf{g}$ and $\mathbf{g}'$ defined by χ

The centre-of-mass velocity is conserved, so that, $\mathbf{G}' = \mathbf{G}$. For the one component gas considered here, $m_1 = m_2$. The variables $(\mathbf{v}_1', \mathbf{v}_2')$ are related to the pair $(\mathbf{v}_1, \mathbf{v_2})$ with the substitution of $\mathbf{g}'$ from Eq. (5.47) into (5.49).

The linearized integral collision operator in Eq. (5.41) can be written in terms of a kernel so that we can recast Eq. (5.46) in the form,

$$\frac{\partial f(\mathbf{v}, t)}{\partial t} = \int K_J(\mathbf{v}, \mathbf{u}) f(\mathbf{u}) d\mathbf{u} - Z(v) f(\mathbf{v}, t), \tag{5.50}$$

where the collision frequency is

$$Z(v) = f(v) \int \int f_1(\mathbf{v}_1) \sigma_t(g) d\mathbf{v}_1. \tag{5.51}$$

The kernel for the hard sphere cross section, $\sigma(g, \Omega) = d^2/4$, expressed in reduced velocity variables, $\mathbf{x} = \mathbf{v}\sqrt{m/2k_BT}$ and $\mathbf{y} = \mathbf{u}\sqrt{m/2k_BT}$, is

$$K_J(x, y, \overline{\mu}) = \frac{Z(0)}{\pi\sqrt{\pi}} e^{-x^2} \left[\frac{2}{\sqrt{x^2 + y^2 - 2xy\overline{\mu}}} \exp\left[\frac{x^2 y^2 (1 - \overline{\mu}^2)}{x^2 + y^2 - 2xy\overline{\mu}} \right] - \sqrt{x^2 + y^2 - 2xy\overline{\mu}} \right], \tag{5.52}$$

where $\overline{\mu} = \cos\theta'$ and θ' is the angle between $\mathbf{x}$ and $\mathbf{y}$ and $Z(0) = n_b \pi d^2 \sqrt{2k_BT/m}$. The derivation of this kernel is lengthy but straightforward and is provided elsewhere (Nielsen and Bak 1964; Monchick and Mason 1967; Chapman and Cowling 1970; Ferziger and Kaper 1972; Williams 1976). For most of the applications presented here, the hard sphere cross section is used, although the kernel in Eq. (5.50) can be written for arbitrary differential scattering cross section (Kapral and Ross 1970; Sospedra-Alfonso and Shizgal 2013).

As the kernel depends only on the angle between $\mathbf{x}$ and $\mathbf{y}$, the operator J is rotationally invariant and diagonal in the Legendre polynomial basis set. It is customary in kinetic theory and radiative transfer theory to expand the kernel in Legendre polynomials in $\overline{\mu}$, that is,

$$K_J(x, y, \overline{\mu}) = \sum_{\ell=0}^{\infty} k_J^{(\ell)}(x, y) P_\ell(\overline{\mu}), \tag{5.53}$$

where the scalar kernels are

$$k_J^{(\ell)}(x, y) = \frac{2\ell + 1}{2} \int_{-1}^{1} K_J(x, y, \overline{\mu}) P_\ell(\overline{\mu}) d\overline{\mu}. \tag{5.54}$$

In radiative transfer theory this is often referred to as a P_N method with the kernel replaced with an analogous photon scattering phase function (Liou 2002; Thomas and Stamnes 2002; Ganapol 2008).

For the hard sphere cross section, the kernels, $k_J^{(\ell)}(x, y)$, are known analytically versus x and y for the lower order ℓ values as provided in Sect. 4.2.1 in the book by Williams (1971) and also by other researchers (Pekeris 1955; Pekeris and Alterman 1957; Desai and Nelkin 1966; Siewert 2002). The kernels can be calculated numerically with a Gauss-Legendre quadrature in Eq. (5.54) (Shizgal 1981a). We use the quadrature algorithms developed in Chap. 2 and discussed further in Chap. 3 to solve the initial value problem, Eq. (5.46), (Hoare and Kaplinsky 1970; Shizgal and Blackmore 1983; Shizgal 1984).

5.4.3 Matrix Representation of the Spherical Component ($\ell = 0$) of J in Sonine-Laguerre Basis Functions

It has been traditional in kinetic theory to solve the integral equations for the transport coefficients with the expansions in the direct product basis set of the Sonine-Laguerre basis functions and the spherical harmonics or Legendre polynomials. The choice of basis function is dictated in part by the fact that the Sonine-Laguerre polynomials are the eigenfunctions of J for the Maxwell molecule collision model as discussed in Sect. 3.6.4, although this is a not a sufficient reason for this choice. However, it is useful to note that the inhomogeneous functions for the Chapman-Enskog integral equations for the transport coefficients, Eqs. (5.44) and (5.45), are low order polynomials in x^2. The resulting inhomogeneous vector of the linear algebraic equations that are inverted in the spectral solution for the viscosity has only one nonzero component (Loyalka et al. 2007).

We restrict the discussion of the initial value problem, Eq. (5.46), to initial isotropic distributions, so that the eigenvalues, λ_n, and eigenfunctions, $\psi_n(x)$, are for $\ell = 0$ unless otherwise noted. We consider only the $\ell = 0$ component of the collision operator and do not show this explicitly to simplify the notation, and write

$$\frac{\partial f(x,t)}{\partial t} = J[f(x,t)]. \tag{5.55}$$

We solve Eq. (5.55) with the expansion of the initial distribution function in the eigenfunctions of J, that is

$$f(x,0) = \sum_{n=0}^{N} c_n \psi_n(x^2), \tag{5.56}$$

where

$$J[\psi_n(x^2)] = -\lambda_n \psi_n(x^2). \tag{5.57}$$

The solution of Eq. (5.55) can be written formally in terms of an evolution operator similar to the time dependent Schrödinger equation, that is

$$\begin{aligned} f(x,t) &= e^{Jt} f(x,0), \\ &= \sum_{n=2}^{\infty} c_n \psi_n(x^2) e^{-\lambda_n t}, \end{aligned} \tag{5.58}$$

where we have used

$$e^{Jt}\psi_n(x^2) = e^{-\lambda_n t}\psi_n(x^2). \tag{5.59}$$

The evolution operator is defined in term of the expansion of the exponential, $e^{Jt} = 1 + Jt + J^2t^2/2 + \cdots$ analogous to the evolution operator in quantum mechanics (Balint-Kurti 2008) discussed in Sect. 4.6.6. In the sections that follow, we are interested in the eigenvalue problem, Eq. (5.57), expressed in terms of a variational theorem. This eigenvalue problem is a fundamental aspect of the kinetic theory of gases, analogous to spectral theory in quantum mechanics.

The matrix elements of the collision operator for isotropic problems are defined by

$$J_{nm}^{(0)} = \int\int\int F_1 F_2 S_1^{(n)} \left[S_1^{(m)'} + S_2^{(m)'} - S_1^{(m)} - S_2^{(m)} \right] \sigma g d\Omega d\mathbf{v}_1 d\mathbf{v}_2, \tag{5.60}$$

which can be shown to be symmetric, that is, $J_{nm}^{(0)} = J_{mn}^{(0)}$. We denote the Sonine-Laguerre polynomials for $\ell = 0$ as $S^{(n)}(x^2)$ given explicitly by

$$\begin{aligned} S^{(n)}(x^2) &= \sum_{k=0}^{n} (-1)^k \frac{\Gamma(n+3/2)}{\Gamma(k+3/2)(n-k)k!} x^{2k}, \\ &= \sum_{k=0}^{n} S_{nk} x^{2k}, \end{aligned} \tag{5.61}$$

and orthogonal in accordance with

$$\int_0^{\infty} e^{-x^2} S^{(n)}(x^2) S^{(m)}(x^2) x dx^2 = \frac{\Gamma(n+3/2)}{n!} \delta_{nm}. \tag{5.62}$$

We evaluate the matrix elements with the generating function for the Sonine-Laguerre polynomials

$$G(t,x^2) = \frac{\exp[tx^2/(t-1)]}{(1-t)^{3/2}} = \sum_{k=0}^{\infty} S^{(k)}(x^2) t^k, \quad |t| < 1. \tag{5.63}$$

The matrix elements $J_{nm}^{(0)}$ are evaluated with the one matrix element between two generating functions, that is the element $\langle G_t|J|G_s\rangle$. This technique was first introduced by Mott-Smith (1954) and used subsequently by other researchers (Ford 1968; Foch and Ford 1970; Shizgal and Karplus 1971; Shizgal and Fitzpatrick 1974; Gust and Reichl 2009; Shizgal and Dridi 2010). The desired matrix element, $J_{nm}^{(0)}$, is then the coefficient of $s^n t^m$ of the expression below.

$$\begin{aligned}\langle G_s|J|G_t\rangle &= \frac{2Z(0)}{\sqrt{\pi}} s^2 t^2 \left(\frac{\sqrt{1-\frac{1}{2}s-\frac{1}{2}t}}{(1-st)^2}\right), \\ &= \sum_{n=2}^{\infty}\sum_{m=2}^{\infty} J_{nm}^{(0)} s^n t^m, \end{aligned} \tag{5.64}$$

Owing to particle number and energy conservation, $J_{nm}^{(0)} = 0$ for $(n, m) = (0, 1)$ and consequently $\lambda_0 = 0$ and $\lambda_1 = 0$. The evaluation of the generating function matrix element, Eq. (5.64), involves the kinematics of binary particle collisions, Eqs. (5.47)–(5.49).

It has been shown (Ford 1968; Foch and Ford 1970; Lindenfeld and Shizgal 1979a; Gust and Reichl 2009) that the matrix elements are given by

$$J_{nm}^{(0)} = \frac{2Z(0)}{\sqrt{\pi}2^{n+m}} \sqrt{\frac{n!m!}{8\Gamma(n+\frac{3}{2})\Gamma(n+\frac{3}{2})}} \sum_{j=0}^{N_m} \frac{4^j B_j \Gamma(n+m-2j-\frac{1}{2})}{(n-j)!(m-j)!}, \tag{5.65}$$

where $B_j = j - 1 + \delta_{j0}$ and $N_m = \min(n, m)$. We use this representation of J in the next section to analyze nonequilibrium effects for a model reactive system and in Sect. 5.5.1 for variational estimates of the eigenvalues and eigenfunctions of the operator.

It is useful to note that the matrix elements given by Eq. (5.65) involve both the integral operator in Eq. (5.50) and the collision frequency, $Z(x)$. For cross sections determined with classical mechanics, the integral operator and the collision frequency are not defined owing to the divergence of the differential scattering cross section at small scattering angles. By contrast, quantum cross sections are finite and the two terms in the collision operator can be considered separately. The matrix elements of the Hamiltonian for a problem in quantum mechanics is the sum of the matrix elements of the kinetic energy operator and the matrix elements of the potential often computed separately. The quadrature evaluations of the matrix elements of the potential in a Schrödinger equation (Harris et al. 1965; Dickinson and Certain 1968) are often cited as the origin of pseudospectral methods in quantum chemistry (Light and Carrington Jr. 2000).

5.4.4 Spectral Solution of the Boltzmann Equation for the Departure from Maxwellian for an Elementary Reaction in a Spatially Uniform System

It is well known that chemical reactions proceed with a concommitant departure of the particle distribution functions from equilibrium. This subject has a long history both for systems with only translational energy (Prigogine and Xhrouet 1949; Shizgal and Karplus 1970; Shizgal and Fitzpatrick 1978; Ross and Mazur 1961; Alves et al. 2011; Kustova and Giordano 2011; Dziekan et al. 2012) as well as for molecular systems with internal vibrational and rotational states (Shizgal 1972; Shizgal and Lordet 1996; Pascal and Brun 1993; Brun 2009). The theoretical treatment of such systems is based on a Boltzmann equation for the velocity distribution and in some instances on a Master equation for the distribution of vibrational and rotational states (Kim and Boyd 2013).

In this section, we consider a one-component atomic system (without internal degrees of freedom) and a single reactive process. We add a single reactive loss term to the Boltzmann eqation, Eq. (5.55), to model the nonequilibrium effects that arise from the reaction. An estimate of the departure from the equilibrium rate of reaction is obtained with a Chapman-Enskog method similar to its application to the calculation of transport coefficients discussed in Sect. 5.4.1. However, for this uniform system the Chapman-Enskog method is more transparent. We also discuss a nonlinear variational approach that provides a different approximate solution of the Boltzmann equation (Present and Morris 1969).

We consider a one component system undergoing a reaction

$$A + A \rightarrow \text{products}, \tag{5.66}$$

with a total reactive cross section, $\sigma_r(g)$, dependent on the relative speed, g, of the reactants. The spatially homogeneous Boltzmann equation for the isotropic distribution function of A is

$$\frac{\partial f(v,t)}{\partial t} = J[f(v,t)] - \epsilon f(v,t) \int f(v_1,t) g \sigma_r(g) d\mathbf{v_1}, \tag{5.67}$$

where a reactive collision term corresponding to the loss of particles by reaction is added to the right hand side of Eq. (5.46). The integral reactive term is the reactive collision frequency, Eq. (3.35), of Sect. 3.6. The parameter ϵ, which is assumed small, multiplies the reactive term and thus the reaction is considered as a small perturbation of the elastic collision term, J. The parameter ϵ is defined in terms of the elastic and reactive cross sections; see after Eq. (5.77).

The particle number is not conserved and we have on integration of Eq. (5.67) that the rate of reaction is

$$\frac{dn}{dt} = -\epsilon \iint f f_1 g \sigma_r(g) d\mathbf{v_1} d\mathbf{v}. \tag{5.68}$$

The local temperature also changes owing to the loss of energetic particles as given by

$$\frac{dT}{dt} = -\epsilon \frac{2T}{3n} \int\int f f_1 \left[\frac{mv^2}{2k_B T} - \frac{3}{2} \right] g \sigma_r(g) d\mathbf{v_1} d\mathbf{v}. \tag{5.69}$$

We employ a Chapman-Enskog approach to determine the departure of the distribution from Maxwellian and the nonequilibrium reaction rate. Since the rate of reactive collisions is much smaller than the rate of elastic collisions and the ratio of these rates to be of the order of ϵ, we set

$$f(v,t) = F[v, n(t), T(t)] \Big[1 + \epsilon \phi(v) \Big], \tag{5.70}$$

where the first term is the local Maxwellian which varies with time implicitly through the time dependence of the density and temperature, that is

$$F[v, n(t), T(t)] = n(t) \left(\frac{m}{2k_B T(t)} \right)^{3/2} \exp \left(-\frac{mv^2}{2k_B T(t)} \right). \tag{5.71}$$

Since the system is assumed to be spatially homogeneous and there is no bulk motion of the gas, the formalism employed here is a simpler version of the Chapman-Enskog method described in Sect. 5.4.1.

The time dependence of the distribution function is implicit through $n(t)$ and $T(t)$, that is

$$\frac{\partial f}{\partial t} = \frac{\partial f}{\partial n} \frac{dn}{dt} + \frac{\partial f}{\partial T} \frac{dT}{dt}. \tag{5.72}$$

With these substitutions into the Boltzmann equation, Eq. (5.67), the term linear in ϵ is the Chapman-Enskog integral equation

$$J[\phi(v)] = F(v) H(v), \tag{5.73}$$

where

$$H(v) = -A_0 \frac{\partial F}{\partial n} + \frac{2T A_1}{3n} \frac{\partial F}{\partial T} + F \int F_1 g \sigma_r(g) d\mathbf{v_1}, \tag{5.74}$$

evaluated with the local Maxwellian, and

$$\begin{aligned} A_0 &= \int\int F F_1 g \sigma_r(g) d\mathbf{v} d\mathbf{v}_1, \\ A_1 &= -\int\int F F_1 \left[x^2 - \frac{3}{2} \right] g \sigma_r(g) d\mathbf{v} d\mathbf{v}_1. \end{aligned} \tag{5.75}$$

A solution of the integral equation, Eq. (5.73), exists if the solutions of the homogeneous equation, namely $J[\psi_0] = 0$ and $J[\psi_1] = 0$, are orthogonal to the inhomogeneous term $F(v)H(v)$. The "summational invariants" for this problem, namely $\psi_0(v) = 1$ and $\psi_1(v) = v^2$, are orthogonal to the inhomogeneous portion of the Chapman-Enskog equation, Eq. (5.73), that is

$$\int F(v)H(v)d\mathbf{v} = 0,$$

and

$$\int F(v)H(v)v^2 d\mathbf{v} = 0.$$

These results are easily verified with the definitions of A_0 and A_1. These are referred to as the auxiliary conditions and were previously discussed in connection with the integral equations for heat conduction and viscosity, namely Eqs. (5.44) and (5.45).

Inspection of the terms in Eq. (5.73) reveals that all terms are of order ϵ. We consider the hard sphere elastic cross section, πd^2, and the line-of-centers reactive cross section, given by

$$\sigma_r(E) = \begin{cases} 0, & E \leq E^*, \\ \pi d_r^2(1 - \frac{E^*}{E}), & E > E^*. \end{cases} \tag{5.76}$$

The equilibrium rate coefficient is

$$k_{eq}(T) = A_0/n^2 = 4\pi d_r^2 \sqrt{\frac{k_B T}{\pi m}} \exp(-E^*/k_B T). \tag{5.77}$$

The expansion parameter can be identified as $\epsilon = (d_r/d)^2$ and thus we must have that $d_r \ll d$ for the Chapman-Enskog perturbative method of solution to be accurate. The inhomogeneous terms of the integral equations for transport processes in Sect. 5.4.1 also satisfy these "auxiliary conditions".

We expand the perturbation of the distribution function, $\phi(x)$, in Sonine-Laguerre polynomials

$$\phi(x) = \sum_{n=2}^{N} a_n S_\alpha^{(n)}(x^2), \tag{5.78}$$

with $\alpha = 1/2$ which is hereafter deleted. This expansion reduces the integral equation to a set of linear equations,

$$\sum_{n=2}^{N} J_{mn}^{(0)} a_n = \alpha_m, \tag{5.79}$$

where

$$\begin{aligned}\alpha_m &= \int F(v)H(v)S^{(m)}(x^2)d\mathbf{v},\\ &= -A_0\delta_{0m} - A_1\delta_{1m} + A_m, \quad m \geq 2,\end{aligned} \tag{5.80}$$

and

$$A_m = \int\int FF_1S_m(x^2)g\sigma_r(g)d\mathbf{v}d\mathbf{v}_1. \tag{5.81}$$

It has been shown (Shizgal and Karplus 1970) that these moments of the reactive collision frequency are given by

$$A_m = \frac{8}{2^m}\sqrt{\frac{\pi k_B T}{m}}\sum_{k=0}^{m} S_{mk}K_k, \tag{5.82}$$

where the S_{mk} coefficients are defined by Eq. (5.61) and

$$K_k = \frac{1}{\pi}\int_0^\infty e^{-\xi^2}\xi^{2k+3}\sigma_r(g)d\xi, \tag{5.83}$$

and $\xi = \sqrt{\mu g^2/2k_BT}$ is the reduced relative speed. For the line of centers reactive cross section, Eq. (5.76), the K_k integrals can be done iteratively with an integration by parts and thus the A_m integrals are known.

The main objective is to calculate with the distribution function, Eq. (5.70), the departure of the nonequilibrium rate coefficient, k_{neq}, Eq. (5.68), from the equilibrium rate coefficient, k_{eq}, that is

$$k_{neq} = k_{eq}(1-\eta), \tag{5.84}$$

where the desired quantity is η given by

$$\eta = -2\sum_{n=0}^{N} a_n\frac{A_m}{A_0}. \tag{5.85}$$

A MATLAB code is used to calculate the matrix elements, Eq. (5.65), and the α_m moments, Eq. (5.80). The code also solves the linear equations, Eq. (5.79), and calculates η with Eq. (5.85).

The rapid convergence of η versus the number of basis functions, N, is shown in Table 5.2. The convergence of η versus N is from below so that each estimate provides a lower bound indicative that a variational theorem is operative although we have not made explicit use of the variational theorem. The extremely small correction for $E^*/k_BT = 32$ is converged to 5 significant figures with 10 basis functions.

Table 5.2 Convergence of the nonequilibrium correction to the reaction rate coefficient for the line-of-centers model cross section

E^*/k_BT	8	16	32
N	$\eta \times 10^2$	$\eta \times 10^3$	$\eta \times 10^6$
1	3.2582	0.2021	0.0004
2	3.6496	0.5600	0.0046
3	3.6507	0.9019	0.0343
4	3.6569	1.0118	0.1581
5	3.6571	1.0167	0.4637
6	3.6571	1.0177	0.9056
7		1.0179	1.2633
8		1.0179	1.4072
9			1.4271
10			1.4271
Nonlinear variational[a]	3.6251	0.8924	0.7665

[a] Present and Morris (1969)

The variation of η with the reduced threshold energy E^*/k_BT is shown by the solid curve in Fig. 5.4(A). The unusual behavior with η decreasing for $E^*/k_BT < 5$ in spite of the increase in the reaction rate has been explained (Shizgal and Karplus 1970) on the basis of the speed dependence of the reactive collision frequency. The nonequilibrium effect vanishes for a reactive collision frequency that varies in such a manner analogous to the way changes in density and temperature change the distribution function. Thus, for a reactive cross section that varies as g or $1/g$, $\eta = 0$. This accounts for the minimum and maximum of η near the E^*/k_BT origin.

It is useful to compare with the nonlinear variational solution of the chemical kinetic Boltzmann equation introduced by Present and Morris (1969). They chose a solution (their Eq. (33)) which is made to satisfy the two auxiliary conditions and parameterized by the variational parameter s, that is

$$\phi(x^2) = C(s)\left[e^{sx^2} - \frac{sx^2 + 1 - \frac{5}{2}s}{\sqrt[5/2]{1-s}}\right]. \tag{5.86}$$

Substitution of this form of the solution into Eq. (5.73) and taking the scalar product with $\phi(x)$ gives an equation for $C(s)$. We then calculate the rate of reaction and divide by the equilibrium rate, Eq. (5.77). The correction to the rate of reaction parametrized by the variational parameter s and $q = E^*/k_BT$ is given by,

$$\eta(q,s) = \frac{2(1-2s)^2 e^{-q}}{s^4\sqrt{1-s}}\left[\sqrt{\frac{2-s}{2}}\exp\left(\frac{sq}{2-s}\right) - \frac{1 - \frac{3}{4}s + \frac{1}{2}sq}{\sqrt{1-s}}\right]. \tag{5.87}$$

The extremum value of $\eta(q,s)$ versus s for fixed q can be determined with a short MATLAB code.

The symbols in Fig. 5.4 show the results with the nonlinear variational approach (Present and Morris 1969) and appear indistinguishable from the spectral solution. However, the comparison of the numerical values with the variational approach and the Sonine polynomial expansion shown in Table 5.2 demonstrates that the variational approach gives poor results for the larger E^*/k_BT values.

The spectral convergence is also demonstrated with the decrease in the expansion coefficients versus n in Fig. 5.4(B) and the accuracy of the expansion for η in Fig. 5.4(C). The "exact" values for η are those calculated with the Sonine polynomial expansion with a sufficient number of terms to get convergence to 16 significant figures.

Explicit time dependent solutions of the Boltzmann equation were carried out to determine the range of validity of the Chapman-Enskog approach for the one component system treated here (Shizgal 1971) as well as for a binary system (Shizgal 1974). These studies suggest that the value of ϵ must be of the order of 10^{-3} to 10^{-4} for the Chapman-Enskog values to be accurate. Shizgal (1981a) used a

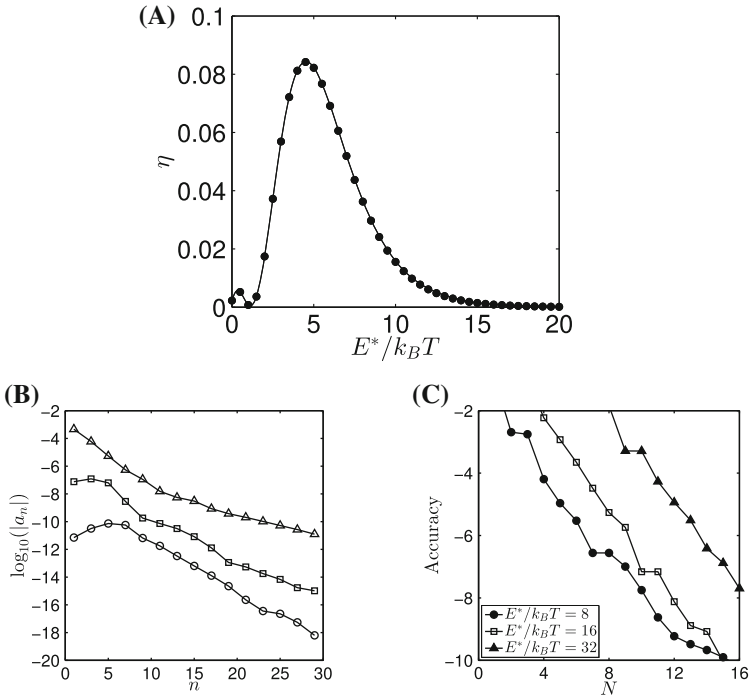

Fig. 5.4 (**A**) Variation of the nonequilibrium connection to the reaction rate, η, versus the reduced activation energy, E^*/k_BT, for the line-of-centers reactive cross section and hard sphere elastic cross section; the *solid symbols* are the results with the variational solution. (**B**) Convergence of the expansion coefficients of $\phi(x)$ versus n, with $E^*/k_BT = 10$ (*triangles*), 20 (*squares*) and 30 (*circles*). (**C**) Accuracy $= \log_{10}[1 - \eta/\eta_{exact}]$ where η_{exact} is determined to 16 significant figures with N sufficiently large

pseudospectral method based on Laguerre quadratures in reduced energy to solve the chemical kinetic Boltzmann equation, Eq. (5.67), but for a binary gas with unit mass ratio and the integral kernel operator, Eq. (5.110). This reactive system was also the basis for the study of the nonequilibrium effects associated with the escape of planetary atmospheres (Lindenfeld and Shizgal 1979b). The loss of atoms from an atmosphere is in the first instance given by the well-known Jeans escape flux (Fahr and Shizgal 1983) analogous to a chemical reaction where the reaction threshold energy is replaced by the escape energy from the planet.

5.4.5 *Pseudospectral Solution of the Boltzmann Equation for Shear Viscosity with the Maxwell Quadrature*

The Chapman-Enskog solution of the Boltzmann equation for the viscosity of a one component gas was summarized in Sect. 5.4.1. The integral equation for the function $B(x)$, Eq. (5.45), for the hard sphere cross section is the solution of the linear integral equation (Shizgal 2011; Siewert 2002)

$$\int_0^\infty e^{-x^2} x^2 k_J^{(2)}(x, y) B(x) dx - Z(y) B(y) = -y^2, \tag{5.88}$$

where the symmetric kernel, $k_J^{(2)}(x, y)$, is given by

$$k_J^{(2)}(x, y) = -\frac{2Z(0)}{x^4 y^4}\left[A(x, y) + C(x, y)\sqrt{\pi} e^{x^2} \mathrm{erf}(x)/2\right], \quad x < y, \tag{5.89}$$

with

$$A(x, y) = \frac{2}{35}x^7 - 3x^3 + 18x - y^2\left(\frac{2}{15}x^5 - 3x\right),$$

$$C(x, y) = -6x^4 + 15x^2 - 18 + y^2(2x^2 - 3),$$

as discussed by Siewert (2002). The kernel $k_J^{(2)}(x, y)$ is the $\ell = 2$ component of the expansion of the anisotropic kernel, Eq. (5.53). Equation (5.88) is equivalent to Eq. (5.45). The function $B(x)$ in this paper corresponds to $x^2 b(x)$ in the papers by Siewert (2002) and by Loyalka et al. (2007). The shear viscosity in reduced units is given in terms of $B(x)$, that is

$$\nu = \frac{16\sqrt{2}}{15} \int_0^\infty e^{-x^2} x^4 B(x) dx. \tag{5.90}$$

The details are provided elsewhere (Siewert 2002; Loyalka et al. 2007; Sharipov and Bertoldo 2009). Our interest here is with the numerical solution of the integral equation, Eq. (5.88) and the calculation of the viscosity, Eq. (5.90).

There have been several different methods used to get accurate solutions of Eq. (5.88). Siewert (2002) used a B-spline technique analogous to a recent work on time dependent solutions of the isotropic Boltzmann equation (Khurana and Thachuk 2012). Sharipov and Bertoldo (2009) have employed a two-dimensional mesh to discretize the Boltzmann integral equation, Eq. (5.45).

Loyalka et al. (2007) employed the expansion of the distribution function in the Sonine-Laguerre polynomials with up to 150 terms to reduce Eq. (5.45) to a set of linear algebraic equations. They used *Mathematica* to calculate the matrix representation of collision operator and invert the resulting set of linear equations algebraically for the function $B(x)$ in Eq. (5.90). This is the Galerkin solution of the integral equation, Eq. (5.88) or equivalently Eq. (5.45). The use of Mathematica avoids the round-off errors that would otherwise occur, and accurate converged solutions to the Boltzmann equation were obtained. Their work serves as an excellent benchmark for the solution of this integral equation and they report the viscosity to 34 significant figures, that is $\nu = 0.44902780628789243460904948953465 45$.

We have noted in Sect. 3.6.3 that the integral for the dimensionless viscosity converges very rapidly with respect to the number, N, of Gauss-Maxwell quadrature points and weights with $w(x) = x^2 e^{-x^2}$. Thus a solution of Eq. (5.88) based on the Gauss-Maxwell quadrature points should converge quickly. With this quadrature procedure, the solution of the integral equation, Eq. (5.88), is given by the inversion of the set of linear algebraic equations

$$\sum_{i=1}^{N} W_i e^{-z_i^2} z_i^2 k_J^{(2)}(z_i, z_j) B(z_i) - Z(z_j) B(z_j) = -z_j^2, \tag{5.91}$$

where $W_i = s w_i / w(x_i)$, $z_i = s x_i$. The scaling parameter s is chosen so that the quadrature points are in the interval $x \in [0, 6]$ for which $B(x)$ is known. The reduced shear viscosity is then given by

$$\nu = \frac{16\sqrt{2}}{15} \sum_{i=1}^{N} W_i e^{-z_i^2} z_i^4 B(z_i). \tag{5.92}$$

The solution to Eq. (5.91), $B(x)$, is shown in Fig. 5.5 and is a very slowly varying function of x. It is not surprising that the convergence of the solution is rapid. A graphically accurate solution is obtained with 16 quadrature points. The convergence is slower for large x but there is a small contribution to ν for $x > 6$ owing to the factor $x^4 e^{-x^2}$ in Eq. (5.90). The convergence of the solution of the Boltzmann equation obtained with the scaled Maxwell quadrature points is shown in Table 5.3 in comparison with the solution reported by Siewert (2002). The pseudospectral solution was spline fitted to the x values reported by Siewert (2002). The major contribution

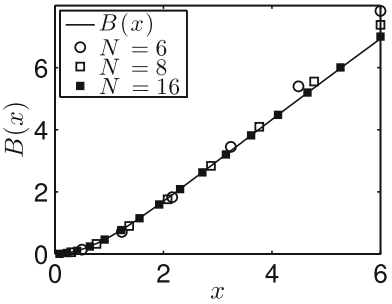

Fig. 5.5 The solution of the Boltzmann equation, Eq. (5.88), for the viscosity function, $B(x)$, versus the number of Maxwell quadrature points, N. The *solid curve* is the result by Loyalka et al. (2007) considered exact

Table 5.3 Solution of the Boltzmann equation for shear viscosity with N speed quadrature points; $(-n) \equiv \times 10^{-n}$

x	Siewert 2002	N = 20	N = 30	N = 40	N = 60
	$x^4 e^{-x^2} B(x)$				
0.3	0.40775 (−3)	0.40629 (−3)	0.40763 (−3)	0.40772 (−3)	0.40775 (−3)
0.4	0.21139 (−2)	0.21101 (−2)	0.21134 (−2)	0.21137 (−2)	0.21139 (−2)
0.5	0.72744 (−2)	0.72686 (−2)	0.72726 (−2)	0.72738 (−2)	0.72742 (−2)
1.0	0.20004	0.19983	0.20000	0.20003	0.20004
1.5	0.57830	0.57780	0.57820	0.57827	0.57829
2.0	0.49722	0.496901	0.49716	0.49720	0.49722
2.5	0.17667	0.17659	0.17665	0.17666	0.17667
3.0	0.30011 (−1)	0.30002 (−1)	0.30009 (−1)	0.30010 (−1)	0.30011 (−1)
3.5	0.26318 (−2)	0.26315 (−2)	0.26317 (−2)	0.26318 (−2)	0.26318 (−2)
4.0	0.12465 (−3)	0.12466 (−3)	0.12465 (−3)	0.12465 (−3)	0.12465 (−3)
ν	0.449027806	0.448816	0.448985	0.449014	0.449025

Reproduced in part from Shizgal (2011) with permission of the American Institute of Physics and from Siewert (2002) with permission from Elsevier

to the integral is approximately in the interval $x \in [0.4, 4.0]$. The scaling of the Gauss-Maxwell points with the parameter s is thus important so as to compute the solution in the range of x that contributes to the viscosity.

Siewert (2002) employed 301 "knots" with the Hermite cubic spline functions and a 4th order Gauss-Legendre quadrature to calculate the integral over subintervals. The final integral for the viscosity, Eq. (5.90), was computed with 100 Gauss-Legendre quadrature points. Sharipov and Bertoldo (2009) solved the Boltzmann equation as a two dimensional problem in two velocity coordinates and used 40 grid points in each velocity direction and 200 points with a Simpson's rule to evaluate ν to the same precision as in Table 2; that is $2\sqrt{\pi} \times 0.126668 = 0.449028$. The application of the speed quadrature points and weights to this problem is very straightforward and the convergence is rapid as seen in Table 5.3 and Fig. 5.5.

5.5 Spectral Theory for the Linearized Boltzmann Collision Operator

The Boltzmann equation, Eq. (5.30), is the basis for modelling transport phenomena in a one component gas. These transport processes include the classic rarefied gas dynamical problems such as the Kramers problem, Poseuille and Couette flow and other similar phenomena discussed elsewhere (Williams 1971; Cercignani 1988; Sharipov and Seleznev 1998; Siewert 2003). These and many other rarefied gas dynamical flows are described in detail in the book by Sone (2007). Spectral methods are employed in the solution of the Boltzmann equation for such systems (Wu et al. 2013; Ghiroldi and Gibelli 2014). These problems are beyond the scope of this book but in Sect. 5.7.2 we discuss the Milne problem for a binary gas that serves as an example of a rarefied gas dynamical problem. The numerical approximation of the linearized collision operator in the Boltzmann equation, J, is important in these applications.

Studies of the mathematical properties of J has a very long history (Alterman et al. 1962; Grad 1963; Foch and Ford 1970; Cercignani 1988) and is ongoing (Mouhot 2007; Dudynski 2013). Some of the mathematical works are directed towards constructive estimates of the first nonzero eigenvalue referred to as the "spectral gap" (Baranger and Mouhot 2005; Mouhot 2007). A comparison of the previously noted mathematical analyses and others (Alexandre 2009; Dudynski 2013) with the numerical estimates (Shizgal 1984; Gust and Reichl 2009) has not been made. The classical differential cross sections diverge at small scattering angle and the total cross section is infinite, except for the hard sphere cross section. For other than the hard sphere cross section, the mathematical treatments involve a cut-off of the divergent classical differential cross section (Grad 1949; Baranger and Mouhot 2005; Mouhot 2007; Alexandre 2009). However, the correct treatment of the elastic scattering is based on quantum theory for which the differential cross section at zero scattering angle is finite as is the total cross section.

The quantum mechanical cross sections can be calculated for physically realistic atomic potentials (Bernstein 1966; Child 1996; Canto and Hussein 2013) and cannot in general be factored as a product of a function of g and a function of θ. Mathematical treatments of the approach to equilibrium for the non-linear Boltzmann equation (see Sect. 5.8) rely on the spectral properties of the linearized operator (Grad 1958; Baranger and Mouhot 2005; Mouhot 2006; Alexandre 2009).

Realistic quantum cross sections have been used in the Boltzmann equation for relaxation processes (Kharchenko et al. 1998; Kharchenko and Dalgarno 2004; Sospedra-Alfonso and Shizgal 2013), in the study of gaseous transport coefficients Zhang et al. (2013), and in modelling electron (Lin et al. 1979a; Pitchford and Phelps 1982; Hagelaar and Pitchford 2005; Robson et al. 2005) and ion transport (Mason and McDaniel 1988; Viehland 1994; Danailov et al. 2008). These works are based on the linear collision operator for binary systems discussed in Sect. 5.6.

We approximate the eigenvalues of the collision operator, J, with a spectral approach in Sect. 5.5.1 and a pseudospectral method in Sect. 5.5.2. It is well known

that the spectrum of the collision operator consists of an infinite number of discrete eigenvalues and a continuum (Grad 1963; Kuščer and Williams 1967; Shizgal 1984; Gust and Reichl 2009). For the Maxwell molecule model with a constant collision frequency the spectrum is completely discrete as discussed in Sect. 3.6.4.

Our main interest in the sections that follow is the eigenvalue problem associated with the initial value problem, Eq. (5.46). There are an infinite number of discrete eigenvalues defined by

$$J\psi_n(x) = -\lambda_n\psi_n(x), \tag{5.93}$$

which satisfy $0 \leq \lambda_n \leq Z(0)$ and continuous eigenvalues, $\lambda > Z(0)$, given by

$$J\psi(x,\lambda) = -\lambda\psi(x,\lambda), \tag{5.94}$$

where $Z(0)$ is the elastic collision frequenxy, Eq. (5.51) at zero reduced speed or energy. This set of eigenstates (taken to be complete) can be used to represent a function, $\phi(x)$, by writing the expansion of the function in terms of the discrete and continuum eigenfunctions as given by,

$$\phi(x) = \sum_{n=0}^{\infty} c_n\psi_n(x) + \int_{Z(0)}^{\infty} C(\lambda)\psi(x,\lambda)d\lambda. \tag{5.95}$$

This property of the eigenvalue spectrum has been discussed elsewhere (Grad 1963; Cercignani 1988; Hoare 1971; Baranger and Mouhot 2005). In Chap. 6, Sect. 6.4.1, we compare this aspect of the spectrum of the Boltzmann equation with a similar behaviour for the Fokker-Planck equation for Coulomb collisions.

5.5.1 *Spectral Calculation of the Eigenvalue Spectrum of J*

In this section, we describe the calculation of the eigenfunctions and eigenvalues of J with a spectral method. The solution of the initial value problem, Eq. (5.46), is not presented here. However, in Sect. 5.6 we consider the solution of an analogous initial value problem for the equilibration of a binary mixture with energy exchange between the components.

We estimate the eigenvalues and eigenfunctions of J with the expansion of the eigenfunctions in the Sonine-Laguerre polynomials, $S_\alpha^{(k)}(x^2)$, with $\alpha = 1/2$, that is

$$\psi_n(x) = \sum_{k=0}^{N} a_k^{(n)} S^{(k)}(x^2). \tag{5.96}$$

where we have deleted the dependence of $S^{(k)}$ on α to simplify the notation. Since these basis functions are the eigenfunctions for the Maxwell molecule model, the usual expectation is that it would be a good choice for other interaction potentials (Phillips 1959; Tompson et al. 2010). However, there is no mathematical reasoning for this supposition.

The expansion coefficients $a_k^{(n)}$ are considered as linear variation parameters. The Rayleigh-Ritz variational approach was discussed in Chap. 1, Sect. 1.2.5. Variational methods are perhaps more familiar in the quantum context (Amore 2006; Balint-Kurti and Pulay 1995) than for kinetic theory problems. However, there has been considerable use of the variational theorem in kinetic theory (Phillips 1959; Cercignani 1969; Driessler 1981) based on maximum entropy principles (Snider 1964; Bobylev and Cercignani 1999).

We use the hard sphere differential cross section for which $\sigma(g, \Omega) = d^2/4$ and πd^2 is the total cross section. We use the expansion, Eq. (5.96), and thus the matrix representation given by Eq. (5.65). The first two eigenvalues are $\lambda_0 = \lambda_1 \equiv 0$ since particle number and energy are conserved, that is, $J_{nm}^{(0)} = 0$ for $(n, m) = 0$ and 1. The numerical diagonalization of the matrix $\mathbf{J}$ of dimension N defined by Eq. (5.65) yields successive approximations to the nonzero eigenvalues.

The convergence of the lower order eigenvalues, λ_2–λ_7, in units of $Z(0)$, is shown in Table 5.4 versus the number of basis functions, N. The convergence of each eigenvalue is from above consistent with a variational calculation. With 80 basis functions there are only 3 discrete nonzero eigenvalues ($\lambda_n < 1$). The other eigenvalues remain unconverged and lie in the continuum (Hoare and Kaplinsky 1970; Hoare 1971). Although this is a spectral method, the convergence of the eigenvalues is very slow with the Sonine-Laguerre basis set.

If we define the columns of the matrix $\mathbf{U}$ as the eigenvectors of the matrix $\mathbf{J}$, then $\mathbf{U}^{(-1)} \cdot \mathbf{J} \cdot \mathbf{U} = \mathbf{\Lambda}$, where $\Lambda_{nm} = \lambda_n \delta_{nm}$. The eigenfunctions can be written in terms of their expansion in the orthonormal Sonine-Laguerre basis functions, that is

Table 5.4 Convergence of the eigenvalues, λ_n, in units of $Z(0)$ of the linearized spherically symmetric ($\ell = 0$) Boltzmann equation with the Sonine-Laguerre basis functions

N	λ_2	λ_3	λ_4	λ_5	λ_6	λ_7
4	0.67660	1.06192	1.58295	2.30219		
6	0.67260	0.98776	1.35808	1.83700	2.41524	3.13509
8	0.67163	0.95494	1.24700	1.62541	2.06912	2.57270
10	0.67136	0.93797	1.18042	1.49760	1.86907	2.28307
20	0.67123	0.91513	1.05183	1.23130	1.45074	1.69800
30	0.67123	0.91226	1.01497	1.13918	1.29772	1.48081
40		0.91173	0.99982	1.09367	1.21770	1.36401
50		0.91161	0.99246	1.06723	1.16878	1.29073
60		0.91158	0.98848	1.05031	1.13600	1.24051
80			0.98477	1.03049	1.09529	1.17634

The eigenvalues, $\lambda_n < 1$, are in the discrete portion of the spectrum

$$\psi_n(x) = \sum_{k=2}^{N} U_{nk} \hat{S}^{(k)}(x^2). \tag{5.97}$$

where $\hat{S}^{(k)}(x^2) = S^{(k)}(x^2)/\sqrt{\Gamma(n+3/2)/n!}$. The orthogonality of the eigenfunctions is given by

$$\begin{aligned}\int_0^\infty w(x)\psi_n(x)\psi_m(x)dx &= \sum_{k=2}^{N}\sum_{\ell=2}^{N} U_{nk}U_{m\ell} \int_0^\infty w(x)\hat{S}^{(k)}(x^2)\hat{S}^{(\ell)}(x^2)dx, \\ &= \sum_{k=2}^{N} U_{nk}U_{mk} = \delta_{nk}, \end{aligned} \tag{5.98}$$

where Eq. (5.62) for the orthogonality of the Sonine-Laguerre polynomials has been used. The result, Eq. (5.98), is a statement of the orthogonality of the eigenvectors, $\mathbf{U}$, of the symmetric matrix $\mathbf{J}$. The eigenfunctions are all normalizable in L^2 with weight function $w(x) = x^2 e^{-x^2}$ whether they belong to the discrete spectrum or the continuum. However, we must address the meaning of the discretized eigenfunctions with $\lambda_n > 1$ as representing the continuum eigenfunctions in some approximate way (Reinhardt 1979).

5.5.2 *Pseudospectral Calculation of the Eigenvalue Spectrum of J*

We reconsider the eigenvalue problem of the previous section (for $\ell = 0$) defined by the equivalent integral equation, that is

$$\int_0^\infty e^{-x^2} x^2 k_J^{(0)}(x, y)\psi_n(x)dx - Z(y)\psi_n(y) = \lambda_n \psi_n(y), \tag{5.99}$$

where the symmetric kernel, $k_J^{(0)}(x, y)$, is given by

$$k_J^{(0)}(x, y) = Z(0) \begin{cases} \left[4e^{x^2}\mathrm{erf}(x) - \frac{4\sqrt{\pi}}{3}(x^2 + 3y^2)\right]/y\Big], & x < y \\ \left[4e^{y^2}\mathrm{erf}(y) - \frac{4\sqrt{\pi}}{3}(3x^2 + y^2)\right]/x\Big], & x > y \end{cases}$$

and discussed by other researchers (Desai and Nelkin 1966; Kuščer and Williams 1967; Yan 1969; Williams 1971; Siewert 2002). The kernel is the $\ell = 0$ component of the expansion Eq. (5.53).

The eigenfunctions are discretized on the grid defined by the Gauss-Maxwell quadrature with $p = 2$ that is with $w(x) = x^2 e^{-x^2}$. With this quadrature, the discretized form of the integral eigenvalue problem is

$$\sum_{j=1}^{N} w_j k_J^{(0)}(x_j, x_i)\psi_n(x_j) - Z(x_i)\psi_n(x_i) = \lambda_n \psi_n(x_i). \tag{5.100}$$

The matrix equation is symmetrized by setting $\hat{\psi}_n(x_i) = \sqrt{w_i}\psi_n(x_i)$ (Gust and Reichl 2010).

The computation of the matrix, $k_J^{(0)}(x_j, x_i)$, is much less prone to numerical round-off errors than the matrix representation with polynomial basis functions, Sect. 5.4.3. This pseudospectral method is more flexible as different quadratures associated with different basis functions can be used with very little additional effort, including a trapezoidal or Simpson rule. We can also scale the quadrature points and weights to improve convergence.

In order to impose detailed balance, that is to ensure that $\lambda_0 = 0$ to machine accuracy, we use the numerical value of the collision frequency, $Z(x_i)$, as determined by the integral over the kernel as discussed in Chap. 3

$$Z(x_i) = \sum_{k=1}^{N} w_k k_J^{(0)}(x_i, x_k). \tag{5.101}$$

The use of this approximate numerical result for $Z(x_i)$ in Eq. (5.99), removes the contribution from the cusp in the kernel and this method has been referred to as the singularity subtraction technique (Loyalka and Naz 2008), and was also discussed by Shizgal (1981a).

However, there is no constraint for λ_1 to be zero. Alternatively, one could define $Z(x_i)$ to ensure that energy conservation is obtained to machine accuracy, that is $\lambda_1 = 0$, but we would then find that $\lambda_0 \neq 0$. In this way, one of the two zero eigenvalues is of the order of 10^{-15} but not both. The other eigenvalue is much larger of the order of 10^{-5}. Recall that the spectral method gives trivially the two zero eigenvalues.

The convergence of the lower order eigenvalues is shown in Table 5.5 versus the number of Gauss-Maxwell quadrature points. The approach of λ_1 to zero is also shown. It is clear that the convergence of the eigenvalues is much faster with the Maxwell polynomials than with the Sonine-Laguerre polynomials except for λ_1 and λ_2. All the eigenvalues shown in the table are in the discrete portion of the spectrum and converged to five significant figures with 80 quadrature points.

There have been many qualitative discussions and diagrams of the approach of the eigenvalues to the continuum boundary (Cercignani 1988; Baranger and Mouhot 2005). An accurate representation is shown in Fig. 5.6. The upper graph depicts the value of each eigenvalue with a vertical line of unit length, the "spectral gap" being $\lambda_1 = 0.67121$. The density of eigenvalues increases very quickly near $\lambda_n = 1$;

Table 5.5 Convergence of the eigenvalues, in units of $Z(0)$, of the linearized spherically symmetric ($\ell = 0$) Boltzmann collision operator, with the Maxwell (p = 2) quadrature points and weights; quadrature points scaled so that $x_{max} = 6$

N	λ_1	λ_2	λ_3	λ_4	λ_5	λ_6	λ_7
10	−0.0182	0.63890	0.88444	0.95485	1.11878	1.48671	2.0014
20	−0.00121	0.66909	0.90988	0.98090	0.99541	1.0075	1.05629
30	−0.000243	0.67080	0.91123	0.98180	0.99673	0.99917	1.00288
40	−0.0000772	0.67120	0.91155	0.98199	0.99690	0.99949	0.99992
80	−0.0000316	0.67122	0.91157	0.98200	0.99691	0.99950	0.99993
BM[a]	0	0.671	0.912	0.982	0.997		
Mouhot[b]	0	0.0047					

[a] Bobylev and Mossberg (2008)
[b] The analytic bound reported by Mouhot (2007) with a constructive approach is $1/(96\sqrt{2e})$

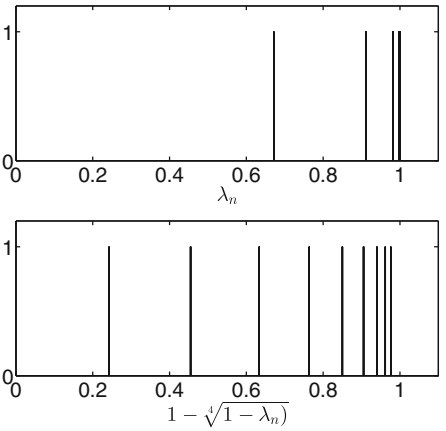

Fig. 5.6 (*Top graph*) The approach of the eigenvalues in units of $Z(0)$ of the linearized spherically symmetric ($\ell = 0$) collision operator, J, to the continuum boundary at $\lambda_n = 1$. (*Bottom graph*) Distorted diagram so as to decrease the density of eigenvalues near the continuum boundary

see Table 5.5. The lower graph is an artificial plot to spread out the eigenvalues near the continuum boundary. It is clear that the density of discrete eigenvalues near the boundary is very high. These discrete or "bound" eigenfunctions, $\psi_n(x)$, $n = 0$–5, are shown in Fig. 5.7 and exhibit $(n - 1)$ nodes. Of particular interest is the rapid variation of the higher eigenfunctions near the origin which explains the slow convergence with the Sonine-Laguerre polynomials. A large number of Sonine-Laguerre basis functions are required in order to accurately describe the behaviour of the eigenfunctions near the origin. The pseudospectral method is more accurate and flexible.

One can transform the integral equation to a differential equation, a procedure which is the opposite to finding a Green function for a differential equation so as to transform it to an integral equation. With this technique, originally developed by Wigner and Wilkins (1944) and subsequently by several other workers (Williams 1966; Kuščer and Corngold 1965; Kuščer and Williams 1967; Hoare 1971; Bobylev

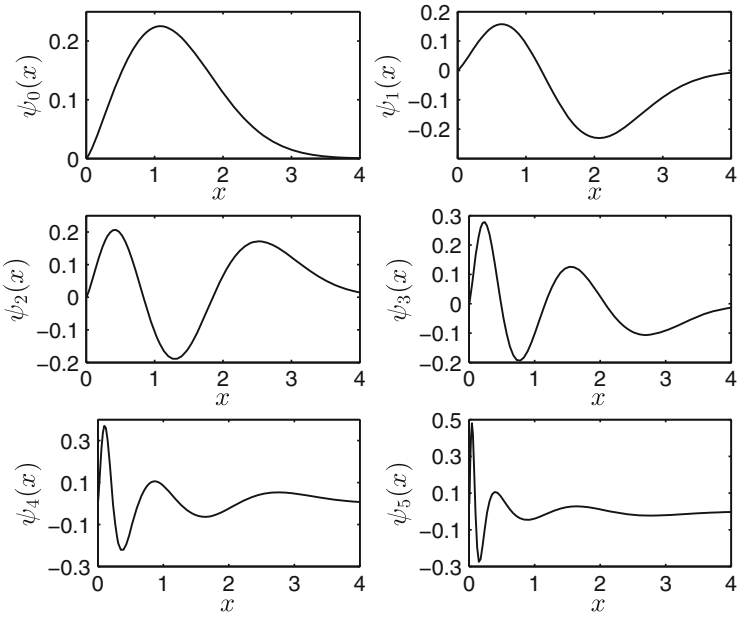

Fig. 5.7 The eigenfunctions, $\psi_n(x)$, of the linearized spherically symmetric ($\ell = 0$) Boltzmann collision operator determined with the Gauss-Maxwell quadratures with $w(x) = x^2 e^{-x^2}$

Table 5.6 Convergence of the eigenvalues of the linearized spherically symmetric ($\ell = 0$) Boltzmann collision operator with the multidomain method; λ_n in units of $Z(0)$

n	λ_n	$\frac{1-\lambda_n}{1-\lambda_{n+1}}$
2	0.67121	3.718
3	0.91156	4.913
4	0.98200	5.816
5	0.996904	6.149
6	0.9994966	6.231
7	0.9999192	6.247
8	0.9999871	6.247
9	0.99999793	6.247
10	0.999999667	6.212
	WKB	6.253

Reprinted from Shizgal (1984) with permission from National Research Council Research Press

and Mossberg 2008), the integral Boltzmann eigenvalue problem can be transformed to a Schrödinger equation. The Schrödinger equation is of an unusual form in that the potential is parameterized by the eigenvalue.

Bobylev and Mossberg (2008) solved the Schrödinger equation with a finite difference method and obtained the eigenvalues with a root searching algorithm.

Their results are shown in Table 5.5 together with the results by Mouhot (2007) with a constructive approach.

This Schrödinger equation in conjunction with a Wentzel-Kramers-Brillouin (WKB) analysis provides an understanding of the nature of the approach of the eigenvalues to the continuum boundary. A clear exposition was provided by Rahman and Sundaresan (1968) with the result that for the linearized collision operator, the eigenvalues obey the asymptotic result

$$\frac{1-\lambda_n}{1-\lambda_{n+1}} \approx \exp\left(\frac{4\pi}{\sqrt{47}}\right) \approx 6.2526. \tag{5.102}$$

In order to accurately verify the behavior of the eigenvalues in accordance with Eq. (5.102), a multidomain spectral method is used (Shizgal 1984). This involves subdividing the semi-infinite domain into many subintervals and the use of Gauss-Mehler quadrature points in each subdomain. Scaled Laguerre quadrature points are used in the last domain which extends to infinity. The division of the semi-infinite interval into subdomains varies from eigenfunction to eigenfunction, with a knowledge of the location of the nodes for each eigenfunction. The grid is thus optimized for each eigenfunction separately. This permits an accurate calculation of the discrete eigenvalues and the approach to the continuum boundary as shown in Table 5.6 in comparison with the WKB approximation. The asymptotic result, Eq. (5.102), appears to be attained by λ_7 or λ_8 but as is clear from the results in the table it is a numerical challenge to calculate accurate eigenvalues extremely close to 1.

5.6 Relaxation to Equilibrium in Binary Gas Mixtures

The approach to equilibrium of the distribution function of a minor constituent of mass m (sometimes referred to as a "test particle") dilutely dispersed in a background gas of mass M at equilibrium is a fundamental problem in kinetic theory (Kuščer and Williams 1967; Yan 1969) with important applications to hot atom relaxation (Park et al. 1989; Cline et al. 1990; Nan and Houston 1992; Matsumi et al. 1994; Nakayama et al. 2005; Zhang et al. 2007; Bovino et al. 2011).

The time dependent Boltzmann equation for a spatially uniform system in the absence of external forces is identical in form to Eq. (5.46) for the one-component gas, that is

$$\frac{\partial f(\mathbf{v},t)}{\partial t} = L[f(\mathbf{v},t)], \tag{5.103}$$

with the linear operator, L, defined by

$$L(f) = \int\int [F_1' f' - F_1 f] g\sigma(g,\theta) d\Omega d\mathbf{v}_1, \tag{5.104}$$

instead of Eq. (5.41) for the linearized collision operator.

The Boltzmann integral equation for this binary gas is of the same form as in Eq. (5.50) but with a different kernel that varies with the mass ratio, γ. In terms of the reduced velocities $\mathbf{x} = \mathbf{u}\sqrt{m/2k_BT}$ and $\mathbf{y} = \mathbf{v}\sqrt{m/2k_BT}$, and the cosine of the angle between the velocity vectors, $\overline{\mu}$, the kernel is given by

$$K_L(x, y, \overline{\mu}) = \frac{Z(0)(\gamma+1)^2}{2\pi\gamma^{3/2}} \frac{1}{\sqrt{x^2+y^2-2xy\overline{\mu}}} \times \exp\left[-x^2 + \frac{\gamma x^2 y^2(1-\overline{\mu}^2)}{x^2+y^2-2xy\overline{\mu}} - \frac{(\gamma-1)^2(x^2+y^2)}{4\gamma} - \frac{(\gamma^2-1)xy\overline{\mu}}{2\gamma}\right], \tag{5.105}$$

where $\gamma = M/m$ is the mass ratio of the two components Shizgal and Blackmore (1983). This result is derived with the definition, Eq. (5.103), and the kinematics of an elastic collision, Fig. 5.3, and Eqs. (5.47)–(5.49) (Chapman and Cowling 1970; Ferziger and Kaper 1972; Khurana and Thachuk 2013). In the sections that follow, we consider spectral and pseudospectral calculations of the eigenvalue spectrum of the integral operator, L, analogous to the results for J in the previous sections.

5.6.1 Spectral Calculation of the Eigenvalue Spectrum of the Linear Collision Operator, L, for a Binary Gas

We proceed as we did in Sect. 5.4.3 for the linearized Boltzmann collision operator. The matrix elements of L in the Sonine-Laguerre basis (for $\ell = 0$) are defined by

$$L_{nm}^{(0)} = \iiint F_1 F_2 S_1^{(n)} \left[S_1^{(m)'} - S_1^{(m)}\right] \sigma g d\Omega d\mathbf{v}_1 d\mathbf{v}_2, \tag{5.106}$$

evaluated as for the linearized case with the generating function for the basis functions, Eq. (5.63) and we have that

$$\langle G_s|L|G_t\rangle = 8\sqrt{\frac{2\pi k_B T_b}{\mu}} \frac{M_1 M_2 st}{(1-st)^2} \left(\frac{\sqrt{1-M_1(s+t)-[1-2M_1]st}}{1-[1-4M_1M_2]st}\right), = \sum_{n=0}^{\infty}\sum_{m=0}^{\infty} L_{nm}^{(0)} s^n t^m, \tag{5.107}$$

where $M_1 = m_1/(m_1+m_2)$, $M_2 = m_2/(m_1+m_2)$ and $\mu = m_1 m_2/(m_1+m_2)$. The matrix elements are evaluated as the coefficients of $s^n t^m$ in the power series expansion of $\langle G_s|L|G_t\rangle$ as in Sect. 5.4.3 for the linearized operator, J. A MAPLE code (Shizgal and Dridi 2010) developed for arbitrary differential cross section can

Table 5.7 Convergence of the eigenvalues, in units of $Z(0)$, of the linear ($\gamma = 1$) spherically symmetric ($\ell = 0$) Boltzmann collision operator with the Sonine-Laguerre basis functions

N	λ_1	λ_2	λ_3	λ_4	λ_5	λ_6
4	0.83191	1.23300	1.80103	2.55781		
6	0.82351	1.13057	1.53697	2.04776	2.64985	3.38573
8	0.82081	1.08006	1.40112	1.80739	2.27335	2.79345
10	0.81980	1.05092	1.31698	1.65904	2.05109	2.48123
20	0.81905	1.00022	1.14237	1.33917	1.57346	1.83352
30	0.81902	0.98819	1.08405	1.22258	1.39305	1.58660
40		0.98384	1.05604	1.16244	1.29671	1.45194
50		0.98192	1.04007	1.12607	1.23674	1.36656
60		0.98099	1.03005	1.10202	1.19613	1.30775

be used to extract the matrix elements based on Eq. (5.107) for the hard sphere cross section. Lindenfeld and Shizgal (1983) also provided a closed form expression for the matrix elements.

The numerical diagonalization of the matrix $\mathbf{L}$ of order N gives the eigenvalues and eigenfunctions. The derivation of the expression for $L_{nm}^{(0)}$ for the hard sphere cross section and arbitrary γ, which requires considerable algebra, is given by Eq. (28) and Appendix A in Lindenfeld and Shizgal (1983).

For $\gamma = 1$, the convergence of the eigenvalues versus the number of basis functions, N, is shown in Table 5.7. The convergence of the eigenvalues is from above consistent with a variational theorem. The smallest eigenvalue, $\lambda_0 = 0$, is consistent with particle conservation. With up to 60 basis functions, there are only two discrete eigenvalues, λ_1 and λ_2, whereas the others shown are in the continuum. Only λ_1 is converged to five significant figures with 30 basis functions. The convergence of the eigenvalues with the Sonine-Laguerre basis set is slow, similar to the results for J in Table 5.4.

5.6.2 *Pseudospectral Calculation of Eigenvalue Spectrum of the Linear Collision Operator, L, for a Binary Gas*

The kernel in the Boltzmann equation for a binary gas mixture is given by Eq. (5.105) and depends on $\overline{\mu}$ and the mass ratio, $\gamma = M/m$. We expand the kernel in Legendre polynomials in $\overline{\mu}$ as given by Eq. (5.53) for the linearized operator. The scalar kernels are denoted by $k_L^{(\ell)}(x, y)$ analogous to the $k_J^{(\ell)}(x, y)$ for the linearized collision operator, J. The eigenvalues and eigenfunctions of the collision operator for given ℓ are defined by the set of integral equations

$$\int_0^\infty k_L^{(\ell)}(x, y)\psi_{n,\ell}(x)dx - Z(y)\psi_{n,\ell}(y) = -\lambda_{n,\ell}\psi_{n,\ell}(y). \tag{5.108}$$

The collision frequency, $Z(x)$, in Eq. (5.108), is given by

$$Z(x) = \int_0^\infty k_L^{(0)}(x, y)dy,$$
$$= \frac{A}{2}\left[e^{-\gamma x^2} + \left[2\sqrt{\gamma}x + \frac{1}{\sqrt{\gamma}x}\right]\frac{\sqrt{\pi}}{2}\text{erf}(\sqrt{\gamma}x)\right], \tag{5.109}$$

where $A = n_b\pi d^2\sqrt{k_B T_b/2m}$ and $Z(0) = 2A$. The kernel $k_L^{(0)}(x, y)$ is the Wigner-Wilkins kernel (Hoare and Kaplinsky 1970) given by

$$k_L^{(0)}(x, y) = \frac{A}{2}Q^2\sqrt{\pi}\Big[\text{erf}[Qy + Rx] + e^{x^2-y^2}\text{erf}[Ry + Qx]$$
$$\pm\Big[\text{erf}[Qy - Rx] + e^{x^2-y^2}\text{erf}[Qy + Rx]\Big]\Big], \tag{5.110}$$

where we have used reduced speeds (x, y) and the $+$ in $\pm$ is for $y < x$ and the $-$ is for $y > x$. The hard sphere cross section is πd^2, $Q = \frac{1}{2}[\frac{1}{\sqrt{\gamma}} + \sqrt{\gamma}]$ and $R = \frac{1}{2}[\frac{1}{\sqrt{\gamma}} - \sqrt{\gamma}]$.

The pseudospectral solution of the eigenvalue problem based on a quadrature reduces Eq. (5.108) to the linear algebraic problem

$$\sum_{j=1}^{N} W_j x_j^2 k_L^{(0)}(x_j, x_i)\psi_{n,\ell}(x_j) - Z_i\psi_{n,\ell}(x_i) = -\lambda_{n,\ell}\psi_{n,\ell}(x_i). \tag{5.111}$$

For the most part, $\psi_n(x)$ and λ_n are for $\ell = 0$, unless otherwise noted. Since particle number is conserved, there is one zero eigenvalue, $\lambda_0 = 0$. The results for the Gauss-Maxwell quadrature is shown in Table 5.8. With 80 quadrature points, we find four discrete eigenvalues converged to 4 significant figures. The results reported by Bobylev and Mossberg (2008) are obtained from the solution of a Schrödinger equation with a potential parametrized by the eigenvalue sought. As a consequence, an iteration is required to converge to each eigenvalue as shown in Figs. 1 and 2 of their paper. The results in the table are also compared with the cubic B-spline solution by Khurana and Thachuk (2012) for which only two discrete eigenvalues are reported.

The study of the approach of the eigenvalues to the continuum boundary requires a very fine grid defined with the subdivision of the semi-infinite interval into 12 sub-intervals with 8 Fejér quadrature points in each interval except the last where a shifted Laguerre quadrature is used (Shizgal 1984). The interval boundaries are chosen to approximately coincide with the roots of the highest bound eigenfunction desired. We refer to this approach as the adaptive multidomain method.

Table 5.8 Convergence of the eigenvalues in units of $Z(0)$ of the linear ($\gamma = 1$) spherically symmetric ($\ell = 0$) Boltzmann collision operator for Gauss-Maxwell quadrature points ($p = 2$)

N	λ_1	λ_2	λ_3	λ_4	λ_5	λ_6
6	0.81359	0.97258	1.16137	1.55419	2.09752	0.00000
8	0.81616	0.97328	1.05678	1.29033	1.65256	2.11734
10	0.81736	0.97672	1.01756	1.15769	1.40627	1.74453
14	0.81831	0.97897	0.99904	1.04972	1.17109	1.36147
20	0.81874	0.97940	0.99772	1.00972	1.05415	1.13938
30	0.81893	0.97963	0.99829	1.00049	1.01072	1.03677
40	0.81898	0.97969	0.99834	0.99984	1.00274	1.01236
60	0.81901	0.97972	0.99838	0.99986	1.00025	1.00223
80	0.81902	0.97973	0.99838	0.99988	1.00001	1.00058
BM[a]	0.8190	0.9795	0.9985	0.999_5		
KT[b]	0.8190	0.9797				

[a] Eigenvalues determined from the solution of the Schrödinger equation (Bobylev and Mossberg 2008)

[b] Cubic B-spline solution of the integral eigenvalue problem with 60 intervals (Khurana and Thachuk 2012)

Table 5.9 Approach to the continuum boundary of the eigenvalues, in units of $Z(0)$, of the linear ($\gamma = 1$) spherically symmetric Boltzmann ($\ell = 0$) collision operator with the multidomain method

n	λ_n	$\frac{1-\lambda_n}{1-\lambda_{n+1}}$
1	0.8190221	
2	0.9797339	5.526
3	0.99838853	8.930
4	0.99988132	12.58
5	0.9999913460	13.58
6	0.99999936318	13.71
7	0.999999958353	13.59
8	0.9999999926736	15.29
	WKB	13.74

The lower order eigenvalues calculated in this way are shown in Table 5.9 in comparison with the WKB asymptotic behaviour (Rahman and Sundaresan 1968)

$$\frac{1-\lambda_{n,\ell}}{1-\lambda_{n+1,\ell}} \approx \exp\left[\frac{4\pi}{\sqrt{6(1+\frac{1}{\gamma})^2-(2\ell+1)^2}}\right], \tag{5.112}$$

which appears to occur by λ_6 or λ_7. It is clear that the calculation of these eigenvalues near to the continuum boundary is a challenging numerical exercise.

The eigenfunctions corresponding to these eigenvalues are shown in Fig. 5.8 and the rapid variation near to the origin is clear. There are several nodes very close to the origin and the others occur for much larger x. We contrast this behaviour

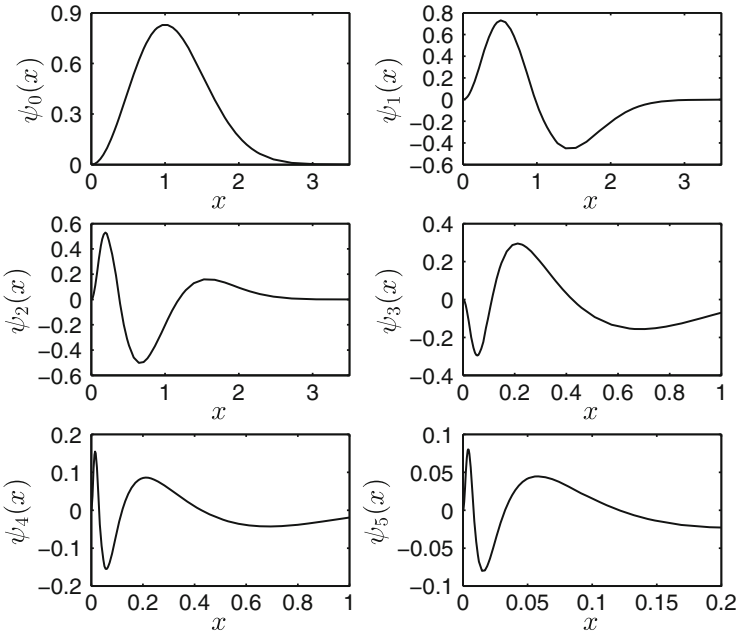

Fig. 5.8 The eigenfunctions, $\psi_n(x)$, of the linear Boltzmann collision operator ($\ell = 0, \gamma = 1$) determined with the adaptive multidomain quadrature

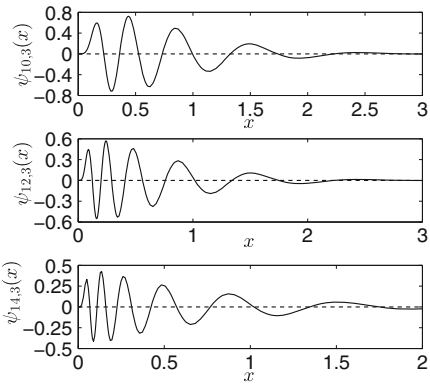

Fig. 5.9 Eigenfunctions of the linear ($\gamma = 1/8$) Boltzmann collision operator with the adaptive multidomain method for $\ell = 3$. The approach of the eigenvalues, $\lambda_{n,3}$, to the continuum boundary is shown in Table 5.10 in comparison with the asymptotic WKB result (Rahman and Sundaresan 1968)

with the eigenfunctions for $\ell = 3$ and $\gamma = 1/8$ in Fig. 5.9. Table 5.10 lists the corresponding eigenvalues and the WKB ratio and it is clear that these eigenvalues below the continuum boundary can be more easily evaluated. The oscillations of the eigenfunctions can be resolved over this larger domain than for the results in Fig. 5.8. With the multidomain approach, the variational theorem is more difficult to verify as the nodes and number of quadrature points between nodes is specific for a particular eigenfunction.

Table 5.10 Approach to the continuum boundary of the eigenvalues, in units of $Z(0)$, of the linear ($\gamma = 1/8$) Boltzmann collision operator with the adaptive multidomain method for $\ell = 3$

n	$\lambda_{n,3}$	$\frac{1-\lambda_{n,3}}{1-\lambda_{n+1,3}}$
1	0.42888	1.4444
2	0.60461	1.4978
3	0.73602	1.5675
4	0.83159	1.6405
5	0.89734	1.6912
6	0.93930	1.7197
7	0.96470	1.7459
8	0.97978	1.7691
9	0.98857	1.7873
10	0.99361	1.8004
11	0.99645	1.8092
12	0.99804	1.8150
13	0.99892	1.8186
14	0.99941	1.8203
	WKB	1.824

5.6.3 *Spectral Method of Solution of the Linear Boltzmann Equation with Quantum Cross Sections; Relaxation to Equilibrium and the Kullback-Leibler Entropy*

In this section, we consider the binary gas mixture defined in the previous section with the application to N-He and Xe-He mixtures for which accurate interatomic interaction potentials are known and the corresponding quantum differential cross sections can be calculated (Sospedra-Alfonso and Shizgal 2013). We write the spherically symmetric distribution function ($\ell = 0$) as $f(x,t) = F[1 + \phi(x,t)]$ and expand $\phi(x,t)$ in Sonine-Laguerre polynomials,

$$\phi(x,t) = \sum_{n=1}^{N} a_n(t) S^{(n)}(x^2), \tag{5.113}$$

and substitute $f(x,t)$ into Eq. (5.103) that defines the initial value problem. With the subsequent multiplication by $S^{(m)}(x^2)$ and integration over $\mathbf{v}$, the Boltzmann equation is reduced to the set of linear ordinary differential equations

$$\frac{d\hat{a}_m(t)}{dt} = \sum_{n=1}^{N} \hat{L}^{(0)}_{mn} \hat{a}_n(t), \tag{5.114}$$

where $\hat{a}_n = \sqrt{N_n} a_n$ such that $\hat{L}^{(0)}_{nm} = L^{(0)}_{nm}/\sqrt{N_n N_m}$ is symmetric, and $N_n = 2\Gamma(n + 3/2)/(n!\sqrt{\pi})$ is the normalization of the Sonine-Laguerre polynomials.

The matrix elements, $L_{nm}^{(0)}$ were previously evaluated, Eq. (5.107), for the hard sphere cross section using the generating function for the Sonine-Laguerre polynomials. This methodology can also be used for realistic cross sections (Shizgal and Dridi 2010) with the result that the matrix elements can be written in terms of the classic Omega integrals of transport theory (Hirschfelder et al. 1954; Chapman and Cowling 1970; Mason and McDaniel 1988) defined by

$$\Omega^{(\ell)}(k) = 2\pi \int_0^\infty \int_0^\pi e^{-z^2} z^{2k+3} (1 - \cos^\ell \theta) \sigma(E, \theta) \sin\theta d\theta dz, \tag{5.115}$$

where $z = \sqrt{E/k_B T_b}$ and

$$L_{nm}^{(0)} = \sum_{\ell=0}^{n} \sum_{k=1}^{n+m-\ell} C_{\ell,k} \Omega^{(\ell)}(k). \tag{5.116}$$

The coefficients, $C_{\ell,k}$ were determined with the generating function method and a MAPLE code is available (Shizgal and Dridi 2010). The differential cross sections vary rapidly with angle (see Fig. 3.19b) and a Simpson's rule integration can be used to accurately calculate the angular integral in $\Omega^{(\ell)}(k)$ and a Gauss-Laguerre quadrature for the reduced speed z. In this way, realistic cross sections can be used in a spectral based solution of the Boltzmann equation.

The time dependent solution is expressed in terms of the discrete eigenvalues, λ_n, and eigenvectors, U_{km}, of $\mathbf{L}$, that is

$$\sum_{k=1}^{N} L_{nk} U_{km} = -\lambda_n U_{nm}. \tag{5.117}$$

We show in Fig. 5.10 the results of a Sonine-Laguerre spectral calculation of the eigenvalue spectrum for the two gas mixtures, namely N in He and Xe in He with realistic quantum cross sections that define the collision operator (Sospedra-Alfonso and Shizgal 2013). The eigenvalues $\lambda_n < Z(0)$ are in the discrete spectrum while the eigenvalues $\lambda_n > Z(0)$ are in the continuum. The comparison with the equivalent hard sphere cross section shown in the figure demonstrates that the hard sphere cross section is a good approximation. For the Xe-He system with the small mass ratio, $\gamma = 0.030$, there are a large number of converged discrete eigenvalues whereas for the N-He system with a larger mass ratio, $\gamma = 0.29$, there are much fewer converged eigenvalues. The three discrete eigenvalues for N-He and the 9 discrete eigenvalues for Xe-He are converged to three significant figures with $N = 30$ and $N = 15$, respectively. This demonstrates the more rapid convergence of the Sonine-Laguerre basis functions for the Xe-He system which is closer to the Rayleigh limit than is N-He. In Chap. 6, we discuss the Fokker-Planck equations in the Rayleigh and Lorentz limits and the choice of basis functions.

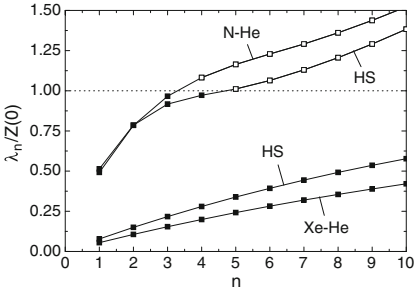

Fig. 5.10 Eigenvalue spectrum of the Boltzmann collision operator for binary mixtures with He as the background gas. The *filled squares* correspond to eigenvalues in the discrete spectrum and *open squares* are unconverged eigenvalues in the continuum. HS denotes the results with the hard sphere cross section, 18 Å^2 for N-He and 27 Å^2 for Xe-He. The other *curves* correspond to the results with a realistic cross section for each pair. Thirty Sonine-Laguerre polynomials were used. Reprinted from Sospedra-Alfonso and Shizgal (2013) with permission from the American Institute of Physics

The time dependent solution of the linear equations, Eq. (5.114), is

$$\hat{a}_n(t) = \sum_{k=1}^{N} c_k U_{nk} e^{-\lambda_k t}, \tag{5.118}$$

and the expansion of $\phi(x, 0)$ defines $\hat{a}_n(0)$. The expansion coefficients, c_k, in Eq. (5.118) are determined from the initial condition

$$c_k = \sum_{n=1}^{N} U_{kn} \hat{a}_n(0). \tag{5.119}$$

The eigenfunctions are given by the expansion in Sonine-Laguerre polynomials

$$\psi_n(x^2) = \sqrt{\frac{2}{\sqrt{\pi}}} \sum_{k=1}^{N} U_{kn} \frac{S^{(k)}(x^2)}{\sqrt{N_k}}, \tag{5.120}$$

and the time dependent distribution function is

$$f(x^2, t) = \frac{2}{\sqrt{\pi}} x^2 e^{-x^2} \left[1 + \sum_{n=1}^{N} c_n e^{-\lambda_n t} \psi_n(x^2) \right]. \tag{5.121}$$

It is readily shown with the orthogonality of the Sonine-Laguerre polynomials that the average energy of the energetic atoms is given exactly in terms of $a_1(t)$, that is

$$E(t) = \frac{3k_B T_b}{2} [1 - a_1(t)]. \tag{5.122}$$

However, the average energy in terms of $a_1(t)$ is coupled to the higher order expansion coefficients, $a_n(t)$ in Eq. (5.114), and the time dependence is multiexponential as given by Eq. (5.118). If the set of moment equations, Eq. (5.114), is truncated at $a_1(t)$, the resulting approximation to the energy relaxation is a pure exponential. Alternatively, we can approximate the distribution function with a local Maxwellian distribution function parametrized by the time dependent temperature (Mozumder 1981; Shizgal 1981b), that is

$$\frac{dT}{dt} = -K_{LM}[T_{eff}(t)]\Big[T(t) - T_b\Big], \tag{5.123}$$

where $T_{eff} = [MT(t) + mT_b]/(M + m)$ and

$$K_{LM}(T_{eff}) = \frac{16}{3\pi} M_1 M_2 \sqrt{\frac{T_{eff}}{T_b}} \int_0^\infty z^5 e^{-z^2} \sigma_{mt}(z^2 k_B T_{eff}) dz. \tag{5.124}$$

The momentum transfer cross section in Eq. (5.124) is defined by

$$\sigma_{mt}(E) = 2\pi \int_0^\pi (1 - \cos\theta)\sigma(E, \theta) \sin\theta d\theta. \tag{5.125}$$

We consider the approach to equilibrium with an initial test particle Gaussian energy distribution of the form

$$f(E, 0) = \frac{C}{\sqrt{k_B T_b}} \sqrt{E} \exp\left[- \alpha \sqrt{\frac{E}{k_B T_b}} - x_0)^2 \right], \tag{5.126}$$

where $T_b = 300\,\mathrm{K}$ and $N_b = 3.27 \times 10^{16}\,\mathrm{cm}^{-3}$ consistent with experimental conditions (Zhang et al. 2007). The parameters $\alpha = 5$ and $x_0 = 2$ are chosen, and C is a normalization. A major difficulty can be the expansion of the initial distribution with Eq. (5.113). The expansion of a Maxwellian at T_b in Sonine-Laguerre polynomials is equivalent to the representation of the Sonine-Laguerre polynomials with the generating function defined by Eq. (4.54) in Sect. 4.5.1. The Sonine-Laguerre expansion of many initial distribution functions, such as a Gaussian, that model energetic distributions with temperatures above the bath temperature will converge very slowly if at all.

The time dependence of the distribution functions is shown in Fig. 5.11(A) for N in He and in Fig. 5.11(B) for Xe in He for an initial energy of 0.12 eV. A sufficient number of basis functions are used so as to fit the initial distribution to three significant figures. Although there are only a few discrete eigenvalues in Eq. (5.121) that converge with an increase in N, there a large number of eigenvalues, $\lambda_n > Z(0)$ that are in the continuum. Nevertheless, the summation in Eq. (5.121) that replaces the

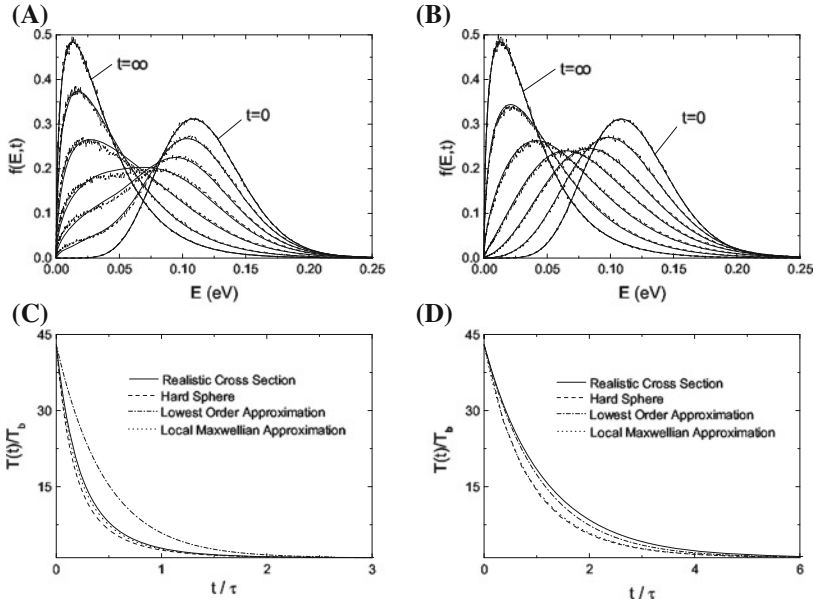

Fig. 5.11 (*Upper graphs*) Energy distribution function for (**A**) N-He and (**B**) Xe-He for $t/\tau = 0.07, 0.16, 0.29, 0.51$ and 0.29 where τ equals (**A**) 76 ns and (**B**) 56 ns; The initial distribution function is a Gaussian with $E(0) = 0.12$ eV; The *dashed curves* are the results with a Monte-Carlo simulation. (*Lower graphs*) Time evolution of the temperature ratio for (**C**) N-He and (**D**) X-He with an initial Gaussian with $E(0) = 1.67$ eV. The results are converged to three significant figures with 30 Sonine-Laguerre polynomials. Reprinted from Sospedra-Alfonso and Shizgal (2013) with permission from the American Institute of Physics

integral over the continuum eigenvalues, converges with an increase in N and thus the solution converges even though λ_k and c_k change with N. The dashed (noisy) curves in the figures are the results of Monte Carlo simulations (Sospedra-Alfonso and Shizgal 2013) that validate the results with the Sonine-Laguerre expansion.

The relaxation of the temperature is shown in Fig. 5.11(C), (D) for N-He and Xe-He mixtures, respectively, with $E(0) = 1.67$ eV. The curve identified as the lowest order approximation with the one moment, $a_1(t)$, is a pure exponential while the other results are multi-exponential curves. A major objective of the kinetic theory is the approach to equilibrium (Ziff et al. 1981; Mouhot 2006). We use the Kullback-Leibler entropy (Kullback and Leibler 1951; Mozumder 1981; Shizgal 2007) defined by

$$\Sigma_{SS}(t) = -4\pi \int v^2 f(v,t) \ln\left[\frac{f(v,t)}{F(v,T_b)}\right] dv, \tag{5.127}$$

and another similar functional that is a measure of the departure of the distribution function from the local Maxwellian F_{LM} and given by

$$\Sigma_{LM}(t) = -4\pi \int v^2 f(v,t) \ln \left[\frac{f(v,t)}{F_{LM}(v, T(t))} \right] dv. \tag{5.128}$$

The local Maxwellian varies with $T(t)$ and it is important to note that $\Sigma_{LM}(t)$ is not an entropy. These are two examples of measures for the departure of one function from another for which there are many choices especially in signal analysis (Cha 2007) analogous to the choice of least squares approximation used in Chap. 4 to analyze the convergence of different expansions.

The time dependence of both quantities is shown in Fig. 5.12 with $\Sigma_{SS}(t)$ as the dashed curves and $\Sigma_{LM}(t)$ as the solid curves for three different initial energies. $\Sigma_{SS}(t)$ is a monotonically increasing function of time consistent with an entropy whereas $\Sigma_{LM}(t)$ can exhibit extremum values as a function of time. The relaxation of the shape of the nonequilibrium distribution function can be determined experimentally with Doppler spectroscopy (Nakayama et al. 2005; Zhang et al. 2007). The translational energy relaxation can also be followed experimentally (Park et al. 1989).

The spectral method of solution of the Boltzmann equation with the Sonine-Laguerre polynomials provides sufficiently converged solutions so as to permit a useful comparison with experiment. The choice of the initial distribution is limited by its expansion in this basis set. Round-off errors can also occur in the calculation of the matrix elements if large basis sets are required.

A pseudospectral approach based on the Gauss-Maxwell or some other quadrature can also be employed with realistic quantum mechanical elastic scattering cross sections. The details of these applications is beyond the scope of this book and can be found elsewhere (Bovino et al. 2009, 2011; Sospedra-Alfonso and Shizgal 2012a), and references therein. The calculation of the spherically symmetric kernel for realistic cross sections requires an integration over E and θ of the differential cross section $\sigma(E, \theta)$ (see Fig. 3.19b). The cusp in the resulting kernel tend to be extremely narrow and the accurate integration over the cusp in the kernel requires a very fine grid (Kharchenko et al. 1998).

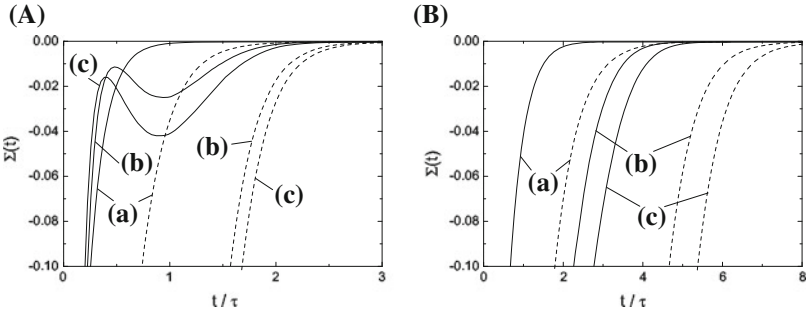

Fig. 5.12 Time evolution of the Kullback-Leibler relative entropies $\Sigma_{SS}(t)$ (*dashed curve*) and $\Sigma_{LM}(t)$ (*solid curve*) for (**A**) N-He ($\tau = 76$ ns) and (**B**) Xe-He ($\tau = 56$ ns). Initial average energies are (*a*) 0.12 eV, (*b*) 0.94 eV and (*c*) 1.67 eV with an initial Gaussian distribution. Reprinted from Sospedra-Alfonso and Shizgal (2013) with permission from the American Institute of Physics

In Chap. 6, we report the eigenvalue spectrum of the Fokker-Planck equation with the Coulomb cross section. We will show that the eigenvalue spectrum has an infinite number of discrete eigenvalues and a continuum. However, in contrast to the behaviour with the Boltzmann equation, the spectrum becomes completely continuous for a particular mass ratio (with the exclusion of $\lambda_0 = 0$). The continuum eigenfunctions are L^2 square integrable discrete eigenfunctions as discussed by Reinhardt (1979) for quantum mechanical problems. In the absence of a single nonzero discrete eigenvalue, that is the "spectral gap", the approach to equilibrium ceases to be a pure exponential (Corngold 1981).

5.7 Two Dimensional Anisotropic Distributions

In the previous sections, we provided a description for the relaxation to equilibrium of isotropic nonequilibrium distributions. In the sections that follow, we consider several physical systems for which the distribution function of the energetic species is anisotropic. Laser photofragmentation of molecules can produce energetic atoms with anisotropic nonequilibrium distributions (Cline et al. 1990; Nicholson et al. 1996). The relaxation of the anisotropy can be followed with Doppler spectroscopy. In Sect. 5.7.1, we consider a spectral solution of the Boltzmann equation with a model initial anisotropic distribution. The decay of the anisotropy can be uncoupled from the energy relaxation in the disparate mass ratio, $\gamma = M/m$, limits. This provides the rationale for the use of the Fokker-Planck equation in the Rayleigh limit, $\gamma \to 0$, and Lorentz limit, $\gamma \to \infty$, (Andersen and Shuler 1964) as discussed in Chap. 6.

In Sect. 5.7.2, we treat the Milne problem for a two component system previously considered in the context of the radiative transfer problem (the one-speed model) in Sect. 5.3. This Milne problem also serves as a model for the escape of planetary atmospheres (Fahr and Shizgal 1983). Both rarefied gas dynamical problems are in three dimensions, namely position, speed and the anisotropy variable, $\mu = \cos\theta$, where θ denotes the orientation of the particle velocity relative to a polar axis. A spectral method is used to solve the Boltzmann equation for the Milne problem whereas a combined spectral/pseudospectral method is used for the planetary escape problem (Shizgal and Blackmore 1986).

5.7.1 Pseudospectral/Spectral Solution of the Boltzmann Equation; Relaxation of Anisotropic Distributions in a Binary Gas

A nonthermal anisotropic distribution function of atoms can be produced in the laboratory by laser photolysis of a molecule producing an energetic atom. The nascent distributions then relax by collisions with background inert gas atoms

and the approach to equilibrium is followed with Doppler spectroscopy (Park et al. 1989; Taatjes et al. 1990). The relaxation of anisotropic nonthermal distributions of I^* produced by photofragamentation of C_3F_7I has been studied experimentally (Cline et al. 1990; Nicholson et al. 1996). It is possible to generate with linearly polarized light an initial distribution that is a product of an isotropic distribution and an anisotropy factor of the form

$$f(v, \mu, 0) = f(v, 0)[1 + \beta(0) P_2(\mu)], \tag{5.129}$$

where $\mu = \cos\theta$ and θ gives the orientation of the velocity vector, $\mathbf{v}$, relative to some polar axis. The parameter $\beta(t)$ is the anisotropy parameter which can also depend on the particle velocity. Matsumi et al. (1994) carried out similar studies of the anisotropy and velocity relaxation of energetic $O(^1D)$ atoms in different moderators.

In this section, we consider a pseudospectral solution of the linear Boltzmann equation with a hard sphere cross section and study the relaxation versus the mass ratio $\gamma = M/m$, with m the test particle mass and M the mass of the background species. We choose for convenience an initial anisotropic nonequilibrium distribution of the form

$$f(x, \mu, 0) = C \frac{(\mu + 1)^\beta}{x} \exp\left[- \alpha(E_0 - x^2)^2 \right], \tag{5.130}$$

where α, β and E_0 are constants to be specified and C is a normalization. The constant β is generally a small integer in keeping with the experimentally generated anisotropic distribution as a single Legendre polynomial, Eq. (5.129).

The Boltzmann equation for this spatially uniform system is given by Eq. (5.103) with the collision operator defined by Eg. (5.104) or equivalently the kernel in Eq. (5.105). The collision frequency is given by

$$Z(y) = 2\pi \int_0^\infty \int_{-1}^{1} K_L(x, y, \overline{\mu}) x^2 d\overline{\mu} dx, \tag{5.131}$$

which is equivalent to Eq. (5.109). The Wigner-Wilkins kernel, Eq. (5.110), is the spherical average of $K_L(x, y, \overline{\mu})$. We expand the kernel, Eq. (5.105), in Legendre polynomials, that is

$$K_L(x, y, \overline{\mu}) = \sum_{\ell=0}^{\infty} k_L^{(\ell)}(x, y) P_\ell(\overline{\mu}), \tag{5.132}$$

where the expansion coefficients are the kernels

$$k_L^{(\ell)}(x, y) = \frac{2\ell + 1}{2} \int_{-1}^{1} K_L(x, y, \overline{\mu}) P_\ell(\overline{\mu}). \tag{5.133}$$

Thus, the relaxation of the anisotropic distribution for the initial distribution given by Eq. (5.130), is described with the set of uncoupled integral equations for each ℓ, that is

$$\frac{\partial f_\ell(x,t)}{\partial t} = \int_0^\infty k_L^{(\ell)}(x,y) f_\ell(y,t) y^2 dy - Z(x) f_\ell(x,t), \tag{5.134}$$

where the initial distributions, $f_\ell(x,0)$, is determined from Eq. (5.130). The spherical components, $f_\ell(x,t)$, of the distribution function are defined as in Eq. (5.138). The kernels, $k_L^{(\ell)}(x,y)$ can be accurately evaluated with a Gauss-Legendre quadrature for the $\overline{\mu}$ integration in Eq. (5.133).

The set of integral equations, Eq. (5.134), can be solved with the Maxwell quadrature points, $\{x_i\}$, and big weights, $\{W_i = w_i/w(x_i)\}$, based on the weight function $w(x) = x^2 e^{-x^2}$ defined in Chap. 3, Sect. 3.3. The discretized version is thus

$$\frac{\partial f_\ell(x_i,t)}{\partial t} = \sum_{j=1}^{N-1} B_{ij} f_\ell(x_i,t), \tag{5.135}$$

where the matrix $\mathbf{B}$ is defined by

$$B_{ij} = W_j k_\ell(x_i,x_j) x_j^2 - Z(x_i)\delta_{ij}. \tag{5.136}$$

As before we express the solution to each integral equation in terms of the eigenvalues $\lambda^{(\ell)}$ and eigenfunctions $\mathbf{U}$, that is

$$\mathbf{B}\cdot\mathbf{U} = \mathbf{U}\cdot\lambda. \tag{5.137}$$

The ℓ dependence of the matrices in Eq. (5.137) is not shown explicitly. The initial values of $f_\ell(x,0)$ are determined from the initial condition, Eq. (5.130). The expansion of $f(x,\mu,t)$ is in Legendre polynomials in μ, that is

$$f(x,\mu,t) = \sqrt{\frac{2\ell+1}{2}} \sum_\ell^\infty f_\ell(x,t) P_\ell(\mu), \tag{5.138}$$

so that

$$f_\ell(x,t) = \sqrt{\frac{2\ell+1}{2}} \int_{-1}^{1} f(x,\mu,t) P_\ell(\mu) d\mu, \tag{5.139}$$

which is evaluated with Gauss-Legendre quadrature points $\{\mu_i\}$ and weights $\{v_i\}$, and written as the transform

$$f_\ell(x,t) = \sum_{i=1}^{N} T_{\ell i}^{(b)} f(x,\mu_i,t), \tag{5.140}$$

where the transformation matrix is

$$T_{\ell i}^{(b)} = \sqrt{\frac{2\ell+1}{2}} v_i P_\ell(\mu_i). \tag{5.141}$$

The inverse of this transformation is

$$f(x,\mu_i,t) = \sum_{\ell=0}^{N-1} T_{i\ell}^{(f)} f_\ell(x,t), \tag{5.142}$$

where

$$T_{i\ell}^{(f)} = \sqrt{\frac{2\ell+1}{2}} P_\ell(\mu_i), \tag{5.143}$$

and $\mathbf{T}^{(b)} \cdot \mathbf{T}^{(f)} = \mathbf{I}$.

The time dependent distribution is expressed in terms of the eigenvalues and eigenfunctions of $\mathbf{B}$, that is

$$f_\ell(y_i,t) = \sum_{j=0}^{N} U_{ij}^{(\ell)} C_j^{(\ell)} \exp(-\lambda_{j\ell} t), \tag{5.144}$$

with the $C_j^{(\ell)}$ evaluated with the initial distributions

$$C_j^{(\ell)} = \sum_{k=0}^{N-1} \left(U^{-1}\right)_{jk} f_\ell(x_k,0). \tag{5.145}$$

We choose $\beta = 2$ in the initial distribution and solve three integral equations, Eq. (5.134), with $\ell = 0, 1$ and 2. For each, 60 Gauss-Maxwell quadrature points were sufficient to give the convergent distributions shown in Figs. 5.13, 5.14 and 5.15. For each ℓ, the collision operator has a discrete and continuous eigenvalue spectrum. The continuous eigenfunctions are square integrable in the discrete L^2 space that is used (Reinhardt 1979). This is another illustration that the discretization of the continuum portion of the spectrum leads to numerically convergent solutions.

The relaxation of the anisotropic distribution is shown in Figs. 5.13, 5.14 and 5.15 for mass ratios $\gamma = 1/16, 1$ and 16, respectively, for the initial condition, Eq. (5.130) with $\beta = 2$, $E_0 = 900$ and $\alpha = 10^{-4}$. The results for the small mass ratio approaching the Rayleigh limit are shown in Fig. 5.13. The anisotropy of the distribution function is maintained while there is a relatively rapid energy exchange.

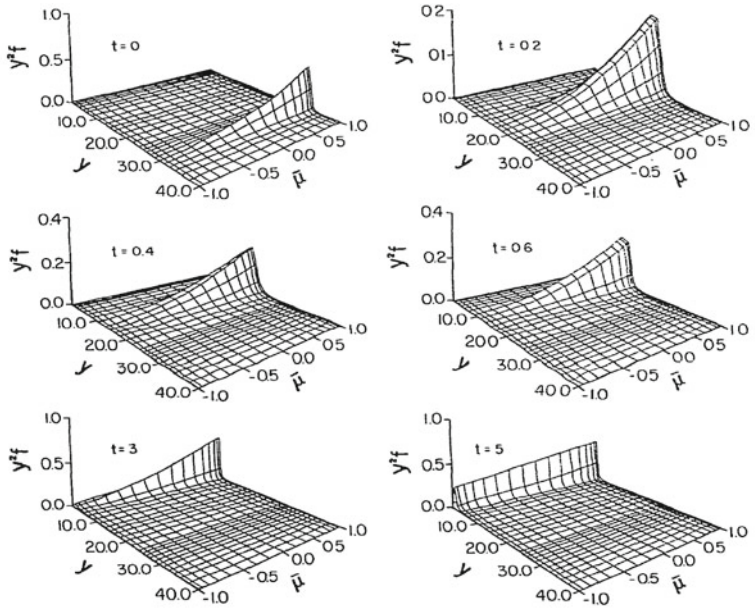

Fig. 5.13 Time evolution of the anisotropic distribution for mass ratio $M/m = 1/16$. The initial distribution is given by Eq. (5.130) with $\beta = 2$, $E_0 = 900$ and $\alpha = 10^{-4}$. The time t is in units of $\tau = [Nd^2\sqrt{2\pi k_B T/M}]^{-1}$. In the figure $\overline{\mu} \equiv \mu$. Reprinted from Shizgal and Blackmore (1983) with permission from Elsevier

There is an efficient transfer of energy on collision relative to the randomization of the particle direction. For the unit mass ratio case in Fig. 5.14, the anisotropy and the energy relaxation appear to occur on the same time scale. In addition, since the energy transfer for equal masses is very efficient; the energy relaxation is rapid as can be seen by the growth of the peak in the distribution in the thermal energy regime. This distribution function in this case is bimodal in speed with a peak at both high and low speeds.

The results in Fig. 5.15 for the larger mass ratio approaching the Lorentz limit, show an efficient change in direction of the light particle on collision. The anisotropy of the distribution disappears quickly and the energy relaxation occurs on a longer time scale. In the limit of very small mass ratios, which is applicable for the relaxation of electrons in atoms, the anisotropy decays many orders of magnitude faster than the energy relaxation. Thus, for electron transport in the Lorentz limit it is often sufficient to use the two-term approximation, that is with $\ell = 0$ and $\ell = 1$ (Pitchford et al. 1981; Pitchford and Phelps 1982; Shizgal and McMahon 1985; Hagelaar and Pitchford 2005); see Chap. 6, Sect. 6.3.

The relaxation of nonthermal distributions for the small and large mass ratio limits is well approximated by a Fokker-Planck equation (Andersen and Shuler 1964) as discussed in Chap. 6, Sect. 6.1.3. The results shown, computed with a

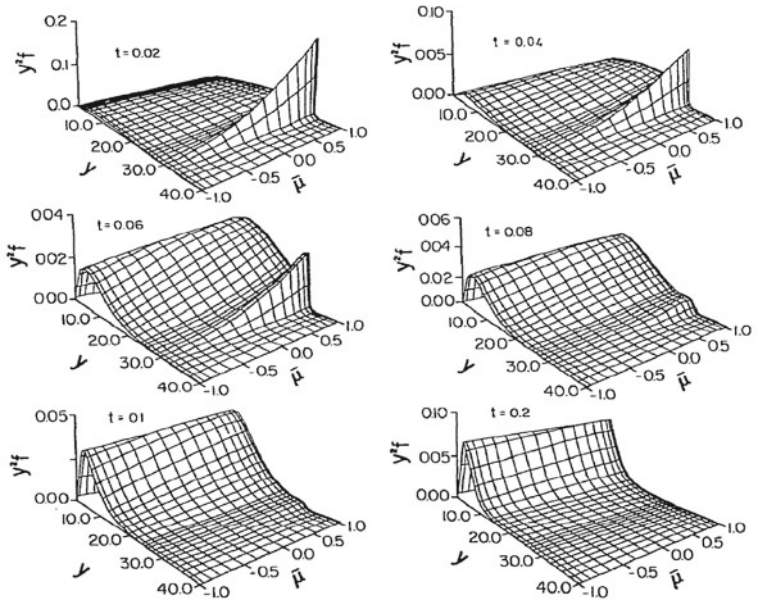

Fig. 5.14 Time evolution of the anisotropic distribution for mass ratio $M/m = 1$. The initial distribution is given by Eq. (5.130) with $\beta = 2$, $E_0 = 900$ and $\alpha = 10^{-4}$. The time t is in units of $\tau = [Nd^2\sqrt{2\pi k_B T/M}]^{-1}$. In the figure $\overline{\mu} \equiv \mu$. Reprinted from Shizgal and Blackmore (1983) with permission from Elsevier

spectral/pseudospectral method, provide useful graphically accurate depictions of the different behaviour in these limits.

5.7.2 *A Spectral Method of Solution of the Milne Problem*

The Milne problem, depicted in Fig. 5.16, refers to the diffusion of a minor constituent of mass m in a background species of mass M considered to be at equilibrium at temperature T_b (Lindenfeld and Shizgal 1983). The vertical line at $r = 0$ separates the medium that occupies the right half-space, $r > 0$, from the vacuum that is in the left half-space $r < 0$. A current density of magnitude **j** directed in the negative r-direction exists in the medium. The problem consists of determining the steady velocity distribution of the minor species within the half-space $r > 0$ and the angular distribution of emerging particles at the boundary subject to the condition that there are no particles incident from the left onto the medium. These boundary conditions are the same as those used for the radiative transfer problem in Sect. 5.3. For $\gamma \to \infty$, we have the Lorentz limit and the one-speed radiative transfer problem. This system is a typical rarefied gas dynamical half-space problem (Williams 1971; Cercignani 1988; Williams 2005).

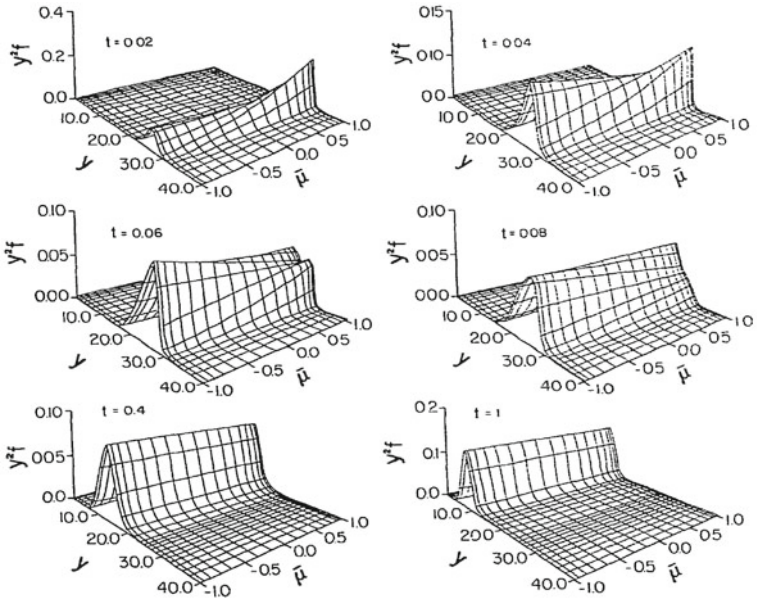

Fig. 5.15 Time evolution of the anisotropic distribution for mass ratio $M/m = 16$. The initial distribution is given by Eq. (5.130) with $\beta = 2$, $E_0 = 900$ and $\alpha = 10^{-4}$. The time t is in units of $\tau = [Nd^2\sqrt{2\pi k_B T/M}]^{-1}$. In the figure $\overline{\mu} \equiv \mu$. Reprinted from (Shizgal and Blackmore 1983) with permission from Elsevier

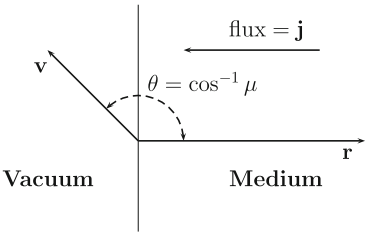

Fig. 5.16 The geometry of the Milne problem; The *vertical line* separates the vacuum from the medium. The orientation of the particle velocity, **v**, relative to the radial direction in space, **r**, is θ. There is a constant source of particles of flux **j** at infinity

Far from the boundary, in the positive r-direction, hydrodynamic equations are valid, which for the present model is the diffusion equation,

$$\overline{j} = -D\frac{dn^{(as)}(r)}{dr}. \tag{5.146}$$

This is the usual diffusion equation in the collision dominated regime that relates the flux $\overline{j}$ and the gradient of the asymptotic density profile, $n^{(as)}(r)$ and D is the diffusion coefficient. One finds that the extrapolation of the linear asymptotic dependence of the actual density profile intersects the r-axis at $r = -q$, where q is the extrapolation length and is a measure of the departure from hydrodynamic behaviour

near the boundary. The calculation of the density and temperature profiles and the extrapolation length are the main objectives.

For steady-state conditions, the Boltzmann equation for the velocity distribution function of test particles, $\overline{f}(r, v, \mu)$, is

$$v\mu \frac{\partial \overline{f}(r, v, \mu)}{\partial r} = n_b(r)\overline{L}[\overline{f}(r, v, \mu)], \tag{5.147}$$

where $\mu = \cos(\theta)$ and θ is the angle between $\mathbf{v}$ and the positive r-axis as shown in Fig. 5.16. In Eq. (5.147), $n_b(r)$ is the number density of the background medium and the linear Boltzmann collision operator for atom-atom collisions is defined by Eq. (5.104) except that the background density appears explicitly. We choose a hard sphere cross section, $\sigma_{el} = \pi d^2$, and rewrite the Boltzmann equation in dimensionless form.

With the transformation to dimensionless spatial variable,

$$z = \pi d^2 \int_0^r n_b(r')dr', \tag{5.148}$$

which is the "optical depth" of the medium, the Boltzmann equation can be written as

$$x\mu \frac{\partial f(z, x, \mu)}{\partial z} = n_b(r)L[f(z, x, \mu)], \tag{5.149}$$

where $L = \overline{L}/(\pi d^2 v_0)$, $f = \overline{f}[v_0/n_b(r)\pi d^2]^3$, $v_0 = \sqrt{2k_B T_b/m}$ and $x = v/v_0$ is the reduced speed.

We seek solutions of this equation subject to the boundary condition that no particles in the positive μ region return to the medium, that is

$$f(0, x, \mu) = 0, \qquad 0 < \mu < 1. \tag{5.150}$$

The general solution is written as the sum of a spatially transient part, f^{tr}, and an asymptotic part, f^{as}, that is

$$f = f^{tr} + f^{as}. \tag{5.151}$$

The transient solution dominates near the $z = 0$ boundary and it is anticipated that it decays out in a distance of the order of a few mean free paths. The asymptotic solution dominates at large distances where hydrodynamics is expected to be valid.

The transient solution is of the form,

$$f^{tr}(z, x, \mu) = \sum_{k=1}^{\infty} a_k e^{\lambda_k z} R_k(x, \mu), \tag{5.152}$$

where λ_k and $R_k(x,\mu)$ are the spatial eigenvalues and eigenfunctions, respectively, given by

$$L[R_k] = (z\mu)\lambda_k R_k. \tag{5.153}$$

We choose basis functions which are products of spherical harmonics and associated Laguerre polynomials, $L_n^{(\ell+1/2)}(x)$, that is

$$\phi_{nl}(x,\mu) = N_{n\ell} L_n^{(\ell+1/2)}(x) P_\ell(\mu), \tag{5.154}$$

where $N_{n\ell} = \sqrt{\frac{\sqrt{\pi}n!(2l+1)}{2\Gamma(n+\ell+\frac{2}{3})}}$ is the combined normalizations of the Sonine-Laguerre and Legendre polynomials. The eigenfunctions and eigenvalues are determined with the expansion of $R_k(x,\mu)$ in the basis functions $\phi_{n\ell}(x,\mu)$

$$R_k(x,\mu) = \frac{\exp(-x^2)}{\pi^{3/2}} \sum_{n=0}^{\infty}\sum_{\ell=0}^{\infty} b_{n\ell}^k \phi_{n\ell}(x,\mu). \tag{5.155}$$

The eigenvalue problem is then converted to the finite set of linear equations,

$$\sum_{n'=0}^{N}\sum_{\ell'=0}^{L}\left(L_{nn'}^{(\ell)}\delta_{\ell\ell'} - \lambda_k M_{n\ell,n'\ell'}\right) b_{n'\ell'}^k = 0. \tag{5.156}$$

The quantities $L_{n,n'}^{(\ell)}$ and $M_{n\ell,n'\ell'}$ are the matrix elements of the collision operator and of $x\mu$ in the drift term on the left hand side of Eq. (5.149), respectively. The matrix elements are defined by

$$\begin{aligned} L_{nn'}^{(\ell)} &= \langle\psi_{n\ell}|L^{(\ell)}|\psi_{n'\ell}\rangle, \\ M_{n\ell,n'\ell'} &= \langle\psi_{n\ell}|x\mu|\psi_{n'\ell'}\rangle. \end{aligned} \tag{5.157}$$

and $M_{n\ell,n'\ell'}$ is given by

$$M_{n\ell,n'\ell'} = \begin{cases} (l+1)\sqrt{(n+\ell+\frac{3}{2})/(2l+1)(2l+3)}, & n'=n,\ l'=l+1 \\ -(\ell+1)\sqrt{n/(2\ell+1)(2\ell+3)}, & n'=n-1,\ l'=\ell+1 \\ \ell\sqrt{(n+\ell+\frac{1}{2})/(4\ell^2-1)}, & n'=n,\ l'=\ell-1 \\ -\ell\sqrt{(n+1)/(4\ell^2-1)}, & n'=n+1,\ \ell'=\ell+1 \\ \\ 0, & \text{otherwise.} \end{cases}$$

and determined with the recurrence relations for the Legendre and associated Laguerre polynomials, namely,

$$\mu P_\ell = \frac{1}{2\ell+1}\Big[(\ell+1)P_\ell(\mu) + \ell P_{\ell-1}\Big],$$
$$x L_{n-1}^{(\ell+1/2)}(x) = n L_{n-1}^{(\ell+1/2)}(x) - n L_n^{(\ell+1/2)}(x) - (n+\ell-1/2) L_{n-1}^{(\ell-1/2)}. \quad (5.158)$$

Numerical diagonalization of the matrices in Eq. (5.156) with a QZ algorithm (Golub and Van Loan 1996), also known as the Schur decomposition, gives approximate eigenvalues and eigenfunctions to order $K = (N+1)(L+1)$. The transient solution is written as

$$f^{tr}(z, x, \mu) = \sum_{k=1}^{\frac{1}{2}K-1} a_k e^{\lambda_k z} R_k(x, \mu). \quad (5.159)$$

The spatial eigenvalues, λ_k, which includes the zero eigenvalue, occur in positive and negative pairs so that the sum over k in Eq. (5.152) includes only nonzero negative λ_k (Lindenfeld and Shizgal 1983; Alterman et al. 1962). This is similar to the radiative transfer problem in Sect. 5.3. If the positive eigenvalues are retained, the solution diverges. Any discretization of the Boltzmann equation without eliminating the positive spatial eigenvalues will lead to spurious results (Pierrard and Lemaire 1998).

The asymptotic solution is written in the form

$$f^{as}(z, x, \mu) = -(j/D) f^M(x)[q + z - \mu U(p)], \quad (5.160)$$

where the dimensionless flux and diffusion coefficient are given by $j = \overline{j}/v_0 [n_1(r)\pi d^2]^3$ and $D = \overline{D}/[v_0/n_1(r)\pi d^2]$, respectively. The function $U(x)$ satisfies the Chapman-Enskog equation for diffusion (Chapman and Cowling 1970), that is

$$L[\mu U(x)] = -x\mu, \quad (5.161)$$

and is solved with the expansion

$$\mu U(x) = \sum_{n'=0}^{\infty} d_{n'} \psi_{n'1}(x, \mu). \quad (5.162)$$

Consequently, the solution of Eq. (5.161) is given by

$$\sum_{n'=0}^{\infty} L^{(1)}_{n',n} d_{n'} = -\frac{1}{\sqrt{2}} \delta_{n,0} \quad (5.163)$$

and the diffusion coefficient is

$$D = \frac{d_0}{\sqrt{2}}. \quad (5.164)$$

The advantage of the associated Laguerre basis functions is that the diffusion coefficient is given in terms of the one expansion coefficient, d_0. However, the matrix equation, Eq. (5.163), must be inverted and the convergence of d_0 verified.

The general solution of the Boltzmann equation is written as the sum of the transient solution and the asymptotic solution, that is

$$f(z,x,\mu) = F(x)\left[\sum_{k=1}^{\frac{1}{2K}-1} a_k e^{\lambda_k z} \sum_{\ell=0}^{L}\sum_{n=0}^{N} b_{n\ell}^{k}\psi_{n\ell}(x,\mu) + \frac{1}{D}\left(q+z-\sum_{n=1}^{N} d_n\psi_{n\ell}(x,\mu)\right)\right]. \tag{5.165}$$

The coefficients $b_{n\ell}^{k}$ and λ_k are determined with the solution of the eigenvalue problem, Eq. (5.156). The d_k coefficients are calculated with the inversion of the Chapman-Enskog equation, Eq. (5.163). The general solution is then completely specified with the $(K/2-1)$ a_k coefficients and the extrapolation length with application of the boundary condition, Eq. (5.150).

However, it should be clear that the expansion Eq. (5.165) cannot satisfy exactly this boundary condition for all x and μ. There are several different methods to use to apply the boundary condition and no one method is a priori better than the others. This is a limitation of a spectral method based on polynomial basis functions. We do not provide the details of this aspect of the problem discussed elsewhere (Lindenfeld and Shizgal 1983; Garcia and Siewert 1996; Ghosh 2014) and references therein. The Marshak boundary condition (Davison 1957; Williams 1971) which sets moments of the distribution function to zero at the boundary provides convergent results with modest sized basis sets ($N = 9$ and $L = 11$).

One of the main objectives is the density profile of the test particle which is shown in Fig. 5.17. The solid lines are the results with the solution of the Boltzmann equation whereas the dashed lines represent the extrapolation of the asymptotic profiles for large x. The intercept on the negative z axis is $-q$.

The extrapolation length, q, versus mass ratio is shown in Table 5.11 with a limited basis set (N = 9, L = 11). The value of the extrapolation length in the one-speed case ($\gamma \to \infty$) is 0.7104 to four significant figures. A more precise value reported by Loyalka and Naz (2008) is 0.710446089599.

The Milne problem was also considered with the Coulomb cross section for collisions between charged particles (Barrett et al. 1992) for which the Boltzmann collision operator is replaced with the Fokker-Planck differential operator. This has been referred to as the Coulomb Milne problem (Lie-Svendsen and Rees 1996) and as a model for the outflow of light ions from the high latitude ionosphere and the solar wind (Echim et al. 2011). The Fokker-Planck equation is also the basis for the study of the plasma sheath problem. This is a Milne problem coupled to the Poisson equation which provides the electric field in the sheath near an electrode (Vasenkov and

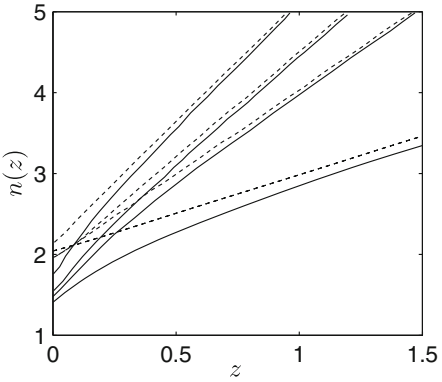

Fig. 5.17 The *solid lines* represent the density profile from the solution of the Boltzmann equation. The *dashed lines* are the asymptotic linear variation extrapolated back to the negative z axis with the intercept equal to $-q$. The mass ratios from *top* to *bottom* are $\gamma = \infty$ (the one-speed case), 10, 1 and 1/9, respectively. Reproduced from Lindenfeld and Shizgal (1983) with permission of the American Physical Society

Table 5.11 The variation of the extrapolation length versus mass ratio γ with the solution of the Boltzmann equation with $N = 9$ Sonine-Laguerre polynomials and $L = 11$ Legendre polynomials

$\gamma = M/m$	q
1	0.9370
1.5	0.8564
2.333	0.7984
4	0.7569
9	0.7278
19	0.7170
39	0.7123
99	0.7097
∞	0.7104

Reproduced in part from Lindenfeld and Shizgal (1983) with permission from the American Physical Society

Shizgal 2000, 2002) analogous to the recent treatment of the behaviour of electric arcs (Lowke and Tanaka 2006).

The Boltzmann equation, Eq. (5.149), may appear similar to the initial value problem whereby z plays the role of t, but there is an important distinction owing to the occurrence of μ on the left hand side. If one were to divide through by $z\mu$ and integrate directly in z there would be spurious results as noted by Pierrard and Lemaire (1998) in their modeling of the terrestrial polar wind.

5.7.3 A Mixed Spectral/Pseudospectral Solution of the Boltzmann Equation for the Escape of Light Atoms from a Planetary Atmosphere

The Milne problem presented in Sect. 5.7.2 also serves as a model for the escape of a minor species from a planetary atmosphere. For the terrestrial atmosphere, this refers to the escape of atomic hydrogen and helium from the high altitude rarefied region of the atmosphere referred to as the exosphere. The bottom of the exosphere is the exobase where the mean free path of the major species, namely atomic oxygen, is equal to the barometric scale height (Fahr and Shizgal 1983). If we assume that the distribution function of escaping species is a Maxwellian, the equilibrium escape flux from the exobase is the Jeans flux given by

$$F_J = 2\pi \int_{v_{esc}}^{\infty} \int_0^{\pi/2} F(v) v \cos\theta \sin\theta d\theta v^2 dv,$$
$$= \frac{n_c}{2}\sqrt{\frac{2kT_c}{m}}\left(1+\lambda_{esc}\right)e^{-\lambda_{esc}}, \tag{5.166}$$

where $\lambda_{esc} = mv_{esc}^2/2k_BT_c$ is the escape parameter, $v_{esc} = 11.2\,\text{km/s}$ is the escape speed and T_c is the temperature at the exobase often referred to as the critical level. The atmosphere above the exobase is assumed to be collisionless. The loss of energetic particles from the atmosphere perturbs the distribution function from Maxwellian such that the nonequilibrium escape flux, F, is less than the equilibrium Jeans escape flux, F_J, and $F/F_J < 1$. This is analogous to the nonequilibrium effects in reactive systems discussed in Sect. 5.4.4 except that in this application we are treating a spatially nonuniform system.

We consider a slab of atmosphere so that a plane parallel model is sufficient. We measure altitude in terms of the atmospheric "optical depth" that is

$$z = -\int_r^{r_{top}} \sigma_{tot} n_b(r') dr', \tag{5.167}$$

where $n_b(r)$ is the density of the heavier background gas bound to the planet. The Boltzmann equation for the distribution function of the minor escaping constituent, with neglect of the gravitational force in the drift term (Shizgal and Blackmore 1986), is Eq. (5.147) as in the Milne problem, that is,

$$x\mu\frac{\partial f}{\partial z} = \tilde{J}[f], \tag{5.168}$$

where $\mu = \cos\theta$ and $\tilde{J} = \sqrt{m/2k_BT_b}J/n_b(r)\pi d^2$. The physical situation is depicted in Fig. 5.18 where the exobase is the dashed line at $z = -1$, where the mean free

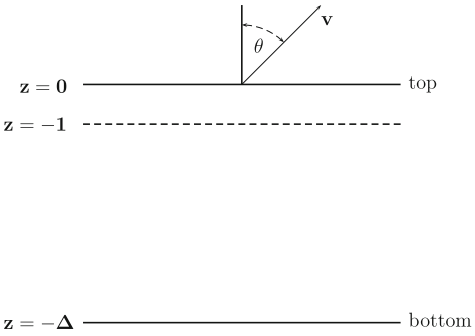

Fig. 5.18 Plane parallel model of an atmosphere with the critical level at $z = -1$ measured in terms of the atmospheric optical depth. The lower boundary at $z = -\Delta$ is in the collision dominated atmosphere whereas the escape of atoms is from the "top" of the atmosphere at $z = 0$

path is equal to the atmospheric scale height. At the lower boundary in the collision dominated region (the asymptotic condition in the Milne problem), the distribution is assumed to be a Maxwellian modified with a drift to account for the flux of particles from below. This is the Chapman-Enskog regime far from the top boundary. Therefore, at $z = -\Delta$, which is sufficiently deep within the collision dominated region, we impose the boundary condition with an anisotropy linear in μ, that is

$$f(x < x_{esc}, \mu, -\Delta) = F(x) + \mu U(x), \tag{5.169}$$

where $F(x)$ is the Maxwellian and $U(x)$ is to be determined.

This is supplemented with boundary conditions at the top taking into account the escape speed from the planet. Particles with less than the escape speed get reflected back down so that

$$f(x < x_{esc}, -\mu, 0) = f(x < x_{esc}, \mu, -\Delta), \quad \mu > 0, \tag{5.170}$$

and there are no incoming particles in excess of the escape speed, so that

$$f(x > x_{esc}, \mu, 0) = 0, \quad \mu < 0. \tag{5.171}$$

Shizgal and Blackmore (1986) used a mixed spectral/pseudospectral method of solution of the Boltzmann equation expressed in terms of the expansion of the anisotropy of the distribution function in Legendre polynomials

$$f(x, \mu, z) = \sum_{\ell=0}^{L} f_\ell(x, z) P_\ell(\mu) \tag{5.172}$$

which yields the set of coupled integral equations

$$\frac{\partial f_\ell(x,t)}{\partial t} + x\left(a_\ell \frac{\partial f_{\ell-1}(x,t)}{\partial z} + a_{\ell+1} \frac{\partial f_{\ell+1}(x,t)}{\partial z}\right) = \int_0^\infty k_L^{(\ell)}(x,y) f_\ell(y,t) dy - Z(x) f_\ell(x,t), \tag{5.173}$$

where $a_\ell = \ell/\sqrt{(2\ell-1)(2\ell+1)}$ and the recurrence relation for the Legendre polynomials has been used. We discretize Eq. (5.173) with the Gauss-Maxwell quadrature. However, in view of the boundary condition dependent on the reduced critical escape speed, $x_{esc} = \sqrt{\lambda_{esc}}$, we divide the semi-infinite speed interval into two subintervals, namely $[0, \sqrt{\lambda_{esc}}]$ and $[\sqrt{\lambda_{esc}}, \infty]$ so as to apply the boundary condition. Two sets of polynomials orthogonal with respect to $w(x) = x^2 e^{-x^2}$ separately on these intervals, together with the associated quadratures are calculated with the methods presented in Chap. 2. This procedure can be compared to the "double Gauss" method in radiative transfer (Sykes 1951; Stamnes et al. 1988) with the half-range Legendre polynomials.

Although we have retained the time dependence in Eq. (5.173), we are interested in the steady state problem. The Boltzmann equation is discretized with Gauss-Legendre quadrature points in z with the transformation of the interval $[-1, 1]$ to $[0, -\Delta]$ with quadrature points at the interval boundaries with the appropriate scaling. The two interval Maxwell quadratures in reduced speed, x, are used to discretize the kernels $k_L^{(\ell)}(x, y)$. The derivative with respect to z is evaluated with the physical space representation of the derivative operator with the transformed Legendre quadratures. As the dimension of the resulting linear matrix equation is large, the time dependence is retained and the steady solution determined with a time iteration. In this scheme the ith iterate is given by

$$\begin{aligned}\Delta f_i^{(\ell)}(x_n, z_m) = \Bigg[&\sum_{j=1}^{N} B_{nj}^{(\ell)} f_i^{(\ell)}(x_j, z_m) \\ &+ x_n \sum_{k=1}^{M} D_{mk} \left(a_\ell f_i^{(\ell-1)}(x_n, z_k) + a_{\ell+1} f_i^{(\ell+1)}(x_n, z_k) \right) \\ &- S[f_i^{(\ell)}(x_n, z_m) - g^{(\ell)}(x_n, z_m)] \Bigg] \Delta t, \end{aligned} \tag{5.174}$$

where $B_{nj}^{(\ell)}$ is the physical space representation of the kernels and D_{mk} is the Gauss-Legendre physical space matrix derivative operator in altitude, z.

An ansatz is made for the form of the initial distribution, given by

$$\begin{aligned} f^{(0)}(x, \mu, z) = F(x) \Bigg(&- \frac{z}{\Delta} \left[1 + \frac{3(1+\lambda)\exp(-\lambda)\mu}{2\sqrt{\pi}} \right] \\ &+ \left[1 + \frac{z}{\Delta} \right] [H(x_c) H(\mu) + h(-\mu)] \Bigg), \end{aligned} \tag{5.175}$$

where the Heaviside function is $H(x) = 1$ for $x > 0$ and $H(x) = 0$ for $x < 0$. Equation (5.175) satisfies the boundary condition at the top ($z = 0$) and the initial form of the anisotropy at the bottom ($z = -\Delta$). The Legendre polynomial expansion of Eq. (5.175) provides the initial Legendre coefficients, $f_0^{(\ell)}(x, z)$.

The term with S at the end of Eq. (5.174) is an added convergence term where at $t = 0$, $g^{(\ell)} = f_0^{(\ell)}$. At each time step, the boundary condition at the top ($z = 0$), Eq. (5.170), is imposed by transforming $f_i^{(\ell)}(x_n, 0)$ to $f_i(x_n, \mu, 0)$ and setting the distribution function for incoming particles ($\mu < 0$) to be equal to outgoing particles ($\mu > 0$) except for values of $x > \sqrt{\lambda_{esc}}$. Once the top boundary condition is imposed, the distribution function is transformed back to the Legendre polynomial basis. When the iterative scheme yields a converged solution $g^{(\ell)} = f_{i-1}^{(\ell)}$ and the last term in small square brackets in Eq. (5.174) will be zero.

This iterative procedure is very similar to the one used by (Lie-Svendsen and Rees 1996) concerning the escape of the minor ion, He^+, in a background of O^+ with the replacement of the integral Boltzmann collision operator with the differential Fokker-Planck operator for Coulomb collisions. The authors refer to this problem as the Coulomb Milne problem (Barrett et al. 1992). Thus the Milne problem serves as the basis for several different physical systems in space and plasma physics.

The principal objective is to determine the reduction of the actual flux, F, from the Jeans' flux, F_J. The ratio $F/F_J < 1$ owing to the depletion of particles with $v > v_{esc}$ in the tail of the Maxwellian. The ratio F/F_J is shown in Fig. 5.19 versus T_c, the temperature at the exobase. The results of the formalism described here are shown as the solid line with solid circles in comparison with two separate Monte Carlo simulations (Chamberlain and Campbell 1967; Brinkman 1970) and from the results reported by Pierrard (2003). The lower boundary condition in (Pierrard 2003) is not the asymptotic Chapman-Enskog distribution for this collisionally dominated regime. It is a Maxwellian with only upward moving ($\mu > 0$) particles. It is reasonable to expect that if the lower boundary is sufficiently deep in the atmosphere, that within a few mean free paths upwards from the lower boundary, the distribution function would attain the same form, Eq. (5.169), used by Shizgal and Blackmore (1986), that

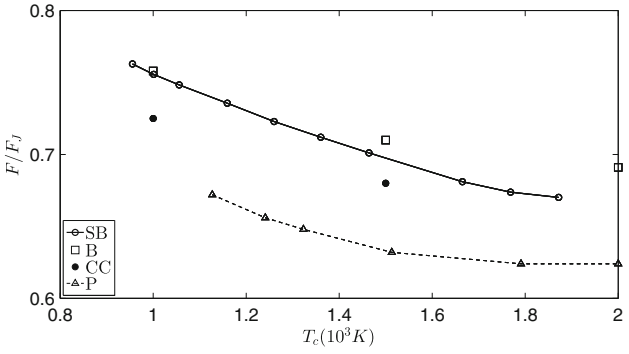

Fig. 5.19 The variation of the nonequilibrium escape flux, F, relative to the equilibrium Jeans flux, F_J versus the temperature at the exobase, T_c; the different results correspond to the work of *SB* (Shizgal and Blackmore 1986), *B* (Brinkman 1970), *CC* (Chamberlain and Campbell 1967) and *P* (Pierrard 2003). Reproduced from Shizgal and Blackmore (1986) and Pierrard (2003) with permission from Elsevier

is, a drifting Maxwellian. With increasing altitude, the distribution function will be further modified owing to the escape of particles at the top.

5.7.4 Electric Field Induced Ion Drift in Buffer Gases; Applications to Ionospheric and Space Physics

A classic problem in kinetic theory is the drift of ions of mass m dilutely dispersed in a background atomic or molecular gas of mass M and density $n_b(r)$ under the influence of an external spatially uniform and steady electrostatic field (Danailov et al. 2008; Viehland and Chang 2012). The distribution function is non-Maxwellian in speed, x, anisotropic in velocity and depends on the electrostatic field strength, E, and the background density, $n_b(r)$. The steady state Boltzmann equation for a gaseous ion in a background of a single atomic gas is

$$\mathbf{v} \cdot \nabla f + \frac{Z_{ion}\mathbf{E}}{m} \cdot \nabla_{\mathbf{v}} f = Lf, \tag{5.176}$$

where Z_{ion} is the ion charge, $\mathbf{E}$ is the electrostatic field directed along the polar axis and L is the linear collision operator given by Eq. (5.104). The anisotropy of the distribution function in velocity is expressed by the dependence on $\mu = \cos\theta$ where θ is the angle between $\mathbf{z}$ and $\mathbf{v}$. The Chapman-Enskog method discussed in Sect. 5.4.1 can be used for small electrostatic field strengths to calculate the diffusion coefficient D and the mobility K that appear in the expression for the ion flux

$$\mathbf{F}_{ion} = D\nabla n_b(r) + n_b(r)K\mathbf{E}. \tag{5.177}$$

The transport coefficients, D and K, are determined with the differential cross section $\sigma(g, \theta)$ for a particular ion-atom system. In this small E limit, the mobility is related to the diffusion coefficient by the Nernst-Townsend-Einstein relation $K = Z_{ion}D/k_BT$ (McDaniel and Mason 1973) and derived also on the basis of Brownian motion (Newburgh et al. 2006).

At higher electrostatic field strengths, the distribution function is more strongly perturbed from a Maxwellian in speed and anisotropy. We assume that the ions diffuse with a spatially uniform distribution and the Boltzmann equation for the distribution function, $f(\mathbf{v})$, is given by

$$\frac{Z_{ion}}{m}\mathbf{E} \cdot \nabla_v f = Lf. \tag{5.178}$$

The distribution function is expanded in the direct product of the Sonine-Laguerre functions in x^2 and Legendre polynomials in μ, that is

$$f(x, \mu) = F(x) \sum_{n=0}^{\infty} \sum_{\ell=0}^{\infty} f_{n,\ell} x^{\ell} S_n^{(\ell+1/2)}(x^2) P_\ell(\mu), \tag{5.179}$$

This procedure is very similar to the one used to treat the Milne problem in Sect. 5.7.2. With the substitution of Eq. (5.179) into (5.178), multiplication by the basis functions and integration over **v**, as we have done previously in other applications, we get the following set of linear equations for the expansion coefficients (see Sect. 6-1-1 in Mason and McDaniel (1988)),

$$\frac{Z_{ion}E}{Nm}\sqrt{\frac{m}{2k_BT}}\left[\ell(\ell+\frac{1}{2}+n)f_{n,\ell-1}-(\ell+1)f_{n-1,\ell+1}\right]=(\ell+\frac{1}{2})\sum_{k=0}L_{nk}^{(\ell)}f_{n,\ell}, \tag{5.180}$$

where the matrix elements of the linear collision operator, $L_{nk}^{(\ell)}$, are given by Eq. (6-1-19), and Table 5-4-2 in McDaniel and Mason (1973). The collision operator matrix elements are diagonal in ℓ and the terms in $\ell+1$ and $\ell-1$ from the drift term on the left hand side are coupled arising from the recurrence relations of the Legendre polynomials. The recurrence relation for the Sonine-Laguerre polynomials has also been used.

This is the spectral Galerkin solution of the Boltzmann equation with the Sonine-Laguerre basis functions orthogonal with the Maxwellian weight function. The mobility is given in terms of the single $f_{0,1}$ coefficient which is coupled to all the higher order coefficients. With increasing electric field strength, the anisotropy and non-Maxwellian features of the distribution function increase and the convergence for the mobility is slow and may even diverge.

To improve the convergence at higher electric field strengths, basis functions orthogonal with a weight function that closely approximates the form of the anticipated solution are preferable. In Chap. 4, we demonstrated the use of the scaling of the quadrature weights and points to improve the convergence of certain test functions with a scaling factor s which we identified with a "scaling" temperature, that is $s^2 = T_s/T$. In the ion-mobility literature (McDaniel and Mason 1973; Lin et al. 1979b; Viehland and Lin 1979; Mason and McDaniel 1988), this procedure is referred to as the two-temperature method with the reduced speed defined with T_s rather than with T. The matrix elements depend on T and T_s where T_s is varied to accelerate the convergence much in the same way as quadrature points are scaled.

However, with further increase in the electric field strength, the two-temperature method also fails to provide accurate results and a different set of basis functions is constructed, motivated again by choosing a weight function that better approximates the anisotropy of the anticipated distribution function. Thus, a drifting bi-Maxwellian weight function in terms of parallel, $v_{||}=v\mu$, and perpendicular, $v_\perp = v\sqrt{1-\mu^2}$, velocity components relative to the electric field direction are used, that is,

$$f(v_\parallel, v_\perp)=4\pi\sqrt{\frac{m}{2k_BT_\parallel}}\left(\frac{m}{2k_BT_\perp}\right)\exp\left(-\frac{mv_\perp^2}{2k_BT_\perp}\right)\exp\left(-\frac{m(v_\parallel-W)^2}{2k_BT_\parallel}\right). \tag{5.181}$$

with an unknown drift velocity W and unkown temperature parameters, $T_\perp$ and $T_\parallel$. The expansion in terms of reduced energies, $y_\perp = mv_\perp^2/2k_BT$ and $y_\parallel = m(v_\parallel - W)^2/2k_BT$, is

$$f(y_\parallel, y_\perp) = e^{-y_\parallel^2 - y_\perp^2} \sum_{n=0}^{\infty} \sum_{m=0}^{\infty} c_{nm} H_n(y_\parallel) S^{(m)}(y_\perp^2), \tag{5.182}$$

with $y_\parallel \in (-\infty, \infty)$ and $y_\perp \in [0, \infty]$. This approach is referred to as the three-temperature model as it depends on $T_\parallel$, $T_\perp$ and T. The basis functions used to model ion velocity distributions in the high-latitude ionosphere (St.-Maurice and Schunk 1976, 1979) are also the classical Laguerre polynomials $L_n^{(0)}(y_\perp)$ and Hermite polynomials, $H_n(y_\parallel)$.

The basis set used by researchers in gaseous ion transport is the product of three Hermite polynomials in the Cartesian velocity coordinates (Lin et al. 1979b; Mason and McDaniel 1988). The matrix elements of the collision operator can be calculated but with greatly increased complexity; see the Appendix in Lin et al. (1979b). The calculations are iterative in that an initial estimate of $T_\perp$, $T_\parallel$ and W must be made and subsequently updated from the moment solution. Thus the calculation has two convergence issues, namely (1) the convergence of the polynomial expansion and (2) the convergence of the iteration.

Viehland (1994) used a Gram-Charlier approach (Blinnikov and Moessner 1998) with a more flexible weight function with several unknown parameters that are updated with an iterative solution of the Boltzmann equation. The parameters in the weight function include as in the other methods W, $T_\parallel$, $T_\perp$ and T_s as well as the skewness and the kurtoses parallel and perpendicular to the electrostatic field. There are still other parameters related to energy and velocity correlations. The calculation of the matrix representation of the collision operator in this basis set defined by this weight function is more involved than for the two and three temperature models. The details of these calculations can be found in the Appendix of Lin et al. (1979b) with the matrix elements are expressed in terms of summations with 25 indices. With this approach, it is possible to compute gaseous ion transport coefficients directly from ab initio potential energy functions for atomic ions in atomic gases, with greater precision and accuracy than they can be measured.

It is clear that the choice of weight function and associated basis functions is crucial in the modelling of ion-mobilities as well as in other similar applications in ionospheric and space science. In the terrestrial ionosphere there is a geomagnetic field, $\mathbf{B}$, perpendicular to the ionospheric electric field $\mathbf{E}$. The use of different weight functions and polynomial basis functions in ionospheric physics was reviewed by St.-Maurice and Schunk (1979). The objective is to derive a small set of partial differential equations in the lower order moments. This approach is very similar to Grad's 13-moment method (Grad 1949; Struchtrup 2005). Models with an increasingly larger number of moments have been developed (Schunk 1977; Ma and St.-Maurice 2008).

The main thrust of the theoretical methods for the solution of the Boltzmann equation is to choose a weight function close to the anticipated solution. A non-classical weight function in $y_\perp$ is derived with the Bahatnager-Gross-Krook relaxation time approximation to the collision operator (Bhatnagar et al. 1954) that yields an analytic solution to the Boltzmann equation (St.-Maurice and Schunk 1974; Hubert 1983). This nonclassical weight function is then used to define a set of polynomials that provide a more rapid convergence than the expansions based on the Sonine-Laguerre polynomials (Shizgal and Hubert 1989). This basis set has also been used to provide lower order approximations of the nonequilibrium speed distributions observed in astrophysical winds (Leblanc and Hubert 1997). This subject is well beyond the scope of this book but we emphasize the strong overlap between these research fields.

5.8 The Nonlinear Isotropic Boltzmann Equation

In Sect. 5.5, we determined the eigenvalue spectrum of the collision operator for the linearized Boltzmann equation with expansions in the Sonine-Laguerre polynomials as well as with a multidomain spectral element method. The time scale of the approach to equilibrium for initial distributions close to the equilibrium Maxwellian distribution is determined by the eigenvalues of the linearized collision operator. In particular the lowest nonzero eigenvalue determines the final approach to equilibrium. In this section, we are concerned with the approach to equilibrium of a one component spatially uniform gas determined with the nonlinear Boltzmann equation given by

$$\frac{\partial f(\mathbf{v},t)}{\partial t} = \int\int \left[f_1(\mathbf{v}_1') f(\mathbf{v}') - f_1(\mathbf{v}_1) f(\mathbf{v}) \right] g\sigma(g,\Omega) d\mathbf{v}_1, \tag{5.183}$$

analogous to Eq. (5.30) without the gradients in space and velocity in the drift term on the left hand side. For this initial value problem, we assume that the distribution function is isotropic.

This problem has been considered by many researchers since the time of Ludwig Boltzmann and a complete review is a daunting task. We highlight here some of the major advances and also provide the results of recent numerical simulations.

The interest in the time evolution of the nonlinear Boltzmann equation increased dramatically with the discovery of an analytic solution for the Maxwell molecule model with the isotropic cross section, $\sigma(g,\Omega) = \kappa/g$. The result was originally reported in the MSc thesis by Krupp (1967) and later published independently by Krook and Wu (1976) and by Bobylev (1976, 1984). This explicit time dependent solution is given by

$$f_{BKW}(x,t) = \frac{2x^2 e^{-x^2/K(t)}}{\sqrt{\pi} K(t)} \left[\frac{5K(t)-3}{K(t)} + \frac{2(1-K(t))}{K^2(t)} x^2 \right],$$

where t is in units of $4\pi n\kappa$ and $K(t) = 1 - \frac{2}{5}e^{-t/6}$, analogous to a time dependent temperature. This model system serves as a benchmark to test different numerical methods for the solution of the nonlinear Boltzmann equation (Filbet et al. 2006; Filbet and Mouhot 2011; Wu et al. 2013; Ghiroldi and Gibelli 2014). The early work on the nonlinear Boltzmann equation was reviewed by Ernst (1981, 1984).

5.8.1 *Finite Difference Method of Solution of the Nonlinear Boltzmann Equation; Approach to Equilibrium*

We restrict our attention to isotropic distributions and the hard sphere collision cross section. Spectral methods with an expansion of the isotropic time dependent distribution function in the Sonine-Laguerre polynomials were employed long ago (Abe 1971; Weinert et al. 1980). Additional results were reported in a series of papers by Kügerl and Schürrer (1990) and by Ender et al. (2011).

The distribution function is expanded in the set of the Sonine-Laguerre polynomials $S^{(n)}(x^2)$, that is

$$f(x,t) = \frac{4}{\sqrt{\pi}} x^2 e^{-x^2} \sum_{n=2}^{\infty} c_n(t) S^{(n)}(x^2), \tag{5.184}$$

where $c_0(t) = 0$ and $c_1(t) = 0$ owing to particle and energy conservation, respectively. The expansion coefficients are given by

$$c_n(t) = \frac{\sqrt{\pi}}{2} \frac{n!}{\Gamma(n+3/2)} \int_0^{\infty} f(x,t) S^{(n)}(x^2) dx. \tag{5.185}$$

With the Sonine-Laguerre expansion, the nonlinear Boltzmann equation is reduced to an infinite set of coupled ordinary differential equations for time dependent $c_j(t)$ coefficients. The substitution of Eq. (5.184) into (5.183) yields the system of nonlinear ordinary differential equations

$$\frac{\mathrm{d}c_n(t)}{\mathrm{d}t} = \sum_{k=2}^{\infty} J_{nk} c_k(t) + \sum_{k=2}^{\infty} \sum_{\ell=2}^{\infty} N_{j,k\ell} c_k(t) c_\ell(t), \quad n \geq 2 \tag{5.186}$$

where the matrix elements of the linearized operator are denoted by $J_{nk} \equiv \langle n|J|k\rangle$ given by Eq. (5.65) and the nonlinear tensor, $N_{n,k\ell}$, is defined by

$$N_{n,k\ell} = \iiint F_1 F_2 S_1^{(n)} \left[S_1^{(k)\prime} S_2^{(\ell)\prime} - S_1^{(k)} S_2^{(\ell)} \right] \sigma g d\Omega d\mathbf{v}_1 \mathbf{v}_2, \tag{5.187}$$

and evaluated as described elsewhere (Shizgal and Karplus 1970; Abe 1971; Shizgal 1971; Kügerl and Schürrer 1990; Weinert et al. 1980). The Maxwellian weight

function in Eq. (5.187) is denoted by F. The spectral method based on the set of equations, Eq. (5.186) is analogous to the solution of the linearized Boltzmann equation in Sect. 5.4.3 with the added nonlinear terms.

The solution of the nonlinear Boltzmann equation is then obtained with the choice of an initial distribution, which provides the initial values of the expansion coefficients, $c_n(0)$, and the subsequent numerical integration of the set of equations, Eq. (5.186). This method of solution is limited to initial distributions close to the equilibrium Maxwellian owing to the difficulty of accurately calculating the nonlinear matrix elements $N_{n,k\ell}$ as well as the convergence of the initial distribution in the Sonine-Laguerre polynomials. The expansion in Sonine-Laguerre polynomials can suffer from spurious oscillations and give distributions that become negative in some regions. However, the method is attractive as the final approach to equilibrium will be determined by the linear terms in Eq. (5.186) and thus the spectral properties of J, discussed in Sect. 5.5.2. This spectral method of solution has been reported by other researchers (Abe 1971; Weinert et al. 1980; Kügerl and Schürrer 1990; Ender et al. 2011).

5.8.2 *Finite Difference Discretization of the Nonlinear Boltzmann Equation*

We solve the nonlinear Boltzmann equation with a stable finite difference method and determine the expansion coefficients, $c_n(t)$, with the numerical solution. For the hard sphere cross section, we define a dimensionless time t in units of $\tau = \sqrt{m/\pi k_B T_b}/(4nd^2)$ and the reduced speed $y = \sqrt{2k_B T/m}$. We rewrite the initial value problem defined by the nonlinear Boltzmann equation in the equivalent form (Kügerl and Schürrer 1990; Kabin and Shizgal 2003),

$$\frac{\partial f(y_1,t)}{\partial t} = \mathcal{F}_{in}(y_1,t) - \mathcal{F}_{out}(y_1,t), \tag{5.188}$$

where

$$\mathcal{F}_{out}(y_1,t) = f(y_1,t)\int_0^\infty S_{out}(y_1,y_2)f(y_2,t)dy_2, \tag{5.189}$$

and

$$\mathcal{F}_{in}(y_1,t) = \int_0^\infty\int_0^\infty S_{in}(y_1' \to y_1; y_2')f(y_1',t)f(y_2',t)dy_1'dy_2'. \tag{5.190}$$

For hard spheres, the scattering kernels can be written as follows (Kügerl and Schürrer 1990):

$$S_{out}(y_1, y_2) = \frac{1}{2}\begin{cases} y_1\left(1+\frac{y_2^2}{3y_1^2}\right) & \text{for } y_1 \geq y_2, \\ y_2\left(1+\frac{y_1^2}{3y_2^2}\right) & \text{for } y_1 \leq y_2, \end{cases}$$

$$S_{in}(y_1' \to y_1, y_2') = \frac{y_1}{y_1' y_2'} \min(y_1, y_2, y_1', y_2') H(y_2^2),$$

where $H(x)$ is the Heaviside step function and from energy conservation we have that $y_1^2 + y_2^2 = y_1'^2 + y_2'^2$. Particle number conservation gives the out-scattering kernel in terms of the in-scattering kernel by an integration, that is

$$S_{out}(y_1, y_2) = \int_0^\infty S_{in}(y_1 \to y_1', y_2) dy_1'.$$

We also have the detailed balance symmetry property

$$S_{in}(y_1' \to y_1, y_2') = S_{in}(y_2' \to y_1, y_1'). \tag{5.191}$$

We define the integral quantities

$$\begin{aligned} F_1(y_1, t) &= \int_0^{y_1} f(y, t) dy, \\ F_2(y_1, t) &= \int_{y_1}^\infty \frac{f(y, t)}{y} dy, \end{aligned} \tag{5.192}$$

so that $\mathcal{F}_{in}$ defined by the double integral (5.190) can be written as

$$\mathcal{F}_{in} = \sqrt{\frac{\pi}{2}}\left[2v_1 F_1(y_1, t) F_2(y_1, t) + y_1^2 F_2^2(y_1, t) + I(y_1, t)\right],$$

where the last term is the integral

$$I(y_1, t) = \iint_{S_0} \frac{y_1 y_2}{y_1' y_2'} f(y_1', t) f(y_2', t) dy_1' dy_2'. \tag{5.193}$$

The two dimensional integral is evaluated over the area S_0 defined by a circle $y_1'^2 + y_2'^2 = y_1^2$ and the straight lines $y_1' = y_1$ and $y_2' = y_1$. This is a significant

simplification of the original expression (5.190) because we have reduced most of the double integrals to the products of single integrals. With the substitution, $\xi_1 = y_1'^2/y_1^2$ and $\xi_2 = y_2'^2/y_1^2$, we get

$$I(y,t) = \frac{y_1^2}{4} \iint\limits_{S_1} \frac{\sqrt{\xi_1 + \xi_2 - 1}}{\xi_1 \xi_2} f(y_1', t) f(y_2', t) d\xi_1 d\xi_2. \tag{5.194}$$

where S_1 is a triangle with the vertices at (1, 0), (1, 1), and (0, 1). This integral can be efficiently evaluated with the cubature rule for a simplex (Stroud 1971).

5.8.3 Time Dependent Solutions

The reduced speed variable, y, is discretized uniformly according to $y_{i+1} = y_i + h$ on the finite interval $[0, y_{max}]$. The time variable is also discretized according to $t_{n+1} = t_n + \Delta t$. We integrate the nonlinear Boltzmann equation, Eq. (5.188), in t with an Euler integration algorithm so that the discretized version of the Boltzmann equation is

$$f^{(n+1)}(y_i) = f^{(n)}(y_i) + \Delta t[\mathcal{F}_{in}^{(n)}(y_i) - \mathcal{F}_{out}^{(n)}(y_i)]. \tag{5.195}$$

The term $\mathcal{F}_{out}^{n}(y_i)$ is determined from Eq. (5.189) with a Simpson rule integration over y_2 on the uniform grid. The double integral over ξ_1 and ξ_2 in Eq. (5.194) over the triangle S_1 is evaluated by dividing the triangle into several smaller triangles. The integral over each of these triangles is evaluated with a cubature for a triangle (Stroud 1971). With this technique, we have simplified the discretization of the in-scattering integral which presents the major challenge for the solution of the nonlinear Boltzmann equation.

Figure 5.20 shows the time evolution of the distribution function with the initial distributions (A) $f(y,0) = y^2 e^{-5y^2} + e^{4(y-3)^2}$ and (B) $f(y,0) = e^{-5\sqrt{|y-1|^2}} + e^{-5\sqrt{|y-3|^2}}$. The first has a large peak at $y = 3$ and a smaller peak at lower speeds. The second has two large peaks at $y = 1$ and 3, respectively. We choose $y_{max} = 8$ and 500 grid points in y. The time step Δt is taken sufficiently small so that the number density and temperature are conserved to 8 significant figures. The time dependent distributions shown in Fig. 5.20 do not drift and the shape evolves to a Maxwellian shown by the dashed curves.

We also consider an initial distribution function $f(x,0) = M(x)\left(\frac{5}{2} - 2x^2 + \frac{4}{5}x^4\right)$ used previously (Kügerl and Schürrer 1990), which corresponds to $c_0(0) = 1$, $c_1(0) = 0$ and $c_n(0) = \frac{4}{5}\delta_{n2}$, $n \geq 2$, in Eq. (5.185). The function $f(x,0)$ is a bimodal distribution with a slightly populated tail. In Fig. 5.21(A), we show the time dependent solution of the nonlinear Boltzmann equation with this initial condition. The dashed curve is the equilibrium Maxwellian. In Fig. 5.21(B), we show the

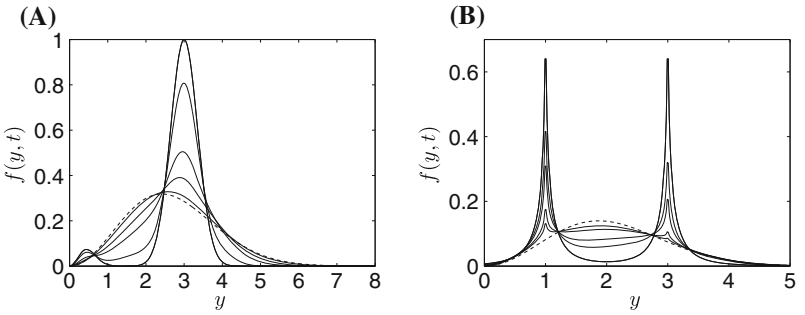

Fig. 5.20 Time evolution of the distribution function for the dimensionless time in units of τ from *top* to *bottom* equal to 0, 0.1, 0.4, 0.7 and 1.4; the *dashed curves* are the equilibrium distributions; (**A**) initial distribution $f(y,0) = y^2 e^{-5y^2} + e^{4(y-3)^2}$; (**B**) $f(y,0) = e^{-5\sqrt{|y-1|}} + e^{-5\sqrt{|y-3|}}$. Reproduced from Kabin and Shizgal (2003) with permission from the American Institute of Physics

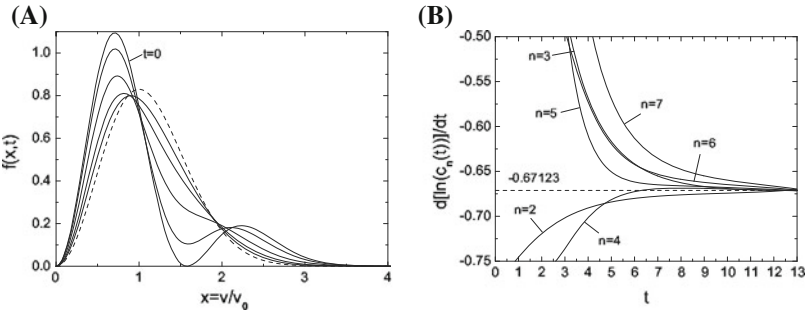

Fig. 5.21 (**A**) Time evolution of the distribution function for $f(x,0) = M(x)\left(\frac{5}{2} - 2x^2 + \frac{4}{5}x^4\right)$; The reduced times from *top* to *bottom* are 0.3, 1, 2 and 3. The *dashed curve* is the equilibrium Maxwellian; (**B**) The time dependence of the time derivative of $\ln c_n(t)$ showing that the approach to equilibrium for all coefficients is given by the "spectral gap", namely λ_2. Reproduced from Sospedra-Alfonso and Shizgal (2012b) with permission from the American Institute of Physics

time dependence of the time derivative of $\ln c_n(t)$ where the expansion coefficients are calculated with Eq. (5.185) and a Simpson rule integration over the distribution function $f^{(n)}(y_i)$ determined with the finite difference solution. It is clear from these results that the rate of approach to equilibrium is asymptotically the same for all coefficients and determined by the "spectral gap", namely $\lambda_2 = 0.67123$ of the linearized collision operator, J. We have used to advantage a finite difference algorithm to calculate the coefficients in a spectral representation of the distribution function without a direct solution of the nonlinear moment equations, Eq. (5.186). A primary objective has been the demonstration of the approach to equilibrium as given by the spectral gap.

The solution of the nonlinear Boltzmann equation for nonuniform systems presents considerable challenges for the accurate representation of distribution

functions that may vary rapidly in position and velocity. The direct simulation Monte Carlo (DSMC) method (Bird 1994) has been used for several decades to study such rarefied gas dynamical problems. The method has been used with success but is not useful for systems approaching the small Knudsen number collision dominated regime. Spectral methods, based on Fourier basis functions, for the nonlinear Boltzmann equation have been reported recently (Filbet et al. 2006; Heintz et al. 2008; Filbet and Mouhot 2011; Wu et al. 2013). The method requires that the velocity and spatial intervals are bounded. The Fourier transform in velocity

$$f^{(N)}(\mathbf{v}) = \sum_{k=-N}^{N} \hat{f}_k e^{\mathbf{k}\cdot\mathbf{v}}, \tag{5.196}$$

$$f_k(t) = \frac{1}{(2\pi)^3} \int f(\mathbf{v}) e^{-i\mathbf{k}\cdot\mathbf{v}} d\mathbf{v}, \tag{5.197}$$

is used to represent the distribution function much in the same way as other basis sets are used. Filbet and Russo (2003) reduced the nonlinear spatially homogeneous Boltzmann equation, Eq. (5.183), to Fourier form as given by

$$\frac{d\hat{f}_k}{dt} = \sum_{m=max(-N,k-N)}^{min(N,k+N)} \hat{f}_{k-m}\hat{f}_m \left[B(k-m,m) - B(m,m)\right] \tag{5.198}$$

where the "kernel modes", $B(n, m)$, are the Fourier transforms of the collision flux $B(g, \theta) = g\sigma(g, \theta)$ in the collision term. The structure of these moment equations is similar to Eq. (5.186) except that in the former, the linear term has been retained.

An excellent review of current numerical methods for the study of rarefied gas dynamical flows modelled with the nonlinear Boltzmann equation was presented by Narayan and Klöckner (2009) where the details of the derivation of Eq. (5.198) can be found. These authors have also provided a bibliography to the current numerical modeling efforts in this research area which is developing rapidly. Other direct methods of solution of the nonlinear homogeneous Boltzmann equation include the discontinous Galerkin method (Aleekseenko and Josyula 2014) and the pseudo-spectral method based on half-range Hermite polynomials (Ghiroldi and Gibelli 2014). A complete discussion of these recent applications with comparisons would require another chapter if not a separate volume.

References

Abe, K.: Sonine polynomial solution of the Boltzmann equation for relaxation of initially nonequilibrium distribution. Phys. Fluids **14**, 492–498 (1971)

Agarwal, R.K., Yun, K.-Y., Balakrishnan, R.: Beyond Navier-Stokes: Burnett equations for flows in the continuum-transition regime. Phys. Fluids **13**, 3061–3085 (2001)

Aleekseenko, A., Josyula, E.: Deterministic solution of the spatially homogeneous Boltzmann equation using discontinuous Galerkin discretizations in the velocity space. J. Comput. Phys. **272**, 170–188 (2014)

Alexandre, R.: A review of the Boltzmann equation with singular kernels. Kinet. Relat. Models **2**, 551–646 (2009)

Alterman, Z., Frankowski, K., Pekeris, C.L.: Eigenvalues and eigenfunctions of the linearized Boltzmann collision operator for a Maxwell gas and for a gas of rigid spheres. Astrophys. J. Suppl. **7**, 291–331 (1962)

Alves, G.M., Kremer, G.M., Marques Jr, W., Soares, A.J.: A kinetic model for chemical reactions without barriers: transport coefficients and eigenmodes. J. Stat. Mech. **2011**, P03014 (2011)

Amore, P.: A variational Sinc collocation method for strong-coupling problems. J. Phys. A: Math. Gen. **39**, L349–L355 (2006)

Andersen, H.C.: Derivation of hydrodynamic equations from the Boltzmann equation. In: Hochstim, A.E. (ed.) Kinetic Processes in Gasses and Plasmas, pp. 25–55. Elsevier, Holland (1969)

Andersen, K., Shuler, K.E.: On the relaxation of a hard sphere Rayleigh and Lorentz gas. J. Chem. Phys. **40**, 633–650 (1964)

Atenzi, S., Meyer-Ter-Vehn, J.: The Physics of Inertial Fusion. Clarendon Press, Oxford (2004)

Atkinson, K.E., Shampine, L.F.: Algorithm 876: solving Fredholm integral equations of the second kind in MATLAB. ACM Trans. Math. Softw. **34**, 21:1–21 (2008)

Balint-Kurti, G.G.: Time-dependent and time-independent wavepacket approaches to reactive scattering and photodissociation dynamics. Int. Rev. Phys. Chem. **27**, 507–539 (2008)

Balint-Kurti, G.G., Pulay, P.: A new grid-based method for the direct computation of excited molecular vibrational-states: test application to formaldehyde. J. Mol. Struct. (Theochem) **341**, 1–11 (1995)

Baranger, C., Mouhot, C.: Explicit spectral gap estimates for the linearized Boltzmann and Landau operators with hard potentials. Rev. Mat. Iberoam. **3**, 819–841 (2005)

Barrett, J., Demeio, L., Shizgal, B.: The Coulomb Milne problem. Phys. Rev. A **45**, 3687–3699 (1992)

Bernstein, R.B.: Quantum effects in elastic molecular scattering. Adv. Chem. Phys. **10**, 75–134 (1966)

Bhatnagar, P.L., Gross, E.P., Krook, M.: A model for collision processes in gases. I. Small amplitude processes in charged and neutral one-component systems. Phys. Rev. **94**, 511–525 (1954)

Binney, J., Tremaine, S.: Galactic Dynamics, 2nd edn. Princeton University Press, New Jersey (2008)

Bird, G.A.: Molecular Gas Dynamics and the Direct Simulation of Gas Flows. Clarendon, Oxford (1994)

Blinnikov, S., Moessner, R.: Expansions for nearly Gaussian distributions. Astron. Astrophys. Suppl. Ser. **130**, 193–205 (1998)

Bobylev, A.V.: A class of invariant solutions of the Boltzmann equation. Dokl. Akad. Nauk SSSR **231**, 571–574 (1976)

Bobylev, A.V.: Exact solutions of the nonlinear Boltzmann equation and the theory of relaxation of a Maxwellian gas. Theor. Math. Phys. **60**, 820–841 (1984)

Bobylev, A.V., Cercignani, C.: On the rate of entropy production for the Boltzmann equation. J. Stat. Phys. **94**, 603–618 (1999)

Bobylev, A.V., Mossberg, E.: On some properties of linear and linearized Boltzmann collision operators for hard spheres. Kinet. Relat. Models **4**, 521–555 (2008)

Bovino, S., Zhang, P., Kharchenko, V., Dalgarno, A.: Trapping hydrogen atoms from a Neon-gas matrix: a theoretical simulation. J. Chem. Phys. **131**, 054302 (2009)

Bovino, S., Zhang, P., Kharchenko, V., Dalgarno, A.: Relaxation of energetic $S(^1D)$ atoms in Xe gas: comparison of ab initio calculations with experimental data. J. Chem. Phys. **135**, 024304 (2011)

Boyd, J.P.: A spectrally accurate quadrature for resolving the logarithmic endpoint singularities of the Chandrasekhar H-function. JQRST **94**, 467–475 (2005)

Boyd, T.J.M., Sanderson, J.S.: The Physics of Plasmas. Cambridge University Press, Cambridge (2003)
Brinkman, R.T.: Departures from Jeans escape rate for H and He in the earth's atmosphere. Planet. Space Sci. **18**, 449–478 (1970)
Brun, R.: Introduction to Reactive Gas Dynamics. Oxford University Press, Oxford (2009)
Buhmann, R.D.: Radial Basis Functions. Cambridge University Press, Cambridge (2004)
Canto, L.F., Hussein, M.S.: Scattering Theory of Molecules. Atoms and Nuclei. Springer, New York (2013)
Case, K.M., Zweifel, P.F.: Linear Transport Theory. Addison-Wesley, Reading (1967)
Cercignani, C.: A variational principle for boundary value problems in kinetic theory. J. Stat. Phys. **1**, 297–311 (1969)
Cercignani, C.: The Boltzmann Equation and Its Applications. Springer, New York (1988)
Cha, S.-H.: Comprehensive survey on distance/similarity measures between probability density functions. Int. J Math. Models Methods Appl. Sci. **1**, 300–307 (2007)
Chamberlain, J.W., Campbell, F.J.: Rate of evaporation of a non-Maxwellian atmosphere. Astrophys. J. **149**, 687–705 (1967)
Chandrasekhar, S.: On the radiative equilibrium of a stellar atmosphere II. Astrophys. J. **100**, 76–86 (1944)
Chandrasekhar, S.: Radiative Transfer. Dover, New York (1960)
Chandrasekhar, S., Breen, F.H.: On the radiative equilibrium of a stellar atmosphere XIX. Astrophys. J. **105**, 143–144 (1947)
Chapman, S., Cowling, T.G.: The Mathematical Theory of Nonuniform Gases. Cambridge University Press, Cambridge (1970)
Child, M.S.: Molecular Collision Theory. Dover, New York (1996)
Cline, J.I., Taatjes, C.A., Leone, S.R.: Diode laser probing of $I(^2P_{1/2})$ Doppler profiles: time evolution of a fast anisotropic velocity distribution in a thermal bath. J. Chem. Phys. **93**, 6543–6553 (1990)
Corngold, N.: Kinetic equation for a weakly coupled test particle. II. Approach to equilibrium. Phys. Rev. A **24**, 656–666 (1981)
Danailov, D.M., Viehland, L.A., Johnson, R., Wright, T.G., Dickinson, A.S.: Transport of O^+ through Argon gas. J. Chem. Phys. **128**, 134302 (2008)
Davidović, D.M., Vukanić, J., Arsenović, D.: Two new analytic approximations of the Chandrasekhar's H function. Icarus **194**, 389–397 (2008)
Davison, B.: Neutron Transport. Oxford University Press, Oxford (1957)
de Groot, S.R., Mazur, P.: Non-equilibrium Thermodynamics. Dover, New York (1984)
Delves, L.M., Mohamed, J.L.: Computational Methods for Integral Equations. Cambridge University Press, Cambridge (1985)
Desai, R.C., Nelkin, M.: Atomic motions in a rigid sphere gas as a problem in neutron transport. Nucl. Sci. Eng. **24**, 142–152 (1966)
Dickinson, A.S., Certain, P.R.: Calculation of matrix elements for one-dimensional quantum-mechanical problems. J. Chem. Phys. **49**, 4209–4211 (1968)
Driessler, W.: On the spectrum of the Rayleigh piston. J. Stat. Phys. **24**, 595–606 (1981)
Driscoll, T.A.: Automatic spectral collocation for integral, integro-differential and integrally reformulated differential equations. J. Comput. Phys. **229**, 5980–5998 (2010)
Dudynski, M.: Spectral properties of the linearized Boltzmann operator in L^p for $1 \leq p \leq \infty$. J. Stat. Phys. **153**, 1084–1106 (2013)
Dziekan, P., Lemarchand, A., Nowakowski, B.: Master equation for a bistable chemical system with perturbed particle velocity distribution function. Phys. Rev. **E85**, 021128 (2012)
Echim, M.M., Lemaire, J., Lie-Svendsen, O.: A review on solar wind modeling: kinetic and fluid aspects. Surv. Geophys. **32**, 1–70 (2011)
Ender, A.Ya., Ender, I.A., Bakaleinikov, L.A., Flegontova, E.Yu.: Matrix elements and kernels of the collision integral in the Boltzmann equation. Tech. Phys. **56**, 452–463 (2011)

Ernst, M.H.: Nonlinear model Boltzmann equations and exact solutions. Phys. Rep. **78**, 1–171 (1981)
Ernst, M.H.: Exact solutions of the nonlinear Boltzmann equation. J. Stat. Phys. **34**, 1001–1017 (1984)
Eskola, L.: Geophysical Interpretation Using Integral Equations. Springer, Netherlands (2012)
Fahr, F.J., Shizgal, B.: Modern exospheric theories and their observational relevance. Rev. Geophys. Space Phys. **21**, 75–124 (1983)
Ferziger, J.H., Kaper, H.G.: Mathematical Theory of Transport Processes in Gases. North-Holland, Amsterdam (1972)
Filbet, F., Mouhot, C.: Analysis of spectral methods for the homogeneous Boltzmann equation. Trans. Am. Math. Soc. **363**, 1947–1980 (2011)
Filbet, F., Russo, G.: High order numerical methods for the space non-homogenous Boltzmann equation. J. Comput. Phys. **186**, 457–480 (2003)
Filbet, F., Mouhot, C., Pareschi, L.: Solving the Boltzmann equation in $N\log_2 N$. SIAM J. Sci. Comput. **28**, 1029–1053 (2006)
Fletcher, A.A.J.: Computational Techniques for Fluid Flow. Springer, New York (1991)
Foch, J.D., Ford, G.W.: The linear Boltzmann equation. In: de Boer, J., Uhlenbeck, G.E. (eds.) Studies in Statistical Mechanics, pp. 127–154. Elsevier, Holland (1970)
Ford, G.W.: Matrix elements of the linearized collision operator. Phys. Fluids **11**, 515–521 (1968)
Gad-el-Hak, M.: The fluid mechanics of microdevices—the Freeman scholar lecture. J. Fluids Eng. **121**, 5–33 (1999)
Ganapol, B.D.: Analytical Benchmarks for Nuclear Engineering Applications. Case Studies in Neutron Transport Theory. Nuclear Energy Agency OECD Publications, Paris (2008)
Garcia, R.D.M., Siewert, C.E.: A stable shifted-Legendre projection scheme generating P_N boundary conditions. Am. Nucl. Energy **23**, 321–332 (1996)
Garcia, R.D.M.: The application of non-classical orthogonal polynomials in particle transport theory. Prog. Nucl. Energy **35**, 249–273 (1999)
Ghiroldi, G.P., Gibelli, L.: A direct method for the Boltzmann equation based on a pseudo-spectral velocity space discretization. J. Comput. Phys. **258**, 568–584 (2014)
Ghosh, K.: Analytical benchmark for non-equilibrium radiation diffusion in finite size systems. Ann. Nucl. Energy **63**, 59–68 (2014)
Golub, G.H., Van Loan, C.F.: Matrix Computations. Johns Hopkins University Press, Baltimore (1996)
Grad, H.: Principles of the kinetic theory. In: Handbook of Physics, pp. 205–294. Springer, Berlin (1958)
Grad, H.: On the kinetic theory of rarefied gases. Commun. Pure Appl. Math. **2**, 331–407 (1949)
Grad, H.: Asymptotic theory of the Boltzmann equation. Phys. Fluids **6**, 147–181 (1963)
Gust, E.D., Reichl, L.E.: Molecular dynamics simulation of collision operator eigenvalues. Phys. Rev. E **79**, 031202 (2009)
Gust, E.D., Reichl, L.E.: Relaxation rates of the linearized Uehling-Uhlenbech equation for bosons. Phys. Rev. E **81**, 061202 (2010)
Hagelaar, G.J.M., Pitchford, L.C.: Solving the Boltzmann equation to obtain electron transport coefficients and rate coefficients for fluid models. Plasma Sources Sci. Technol. **14**, 722–733 (2005)
Harris, D.O., Engerholm, G.G., Gwinn, W.D.: Calculation of matrix elements for one-dimensional quantum-mechanical problems and the application to anharmonic oscillators. J. Chem. Phys. **43**, 1515–1517 (1965)
Hebert, A.: Applied Reactor Physics. Presse Internationales Polytechnique, Montréal (2009)
Heintz, A., Kowalczyk, P., Grzhibovskis, R.: Fast numerical method for the Boltzmann equation on non-uniform grids. J. Comput. Phys. **227**, 6681–6695 (2008)
Hiroi, T.: Recalculation of the isotropic H functions. Icarus **109**, 313–317 (1994)
Hirschfelder, J.O., Curtiss, C.F., Bird, B.: The Molecular Theory of Gases and Liquids. Wiley, New York (1954)

Hoare, M.R.: The linear gas. Adv. Chem. Phys. **20**, 135–214 (1971)
Hoare, M.R., Kaplinsky, C.H.: Linear hard sphere gas: variational eigenvalue spectrum of the energy kernel. J. Chem. Phys. **52**, 3336–3353 (1970)
Huang, K.: Statistical Mechanics. Wiley, New York (1967)
Hubert, D.: Auroral ion velocity distribution function: generalized polynomial solution of Boltzmann's equation. Planet. Space Sci. **31**, 119–127 (1983)
Jablonski, A.: Improved algorithm for calculating the Chandrasekhar function. Comput. Phys. Commun. **184**, 440–442 (2013)
Jerri, A.J.: Introduction to Integral Equations with Applications, 2nd edn. Wiley, New York (1999)
Jüngel, A.: Transport Equations for Semiconductors. Springer, New York (2009)
Kabin, K., Shizgal, B.D.: Exact evaluation of collision integrals for the nonlinear Boltzmann equation. AIP Conf. Proc. **663**, 35–42 (2003)
Kan, M.W.K., Yu, P.K.N., Leung, L.H.T.: A review on the use of grid-based Boltzmann equation solvers for dose calculation in external photon beam treatment planning. Biomed. Res. Int. **2013**, 692874 (2013)
Kapral, R., Ross, J.: Relaxation in a dilute binary gas mixture. J. Chem. Phys. **52**, 1238–1243 (1970)
Kawabata, K., Limaye, S.S.: Rational approximation formula for Chandrasekhar's H-function for isotropic scattering. Astrophys. Space Sci. **332**, 365–371 (2011)
Kawabata, K., Satoh, T., Ueno, S.: A direct numerical approach to the Chandrasekhar's H-function for arbitrary characteristic functions. Astrophys. Space Sci. **182**, 249–260 (1991)
Kharchenko, V., Dalgarno, A.: Thermalization of fast O(^{1}D) atoms in the stratosphere and mesosphere. J. Geophys. Res. **109**, D18311 (2004)
Kharchenko, V., Balakrishnan, N., Dalgarno, A.: Thermalization of fast nitrogen atoms in elastic and inelastic collisions with molecules of atmospheric gases. J. Atmos. Terr. Phys. **60**, 95–106 (1998)
Khazanov, G.V.: Kinetic Theory of the Inner Magnetospheric Plasma. Springer, New York (2011)
Khurana, S., Thachuk, M.: A numerical solution of the linear Boltzmann equation using cubic B-splines. J. Chem. Phys. **136**, 094103 (2012)
Khurana, S., Thachuk, M.: Kernels of the linear Boltzmann equation for spherical particles and rough hard sphere particles. J. Chem. Phys. **139**, 164122 (2013)
Kim, J.G., Boyd, I.D.: State-resolved master equation analysis of thermochemical nonequilibrium of nitrogen. Chem. Phys. **415**, 237–246 (2013)
Kourganoff, V.: Basic Methods in Transfer Problems. Oxford University Press, Oxford (1963)
Kremer, G.M.: An Introduction to the Boltzmann Equation and Transport Processes in Gases. Springer, New York (2010)
Krook, M., Wu, T.T.: Formation of Maxwellian tails. Phys. Rev. Lett. **36**, 1107–1109 (1976)
Krupp, R.S.: A nonequilibrium solution of the Fourier transformed Boltzmann equation. MSc thesis, MIT (1967)
Kügerl, G., Schürrer, F.: On the relaxation of binary hard-sphere gases. Phys. Fluids **2**, 609–618 (1990)
Kullback, S., Leibler, R.A.: On information and sufficiency. Ann. Math. Stat. **22**, 79–86 (1951)
Kundu, P., Cohen, I.M., Dowling, D.R.: Fluid Mechanics, 6th edn. Academic Press, Waltham (2012)
Kuščer, I., Corngold, N.: Discrete relaxation times in neutron transport. Phys. Rev. **139**, A981–A990 (1965)
Kuščer, I., Williams, M.M.R.: Relaxation constants of a uniform hard sphere gas. Phys. Fluids **10**, 1922–1927 (1967)
Kuščer, I., McCormick, N.J.: Some analytical results for radiative transfer in thick atmospheres. Trans. Theory Stat. Phys. **20**, 351–381 (1991)
Kustova, E.V., Giordano, D.: Cross-coupling effects in chemically non-equilibrium viscous compressible flows. Chem. Phys. **379**, 83–91 (2011)
Kythe, P.K., Puri, P.: Computational Methods for Linear Integral Equations. Birkhauser, Berlin (2002)

Leblanc, F., Hubert, D.: A generalized model for the proton expansion in astrophysical winds. I. The velocity distribution function representation. Astrophys. J. **483**, 464–474 (1997)
Lemaire, J.: Half a century of kinetic solar wind models. AIP Conf. Proc. **1216**, 8–13 (2010)
Lemaire, J., Scherer, M.: Model of the polar ion exosphere. Planet. Space Sci. **18**, 103–120 (1970)
Lemaire, J., Scherer, M.: Kinetic models of the solar and polar winds. Rev. Geophys. Space Phys. **11**, 427–468 (1973)
Liang, S.: Quantitative Remote Sensing of Land Surfaces. Wiley, New Jersey (2005)
Liboff, R.L.: Kinetic Theory: Classical, Quantum, and Relativistic Descriptions, 3rd edn. Springer, New York (2003)
Lie-Svendsen, O., Rees, M.H.: An improved kinetic model for the polar outflow of a minor ion. J. Geophys. Res. **101**, 2415–2433 (1996)
Light, J.C., Carrington Jr, T.: Discrete variable representations and their utilization. Adv. Chem. Phys. **114**, 263–310 (2000)
Lightman, A.P., Shapiro, S.L.: The dynamical evolution of globular clusters. Rev. Mod. Phys. **50**, 437–481 (1978)
Lin, S.R., Robson, R.E., Mason, E.A.: Moment theory of electron drift and diffusion in neutral gases in an electrostatic field. J. Chem. Phys. **71**, 3483–3498 (1979a)
Lin, S.Y., Viehland, L.A., Mason, E.A.: Three temperature theory of gaseous ion transport. Chem. Phys. **37**, 411–424 (1979b)
Lindenfeld, M.J., Shizgal, B.: Matrix elements of the Boltzmann collision operator for gas mixtures. Chem. Phys. **41**, 81–95 (1979a)
Lindenfeld, M.J., Shizgal, B.: Non-Maxwellian effects associated with the thermal escape of a planetary atmosphere. Planet. Space Sci. **27**, 739–751 (1979b)
Lindenfeld, M.J., Shizgal, B.: The Milne problem: a study of the mass dependence. Phys. Rev. **A27**, 1657–1670 (1983)
Liou, K.-N.: A numerical experiment on Chandrasekhar's discrete-ordinate method for radiative transfer: applications to cloudy and hazy atmospheres. J. Atmos. Sci. **30**, 1303–1326 (1973)
Liou, K.N.: An Introduction to Atmospheric Radiation. Elsevier, Amsterdam (2002)
Lowke, J.J., Tanaka, M.: LTE-diffusion approximation for arc calculations. J. Phys. D: Appl. Phys. **39**, 3634–3643 (2006)
Loyalka, S.K., Naz, S.: Milne's half-space problem: a numerical solution of the related integral equation. Ann. Nucl. Energy **35**, 1900–1902 (2008)
Loyalka, S.K., Tipton, E.L., Tompson, R.V.: Chapman-Enskog solutions to arbitrary order in Sonine polynomials I: simple, rigid-sphere gas. Phys. A **379**, 417–435 (2007)
Ma, J.Z.G., St.-Maurice, J.-P.: Ion distribution functions in cylindrically symmetric electric fields in the auroral ionosphere: the collision-free case in a uniformly charged configuration. J. Geophys. Res. **113**, A05312 (2008)
Mason, E.A., McDaniel, E.W.: Transport Properties of Ions in Gases. Wiley, New York (1988)
Matsumi, Y., Shamsuddin, S.M., Sato, Y., Kawasaki, M.: Velocity relaxation of hot $O(^1D)$ atoms by collisions with rare gases, N_2, and O_2. J. Chem. Phys. **101**, 9610–9618 (1994)
McCormick, N.J., Kuščer, I.: Singular eigenfunction expansions in neutron transport problems. Adv. Nucl. Sci. Technol. **7**, 181–282 (1973)
McCourt, F.R.W., Beenakker, J.J.M., Köhler, W.E.E., Kuščer, I.: Nonequilibrium Phenomena in Polyatomic Gases Volume 2: Cross Sections, Scattering, and Rarefied Gases. Oxford University Press, Oxford (1991)
McDaniel, E.W., Mason, E.A.: The Mobility and Diffusion of Ions in Gases. Wiley, New York (1973)
Milne, E.A.: Radiative equilibrium in the outer layers of a star; the temperature distribution and the law of darkening. Mon. Not. R. Astron. Soc. **81**, 361–375 (1921)
Monchick, L., Mason, E.A.: Free flight theory of gas mixtures. Phys. Fluids **10**, 1377–1390 (1967)
Mott-Smith, H.M.: A new approach in the kinetic theory of gases. MIT Linc. Lab. **V2**, 1–1 (1954)
Mouhot, C.: Rate of convergence to equilibrium for the spatially homogeneous Boltzmann equation for hard potentials. Commun. Math. Phys. **261**, 629–672 (2006)

Mouhot, C.: Quantitative linearized study of the Boltzmann collision operator and applications. Commun. Math. Sci. **1**, 73–86 (2007)
Mozumder, A.: Electron thermalization in gases. III epithermal electron scavenging in rare gases. J. Chem. Phys. **74**, 6911–6921 (1981)
Nakayama, T., Takahashi, K., Matsumi, Y.: Thermalization cross sections of suprathermal N(^{4}S) atoms in collisions with atmospheric molecules. Geophys. Res. Lett. **32**, L24803 (2005)
Nan, G., Houston, P.L.: Velocity relaxation of S(^{1}D) by rare gases measured by Doppler spectroscopy. J. Chem. Phys. **97**, 7865–7872 (1992)
Narayan, A., Klöckner, A.: deterministic numerical schemes for the Boltzmann equation, 1–51 (2009) ArXiv e-prints
Newburgh, R., Peidle, J., Rueckner, W.: Einstein, Perrin, and the reality of atoms: 1905 revisited. Am. J. Phys. **74**, 478–481 (2006)
Nicholson, J.W., Rudolph, W., Hager, G.: Using laser pulse dynamics to probe velocity distribution of excited iodine. J. Chem. Phys. **104**, 3537–3545 (1996)
Nielsen, S.E., Bak, T.A.: Hard sphere model for the dissociation of diatomic molecules. J. Chem. Phys. **41**, 665–674 (1964)
Oh, S.-K.: Modified Lennard-Jones potentials with a reduced temperature-correction parameter for calculating thermodynamic and transport properties: noble gases and their mixtures (He, Ne, Ar, Kr, and Xe). J. Thermodyn. **2013**, 828620 (2013)
Park, J., Shafer, N., Bersohn, R.: The time evolution of the velocity distribution of hydrogen atoms in a bath gas. J. Chem. Phys. **91**, 7861–7871 (1989)
Parker, E.N.: Dynamical theory of the solar wind. Space Sci. Rev. **4**, 666–708 (1965)
Parker, E.N.: Kinetic and hydrodynamic representations of coronal expansion and the solar wind. AIP Conf. Proc. **1216**, 3–7 (2010)
Pascal, S., Brun, R.: Transport properties of nonequilibrium gas mixtures. Phys. Rev. E **47**, 3251–3267 (1993)
Pekeris, C.L.: Solution of the Boltzmann-Hilbert integral equation. Proc. Natl. Acad. Sci. **41**, 661–669 (1955)
Pekeris, C.L., Alterman, Z.: Solution of the Boltzmann-Hilbert integral equation II; the coefficients of viscosity and heat transfer. Proc. Natl. Acad. Sci. **43**, 998–1007 (1957)
Peraiah, A.: Radiative transfer—Chandrasekhar—and after. Bull. Astron. Soc. India **24**, 397–536 (1996)
Phillips, N.J.: Collisional relaxation in gases. Proc. Phys. Soc. **73**, 800–806 (1959)
Pierrard, V.: Evaporation of hydrogen and helium atoms from the atmospheres of Earth and Mars. Planet. Space Sci. **51**, 319–327 (2003)
Pierrard, V., Lazar, V.: Kappa distributions; theory and applications in space plasmas. Sol. Phys. **267**, 153–174 (2010)
Pierrard, V., Lemaire, J.: A collisional model of the polar wind. J. Geophys. Res. **103**, 11701–11709 (1998)
Pitchford, L.C., ONeil, S.V., Rumble Jr, J.R.: Extended Boltzmann analysis of electron swarm experiments. Phys. Rev. A **23**, 294–304 (1981)
Pitchford, L.C., Phelps, A.V.: Comparative calculations of electron-swarm properties in N_2 at moderate E/N values. Phys. Rev. A **25**, 540–554 (1982)
Present, R.D., Morris, B.M.: Variational solution of the chemical kinetic Boltzmann equation. J. Chem. Phys. **50**, 151–160 (1969)
Prigogine, I., Xhrouet, E.: On the perturbation of Maxwell distribution function by chemical reactions in gases. Physica **15**, 913–932 (1949)
Rahman, M., Sundaresan, M.K.: Discrete relaxation modes for a hard sphere gas. Can. J. Phys. **46**, 2463–2469 (1968)
Reinhardt, W.P.: L^2 discretization of atomic and molecular electronic continua: moment, quadrature and J-matrix techniques. Comput. Phys. Commun. **17**, 1–21 (1979)
Robson, R.E., White, R.D., Petrović, Z.L.: Colloquium: physically based fluid modeling of collisionally dominated low-temperature plasmas. Rev. Mod. Phys. **77**, 1303–1320 (2005)

Ross, J., Mazur, P.: Some deductions from a formal statistical mechanical theory of chemical kinetics. J. Chem. Phys. **35**, 19–28 (1961)
Rybicki, G.B., Lightman, A.P.: Radiative Processes in Astrophysics. Wiley Interscience, New York (1979)
Rybicki, G.B.: Radiative transfer. J. Astrophys. Astron. **17**, 95–112 (1996)
Schunk, R.W.: Mathematical structure of transport equations for multispecies flows. Rev. Geophys. Space Phys. **15**, 429–445 (1977)
Sharipov, F., Seleznev, V.: Data on internal rarefied gas flows. J. Phys. Chem. Ref. Data **27**, 657–706 (1998)
Sharipov, F., Bertoldo, G.: Numerical solution of the linearized Boltzmann equation for an arbitrary intermolecular potential. J. Comput. Phys. **228**, 3345–3357 (2009)
Shizgal, B.: Nonequilibrium contributions to the rate of reaction. IV. Explicit time-dependent solutions. J. Chem. Phys. **55**, 76–83 (1971)
Shizgal, B.: Vibrational nonequilibrium effects in the (H_2-H_2) reactive system. J. Chem. Phys. **57**, 3915–3928 (1972)
Shizgal, B.: Time dependent solution of the chemical kinetic Boltzmann equation; two component isothermal system. Chem. Phys. **5**, 129–135 (1974)
Shizgal, B.: A Gaussian quadrature procedure for the use in the solution of the Boltzmann equation and related problems. J. Comput. Phys. **41**, 309–328 (1981a)
Shizgal, B.: Nonequilibrium time dependent theory of hot atom reactions. III. Comparison with the Estrup-Wolfgang theory. J. Chem. Phys. **741**, 1401–1408 (1981b)
Shizgal, B.: Discrete versus continuum relaxation modes of a hard sphere gas. Can. J. Phys. **62**, 97–103 (1984)
Shizgal, B., Blackmore, R.: Eigenvalues of the Boltzmann collision operator for binary gases and relaxation of anisotropic distributions. Chem. Phys. **77**, 417–427 (1983)
Shizgal, B., Blackmore, R.: A collisional kinetic theory of a plane parallel evaporating planetary atmosphere. Planet. Space Sci. **34**, 279–291 (1986)
Shizgal, B., Fitzpatrick, J.M.: Matrix elements of the linear Boltzmann collision operator for systems of two components at different temperatures. Chem. Phys. **6**, 54–65 (1974)
Shizgal, B., Fitzpatrick, J.M.: Possible failure of relaxation-time comparisons in the justification of local thermodynamic equilibrium. Phys. Rev. A **18**, 267–276 (1978)
Shizgal, B., Hubert, D.: The nonequilibrium nature of ion distribution functions in the high latitude auroral ionosphere. In: Muntz, E.P., Weaver, D.P., Campbell, D.H. (eds.) Proceedings of the 16th International Symposium on Rarefied Gas Dynamics, pp. 3–22. AIAA, Washington (1989)
Shizgal, B., Karplus, M.: Nonequilibrium contributions to the rate of reaction. I. Perturbation of the velocity distribution function. J. Chem. Phys. **52**, 4262–4278 (1970)
Shizgal, B., Karplus, M.: Nonequilibrium contributions to the rate of reaction. II. Isolated multicomponent systems. J. Chem. Phys. **54**, 4345–4356 (1971)
Shizgal, B., McMahon, D.R.A.: Electric field dependence of transient electron transport properties in rare gas moderators. Phys. Rev. A **32**, 3669–3680 (1985)
Shizgal, B.D., Lordet, F.: Vibrational nonequilibrium in a supersonic expansion with reaction: application to O_2-O. J. Chem. Phys. **104**, 3579–3597 (1996)
Shizgal, B.D.: Suprathermal particle distributions in space physics: Kappa distributions and entropy. Astrophys. Space Sci. **312**, 227–237 (2007)
Shizgal, B.D.: Pseudospectral methods of solution of the linear and linearized Boltzmann equations; transport and relaxation. AIP Conf. Proc. **1333**, 986–991 (2011)
Shizgal, B.D., Arkos, G.G.: Nonthermal escape of the atmospheres of Venus, Earth, and Mars. Rev. Geophys. **34**, 483–505 (1996)
Shizgal, B.D., Dridi, R.: Maple code for the calculation of the matrix elements of the Boltzmann collision operators for mixtures. Comput. Phys. Commun. **181**, 1633–1640 (2010)
Shore, S.N.: Blue sky and hot piles: the evolution of radiative transfer theory from atmospheres to nuclear reactors. Hist. Math. **29**, 463–489 (2002)

Siewert, C.E.: A concise and accurate solution to Chandrasekhar's basic problem in radiative transfer. JQRST **64**, 109–130 (2000)
Siewert, C.E.: On computing the Chapman-Enskog functions for viscosity and heat transfer and the Burnett functions. JQRST **74**, 789–796 (2002)
Siewert, C.E.: The linearized Boltzmann equation: concise and accurate solutions to basic flow problems. Z. angew. Math. Phys. **54**, 273–303 (2003)
Singh, G.S., Prasad, N., Kumar, B.: Transport properties of a binary gas mixture of molecules with internal energy. II. Thermal conductivity. J. Chem. Phys. **105**, 1537–1545 (1996)
Slevinsky, M., Safouhi, H.: Numerical treatment of a twisted tail using extrapolation methods. Numer. Algorithms **48**, 301–316 (2008)
Snider, R.F.: Quantum-mechanical modified Boltzmann equation for degenerate internal states. J. Chem. Phys. **32**, 1051–1060 (1960)
Snider, R.F.: Variational methods for solving the Boltzmann equation. J. Chem. Phys. **41**, 591–595 (1964)
Sone, Y.: Molecular Gas Dynamics: Theory, Techniques and Applications. Birkhauser, Boston (2007)
Sospedra-Alfonso, R., Shizgal, B.D.: Henyey-Greenstein model in the shape relaxation of dilute gas mixtures. Trans. Theory Stat. Phys. **41**, 368–388 (2012a)
Sospedra-Alfonso, R., Shizgal, B.D.: Hot atom populations in the terrestrial atmosphere. A comparison of the nonlinear and linearized Boltzmann equation. AIP Conf. Proc. **1501**, 91–98 (2012b)
Sospedra-Alfonso, R., Shizgal, B.D.: Energy and shape relaxation in binary atomic systems with realistic quantum cross sections. J. Chem. Phys. **139**, 044113 (2013)
Spitzer, L.J., Härm, R.: Evaporation of stars from open clusters. Astrophys. J. **127**, 544–550 (1958)
St.-Maurice, J.-P., Schunk, R.W.: Behaviour of ion velocity distributions for a simple collision model. Planet. Space Sci. **22**, 1–18 (1974)
St.-Maurice, J.-P., Schunk, R.W.: Use of generalized orthogonal polynomial solutions of Boltzmanns equation in certain aeronomy problems, Auroral ion velocity distributions. J. Geophys. Res. **81**, 2145–2154 (1976)
St.-Maurice, J.-P., Schunk, R.W.: Ion velocity distributions in the high-latitude ionosphere. Rev. Geophys. **17**, 99–134 (1979)
Stamnes, K., Tsay, S.-C., Wiscombe, W., Jayaweera, K.: Numerically stable algorithm for discrete-ordinate-method radiative transfer in multiple scattering and emitting layered media. Appl. Opt. **27**, 2502–2509 (1988)
Stroud, A.H.: Approximate Calculation of Multiple Integrals. Prentice Hall, Engelwood Cliffs (1971)
Struchtrup, H.: Macroscopic Transport Equations for Rarefied Gas Flows; Approximation Methods in Kinetic Theory. Springer, New York (2005)
Sykes, J.B.: Approximate integration of the equation of transfer. Mon. Not. R. Astron. Soc. **111**, 377–386 (1951)
Taatjes, C.A., Cline, J.I., Leone, S.R.: A general method for Doppler determination of cylindrically symmetric velocity distributions: an application of Fourier transform Doppler spectroscopy. J. Chem. Phys. **93**, 6554–6559 (1990)
Thomas, G.E., Stamnes, K.: Radiative Transfer in the Atmosphere and Ocean. Cambridge University Press, Cambridge (2002)
Tompson, R.V., Tipton, E.L., Loyalka, S.K.: Chapman-Enskog solutions to arbitrary order in Sonine polynomials V: summational expressions for the viscosity-related bracket integrals. Eur. J. Mech. B/Fluids **29**, 153–179 (2010)
Tricomi, F.G.: Integral Equations. Dover, New York (1985)
Vasenkov, A., Shizgal, B.D.: Nonhydrodynamic aspects of electron transport near a boundary: the Milne problem. Phys. Rev. E **63**, 016401 (2000)
Vasenkov, A., Shizgal, B.D.: Numerical study of a direct current plasma sheath based on kinetic theory. Phys. Plasmas **9**, 691–700 (2002)

Ven Den Eynde, G., Beauwens, R., Mund, E.: Calculating the discrete spectrum of the transport operator with arbitrary order anisotropic scattering. Trans. Theory Stat. Phys. **36**, 179–197 (2007)
Viehland, L.A.: Velocity distribution functions and transport coefficients of atomic ions in atomic gases by a Gram-Charlier approach. Chem. Phys. **179**, 71–92 (1994)
Viehland, L.A., Lin, S.L.: Application of the three temperature theory of ion transport. Chem. Phys. **43**, 135–144 (1979)
Viehland, L.A., Chang, Y.: Beyond the Monchick-Mason approximation: the mobility of Li ions in H_2. Mol. Phys. **110**, 259–266 (2012)
Volakis, J., Sertel, K.: Integral Equation Methods for Electromagnetics. Scitech, North Carolina (2012)
Wang-Chang, C.S., Uhlenbeck G.S.: Solution of the transport equation by S_N approximation. Technical Report CM-681, University of Michigan (1951)
Weinert, U., Lin, S.L., Mason, E.A.: Solutions of the nonlinear Boltzmann equation describing relaxation to equilibrium. Phys. Rev. A **22**, 2262–2269 (1980)
Wick, G.C.: Über ebene diffusionsprobleme. Z. Phys. **121**, 702–718 (1943)
Wigner, E.P., Wilkins Jr, J.E.: Effect of temperature of the moderator on the velocity distribution of neutrons with numerical calculations for H as moderator. Technical Report AECD-2275, US Atomic Energy Commission (1944)
Williams, M.M.R.: The Slowing Down and Thermalization of Neutrons. North-Holland, Amsterdam (1966)
Williams, M.M.R.: Mathematical Methods in Particle Transport Theory. Wiley-Interscience, New York (1971)
Williams, M.M.R.: The Boltzmann equation for fast atoms. J. Phys. A: Math. Gen. **9**, 771–783 (1976)
Williams, M.M.R.: The development of nuclear reactor theory in the Montreal laboratory of the National Research Council of Canada (Division of Atomic Energy) 1943–1946. Prog. Nucl. Energy **36**, 239–322 (2000)
Williams, M.M.R.: The Milne problem with Fresnel reflection. J. Phys. A: Math. Gen. **38**, 3841–3850 (2005)
Wu, L., White, C., Scanlon, T.J., Reese, J.M., Zhang, Y.: Deterministic numerical solutions of the Boltzmann equation using the fast spectral method. J. Comput. Phys. **250**, 27–52 (2013)
Yan, C.C.: Relaxation rate spectrum of the linearized Boltzmann equation for hard spheres. Phys. Fluids **12**, 2306–2312 (1969)
Yilmazer, A., Kocar, C.: Some benchmark results in spherical media radiative transfer problems. Trans. Theory Stat. Phys. **38**, 273–292 (2009)
Zhang, P., Kharchenko, V., Dalgarno, A.: Thermalization of suprathermal N(^{4}S) atoms in He and Ar gases. Mol. Phys. **105**, 1487–1496 (2007)
Zhang, X.-N., Li, H.-P., Murphy, A.B., Xia, W.-D.: A numerical model of non-equilibrium thermal plasmas. I. Transport properties. Phys. Plasmas **20**, 033508 (2013)
Ziff, R.M., Merajver, S.D., Stell, G.: Approach to equilibrium of a Boltzmann-equation solution. Phys. Rev. Lett. **47**, 1493–1496 (1981)

Chapter 6
Spectral and Pseudospectral Methods of Solution of the Fokker-Planck and Schrödinger Equations

Abstract Spectral and pseudospectral methods based on classical and nonclassical polynomial basis sets are used for the solution of the Fokker-Planck and Schrödinger equations. Fokker-Planck equations describe many different processes in chemistry and physics, and their study has attracted considerable attention by researchers in many different fields including astrophysics, finance and biology. Pseudospectral methods of solution of the Fokker-Planck equation are presented for several systems such as the Ornstein-Uhlenbeck model for Brownian motion, electron thermalization in atomic moderators, charged particle relaxation in plasmas and models for chemical reactions based on Kramers' equation. A Fokker-Planck equation can be transformed to a Schrödinger equation with a potential that belongs to the class of potentials in supersymmetric quantum mechanics and expressed in terms of the superpotential. The quantum harmonic oscillator and the Morse potential belong to this class of Schrödinger equations. The pseudospectral methods developed for the solution of the Fokker-Planck equation based on nonclassical basis sets are also applied to a large number of the Schrödinger equations including the Henon-Heles potential. Fundamental aspects of different pseudospectral methods such as the Discrete Variable Representation, the Quadrature Discretization method, the Lagrange mesh method and Fourier grid methods are discussed.

6.1 The Fokker-Planck Equation in Chemistry, Physics, Astrophysics and Other Fields

The Fokker-Planck equation is a partial differential equation for a probability density function, $P(\mathbf{v}, \mathbf{r}, t)$, analogous to a distribution function of kinetic theory discussed in Chap. 5. The linear integral Boltzmann equation for a binary gas of test particles of mass m dilutely dispersed in bath particles of mass M at T_b can be approximated by Fokker-Planck equations in the disparate mass limits ($\gamma = M/m \to 0$ or $\gamma \to \infty$) as a consequence of the small energy transfers in particle collisions (Andersen and Shuler 1964). A similar approximation is used in plasma physics for which charged particle Coulomb collisions involve predominantly large impact parameter grazing collisions (Rosenbluth et al. 1957; Spitzer 1962; Mitchner and Kruger 1973; Hinton 1983). These approximations are examples of a large class of Master equations for

B. Shizgal, *Spectral Methods in Chemistry and Physics*, Scientific Computation,
DOI 10.1007/978-94-017-9454-1_6

which a Fokker-Planck equation can be derived with the Kramers-Moyal expansion (Gillespie 1980; Knessl et al. 1984; Kuczka et al. 1995; Risken 1996; Frank 2007; van Kampen 2007).

An alternate derivation of the Fokker-Planck equation is based on stochastic differential equations such as the Langevin equation to model "Brownian" motion as discussed in the next section and in greater detail in several references (Chandrasekhar 1949; Risken 1996; Gardiner 2003; van Kampen 2007; Reif 2008; Paul and Baschnagel 2013). For most of the applications in this chapter, we will consider a Fokker-Planck equation in two variables and a probability density function, $P(x, t)$, where t is the time and x is an independent variable that represents the reduced speed or energy of a particle, the particle position or some other independent variable.

The equation is named after Adrian Fokker[1] and Max Planck.[2] Fokker (1914) studied the relationship between the fluctuations of the rotational motion of dipoles in an electric field and the steady state probability density function. Planck (1917) developed the time dependent equation and provided the relationship between the drift and diffusion coefficients and the random fluctuations inherent in the system.

Fokker-Planck equations are used to model numerous systems in physics, astrophysics, chemistry, biology, engineering, finance and other research fields. Fokker-Planck equations have also been used to model processes in space science, notably the solar and polar wind expansions (Lie-Svendsen and Rees 1996; Pierrard and Lemaire 1998; Marsch 2006; Echim et al. 2011). A large number of chemically reactive systems can be modelled with a Fokker-Planck equation proposed by Kramers (1940). Many aspects of turbulence are modelled as stochastic processes leading to a Fokker-Planck equation (Pope 2000). The applications of the Fokker-Planck equation to stellar dynamics and astrophysics (Chandrasekhar 1942; Spitzer 1998; Chavanis 2006; Binney and Tremaine 2008) overlap applications to plasma physics (Rosenbluth et al. 1957; Spitzer 1962; Boyd and Sanderson 2003). The set of coupled rate equations for the growth of a cluster in nucleation theory is often modelled with a Fokker-Planck equation (Shizgal and Barrett 1989; Demeio and Shizgal 1993a). The Black-Scholes model in mathematical finance (Black and Scholes 1973; Paul and Baschnagel 2013) is based on a Fokker-Planck equation. These are just a few examples of the many different Fokker-Planck equations that arise in diverse applications. Additional discussion of these topics can be found in several textbooks (Risken 1996; Gardiner 2003; Reif 2008) and review papers (Chandrasekhar 1949; Lightman and Shapiro 1978).

---

[1] Adrian Fokker (1887–1972) was a Dutch physicist who made contributions to relativity and statistical mechanics in collaboration with Albert Einstein. The Fokker-Planck equation used to model numerous processes in physics, astrophysics, chemistry, finance and biology bears his name. He also made numerous contributions to music theory.

[2] Max Planck (1858–1947) was a German physicist and the 1918 Nobel laureate for his contributions to the explanation of the photoelectric effect, energy quantization and the introduction of the Planck constant. The basis for this work was his doctoral work on thermodynamics as related to black body radiation at equilibrium. Planck and Fokker independently derived the Fokker-Planck equation of statistical physics.

In Chap. 5, we expressed the solutions of the linearized and linear Boltzmann equations in terms of the eigenvalues of the collision operators involved. For the linearized collision operator and the linear collision operator with unit mass ratio ($\gamma = 1$), the integral operator can be transformed to a Schrödinger equation (Kuščer and Williams 1967; Bobylev and Mossberg 2008). The Fokker-Planck equations discussed in the sections that follow can be transformed to Schrödinger equations with well defined potential functions (Risken 1996). The potentials belong to the class of Schrödinger equations in supersymmetric quantum mechanics (Bernstein and Brown 1984; Comtet et al. 1985; Dutt et al. 1988; Cooper et al. 1995).

6.1.1 From the Langevin Equation to the Fokker-Planck Equation; Brownian Motion

We begin the discussion with the classic treatment of Brownian motion. We consider a subsystem of particles of mass m that interact solely with the particles of a background medium at equilibrium at temperature T_b. The origin of this approach is the work of the botanist Robert Brown[3] who observed the random movement of a pollen grain in a fluid at some temperature T_b. The movement of the so-called "Brownian" particle is random owing to the multitude of collisions of the molecules of the background fluid with the grain. Thus the scalar force, $F(t)$, on the Brownian particle is random in time. However, there is also a steady component that corresponds to the friction involved in the steady movement of the Brownian particle through the fluid. Thus we write $F(t) = F_s(t) + F_r(t)$ where $F_s(t)$ is the steady component related to the viscosity of the fluid and $F_r(t)$ is a largely unknown random or "stochastic" force. The steady component of the force is $F_s(t) = -\alpha v(t)$ where v is the particle velocity in one dimension and α is the friction coefficient that slows the particle as it moves through the fluid. We write the "stochastic" differential equation of motion for the Brownian particle as Newton's law with a random force, that is,

$$m\frac{dv}{dt} = -\alpha v(t) + F_r(t). \tag{6.1}$$

Equation (6.1) is known as the Langevin[4] equation for Brownian motion that was treated previously by Einstein (1906). The main difficulty with Eq. (6.1) is that the detailed time variation of $F_r(t)$ is largely unknown. What is remarkable with this approach is that the friction coefficient α in Eq. (6.1) is related to the properties of

[3] Robert Brown (1773–1858) was a Scottish botanist who made important contributions to botany and statistical physics from his use of a microscope to observe the random motion of pollen grains which was later referred to as Brownian motion.

[4] Paul Langevin (1872–1946) was a French physicist and doctoral student with J.J. Thompson at the Cavendish Laboratory and Pierre Curie in Paris. He worked extensively on paramagnetism and diamagnetism as well as in kinetic theory and theory of Brownian motion following on Einstein's work.

$F_r(t)$ (Reif 2008). Alternative methods are based on computer simulations that follow the time history of the particle positions and velocities (Gunther and Weaver 1978; Gillespie 1996). Monte Carlo simulations have become common in statistical physics and chemistry for the study of multidimensional complex systems in equilibrium and nonequilibrium situations (Bird 1994; Landau and Binder 2009).

An alternative approach to computer simulations is one based on the probability density of the random variable leading to a deterministic Fokker-Planck equation. The stochastic force, $F_r(t)$, is assumed to satisfy two important relations, (1) that the time (or "ensemble") average is zero and (2) the correlation in time has a definite strength, that is

$$\begin{aligned} \overline{F_r(t)} &= 0, \\ \overline{F_r(t)F_r(t')} &= 2\alpha k_B T_b \delta(t-t'), \end{aligned} \tag{6.2}$$

where k_B is the Boltzmann constant and T_b is the temperature of the background. The overbars indicate time or ensemble averages; see Sect. 15.5 in Reif (2008). In addition to the textbooks referenced earlier, excellent discussions of the historical development of stochastic processes are available (Uhlenbeck and Ornstein 1930; Hänggi et al. 1990; Risken 1996; Abbott 2001; Gardiner 2003; van Kampen 2007; Dunkel and Hänggi 2009; Paul and Baschnagel 2013).

Brownian motion and other stochastic processes are modelled with a probability density, $P(v,t)$, corresponding to the values of $v(t)$ sampled in a sufficiently long sequences of realizations of $v(t)$. Thus $P(v,t)$ is similar to the velocity distribution function $f(v,t)$ in kinetic theory in Chap. 5. It has been shown (Uhlenbeck and Ornstein 1930; Chandrasekhar 1949; Reif 2008) that the Fokker-Planck equation for the probability density (equivalently the velocity distribution) of the Brownian particle is given by the Ornstein–Uhlenbeck equation,

$$\frac{\partial P(v,t)}{\partial t} = \nu \frac{\partial}{\partial v}\left[vP(v,t) + \frac{k_B T_b}{m}\frac{\partial P(v,t)}{\partial v}\right], \qquad v \in (-\infty, \infty), \tag{6.3}$$

where the drift and diffusion coefficients, defined in what follows are νv and $\nu k_B T_b/m$, respectively, and $\nu = \alpha/m$ is a collision frequency.

A stochastic process which includes multiplicative as well as additive noise (Chandrasekhar 1949; Lax 1966; Brey et al. 1987; Gitterman 1999; Biró and Jakovác 2005) yields a Fokker-Planck equation with a velocity dependent diffusion coefficient. For this more general stochastic process we have the Langevin equation of the form

$$\frac{dv}{dt} = f(v) + g(v)\xi(t) + \eta(t), \tag{6.4}$$

with $f(v)$ and $g(v)$ are known but unspecified functions. The additive and multiplicative Gaussian random variables, $\eta(t)$ and $\xi(t)$ have zero mean,

$$\overline{\eta(t)} = 0 \qquad \text{and} \qquad \overline{\xi(t)} = 0, \tag{6.5}$$

and correlations given by,

$$\overline{\eta(t)\eta(t')} = 2D\delta(t-t') \qquad \overline{\xi(t)\xi(t')} = 2\beta\delta(t-t'). \tag{6.6}$$

The Fokker-Planck equation for $P(v,t)$ corresponding to this stochastic process is of the form

$$\frac{\partial P(v,t)}{\partial t} = \frac{\partial}{\partial v}\left[A(v)P(v,t) + \frac{\partial B(v)P(v,t)}{\partial v}\right], \tag{6.7}$$

where $A(v)$ and $B(v)$ are the time-independent drift and diffusion coefficients, respectively, given by,

$$\begin{aligned} A(v) &= f(v) + \beta g(v)\frac{dg(v)}{dv}, \\ B(v) &= D + \beta g^2(v). \end{aligned} \tag{6.8}$$

where $f(v)$, $g(v)$, D and β are defined by Eqs. (6.4) and (6.6). Additional details of this derivation are in the references cited.

Given some initial condition, $P(v,0)$, the distribution $P(v,t)$ varies in time as deduced with Eq. (6.7) and attains a steady distribution at infinite time for which $\partial P(v,t)/\partial t = 0$ and denoted by $P_0(v)$. For most of the applications to be discussed, the reduced speed, $x = \sqrt{mv^2/2k_BT_b}$ is used and generally $x \in (-\infty, \infty)$. From Eq. (6.7), this equilibrium probability density is

$$P_0(v) = \frac{1}{B(v)}\exp\left(-\int_{-\infty}^{v}\frac{A(v')}{B(v')}dv'\right), \tag{6.9}$$

and is not in general a Maxwellian.

6.1.2 *Spectral Solution of the Ornstein-Uhlenbeck Fokker-Planck Equation*

The equilibrium distribution analogous to Eq. (6.9) for the Brownian motion Fokker-Planck equation, Eq. (6.3), is defined by

$$\left[vP_0(v) + \frac{k_BT_b}{m}\frac{\partial P_0(v)}{\partial v}\right] = 0,$$

and the steady state distribution of Eq. (6.3) is a Maxwellian,

$$P_0(v) = \sqrt{\frac{m}{2\pi k_BT_b}}e^{-mv^2/2k_BT_b}. \tag{6.10}$$

normalized such that

$$\int_{-\infty}^{\infty} P_0(v)dv = 1.$$

We consider an initial condition whereby all the particles start with a specific speed v_0 that is

$$P(v, 0) = \delta(v - v_0). \tag{6.11}$$

The solution of this Fokker-Planck equation is readily determined with the transformation to a strict diffusion equation where the diffusion coefficient is $D = \mu k_B T_b/m$. We redefine the variables so as to remove the term in $\partial P/\partial v$ in Eq. (6.3) in a manner analogous to the transformation of the Fokker-Planck equation to a Schrödinger equation discussed in Sect. 6.3.2. We make the change of variable $u = ve^{\nu t}$ and set $P(v, t) = e^{\nu t} Q(u, t)$. With these substitutions, the Fokker-Planck equation can be written in terms of $Q(u, t)$, that is

$$\frac{\partial Q(u, t)}{\partial t} = De^{2\nu t} \frac{\partial^2 Q(u, t)}{\partial u^2}. \tag{6.12}$$

With the change in the time variable to $\tau = (e^{2\nu t} - 1)/\nu$, we transform the Fokker-Planck equation to the diffusion equation, that is

$$\frac{\partial Q(u, \tau)}{\partial \tau} = D \frac{\partial^2 Q(u, \tau)}{\partial u^2}. \tag{6.13}$$

This equation could be considered as a Fokker-Planck equation without drift which is referred to as a Weiner process (Risken 1996; Gillespie 1996).

We have solved the diffusion equation with a Fourier transform method in Chap. 4, Sect. 4.6.5 and the solution of Eq. (6.13) is

$$Q(u, \tau) = \frac{1}{\sqrt{4\pi D\tau}} e^{-(u-u_0)^2/4D\tau}. \tag{6.14}$$

With this result, the solution to the Ornstein–Uhlenbeck, Eq. (6.13), in the reduced speed, $x = \sqrt{mv^2/2k_B T_b}$, is

$$P(x, t) = \left[\frac{1}{\pi(1 - e^{-2\nu t})}\right]^{1/2} \exp\left[-\frac{(x - x_0 e^{-\nu t})^2}{(1 - e^{-2\nu t})}\right]. \tag{6.15}$$

A spectral solution of Eq. (6.3) can be expressed in Hermite polynomials in x by substituting $P(x, t) = e^{-x^2} g(x, t)$ into Eq. (6.3) written in terms of x. The result is the differential equation

$$\frac{\partial g(x,t)}{\partial t} = \nu e^{x^2} \frac{\partial}{\partial x}\left[e^{-x^2} \frac{\partial g(x,t)}{\partial x} \right],$$
$$= \nu \left[-2x \frac{\partial g}{\partial x} + \frac{\partial^2 g}{\partial x^2} \right]. \tag{6.16}$$

With the expansion in Hermite polynomials

$$g(x,t) = \sum_{n=0}^{\infty} c_n(t) H_n(x), \tag{6.17}$$

Eq. (6.16) can be written as

$$\sum_{n=0}^{\infty} H_n(x) \frac{dc_n}{dt} = \nu \sum_{n=0}^{\infty} c_n(t) \left[-2x H_n'(x) + H_n''(x) \right]. \tag{6.18}$$

With the relation $-2x H_n' + H_n'' = -2n H_n$, the time dependence of the coefficients is given by

$$\frac{dc_n(t)}{dt} = -2n\nu c_n(t). \tag{6.19}$$

With the expansion of the initial condition in the Hermite polynomials, the spectral solution is given by

$$P(x,t) = e^{-x^2} \sum_{n=0}^{\infty} \frac{1}{2^n n! \sqrt{\pi}} H_n(x_0) H_n(x) e^{-2n\nu t}. \tag{6.20}$$

Equations (6.15) and (6.20) can be used to study the rate of convergence of the expansion in Hermite polynomials (Wei et al. 1997). A study of the use of orthogonal expansions for the solution of Fokker-Planck equations was reported by Cukier et al. (1973). An eigenfunction analysis of the three-dimensional Ornstein-Uhlenbeck process with expansions in associated Laguerre polynomials and spherical harmonics was reported recently by Wilkinson and Pumir (2011).

6.1.3 *Rayleigh and Lorentz Fokker-Planck Equations from the Boltzmann Equation; The Kramers-Moyal Expansion*

In Chap. 3 (Eq. (3.49)) and Chap. 5 (Eq. (5.110)), we discussed the Wigner-Wilkins kernel (Wigner 1943; Wigner and Wilkins 1944; Hoare and Kaplinsky 1970; Hoare 1971) for the linear Boltzmann integral operator for a hard sphere cross section. This

Boltzmann equation models the relaxation of an ensemble of test particles of mass m dilutely dispersed in a second gas of particles of mass M which is taken to be at equilibrium with a Maxwellian distribution at temperature T_b.

The hard sphere collision operator in the Boltzmann equation for a binary gas mixture can be approximated by Fokker-Planck equations in the mass ratio limits $\gamma = M/m \to \infty$ (the "Lorentz" limit) or $\gamma \to 0$ (the "Rayleigh" limit), respectively as shown by Andersen and Shuler (1964). The derivation is based on the expansion of the kernel in the small energy transfer on collision for these disparate mass ratios. The integral operator is expanded up to second order in the small energy transfer and this transformation of the integral equation to a Fokker-Planck equation is known as the Kramers-Moyal expansion (Risken 1996; Knessl et al. 1984; van Kampen 2007).

For the disparate mass ratio limit, $\gamma \to 0$, the Rayleigh Fokker-Planck equation is

$$\frac{\partial P(y,t)}{\partial t} = \frac{\partial}{\partial y}\left[(y-3)P(y,t) + \frac{\partial}{\partial y}[yP(y,t)]\right], \tag{6.21}$$

where $y = mv^2/k_BT_b$ is the reduced energy and t is in units of τ given by $1/\tau = K_R = \frac{16}{3}Mmn_b\sigma_0\sqrt{2k_BT_b/\pi M}$. For $\gamma \to \infty$, the Lorentz Fokker-Planck equation is

$$\frac{\partial P(x,t)}{\partial t} = \frac{1}{4}\frac{\partial}{\partial x}\left[(2x^2-3)P(x,t) + \frac{\partial}{\partial x}[xP(x,t)]\right], \tag{6.22}$$

where $x = \sqrt{mv^2/2k_BT_b}$ is the reduced speed and $1/\tau = K_L = 2\sqrt{m/M}n_b\sigma_0$ $\sqrt{2k_BT_b/M}$. The hard sphere cross section is denoted by σ_0 and n_b is the density of the background gas. A spectral solution of the Rayleigh Fokker-Planck equation in terms of Hermite polynomials is described in the next section. There is no known spectral solution of the Lorentz Fokker-Planck equation in terms of classical polynomials.

6.1.4 Spectral Solution of the Rayleigh Fokker-Planck Equation

We consider an analysis similar to the one in Sect. 6.1.2. If we set $P(y,t) = P_0(y)g(y,t)$ where $P_0(y) = (2/\sqrt{\pi})\sqrt{y}e^{-y}$ in dimensionless units and we get the differential equation

$$\frac{\partial g(y,t)}{\partial t} = \frac{1}{P_0(y)}\frac{\partial}{\partial y}\left[yP_0(y)\frac{\partial g(y,t)}{\partial y}\right]. \tag{6.23}$$

The evaluation of the partial derivative in the square bracket gives

$$\frac{\partial g(y,t)}{\partial t} = y\frac{\partial^2 g(y,t)}{\partial y^2} + (\frac{3}{2}-y)\frac{\partial g(y,t)}{\partial y}. \tag{6.24}$$

The differential operator on the right hand side is related to the eigenvalue problem for the associated Laguerre polynomials, $L_n^{(\frac{1}{2})}(y)$, that is

$$y\frac{d^2L_n^{(\frac{1}{2})}(y)}{dy^2} + (\frac{3}{2} - y)\frac{dL_n^{(\frac{1}{2})}(y)}{dy} = -ny. \tag{6.25}$$

Thus, the spectral solution is represented by the expansion in the associated Laguerre polynomials

$$g(y,t) = \sum_{n=0}^{\infty} c_n L_n^{(\frac{1}{2})}(y)e^{-nt}, \tag{6.26}$$

where the coefficients for a δ-function initial condition, $P(y,0) = \delta(y - y_0)$, are

$$c_n = \frac{\Gamma(n+1)}{\Gamma(n+\frac{3}{2})} L_n^{(\frac{1}{2})}(y_0). \tag{6.27}$$

Analogous to the expansion of the Ornstein-Uhlenbeck Fokker-Planck equation in Hermite polynomials, the solution of Eq. (6.21) can be expanded in Laguerre polynomials, that is

$$P(y,t) = \sqrt{y}e^{-y} \sum_{n=0}^{\infty} \frac{\Gamma(n+1)}{\Gamma(n+3/2)} L_n^{(\frac{1}{2})}(y_0) L_n^{(\frac{1}{2})}(y)e^{-nt}. \tag{6.28}$$

Andersen and Shuler (1964) summed this series and found the analytic result,

$$P(y,t) = \frac{e^{t/2}}{2\sqrt{\pi y_0(1-e^{-t})}} \left\{ \exp\left[-\frac{(\sqrt{y} - \sqrt{y_0 e^{-t}})^2}{1-e^{-t}} \right] - \exp\left[-\frac{(\sqrt{y} + \sqrt{y_0 e^{-t}})^2}{1-e^{-t}} \right] \right\}, \tag{6.29}$$

analogous to Eq. (6.15) for the Ornstein-Uhlenbeck equation. This provides another opportunity to study the rate of convergence of the Laguerre expansions.

For an initial Maxwellian distribution at temperature $T(0) > T_b$, the expansion in Laguerre polynomials can be summed in closed form (Andersen and Shuler 1964) to give

$$P(y,t) = \frac{2}{\sqrt{\pi}} \left[\frac{T_b}{T(t)} \right]^{3/2} \sqrt{y} \exp[-\frac{T_b}{T(t)} y], \tag{6.30}$$

which is a Maxwellian distribution with the time dependent temperature $T(t)$. Equation (6.30) also defines the intial Maxwellian at $T(0)$. An important property of

this Fokker-Planck equation is that if the initial distribution function is a Maxwellian at some temperature $T(0) > T_b$, the time dependent distribution remains Maxwellian with a time dependent temperature. This property of the Rayleigh Fokker-Planck equation is referred to as canonical invariance (Andersen et al. 1964; Andersen and Shuler 1964). This is a consequence of the fact that for this Rayleigh Fokker-Planck equation the moments of the distribution function in the Laguerre basis set are uncoupled and the temperature relaxation is a pure exponential given by

$$\frac{T(t) - T_b}{T(0) - T_b} = e^{-t}. \tag{6.31}$$

6.2 Numerical Methods for the Solution of the Fokker-Planck Equation

We have expressed the spectral solutions of the Ornstein-Uhlenbeck Fokker-Planck equation in Hermite polynomials and of the Rayleigh Fokker-Planck equation in Laguerre polynomials. Analogous pseudospectral solutions can also be derived which provide identical numerical results. We present in the next section a formalism for the use of nonclassical basis functions for the solution of the general Fokker-Planck equation in Eq. (6.7) with arbitrary drift and diffusion coefficients, $A(v)$ and $B(v)$, respectively. In Sect. 6.2.2, an equivalent pseudospectral formalism is presented.

6.2.1 Spectral Methods with Nonclassical Basis Functions

We consider a solution of the Fokker-Planck equation with a spectral method and with a basis set analogous to the solution of the Ornstein-Uhlenbeck equation in Sect. 6.1.2. The polynomial basis set is defined with the steady distribution $P_0(x)$ as the weight function. If we set $P(x,t) = P_0(x)g(x,t)$ in the Fokker-Planck equation, Eq. (6.7), where $P_0(x)$ is given by Eq. (6.9), then the equation for $g(x,t)$ becomes

$$\begin{aligned}\frac{\partial g(x,t)}{\partial t} &= \frac{1}{P_0(x)}\frac{\partial}{\partial x}\left[B(x)P_0(x)\frac{\partial g(x,t)}{\partial x}\right], \quad x \in [0,\infty)\\ &= -A(x)\frac{\partial g(x,t)}{\partial x} + B(x)\frac{\partial^2 g(x,t)}{\partial x^2},\\ &= -Lg(x,t),\end{aligned} \tag{6.32}$$

where the definition of $P_0(x)$ has been used. The term in square brackets in Eq. (6.32) can be considered as a flux. With the form of the operator, L, in the first line of

Eq. (6.32), L is self-adjoint with respect to $P_0(x)$ as the weight function provided that the zero flux boundary condition

$$P_0(x)B(x)\frac{\partial g(x)}{\partial x}\bigg|_0^\infty = 0, \tag{6.33}$$

is imposed. The linear time dependent Fokker-Planck equation, Eq. (6.32), admits a solution in terms of the eigenfunctions, $\psi_n(x)$, and eigenvalues, λ_n, defined by

$$L\psi_n(x) = \lambda_n\psi_n(x), \tag{6.34}$$

and the solution can be written as

$$P(x,t) = P_0(x)\sum_{n=0}^{\infty} a_n e^{-\lambda_n t}\psi_n(x), \tag{6.35}$$

where the a_n coefficients are determined from the initial distribution, $P(x,0)$. The self-adjoint property of L can be verified by calculating the matrix element $\langle\phi_1|L|\phi_2\rangle$ with L defined as in Eq. (6.32). With an integration by parts, it is easily shown that $\langle\phi_1|L|\phi_2\rangle = \langle\phi_2|L|\phi_1\rangle$ provided Eq. (6.33) is satisfied.

The eigenvalues and eigenfunctions are determined with a Galerkin spectral method and nonclassical basis sets and we use the basis set $\{S_n(x)\}$ orthonormal with $P_0(x)$ as weight function, that is

$$\int_0^\infty P_0(x)S_n(x)S_m(x)dx = \delta_{nm}. \tag{6.36}$$

The set $\{S_n(x)\}$, introduced in this chapter, is used to denote a general basis set of nonclassical polynomials orthonormal with respect to different equilibrium density functions, $P_0(x)$, defined by a specific physical problem. The matrix elements of the Fokker-Planck operator L in this basis set are given by

$$\begin{aligned} L_{nm}^{(sp)} &= \int_0^\infty P_0(x)S_n(x)LS_m(x)dx \\ &= -\int_0^\infty P_0(x)S_n(x)\frac{1}{P_0(x)}\frac{d}{dx}\left[P_0(x)B(x)\frac{dS_m(x)}{dx}\right]dx, \end{aligned} \tag{6.37}$$

where the superscript (sp) denotes the polynomial spectral representation. With an integration by parts, we get the symmetric matrix representation of the Fokker-Planck operator,

$$\boxed{L_{nm}^{(sp)} = -\int_0^\infty P_0(x)B(x)S_n'(x)S_m'(x)dx, \qquad (n,m) = 0,1,\ldots,N-1} \tag{6.38}$$

where zero flux boundary conditions are satisfied, Eq. (6.33). We highlight this important result showing the self-adjoint property of the Fokker-Planck equation subject to zero flux boundary conditions. The eigenvalues, λ_n, and eigenfunctions, $\psi_n(x)$, are determined with a numerical diagonalization of the matrix $\mathbf{L}^{(sp)}$ of dimension N. Although we have not demonstrated this explicitly here, the numerical results will show that the coefficients of the expansion $\psi_n(x)$ in the $S_n(x)$ basis set are linear variational parameters. Thus, the variational theorem is applicable and this spectral method will provide an upper bound to the eigenvalues for each N and converge from above. The time dependent solution of the Fokker-Planck equation is given by Eq. (6.35).

We will use L to denote several different Fokker-Planck operators in the sections that follow and each is defined at the outset. Otherwise the notation would become excessive.

6.2.2 *Pseudospectral Methods with Nonclassical Quadratures*

We introduce the basis set $R_n(x)$ orthonormal with respect to $w(x)$ defined by

$$R_n(x) = \sqrt{\frac{P_0(x)}{w(x)}}S_n(x), \tag{6.39}$$

and evaluate the derivative $S'(x) \equiv dS(x)/dx$,

$$S_n'(x) = \sqrt{\frac{w}{P_0}}\left(\frac{w'}{2w} - \frac{P_0'}{2P_0}\right)R_n(x) + \sqrt{\frac{w}{P_0}}R_n'(x). \tag{6.40}$$

Thus, the matrix elements of the Fokker-Planck operator, Eq. (6.38), are given by

$$L_{nm}^{(sp)} = -\int_0^\infty w(x)B(x)\left[R_n'(x) + h(x)R_n(x)\right]\left[R_m'(x) + h(x)R_m(x)\right]dx, \tag{6.41}$$

where

$$\boxed{h(x) = \frac{w'(x)}{2w(x)} - \frac{P_0'(x)}{2P_0(x)},} \tag{6.42}$$

and is a measure of the departure of $w(x)$ from $P_0(x)$. This result is highlighted as it shows that an optimal choice of weight function might be $w(x) = P_0(x)$ giving $h(x) = 0$.

The matrix elements are evaluated with the quadrature based on the weight function $w(x)$, that is

$$L_{nm}^{(sp)} = -\sum_{k=1}^{N} w_k B(x_k)[R_n'(x_k) + h(x_k)R_n(x_k)][R_m'(x_k) + h(x_k)R_m(x_k)], \quad (6.43)$$

where x_k and w_k are the quadrature points and weights associated with the polynomials orthogonal with respect to the weight function, $w(x) = P_0(x)$. To express this spectral representation in the equivalent physical space representation, we transform

$$L_{ij}^{(ps)} = \sum_{m=0}^{N-1}\sum_{n=0}^{N-1} T_{in} L_{nm}^{(sp)} T_{jm}, \quad (6.44)$$

where the superscript (ps) denotes the discrete pseudospectral representation and the transformation matrix between physical and spectral space is defined as in Chap. 3, namely

$$T_{in} = \sqrt{w_i} R_n(x_i).$$

We need only consider the first transformation with the sum over n as the second over m is similar. With the definition of T_{in}, the term in $R_n(x_k)$ is transformed as

$$\begin{aligned} h(x_k)\sum_{n=0}^{N-1} T_{in} R_n(x_k) &= h(x_k)\sum_{n=0}^{N-1} \sqrt{w_i} R_n(x_i) R_n(x_k), \\ &= \frac{h(x_k)}{\sqrt{w_k}}\delta_{ik}. \end{aligned} \quad (6.45)$$

The transformation of $R_n'(x_k)$ employs the derivative matrix operator giving

$$\begin{aligned} \sum_{n=0}^{N-1} T_{in} R_n'(x_k) &= \sum_{n=0}^{N-1} \sqrt{w_i} R_n(x_i) \sum_{\ell=1}^{N} D_{k\ell}\sqrt{\frac{w_\ell}{w_k}} R_n(x_\ell), \\ &= \sum_{\ell=1}^{N} D_{k\ell}\sqrt{\frac{w_i w_\ell}{w_k}} \sum_{n=0}^{N-1} R_n(x_i) R_n(x_\ell), \\ &= \sum_{\ell=1}^{N} D_{k\ell}\sqrt{\frac{w_i w_\ell}{w_k}} \frac{\delta_{i\ell}}{w_i}, \\ &= \frac{D_{ki}}{\sqrt{w_k}}. \end{aligned} \quad (6.46)$$

The transformation with T_{jm} yields similar results and we find the discrete pseudospectral representation

$$\boxed{L_{ij}^{(ps)} = -\sum_{k=1}^{N} B(x_k)[D_{ki} + h(x_k)\delta_{ki}][D_{kj} + h(x_k)\delta_{kj}], \quad (i, j) = 1, 2, \ldots, N.} \tag{6.47}$$

This result is also highlighted because for the quadrature defined with the stationary distribution, $w(x) = P_0(x)$, for which $h(x_k) = 0$, the representation of L_{ij} has the simpler form,

$$L_{ij}^{(ps)} = -\sum_{k=1}^{N} B(x_k) D_{ki} D_{kj}. \tag{6.48}$$

The representation of the Fokker-Planck operator given by Eq. (6.48) is straightforward to program in MATLAB for different choices of the basis set and associated quadrature points and weights. The derivative matrix operator, D_{ki}, is calculated as discussed in Chap. 3, Eqs. (3.138) and (3.139).

The pseudospectral solution of the Ornstein–Uhlenbeck Fokker-Planck equation is equivalent to the solution of the Schrödinger equation for the quantum harmonic oscillator. The drift coefficient, $B(x) = 1$, (Eq. 6.16), and $P_0(x) = w(x) = e^{-x^2}$, $x \in (-\infty, \infty)$, so that the derivative matrix operator, D_{ki}, is defined in terms of the Hermite polynomials as discussed in Chap. 4. The eigenvalues of the self-adjoint representation of the Fokker-Planck operator $\mathbf{L}^{(ps)}$ (Eq. 6.48) are $\lambda_n = n$ and the eigenfunctions are the Hermite polynomials.

For the Rayleigh Fokker-Planck equation $B(y) = y$, and with the Gauss Laguerre quadrature weights and points defined with $P_0(y) = w(y) = \sqrt{y}e^{-y}$, $y \in [0, \infty)$, the eigenvalues of $\mathbf{L}^{(ps)}$ are $\lambda_n = n$ and the eigenfunctions are the Laguerre polynomials. This is consistent with the spectral solutions given by Eqs. (6.20) and (6.28).

6.2.3 *The Chang-Cooper Finite Difference Method of Solution of the Fokker-Planck Equation*

The finite difference algorithm by Chang and Cooper (1970) has found numerous applications for the solution of the Fokker-Planck equation in many different applications (Larsen et al. 1985; Park and Petrosian 1996; Buet and Dellacherie 2010; Abolhassani and Matte 2012).

The self-adjoint form of the Fokker-Planck equation, Eq. (6.32), was shown to be consistent with zero flux at the boundaries, Eq. (6.33). This boundary condition is also related to particle conservation

$$\frac{\partial}{\partial t}\int_0^\infty P_0(x)g(x,t)dx = P_0(x)B(x)\frac{\partial g(x,t)}{\partial x}\Big|_{x=0}^{\infty} = 0. \tag{6.49}$$

Any useful discretization would have to ensure particle conservation which yields, $\lambda_0 = 0$.

We discretize the speed variable according to $0 = x_1 < x_2 < x_3 \cdots < x_N = x_{max}$ with $x_{i+1} = x_i + \Delta x$, and $\Delta x = x_{max}/(N-1)$ where x_{max} is the speed point chosen large enough so that the flux boundary condition is satisfied. We also introduce a shifted grid at the midpoint defined by $x_{i+1/2} = x_i + \Delta x/2$. With a centered difference for the derivative,

$$\frac{\partial g(x,t)}{\partial x}|_{x_{i+1/2}} \approx \frac{g(x_{i+1},t) - g(x_i,t)}{\Delta x}, \tag{6.50}$$

the finite difference representation of the eigenvalue problem is,

$$\sum_{j=1}^{N} L_{ij}\phi_n(x_j) = \lambda_n \phi_n(x_i), \tag{6.51}$$

where

$$Ł_{ii} = \frac{1}{(\Delta x)^2}\frac{x_i^2 P_0(x_i)B_i + x_{i+1}^2 P_0(x_{i+1})B_{i+1}}{x_{i+1/2}^2 P_0(x_{i+1/2})}, \quad i = 1,\ldots,N, \tag{6.52}$$

$$Ł_{i,i-1} = -\frac{1}{(\Delta x)^2}\frac{x_i^2 P_0(x_i)B_i}{x_{i+1/2}^2 P_0(x_{i+1/2})}, \quad i = 2,\ldots,N, \tag{6.53}$$

$$Ł_{i,i+1} = -\frac{1}{(\Delta x)^2}\frac{x_{i+1}^2 P_0(x_{i+1})B_{i+1}}{x_{i+1/2}^2 P_0(x_{i+1/2})}, \quad i = 1,\ldots,N-1, \tag{6.54}$$

with the understanding that the first term in the fraction on the right hand side of Eq. (6.52) vanishes for $i = 1$ and the second term vanishes for $i = N$ in order to enforce the boundary conditions.

We use a forward Euler difference algorithm for the time derivative, that is

$$\frac{\partial g(x_i,t)}{\partial t} = \frac{g_i^{(n+1)} - g_i^{(n)}}{\Delta t}, \tag{6.55}$$

where $t = n\Delta t$ and $g_i^{(n)} = g(x_{i+1/2}, n\Delta t)$. The Chang-Cooper finite difference algorithm for the Fokker-Planck equation is

$$g_i^{(n+1)} = g_i^{(n)} + \Delta t \frac{x_{i+1}^2 P_0(x_{i+1}) B_{i+1}[g_{i+1}^{(n+1)} - g_i^{(n+1)}] - x_i^2 P_0(x_i) B_i[g_i^{(n+1)} - g_{i-1}^{(n+1)}]}{(\Delta x)^2 x_{i+1/2}^2 P_0(x_{i+1/2})}. \tag{6.56}$$

This result can be rewritten compactly as the matrix equation

$$\sum_{j=1}^{N} V_{ij} g_j^{(n+1)} = g_i^{(n)}, \tag{6.57}$$

where the matrix $\mathbf{V}$ is tridiagonal with elements

$$\begin{aligned} V_{i,i} &= 1 + \Delta t L_{i,i}, \quad i = 1, \ldots, N, \\ V_{i,i-1} &= \Delta t L_{i,i-1}, \quad i = 2, \ldots, N, \\ V_{i,i+1} &= \Delta t L_{i,i+1}, \quad i = 1, \ldots, N-1 \end{aligned} \tag{6.58}$$

At each time step, the updated values $g_i^{(n+1)}$ are obtained with the inversion of Eq. (6.57).

The Chang-Cooper finite difference scheme, as a discrete representation of L, does not give rapidly convergent eigenvalues and eigenfunctions (Leung et al. 1998). However, with the algorithm Eq. (6.56), the probability density function remains positive, entropy increases with time and a Maxwellian is recovered at equilibrium (Buet and Dellacherie 2010). We use this algorithm in Sect. 6.4.2 to solve the Fokker-Planck equation for a model that involves heating of a plasma by wave-particle interactions.

6.3 Electron Thermalization; The Lorentz Fokker-Planck Equation Revisited

The degradation or thermalization of energetic electrons in atomic and molecular moderators is an important aspect of radiation chemistry and physics (Mozumder 1999; Robson 2006), plasma processing of semiconductor devices (Petrović et al. 2009), the physics of the aurora (Stamnes 1980; Basu et al. 1993; Solomon 2001; Shematovich et al. 2008) fundamental aspects of the approach to equilibrium (Trunec et al. 2003; Sospedra-Alfonso and Shizgal 2011) and thermalization in condensed matter (Sakai 2007; White et al. 2010).

The electron anisotropic nonequilibrium distribution functions are often expanded in the direct product of the spherical harmonics in (θ, ϕ) and the Sonine–Laguerre polynomials for the reduced speed or reduced energy dependence (Kumar et al. 1980; Robson and Ness 1986; Robson 2006; White and Robson 2011; Abolhassani and Matte 2012). This methodology requires the matrix elements of the collision operator

in the Boltzmann equation as discussed in Chap. 5. There have also been solutions of the electron Boltzmann equation with a B spline representation (Pitchford and Phelps 1982) as well as with Monte Carlo methods (Koura 1983; Solomon 2001; Shematovich et al. 2008).

For molecular moderators such as N_2, O_2 and CH_4, inelastic collisions that involve changes in the rotational and/or vibrational states of the moderator (Pitchford and Phelps 1982; Kowari et al. 1992) and electron attachment to electronegative gases such as SF_6 and CCl_4 must be included (Kowari and Shizgal 1996; Kowari et al. 1998).

The relaxation of electrons of moderate energy in atomic moderators for which only elastic collisions need be included (Mozumder 1981; Knierim et al. 1982; Risken and Voigtlaender 1984; McMahon and Shizgal 1985; Shizgal and McMahon 1985) is presented in this section. In atomic moderators, there have been two notable phenomena exhibited, namely the transient negative mobility (Shizgal and McMahon 1985; Dyatko et al. 2001; Dyatko 2007) and the negative differential conductivity effect in gas mixtures (Shizgal 1990) previously thought to occur only for polyatomic gases with internal degrees of freedom.

Owing to the small electron mass m_e to moderator mass M ratio, the Boltzmann collision operator can be replaced by the Fokker-Planck operator corresponding to the Lorentz limit discussed in Sect. (6.1.3). The Boltzmann equation or the Fokker-Planck equation have been used in the study of electron thermalization in rare gases (Lin et al. 1979; Knierim et al. 1982; McMahon and Shizgal 1985; Shizgal and McMahon 1985). The physics of the problem is defined by the energy dependent momentum transfer cross section $\sigma_{mt}(v)$ for electron-atom collisions and the strength of the applied electric field, E. The electric field results in a drift of the electrons with a mobility determined by the electron-atom cross section.

To account for the electron drift in the applied electric field, there is a small anisotropy of the electron velocity distribution function which is expressed by the expansion in Legendre polynomials, that is,

$$f(\mathbf{v}, t') = \sum_{\ell=0}^{\infty} f_\ell(v, t') P_\ell(\cos\theta), \tag{6.59}$$

where θ is the angle between $\mathbf{v}$ and the polar axis taken in the direction of the electric field. Owing to the small mass ratio, m_e/M, the anisotropy of the distribution remains small and only the terms in $\ell = 0$ and $\ell = 1$ in Eq. (6.59) need to be retained. This is referred to as the "two-term" approximation (Hagelaar and Pitchford 2005). The coupled equations for the first two terms, f_0 and f_1, are

$$\begin{aligned} \frac{\partial f_0}{\partial t'} + \frac{eE}{3m_e}\left(\frac{\partial}{\partial v} + \frac{2}{v}\right) f_1 &= \frac{m_e}{Mv^2}\frac{\partial}{\partial v}\left[v^3\gamma(v)\left(1 + \frac{k_B T_b}{m_e v}\frac{\partial}{\partial v}\right)\right] f_0, \\ \frac{\partial f_1}{\partial t'} + \frac{eE}{m_e}\frac{\partial f_0}{\partial v} &= -\gamma(v) f_1, \end{aligned} \tag{6.60}$$

where $\gamma(v) = N_b v \sigma_{mt}(v)$ and N_b is the density of the moderator. There is an initial fast transient that we ignore and thus we set $\partial f_1/\partial t' = 0$. This aspect of relaxation in the Lorentz limit was illustrated in Chap. 3; see Fig. 5.15.

We also define the reduced speed $x = v\sqrt{m_e/2k_B T_s}$ with an arbitrary scaling temperature T_s and dimensionless time $t = t'/\tau$ where

$$\tau = \left[\frac{nm_e\sigma_0}{2M}\sqrt{\frac{2k_B T_b}{m_e}}\right]^{-1}. \tag{6.61}$$

A representative hard sphere cross section is denoted by σ_0. We also consider a scaling of the speed variable in anticipation of the use of a quadrature based solution of the Fokker-Planck equation so that we define $s^2 = T_s/T_b$. With these definitions and the steady state value of f_1 given by

$$f_1 = -\frac{eE}{\gamma m_e}\frac{\partial f_0}{\partial v}, \tag{6.62}$$

we have the Fokker-Planck equation for f_0, that is

$$\frac{\partial f_0}{\partial t} = \frac{s}{x^2}\frac{\partial}{\partial x}\left[2x^4\hat{\sigma}(x)f_0 + \frac{x^2}{s^2}B(x)\frac{\partial f_o}{\partial x}\right], \tag{6.63}$$

where

$$B(x) = x\hat{\sigma}x) + \frac{(\alpha/s)^2}{x\hat{\sigma}(x)}, \tag{6.64}$$

and the field strength parameter is

$$\alpha^2 = \frac{M}{6m_e}\left[\frac{eE}{n\sigma_0 k_B T_b}\right]^2. \tag{6.65}$$

In Eq. (6.63), $\hat{\sigma}(x) = \sigma_{mt}(x)/\sigma_0$ is a dimensionless cross section written as a function of reduced speed. The steady state distribution is from Eq. (6.63) given by

$$f_0(x,\infty) = D(x) = C\exp\left[-2s^2\int_0^x \frac{(x')^2\hat{\sigma}(x')}{B(x')}dx'\right]. \tag{6.66}$$

The steady solution, $D(x)$ given by Eq. (6.66), is precisely $P_0(x)$ in Sect. 6.2.1. The distribution, $D(x)$, is referred to as the Davydov distribution which reduces to a Maxwellian in the absence of an electric field. If we set $f(x,t) = D(x)g(x,t)$, the equation for $g(x,t)$ is given by

$$\frac{\partial g}{\partial t} = \frac{s}{D(x)x^2}\frac{\partial}{\partial x}\left[\frac{x^2}{s}B(x)D(x)\frac{\partial g}{\partial x}\right] = -Lg, \quad x \in [0,\infty). \tag{6.67}$$

The linear operator on the right hand side of Eq. (6.67) that we have denoted by L is self adjoint with $D(x)$ as weight function with zero flux boundary conditions, that is,

$$x^2 D(x)B(x)\frac{\partial g(x,t)}{\partial x}\Big|_{x=0}^{x=\infty} = 0. \tag{6.68}$$

We are interested in the eigenvalue problem defined by

$$L\psi_n(x) = \lambda_n \psi_n(x). \tag{6.69}$$

6.3.1 Hard Sphere Cross Section and Zero Electric Field, $E = 0$

If there is no external electric field and the cross section is a hard sphere $\sigma(x) = \sigma_0$, then $B(x) = x$ and the equilibrium distribution is the Maxwellian $P_0(x) = x^2\exp(-x^2)$. We consider a calculation of the eigenvalue spectrum of this Fokker-Planck operator with the Maxwell polynomials orthonormal with respect to the weight function $w(x) = x^2\exp(-x^2)$. The "traditional" method of solution of the Boltzmann equation involves the representation of the collision operator in the Sonine-Laguerre polynomials (Knierim et al. 1982) denoted by $L_{nm}^{(SL)}$.

The calculation of this matrix representation of the collision operator in the Boltzmann equation defined by $L_{nm}^{(SL)} = \langle L_n^{(\frac{1}{2})}|L|L_m^{(\frac{1}{2})}\rangle$ with weight function $w(y) = \sqrt{y}e^{-y}$ is straightforward but algebraically tedious (Shizgal and Fitzpatrick 1974) and the final expressions obtained can lead to considerable round-off errors in the numerical calculation of the matrix elements. In the Lorentz limit, the result is simpler and we have that

$$L_{nm}^{(SL)} = -2\sqrt{\pi}A\frac{m_e}{M}\sqrt{\frac{m!n!}{\Gamma(n+\frac{3}{2})\Gamma(m+\frac{3}{2})}}\sum_{r=1}^{min(n,m+1)} r(r+1)N(n-r)N(m-r) \tag{6.70}$$

where $N(\ell) = \Gamma(\ell-\frac{1}{2})/(2\ell!\sqrt{\pi})$ and $A = 2n_b\pi d^2\sqrt{2k_BT_b/m_e}$. The matrix $\mathbf{L}^{(SL)}$ in the Sonine-Laguerre representation is a full matrix.

Our main objective is to compare the convergence of the eigenvalues of the Boltzmann collision operator as calculated with the representation given by Eq. (6.70) and a pseudospectral method of solution based on the non-classical polynomials orthogonal with respect to weight function $w(x) = P_0(x) = x^2\exp(-x^2)$.

The matrix representation of the Lorentz Fokker-Planck operator in the Maxwell polynomials, $M_n(x)$, $p = 2$, orthonormal with respect to a weight function $w(x) = x^2 e^{-x^2}$ is defined by $L_{nm}^{(MP)} = \langle M_n | L | M_m \rangle$ where the scalar product is with respect to $w(x)$. Lo and Shizgal (2006) derived the explicit tridiagonal form of this spectral representation as

$$L_{mn}^{(MP)} = \begin{cases} (n-1)\alpha_{n-1} + \sum_{k=0}^{n-2} \alpha_k, & m = n > 1, \\ 2(n-1)\sqrt{\beta_n}, & m = n+1, \\ 2(m-1)\sqrt{\beta_m}, & m = n-1, \\ 0, & \text{otherwise.} \end{cases} \tag{6.71}$$

where α_n and β_n are the coefficients in the three term recurrence relation discussed in Chap. 2. It should be clear that the transformation of $L_{nm}^{(MP)}$ with the transformation $T_{in} = \sqrt{w_i} M_n(x_i)$, yields the discrete pseudospectral (ps) representation $L_{ij}^{(ps)}$ given by

$$L_{ij}^{(ps)} = -\sum_{k=1}^{N} x_k D_{ki} D_{kj}, \tag{6.72}$$

where in Eq. (6.48), $B(x_k) = x_k$. An equivalent pseudospectral representation can also be calculated for the Sonine-Laguerre quadratures.

A comparison of the convergence of the eigenvalues of the Fokker-Planck operator for a hard sphere cross section versus the size of the basis set N is shown in Table 6.1. It is clear that the convergence of the eigenvalues is much faster with the Maxwell polynomials as basis functions. The first nonzero eigenvalue, λ_1, requires

Table 6.1 Convergence of the eigenvalues of the hard sphere Lorentz Fokker-Planck equation with the Sonine-Laguerre polynomial basis set (*left*) in comparison with the Maxwell polynomial basis set (*right*)

$w(y) = \sqrt{y}e^{-y}$ (Laguerre)					$w(x) = x^2 e^{-x^2}$ (Maxwell)				
N	λ_1	λ_2	λ_3	λ_5	N	λ_1	λ_2	λ_3	λ_5
1	6.018				1	4.976			
2	5.317	16.35			2	4.716	11.52		
3	5.066	13.85	30.66		3	4.68704	10.40	19.84	
5	4.872	12.10	23.61	68.94	4	4.68378	10.16	17.40	
7	4.797	11.41	21.22	53.80	5	4.68343	10.121	16.68	41.28
10	4.748	10.91	19.56	45.96	6	4.68340	10.1137	16.485	35.55
20	4.7032	10.406	17.75	38.29	7	4.68340	10.1127	16.4401	33.11
30	4.6930	10.267	17.19	35.87	8		10.1125	16.4314	32.05
50	4.6871	10.178	16.79	33.94	9		10.1125	16.4300	31.64
75	4.6851	10.145	16.62	32.97	10			16.4297	31.512
100	4.6840	10.132	16.550	32.50	11			16.4297	31.4765
125	4.6840	10.125	16.512	32.231	12				31.4683
150	4.6839	10.122	16.490	32.056	13				31.4666

Reprinted from (Lo and Shizgal 2006) with permission from the American Institute of Physics

150 Laguerre polynomials for convergence to five significant figures whereas only 6 Maxwell polynomials are required. The higher eigenvalues also converge very quickly with the Maxwell polynomial basis set.

Risken and Voigtlaender (1984) introduced the Maxwell polynomials in the transformation of the Fokker-Planck eigenvalue problem to a Schrödinger equation presented in the following section. They studied the relaxation of neutrons in a heavy gas moderator with the assumption that the Lorentz Fokker-Planck equation is applicable. They report eigenvalues in agreement with the results listed in Table 6.1 calculated with a continued fraction method (Risken and Till 1996).

The pseudospectral method of solution of the Lorentz Fokker-Planck equation is applicable also to realistic energy dependent momentum transfer cross sections (McMahon and Shizgal 1985) and also with a nonzero electric field (Shizgal and McMahon 1985). In these applications, the nonclassical polynomial basis sets that are used for the eigenvalue problem are orthonormal with respect to $P_0(x)$ parametrized by the momentum transfer cross section and the electric field strength, Eq. (6.66). The method was also applied to the relaxation of positrons in He and Ne (Shizgal and Ness 1987), for an oscillatory electric field (Viehland et al. 1988) and in systems with an admixture of a strongly electron attaching gas such as SF_6 and CCl_4 (Shizgal 1988). A review of this subject was presented by Shizgal et al. (1989).

6.3.2 *Transformation of the Fokker-Planck Eigenvalue Problem to a Schrödinger Equation; Supersymmetric Quantum Mechanics*

The eigenvalue problem of the Fokker-Planck equation is

$$A(x)\frac{d\psi_n}{dx} - B(x)\frac{d^2\psi_n}{dx^2} = \lambda_n \psi_n. \tag{6.73}$$

We transform the independent variable x to a new variable z defined by

$$z = \int^x \frac{1}{\sqrt{B(x')}} dx',$$

so that

$$\frac{dz}{dx} = \frac{1}{\sqrt{B}} \qquad \text{and} \qquad \frac{d}{dx} = \frac{1}{\sqrt{B}}\frac{d}{dz},$$

giving

$$\frac{A}{\sqrt{B}}\frac{d\psi_n}{dz} - \sqrt{B}\left(-\frac{B'}{2B^{3/2}}\frac{d\psi_n}{dz} + \frac{1}{\sqrt{B}}\frac{d^2\psi_n}{dz^2}\right) = \lambda_n \psi_n.$$

where the prime, ($B' \equiv dB[x(z)]/dz$), denotes differentiation with respect to z. The eigenvalue equation in the new variable z is

$$-\frac{d^2\psi_n}{dz^2} + \left(\frac{A}{\sqrt{B}} + \frac{B'}{2B}\right)\frac{d\psi_n}{dz} = \lambda_n \psi_n. \tag{6.74}$$

A function $C(z)$ is defined by

$$\psi_n(z) = e^{C(z)}\phi_n(z),$$

where the functions $\phi_n(z)$ will be shown to satisfy a Schrödinger equation. With $\psi_n'(z) \equiv d\psi_n(z)/dz$, we have that

$$\psi_n' = C' e^C \phi_n + e^C \phi_n',$$

and

$$\psi_n'' = C'' e^C \phi_n + (C')^2 e^C \phi_n + 2C' e^C \phi_n' + e^C \phi_n''.$$

The Fokker-Planck eigenvalue equation, Eq. (6.74), is rewritten in terms of $\phi_n(z)$ as

$$-\left[C''\phi_n + (C')^2\phi_n + 2C'\phi_n' + \phi_n''\right] + \left(\frac{A}{\sqrt{B}} + \frac{B'}{2B}\right)(C'\phi_n + \phi_n') = \lambda_n \phi_n. \tag{6.75}$$

We set the coefficient of ϕ_n' to zero and get the defining equation for $C(z)$, that is,

$$\frac{dC(z)}{dz} = \frac{1}{2}\left(\frac{A}{\sqrt{B}} + \frac{B'}{2B}\right), \tag{6.76}$$

which when integrated gives

$$C(z) = \frac{1}{2}\int^z \frac{A(z')}{\sqrt{B(z')}}dz' + \frac{1}{4}\ln B(z). \tag{6.77}$$

With these definitions, the partial differential equation, Eq. (6.75), for $\phi_n(z)$ is the Schrödinger equation

$$-\frac{d^2\phi_n}{dz^2} + V(z)\phi_n(z) = \lambda_n \phi_n(z), \tag{6.78}$$

where Eq. (6.76) has been used and the coefficient of ϕ_n in Eq. (6.75) is the potential $V(z)$, given by

$$V(z) = (C'(z))^2 - C''(z). \tag{6.79}$$

The orthonormality of the eigenfunctions $\psi_n(x)$ is defined in terms of $P_0(x)$ and given by

$$\int_0^\infty P_0(x)\psi_n(x)\psi_m(x)dx = \delta_{nm},$$

$$\int_0^\infty P_0[x(z)]e^{C(z)}\phi_n(z)e^{C(z)}\phi_m(z)\sqrt{B(x(z))}dz = \delta_{nm}, \tag{6.80}$$

which is consistent with the normalization

$$\int_0^\infty \phi_n(z)\phi_m(z)dz = \delta_{nm}, \tag{6.81}$$

so that

$$P_0[x(z)]e^{2C(z)}\sqrt{B[x(z)]} = 1, \tag{6.82}$$

which is consistent with the definition of $C(z)$. Moreover, if we set $W(z) = 2C'(z)$ we have that

$$\boxed{V(z) = \frac{W(z)^2}{4} - \frac{W(z)'}{2},} \tag{6.83}$$

and

$$W(z) = \frac{A}{\sqrt{B}} + \frac{B'}{2B}. \tag{6.84}$$

Thus the equilibrium solution of the Fokker-Planck equation can be expressed as

$$P_0(x) = \exp[-\frac{1}{2}\int^x W[z(x')]dx'], \tag{6.85}$$

and is the ground state of the Fokker-Planck equation with $\lambda_0 = 0$ as can be easily verified by differentiating $P_0(x)$ twice.

The function $W(z)$ is the "superpotential" of supersymmetric quantum mechanics. We have derived the formal relationship between the Fokker-Planck equation and the Schrödinger equation (Comtet et al. 1985; Cooper et al. 1995; Risken and Till 1996; Feizi et al. 2011). This close relationship between these two large classes of problems has been exploited to advantage in the study of nucleation (Demeio and Shizgal 1993a), electron relaxation in molecular gases (Demeio and Shizgal 1993b), relaxation in plasmas (Shizgal 1992) and other applications (Gomez-Ullate et al. 2009).

6.3.3 Pseudospectral Representation of the Schrödinger Equation; Supersymmetric Quantum Mechanics

The spectral representation of the Hamiltonian in the Schrödinger equation, Eq. (6.78), for a basis set $\{S_n(y)\}$ orthonormal with unit weight function is

$$H_{nm}^{(sp)} = -\int_0^\infty S_n(y) S_m''(y) dy + \int_0^\infty S_n(y) V(y) S_m(y) dy. \tag{6.86}$$

We integrate the first integral by parts so that

$$H_{nm}^{(sp)} = \int_0^\infty S_n'(y) S_m'(y) dy + V_{nm}, \tag{6.87}$$

where the potential matrix element is $V_{nm} = \int S_n(y) V(y) S_m(y) dy$. Define a second polynomial set $\{F_n\}$ orthogonal with weight function $w(y)$, that is,

$$S_n(y) = \sqrt{w(y)} F_n(y), \tag{6.88}$$

where the weight function is defined as $w(y) = \exp(-\int W(y')dy')$ analogous to the equilibrium distribution for the Fokker-Planck equation, Eq. (6.85). Equation (6.87) can then be rewritten as,

$$H_{nm}^{(sp)} = \int w[F_m' + \frac{w'}{2w} F_m][F_n' + \frac{w'}{2w} F_n] dy + V_{nm}. \tag{6.89}$$

If one of the cross terms, $F_m' F_n$, in the integrand above is integrated by parts we find that,

$$H_{nm}^{(sp)} = \int w F_n' F_m' dy + [V_{nm} - \tilde{V}_{nm}], \tag{6.90}$$

where $\tilde{V}_{nm}$ are the matrix elements of the potential

$$\tilde{V}(y) = \frac{1}{4} W^2(y) - \frac{1}{2} W'(y), \tag{6.91}$$

defined in terms of the "superpotential", $W(y)$, in supersymmetric quantum mechanics. We transform the spectral representation $H_{nm}^{(sp)}$ to the discrete representation with the transformation $\mathbf{T}$, that is,

$$H_{ij}^{(ps)} = \sum_{n=0}^{N-1} \sum_{m=0}^{N-1} T_{in} H_{nm}^{(sp)} T_{jm}, \tag{6.92}$$

to give the final desired result, namely

$$\boxed{H_{ij}^{(ps)} = \sum_{k=1}^{N} D_{ki} D_{kj} + [V(y_i) - \tilde{V}(y_i)]\delta_{ij},} \tag{6.93}$$

If the potential of interest can be written as in Eq. (6.91), then a useful weight function for the definition of the basis set is given by the equilibrium distribution function or the ground state wave function, Eq. (6.85). For this choice, $\tilde{V}(y) = V(y)$, and the pseudospectral representation of the Hamiltonian reduces to

$$H_{ij}^{(ps)} = \sum_{k=1}^{N} D_{ki} D_{kj}. \tag{6.94}$$

This approach has been described in detail by Shizgal and Chen (1996) and Lo and Shizgal (2006).

6.4 Relaxation and Wave-Particle Heating in Space Plasmas

The Fokker-Planck equation plays a dominant role in plasma physics (Chandrasekhar 1942; Spitzer 1962; Hinton 1983; Shoub 1987) and stellar astrophysics (Spitzer and Härm 1958; Binney and Tremaine 2008; Lemou and Chavanis 2010). We consider as was done in Chap. 5, the kinetic theory of a test particle of mass m and charge Z dilutely dispersed in a large excess of a second species of mass M and charge Z_b at equilibrium with temperature T_b and number density N_b. The Coulomb differential scattering cross section for collisions between the charged particles interacting via a Coulomb potential is given by

$$\sigma(g, \theta) = \left(\frac{Z_b Z e^2}{2\mu g^2}\right)^2 \frac{1}{\sin^4(\theta/2)}. \tag{6.95}$$

The cross section varies inversely as the fourth power of the relative velocity, g, and diverges for small scattering angle, θ.

The Coulomb Fokker-Planck equation finds numerous applications in space science and in particular for the modelling of the solar and polar winds. The solar wind consists primarily of protons and electrons that escape the solar gravitational field. The polar wind (Lie-Svendsen and Rees 1996; Pierrard and Lemaire 1998) is analogous to the solar wind (Parker 1965; Vocks 2002) and represents the escape of ions from the ionosphere along open magnetic field lines at high latitudes (Marsch 2006; Echim et al. 2011).

6.4.1 Pseudospectral Solution of the Coulomb Fokker-Planck and Associated Schrödinger Equations; The Approach to Equilibrium and the Continuous Spectrum

The Fokker-Planck equation for Coulomb collisions is derived from the Boltzmann equation with the differential cross section, Eq. (6.95), with the assumption of small energy transfers in individual binary collisions between charged particles. The small energy transfer collisions are those with large impact parameters. Consistent with this approximation, the small angle singularity in the momentum transfer differential cross section is eliminated by restricting the scattering angle such that $\theta > \theta_{min}$ where $\sin^2(\theta_{min}/2) = [1 + \Lambda]^{-1}$, where $\Lambda = \lambda_D/b_0$; λ_D is the Debye length and $b_0 = ZZ_b e^2/2k_B T_b$, the impact parameter that corresponds to the scattering angle $\theta = \pi/2$ (Spitzer 1962; Mitchner and Kruger 1973; Hinton 1983).

The Fokker-Planck equation derived from the Boltzmann equation as discussed in the previous paragraph is

$$\frac{\partial f(v,t')}{\partial t'} = \frac{A}{v^2}\frac{\partial}{\partial v}\left[G(v)\left(1 + \frac{kT_b}{mv}\frac{\partial}{\partial v}\right)\right] f(v,t'), \tag{6.96}$$

where $A = (4\pi N_b e^4 Z^2 Z_b^2/mM)\ln\Lambda$ and the diffusion coefficient is

$$G(v) = \text{erf}(\sqrt{\frac{Mv^2}{2kT_b}}) - \sqrt{\frac{2Mv^2}{\pi kT_b}}\exp(-\frac{Mv^2}{2kT_b}), \tag{6.97}$$

as discussed elsewhere (Karney 1986; Shizgal 2004; Chavanis 2006).

The steady state distribution from Eq. (6.96) is a Maxwellian. A dimensionless time $t' = t/\tau$ is defined with $\tau = ([2A/3\sqrt{\pi}][M/2k_B T_b]^{3/2})^{-1}$ and the reduced speed $x = v\sqrt{m/2k_B T_s}$ where the temperature parameter $T_s = s^2 T_b$. The parameter s is the quadrature scaling parameter introduced in Chap. 3. With these definitions, the Fokker-Planck equation is

$$\frac{\partial f(x,t)}{\partial t} = \frac{2}{s^3 x^2}\frac{\partial}{\partial x}\left[G_1(sx)\left(1 + \frac{1}{2xs^2}\frac{\partial}{\partial x}\right)\right] f(x,t), \tag{6.98}$$

where $G_1(sx) = h(\gamma)G(v)$, $\gamma = \sqrt{M/m}$ and $h(\gamma) = 3\sqrt{\pi}/4\gamma^{3/2}$.

If we set $f(x,t) = e^{-s^2x^2} g(x,t)$, the Fokker-Planck equation is

$$\frac{\partial g}{\partial t} = \frac{1}{s^2}\left[A(x)\frac{\partial g}{\partial x} - B(x)\frac{\partial^2 g}{\partial x^2}\right] = Lg, \tag{6.99}$$

with $B(x) = G_1(sx)/(sx)^3$. The drift coefficient in terms of $B(x)$ is

$$A(x) = 2s^2 x B(x) - \frac{2B(x)}{x} - \frac{dB(x)}{dx}. \tag{6.100}$$

We are concerned with the eigenvalue problem

$$L\psi_n(x) = -\lambda_n \psi_n(x),$$

with L defined with Eq. (6.99). The physical space pseudospectral representation of this Fokker-Planck operator is

$$L_{ij}^{(ps)} = \frac{1}{s^2} \sum_{k=1}^{N} B(x_k)[D_{ki} + x_k(s^2 - 1)\delta_{ki}][D_{kj} + x_k(s^2 - 1)\delta_{kj}]. \tag{6.101}$$

If the scaling parameter, $s = 1$, Eq. (6.101) reduces to Eq. (6.48).

The eigenvalues are determined with the numerical diagonalization of the matrix $\mathbf{L}^{(ps)}$ of dimension N. The convergence of the lower order eigenvalues is shown in Table 6.2 and the rapid convergence is clear.

We transform the Fokker-Planck eigenvalue equation to a Schrödinger equation as discussed in Sect. 6.3.3 and derive, after some algebra, the potential in x, that is

$$V_-(x) = \frac{G_1(x)}{x}\left(1 - \frac{9}{16x^4}\right) - 3\left[1 + \frac{\gamma^2}{2} - \frac{3}{8x^2}\right]e^{-\gamma^2 x^2} - \frac{9x}{16G_1(x)}e^{-2\gamma^2 x^2}. \tag{6.102}$$

The potentials are shown in Fig. 6.1 for two mass ratios, $M/m = 0.01$ and 0.04, and the eigenvalues (bound states) are indicated with the horizontal lines. There are a finite number of discrete eigenvalues and the number of states diminishes with increasing mass ratio. Since the potential barrier is finite, the eigenstates are not true bound states (Corngold 1981) and could be referred to as "quasi-bound" states. The only bound state is the ground state with $\lambda_0 = 0$. However, it is readily verified that

Table 6.2 Convergence of the eigenvalues of the pseudospectral representation of the Coulomb Fokker-Planck operator, Eq. (6.101), for mass ratio, $\gamma = 0.3$

N	λ_1	λ_2	λ_3	λ_4	λ_5	λ_6	λ_7
4	3.82049	7.522947	18.6937				
6	3.82023	7.35052	10.7565	16.6796	47.3754		
8	3.82023	7.34943	10.5866	13.7437	18.4730	30.7286	96.2670
10		7.34943	10.5828	13.5261	16.4786	20.7524	20.3964
20				13.5139	16.1314	18.4301	20.3807
30				13.5139	16.1341	18.4301	20.3897
40						18.4301	20.3807
SWKB	3.82031	7.34954	10.5831	13.5144	16.1348	18.4313	20.3829
WKB	3.82834	7.35710	10.5900	13.5208	16.1407	18.4366	20.3875

Reproduced from Shizgal (1992) with permission from Taylor and Francis

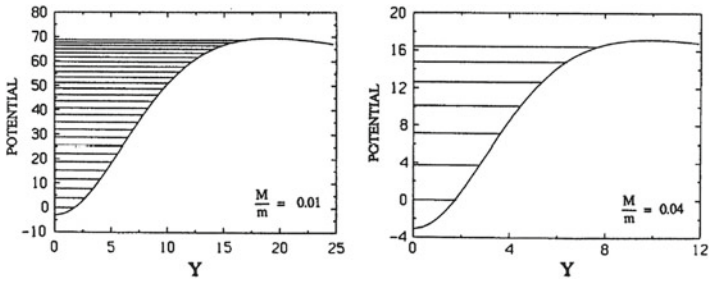

Fig. 6.1 Potential, $V_-(y)$, in the Schrödinger equation corresponding to the Coulomb Fokker-Planck equation for mass ratios $M/m = 0.01$ and 0.04. There are a finite number of eigenstates which are strictly not discrete. Reproduced from Shizgal (1991) with permission from Beylich A.E.: Rarefied gas dynamics. In: Proceedings of the 17th International Symposium on Rarefied Gas Dynamics, Wiley-VCH Verlag GmbH and Co. KGaA. pp. 22–29, (1991)

in the Rayleigh limit, $\gamma = 0$, $V_-(x) = x^2 - 3$ and the eigenvalues are all discrete and given by $\lambda_n = 4n$, the harmonic oscillator eigenvalues.

The converged eigenvalues in the table are compared with the semiclassical Wentzel-Kramers-Brillouin (WKB) eigenvalues (Miller and Good 1953), namely

$$\int_{x_1}^{x_2} \sqrt{\lambda_n - V_-(x)}dx = \left(n + \frac{1}{2}\right)\pi, \tag{6.103}$$

and the corresponding supersymmetric, SWKB, eigenvalues (Fricke et al. 1988)

$$\int_{x_1'}^{x_2'} \sqrt{\lambda_n - W^2(x)}dx = n\pi, \tag{6.104}$$

where the integral limits are the classical turning points. The agreement with the SWKB and WKB approximations is very good.

We expand the solution in the eigenfunctions of L and the time dependence of the average energy is

$$\frac{E(t')}{E_{th}} = \sum_{k=0}^{\infty} c_k e^{-\lambda_k t'}, \tag{6.105}$$

where $E_{th} = 3k_B T_b/2$ is the thermal energy and the coefficients are

$$c_k = \frac{2}{3}s^5 a_k \int_0^{\infty} e^{-s^2x^2}\psi_k(x)x^4 dx. \tag{6.106}$$

The coefficients a_k are the expansion coefficients of the intial condition

$$g(x,0) = \sum_{k=0}^{\infty} a_k \phi_k(x).$$

The 7 eigenvalues for $\gamma = 0.3$ are shown in Table 6.2 as the horizontal lines in the potential functions $V_-(x)$ and $W^2(x)$ in Fig. 6.2. The additional eigenvalue in $V_-(y)$ is $\lambda_0 = 0$. The eigenfunctions $\psi_4(x)$ and $\psi_6(x)$ are also shown in Fig. 6.2 with the WKB eigenfunctions denoted with the symbols. Two examples of continuum eiegenfunctions are shown in Fig. 6.3. The symbols that coincide with the solid curves are the results with the WKB approximation. These numerical eigenfunctions are L^2 square integrable with the discrete quadrature (Reinhardt 1979) defining the norm.

The relaxation of the temperature is given by $T(t') = 2E(t')/3k_B$ with $E(t')$ as in Eq. (6.105). The time variation of $T(t')/T_b$ is shown in Fig. 6.4 for four mass ratios includes the sum over discrete and continuous eigenvalues and is convergent. For mass ratio $M/m = 0.4$, there are no bound states and the discrete sum is over the continuous spectrum.

In Chap. 5, we discussed the properties of the discrete and continuous portions of the eigenvalue spectra of the Boltzmann integral collision operators. It is these spectral properties that determine the time dependent approach to equilibrium (Sospedra-Alfonso and Shizgal 2013). For the Boltzmann equation, there is always a discrete

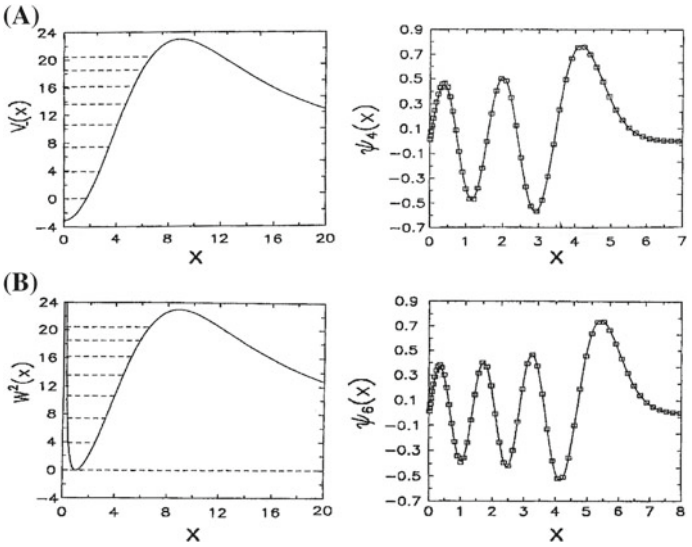

Fig. 6.2 (*Left hand graphs*) **(A)** The potential $V_-(y)$ in the Schrödinger potential; **(B)** The super potential $W^2(y)$ with a minimum value of 0. The bound states are shown with the *dashed horizontal lines*. (*Right hand graphs*) Eigenfunctions of the Fokker-Planck equation **(A)** $\psi_4(x)$ and **(B)** $\psi_6(x)$. The symbols are the WKB approximations (Miller and Good 1953). Reproduced from Shizgal (1992) with permission from Taylor and Francis

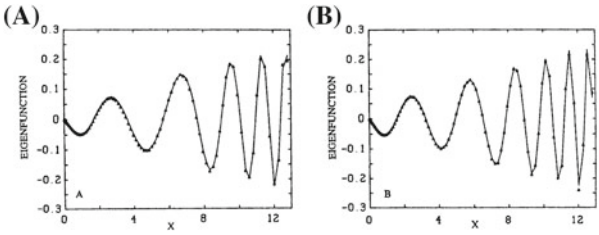

Fig. 6.3 The continuum eigenfunction of the Fokker-Planck collision operator for Coulomb collisions (symbols) in comparison with the WKB approximation (*solid curve*) with $T_b = 300\,\mathrm{K}$, $s = 0.6042$ and $\gamma = 0.04$; **(A)** $\lambda = 5.855$ and **(B)** $\lambda = 7.603$. Reproduced from Shizgal (1992) with permission Beylich A.E.: Rarefied gas dynamics. In: Proceedings of the 17th International Symposium on Rarefied Gas Dynamics, Wiley-VCH Verlag GmbH and Co. KGaA. pp. 22–29, (1991)

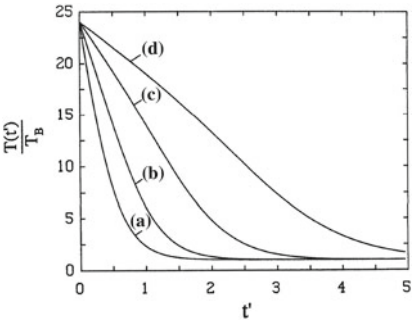

Fig. 6.4 Temperature relaxation for $T(0)/T_b = 24$ and $\gamma = a\,0.2, b\,0.3, c\,0.4$ and $d\,0.5$. Reproduced from Shizgal (1991) with permission Beylich A.E.: Rarefied gas dynamics. In: Proceedings of the 17th International Symposium on Rarefied Gas Dynamics, Wiley-VCH Verlag GmbH and Co. KGaA. pp. 22–29, (1991)

spectrum whereas for the Coulomb Fokker-Planck equation we have demonstrated that the spectrum can be completely continuous, except for $\lambda_0 = 0$. The approach to equilibrium is an exponential if there is at least one discrete eigenvalue, that is "the spectral gap" as discussed in Chap. 5. For mass ratios for which there are no discrete "quasi-bound" states, the approach to equilibrium can be a complicated non-exponential function of time (Corngold 1981). This may be the case for curve d in Fig. 6.4.

We consider the variation of the energy coefficients in the energy relaxation, Eq. (6.105), versus the numerical continuous eigenvalues. This variation of $c(\lambda)$ versus λ is shown in Fig. 6.5 for different scaling parameters. The discrete values of λ_k and c_k (or λ and $c(\lambda)$) in the continuum vary with a change in the scaling parameter, s, or with a change in the number of quadrature points, N, but the variation of $c(\lambda)$ versus λ is on the same curve as shown in Fig. 6.5. As a consequence, the pseudospectral solution of the Fokker-Planck equation provides a converged solution even though the continuum has not been treated rigorously. However, the analytic form of the time variation of the average energy, equivalently the temperature, very close to equilibrium (Corngold 1981; Shizgal 1991) has not been confirmed.

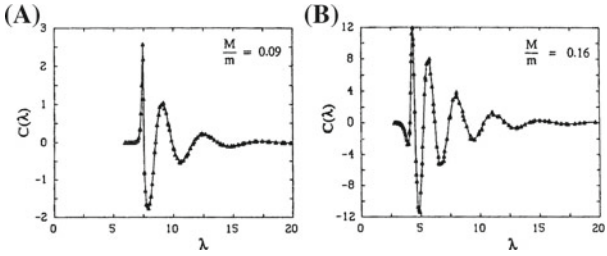

Fig. 6.5 Variation of the coefficients, $c(\lambda)$ (in units of 10^3) for the temperature relaxation versus the continuous eigenvalue, λ. $T(0)/T_b = 24$. The symbols are the numerical results for 4 different values of the scaling parameter. Reproduced from Shizgal (1991) with permission Beylich A.E.: Rarefied gas dynamics. In: Proceedings of the 17th International Symposium on Rarefied Gas Dynamics, Wiley-VCH Verlag GmbH and Co. KGaA. pp. 22–29, (1991)

6.4.2 *Fokker-Planck Equation for Wave Particle Heating of Ions; Kappa Distributions, and Tsallis Nonextensive Entropy*

Tsallis (1995) derived the Kappa distribution

$$f_\kappa(x) = C_\kappa \left[\frac{1}{1+\frac{x^2}{\kappa+1}}\right]^{\kappa+1}, \tag{6.107}$$

in the development of a new form of entropy functional for problems in statistical mechanics. In Eq. (6.107), $C_\kappa = 2\pi\Gamma(\kappa+1)/[\sqrt{\pi(\kappa+1)}]^3\Gamma(\kappa-\frac{1}{2})$ is a normalization such that $4\pi\int_0^\infty f_\kappa(x)x^2dx = 1$. In the limit, $\kappa \to \infty$, the Kappa distribution tends to a Maxwellian. The Tsallis nonextensive entropy formalism is a controversial topic (Nauenberg 2003; Tsallis 2004; Lutsko and Boon 2011).

In Chap. 4, we discussed the expansion of the Kappa distribution function, in Laguerre polynomials, Eq. (4.60). We demonstrated that the expansion in Laguerre polynomials is a divergent asymptotic series as the decay of $f_\kappa(x)$ as $x \to \infty$ is slower than that of the Laguerre weight function, $w(x) = \sqrt{x}e^{-x}$; see Fig. 4.9 (Mintzer 1965; Leblanc and Hubert 1997). It is clear that the normalization C_κ does not exist for $\kappa \to 1/2$. The average kinetic energy, that is the average of $mv^2/2$ with $f_\kappa(x)$, defines the nonequilibrium "temperature"

$$\frac{T_\kappa}{T_b} = \frac{\kappa+1}{\kappa-\frac{3}{2}}, \tag{6.108}$$

which also diverges for $\kappa \to 3/2$. A nonphysical feature of the Kappa distribution is that the nth moment diverges for $\kappa \to (n+1)/2$ (Treumann et al. 2004; Shizgal 2007). For this reason, Magnus and Pierrard (2008) could not generate the Gaussian quadrature weights and points for the Kappa distribution and used instead modified weight functions.

In space physics, the Kappa distribution has been employed to explain the nature of energetic distributions in space physics (Meyer-Vernet 2001; Livadiotis and McComas 2009), the heating of the solar chromosphere (Scudder 1994), the escape of charged particles from the solar atmosphere and from the high latitude terrestrial ionosphere known as the solar and polar winds, respectively (Pierrard et al. 2004; Pierrard and Lazar 2010). There is an ongoing effort in space physics to better understand the complex mechanism for the energization of ions and electrons by plasma waves (Schulz and Lanzerotti 1974; Stix 1992; Gary 1993).

One approach is based on a Fokker-Planck equation where the wave-particle interactions are modelled with a second diffusion operator (Nicholson 1983) that is

$$\frac{\partial f(x,t)}{\partial t} = \sqrt{\frac{m}{M}}\left(\frac{1}{x^2}\frac{\partial}{\partial x}\left[D_1(v_{th}x)(1+\frac{1}{2x}\frac{\partial}{\partial x})\right]f(x,t) + \frac{\alpha v_{th}}{2}\frac{1}{x^2}\frac{\partial}{\partial x}\left[x^2 D_2(v_{th}x)\frac{\partial}{\partial x}f(x,t)\right]\right), \tag{6.109}$$

where in the second differential operator term the parameter α is an adjustable parameter that controls the strength of the wave-particle interactions relative to the Coulomb collision rate. It is clear that for $\alpha = 0$, the steady state distribution is a Maxwellian. Equation (6.109) has been written in dimensionless time, $t = t'/t_0$, where $t_0 = [2N\sigma_{eff}\sqrt{2kT_b/M}]^{-1}$ and $\sigma_{eff} = [4\pi N Z^2 Z_b^2 e^4 \ln\Lambda]/(2kT_b)^2$.

The steady distribution obtained by setting $\partial f/\partial t = 0$ in Eq. (6.109) is given by

$$\frac{df_{ss}(x)}{f_{ss}(x)} = -\left[\frac{2x}{1+\alpha v_{th}x^3\frac{D_2(v_{th}x)}{\hat{D}_1(z)}}\right]dx, \tag{6.110}$$

where

$$\hat{D}_1(z) = \mathrm{erf}(z) - \frac{2z}{\sqrt{\pi}}e^{-z^2}, \tag{6.111}$$

with $z = \sqrt{\gamma}x$, $\gamma = M/m$. As a consequence of the wave-particle interaction diffusion term, the steady state solution of Eq. (6.109), $f_{ss}(v)$, is no longer a Maxwellian and depends on the ratio of the strength of the wave-particle diffusion term relative to the strength of Coulomb collisional relaxation, that is on α, as well as the mass ratio M/m. The velocity dependence of this steady-state distribution function depends on both $\hat{D}_1(z)$ and $D_2(v_{th}x)$.

The choice of the wave-particle diffusion coefficient has been discussed in the literature (Crew and Chang 1985; Stix 1992; Ma and Summers 1999; Vocks 2002; Shizgal 2007). There is at present no theoretical model for the occurrence of a Kappa distribution except for the works of Ma and Summers (1999) and Hasegawa et al. (1985). We consider the wave-particle diffusion coefficient to be of the form $D_2(v_{th}x) = 1/(v_{th}x)$ following on the work of Ma and Summers (1999). To reproduce the result obtained by them, one has to choose $D_2(v_{th}x) = 1/(v_{th}x)$ and

$v \gg v_{th}$, that is $\gamma \to \infty$ in which case $\hat{D}_1(z) \to 1$. Thus the mass dependence and the behaviour $\hat{D}_1(z) \approx z^{-3}$ as $z \to 0$ are not retained by setting $\hat{D}_1(z) \equiv 1$.

The steady state distribution function that is obtained in this limit is

$$\frac{df_\kappa(x)}{f_\kappa(x)} = -\left[\frac{2x}{1+\alpha x^2}\right] dx, \tag{6.112}$$

and when integrated leads to the Kappa distribution, Eq. (6.107). In this way, the adjustable κ parameter in exospheric models is interpreted in terms of the strength of wave-particle interactions and $\kappa = (1-\alpha)/\alpha$.

The steady state distribution, $f_{ss}(x)$, the Kappa distribution, $f_\kappa(x)$ and the Maxwellian are compared in Fig. 6.6 for two mass ratios and the arbitrary choice $\alpha = 1/8$. The steady state distribution has a more extended high energy tail than either the Kappa distribution or the Maxwellian. The mass ratios chosen correspond to O^+ and Fe^+ in the solar atmosphere. For the larger mass ratio the tail of the steady distribution is more extended than for the smaller mass consistent with the observed heating of the heavy minor ions in the solar atmosphere.

For this application, we use the Chang-Cooper finite difference algorithm described in Sect. 6.2.3 to integrate the Fokker-Planck equation given by Eq. (6.109) with an initial Maxwellian distribution. With this numerical method, there is no reference to the eigenvalue spectrum of the operator in Eq. (6.109) as we have done for all the other applications. The solutions converge provided that the grid spacing in the finite difference reduced speed discretization and the time step are sufficiently small. The evolution of the distribution functions showing the heating of the tail of the distributions is shown in Fig. 6.7a, b for $m/M = 16$ and 55.85, respectively. The increase in the temperature is shown in Fig. 6.7c for several heavy ions in the solar atmosphere. This heating is consistent with observations that the temperature of the

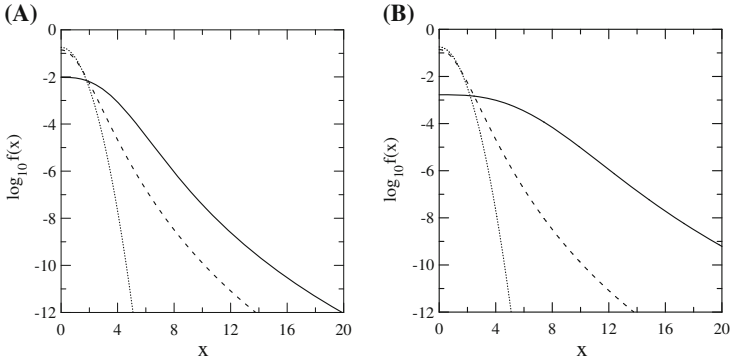

Fig. 6.6 Comparison of the Maxwellian (*dotted curve*), Kappa (*dashed curve*) and steady, $f_{st}(x)$ (*solid curve*) distributions. The diffusion coefficient for wave-particle interactions is $\hat{D}_2(x) = 1/x$, the mass ratio m/M and α are **(A)** 16, 1/8 **(B)** 55.845, 1/8. For the Kappa distribution, $\kappa = (1-\alpha)/\alpha$. Reprinted from Shizgal (2007) with permission from Springer

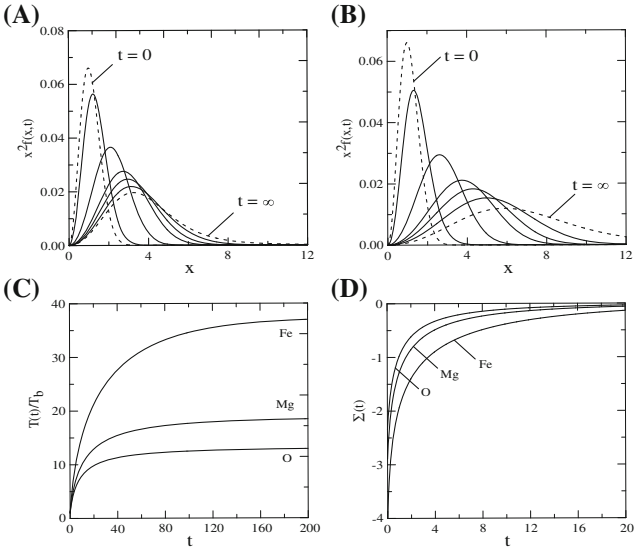

Fig. 6.7 Approach to a steady state distribution, $f_{ss}(x)$, with an initial Maxwellian and the inclusion of wave-particle energization; $\alpha = 0.25$ and $\hat{D}_2(x) = 1/x$. Successive distributions are at reduced times equal to 0.4, 2, 6, 10 and 20 for m/M equal to **(A)** 16 and **(B)** 55.85. **(C)** The heating of the gas is shown as $T(t)/T_b$ and **(D)** the Kulback entropy increases with time. The mass ratio, m/M, is equal to (O) 16, (Mg) 24.3 and (Fe) 55.85. Reprinted from (Shizgal 2007) with permission from Springer

minor ions in the solar atmosphere increases with mass (Pierrard et al. 2004).

In Fig. 6.7d, we show the monotonic increase in the Kullback–Leibler entropy functional defined by

$$\Sigma(t) = 4\pi \int x^2 f(x,t) \ln \frac{f(x,t)}{f_{ss}(x)} dx. \tag{6.113}$$

This final result demonstrates that the usual notions of entropy rationalizes the generation of a non-equilibrium distribution which is neither a Maxwellian nor a Kappa distribution. The nonextensive entropy formalism of Tsallis (1995) is not required as previously suggested (Collier 2004; Leubner and Vörös 2005) and references therein. A pseudospectral solution of the Fokker–Planck operator equation, Eq. (6.109), is of considerable interest, especially with concern to the properties of the eigenvalue spectrum of the operator with wave-particle interactions ($\alpha \neq 0$).

6.5 Fokker-Planck or Smoluchowski Equation for Bistable Potentials

Potentials $U(y)$, where y denotes a coordinate for internal rotation in a molecule about some symmetry axis, are known for many molecules including for example butane, C_4H_{10}, (Ryckaert and Bellemans 1978; Montgomery et al. 1979; Blackmore and Shizgal 1985b; Pastor and Karplus 1989; Travis and Searles 2006), hydrogen peroxide, HOOH, (Koput et al. 2001; Lin and Guo 2003; Lynch et al. 2004; Le et al. 2009) and chlorine peroxide, ClOOCl (Gomes and Pacios 1996). The cis-trans isomerization kinetics for such molecules can be modelled with a Fokker-Planck or Smoluchowski[5] equation of the form

$$\frac{\partial P(y,t)}{\partial t} = \frac{\partial}{\partial y}\left[U(y)P(y,t) + \frac{\partial B(y)P(y,t)}{\partial y}\right] = LP(y,t), \quad y \in (-\infty,\infty), \tag{6.114}$$

where y is a reaction coordinate.

A simple model for the isomerization kinetics used by many researchers (Larson and Kostin 1978; Bernstein and Brown 1984; Voigtlaender and Risken 1985; Blackmore and Shizgal 1985a, b; Cartling 1987; Drozdov 1999; Drozdov and Tucker 2001; Felderhof 2008) is defined with the drift and diffusion coefficients given by

$$U(y) = y^3 - y, \qquad B(y) = \epsilon. \tag{6.115}$$

This model potential is bimodal with two minima at $y = \pm 1$. The steady distribution is

$$P_0(y) = C\exp[-\frac{y^4}{4\epsilon} + \frac{y^2}{2\epsilon}], \tag{6.116}$$

and has two sharp maxima at $y = \pm 1$, especially for ϵ small as shown in Fig. 6.8. The constant C is a normalization. The model is also referred to as the quartic potential because of the form of $P_0(y)$. This type of Fokker-Planck equation with two stable states also has application to climate models (Nicolis and Nicolis 1981; Nicolis 1982; Shizgal and Chen 1997) and laser physics (Blackmore et al. 1986; Shizgal and Chen 1997). The recent work by (Blaise et al. 2012) provides an extensive bibliography on diffusion in a double well potential.

We study the time evolution of this system in terms of the eigenfunction expansion discussed in Sect. 6.2. The eigenvalues and eigenfunctions can be calculated numerically with the diagonalization of the spectral matrix representation of the linear

[5] Marian Smoluchowski (1872–1917) was a Polish physicist who was responsible for the development of fundamental concepts in statistical physics, kinetic theory and Brownian motion. His name is associated with integral equations for coagulation and a Fokker-Planck equation for chemical reactions.

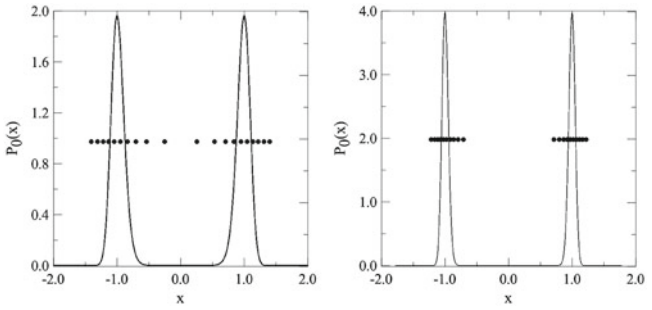

Fig. 6.8 Steady state bimodal distribution $P_0(x) = C\exp[-\frac{1}{\epsilon}(x^4/4 - x^2/2)]$ for $\epsilon = 0.02$ on the *left* and $\epsilon = 0.005$ on the *right*. The distribution of quadrature points with $N = 20$ is also shown

Fokker-Planck operator, L, defined by Eq. (6.114), that is

$$L_{mn}^{(sp)} = \int_{-\infty}^{\infty} w(y) B_n(y) L B_m(y) dy, \tag{6.117}$$

where the nonclassical polynomials, $B_n(y)$, are orthonormal with respect to the weight function, $w(y) = P_0(y)$, that is

$$\int_{-\infty}^{\infty} \exp\left[-\frac{1}{\epsilon}\left(\frac{y^4}{4} - \frac{y^2}{2}\right)\right] B_n(y) B_m(y) dx = \delta_{nm}, \tag{6.118}$$

as discussed in Chap. 2, Sect. 2.5.2.

Since $w(y)$ is even and the integrals are evaluated over $(-\infty, \infty)$, the recurrence coefficients, $\alpha_n = 0$. The polynomials $B_n(y)$ are even when n is an even number and odd when n is an odd number. After some detailed algebraic manipulations presented in Appendix B of Lo and Shizgal (2006), the symmetric matrix representation of the Fokker-Planck operator is given by

$$L_{mn}^{(sp)} = \begin{cases} -(\beta_2 + \beta_1 - 1), & m = n = 2, \\ (n-1)(\beta_n + \beta_{n-1} - 1) + 2\sum_{k=1}^{n-2} \beta_k, & m = n > 2, \\ (n-1)\sqrt{\beta_{n+1}\beta_n}, & m = n + 2, \\ (m-1)\sqrt{\beta_{m+1}\beta_m}, & m = n - 2, \\ 0 & \text{otherwise}, \end{cases} \tag{6.119}$$

where β_n are the recurrence coefficients in the three term recurrence relation discussed in Chap. 2. The eigenvalue problem is $L\psi_n(y) = -\lambda_n \psi_n(y)$, with L as defined by Eq. (6.114).

This matrix representation of the Fokker-Planck operator for the bimodal model is pentadiagonal where the off-diagonal elements for $m \neq n \pm 2$ are zero. As a

consequence, the eigenfunctions are odd or even and there is no coupling between them. Thus, the matrix representation $L_{nm}^{(sp)}$ can be split into two separate matrices, $\mathbf{L}^{even}$ with even n and m and $\mathbf{L}^{odd}$ with odd n and m. The spectrum of the Fokker-Planck operator is composed of a set of singlet and nearly degenerate triplets. With $B(y_i) = \epsilon$, the pseudospectral discrete matrix representation of the Fokker-Planck operator is given by Eq. (6.48)

$$L_{ij}^{(ps)} = -\epsilon \sum_{k=1}^{N} D_{ki} D_{kj}, \tag{6.120}$$

and yields the same eigenvalues and eigenfunctions as obtained with the spectral representation. However, $L_{ij}^{(ps)}$, is a full matrix and the symmetry properties of the problem as determined from the structure of $L_{nm}^{(sp)}$ are not apparent. As demonstrated in Chap. 2, the quadrature points are distributed nonuniformly within the domain, as shown in Fig. 6.8 for two choices of ϵ. Therefore, the pseudospectral approach is more flexible than the polynomial based spectral method as different weight functions can be easily used to improve the convergence. The matrix elements for such nonclassical basis functions may be difficult to calculate analytically as given by Eq. (6.119).

The convergence of the lower order eigenvalues for $\epsilon = 0.01$ is shown in Table 6.3 versus the number of quadrature grid points, N, for three different grids as defined by the weight functions shown in the table. As can be seen, the first nonzero eigenvalue λ_1 is extremely small relative to the other eigenvalues. The reciprocal of this eigenvalue represents the isomerization rate as discussed later. The three eigenvalues $\lambda_3 - \lambda_5$ are nearly degenerate and converge at different rates. The first set of results are obtained with the grid defined by $w_a(y) = P_0(y),\ \ y \in (-\infty, \infty)$.

The convergence can be improved by taking advantage of the symmetry of the eigenstates and calculating the even and odd eigenvalues with different weight functions, $w_b^{(e)}(y)$ and $w_b^{(o)}(y)$, $y \in [0, \infty)$, as shown in the middle of the table. The convergence requires about half the number of quadrature points as with $w_a(y) = P_0(y)$ over the whole interval. The bottom portion of the table shows the convergence with the uniform grid for the Sinc collocation method (SCM) (Wei 1999; Amore 2006) as well as a comparison with the limited results by Dekker and van Kampen (1979).

The convergence of the eigenvalues for $\epsilon = 0.001$ is shown in Table 6.4 and a third weight function is chosen in order to accelerate the convergence. The weight function is $w_c(y) = P_0(y) + \exp(-\frac{y^2}{2\epsilon})$ where the added exponential term yields quadrature points in the middle of the interval near the origin. The convergence of the eigenvalues is extremely rapid relative to the Sinc collocation method with a uniform grid.

The distribution of quadrature points relative to the bimodal potential is shown in Fig. 6.9 for three values of ϵ. The distribution of grid points is uniform for all three values with the SCM. The quadrature points labelled QDM (a) are densely distributed over the region of the outermost potential wells. The acronym QDM is for the Quadrature Discretization Method which is the pseudspectral representation given by Eq. (6.120). The quadrature points for QDM (b) are defined over the interval

$x \in [0, \infty)$ and are more densely distributed near the origin. The points for QDM (c) are distributed densely about the origin. The rate of convergence of the eigenvalues in Tables 6.3 and 6.4 is consistent with the distribution of the quadrature points for these different weight functions.

The structure of the eigenvalue spectrum is made clearer by considering the transformation to a Schrödinger equation and one finds the potential

$$V(y) = \frac{y^2(y^2-1)^2}{4\epsilon} - \frac{1}{2}(3y^2-1), \tag{6.121}$$

which has three minima at

$$y^0 = 0, \quad y^{\pm} = \pm\sqrt{\left[\frac{2}{3} + \sqrt{\frac{1}{9} + 2\epsilon}\right]}. \tag{6.122}$$

Table 6.3 Convergence of the eigenvalues of the Fokker-Planck operator with the bistable potential, $U(y) = y^3 - y$; $\epsilon = 0.01$

N	λ_1	λ_2	λ_3	λ_4	λ_5
$w_a(y) = \exp[-(\frac{y^4}{4\epsilon} - \frac{y^2}{2\epsilon})]/\exp(1/4\epsilon)$; $y \in (-\infty, \infty)$					
12	5.0833 (−8)		1.866176	1.865861	
24	3.6651 (−11)		1.865757	1.865753	
36	7.0354 (−12)	1.388230	1.865752	1.865758	2.664871
48	6.1809E-12	0.994289	1.865735	1.865754	1.956370
60	6.15499 (−12)	0.968472	1.865337		1.869329
72	6.15466 (−12)	0.967870	1.864560		1.866993
84	6.15465 (−12)	0.967865	1.864542		1.866975
$w_b^{(e)}(y) = w_a(y)$; $w_b^{(o)}(y) = y^2 w_a(y)$; $y \in [0, \infty)$					
12	6.4259 (−12)	1.256087	1.865747	1.865757	2.113341
15	6.1656 (−12)	0.990778	1.865720	1.865754	1.913825
18	6.1405 (−12)	0.969092	1.865601		1.875631
24	6.1424 (−12)	0.967879	1.864549		1.866982
27	6.1436 (−12)	0.967865	1.864542		1.866975
30	6.1427 (−12)	0.967864			
Sinc collocation method $x_{max} = 2.2$					
12	7.4085 (−1)	1.076821	3.336192	3.321671	1.574892
24	3.3865 (−3)	0.967915	1.931199	1.930972	1.865051
36	−4.8093 (−5)	0.967864	1.864066	1.864927	1.866629
48	1.7533 (−8)		1.864542	1.865754	1.866975
60	7.9956 (−12)				
DvK[a]		0.968	1.862		1.867

Reprinted from Lo and Shizgal (2006) with permission of the American Institute of Physics
[a] Dekker and van Kampen (1979)

Table 6.4 Convergence of the eigenvalues of the Fokker-Planck operator with the bistable potential, $U(x) = x^3 - x$; $\epsilon = 0.001$

N	λ_2	λ_3	λ_4	λ_5
$w_c(y) = \exp[-(\frac{y^4}{4\epsilon} - \frac{y^2}{2\epsilon})]/\exp(\frac{1}{4\epsilon}) + \exp(-\frac{y^2}{2\epsilon})$				
6	0.9980526	2.0000470	2.0200067	2.0694590
12	0.9969809	1.9878205	1.9880010	1.9881554
18	0.9969817	1.9878873	1.9878903	1.9878937
24		1.9878896	1.9878896	1.9878893
30				1.9878896
Sinc collocation method $x_{max} = 1.2$				
12	3.4140030	21.7611343	21.7517512	3.4979300
24	1.2875835	8.5716393	8.5704015	1.6476678
36	1.0279928	4.1568953	4.1569000	1.7776398
48	0.9984717	2.5344712	2.5345542	1.9649680
60	0.9970079	2.0928734	2.0928574	1.9872886
72	0.9969819	1.9995592	1.9995565	1.9878842
84	0.9969817	1.9884160	1.9884156	1.9878896
96		1.9878838	1.9878838	
108		1.9878884	1.9878884	
120		1.9878896	1.9878896	

Reprinted from Lo and Shizgal (2006) with permission of the American Institute of Physics

In the limit $\epsilon \to 0$, the potential barriers between the two minima become larger and the potentials near the minima are quadratic, that is,

$$\lim_{\epsilon\to 0} V^{\pm}(y) \to \frac{(y - y^{\pm})^2}{\epsilon} - 1, \quad y \approx y^{\pm}, \tag{6.123}$$
$$\lim_{\epsilon\to 0} V^{0}(y) \to \frac{y^2}{4\epsilon} + \frac{1}{2} \quad y \approx 0.$$

and the corresponding eigenvalues are

$$\lim_{\epsilon\to 0} \lambda_k^{\pm} \to 2k, \quad k = 0, 1, 2, \ldots \tag{6.124}$$
$$\lim_{\epsilon\to 0} \lambda_k^{0} \to k + 1, \quad k = 0, 1, 2, \ldots$$

Thus in the very small ϵ limit the eigenvalues approach integer values, the zero eigenvalue is doubly degenerate and the remaining even eigenvalues are triply degenerate.

The importance of the distribution of grid points is illustrated in Fig. 6.9 where the grid points are shown in relation to the potentials in the Schrödinger equation. For $\epsilon = 0.1$ in Fig. 6.9a, the grid points are well distributed in the two wells of the potential. For $\epsilon = 0.01$, the potential has a minimum near the origin and $w_a(y) = P_0(y)$ does not properly capture the eigenfunction in this region whereas the quadrature

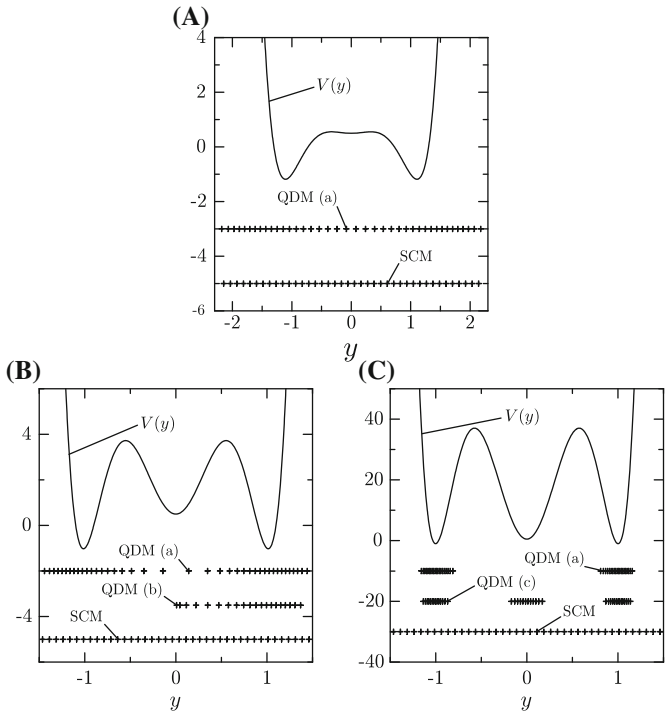

Fig. 6.9 The bimodal potential, $V(y)$, for ϵ equal to **(A)** 0.1, **(B)** 0.01 and **(C)** 0.001. The quadrature points with weight functions $w_a(y) = \exp[-(\frac{y^4}{4\epsilon} - \frac{y^2}{2\epsilon})]/\exp(1/4\epsilon)$; $y \in (-\infty, \infty)$, $w_b^{(e)}(y) = w_a(y) \quad y \in [0, \infty)$; $w_b^{(o)}(y) = y^2 w_a(y)$; $y \in [0, \infty)$ and $w_c(y) = \exp[-(\frac{y^4}{4\epsilon} - \frac{y^2}{2\epsilon}]\exp(\frac{1}{4\epsilon}) + \exp(-\frac{y^2}{2\epsilon})$ are shown. Reprinted from Lo and Shizgal (2006) with permission of the American Institute of Physics

over the positive interval defined with $w_b(y), \quad y \in [0, \infty)$ has more quadrature points close to the origin than does $w_a(y), \quad y \in (-\infty, \infty)$. For $\epsilon = 0.001$, we use a weight function centred about the origin together with $w_a(y)$. These results illustrate the flexibility of a pseudospectral method based on nonclassical weight functions that accelerate the convergence.

The variation of the eigenvalues versus ϵ is shown in Fig. 6.10. The top graph illustrates the very rapid decrease of λ_1 with decreasing ϵ. This eigenvalue represents the slowest mode and the reciprocal can be identified with the long time isomerization rate coefficient. The division of the other eigenvalues into singlet and triplet states is shown in the bottom graph with the triplet states converging to integer values for $\epsilon \to 0$. The objective of such modelling is to determine the nonequilibrium isomerization rate coefficient.

The cis-trans isomerization of n-butane has been studied by numerous researchers (Ryckaert and Bellemans 1978; Montgomery et al. 1979; Pastor and Karplus 1989; Shizgal et al. 1991; Travis and Searles 2006) with a particular potential reported by Montgomery et al. (1979) and also used by Marechal and Moreau (1984).

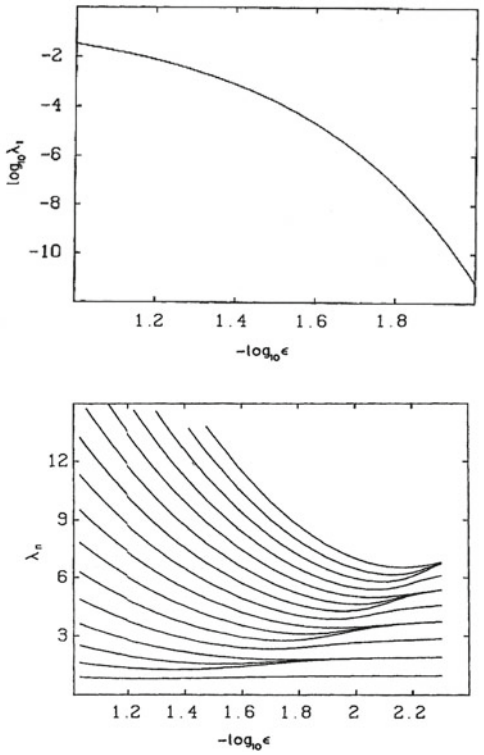

Fig. 6.10 Eigenvalue spectrum of the Fokker-Planck operator for the bistable potential; (*Top graph*) Variation of the smallest nonzero λ_1 eigenvalue versus ϵ. (*Bottom graph*) Variation of the higher eigenvalues showing the splitting into singlet and triplet states. Reprinted from Blackmore and Shizgal (1985a); Copyright 1985 by the American Physical Society

The solution of the time dependent Fokker-Planck equation for an initial delta function, $\delta(y - y_0)$, with all of the particles in one well at y_0 is given by

$$P(y,t) = \sum_{n=0}^{\infty} \psi_n(y_0)\psi_n(y)e^{-\lambda_n t}, \tag{6.125}$$

where λ_n are the eigenvalues of the Smoluchowski operator, L, in Eq. (6.114). The eigenvalues are calculated with the pseudospectral method with quadrature points and weights defined with the equilibrium density, $P_0(y)$ and the associated discrete derivative operator in physical space (Blackmore and Shizgal 1985a).

The number density of isomers in the potential well on the right for $y \in [0, \infty)$ is denoted by $N_A(t)$ and the isomerization rate equation is defined by

$$\frac{dN_A(t)}{dt} = -k(t)\left[N_A^{eq} - N_A(t)\right]. \tag{6.126}$$

where the nonequilibrium time dependent rate coefficient is determined from the time dependent reactive flux over the barrier. From a correlation function formalism (Montgomery et al. 1979; Marechal and Moreau 1984; Blackmore and Shizgal 1985a), the time dependent nonequilibrium rate coefficient can be written in the form

$$k(t) = \sum_{n=0}^{\infty} A_n e^{-\lambda_n t}, \tag{6.127}$$

with the A_n coefficients given by

$$A_n = \lambda_n \left[\int_0^{\infty} \psi_n(y) dy \right]^2, \tag{6.128}$$

and determined numerically with the nonclassical quadrature points. The details of this calculation were provided by Blackmore and Shizgal (1985a).

The nonequilibrium rate coefficient is compared with the transition state theory estimate given by

$$k_{tst} = S(0)\sqrt{\frac{k_B T_b}{2\pi m}}, \tag{6.129}$$

where

$$S(y) = \frac{e^{-U(y)/k_B T_b}}{\int_{-\infty}^{\infty} e^{-U(y)/k_B T_b} dy}.$$

The time dependent rate coefficient for butane isomerization in the potential reported by Montgomery et al. (1979) is summarized in Fig. 6.11. The time dependent rate coefficient given by Eq. (6.127) relative to the equilibrium transition state theory (tst) rate coefficient, Eq. (6.129), is shown in the figure as the solid curves *(a)* and *(b)*. The curve labelled *(b)* is for the potential as reported and the one labelled *(a)* is for an harmonic fit to this potential. The curve denoted by MM and MCB are the results by Marechal and Moreau (1984) and the simulations by Montgomery et al. (1979), respectively. There are many reactive systems and diffusion processes that are modelled with the Smoluchowski equation (Szabo et al. 1980; Bagchi et al. 1983; Chavanis 2006; Felderhof 2008) including protein folding (Bicout and Szabo 2000), dielectric relaxation (Coffey et al. 2009) and a Smoluchowski equation with a capture term (Spendier et al. 2013) that overlaps in some respects the studies of the nonequilibrium reactive system in Sect. 5.4.4.

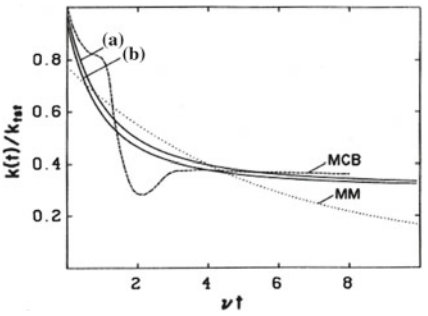

Fig. 6.11 The time dependent nonequilibrium rate coefficient for butane isomerization with the potential reported by Montgomery et al. (1979) *(b)* and with an harmonic fit to the potential *(a)*. The *dashed curve* (MM) is the result by Marechal and Moreau (1984) and the *dotted curve* (MCB) is the result by Montgomery et al. (1979). The collision frequency $\nu = 3 \times 10^{12}$ sec^{-1}. Reprinted with permission from Blackmore and Shizgal (1985a); Copyright 1985 by the American Institute of Physics

6.6 Kramers Equation and Nonequilibrium Chemical Kinetics; A Spectral Solution

It has been long recognized that reactive processes for gaseous systems proceed with the perturbation of the species velocity distribution functions from Maxwellian (Ross and Mazur 1961; Shizgal and Karplus 1970; Shizgal and Napier 1996; Kustova and Giordano 2011; Dziekan et al. 2012). These analyses of the departure from Maxwellian are based on the Boltzmann equation. The fundamental quantities that define the Boltzmann equation are the cross sections for elastic and reactive collisional processes. We considered spectral methods of solution of the chemical kinetic Boltzmann equation in Chap. 5, Sect. 5.4.4. The theoretical description of the kinetics of isomerization reactions presented in Sect. 6.5 based on the Fokker-Planck or equivalently the Smoluchowski equation in position space assumed a Maxwellian distribution function of the particles in velocity space.

The Kramers equation (Kramers 1940) for the distribution function, $f(r, v, t)$, of a test particle at position r and velocity v, at time t in the potential $U(r)$ is given by

$$\frac{\partial f}{\partial t} - v\frac{\partial f}{\partial r} - \frac{F}{m}\frac{\partial f}{\partial v} = \nu\frac{\partial}{\partial v}\left(v + \frac{k_B T_b}{m}\frac{\partial}{\partial v}\right) f. \tag{6.130}$$

The equation is comparable to the Boltzmann equation in Chap. 5, Eq. (5.30) with a drift term on the left hand side and a collision term on the right hand side. The force $F = -\partial U(r)/\partial r$ is derivable from an internal potential $U(r)$. The collision term is a particular choice which can be recognized as the Ornstein-Uhlenbeck Fokker-Planck operator in Sect. 6.1.2. The strength of the collision operator is denoted by the collision frequency ν. Kramers equation is generally used to model isomerization reactions in liquids for which the potential is the internal molecular torsional potential

about a symmetry axis in a molecule with cis-trans isomers. The frequency ν is related to the viscosity of the background liquid in which the isomerization rate is measured. There exists experimental data of the isomerization rates versus the viscosity of the liquid. The magnitude of ν reflects the strength of the coupling of the nonequilibrium system with the surroundings at equilibrium. When ν is large, the coupling is strong and the velocity distribution function approaches the equilibrium Maxwellian distribution at the heat bath temperature, T_b.

We continue the analogy of Kramers equation with the Boltzmann equation and relate the problem to rarefied gas dynamical problems where instead of ν we have the Knudsen number, 1/Kn, playing a similar role. In the small Kn collision dominated regime, departures from equilibrium are small and pertubation type methods such as the Chapman-Enskog method work remarkably well. The other extreme is the almost fully collisionless situation when Kn is very large and the Boltzmann equation can be solved with Liouville's theorem. It is the intermediate situation when Kn ≈ 1 that is the most difficult to treat theoretically.

A review of the many different applications of Kramers equation in chemistry and physics is beyond the scope of this book. The reader is directed to the excellent review by Hänggi et al. (1990) that provides a large bibliography up to about 1990. Another good overview is the book by Risken and Till (1996). A more recent summary was provided by Pollak and Talkner (2005). References 1–40 in the introduction section of the paper by Voigtlaender and Risken (1985) refers to a large number of applications of the Kramers equation. Numerical methods for the efficient solution of the Kramers equation are of considerable importance (Berezhkovskii et al. 1996; Bicout et al. 2001; Schindler et al. 2005; Bi and Chakraborty 2009; Coffey et al. 2009; Müller et al. 2012).

In this section we describe a particular pseudospectral method of solution of the Kramers equation with the symmetric bistable double Morse potential introduced by Garrity and Skinner (1983) given by

$$U(r) = \frac{U_m}{[1 - e^{-br_0}]^4}\left[1 - e^{-b(r_0+r)}\right]^2\left[1 - e^{-b(r_0-r)}\right]^2, \tag{6.131}$$

where r is an internal spatial coordinate, r_0 and $-r_0$ are the positions of the minima and br_0 is a parameter which controls the width of the barrier of height U_m that separates cis-trans isomers, as in the previous section. The potential is shown for two values of br_0 in Fig. 6.12.

The "collision" operator on the right hand side of Eq. (6.130) that describes the coupling of the system with the surrounding heat bath is the Ornstein-Uhlenbeck Brownian motion Fokker-Planck operator discussed in Sect. 6.1.2. This is not the only choice for the operator that couples the reactive system with the surrounding heat bath. Garrity and Skinner (1983) used the Bhatnagar–Gross–Krook (Bhatnagar et al. 1954) model of the Boltzmann collision operator. The correspondence between the Boltzmann equation and the Kramers equation was made in the paper by Skinner and Wolynes (1980) and they proposed alternate collision operators in the Kramers equation that couple the reactive system with the heat bath.

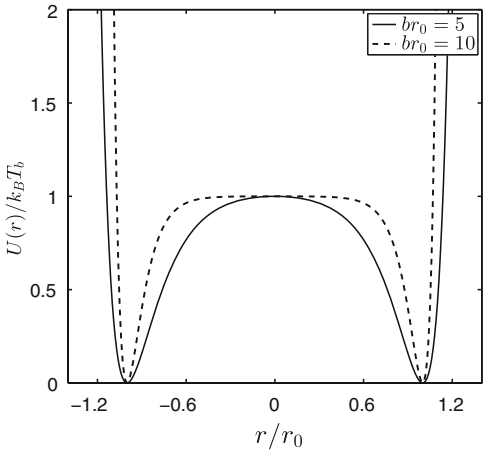

Fig. 6.12 The model bimodal double Morse potential (Garrity and Skinner 1983)

In the high collision frequency limit, $\nu \rightarrow \infty$, the Kramers equation can be transformed to the Smoluchowski equation (Risken 1996; Gardiner 2003) for the distribution in r. This transformation involves the integration over the Maxwellian velocity distribution for the probability density in position (Blackmore 1985)

$$P(r,t) = \int_{-\infty}^{\infty} f(r,v,t)dv, \tag{6.132}$$

and the result is the Smoluchowski equation

$$\frac{\partial P}{\partial t} = L_S P, \tag{6.133}$$

where L_S is defined by,

$$L_S P = \frac{1}{\nu m}\frac{\partial U^{'}(r)P}{\partial r} + D\frac{\partial^2 P}{\partial r^2}, \tag{6.134}$$

and $D = k_B T_b/m\nu$ is the diffusion coefficient as treated in the previous section.

The theoretical maximum reaction rate is the transition state theory (tst) estimate. The extent of the nonequilibrium reactive effects is determined by the magnitude of the coupling of the reactive system with the heat bath. If the coupling is strong, the nonequilibrium effects are small and conversely if the coupling is weak, the nonequilibrium effects can be large. This is similar to the treatment in Chap. 5 with the chemical kinetic Boltzmann equation where the elastic cross section controls the coupling with the heat bath.

The collision frequency ν plays the same role in Kramers equation as does 1/Kn in gas kinetic theory. We are interested in the solution of Kramers equation over the whole range of friction coefficient. In the large collision frequency limit, the Kramers equation is approximated by the Smoluchowski equation.

The Kramers equation in dimensionless variables, $x = v\sqrt{m/2kT}$, $\rho = r/r_0$, and $t' = t\nu/2$, is

$$\begin{aligned}\frac{\partial P(x,\rho,t)}{\partial t'} &= \frac{\partial}{\partial x}\left[\frac{\partial}{\partial x} + 2x\right]P(x,\rho,t) - \frac{1}{\nu}\left[2\nu\frac{\partial}{\partial \rho} - V(\rho)\frac{\partial}{\partial x}\right]P(x,\rho,t)\\ &= L_K P(x,\rho,t),\end{aligned} \tag{6.135}$$

where $\gamma = \sqrt{mr_0^2\nu^2/2kT}$ is the friction coefficient and

$$V[\rho(r)] = -\frac{1}{kT}\frac{dU(r)}{dr}. \tag{6.136}$$

We expand the probability density in the eigenfunctions of the Kramers operator, L_K. The eigenfunctions and eigenvalues can be complex as the Kramers operator is not Hermitian. We expand the eigenfunctions in Hermite polynomials in velocity v and in the eigenfunctions of the Smoluchowski operator in the spatial coordinate ρ. The Hermite polynomials are the eigenfunctions of the Ornstein-Uhlenbeck "collision" operator as discussed in Sect. 6.1.2.

The system is initially prepared to be entirely in one of the potential wells, that is

$$P(x,\rho,0) = \begin{cases} P_0(x,\rho), & \rho > 0,\\ 0, & \text{otherwise,}\end{cases} \tag{6.137}$$

where the equilibrium distribution is

$$P_0(x,\rho) = Ne^{-x^2}\exp\left(\int^{\rho} V(\rho')d\rho'\right), \tag{6.138}$$

and N is a normalization constant.

We expand $P(x,\rho,t)$ in the eigenfunctions of L_K,

$$P(x,\rho,t') = \sum_{n=0}^{\infty} a_n e^{-\lambda_n t'}\Psi_n(x,\rho), \tag{6.139}$$

where

$$L_K\Psi_n(x,\rho) = -\lambda_n\Psi_n(x,\rho). \tag{6.140}$$

The expansion coefficients, a_n, are determined by the initial condition,

$$a_n = \int_{-\infty}^{\infty}\int_{-\infty}^{\infty} P(x,\rho,0)\Psi_n^*(x,\rho)/P_0(x,\rho)dxd\rho,$$
$$= \int_{0}^{\infty}\int_{-\infty}^{\infty} \Psi_n^*(x,\rho)dxd\rho. \tag{6.141}$$

With Eq. (6.139), it can be shown (Shizgal et al. 1991) that the time dependent relaxation time is given by

$$\tau^{-1}(t') = \sum_{n=0}^{\infty} A_n \exp(-\lambda_n^r t')\left[\lambda_n^r \cos(\lambda_n^i t') + |\lambda_n^i| \sin(|\lambda_n^i| t')\right], \tag{6.142}$$

where $\lambda_n = \lambda_n^r + i\lambda_n^i$ are the complex eigenvalues and

$$A_n = a_n \int_{-\infty}^{\infty}\int_{0}^{\infty} P_n(x,\rho)dxd\rho.$$

For a sufficiently large barrier separating the two minima, λ_1 will be much less than the higher eigenvalues and the relaxation time will tend to the limiting value,

$$\frac{1}{\tau} \to \lambda_1 A_1, \tag{6.143}$$

as $t \to \infty$. This result also requires that A_1 is of the order of unity and the remaining coefficients A_n are very much smaller (Blackmore and Shizgal 1985b).

We compare the results obtained with Eq. (6.143) with the transition state theory (tst) value of the relaxation time

$$\frac{1}{\tau_{tst}} = S(0)\sqrt{kT/2\pi m}, \tag{6.144}$$

where

$$S(r) = e^{-U(r)/kT} / \int_{-\infty}^{\infty} \exp[-U(r')/kT]dr'. \tag{6.145}$$

It is important to note that this result is independent of ν.

The eigenvalue equation for the Kramers operator, $L_K \Psi_n = -\lambda_n \Psi_n$, is written in terms of the eigenfunctions, $\phi_n(x, \rho) = \Psi_n / P_0$ which satisfy the eigenvalue problem,

$$\tilde{L}_K \phi_n = [\frac{\partial}{\partial x} - 2x]\frac{\partial}{\partial x}\phi_n - \frac{1}{\gamma}[2x\frac{\partial}{\partial \rho} - V(\rho)\frac{\partial}{\partial x}]\phi_n = -\lambda_n \phi_n. \tag{6.146}$$

Since the first operator in x alone is diagonal in the Hermite polynomials, $H_j(x)$ (normalized to unity), we consider the expansion

$$\phi_n(x, \rho) = \sum_{j=0}^{\infty} c_j(\rho) H_j(x), \tag{6.147}$$

in Eq. (6.146) and find that the coefficients satisfy the set of operator equations (Brinkmann 1956; Risken and Till 1996; Blackmore and Shizgal 1985b; Shizgal et al. 1991),

$$\sum_{j=0}^{\infty}\left(2j\delta_{jk} + \frac{\sqrt{2j}}{\gamma}\left[\frac{\partial}{\partial x}\delta_{j,k-1} + (\frac{\partial}{\partial \rho} - V(\rho))\delta_{j,k+1}\right]\right) c_j(\rho) = \lambda_n c_k(x). \tag{6.148}$$

Equation (6.148) is a tri-diagonal system of coupled differential operator equations in the spatial variable (Brinkmann 1956; Risken and Till 1996).
The eigenfunctions, $S_\ell(x)$, of the Smoluchowski operator, $\tilde{L}_S$, defined by,

$$\tilde{L}_S S_\ell(\rho) = -\frac{1}{\gamma^2}\left[\phi(\rho) - \frac{\partial}{\partial \rho}\right]\frac{\partial}{\partial \rho} = -\lambda_\ell^S S_\ell(\rho), \tag{6.149}$$

are used as nonclassical basis functions to expand

$$c_j(\rho) = \sum_{\ell=0}^{\infty} d_{j\ell} S_\ell(\rho). \tag{6.150}$$

The set of eigenvalue differential operator equations, Eq. (6.148), reduces to the matrix eigenvalue equation

$$\sum_{k'=0}^{\infty}\sum_{\ell'=0}^{\infty}\left(2k\delta_{k,k'}\delta_{\ell,\ell'} - \sqrt{2(k+1)}\delta_{k',k+1}G_{\ell',\ell}/\gamma + \sqrt{2k}\delta_{k',k-1}G_{\ell,\ell'}/\gamma\right) d_{k',\ell'} = \lambda d_{k,\ell}. \tag{6.151}$$

The quantities

$$G_{\ell,\ell'} = \int_{-\infty}^{\infty} v(\rho) S_\ell(\rho) \frac{dS_{\ell'}(\rho)}{d\rho} d\rho, \tag{6.152}$$

are the matrix elements of the derivative operator over the spatial variable with the eigenfunctions of the Smoluchowski operator, where the weight function is $v(\rho) = \exp(-\int^{\rho} V(\rho')d\rho')$. These eigenfunctions form the nonclassical basis set for the solution of the Kramers equation.

The eigenfunctions of the Smoluchowsi operator which define the $G_{\ell,\ell'}$ matrix elements are determined with the pseudospectral solution of the Smoluchowski equation as discussed in Sect. 6.5. This particular numerical approach permits the efficient numerical evaluation of the derivative of the eigenfunctions with the derivative matrix operator, **D**, and the evaluation of the matrix elements with the associated quadrature. These matrix elements are evaluated with the derivative operator and quadrature as

$$\boxed{G_{\ell\ell'} = \sum_{m=1}^{M} w_m \frac{v(x_m)}{w(x_m)} S_\ell(x_m) \sum_{m'=1}^{M} D_{mm'} S_{\ell'}(x_m),} \tag{6.153}$$

where

$$w(x) = \exp[-U_m(x^4 - 2x^2)/(k_B T_b)],$$

defines the quadrature points, x_m and weights, w_m. Thus we make use of both the pseudospectral derivative evaluation and the Gaussian quadrature, both for the nonclassical Smoluchoski eigenfunctions as basis functions. It is useful to mention that the matrix elements $G_{\ell\ell'}$ are the representations of the derivative operator in the basis set of Smoluchowski eigenfunctions.

A detailed consideration of the form of Eq. (6.151) shows that the characteristic polynomial which determines the eigenvalues factors into two polynomials, with eigenvalues that correspond to even and odd eigenfunctions (Voigtlaender and Risken 1985), and the dimensionality of the eigenvalue problem is reduced. The reaction rate, which is given by λ_1, is of primary interest. Consequently, the eigenfunction corresponding to this eigenvalue must satisfy the conditions, $P_1(x, -\rho) = -P_1(x, \rho)$ and $P_1(-x, \rho) = P_1(x, \rho)$. Since the overall parity is odd, the eigenvalue λ_1 can be determined by restricting the calculation to the space of odd eigenfunctions.

Table 6.5 shows the convergence of λ_1 versus the number of Hermite polynomials M and the number of Smoluchowski eigenfunctions N for $br_0 = 4$. The convergence of this eigenvalue is very rapid for large γ as expected in view of the use of the Smoluchowski eigenfunctions as basis functions. We show the results only for an even number of Smoluchoswki basis functions, N even. The results for N odd are nonphysical as λ_1 increases with N. This feature of the matrix representation of the Kramers operator has been interpreted and discussed in detail by Shizgal et al. (1991).

Table 6.5 Convergence of λ_1 of the Kramers operator in units of 10^{-2} ($\sqrt{k_B T_b/2m}/r_0$); $br_0 = 4$; $U_m/k_B T_b = 5$

N/M	4	10	16	22
$\gamma = 2$				
4	1.876			
10	2.256	2.043		
16	2.268	2.050	2.049	
22	2.267	2.049		
$\gamma = 1$				
4	2.295	2.158		
10	2.968	2.317	2.119	
16	3.020	2.118	2.159	2.157
22	3.022	2.172	2.154	2.153
$\gamma = 0.4$				
4	3.202	2.525		
10	2.572	1.529	1.377	1.359
16	2.669	1.637	1.506	1.478
22	2.679	1.623	1.497	1.470
$\gamma = 0.1$				
4	4.742	1.474		
10	2.003	0.6823	0.470	0.448
16	2.099	0.828	0.665	0.599
22	2.110	0.790	0.634	0.574

Reproduced from (Shizgal et al. 1991) with permission Beylich A.E.: Rarefied gas dynamics. In: Proceedings of the 17th International Symposium on Rarefied Gas Dynamics, Wiley-VCH Verlag GmbH and Co. KGaA. pp. 85–92, (1991)

The variation of the relaxation rate relative to the transition state estimate is shown in Fig. 6.13 versus the friction coefficient. The present method of calculation of these isomerization rates gives reliable estimates down to $\gamma = 0.05 - 0.1$. This variation of the reaction rate with γ with a maximum at some intermediate γ is referred to as the "turnover" problem that has been investigated experimentally and theoretically since the publication of Kramers paper (Kramers 1940). It is the turnover of the graph in the Figure that has been difficult to calculate. With increasing γ, the convergence becomes more rapid.

There have been and continue to be many experimental studies of the isomerization rates in different solvents with different viscosities. The viscosity is related to the friction coefficient, γ, and thus the turnover in Fig. 6.13 has been verified experimentally (Pollak et al. 1989; Anna and Kubarych 2010; Pollak and Ianconescu 2014).

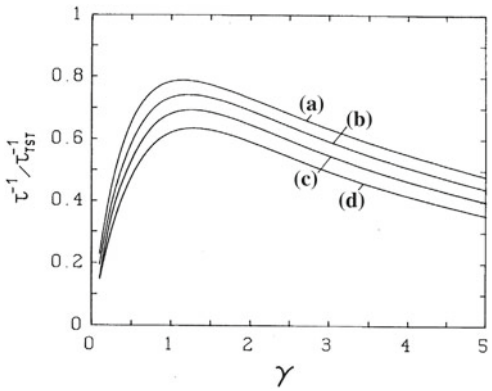

Fig. 6.13 The ratio $\tau^{-1}/\tau_{TST}^{-1}$ versus the friction coefficient γ demonstrates the classic "turnover problem". The value of br_0 is equal to *(a)* 0, *(b)* 2, *(c)* 3 and *(d)* 4. Reproduced from (Shizgal et al. 1991) with permission Beylich A.E.: Rarefied gas dynamics. In: Proceedings of the 17th International Symposium on Rarefied Gas Dynamics, Wiley-VCH Verlag GmbH and Co. KGaA. pp. 85–92, (1991)

6.7 Sturm-Liouville Problems and the Schrödinger Equation

The Sturm-Liouville problem (Pryce 1993; Al-Gwaiz 2008) refers to the solution, either analytically or numerically, of the eigenvalue problem

$$L\psi_n(x) = \lambda_n w(x)\psi_n(x), \tag{6.154}$$

where $w(x) > 0$ is a weight function and L is the second order differential operator, defined by

$$Lf(x) = \frac{d}{dx}\left[p(x)\frac{df(x)}{dx}\right] + q(x)f(x). \tag{6.155}$$

It is useful to notice that this operator is in the form of a diffusion equation where $p(x)$ is a diffusion coefficient in a Fokker-Planck equation and $q(x)$ is a gain or loss term. We assume that $p(x) > 0$, $dp(x)/dx$, $q(x)$ and $w(x) > 0$ are real valued and piecewise continuous. Any linear second order differential equation can be written in this form. The eigenfunction, $\psi_n(x)$, defined on the interval $[a, b]$ is subject to two homogeneous boundary conditions which are linear combinations of the value of the function and derivative at the two interval end points and are of the form

$$\begin{aligned} A_1\psi_n(a) + B_1\psi_n'(a) &= 0, \\ A_2\psi_n(b) + B_2\psi_n'(b) &= 0, \end{aligned} \tag{6.156}$$

where for $A_k = 0$ we have a Neumann boundary condition and if $B_k = 0$ we have a Dirichlet boundary condition.

In Sect. 6.2.1 we demonstrated the self-adjoint property of the Fokker-Planck operators subject to zero flux boundary conditions. The linear operator defined by the Sturm-Liouville problem is self-adjoint with respect to the boundary conditions, Eq. (6.156).

With the transformation of the independent variable from x to y,

$$y = \int \sqrt{w(x)/p(x)}dx, \tag{6.157}$$

and the transformation of the dependent variable $\psi_n(x)$ to $\phi_n(y)$ of the form

$$\psi_n(x) = m(x)\phi_n[y(x)], \tag{6.158}$$

where $m(x) = [p(x)w(x)]^{-1/4}$, the Sturm-Liouville equation can be written in so-called Liouville normal form which is identical to a Schrödinger equation of the form

$$-\frac{d^2\phi_n(y)}{dy^2} + V(y)\phi_n(y) = \lambda_n\phi_n(y), \tag{6.159}$$

where the potential function $V(y)$ is

$$V(y) = \frac{q[x(y)]}{w[x(y)]} + m[x(y)]\frac{d^2}{dy^2}\left(\frac{1}{m[x(y)]}\right). \tag{6.160}$$

as derived by Pryce (1993).

6.7.1 Classical Polynomials as Eigenfunctions of the Sturm-Liouville and Schrödinger Equations

The classical polynomials discussed in this chapter (and other orthogonal polynomials) satisfy a Sturm-Liouville eigenvalue problem related to an associated Schrödinger equation. Many of the details of these relationships can be found in standard textbooks so we here outline the main results and the reader is referred to other references for a complete development. We presented a preliminary discussion in Sect. 3.9.3.

6.7.2 Legendre Polynomials; Quantized Rotational States of a Rigid Rotor

The rigid rotor model for a diatomic molecule has a fixed internuclear distance at r_e and it is only the orientation of $\mathbf{r} = (r_e, \theta, \phi)$ in terms of the spherical coordinates

that is of concern. The dependence on the azimuthal angle ϕ does not influence the rotational energy and thus only the dependence on θ is considered. The Schrödinger equation is

$$-\frac{\hbar^2}{2I}\left[\frac{1}{\sin\theta}\frac{d}{d\theta}(\sin\theta\frac{d\psi(\theta)}{d\theta})\right] = E\psi(\theta), \tag{6.161}$$

where E is quantized, I is the moment of inertia and the differential operator in θ is from the form of ∇^2 in spherical polar coordinates. With the substitution $x = \cos\theta$, Eq. (6.161) can be expressed as

$$H\psi_\ell(x) = -\frac{d}{dx}\left[(1-x^2)\frac{d\psi_\ell(x)}{dx}\right] = \lambda_\ell\psi_\ell(x), \tag{6.162}$$

where H is the dimensionless Hamiltonian, $E_\ell = \lambda_\ell\frac{\hbar^2}{2I}$ is the energy eigenvalue and

$$\lambda_\ell = \ell(\ell+1). \tag{6.163}$$

These rigid rotor energy eigenvalues are precisely the eigenvalues of the total angular momentum operator L^2. There are two aspects that are important to note. The differential operator in Eq. (6.163) is of the Sturm-Liouville type and the differential operator on the left hand side is self-adjoint on the interval $x \in [-1, 1]$. The eigenvalue equation, Eq. (6.163), is the defining equation for the Legendre polynomials, that is

$$\frac{d}{dx}\left[(1-x^2)\frac{dP_\ell(x)}{dx}\right] = -\ell(\ell+1)P_\ell(x). \tag{6.164}$$

Thus, the solution of this problem is $\psi_\ell(x) \equiv P_\ell(x)$. We have found the basis for which the Hamiltonian is diagonal $H_{\ell,\ell'} = \ell(\ell+1)\delta_{\ell,\ell'}$. This is the physical space representation. The discrete space representation can be obtained with the transformation $T_{\ell j}$ defined in terms of the Legendre polynomials $P_\ell(x)$, that is

$$H_{ij}^{(ps)} = \sum_{\ell=0}^{N-1}\sum_{\ell'=0}^{N-1} T_{i\ell}H_{\ell\ell'}T_{\ell' i}. \tag{6.165}$$

With the transformation, $T_{i\ell} = \sqrt{w_i}P_\ell(x_i)$, one can show that

$$H_{ij}^{(ps)} = \sum_{k=1}^{N}(1-x_k^2)D_{ki}D_{kj}, \tag{6.166}$$

where $\mathbf{D}$ is the derivative matrix operator. The numerical diagonalization of this discrete matrix representation of the Hamiltonian of order N gives N eigenvalues

$\lambda_\ell = \ell(\ell+1)$ exactly. This formalism was introduced in Chap. 3, Sect. 3.9.3, and Fig. 3.26 shows the exact eigenfunction obtained with Eq. (6.166). For Legendre polynomials, $P_\ell(x)$, defined in $x \in [-1, 1]$ with $w(x) = 1$, $p(x) = (1 - x^2)$ and $q(x) = 0$, we find easily from Eq. (6.155) that

$$-(1-x^2)P_\ell^{''}(x) + 2xP_\ell^{'} = \ell(\ell+1)P_\ell(x) \tag{6.167}$$

which is the defining differential equation for Legendre polynomials.

6.7.3 Hermite Polynomials; Quantum Harmonic Oscillator

The Hermite polynomials $H_n(x)$ on $x \in (-\infty, \infty)$, satisfy a Sturm-Liouville problem defined by $w(x) = p(x) = e^{-x^2}$ and $q(x) = 0$ in the general form Eq. (6.155). With these definitions, Eq. (6.155) gives the differential equation

$$H_n^{''}(x) - 2xH_n^{'} = -2nH_n(x). \tag{6.168}$$

This differential equation can be written as a Schrödinger equation in terms of $h_n(x) = e^{-x^2/2}H_n(x)$. Notice that where $H_n(x)$ polynomials are orthogonal with respect to $w(x) = e^{-x^2}$, the basis functions $h_n(x)$ are orthogonal with unit weight function. The defining Schrödinger differential equation for these functions from Eq. (6.168) is

$$-h_n^{''}(x) + x^2 h_n = (2n+1)h_n(x), \tag{6.169}$$

where the term in $h_n^{'}(x)$ does not appear. This is precisely the dimensionless Schrödinger equation for a quantum harmonic oscillator as a simple model for the vibrational states of a non-rotating diatomic molecule.

If the interaction potential between the nuclei of a diatom is $V(r)$ where r is the internuclear separation, the harmonic oscillator model involves the quadratic approximation of the potential at the minimum of the potential, that is,

$$V(r) \approx V(r_e) + \frac{1}{2}\frac{d^2V}{dr^2}\bigg|_{r=r_e}(r - r_e)^2. \tag{6.170}$$

If we define the force constant as $k = \frac{dV}{dr}|_{r=r_e}$ and the displacement from r_e as $x = r - r_e$, the one-dimensional Schrödinger equation is given by

$$-\frac{\hbar^2}{2\mu}\psi_n^{''}(x) + \frac{kx^2}{2}\psi_n(x) = E_n\psi_n(x), \tag{6.171}$$

where $\hbar$ is the Planck constant and $\mu = m_1 m_2/(m_1 + m_2)$ is the reduced mass with m_1 and m_2 the masses of the two nuclei. Comparing Eqs. (6.171) and (6.169), we get the quantized vibrational states given by

$$E_n = (n + \frac{1}{2})\hbar\omega, \tag{6.172}$$

where $\omega = \sqrt{k/\mu}$ is the fundamental frequency of the oscillator.

The harmonic oscillator is a typical benchmark problem for which a variety of different discretizations are compared. One such method is based on the representation of the second derivative operator on $x \in (-\infty, \infty)$ with a uniform grid with spacing Δx. The grid points are thus $x_i = i\Delta x, i = 0, \pm 1, \pm 2, \ldots, \pm N/2$, on the finite interval $[-N\Delta x/2, N\Delta x/2]$. This representation of the second derivative operator

$$D^2_{ij} = \begin{cases} \pi^3/3, & i = j, \\ 2(-1)^{(i-j)}/(i-j)^2, & i \neq j, \end{cases} \tag{6.173}$$

has been reported by Schwartz (1985); Colbert and Miller (1992); Mazziotti (1999); Amore (2006); Baye (2006) and others. The Hamiltonian matrix for the dimensionless quantum harmonic oscillator (Colbert and Miller 1992) is approximated by

$$H_{ij} = \frac{1}{2(\Delta x)^2} \left\{ \begin{matrix} -\pi^3/3, & i = j, \\ -2(-1)^{(i-j)}/(i-j)^2, & i \neq j. \end{matrix} \right\} + \frac{x_i^2}{2}\delta_{ij}. \tag{6.174}$$

The relative accuracy of the approximate harmonic oscillator eigenvalues determined with the diagonalization of the matrix H_{ij} of dimension $N \times N$ given by Eq. (6.174) is shown in Fig. 6.14(A) versus the quantum number n. The lower order eigenstates are well approximated but the error increases with increasing n. The size of the matrix is increased by halving the step size and keeping the interval fixed as

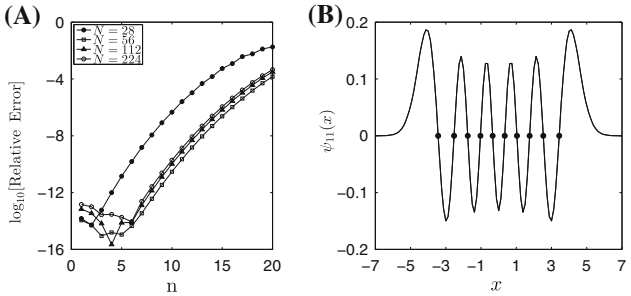

Fig. 6.14 **(A)** Relative accuracy $= 1 - \lambda_n/(n + 1/2)$ for eigenvalues of the quantum harmonic oscillator versus the vibrational quantum number n obtained with the diagonalization of the H_{ij} matrix (Eq. (6.174)) of dimension N; $x \in [-7, 7]$. **(B)** The eigenfunction, $\psi_{11}(x)$, with the 10 Hermite quadrature points shown as the *solid circles*; $N = 112$

shown in the figure and there is not much change for $N = 56$ to $N = 224$. Of interest is the variation of $\psi_{11}(x)$ in Fig. 6.14(B) with $N = 112$. The filled circles are the 10 Hermite quadrature points which coincide rather well with the nodes of the wave function. In order to get a good result for the higher eigenstates the interval has to be made larger.

The optimal basis functions are the Hermite polynomials which are the eigenfunctions of the harmonic oscillator Hamiltonian and the matrix representation of the Hamiltonian in this basis set is diagonal, $\langle n|H|m\rangle = (n+1/2)\delta_{nm}$, and provides the exact result. This result can be derived with the recurrence relations for the Hermite polynomials. This is the spectral solution of this elementary problem.

Baye and Heenen (1986) use a pseudospectral method (a Lagrange mesh method) based on the discrete physical space representation of the second derivative matrix operator in the Hermite polynomial basis

$$H_{ij} = \left\{ \begin{array}{ll} (4N - 1 - 2x_i^2)/12, & i = j, \\ (-1)^{(i-j)}\left[\frac{1}{(x_i - x_j)^2} - \frac{1}{4}\right] & i \neq j. \end{array} \right\} + \frac{x_i^2}{2}\delta_{ij}. \tag{6.175}$$

The diagonalization of this discrete matrix representation gives the eigenvalues $\lambda_n = n+1/2$ to machine accuracy for all but one eigenvalue even though the basis functions used are the exact eigenfunctions of the Hamiltonian. The results of this calculation are summarized in Table 6.6. The four eigenvalues, λ_0 to λ_3, for $N = 6$ to 9 are determined to machine accuracy, although only shown to three significant figures. For each N there is a nonphysical eigenvalue referred to as a"ghost" level (Wei 1997; Willner et al. 2004; Kallush and Kosloff 2006) that are framed in the table. For the harmonic oscillator problem, $\lambda_{ghost} = (3N - 2)/4$, and for $N = 8$ this coincides with an eigenvalue so there are two degenerate eigenvalues. This pattern repeats for $N = 10$ to 13, 14 to 18, etc.

Table 6.6 *Ghost* levels of the quantum harmonic oscillator determined with Eq. (6.175)

n	$\lambda_n = n + \frac{1}{2}$	$N = 6$	$N = 7$	$N = 8$	$N = 9$
01	0.50	0.50	0.50	0.50	0.50
1	1.50	1.50	1.50	1.50	1.50
2	2.50	2.50	2.50	2.50	2.50
3	3.50	3.50	3.50	3.50	3.50
4	4.50	4.00	4.50	4.50	4.50
5	5.50	4.50	4.75	5.50	5.50
6	6.50		5.50	5.50	6.25
7	7.50			6.50	6.50
8	8.70				7.50

The last eigenvalue is replaced with a nonphysical state highlighted by the framed numbers. For $N = 8$, there is a degenerate pair of eigenvalues. $\lambda_5 = \lambda_6 = 5.50$

The reason for the appearance of nonphysical eigenvalues is often attributed to the inexact calculation of the matrix elements of the harmonic potential with the quadrature of order N represented by the diagonal physical space matrix $V(x_i) = (x_i^2/2)\delta_{ij}$. The potential energy matrix elements

$$V_{nm} = \frac{1}{2}\int_{-\infty}^{\infty} e^{-x^2} H_n(x) x^2 H_m(x) dx, \tag{6.176}$$

evaluated with an Nth order quadrature

$$V_{nm}^{(N)} \approx \frac{1}{2}\sum_{i=1}^{N} w_i H_n(x_i) x_i^2 H_m(x_i), \tag{6.177}$$

is not exact. For the element $n = m = N$, the integrand is a polynomial of degree $2N+2$. The quadrature of order N is exact only for polynomials of order up to $2N+1$. We have considered this calculation in detail in Chap. 3, Sect. 3.7.2. The transformation to spectral space of the physical space representation of the multiplicative potential operator with the diagonal matrix $V(x_i)\delta_{ij}$ gives an inaccurate result for the $V_{N,N}$ matrix element. The result with a quadrature of order N in Eq. (6.177) is not correct.

The physical space pseudospectral representation of the harmonic oscillator Hamiltonian based on the Hermite polynomials is

$$H_{ij}^{(ps)} = \frac{1}{2}\sum_{k=1}^{N} D_{ki} D_{kj}. \tag{6.178}$$

where D_{kj} is given by Eq. (3.139). This representation does not have explicit reference to the harmonic potential as does Eq. (6.175). The usual concerns about the accuracy of the quadrature evaluated matrix elements of the potential related to the physical space representation as $V(x_i)\delta_{ij}$ do not play a role (Harris et al. 1965; Dickinson and Certain 1968).

A short MATLAB code constructs the derivative matrix operator $\mathbf{D}$ for the Hermite polynomials. The diagonalization of physical space matrix representation $\frac{1}{2}\mathbf{D}^t \cdot \mathbf{D}$ gives exactly $\lambda_n \equiv n$ relative to the ground state and $\psi_n(x_i) \equiv H_n(x_i)e^{-x^2/2}$. The solid curve in Fig. 6.15 shows the exact $H_{12}(x)e^{-x^2/2}$. The corresponding eigenfunction, $\psi_{12}(x_i)$, from the diagonalization of $\frac{1}{2}\mathbf{D}^t \cdot \mathbf{D}$ with $N = 12$ is shown with the symbols evaluated at the quadrature points. There is exact agreement between the numerical and analytical result.

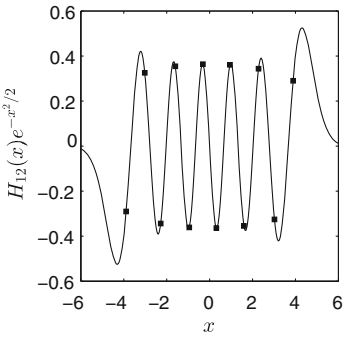

Fig. 6.15 The *solid curve* is the exact Hermite polynomial whereas the symbols represent the values of the 12th eigenfunction of $\mathbf{D}^t \cdot \mathbf{D}$ calculated at 12 quadrature points defined by the Hermite weight function, $w(x) = e^{-x^2}$

6.7.4 The Schrödinger Equation for the Electron Relaxation Problem

We return to the electron relaxation problem discussed in Sect. 6.3 for the hard sphere cross section, $\hat{\sigma} = 1$, and zero electrostaic field, $\alpha = 0$. The Fokker-Planck equation, Eq. (6.63), leads to the eigenvalue problem Eq. (6.73) with $B(x) = x$ and $A(x) = 2x^2 - 3$ (Shizgal 1979). The transformation to the new variable z in Sect. 6.3.2 which is y in this section is defined by

$$y = \int^x \frac{1}{\sqrt{B(x')}} dx' = 2\sqrt{x}.$$

The coefficients in the Fokker-Planck eigenvalue problem are in terms of y,

$$A(y) = \frac{y^4}{2} - 3,$$

and

$$B(y) = \frac{y^2}{4}.$$

The superpotential given by Eq. (6.84) is

$$W(y) = \frac{y^3}{4} - \frac{5}{y}.$$

The potential $V_-(y)$ in the Schrödinger equation

$$-\frac{d^2\psi_n(y)}{dy^2} + V_-(y)\psi_n(y) = \lambda_n\psi_n(y), \tag{6.179}$$

is defined in terms of $W(y)$ in Eq. (6.83) and

$$V_-(y) = \frac{y^6}{64} - y^2 + \frac{15}{4y^2}, \qquad y \in [0, \infty). \tag{6.180}$$

The notation $V_-(y)$ refers to one of the partner potentials in supersymmetric quantum mechanics, the other being $V_+(y)$. We refer the reader to references (Comtet et al. 1985; Cooper et al. 1995, 1987) for further details.

The potential in Eq. (6.180) is shown in Fig. 6.16. The horizontal lines indicate the positions of the eigenvalues calculated as discussed below. At first glance one might consider the basis set of associated Laguerre polynomials or the discrete representation based on the Laguerre quadrature points. However, the optimal polynomial basis set is defined with the weight function equal to the known ground state wave function, that is

$$w(y) = \begin{cases} \exp\left[-\int^y \sqrt{W(y')}dy'\right], \\ y^5 e^{-y^4/16}, \end{cases} \tag{6.181}$$

which gives $V(y) = \tilde{V}(y)$ in Eq. (6.93) and the pseudospectral matrix representation is as in Eq. (6.94) with the physical space derivative operator defined by the weight function Eq. (6.181).

A MATLAB code provides the recurrence coefficients for the polynomials orthogonal with respect to this weight function and the physical space derivative operator. The representation of the Hamitonian for this potential is $\mathbf{H} = \mathbf{D}^t \cdot \mathbf{D}$ given by

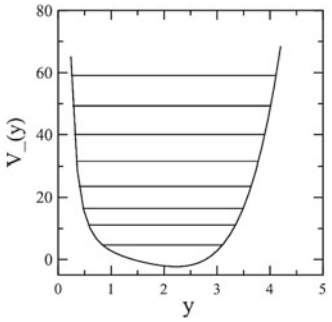

Fig. 6.16 Supersymmetric potential $V_-(y)$, Eq. (6.180), in the Schrödinger equation corresponding to the hard sphere Lorentz Fokker-Planck equation. The *horizontal lines* show the ordering of the eigenvalues in the potential

Table 6.7 Convergence of the eigenvalues of the Schrödinger equation with the potential, Eq. (6.180), with the quadrature defined with the weight function $w(y) = y^5 e^{-y^4/16}$ and the pseudospectral representation $\mathbf{H} = \mathbf{D}^t \cdot \mathbf{D}$, Eq. (6.94)

N	λ_1	λ_2	λ_3	λ_6	λ_{10}	λ_{15}	λ_{20}	λ_{30}
4	4.68598	10.21673	16.86293					
5	4.68346	10.13276	16.83567					
6	4.68340	10.11291	16.48805					
8		10.11257	16.43271	42.95019				
10		10.11252	16.42971	40.95019				
15			16.42968	40.05250	80.91828			
20				40.05238	80.44866	148.9082		
25					80.44794	142.5387	227.5833	
30						142.4463	215.1651	453.450
40							215.1631	397.036
45								388.021
50								387.626
60								387.623
$w(x) = x^2 e^{-x^2}$	4.68340	10.11251	16.42968	40.05238	80.44794	142.44461	215.1631	387.623

The results in the bottom row are the converged eigenvalues for the hard sphere Lorentz Fokker-Planck equation computed with the quadrature defined by $w(x) = x^2 e^{-x^2}$

Eq. (6.94). With the use of this nonclassical basis set and associated quadrature the matrix elements of the potential are not required as with other pseudospectral methods (Harris et al. 1965; Dickinson and Certain 1968).

The convergence of the eigenvalues calculated in this way versus the number of quadrature points is shown in Table 6.7. The convergence is rapid and from above so that the calculation is variational. At each order N an upper bound to the eigenvalue is obtained. There is no occurrence of ghost levels. The bottom row of the table shows the eigenvalues obtained with the solution of the Fokker-Planck eigenvalue problem in complete agreement with the calculations based on the Schrödinger equation. The eigenfunctions corresponding to four eigenvalues are shown in Fig. 6.17. With $N = 80$, the oscillations of these converged eigenfunctions are well resolved.

6.7.5 *Quantum Mechanics for the Vibrational States of a Diatomic Molecule; Morse Potential*

The Morse interatomic potential for a diatomic molecule (Morse 1929) is given by

$$V(r) = D_e \left[1 - e^{-\alpha(y - y_e)} \right]^2, \tag{6.182}$$

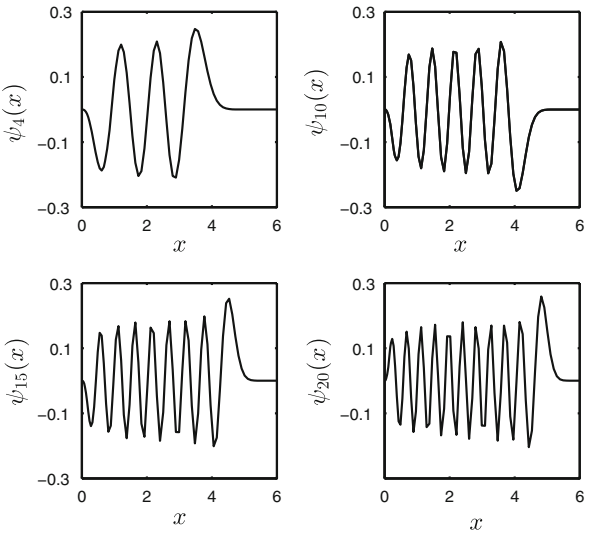

Fig. 6.17 Eigenfunctions of the Schrödinger equation for the potential, $V(y) = \frac{y^6}{64} - y^2 + \frac{15}{y^2}$ that arises from the transformation of the hard sphere Lorentz Fokker-Planck equation to the Schrödinger equation. Eigenfunctions calculated with the diagonalization $\mathbf{H} = \mathbf{D}^t \cdot \mathbf{D}$ with the pseudospectral derivative matrix operator based on the quadrature defined with the weight function $w(y) = y^5 e^{-y^4/16}$, $N = 80$

where D_e is the dissociation energy and α determines the spatial variation relative to the equilibrium position y_e. The exact vibrational eigenvalues with $\hbar = 1$ and reduced mass $\mu = 1$ are

$$\epsilon_n = \left[2\alpha\sqrt{D_e} - \alpha^2\right]n - \alpha^2 n^2, \quad n = 1, 2, \ldots, n_{max}, \tag{6.183}$$

relative to the ground state. There are a finite number of bound states denoted by n_{max}. Table 6.8 lists several diatomic molecules that have been studied by researchers to benchmark numerical methods of solution of the Schrödinger equation. For most of these studies, the interatomic potential is approximated with a Morse potential (Morse 1929). The numerical methods include finite difference methods, pseudospectral methods, methods based on B splines, the Discrete Variable Representation, the Lagrange mesh method, the Fourier grid method, the Sinc interpolation, and the Quadrature Discretization Method. Each method is based on the physical space representation of the derivative operator as determined with an interpolation. The methods are all variants of a pseudospectral method (Gottlieb and Orszag 1977; Francisco 1995; Fornberg 1996; Boyd 2001; Canuto et al. 2006b).

The numerical methods differ primarily with regards to the choice of the basis functions and the application of boundary conditions. Fourier methods are applied on a uniform grid and the number of grid points per wavelength of the eigenfunction is an

Table 6.8 References to numerical solutions of the Schrödinger equation for the vibrational states of diatomic molecules

Molecule	References	Numerical method
HF	Light et al. (1985)	Discrete variable representation
	Hamilton and Light (1986)	Discrete variable representation
	Yang and Peet (1988)	Collocation
	Balint-Kurti and Pulay (1995)	Fourier grid method
	Shizgal and Chen (1996)	Quadrature discretization method
	Guantes and Farantos (1999)	Finite difference
I_2	Braun et al. (1996)	Chebyshev Lanczos
	Shizgal (1997)	Quadrature discretization method
	Wei et al. (1997)	Lagrange interpolation
	Baye and Vincke (1999)	Lagrange mesh method
	Mazziotti (1999)	Spectral difference method
	Wei (2000)	Discrete singular convolution (Sinc)
	Chen and Shizgal (2001)	Quadrature discretization method
	Lo and Shizgal (2008b)	Quadrature discretization method
H_2	Johnson (1977)	Finite difference
	Marston and Balint-Kurti (1989)	Fourier grid method
	Baye (1995)	Lagrange mesh method
H_2^+	ONeil and Reinhardt (1978)	B-spline
	Layton (1993)	Fourier
Cs_2	Kokoouline et al. (1999)	Discrete variable representation
	Willner et al. (2004)	Mapped grid methods
	Lo and Shizgal (2008a)	Quadrature discretization method
	Derevianko et al. (2009)	B-spline
He_2, Ne_2, Ar_2, HeAr, HeNe, etc.	Shizgal (1997)	Quadrature discretization method
He_2, Ne_2, Ar_2	Lo and Shizgal (2006)	Quadrature discretization method

important parameter (Colbert and Miller 1992). Associated with some of the methods is a variational theorem so that the Nth approximation represents an upper bound. For some methods there are nonphysical eigenvalues calculated that are referred to as "ghost" levels (Wei 1997; Kokoouline et al. 1999; Willner et al. 2004).

The Morse potential belongs to the class of potentials in supersymmetric quantum mechanics (Dutt et al. 1988; Cooper et al. 1995). The basis set defined with the weight function

$$w(x) = \exp\left[-2\sqrt{D_e}(x + \frac{e^{-\alpha x}}{\alpha}) + \alpha x \right], \tag{6.184}$$

for which the ground state wavefunction is $\psi_0(x) = \sqrt{w(x)}$ and $V(x) = \tilde{V}(x)$. The pseudospectral representation of the Hamiltonian, Eq. (6.93), reduces to Eq. (6.94).

Table 6.9 Convergence of the eigenvalues in cm^{-1} for the Morse oscillator for HF with $D_e = 49383.407073\,\text{cm}^{-1}$, $\beta = 1.1741 a_0^{-1}$, $x_e = 1.7329 a_0$ and $\mu = 1744.4453572532 m_e$

N	ϵ_2	ϵ_8	ϵ_{14}
4	9819.11761		
6	9805.01756		
8	9805.00714		
10		33041.31574	
12		29960.19345	
14		29067.91526	
16		28925.47987	62676.28749
18		28914.83536	53058.24677
20		28914.43671	48112.83259
25		28914.42738	43025.97932
30			41879.68669
35			41781.77734
40			41780.18827
45			41780.18145
Exact	9805.0714	28914.42738	41780.18143

The quadrature is defined in terms of the weight function, Eq. (6.184) and the eigenvalues determined with the diagonalization of $\mathbf{D}^t \cdot \mathbf{D}$, Eq. (6.94). Reprinted from (Shizgal 1997) with permission from Elsevier

The diagonalization of $\mathbf{D}^t \cdot \mathbf{D}$ gives the eigenvalues and eigenfunctions.

The convergence of the vibrational energies ϵ_2, ϵ_8 and ϵ_{14} for the Morse potential for HF calculated with the quadrature defined with $w(x)$, Eq. (6.184), are shown in Table 6.9 and the rapid convergence of the eigenvalues is evident. It is clear that there is a variational theorem inherent in the method as the convergence of the eigenvalues is from above. For each N, an upper bound to the vibrational state is obtained.

The convergence demonstrated here is faster than reported by other researchers (Balint-Kurti and Pulay 1995; Braun et al. 1996; Hoffman et al. 1998; Baye and Vincke 1999) with different numerical methods. The spectral convergence of the eigenvalues is shown in Fig. 6.18 and several eigenfunctions are shown in Fig. 6.19. Unlike Fourier methods, this high order pseudospectral method with the particular basis set constructed with $w(x) = \psi_0^2(x)$, does not require a particularly dense distribution of quadrature points to accurately calculate the higher order oscillatory vibrational eigenfunctions (Gottlieb and Orszag 1977; Francisco 1995; Fornberg 1996; Boyd 2001; Canuto et al. 2006b).

An important aspect of these benchmark calculations is the total number of bound states for the potential chosen. If the potential supports n_{max} states, the calculation of the lower states up to vibrational quantum number $n \approx 3n_{max}/4$ are relatively easy to calculate in spite of the oscillatory form of the eigenfunctions. It is the vibrational states close to the dissociation limit that are the most difficult to calculate.

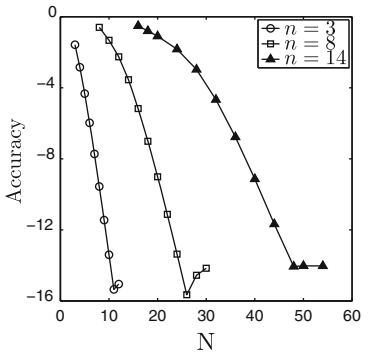

Fig. 6.18 The convergence of the lower order eigenvalues, λ_n, of the Morse potential with diagonalization of $\mathbf{D}^t \cdot \mathbf{D}$; Morse potential for HF with $D_e = 49383.407073\,\mathrm{cm}^{-1}$, $\beta = 1.1741 a_0^{-1}$, $x_e = 1.7329 a_0$ and $\mu = 1744.4453572532 m_e$; Accuracy $= \log_{10} |1 - \lambda_n^{(N)}/\lambda_n^{(exact)}|$

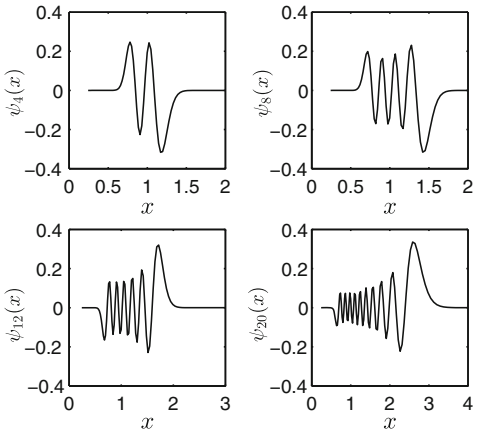

Fig. 6.19 Eigenfunctions determined from the diagonalization of $\mathbf{D}^t \cdot \mathbf{D}$ for selected vibrational states of HF versus x in angstroms

We illustrate this feature with the model Morse potential employed by Pryce (1993) and Weideman (1999)

$$V(x) = 9(1 - e^{-x})^2 - 9,$$

which supports only three bound states,

$$\lambda_n = -n^2 + 5n - \frac{25}{4}, \quad n = 0, 1 \text{ and } 2.$$

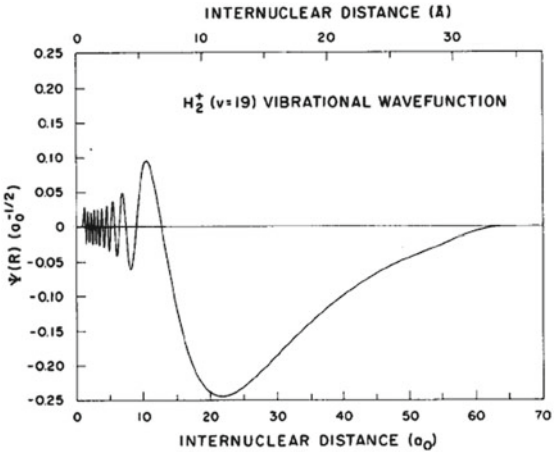

Fig. 6.20 Variational approximation to the $n = 19$ vibrational eigenfunction of H_2^+ with the potential from Wind (1965) with 100 B splines (Shore 1973). Reproduced from ONeil and Reinhardt (1978) with permission of the American Physical Society

The vibrational states are determined with the quadrature based on the weight function

$$w(x) = \exp(-5x + 6e^{-x})$$

for which $V(x) = \tilde{V}(x)$ and pseudospectral representation of the Hamiltonian is $\mathbf{D}^t \cdot \mathbf{D}$. The convergence of the 3 states to 14 significant figures requires 2, 20 and 55 quadrature points (Chen and Shizgal 2001). The numerical difficulty in the accurate calculation of the highest state with only two nodes is the diffuse nature of the eigenfunction just below the dissociation limit. This is illustrated in Fig. 6.20 for a higher order eigenfunction for H_2^+ determined with 100 B splines (ONeil and Reinhardt 1978). The numerical challenge is to capture both the oscillatory behaviour at small internuclear distance as well as the variation on a much larger scale for larger ($r > 20\, a_0$) distances. This behaviour was also demonstrated in Fig. 1 of Meshkov et al. (2008) for the eigenfunctions for a Lennard–Jones potential.

The diatoms, He_2 and Ne_2, with 1 and 3 bound states, respectively, illustrate the same difficulty in the accurate representation of the highest bound state. The potentials for He_2 and Ne_2 were reported by Aziz and Slaman (1991) and Tang and Toennies (2003), respectively. A Morse potential that approximates the true potential (Lo and Shizgal 2008a) is used to define a quadrature based on the weight function, Eq. (6.184). For this realistic potential, $V(y) \neq \tilde{V}(y)$ and the pseudospectral representation of the Hamiltonian given by Eq. (6.93) is diagonalized.

In addition, a mapping, $u = \rho(x)$, is used to redistribute the points so as to best capture the variation of the wave function. Two such mappings are

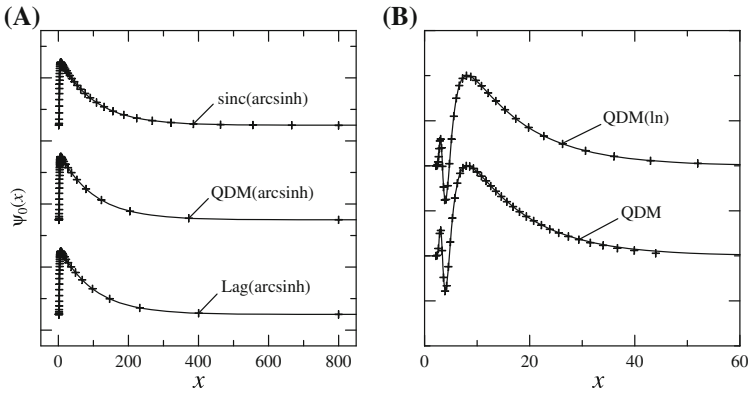

Fig. 6.21 (*Left hand panel*) Single bound state eigenfunction, $\psi_0(x)$, for He_2 with the Aziz and Slaman (1991) interatomic potential. QDM is the quadrature discretization method with a nonclassical weight function with the mapping, Eq. (6.186); Lag refers to the Lagrange mesh method with the same map. (*Right hand panel*) The second excited state eigenfunction, $\psi_2(x)$, for Ne_2 with the Tang and Toennies (2003) potential determined with the QDM, with and without the mapping, Eq. (6.185). Reproduced from Lo and Shizgal (2008a) with permission of the American Institute of Physics

$$\rho(x) = s_1 \ln\left(\frac{x - b_2}{s_2}\right) \tag{6.185}$$

$$\rho(x) = s_1 \sinh^{-1}\left(\frac{x - b_2}{s_2}\right) + b_1, \tag{6.186}$$

where s_1, s_2, b_1 and b_2 are adjustable parameters chosen empirically.

The single ground vibrational state for He_2 and the second excited vibrational state for Ne_2 are shown in Fig. 6.21. The variation of the wave function of the one bound state for He_2 occurs on two different spatial scales. There is a rapid variation near the origin and a very slow decay over a very large distance. The collocation points shown in the figure are distributed nonuniformly on the large interval of interest. The curves labelled QDM are calculated with the quadrature discretization method (Lo and Shizgal 2008a) and the two mappings above. The curves labelled by "Lag" refer to the Lagrange mesh method (Baye 2006).

Pseudospectral methods applied to the entire interval or in subdomains of interest in which case it is referred to as a spectral element method (Deville et al. 2002; Pasquetti and Rapetti 2004) belong to that class of spectral and higher order numerical methods (Azaez et al. 2012). In every application in chemistry, physics and engineering, there are important applications to three and multidimensional problems. The extension from one-dimension to several dimensions generally involves a direct product of several one-dimensional polynomial basis sets. The size of the matrices for such problems increases dramatically with an increase with the number of degrees of freedom especially for the calculation of the rotational–vibrational states of polyatomic molecules (Friesner et al. 1993; Littlejohn et al. 2002; Dawes

and Carrington 2004, 2005; Cassam-Chenaï and Liévin 2012). The numerics is then a problem in linear algebra to find the eigenvalues of a very large matrix.

A reduction in the dimensionality of the problem can be achieved by making use of available symmetries and with other techniques. Also, with a judicious choice of basis functions and/or grid points the number for each vibrational mode can be significantly decreased so as to achieve computational economy. In their case study of the vibrational states of methane, Mielke et al. (2013) introduce the use of optimized vibrational quadratures for the efficient computation of one-dimensional matrix elements. Any reduction in the number of grid points for each degree of freedom could dramatically decrease the dimension of the matrices resulting from the direct product of the different spaces for multidimensional problems. There are ongoing efforts to develop more efficient schemes for the development of sparse grids with algorithms related to cubatures discussed in Chap. 2, Sect. 2.8 (Avila and Carrington 2013; Lauvergnat and Nauts 2014).

6.7.6 *Pseudospectral Solution of the Two Dimensional Schrödinger Equation for the Henon-Heles Potential; Nonclassical Basis Sets*

Quantum problems in two and higher dimensions are often solved with a direct product of the basis sets for each one dimensional variable (Parrish and Hohenstein 2013) (and references therein). The resulting matrix representation of the Hamiltonian for a multidimensional system in either the spectral space or the physical space is the product of matrix representations for each dimension. Consequently the size of the matrices involved can increase very quickly if many basis functions or grid points are required in each dimension. This becomes a computationally challenging problem in order to reduce the dimensionality of the matrices by applying symmetries or particular numerical algorithms to reduce memory requirements and computational speed. The Milne problem (Lindenfeld and Shizgal 1983) and the associated planetary escape problem (Shizgal and Blackmore 1986) discussed in Chap. 5 are examples of problems in kinetic theory in three dimensions.

In this section, we consider the calculation of the eigenvalues of the two dimensional Hamiltonian

$$-\frac{1}{2}\left[\frac{\partial^2\psi_{nm}(x,y)}{\partial x^2}+\frac{\partial^2\psi_{nm}(x,y)}{\partial y^2}\right]+V(x,y)\psi_{nm}(x,y)=\lambda_{nm}\psi_{nm}(x,y), \tag{6.187}$$

where the potential is the Henon-Heles potential

$$V(x,y)=\frac{x^2+y^2}{2}-\lambda x(\frac{x^3}{3}-y^2). \tag{6.188}$$

This potential was introduced by Henon and Heiles (1964) in their study of the motion of a star in the potential of the galaxy and the determination of a third conserved integral of the classical two dimensional motion with this Hamiltonian. The potential, Eq. (6.188), was chosen for its analytic simplicity so as to make the trajectory computations easy and to obtain interesting dynamical results. This system has received considerable attention as a model for classical and quantum chaotic behaviour. For $\lambda = 0$, the problem reduces to two uncoupled harmonic oscillators.

For the two dimensional Schrödinger equation, we choose basis functions

$$\begin{aligned} X_n(x) &= \sqrt{u(x)}G_n(x), \\ Y_n(y) &= \sqrt{v(y)}H_m(y), \end{aligned} \tag{6.189}$$

where $u(x)$ and $v(y)$ are the weight functions and we denote the logarithmic derivatives of the weight functions by

$$\begin{aligned} U(x) &= -\frac{u'(x)}{u(x)}, \\ V(x) &= -\frac{v'(x)}{v(x)}, \end{aligned} \tag{6.190}$$

We extend the pseudospectral analysis of the one-dimensional applications presented in Sect. 6.3.3 to two dimensions by defining the spectral space representation of the Hamiltonian as

$$\begin{aligned} H_{n'm',nm} = \delta_{m'm} \int u(x) G'_{n'}(x) G'_n(x) dx + \delta_{n'n} \\ \int v(y) H'_{m'}(y) H'_m(y) dy + (V_{n'm',nm} - \tilde{V}_{n'm',nm}). \end{aligned} \tag{6.191}$$

The potential matrix elements are $V_{n'm',nm} = \langle X_{n'} Y_{m'} | V(x, y) | X_n Y_m \rangle$ and the matrix elements of the reference potential are

$$\begin{aligned} \tilde{V}_{n'm',nm} = \delta_{m'm} \int \left(\frac{U^2(x)}{4} - \frac{U'(x)}{2} \right) u(x) G_{n'}(x) G_n(x) dx \\ + \delta_{n'n} \int \left(\frac{V^2(y)}{4} - \frac{V'(y)}{2} \right) v(y) H_{m'}(y) H_m(y) dy. \end{aligned} \tag{6.192}$$

We transform this spectral space representation with the appropriate transformation matrices, Eq. (1.24), and obtain the discrete physical space representation

$$H_{ij,k\ell} = \delta_{k\ell} \sum_{k'=0}^{N_x} D_{k'i} D_{k'j} + \delta_{ij} \sum_{k'=0}^{N_y} D_{k'k} D_{k'\ell} + \left[V(x_i, y_j) - \tilde{V}(x_i, y_k) \right], \tag{6.193}$$

where

$$\tilde{V}(x, y) = \left(\frac{U^2(x)}{4} - \frac{U'(x)}{2}\right) + \left(\frac{V^2(y)}{4} - \frac{V'(y)}{2}\right). \tag{6.194}$$

is the usual reference potential in two-dimensions. The pseudospectral representation, Eq. (6.193) is the two-dimensional analog of the one-dimensional representation, Eq. (6.93). The details are similar to the transformations for the Fokker-Planck operator in Sect. 6.2.2.

Two sets of quadratures were used; (1) Hermite quadratures for both dimensions and (2) a quadrature in x based on a nonclassical weight function, $u(x) = \exp[-x^2 + 2\lambda x^3/9]$, chosen empirically and Hermite quadratures in y. With the Hermite quadrature in both dimensions, the lowest order eigenvalues required as few as 8 quadrature

Table 6.10 Eigenvalues of the Henon-Heles potential with $\lambda = \sqrt{0.0125}$ with $u(x) = \exp[-x^2 + 2\lambda x^3/9]$ and $v(y) = \exp(-y^2)$; $N_x = N_y = 32$

n	ℓ	Feit et al. (1982)	Shizgal and Chen (1996)	Echave and Clary (1992)
3	3	3.9825	3.982417	
	−3	3.9859	3.985761	
5	3	5.8672	5.867 015	
	−3	5.8816	5.881 446	
6	6	6.9991	6.998 932	
	−6	6.9996	6.999 387	
7	3	7.6979	7.697 721	
	−3	7.7371	7.736 885	
8	6	8.8116	8.811 327	
	−6	8.8154	8.815 188	
9	3	9.4670	9.466 773	
	−3	9.5526	9.552 382	
9	9	10.0356	10.035 413	
	−9	10.0359	10.035 592	
10	6	10.5727	10.572 480	
	−6	10.5907	10.590 470	
11	3	11.1603	11.160 259	11.160 258
	−3	11.3253	11.325 231	11.325 231
11	9	11.7497	11.749 519	11.749 518
	−9	11.7525	11.752 297	11.752 297
12	6	12.3335	12.333 786	12.333 780
	−6	12.2771	12.277 192	12.277 192
12	12	12.7474	12.748 520	12.748 183
	−12	13.0310	13.032 065	13.032 060
13	3	13.0868	13.086 873	13.086 873
	−3	13.0800	13.081 199	13.081 191

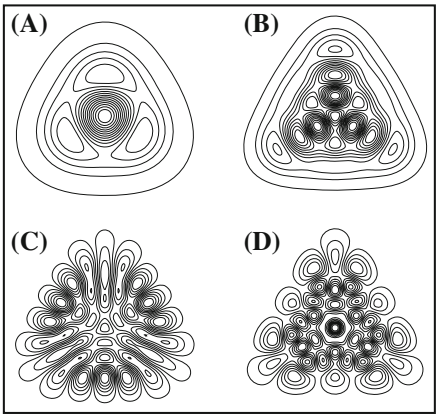

Fig. 6.22 Contour plots of the eigenfunctions of the Schrödinger equation for the Henon-Heles potential with n and ℓ equal to **(A)** 2, 0 **(B)** 6, 0 **(C)** 9, −9 and **(D)** 10, 6; Hermite quadratures were used, $N_x = N_y = 32$; the vertical scale is y and the horizontal scale is x, both in the interval [−7, 7]. Reproduced from Shizgal and Chen (1997) with permission of the American Institute of Physics

points in each variable to get convergence to 5 significant figures and up to 50 quadrature points for the higher states to the same accuracy. The nonclassical weight function provides faster convergence giving 8 significant figure accuracy with 32 quadrature points in each dimension.

The eigenvalues calculated in this way are listed in Table 6.10 in comparison with the previous calculations. Echave and Clary (1992) used Fourier basis functions to solve two one-dimensional reference problems and used the eigenfunctions of these hamiltonians as basis functions for the two-dimensional Henon-Heiles potential. They refer to this method that follows on the earlier work by Hamilton and Light (1986) as the potential optimized discrete variable representation. The results listed in the table are also in agreement with the results by Wei (1999) who used a collocation method referred to as a discrete singular convolution analogous to a Sinc interpolation as used by Amore (2006) and Amore et al. (2009). We discussed the Sinc interpolation in Chap. 2. We list the eigenvalues in the same manner as done by Noid and Marcus (1977). The results are in agreement to the accuracy in the table except for the (12,12) state for which Wei (1999) reports the value of 12.748431. The reason for this discrepancy is not known.

The contour plots of several eigenfunctions are shown in Fig. 6.22 and converged with 50 Hermite basis functions in each variable. The C_{3v} symmetry is evident from the figure and several fine details of the eigenfunctions are recovered. It should be mentioned that this model system with the small value of $\lambda = \sqrt{0.0125}$ is very close to two uncoupled harmonic oscillators in each variable. The convergence of the Hermite polynomial basis set for each dimension for the lower states works as well as it does owing to the small value of λ. It would be of interest to consider larger values and experiment with nonclassical basis sets that might provide faster convergence.

References

Abbott, D.: Overview: unsolved problems of noise and fluctuations. Chaos **11**, 526–538 (2001)

Abolhassani, A.A.H., Matte, J.P.: Multi-temperature representation of electron velocity distribution functions. I. Fits to numerical results. Phys. Plasmas **19**, 102103 (2012)

Al-Gwaiz, M.A.: Sturm-Liouville Theory and Its Applications. Springer, Berlin (2008)

Amore, P.: A variational Sinc collocation method for strong-coupling problems. J. Phys. A: Math. Gen. **39**, L349–L355 (2006)

Amore, P., Fernandez, F.M., Saenz, R.A., Salvo, K.: Collocation on uniform grids. J. Phys. A: Math. Theor. **42**, 115302 (2009)

Andersen, K., Shuler, K.E.: On the relaxation of a hard sphere Rayleigh and Lorentz gas. J. Chem. Phys. **40**, 633–650 (1964)

Andersen, H.C., Oppenheim, I., Shuler, K.E., Weiss, G.H.: Exact condition for the preservation of a canonical distribution in Markovian relaxation process. J. Math. Phys. **5**, 522–536 (1964)

Anna, J.M., Kubarych, K.J.: Watching solvent friction impede ultrafast barrier crossings: a direct test of Kramers theory. J. Chem. Phys. **133**, 174506 (2010)

Avila, G., Carrington Jr, T.: Solving the Schrödinger equation using Smolyak interpolants. J. Chem. Phys. **139**, 134114 (2013)

Azaez, M., El Fekih, H., Hesthaven, J.S.: Spectral and High Order Methods for Partial Differential Equations-ICOSAHOM. Springer, New York (2012)

Aziz, R.A., Slaman, M.J.: An examination of ab initio results for the helium potential energy curve. J. Chem. Phys. **94**, 8047–8053 (1991)

Bagchi, B., Fleming, G.R., Oxtoby, D.W.: Theory of electronic relaxation in solution in the absence of an activation barrier. J. Chem. Phys. **78**, 7375–7385 (1983)

Balint-Kurti, G.G., Pulay, P.: A new grid-based method for the direct computation of excited molecular vibrational-states: test application to formaldehyde. J. Mol. Struct. (Theochem) **341**, 1–11 (1995)

Basu, B., Jasperse, J.R., Strickland, D.J., Daniel, R.E.: Transport-theoretic model for the electron-proton-hydrogen atom aurora. J. Geophys. Res. **98**, 21517–21532 (1993)

Baye, D.: Constant-step Lagrange meshes for central potentials. J. Phys. B: At. Mol. Opt. Phys. **28**, 4399–4412 (1995)

Baye, D.: Lagrange-mesh method for quantum-mechanical problems. Phys. Stat. Sol. B **243**, 1095–1109 (2006)

Baye, D., Heenen, P.H.: Generalized meshes for quantum-mechanical problems. J. Phys. A: Math. Gen. **19**, 2041–2059 (1986)

Baye, D., Vincke, V.: Lagrange meshes from nonclassical orthogonal polynomials. Phys. Rev. E **59**, 7195–7199 (1999)

Berezhkovskii, A.M., Zitserman, V.Yu., Polimenob, A.: Numerical test of Kramers reaction rate theory in two dimensions. J. Chem. Phys. **105**, 6342–6357 (1996)

Bernstein, M., Brown, L.S.: Supersymmetry and the bistable Fokker-Planck equation. Phys. Rev. Lett. **52**, 1933–1935 (1984)

Bhatnagar, P.L., Gross, E.P., Krook, M.: A model for collision processes in gases. I. Small amplitude processes in charged and neutral one-component systems. Phys. Rev. **94**, 511–525 (1954)

Bi, C., Chakraborty, B.: Rheology of granular materials: dynamics in a stress landscape. Philos. Trans. R. Soc. A **367**, 5073–5090 (2009)

Bicout, D.J., Szabo, A.: Entropic barriers, transition states, funnels, and exponential protein folding kinetics: a simple model. Protein Sci. **9**, 452–465 (2000)

Bicout, D.J., Berezhkovskii, A.M., Szabo, A.: Irreversible bimolecular reactions of Langevin particles. J. Chem. Phys. **114**, 2293–2303 (2001)

Binney, J., Tremaine, S.: Galactic Dynamics, 2nd edn. Princeton University Press, New Jersey (2008)

Bird, G.A.: Molecular Gas Dynamics and the Direct Simulation of Gas Flows. Clarendon, Oxford (1994)

Biró, T.S., Jakovác, A.: Power-law tails from multiplicative noise. Phys. Rev. Lett. **94**, 132302 (2005)
Black, F., Scholes, M.: The pricing of options and corporate liabilities. J. Polit. Econ. **81**, 637–654 (1973)
Blackmore, R.S.: (1985) Theoretical studies in stochastic processes. PhD thesis, UBC, http://circle.ubc.ca/handle/2429/25554
Blackmore, R., Shizgal, B.: Discrete ordinate method of solution of Fokker-Planck equations with nonlinear coefficients. Phys. Rev. A **31**, 1855–1868 (1985a)
Blackmore, R., Shizgal, B.: A solution of Kramers equation for the isomerization of n-butane in CCl_4. J. Chem. Phys. **83**, 2934–2941 (1985b)
Blackmore, R., Weinert, U., Shizgal, B.: Discrete ordinate solution of a Fokker-Planck equation in laser physics. Trans. Theory Stat. Phys. **15**, 181–210 (1986)
Blaise, P., Kalmykov, Y.P., Velcescu, A.A.: Extended diffusion in a double well potential: transition from classical to quantum regime. J. Chem. Phys. **137**, 094105 (2012)
Bobylev, A.V., Mossberg, E.: On some properties of linear and linearized Boltzmann collision operators for hard spheres. Kinet. Relat. Models **4**, 521–555 (2008)
Boyd, J.P.: Chebyshev and Fourier Spectral Methods. Dover, New York (2001)
Boyd, T.J.M., Sanderson, J.S.: The Physics of Plasmas. Cambridge University Press, Cambridge (2003)
Braun, M., Sofianos, S.A., Papageorgiou, D.G., Lagaris, I.E.: An efficient Chebyshev-Lanczos method for obtaining eigensolutions of the Schrödinger equation on a grid. J. Comput. Phys. **126**, 315–327 (1996)
Brey, J.J., Casado, J.M., Morillo, M.: Combined effects of additive and multiplicative noise in a Fokker-Planck model. Z. Phys. B—Condens. Matter **66**, 263–269 (1987)
Brinkmann, H.C.: Brownian motion in a field of force and the diffusion theory of chemical reactions. Physica A **22**, 29–34 (1956)
Buet, C., Dellacherie, S.: On the Chang Cooper scheme applied to a linear Fokker Planck equation. Commun. Math. Sci. **8**, 1079–1090 (2010)
Canuto, C., Hussaini, M.Y., Quarteroni, A., Zang, T.A.: Spectral Methods: Fundamentals in Single Domains. Springer, New York (2006b)
Cartling, B.: Kinetics of activated processes from nonstationary solutions of the Fokker-Planck equation for a bistable potential. J. Chem. Phys. **87**, 2638–2648 (1987)
Cassam-Chenaï, P., Liévin, J.: Ab initio calculation of the rotational spectrum of methane vibrational ground state. J. Chem. Phys. **136**, 174309 (2012)
Chandrasekhar, S.: Principles of Stellar Dynamics. Dover, New York (1942)
Chandrasekhar, S.: Brownian motion, dynamical friction, and stellar dynamics. Rev. Mod. Phys. **21**, 383–388 (1949)
Chang, J.C., Cooper, G.: A practical difference scheme for Fokker-Planck equations. J. Comput. Phys. **6**, 1–16 (1970)
Chavanis, P.H.: Relaxation of a test particle in systems with long-range interactions: diffusion coefficient and dynamical friction. Eur. J. Phys. B **52**, 61–82 (2006)
Chen, H., Shizgal, B.D.: A spectral solution of the Sturm-Liouville equation: comparison of classical and nonclassical basis sets. J. Comput. Appl. Math. **136**, 17–35 (2001)
Coffey, W.T., Kalmykov, Y.P., Titov, S.V., Cleary, L.: Quantum effects in the Brownian motion of a particle in a double well potential in the overdamped limit. J. Chem. Phys. **131**, 084101 (2009)
Colbert, D.T., Miller, W.H.: A novel discrete variable representation for quantum-mechanical reactive scattering via the S-Matrix Kohn method. J. Chem. Phys. **96**, 1982–1991 (1992)
Collier, M.R.: Are magnetospheric suprathermal particle distributions (κ functions) inconsistent with maximum entropy considerations. Adv. Space Res. **33**, 2108–2112 (2004)
Comtet, A., Bandrauk, A.D., Campbell, D.K.: Exactness of semiclassical bound-state energies for supersymmetric quantum-mechanics. Phys. Lett. B **150**, 159–162 (1985)
Cooper, F., Ginocchio, J.N., Khare, A.: Relationship between supersymmetry and solvable potentials. Phys. Rev. D **36**, 2458–2473 (1987)

Cooper, F., Khare, A., Sukhatme, U.: Supersymmetry and quantum mechanics. Phys. Rep. **251**, 267–385 (1995)
Corngold, N.: Kinetic equation for a weakly coupled test particle. II. Approach to equilibrium. Phys. Rev. A **24**, 656–666 (1981)
Crew, G.B., Chang, T.S.: Asymptotic theory of ion conic distributions. Phys. Fluids **28**, 2382–2394 (1985)
Cukier, R.I., Lakatos-Lindenberg, K., Shuler, K.E.: Orthogonal polynomial solutions of the Fokker-Planck equation. J. Stat. Phys. **9**, 137–144 (1973)
Dawes, R., Carrington Jr, T.: A multidimensional discrete variable representation basis obtained by simultaneous diagonalization. J. Chem. Phys. **121**, 726–736 (2004)
Dawes, R., Carrington, T.: How to choose one-dimensional basis functions so that a very efficient multidimensional basis may be extracted from a direct product of the one-dimensional functions: energy levels of coupled systems with as many as 16 coordinates. J. Chem. Phys. **122**, 134101 (2005)
Dekker, H., van Kampen, N.G.: Eigenvalues of a diffusion process with a critical point. Phys. Lett. A **73**, 374–376 (1979)
Demeio, L., Shizgal, B.: Time dependent nucleation. II. A semiclassical approach. J. Chem. Phys. **98**, 5713–5719 (1993a)
Demeio, L., Shizgal, B.: A uniform Wentzel-Kramers-Brillouin approach to electron transport in molecular gases. J. Chem. Phys. **99**, 7638–7651 (1993b)
Derevianko, A., Luc-Koenig, E., Masnou-Seeuws, F.: Application of B-splines in determining the eigenspectrum of diatomic molecules: robust numerical description of Halo-state and Feshbach molecules. Can. J. Phys. **87**, 67–74 (2009)
Deville, M.O., Fisher, P.F., Mund, E.H.: High Order Methods for Incompressible Fluid Flow. Cambridge University Press, Cambridge (2002)
Dickinson, A.S., Certain, P.R.: Calculation of matrix elements for one-dimensional quantum-mechanical problems. J. Chem. Phys. **49**, 4209–4211 (1968)
Drozdov, A.N.: Two novel approaches to the Kramers rate problem in the spatial diffusion regime. J. Chem. Phys. **111**, 6481–6491 (1999)
Drozdov, A.N., Tucker, S.C.: An improved reactive flux method for evaluation of rate constants in dissipative systems. J. Chem. Phys. **115**, 9675–9684 (2001)
Dunkel, J., Hänggi, P.: Relativistic Brownian motion. Phys. Rep. **471**, 1–73 (2009)
Dutt, R., Khare, A., Sukhatme, U.P.: Supersymmetry, shape invariance and exactly solvable potentials. Am. J. Phys. **56**, 163–168 (1988)
Dyatko, N.A.: Negative electron conductivity in gases and semiconductors. J. Phys.: Conf. Ser. **71**, 012005 (2007)
Dyatko, N.A., Loffhagen, D., Napartovich, A.P., Winkler, R.: Negative electron mobility in attachment dominated plasmas. Plasma Chem. Plasma Proc. **21**, 421–439 (2001)
Dziekan, P., Lemarchand, A., Nowakowski, B.: Master equation for a bistable chemical system with perturbed particle velocity distribution function. Phys. Rev. **85**, 021128 (2012)
Echave, J., Clary, D.C.: Potential optimized discrete variable representation. Chem. Phys. Lett. **190**, 225–230 (1992)
Echim, M.M., Lemaire, J., Lie-Svendsen, O.: A review on solar wind modeling: kinetic and fluid aspects. Surv. Geophys. **32**, 1–70 (2011)
Einstein, A.: Zur theorie der brownschen bewegung. Ann. Phys. **19**, 371–381 (1906)
Feit, M.D., Fleck Jr, J.A., Steiger, A.: Solution of the Schrödinger equation by a spectral method. J. Comput. Phys. **47**, 412–433 (1982)
Feizi, H., Rajabi, A.A., Shojaei, M.R.: Supersymmetric solution of the Schrödinger equation for the Woods-Saxon potential using the Pekeris approximation. Acta Phys. Pol. B **42**, 2143–2152 (2011)
Felderhof, B.U.: Diffusion in a bistable potential. Phys. A **387**, 5017–5023 (2008)
Fokker, A.D.: Die mittlere energie rotierender elektrischer dipole im strahlungsfeld. Ann. Phys. **348**, 810–820 (1914)

Fornberg, B.: A Practical Guide to Pseudospectral Methods. Cambridge University Press, Cambridge (1996)
Francisco, J.F.: Internal rotational barriers of ClOOCl. J. Chem. Phys. **103**, 8921–8923 (1995)
Frank, T.D.: Kramers-Moyal expansion for stochastic differential equations with single and multiple delays: applications to financial physics and neurophysics. Phys. Lett. A **360**, 552–562 (2007)
Fricke, S.H., Balantekin, A.B., Hatchell, P.J., Uzer, T.: Uniform semiclassical approximation to supersymmetric quantum mechanics. Phys. Rev. A **37**, 2797–2804 (1988)
Friesner, R.A., Bentley, J.A., Menou, M., Leforestier, C.: Adiabatic pseudospectral methods for multidimensional vibrational potentials. J. Chem. Phys. **99**, 324–335 (1993)
Gardiner, C.W.: Handbook of Stochastic Methods. Springer, Berlin (2003)
Garrity, D.K., Skinner, J.L.: Effect of potential shape on isomerization rate constants for the BGK model. Chem. Phys. Lett. **95**, 46–51 (1983)
Gary, S.P.: Theory of Space Plasma Microinstabilities. Cambrigde University Press, Cambridge (1993)
Gillespie, G.T.: Approximating the master equation by Fokker-Planck type equations for single variable chemical systems. J. Chem. Phys. **72**, 5363–5370 (1980)
Gillespie, G.T.: Exact numerical simulation of the Ornstein-Uhlenbeck process and its integral. Phys. Rev. E **54**, 2084–2091 (1996)
Gitterman, M.: Simple treatment of correlated multiplicative and additive noises. J. Phys. A: Math. Gen. **32**, L293–L297 (1999)
Gomes, P.C., Pacios, L.F.: The torsional barrier of ClOOCl. J. Phys. Chem. **100**, 8731–8736 (1996)
Gomez-Ullate, D., Kamran, N., Milson, R.: An extended class of orthogonal polynomials defined by a Sturm-Liouville problem. J. Math. Anal. Appl. **359**, 352–376 (2009)
Gottlieb, D., Orszag, S.: Numerical Analysis of Spectral Methods: Theory and Applications. SIAM, Philadelphia (1977)
Guantes, R., Farantos, S.C.: High order finite difference algorithms for solving the Schrödinger equation. J. Chem. Phys. **111**, 10827–10835 (1999)
Gunther, L., Weaver, D.L.: Monte Carlo simulation of Brownian motion with viscous drag. Am. J. Phys. **46**, 543–545 (1978)
Hagelaar, G.J.M., Pitchford, L.C.: Solving the Boltzmann equation to obtain electron transport coefficients and rate coefficients for fluid models. Plasma Sources Sci. Technol. **14**, 722–733 (2005)
Hamilton, I.P., Light, J.C.: On distributed Gaussian bases for simple model multidimensional vibrational problems. J. Chem. Phys **84**, 306–317 (1986)
Hänggi, P., Talkner, P., Borkovec, M.: Reaction rate theory: fifty years after Kramers. Rev. Mod. Phys. **62**, 251–341 (1990)
Harris, D.O., Engerholm, G.G., Gwinn, W.D.: Calculation of matrix elements for one-dimensional quantum-mechanical problems and the application to anharmonic oscillators. J. Chem. Phys. **43**, 1515–1517 (1965)
Hasegawa, A., Mima, K., Duong-van, M.: Plasma distribution function in a superthermal radiation field. Phys. Rev. Lett. **54**, 2608–2610 (1985)
Henon, M., Heiles, C.: The applicability of the third integral of motion: some numerical experiments. Astron. J. **69**, 73–79 (1964)
Hinton, F.L.: Collisional transport in plasma. In: Galeev, A.A., Sagdeev, R.Z. (eds.) Handbook of Physics, Basic Plasma Physics, pp. 147–197. Elsevier, The Netherlands (1983)
Hoare, M.R.: The linear gas. Adv. Chem. Phys. **20**, 135–214 (1971)
Hoare, M.R., Kaplinsky, C.H.: Linear hard sphere gas: variational eigenvalue spectrum of the energy kernel. J. Chem. Phys. **52**, 3336–3353 (1970)
Hoffman, D.K., Wei, G.W., Zhang, D.S., Kouri, D.J.: Interpolating distributed approximating functionals. Phys. Rev. E **57**, 6152–6160 (1998)
Johnson, B.R.: New numerical methods applied to solving the one dimensional eigenvalue problem. J. Chem. Phys. **67**, 4086–4093 (1977)

Kallush, S., Kosloff, R.: Improved methods for mapped grids: applied to highly excited vibrational states of diatomic molecules. Chem. Phys. Lett. **433**, 221–227 (2006)
Karney, C.F.F.: Fokker-Planck and quasi-linear codes. Comput. Phys. Rep. **4**, 183–244 (1986)
Knessl, C., Mangel, M., Matkowsky, B.J., Schuss, Z., Tier, C.: Solution of Kramers-Moyal equations for problems in chemical physics. J. Chem. Phys. **81**, 1285–1293 (1984)
Knierim, K.D., Waldman, M., Mason, E.A.: Moment theory of electron thermalization in gases. J. Chem. Phys. **77**, 943–950 (1982)
Kokoouline, V., Dulieu, O., Kosloff, R., Masnou-Seeuws, F.: Mapped Fourier methods for long-range molecules: application to perturbations in the $Rb_2(0_u^+)$ photoassociation spectrum. J. Chem. Phys. **110**, 9865–9876 (1999)
Koput, J., Carter, S., Handy, N.C.: Ab initio prediction of the vibrational-rotational energy levels of hydrogen peroxide and its isotopomers. J. Chem. Phys. **115**, 8345–8350 (2001)
Koura, K.: Nonequilibrium electron velocity distribution and temperature in thermalization of low energy electrons in molecular hydrogen. J. Chem. Phys. **79**, 3367–3372 (1983)
Kowari, K., Demeio, L., Shizgal, B.: Electron degradation and thermalization in CH_4 gas. J. Chem. Phys. **97**, 2061–2074 (1992)
Kowari, K., Shizgal, B.: On the existence of a steady electron distribution for systems with electron attachment: Ar-CCl_4 mixtures. Chem. Phys. Lett. **260**, 365–370 (1996)
Kowari, K.-I., Leung, K., Shizgal, B.D.: The coupling of electron thermalization and electron attachment in CCl_4/Ar and CCl_4/Ne mixtures. J. Chem. Phys. **108**, 1587–1600 (1998)
Kramers, H.A.: Brownian motion in a field of force and the diffusion model of chemical reactions. Physica **7**, 284–304 (1940)
Kuczka, J., Hänggi, P., Gadmski, A.: Non-Markovian process driven quadratic noise: Kramers-Moyal expansion and Fokker-Planck modeling. Phys. Rev. E **51**, 2933–2938 (1995)
Kumar, K., Skullerud, H.R., Robson, R.E.: Kinetic theory of charged particle swarms in neutral gases. Aust. J. Phys. **33**, 343–448 (1980)
Kuščer, I., Williams, M.M.R.: Relaxation constants of a uniform hard sphere gas. Phys. Fluids **10**, 1922–1927 (1967)
Kustova, E.V., Giordano, D.: Cross-coupling effects in chemically non-equilibrium viscous compressible flows. Chem. Phys. **379**, 83–91 (2011)
Landau, D.P., Binder, K.: A Guide to Monte Carlo Simulations in Statistical Physics, 3rd edn. Cambridge University Press, Cambridge (2009)
Larsen, E.W., Livermore, C.D., Pomraning, G.C., Sanderson, J.G.: Discretization methods for one-dimensional Fokker-Planck operators. J. Comput. Phys. **61**, 359–390 (1985)
Larson, R.S., Kostin, M.D.: Kramers's theory of chemical kinetics: eigenvalue and eigenfunction analysis. J. Chem. Phys. **69**, 4821–4829 (1978)
Lauvergnat, D., Nauts, A.: Quantum dynamics with sparse grids: a combination of Smolyak scheme and cubature. Application to methanol in full dimensionality. Spectrochim. Acta, A **119**, 18–25 (2014)
Lax, M.: Classical noise IV: Langevin method. Rev. Mod. Phys. **38**, 541–566 (1966)
Layton, E.G.: The Fourier-grid formalism: philosophy and application to scattering problems using R-matrix theory. J. Phys. B: At. Mol. Opt. Phys. **36**, 2501–2522 (1993)
Le, H.M., Huynh, S., Raff, L.: Molecular dissociation of hydrogen peroxide (HOOH) on a neural network ab initio potential surface with a new configuration sampling method involving gradient fitting. J. Chem. Phys. **131**, 014107 (2009)
Leblanc, F., Hubert, D.: A generalized model for the proton expansion in astrophysical winds. I. The velocity distribution function representation. Astrophys. J. **483**, 464–474 (1997)
Lemou, M., Chavanis, P.H.: Escape of stars from gravitational clusters in the Chandrasekhar model. Phys. A **389**, 1021–1040 (2010)
Leubner, M.P., Vörös, Z.: A nonextensive entropy approach to solar wind intermittency. Astrophys. J. **618**, 547–555 (2005)

Leung, K., Shizgal, B.D., Chen, H.: The quadrature discretization method QDM in comparison with other numerical methods of solution of the Fokker-Planck equation for electron thermalization. J. Math. Chem. **24**, 291–319 (1998)

Lie-Svendsen, O., Rees, M.H.: An improved kinetic model for the polar outflow of a minor ion. J. Geophys. Res. **101**, 2415–2433 (1996)

Light, J.C., Hamilton, I.P., Lill, J.V.: Generalized discrete variable approximation in quantum mechanics. J. Chem. Phys. **82**, 1400–1409 (1985)

Lightman, A.P., Shapiro, S.L.: The dynamical evolution of globular clusters. Rev. Mod. Phys. **50**, 437–481 (1978)

Lin, S.Y., Guo, H.: Exact quantum mechanical calculations of rovibrational energy levels of hydrogen peroxide (HOOH). J. Chem. Phys. **119**, 5867–5873 (2003)

Lin, S.R., Robson, R.E., Mason, E.A.: Moment theory of electron drift and diffusion in neutral gases in an electrostatic field. J. Chem. Phys. **71**, 3483–3498 (1979)

Lindenfeld, M.J., Shizgal, B.: The Milne problem: a study of the mass dependence. Phys. Rev. **A27**, 1657–1670 (1983)

Littlejohn, R.G., Cargo, M., Carrington Jr, T., Mitchell, K.A., Poirier, B.: A general framework for discrete variable representation basis sets. J. Chem. Phys. **116**, 8691–8703 (2002)

Livadiotis, G., McComas, D.J.: Beyond Kappa distributions: exploiting Tsallis statistical mechanics in space plasmas. J. Geophys. Res. **114**, A11105 (2009)

Lo, J.Q.-W., Shizgal, B.D.: Spectral convergence of the quadrature discretization method in the solution of the Schrödinger and Fokker-Planck equations: comparison with Sinc methods. J. Chem. Phys. **125**, 194108 (2006)

Lo, J.Q.-W., Shizgal, B.D.: An efficient mapped pseudospectral method for weakly bound states: vibrational states of He_2, Ne_2, Ar_2 and Cs_2. J. Phys. B: At. Mol. Opt. Phys. **41**, 185103 (2008a)

Lo, J.Q.-W., Shizgal, B.D.: Pseudospectral methods of solution of the Schrödinger equation. J. Math. Chem. **44**, 787–801 (2008b)

Lutsko, J.F., Boon, J.P.: Questioning the validity of non-extensive thermodynamics for classical Hamiltonian systems. EPL **95**, 20006 (2011)

Lynch, V.A., Mielke, S.L., Truhlar, D.G.: Accurate vibrational-rotational partition functions and standard-state free energy values for H_2O_2 from Monte Carlo path-integral calculations. J. Chem. Phys. **121**, 5148–5162 (2004)

Ma, C.-Y., Summers, D.: Formation of power-law energy spectra in space plasmas by stochastic acceleration due to Whistler-mode waves. Geophys. Res. Lett. **26**, 1121–1124 (1999)

Magnus, A.P., Pierrard, V.: Formulas for the recurrence coefficients of orthogonal polynomials related to Lorentzian-like weights. J. Comput. Appl. Math. **219**, 431–440 (2008)

Marechal, E., Moreau, M.: On the microscopic kinetic theory of a chemical reaction in the limit of high collision frequency. Mol. Phys. **51**, 133–140 (1984)

Marsch, E.: Kinetic physics of the solar corona and solar wind. Living Rev. Sol. Phys. **3**, 1–100 (2006)

Marston, C.C., Balint-Kurti, G.G.: The Fourier grid Hamiltonian method for bound state eigenvalues and eigenfunctions. J. Chem. Phys. **91**, 3571–3576 (1989)

Mazziotti, D.A.: Spectral difference methods for solving differential equations. Chem. Phys. Lett. **299**, 473–480 (1999)

McMahon, D.R.A., Shizgal, B.: Hot-electron zero-field mobility and diffusion in rare-gas moderators. Phys. Rev. A **31**, 1894–1905 (1985)

Meshkov, V.V., Stolyarov, A.V., Le Roy, R.J.: Adaptive analytical mapping procedure for efficiently solving the radial Schrödinger equation. Phys. Rev. A **78**, 052510 (2008)

Meyer-Vernet, N.: Large scale structure of planetary environments: the importance of not being Maxwellian. Planet. Space Sci. **49**, 247–260 (2001)

Mielke, S.L., Chakraborty, A., Truhlar, D.G.: Vibrational configuration interaction using a tiered multimode scheme and tests of approximate treatments of vibrational angular momentum coupling: a case study for Methane. J. Phys. Chem. A **117**, 7327–7343 (2013)

Miller, S.C., Good Jr, R.H.: A WKB-type approximation to the Schrödinger equation. Phys. Rev. **91**, 174–179 (1953)
Mintzer, D.: Generalized orthogonal polynomial solutions of the Boltzmann equation. Phys. Fluids **8**, 1076–1090 (1965)
Mitchner, M., Kruger, C.H.J.: Partially Ionized Gases. Wiley, New York (1973)
Montgomery, J.A., Chandler, D., Berne, B.J.: Trajectory analysis of a kinetic theory for isomerization dynamics in condensed phases. J. Chem. Phys. **70**, 4056–4066 (1979)
Morse, P.M.: Diatomic molecules according to the wave mechanics II. Vibrational levels. Phys. Rev. **34**, 57–64 (1929)
Mozumder, A.: Electron thermalization in gases. III epithermal electron scavenging in rare gases. J. Chem. Phys. **74**, 6911–6921 (1981)
Mozumder, A.: Fundamentals of Radiation Chemistry. Academic Press, London (1999)
Müller, P.L.G., Hernandez, R., Benito, R.M., Borondo, F.: Detailed study of the direct numerical observation of the Kramers turnover in the LiNC⇌LiCN isomerization rate. J. Chem. Phys. **137**, 204301 (2012)
Nauenberg, M.: Critique of q-entropy for thermal statistics. Phys. Rev. E **67**, 036114 (2003)
Nicholson, D.R.: Introduction to Plasma Theory. Wiley, New York (1983)
Nicolis, C.: Stochastic aspects of climatic transitions—response to a periodic forcing. Tellus **34**, 1–9 (1982)
Nicolis, C., Nicolis, G.: Stochastic aspects of climatic transitions—additive fluctuations. Tellus **33**, 225–234 (1981)
Noid, D.W., Marcus, R.A.: Semiclassical calculation of bound states in a multidimensional system for nearly 1:1 degenerate systems. J. Chem. Phys. **67**, 559–567 (1977)
ONeil, S.V., Reinhardt, W.P.: Photoionization of molecular hydrogen. J. Chem. Phys. **69**, 2126–2142 (1978)
Park, B.T., Petrosian, V.: Fokker-Planck equations of stochastic acceleration: a study of numerical methods. Astrophys. J. Suppl. Ser. **103**, 225–267 (1996)
Parker, E.N.: Dynamical theory of the solar wind. Space Sci. Rev. **4**, 666–708 (1965)
Parrish, R.M., Hohenstein, E.G., Martnez, T.J., Sherrill, C.D.: Discrete variable representation in electronic structure theory: quadrature grids for least-squares tensor hypercontraction. J. Chem. Phys. **138**, 194107 (2013)
Pasquetti, R., Rapetti, F.: Spectral element methods on triangles and quadrilaterals: comparisons and applications. J. Comput. Phys. **198**, 349–362 (2004)
Pastor, R.W., Karplus, M.: Inertial effects in butane stochastic dynamics. J. Chem. Phys. **91**, 211–218 (1989)
Paul, W., Baschnagel, J.: Stochastic Processes; From Physics to Finance, 2nd edn. Springer, Berlin (2013)
Petrović, Z.L., Dujko, S., Marić, D., Malović, G., Nikitović, Ž., Šašič, O., Jovanović, J., Stojanović, V., Radmilović-Radenović, M.: Measurement and interpretation of swarm parameters and their application in plasma modelling. J. Phys. D: Appl. Phys. **42**, 194002 (2009)
Pierrard, V., Lemaire, J.: A collisional model of the polar wind. J. Geophys. Res. **103**, 11701–11709 (1998)
Pierrard, V., Lazar, V.: Kappa distributions; theory and applications in space plasmas. Sol. Phys. **267**, 153–174 (2010)
Pierrard, V., Lamy, H., Lemaire, J.: Exospheric distributions of minor ions in the solar wind. J. Geophys. Res. **109**, A02118 (2004)
Pitchford, L.C., Phelps, A.V.: Comparative calculations of electron-swarm properties in N_2 at moderate E/N values. Phys. Rev. A **25**, 540–554 (1982)
Planck, M.: Ueber einen satz der statistichen dynamik und eine erweiterung in der quantumtheorie. Sitzber. Preuß. Akad. Wiss. pp. 324–341 (1917)
Pollak, E., Talkner, P.: Reaction rate theory: what it was, where is it today, and where is it going? Chaos **15**, 026116 (2005)

Pollak, E., Ianconescu, R.: Finite barrier corrections to the PGH solution of Kramers turnover theory. J. Chem. Phys. **140**, 154108 (2014)
Pollak, E., Grabert, H., Hänggi, P.: Theory of activated rate processes for arbitrary frequency dependent friction: solution of the turnover problem. J. Chem. Phys. **91**, 4073–4087 (1989)
Pope, S.B.: Turbulent Flows. Cambridge University Press, Cambridge (2000)
Pryce, J.D.: Numerical Solution of Sturm-Liouville Problems. Oxford University Press, Oxford (1993)
Reif, F.: Fundamentals of Statistical and Thermal Physics. Waveland Press, Illinois (2008)
Reinhardt, W.P.: L^2 discretization of atomic and molecular electronic continua: moment, quadrature and J-matrix techniques. Comput. Phys. Commun. **17**, 1–21 (1979)
Risken, H.: The Fokker-Planck Equation: Methods of Solution and Applications, 2nd edn. Springer, Berlin (1996)
Risken, H., Voigtlaender, K.: Solutions of the Fokker-Planck equation describing thermalization of neutrons in a heavy gas moderator. Z. Phys. B—Condens. Matter **54**, 253–262 (1984)
Risken, H., Till, F.: The Fokker-Planck equation: Methods of solution and applications, 2nd edn. Springer, Berlin (1996)
Robson, R.E.: Introductory Transport Theory for Charges Particles in Gases. World Scientific, Singapore (2006)
Robson, R.E., Ness, K.F.: Velocity distribution and transport coefficients of electron swarms in gases: spherical-harmonic decomposition of Boltzmann's equation. Phys. Rev. A **33**, 2068–2077 (1986)
Rosenbluth, M., Macdonald, F.W.M., Judd, D.L.: Fokker-Planck equation for an inverse-square force. Phys. Rev. **107**, 1–6 (1957)
Ross, J., Mazur, P.: Some deductions from a formal statistical mechanical theory of chemical kinetics. J. Chem. Phys. **35**, 19–28 (1961)
Ryckaert, J.-P., Bellemans, A.: Molecule dynamics of liquid alkanes. Faraday Discuss. Chem. Soc. **66**, 95–106 (1978)
Sakai, Y.: Quasifree electron transport under electric field in nonpolar simple-structured condensed matters. J. Phys. D: Appl. Phys. **40**, R441–R452 (2007)
Schindler, M., Talkner, P., Hänggi, P.: Escape rates in periodically driven Markov processes. Physica A **351**, 40–50 (2005)
Schulz, M., Lanzerotti, M.L.: Particle Diffusion in the Radiation Belts. Springer, Berlin (1974)
Schwartz, C.: High-accuracy approximation techniques for analytic functions. J. Math. Phys. **26**, 411–415 (1985)
Scudder, J.D.: Ion and electron suprethermal tail strengths in the transition region for the velocity filtration model of the corona. Astrophys. J. **427**, 446–452 (1994)
Shematovich, V.I., Bisikalo, D.V., Gérard, J.-C., Cox, C., Bougher, S.W.: Monte Carlo model of electron transport for the calculation of mars dayglow emissions. J. Geophys. Res. **113**, E02011 (2008)
Shizgal, B.: Eigenvalues of the Lorentz Fokker-Planck equation. J. Chem. Phys. **70**, 1948–1951 (1979)
Shizgal, B.: The coupling of electron thermalisation and electron attachment; SF_6 and $CC1_4$ in rare-gas moderators. J. Phys. B: At. Mol. Opt. Phys. **21**, 1699–1715 (1988)
Shizgal, B.: Negative differential conductivity of electrons in He-Xe and He-Kr mixtures. Chem. Phys. **147**, 271–279 (1990)
Shizgal, B.: Relaxation in ionized gases: the role of the spectrum of the collision operator. In: Beylich, A.E. (ed.) Proceedings of the 17th International Symposium on Rarefied Gas Dynamics, pp. 22–29. VCH Verlagsgesellschaft GmbH, Berlin (1991)
Shizgal, B.: Spectral theory and the approach to equilibrium in a plasma. Trans. Theory Stat. Phys. **21**, 645–665 (1992)
Shizgal, B.D.: The quadrature discretization method (QDM) in the calculation of the rotational-vibrational transitions in rare gas dimers. J. Mol. Struct. (Theochem) **391**, 131–139 (1997)

Shizgal, B.D.: Coulomb collisional processes in space plasmas; relaxation of suprathermal particle distributions. Planet. Space Sci. **52**, 923–933 (2004)
Shizgal, B.D.: Suprathermal particle distributions in space physics: kappa distributions and entropy. Astrophys. Space Sci. **312**, 227–237 (2007)
Shizgal, B., Karplus, M.: Nonequilibrium contributions to the rate of reaction. I. Perturbation of the velocity distribution function. J. Chem. Phys. **52**, 4262–4278 (1970)
Shizgal, B., Fitzpatrick, J.M.: Matrix elements of the linear Boltzmann collision operator for systems of two components at different temperatures. Chem. Phys. **6**, 54–65 (1974)
Shizgal, B., McMahon, D.R.A.: Electric field dependence of transient electron transport properties in rare gas moderators. Phys. Rev. A **32**, 3669–3680 (1985)
Shizgal, B., Blackmore, R.: A collisional kinetic theory of a plane parallel evaporating planetary atmosphere. Planet. Space Sci. **34**, 279–291 (1986)
Shizgal, B., Ness, K.: Thermalisation and annihilation of positrons in helium and neon. J. Phys. B: At. Mol. Phys. **20**, 847–865 (1987)
Shizgal, B., Barrett, J.C.: Time dependent nucleation. J. Chem. Phys. **91**, 6506–6518 (1989)
Shizgal, B.D., Chen, H.: The quadrature discretization method (QDM) in the solution of the Schrödinger equation with nonclassical basis functions. J. Chem. Phys. **104**, 4137–4150 (1996)
Shizgal, B.D., Napier, D.G.: Nonequilibrium effects in reactive systems: the effect of reaction products and the validity of the Chapman-Enskog method. Physica A **223**, 50–86 (1996)
Shizgal, B.D., Chen, H.: The quadrature discretization method in the solution of the Fokker-Planck equation with nonclassical basis functions. J. Chem. Phys. **107**, 8051–8063 (1997)
Shizgal, B., McMahon, D.R.A., Viehland, L.A.: Thermalization of electrons in gases. Radiat. Phys. Chem. **34**, 35–50 (1989)
Shizgal, B., Weinert, U., Blackmore, R.: The QDM in the solution of the Kramers equation for symmetrical potentials. In: Beylich, A.E. (ed.) Proceedings of the 17th International Symposium on Rarefied Gas Dynamics, pp. 85–92. Wiley, Weinheim (1991)
Shore, B.W.: Solving the radial Schrödinger equation by using cubic-spline basis functions. J. Chem. Phys. **58**, 3855–3866 (1973)
Shoub, E.C.: Failure of the Fokker-Planck approximation to the Boltzmann integral for 1/r potentials. Phys. Fluids **30**, 1340–1352 (1987)
Skinner, J,l, Wolynes, P.G.: General kinetic models of activated processes in condensed phases. J. Chem. Phys. **71**, 4913–4927 (1980)
Solomon, S.C.: Auroral particle transport using Monte Carlo and hybrid methods. J. Geophys. Res. **106**, 107–116 (2001)
Sospedra-Alfonso, R., Shizgal, B.D.: Kullback-Leibler entropy in the electron distribution shape relaxation for electron-atom thermalization. Phys. Rev. E **84**, 041202 (2011)
Sospedra-Alfonso, R., Shizgal, B.D.: Energy and shape relaxation in binary atomic systems with realistic quantum cross sections. J. Chem. Phys. **139**, 044113 (2013)
Spendier, K., Sugaya, S., Kenkre, V.M.: Reaction-diffusion theory in the presence of an attractive harmonic potential. Phys. Rev. E **88**, 062142 (2013)
Spitzer, L.J.: Physics of Fully Ionized Gases. Interscience, New York (1962)
Spitzer, L.J.: Physical Processes in the Interstellar Medium. Wiley, New York (1998)
Spitzer, L.J., Härm, R.: Evaporation of stars from open clusters. Astrophys. J. **127**, 544–550 (1958)
Stamnes, K.: Analytic approach to auroral electron transport and energy degradation. Planet. Space Sci. **28**, 427–441 (1980)
Stix, T.H.: Waves in Plasmas. Springer, New York (1992)
Szabo, A., Schulten, K., Schulten, Z.: First passage time approach to diffusion controlled reactions. J. Chem. Phys. **72**, 4350–4357 (1980)
Tang, K.T., Toennies, J.P.: The van der Waals potentials between all the rare gas atoms from He to Rn. J. Chem. Phys. **118**, 4976–4983 (2003)
Travis, K.P., Searles, D.J.: Effect of solvation and confinement on the trans-gauche isomerization reaction in n-butane. J. Chem. Phys. **125**, 164501 (2006)

Treumann, R.A., Jaroschek, C.H., Scholer, M.: Stationary plasma states far from equilibrium. Phys. Plasmas **11**, 1317–1325 (2004)
Trunec, D., Španěl, P., Smith, D.: The influence of electron-electron collisions on electron thermalization in He and Ar afterglow plasmas. Chem. Phys. Lett. **372**, 728–732 (2003)
Tsallis, C.: Non-extensive thermostatics: brief review and comments. Phys. A **221**, 277–290 (1995)
Tsallis, C.: Comment on Critique of q-entropy for thermal statistics. Phys. Rev. E **69**, 038101 (2004)
Uhlenbeck, G.E., Ornstein, L.S.: On the theory of the Brownian motion. Phys. Rev. **36**, 823–841 (1930)
van Kampen, N.G.: Stochastic Processes in Physics and Chemistry, 3rd edn. North Holland, Amsterdam (2007)
Viehland, L.A., Ranganathan, B., Shizgal, S.: Transient microwave conductivity of electrons in helium and argon. J. Chem. Phys. **88**, 362–370 (1988)
Vocks, C.: A kinetic model for ions in the solar corona including wave-particle interactions and Coulomb collisions. Astrophys. J. **568**, 1017–1029 (2002)
Voigtlaender, K., Risken, H.: Solutions of the Fokker-Planck equation for a double-well potential in terms of continued fractions. J. Stat. Phys. **40**, 397–429 (1985)
Wei, H.: Ghost levels and near-variational forms of the discrete variable representation: application to H_2O. J. Chem. Phys. **106**, 6885–6900 (1997)
Wei, G.W.: Discrete singular convolution for the solution of the Fokker Planck equation. J. Chem. Phys. **110**, 8930–8942 (1999)
Wei, G.W.: Solving quantum eigenvalue problems by discrete singular convolution. J. Phys. B: At. Mol. Opt. Phys. **33**, 343–352 (2000)
Wei, G.W., Zhang, D.S., Kouri, D.J., Hoffman, D.K.: Lagrange distributed approximating functionals. Phys. Rev. Lett. **79**, 775–779 (1997)
Weideman, W.A.C.: Spectral methods based on non-classical polynomials. In: Gautschi, G., Golub, G.H., Opfer, G. (eds.) Approximations and Computation of Orthogonal Polynomials, pp. 239–251. birkhauser, Basel (1999)
White, R.D., Dujko, S., Robson, R.E., Petrović, Z.L., McEachran, R.P.: Non-equilibrium transport of positron and electron swarms in gases and liquids. Plasma Sources Sci. Technol. **19**, 034001 (2010)
White, R.D., Robson, R.E.: Multiterm solution of a generalized Boltzmann kinetic equation for electron and positron transport in structured and soft condensed matter. Phys. Rev. E **84**, 031125 (2011)
Wigner, E.P.: A solution of Boltzmann's equation for monoenergetic neutrons in an infinite medium. Technical Report AECD-3125, U.S. Atomic Energy Commission (1943)
Wigner, E.P., Wilkins Jr, J.E.: Effect of temperature of the moderator on the velocity distribution of neutrons with numerical calculations for H as moderator. Technical Report AECD-2275, U.S. Atomic Energy Commission (1944)
Wilkinson, M., Pumir, A.: Spherical Ornstein-Uhlenbeck process. J. Stat. Phys. **145**, 113–142 (2011)
Willner, K., Dulieu, O., Masnou-Seeuws, F.: Mapped grid methods for long-range molecules and cold collisions. J. Chem. Phys. **120**, 548–561 (2004)
Wind, H.: Electron energy for H_2^+ in the ground state. J. Chem. Phys. **42**, 2371–2373 (1965)
Yang, W., Peet, A.C.: The collocation method for bound solutions of the Schrödinger equation. Chem. Phys. Lett. **153**, 98–104 (1988)

Index

B. Shizgal, *Spectral Methods in Chemistry and Physics*, Scientific Computation,
DOI 10.1007/978-94-017-9454-1